Universitat Autònoma de Barcelona

Antimicrobial and immune-modulation action within the RNase A superfamily using macrophage infection models

LU LU

Universitat Autònoma de Barcelona

DOCTORAL THESIS

Antimicrobial and immune-modulation action within the RNase A superfamily using macrophage infection models

LU LU

March 2020

Universitat Autònoma de Barcelona

Thesis presented by **Lu Lu** to obtain the degree of doctor in

Biochemistry and molecular biology

Supervised by:

Ester Boix

Dr. **Ester Boix** **Lu Lu**

Biochemistry and Molecular Biology department

Biosciences Faculty,

Campus UAB

Cerdanyola del Vallès, Spain

March 2020

List of papers included in the thesis:

1. Arranz-Trullén J, **Lu L**, Pulido D, Bhakta S, Boix E. Host Antimicrobial Peptides: The Promise of New Treatment Strategies against Tuberculosis. *Frontiers in Immunology*. doi:10.3389/fimmu.2017.01499.
2. **Lu L**, Li J, Moussaoui M, Boix E. Immune Modulation by Human Secreted RNases at the Extracellular Space. *Frontiers in Immunology*. doi:10.3389/fimmu.2018.01012.
3. **Lu L**, Arranz-Trullén J, Prats-Ejarque G, Pulido D, Bhakta S, Boix E. Human Antimicrobial RNases inhibit intracellular bacterial growth and induce Autophagy in Mycobacteria-Infected Macrophages. *Frontiers in Immunology*. doi: 10.3389/fimmu.2019.01500.
4. **Lu L**, Wei RL, Goetz-Antico M, Prats-Ejarque G, Wang G, Torrent M, Boix E. Immunomodulatory action of RNase3/ECP in a macrophage infection model related and unrelated to catalytic activity. (Manuscript submitted to *Cellular and Molecular Life Sciences*)
5. **Lu L**, Wei RL, Goetz-Antico M, Pablo Fernandez-Millan, Boix E. RNase2 antiviral activity against human respiratory syncytial virus through macrophage immunomodulation and targeting of tRNA. (Manuscript in preparation)
6. Prats-Ejarque G, **Lu L**, Salazar VA, Moussaoui M, Boix E. Evolutionary Trends in RNA Base Selectivity Within the RNase A Superfamily. *Frontiers in Pharmacology*, 2019. doi: 10.3389/fphar.2019.01170

ACKNOLDGEMENTS

I would like to give special thanks to my supervisor, Ester Boix. She has provided excellent support as my supervisor and it would be hard to find a person with more dedication to science and her students. She has provided expert knowledge to all work regarding experimental procedures and supported me during all aspects of my PhD.

To my committee members, Prof. Victoria Nogues, Prof. Marc Torrent and Prof. Ester Carreras for their support and helpful suggestions regarding my project.

Much of the work in this thesis could not have been carried out without the work of Mohhammed, Guillem and Pablo.

To my "students", Maria Goetz and Eva Garcia Moro, for their intensive and excellent works.

To my lab mates, Clara, Javier, Helena, Jiarui, Sergi, Vivian.

To Fransisco, Laura, Anna Genesca, Marina and Marcos, generously offered help with the experiment.

Yo no hablo mucho español, ni Catalan, pero entiendo lo que significa cuando dije que te quiero. Al menos esta vez, deseo expresar mi agradecimiento con mi armor a Jofre, Gisela, Gabriel, Alejandro, Jordi, Marcos, Valentin, Fransica, Jaime, Samuel, Raquel, Joan, Shuang, Pilar, Lucia, Ana Paula, Nuria, Salvador, Santiago, Elena, Magda, Juan Carlos, Maria.

The last, to my country and families who provide solid support, economically and mentally.

Contents

Abbreviations

AMP: antimicrobial peptide

APD: antimicrobial peptide database

CRISPR: clustered regularly interspaced short palindromic repeats

DC: dendritic cell

DEGs: differential expressed genes

ECP: eosinophil cationic protein

EDN: eosinophil derived neurotoxin

EGFR: epidermal growth factor receptor

exRNAs: extracellular RNAs

HDP: host defense peptide

HIV: human immunodeficiency virus

HPLC: high performance liquid chromatography

LPS: lipopolysaccharide

MIC: minimum inhibitory concentration

MAC: minimum aggregation concentration

ncRNAs: non-coding RNAs

RI: ribonuclease inhibitor

RSV: respiratory syncytial virus

TLR: toll-like receptor

tiRNAs: tRNA-derived stress-induced small RNAs

tRFs: tRNA fragments

SUMMARY

My PhD project focused on the biological function analysis of human RNases, emphasizing the immune-regulation action within human macrophages to fight pathogen infection and the potential molecular mechanisms involved. Our laboratory has extensively studied human RNases and found that RNases have a direct antimicrobial activity against diverse bacterial species *in vitro*, suggesting a physiological host-defense function. In this doctoral thesis, the main goal is to understand how human RNases function in human innate cells against pathogen infection.

The majority of the research presented in this thesis is taken from 4 published papers, 1 manuscript submitted and 1 in preparation. Below is a description of each chapter within this thesis:

CHAPTER I:

A version of Chapter 1 has been published as:

Arranz-Trullén J, **Lu L**, Pulido D, Bhakta S, Boix E. Host Antimicrobial Peptides: The Promise of New Treatment Strategies against Tuberculosis. 2017, 8, 1499, *Frontiers in Immunology*. This chapter mainly summarized the antipathogenic mechanism of human antimicrobial peptides and proteins in mycobacterial infections and their applied therapies against tuberculosis.

CHAPTER II:

A version of Chapter 2 has been published as:

Lu L, Li J, Moussaoui M, Boix E. Immune Modulation by Human Secreted RNases at the Extracellular Space. 2018, 9, 1012, *Frontiers in Immunology*. This chapter reviewed the immune-regulation functions of human RNase superfamily. 8 human RNase A family members were summarized based on their contribution to innate immunity at the extracellular space.

CHAPTER III:

A version of Chapter 3 has been published as:

Lu L, Arranz-Trullén J, Prats-Ejarque G, Pulido D, Bhakta S, Boix E. Human Antimicrobial RNases inhibit intracellular bacterial growth and induce Autophagy in Mycobacteria-Infected Macrophages. 2019, 10, 1500, *Frontiers in Immunology*. This chapter focused on screening the antimicrobial profiles of human RNases against *M. aurum* and identifying their ability to induce autophagy in infected macrophages. Moreover, we found that the antimicrobial and autophagy activities were not dependent on the RNase enzymatic activity.

CHAPTER IV:

A version of Chapter 4 is currently being prepared for submission as: **Lu L**, Wei RL, Goetz M, Prats-Ejarque G, Wang G, Torrent M, Boix E. Immunomodulatory action of RNase3/ECP in a macrophage infection model related and unrelated to catalytic activity. In this chapter, the transcriptome of macrophages treated with RNase3 and RNase3-H15A (a catalytic defective mutant) were compared to identify the molecular mechanism of the immune-regulation action of RNase3. Moreover, we overexpressed the endogenous RNase3 in THP1 derived-macrophage cells and analyzed its effect on the infectivity by *Mycobacterium aurum* and the Respiratory Syncytial Virus. We identified RNase3 immune-regulation activities on macrophages, either in a

ribonucleolytic-dependent or independent manner. We propose that RNase3 directly targets the EGFR receptor. On the other hand, the RNA products cleaved by RNase3 may be responsible for the ribonucleolytic-dependent macrophage immune response.

CHAPTER V:
A version of Chapter 5 is currently being prepared for publication as:
Lu L, Wei RL, Goetz M, Boix E. RNase2 antiviral activity against human respiratory syncytial virus through macrophage immunomodulation and targeting of tRNA.
In this chapter, CRISPR/Cas9 gene editing tool was applied to knock out RNase2 in macrophage THP1 cells. Then, RSV infectivity, transcriptome change, and tRNA population were compared in cells with and without endogenous RNase2. Our results indicated that RNase2 is crucial in controlling the macrophage intracellular RSV infection. Transcriptome analysis suggests a direct interaction of RNase2 with the EGFR receptor. In addition, by screening a library of tRNA fragments we identified the tRNA fragments produced by RNase2 that might participate in the virus infection inhibition.

CHAPTER VI:
A version of Chapter 6 has been published as:
Prats-Ejarque G, **Lu L**, Salazar VA, Moussaoui M, Boix E. Evolutionary Trends in RNA Base Selectivity Within the RNase A Superfamily. 2019, 10, 1170, *Frontiers in Pharmacology.*
In this chapter, we analyzed the enzyme substrate specificity at the secondary nucleotide base binding site and performed a kinetic characterization of the canonical RNase types together with a molecular dynamic simulation of the selected representative family members. The results highlight an evolutionary trend from lower to higher order vertebrates towards an enhanced discrimination for adenine respect to guanine preference, The RNase binding involves specific bidentate polar and electrostatic interactions: Asn to N1/N6 and N6/N7 adenine groups in mammals versus Glu/Asp and Arg to N1/N2, N1/O6 and O6/N7 guanine groups in non-mammals. The study aims to identify the structural basis for the specific recognition of cellular RNA substrates.
In conclusion, the results presented in this thesis contribute to understand the role of RNases in innate immune cells and how they facilitate the host clearance of pathogens, which is crucial for designing and developing new therapeutic agents.

1 INTRODUCTION

Drug-resistant bacteria are becoming a major world health issue(1). Host defense peptides (HDPs), also named as antimicrobial peptides (AMPs), represent a promising alternative to conventional antibiotics(2). HDPs are gene coded and produced by a wide variety of animals, plants, fungi, protists, archaea, bacteria and viruses(3,4). Instead of AMP, HDP is a better term to define these peptides, as recent studies have demonstrated that most AMPs are endowed with a wide range of activities. Apart from their mere antimicrobial properties, AMPs display a variety of immune-modulating activities and participate in the natural host defense system(3). In fact, HDPs are key components of the innate immunity and they play a critical role in cleaning invading pathogens. Moreover, HDPs can possess other complementary biological functions, such as apoptosis induction, wound healing, and tissue remodeling(3,5).

1.1 Diversity of HDPs

1.1.1 Identification of HDPs

Since cecropin was identified in *Hyalophora cecropia* moth, more than 3000 antimicrobial peptides with diverse sequences and structures are now compiled in the antimicrobial Peptide Database (APD3, http://aps.unmc.edu/AP/main.php). Two major methods were utilized for AMP identification, chromatographic and bioinformatic approaches. Initially, chromatographic approaches were used to isolate and characterize new peptides, for example, identification and purification of HDP from frog skin secretions. Briefly, the peptide components in the secretions can be separated using reverse-phase high performance liquid chromatography (HPLC), of which the peptides with antimicrobial activity are then identified. Individual peptides with antimicrobial activity are further characterized structurally by an automated Edman assay and mass spectrometry(6,7).

With the recognition of conserved peptide sequence motifs, bioinformatic approaches were later developed to identify HDPs at the genomic level(8). The genomic and transcriptome databases are valuable sources to identify gene sequences involved in the biosynthesis of HDPs. A number of HDP prediction tools have been designed and made freely available online, and an empirical comparison of those tools have been well conducted(9). The *in silico* analysis of protein sequences or gene databases are strategies used to predict peptides of therapeutic interest(10). The search for peptides using this strategy is performed by using sophisticated computational programs that scan the databases, correlating the antimicrobial peptide features previously described in the literature with the amino acid sequences. Since the main characteristics of antimicrobial peptides are already known, the pursuit of these similarities *in silico* in the available databases is a tool to facilitate the identification and selection of new HDPs. To certify the *in silico* identified peptides, the selected sequences must be synthesized and evaluated *in vitro* against selected microorganisms to explore their antimicrobial potential. Besides, once the sequences are identified, it is also possible to make chemical variations in their amino acid residues, in order to improve their antimicrobial activity. Recently, a new deep neutral network classifier was developed which can better recognize HDP compared to the existing methods(11).

1.1.2 Classification of HDPs

Natural HDPs can be arbitrarily classified based on peptide size: ultra-short (2-10 aa), short (10-24 aa), medium (25-50 aa), and long (50-100 aa). HDPs greater than 100 aa are classified as antimicrobial proteins, as for example, lysozyme or RNase7. HDPs can

also be classified in numerous ways based on their biological sources biological functions (antibacterial, antiviral, antifungal, antiparasitic, insecticidal, chemotactic, etc), physicochemical properties (charge, hydrophobicity, amino acid composition, length), primary structure (covalent bonding pattern, linear or circular main chains), secondary and three dimensional structure (alpha helical, beta strand and random coil content) as well as their molecular targets (cell surface and intracellular targeting).

1.1.3 Structural determinants of HDPs

Sequence composition and structural propensity, cationicity, hydrophobicity and amphipathicity are the most important structural determinants for HDPs microbicidal and cytotoxic activities.

1.1.3.1 Sequence and structure

Although HDPs show a high variability in their amino acid composition, some common traits have been found. For example, lysine and arginine are the most frequent residues and have an important role in HDPs interaction with negative membrane components(12). However, it is considered that it is the overall amino acid composition and physicochemical features that determines the antimicrobial activity of HDPs, rather than their specific amino acid sequences or peptide structures(13–16). Notwithstanding, the peptides' overall features are intrinsically dependent to specific amino acids. Subtle changes of specific amino acids and their relative positioning may lead to major functional differences in their antimicrobial activity and cytotoxicity toward host cells.

Besides, the structures and conformations have been recognized as one of the key factors determining the antimicrobial activity of HDPs. During the process of interacting with biological membranes, the main secondary structures adopted by HDPs are α-helical and β-sheet(17). Most cationic amphipathic peptides do not present specific structures in a polar hydrophilic medium, while the amphipathic sequence tends to reorganize after the initial contact with the membrane through electrostatic interactions. In particular, the stable helical secondary structure is optimal for HDPs interactions with the membrane core, resulting in destabilizing and/or penetrating into the cell(18). β-sheet structures are the second most common structure for HDPs. The disulfide bond makes these molecules more resistance to degradation by peptidases(19).

Nevertheless, the modification of amino acids of HDPs should not be ignored. Especially, in the design of synthetic peptides, chemical modifications such as halogenation, oxidation, reduction, or introduction of unnatural amino acids, can broaden the functional scope of naturally occurring peptides(17). For example, modifying amino acids can increase the stability of peptides through increasing the resistance to proteolytic degradation. Moreover, it can fulfill specific requirements during peptide design, such as ensuring a proper balance of cationic and hydrophobic regions.

1.1.3.2 Cationicity

High cationicity is mostly required for interaction with bacterial surface. Gram-positive bacteria cell wall is rich in peptidoglycans and other polymers such as teichoic acids, teichuronic acids, lipoteichoic acids, and glycolipids. On their side, Gram-negative bacteria are more complex, consisting of an outer membrane (composed of lipopolysaccharides and phospholipids), a layer between the outer and inner membranes (composed of peptidoglycans) and the inner membrane (composed of phospholipids and proteins)(20). Those components of bacterial membranes have large quantities of

negatively charged molecules that influence their interactions with HDPs. HDPs vary in cationicity, but most active peptides fall into an range from +2 to +11 net charge(21). Some studies have shown that there is a correlation between charge and potency, but no optimal structure-function profiles have been determined because additional parameters (secondary interactions, solvation and composition) have to be considered(17,22).

1.1.3.3 Hydrophobicity

Hydrophobicity is another important feature determining the antimicrobial activity of HDPs, because it facilitates its interaction with the membrane lipids. The percentage of hydrophobic residues in natural HDPs varies between 40% and 60%, this is consistent with the requirement for energetically stable amphipathic structures for antimicrobial function.

Hydrophobicity governs the partition degree of a peptide from water to the lipid bilayer, thus it is crucial for the specificity toward a class of microorganism or enhanced antimicrobial activity of HDPs. For example, a reduction of hydrophobicity will impair the antimicrobial profile while an increase causes a loss in selectivity towards microbial membranes, inducing the hemolytic activity of eukaryotic cells(23,24). It is important to note that a fine balance of charge and hydrophobicity should be considered in designing synthetic peptides.

1.1.3.4 Amphipathicity

Amphipathicity of HDPs is quantified by calculating the vectorial sum of individual amino acid hydrophobicity vectors and normalizing to an ideal helix(25). Thus, HDP amphipathicity is commonly described as peptide helicity. However, amphipathic structures are not limited to helical molecules because β-turn or β-sheets can also present amphipathicity(26). Cationic moieties and hydrophobic moieties, the common features of these amphipathic molecules, are responsible for initial peptide-membrane electrostatic interaction and subsequent interaction with hydrocarbon chains of lipids. Most peptides are unstructured and will fold into a defined structure until hydrophobic interactions happen and become prevalent. Amphipathicity is considered the feature most relevant to the antimicrobial activity of HDPs, affecting the mechanism of action(27,28). Likewise, amphipathicity is also crucial for antifungal(29), antiparasitic(29), and anticancer activities(30).

1.2 Antimicrobial action of HDP against microorganisms

The evolutionarily widespread distribution and the extreme diversity of HDPs highlight their prominent role in immune defense. The main mode of the antimicrobial action for most HDPs is through non-specific physical disruption of bacterial wall or cytoplasmic membranes(31).

1.2.1 Membrane target

Most HDPs act on cytoplasmic membrane of microorganisms. Important mechanisms of action of HDPs are carpet-like, barrel stave, or toroidal pore formation(32,33). Electrostatic interactions between HDPs and bacterial membrane components initiated the physical disruption of membranes. Firstly, negatively charged microbial membranes components such as lipopolysaccharide (LPS) of Gram-negative bacteria, lipoteichoic acids of Gram-positive bacteria, and peptidoglycan of both Gram-negative bacteria and Gram-negative bacteria drive the electrostatic interaction with cationic HDPs. The electrostatic interactions between anionic phospholipid head groups of the outer layer of

the lipid membrane and HDPs will happen once HDPs reached the cytoplasmic membrane. The HDPs are then induced to adopt amphipathic structures with the charged side facing outward towards the phospholipid head groups and the hydrophobic part embedded into the acyl tail core, which further leads to cell depolarization, leakage of cellular contents and ultimate cell death. Other specific mechanisms targeting membrane have also been reported, such as membrane thinning(34) and non-lytic membrane depolarization(35).

1.2.2 Intracellular target

In addition to acting at the bacterial membrane level at high concentrations above the minimal inhibitory concentration (MIC), many HDPs have the ability to cross the membrane and interact with intracellular components without excessively disrupting the cell membrane(33,36). Those HDPs enter the pathogen cells and targets cellular processes and metabolic pathways, such as DNA replication, RNA transcription or protein synthesis and folding. We find HDPs that specifically inactivate chaperone proteins(36) or inhibit the bacterial cell wall synthesis(37). An illustration of the AMPs targeting intracellular sites is detailed in Figure1.

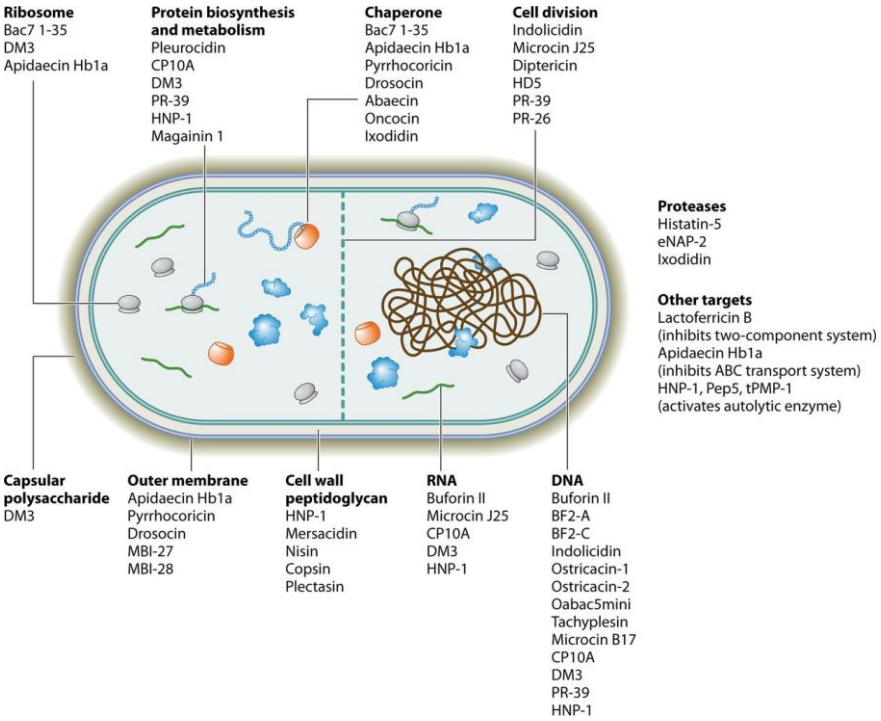

Figure1. Illustration showing the major pathways targeted by HDPs in bacterial cells. A few HDPs can inhibit multiple intracellular targets to achieve high antibacterial efficiency. Taken from(36).

1.3 Host immune-modulation action of HDPs

Most HDPs were found to have direct antimicrobial activity against microorganisms *in vitro* and this was long time considered their primary biological role *in vivo*. However, many natural HDPs play immune-modulation roles towards the host cells and many of them exhibit regulatory activities at concentrations that are much lower than those necessary for direct antimicrobial activity(38). Generally, HDPs interact with or act on target cells including monocytes, macrophages, dendritic cells, epithelial cells, neutrophils, and keratinocytes(39). Those HDPs can cross the plasma membrane of cells and/or interact with membrane receptors such as TLRs, CXCR2(40,41); while some

HDPs can bind to intracellular receptors such as GAPDH and SQSTM1(42–44). The interaction with those receptors will stimulate a variety of signal transduction pathways important in the innate immune response including the p38, Erk1/2, and JNK, MAP-kinases, NFkB, PI3-kinase, Src family kinase, TRIF-IRF, TREM pathways, as well as autophagy. Those signaling will activate downstream transcription factors such as NFkB, Creb, IRF4, AP-1, AP-2, Are, E2F1, SP1, Gre, Elk, PPARγ, STAT3, resulting in the alteration of host transcriptome(3,42). The immune-regulation activities include: expression of cytokines; expression of chemokines; stimulation of angiogenesis; leukocyte differentiation and activation of autophagy, as illustrated in Figure2.

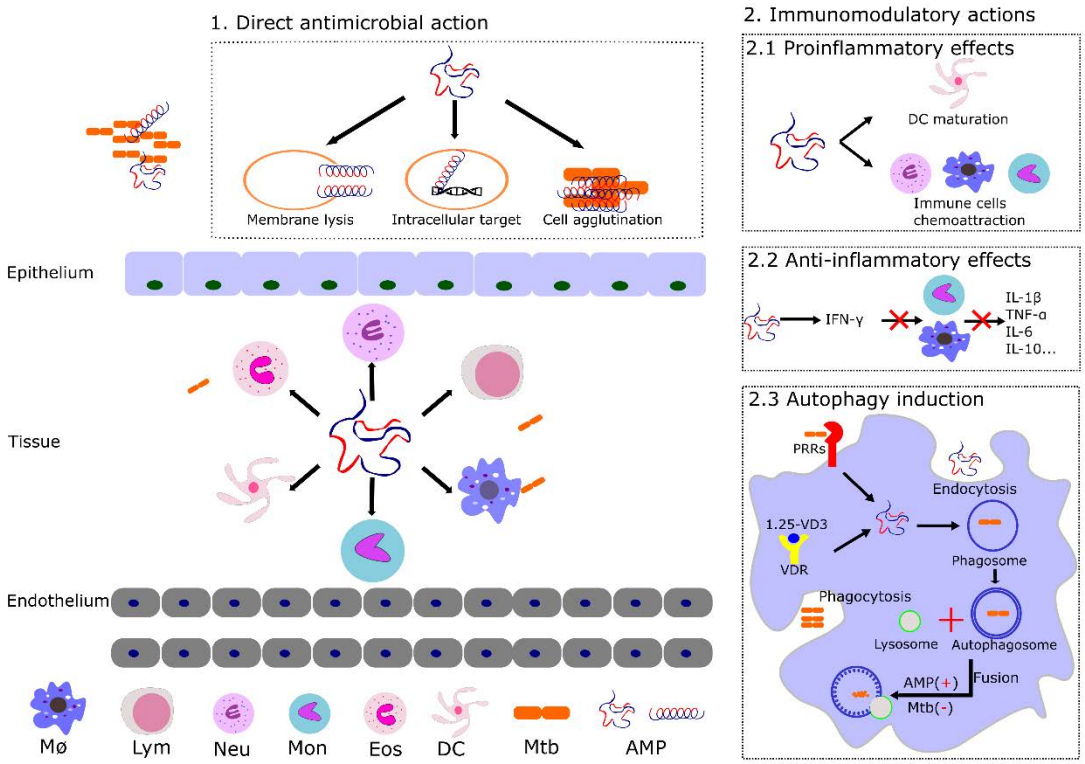

Figure 2. Illustration of the distinct reported mechanism of action of HDPs/AMPs expressed by the vertebrate innate immune cells. The main peptide antimicrobial and immune-regulation activities are showed(45).

1.3.1 Modulation of inflammation

Inflammation is a natural response system to injury, which allows the host organism to kill infective microbes, remove damaged cells or heal damaged tissues(46). Infection or local tissue damage usually trigger inflammation, resulting in immune cells chemoattraction and activation and the loosening of blood vessel walls to ease blood immune cells passage. Dendritic cells, recruited neutrophils, monocytes, lymphocytes, and resident tissue macrophages are the main immune cells involved in inflammatory responses, and activation of these cells leads to the transcription of numerous proteins including cytokines, chemokines, acute-phase proteins, cell adhesion molecules, costimulatory molecules and HDPs(42,47).

HDPs can enhance inflammation by enhancing production of chemokines, polarizing macrophage and dendritic cell (DC) differentiation, promoting phagocytosis, and attracting neutrophils or other immune cells(39). On the other hand, HDPs can also exhibit anti-inflammatory activities by dampening pro-inflammatory cytokine responses

via various mechanisms, such as inducing anti-inflammatory cytokines, and blocking LPS binding to receptor proteins or LPS-binding protein(48). HDPs are neither pro-inflammatory nor anti-inflammatory, they are indeed selectively modulating inflammatory mechanisms.

1.3.2 Direct chemoattractant activity

Although many of the inflammatory modulation of HDPs are related to their indirect recruitment of immune cells, some HDPs such as, LL-37, cathelicidins and defensins show direct chemoattractant action to immune cells(49–53). The structural similarities between HDPs and chemokines may help to elucidate the structure-function relationships that allow HDPs to have chemoattractant properties(54). For example, defensins share various characteristics with chemokines, including size, structure, disulfide bonds, and cationic charge(50,55,56).

1.3.3 Promotion of wound healing

Wound healing, involving multiple steps from inflammation to regeneration, is another process that can be enhanced by HDPs. Vascular permeability increases and platelet and fibrin aggregation occur when skin injury happens. Then, several growth factors are released from platelets and attract neutrophils to the wound and induce inflammation. Presence of HDPs is frequent around oral and cutaneous wounds, and they have been found to play various roles in promoting wound healing, such as reducing the bacterial burden, increasing neutrophil and macrophage recruitment, interacting with growth factors, inducing chemotaxis of epithelial cells, and promoting angiogenesis(39,48). Expression of natural HDPs can be induced in wounded keratinocytes by growth factors. The presence of LL-37 at wound sites has been shown to induce migration and proliferation of fibroblasts, human microvascular endothelial cells, and human umbilical vein endothelial cells(57). Human beta-defensin 2 promotes keratinocyte migration and proliferation through the phosphorylation of the epidermal growth factor receptor and activation of STAT1 and STAT3(56,58).

1.3.4 Modulation of Autophagy and apoptosis

Autophagy is a natural process of cells to recycle dysfunctional cellular components and preserve cellular energy and is considered a part of the innate defense mechanism(59). The autophagy process involves the sequestration of cellular components into autophagosome vesicles that fuse with lysosomes to hydrolyze and recycle cytosolic materials. The process depends on signaling pathways and highly conserved autophagy-related genes. Autophagy is often activated upon intracellular organisms infection, such as *Mycobacterium. tuberculosis*(60). Alternatively, cells can undergo apoptosis which is a programmed cell death process(59). Some HDPs are known to be able to promote these two modes of cellular degradation pathways.

LL-37 can induce autophagy in neutrophils through nucleotide scavenging receptor P2X7 and G-protein-coupled receptors(61). Moreover, vitamin D3 induction of autophagy by activating Beclin-1 and Atg5 is mediated by LL-37(62). In addition, LL-37 can induce cellular apoptosis through activation of caspase3 and caspase9 upon *P. aeruginosa* infection in the airway epithelium, promoting thereby pathogen clearance(61,63). Conversely, LL-37 has been found to suppress caspase3 activity through upregulating cyclooxygenase-2 in keratinocytes(64). Although the role of HDPs on apoptosis and autophagy is complex, their ability to promote either cell death

or cellular recycling could potentially be used to treat intracellular resident infections or directly the clearance of infected cells.

1.4 Human antimicrobial RNases

The bovine pancreatic RNase (RNaseA) is the first ribonuclease discovered and characterized, thanks to its abundance at bovine pancreas and high stability(65,66). Thus, RNaseA was taken as the reference member of a vertebrate specific superfamily. Although varying from 20 to nearly 100% in sequence, the RNase A family proteins share specific elements of sequence identity (containing a CKXXNTF signature motif), a common 3D kidney shaped structure (Figure3) and the catalytic active center (conformed by 2 histidine and 1 lysine key residues). In humans, 13 homologous gene members were identified, but only 8 enzymatically functional members have been isolated, known as "canonical RNases". In addition to their ribonuclease activity, those RNases were reported to have antibacterial, antiviral, antifungal, and antitumor activities even though each protein attributes to different biological effects(67). Moreover, the immune-regulation properties of human RNases in host defense cannot be disregarded(68).

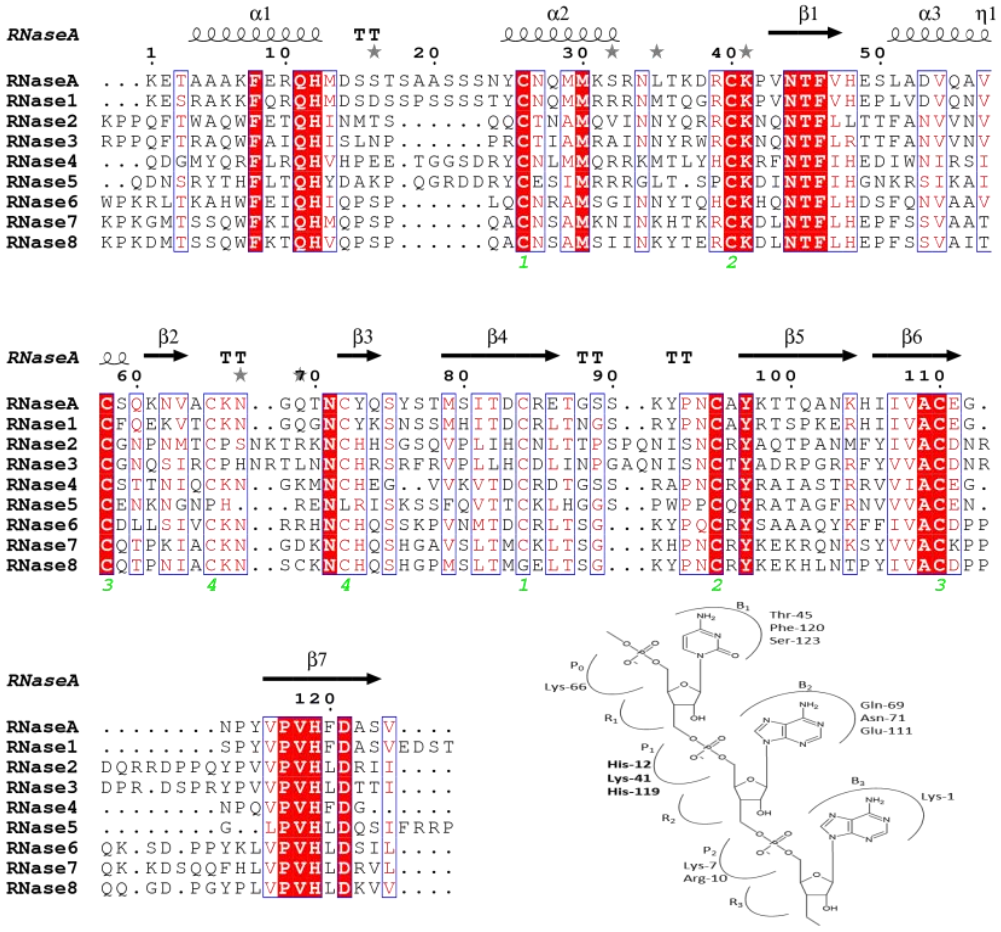

Figure 3. Alignment of human homologous RNases with bovine RNaseA. The alignment was performed using Clustal W (https://www.ebi.ac.uk/Tools/msa/clustalo/), and the picture was drawn with the ESPript online tool (http://espript.ibcp.fr/ESPript/cgi-bin/ESPript.cgi) using as a reference bovine RNaseA

3D structure. Disulfide pairs are labelled in green. The substrate-binding sites of RNaseA are illustrated at the bottom right corner， taken and modified from Parés(69).

1.4.1 Expression

Human RNase1 is expressed in almost all tissues and is particularly abundant in endothelial cells(70–72). Human RNase2 (also known as the eosinophil-derived neurotoxin, EDN), together RNase3, is one of the main secretory proteins stored in eosinophil secondary granules(73,74). In addition, the high expression of RNase2 can also be detected in other blood cells such as monocytes and other tissues such as lung and liver. RNase2 has a high antiviral activity mediated by its catalytic activity(75) and induced by viral infection(68,73,74). Moreover, the release of the eosinophil RNases can be induced by cytokines such as CCL11 and CCL24 through the PI3K/MAPK pathway in human and mice(76). RNase3, also called the eosinophil cationic protein (ECP), is the other eosinophil RNase abundant in the secondary secretory granule. RNase3 can be induced by infection as well as by inflammation. The concentration of RNase3 circulating in biological fluids is correlated with eosinophil degranulation, which is used as a clinical marker for the diagnosis and monitoring of inflammatory disorders(77,78). RNase4 was detected in most human tissues and was found particularly abundant in liver and lung. Interestingly, cytoplasmic granules of monocytes also contain RNase4(79). RNase5 is the most ancient RNase A family member(80). The expression of RNase5 can be found in embryonic somatic cells and epithelial cells, and it can be induced during inflammation(81,82). Transcriptional expression of RNase6 showed a nearly ubiquitous distribution in all tissues, including monocytes and neutrophils(83). Bacterial infection caused the upregulation of RNase6 in genitourinary tract(84), while HIV infection caused the downregulation in Th17 polarized cells(85). RNase7 is one of the most abundant AMPs purified from skin(86,87). The protein is secreted by various epithelial cells, and can be induced by various factors such as infection, inflammation signaling molecules, and insulin(88–90). RNase8 is the last identified canonical member of the RNase A superfamily. RNase8 was first uniquely identified in the placenta, and later on it was also reported in lung, liver, and testes(91,92).

1.4.2 Ribonuclease catalytic activity

All eight human RNase A superfamily member harbor detectable ribonucleolytic activities. The conserved catalytic triad, consisted by 1 lysine and 2 histidine residues, is the structural base of the endoribonuclease enzyme activity of RNaseA via acid-base catalysis(93). RNase A catalyzes the cleavage of the P-O5’ bond of RNA specifically on the 3’ side of pyrimidine nucleotides, and this pyrimidine specificity is mediated by Thr45 and Phe120 of the B1 subsite. The cleavage process of RNA substrate catalyzed by RNaseA takes place in two steps: first the transphosphorylation step and formation of a 2’,3’-cyclic nucleotide at 3’-terminus of one product and a 5’-hydroxyl group at 5’-terminus of the other product; and secondly, the hydrolysis step from the 2’,3’ -cyclic phosphate nucleotide into a 3’-phosphate mononucleotide end(93). This mechanism is conserved in all canonical RNaseA superfamily members, with the participation of equivalent His and Lys active site counterparts to residues His12, Lys41, and His119 in RNaseA. Although the eight human canonical RNaseA family members strictly conserve their catalytic triad they vary a lot in the catalytic efficiency against diverse RNA substrates(94).

1.4.2.1 Substrate binding pattern

RNaseA binds nucleic acids through multiple electrostatic interactions between the phosphates of the polynucleotide and the positive groups of the protein subsites(69,95). In addition, hydrogen bond and van der Waals interactions contribute to shape the nucleotide recognition pattern. The RNase subsites that interact with nitrogenous base, ribose, phosphate are defined as Bn, Rn, and Pn, respectively (Figure3). In addition to the main phosphate active site P1 (consisted by His12, Lys41, and His119), there are two more main noncatalytic phosphate-binding subsites, the P0 (consisted by Lys66) and P2 site (consisted by Lys7 and Arg10), that bind the phosphate group of the nucleotide adjacent upstream to the active site and the phosphate group of the corresponding adjacent nucleotide at the 3' side, respectively(96). The main base site (B1, consisted by Thr45, Phe120, and Ser123) prefers pyrimidines and the secondary site (B2, consisted by Gln69, Asn71, and Glu111) favors purines binding(93,97). Altogether, the subsites facilitate RNA binding to form the enzyme-substrate complex and facilitate the endonuclease cleavage. The comprehensive structural evolutionary analysis and preliminary kinetic characterization indicate a conservation binding pattern at the main B1 and P1 sites but a higher variability at the secondary base and phosphate subsites(98,99).

1.4.2.2 Role in RNA metabolism

RNA metabolism refers to any modification of RNA molecules, including splicing, maturation, and degradation. RNA alteration is related to the pathogenesis of many diseases, such as cancers and neurodegeneration(100,101). Messenger RNAs (mRNAs) convey genetic information to direct the assembly of protein of the ribosomes in protein synthesis of cellular organisms. This process is regulated by abundant and functional non-coding RNAs (ncRNAs), including tRNAs, ribosomal RNAs, microRNAs, tRNA-derived stress-induced small RNAs (tiRNAs), small interfering RNAs (siRNAs), small nuclear RNAs (snRNAs), Piwi-interacting RNAs (piRNAs), small nucleolar RNAs (snoRNAs), and long ncRNAs (lncRNAs)(102,103). In addition to the intracellular functions, some types of RNAs such as mRNAs and most of ncRNAs are also found outside the cells either in a free form or within vesicles, and are termed extracellular RNAs (exRNAs). ExRNAs can serve as intercellular communicators and are used as biomarkers for certain diseases(104,105).

Human RNaseA superfamily may mainly exert its ribonucleolytic activity toward free forms of exRNAs for body fluid cleaning(106). The proteins are synthesized with an N-terminal signal peptide that guides their secretory route towards the extracellular space. Besides, the cell cytoplasm is protected against their potentially toxic ribonucleolytic action by the presence of the abundant and ubiquitous RNase inhibitor (RI)(107). Although the relative catalytic activity of the human RNase A members is dependent on the substrate, RNase1, the human homologue of bovine RNaseA, is the most active one. RNase2 and RNase7 also have a quite high activity compared to RNase3 and RNase6, RNase5 has very low activity and RNase8 shows the lowest ribonucleolytic activity(91,108–110). More and more evidences indicate that the ribonucleolytic activity of RNases is required for some but not all their biological functions (Table1).

Human RNase1 is conventionally ascribed as the direct orthologue of bovine RNaseA based on their sequence identity, although a distinct biological role is being attributed. RNaseA was previously reported to be essential for the digestion of dietary RNAs in ruminants(66,71). On its side, human RNase1 is secreted abundantly in the blood circulatory system, where it can modulate the content of exRNAs. Those processes strictly require the ribonucleolytic activity of RNase1(106). Human RNase1 possess the

ability to degrade single and double strand RNAs, and RNA: DNA hybrid(111,112). Human RNase2 and RNase3 are derived by gene duplication from a common ancestor that took place during primate evolution. Although they share 67% in protein sequence and 88% in gene sequence identities(113,114), RNase2 harbors about 10 times higher ribonucleolytic activities than RNase3(115). One of the best characterized biological roles of RNase2, its activity against RNA viruses, is dependent on its ribonucleolytic activity(73,116). RNase3 is tightly associated with innate host defense involving antibacterial, antihelminthic, and cytotoxic roles(68,117). It is worth to note that the antiviral and antihelminthic activities of RNase3 require the ribonucleolytic activity whereas the bactericidal and cytotoxic effects do not(75,118).

Table1. Ribonucleolytic activity and biological properties of human RNases reported to work in a dependent or independent manne.

Ribonuclease	Dependent	Independent	Not defined
RNase1	Extracellular RNA degradation(106)		Dendritic cell maturation(119); Antiviral(120)
RNase2	Antiviral activity(73)		Dendritic cell chemotaxis and activation(73,119)
RNase3	Antiviral activity & Antihelminthic activity(75,118)	Antibacterial activity(106); Cytotoxic activity(106); Promote bacterial cell agglutination(98)	Tissue remodeling(121); Chemotaxis of fibroblasts(122)
RNase4			Angiogenesis(123); Antiviral(124); Antimicrobial(125); neuroprotective(123)
RNase5	Angiogenic activity(126); Cell proliferation by stimulation of rRNA metabolism [125], Cell stress response by tRNA cleavage[124,]	EGFR binding(129)	Inhibits neutrophil degranulation(130); Modulated inflammatory response(131); Tissue remodeling(132), Neuroprotective(133)
RNase6	Antiviral activity(85)	Antibacterial activity(84); Promote bacterial cell agglutination(98)	
RNase7		Antibacterial acitivity(134,135)	Promote inflammation(132); Chemotaxis of immune cells(136); Tissue remodeling(137)
RNase8			Antimicrobial activity(138)

On its side, RNase4 shows a very high sequence conservation within the family lineage, suggesting an essential physiological role. Besides, RNase4 has a particularly

pronounced specificity for uridine at the B1 site(139), suggesting a strong RNA selectivity. Cleaning of cellular RNA was first proposed for the protein functional role, but still little information is available. Although RNase5 harbors significantly lower ribonucleolytic activities, the limited ribonucleolytic activity of RNase5 is essential for its role in angiogenesis and ncRNA cleavage(140,141), illustrated in Figure 4. For example, the tRNA fragments (tRFs), are produced from pre-tRNAs as well as mature tRNAs. Beside RNase5, other RNases are involved in cleaving tRNA and producing functional tRFs (Figure 4). For example, 5-tRFs are generated from cleavage in the D-loop of tRNAs by Dicer; 3-tRFs are generated from cleavage in the T-loop by Dicer, RNase5/ANG; TF-1s are generated from cleavage of the 3'-trailer fragment of pre-tRNAs by RNase Z or its cytoplasmic homologue ELAC2; tiRNAs (also referred as tRNA halves) are generated by the cleavage in or near the anticodon loop of a tRNA, RNase5/ ANG, and Rny1p, a member of the ribonuclease T2 family, are responsible fo the production of tiRNAs in mammal and yeast cells, respectively(142–145). tiRNAs can be induced under stress conditions such as amino acid deficiency, phosphate starvation, UV radiation, heat shock, hypoxia, oxidative damage, and viral infection. tiRNAs are mainly located in the cytoplasm, with a small amount in the nucleus and mitochondria, and can also be detected in the circulation system(127,141,145–148). RNase6, on its side, has a second catalytic triad that favor its endonuclease cleavage specificity with polynucleotide substrate(149). However, whether this catalytically specificity is associated to a physiological target *in vivo* is still unknown.

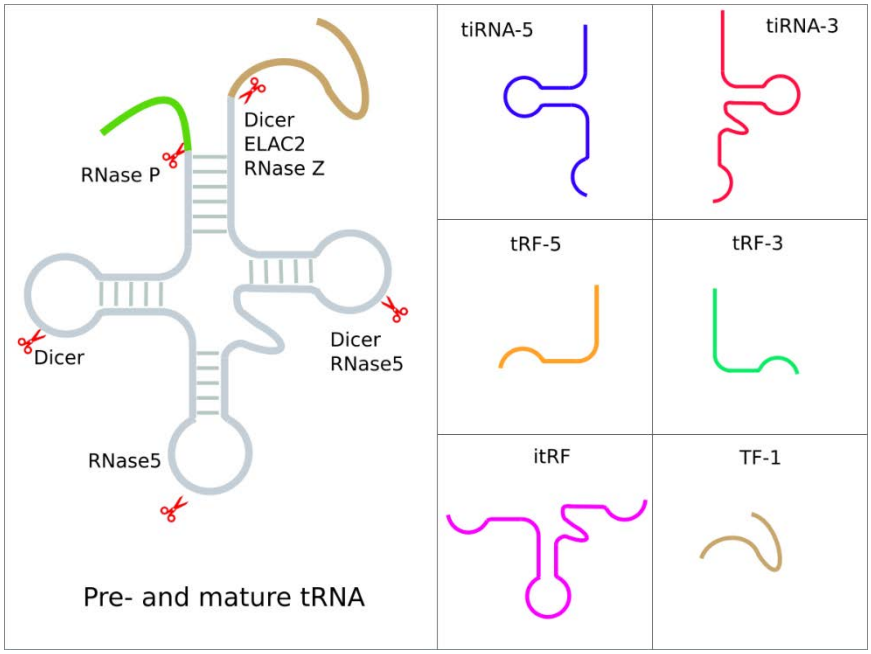

Figure 4. RNases involved in specific tRNAs cleavage. The types of tRNAs are classified by size and sequence location in the tRNA structure. Biogenesis of tRFs/tiRNAs. tRF-1 is generated from the 3'-trailer of primary tRNA. tRF-5, i-tRF and tRF-3 are produced from the 5'-, internal- and 3'-portions of the mature tRNA, respectively. When the cleavage site is within the anticodon loop, two fragments are generated as tiRNAs for the 5'- and 3'- tRNA halves. Unpublished work.

1.4.3 Antimicrobial activity

In addition to the ribonucleolytic activities, RNaseA superfamily proteins display a wide spectrum of antimicrobial activities against various microorganisms. RNase1 is not recognized as a high antimicrobial protein, but it was reported that recombinant

RNase1 and the native protein from urinary samples showed activity against the human immunodeficiency virus (HIV-1)(120,150). RNase2 is mainly recognized to display a broad antiviral activity, in particular against ssRNA viruses, by inhibiting the replication of respiratory syncytial virus (RSV), HIV-1, and hepatitis B DNA virus(120,150,151). Together with RNase2, RNase3 is the other RNase in the eosinophil secondary secretory granule. In addition to share neurotoxic and antiviral activities with RNase2, RNase3 has unique bacterial properties(152). The protein has an aggregation-prone region that promotes the protein self-aggregation and the agglutination of bacterial cells. Moreover, bacterial cell agglutination is further enhanced by high biding affinity of the protein to anionic LPS present at the Gram-negative bacterial wall(153). The antimicrobial activity of RNase4 is not well defined yet. Notwithstanding, few studies suggested RNase4, along with RNase5, are the soluble factors secreted by T cells showing anti-HIV activity(124). RNase5 apart from its role in promoting neovascularization and angiogenesis, displays toxicity toward the yeast *Candida albicans* and *Streptococcus Pneumonia, Enterococcus faecalis, Listeria Moncocytogenes* bacteria(132,154). It has also been implicated in inhibiting HIV-1 replication(124). Recently, RNase6 is reported to have bactericidal activity against Gram-positive and Gram-negative bacteria(84,155). The antimicrobial mechanisms of RNase6 is similar to RNase3 in the sense that it induces bacterial agglutination and membrane depolarization in Gram-negative bacteria(155). Moreover, RNase6 inhibits HIV replication and is downregulated in Th17 cells upon HIV infection(85).

RNase7 is one of the most abundant antimicrobial proteins purified from skin, which has high antimicrobial activity against a wide variety of infective microorganisms(86,89,156,157). RNase8 is the last canonical RNaseA superfamily member, and the recombinant protein exhibits sub-micromolar toxicity to microorganisms such as Gram-positive and Gram-negative bacteria, and yeast(138).

1.4.4 Immune modulation activity

HDPs also participate in host defense response by playing an immune modulation role. HDPs can target a variety of cell types, including epithelial cells, keratinocytes, and immune cells of myeloid or lymphoid origin.

Although no direct antibacterial action is detected for RNase1, the protein may mediate the host anti-pathogen response by activating human dendritic cells, resulting in the production of inflammatory cytokines, chemokines, growth factors, and soluble receptors(119). RNase2 can promote leukocyte activation, maturation, and chemotaxis(73). Moreover, RNase2 contribute to host immunity as an alarmin through activating DCs mediated by TLR2-MyD88(116,119,158). Together with direct hRNase3 action on pathogens, a series of immune-modulating activities are observed. For example, RNase3 has remodeling activity that is partly mediated by inducing the expression of epithelial insulin-like growth factor1 (IGF-1) expression(122). In addition, RNase3 can enhance fibroblast chemotaxis to the site of injury to facilitate tissue repair(159). More recently, RNase3 was proven to be able to exert antimicrobial activity against *M. aurum* intracellular infection in macrophages, which is related to its ability to induce autophagy. The role of RNase5 in immunomodulation has been broadly investigated. It has been postulated that RNase5 regulates inflammatory states by inhibiting TKB1-mediated NF-kB nuclear translocation, thus decreasing levels of TNFa and IL-1b(132,160,161). RNase5 is also implicated in modulating inflammatory responses owing to its ability to stimulate leukocytes to produce the pro-inflammatory cytokines IL-6 and TNF-a. In addition, RNase5 can promote cell survival in stress

conditions by inducing tiRNA, which inhibits global protein translation(162). Very recently, RNase5 was found to serve as a ligand for epidermal growth factor receptor (EGFR, a member of the tyrosine kinase receptor family) in pancreatic ductal adenocarcinoma(129). The RNase5-EGFR pair complex is a novel example of a ligand-receptor relationship between families of RNase A and tyrosine kinase receptors(163) (Figure 5).

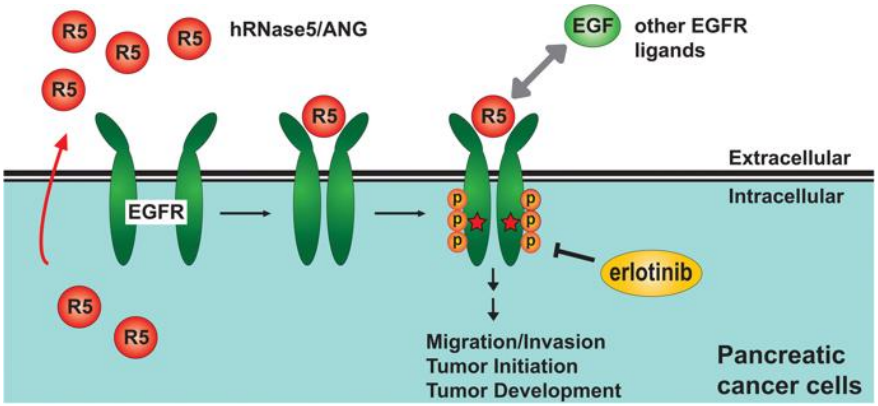

Figure 5. A diagram of RNase5/ANG as an EGFR ligand and a serum biomarker for prediction of erlotinib sensitivity in pancreatic cancer(163).

RNase7 can selectively suppress TH2 cytokine production by reducing GATA3 activation(164,165). It has further been indicated that RNase7 promoted inflammation and chemotaxis in acne and cutaneous wound healing(166). Moreover, recent data indicates that RNase7 acts as an alarmin by converting self-DNA released from dying host cells into a danger signal that rapidly activates interferon genes and antimicrobial immune responses(117). Nevertheless, RNase7 facilitates microbial clearance or drive autoimmunity in chronic inflammatory skin conditions by permitting recognition of self-DNA by plasma dendritic cells(136).

2 AIMS OF THE THESIS

The main objective of the present work is to investigate the antimicrobial mechanism of human ribonucleases, emphasizing on the immune-regulation role and the related molecular mechanism in host defense. Particularly, the specific aims of the thesis are:

Chapter 1:

- To review the antimicrobial action of host antimicrobial peptides against tuberculosis.

Chapter 2:

- To review the immune-regulation role of human secretory RNases and their role at the extracellular space.

Chapter 3:

- To screen the anti-mycobacterial activity of human RNase A family members and further investigate the mechanism involved in removal of macrophage intracellular infection, mediated by autophagy induction.

Chapter 4:

- To explore the immune modulation action of RNase3 in THP1-derived macrophages and the catalytic dependent and independent mechanisms.

Chapter 5:

- To investigate the antiviral action of RNase2 and its mechanism by RNase2 knock-out THP1-derivedmacrophages and analyze the cellular ncRNA products. To compare the tRFs population in native and RNase2 knock-out cells in the presence and absence of RSV challenge.

Chapter 6:

- To identify the evolutionary trend in substrate specificity at the secondary base binding site of RNase A superfamily by a kinetic and structural comparative analysis of representative family members. The characterization of the RNases substrate specificities should help us to identify the protein physiological cell RNA substrates related to their biological role.

3 GENERAL DISCUSSION AND FUTURE PERSPECTIVES

Antimicrobial RNases are small cationic proteins belonging to the vertebrate secreted RNase A superfamily. Eight members, known as "canonical RNases" have been identified in humans. Despite of the shared RNase catalytic activity, RNases were also reported to possess other biological activities, such as antimicrobial, antiparasitic, antiviral, antitumoral, angiogenic and immune-regulation properties(167,168). It has been reported that RNase3, RNase6 and RNase7 are the most effective antimicrobial members within the superfamily and RNase3 and RNase7 were proven to have an effective mycobactericidal action at low micromolar concentration *in vitro*(157). These characteristics are the basis to consider human RNases as potential drug molecules against pathogens.

In this thesis work, we first screened the antimycobacterial activity of seven human canonical RNases. Applying the semi-solid agar-based spot-culture growth inhibition assay-high-through screening (SPOTi-HTS), the protein activities were evaluated both *in vitro* and *ex vivo*. Our data demonstrated that RNase3, RNase6 and RNase7 were active against extracellular bacteria, moreover the protein can be phagocyted into macrophage and then eradicate intracellular macrophages-dwelling mycobacteria. The data corroborated that RNase3 is the most active among the family members. Moreover, the protein cell agglutination activity was determined *in vitro* against three distinct *Mycobacterium* species: *M. smegmatis mc²155*, *M. aurum* and *M. bovis BCG*. RNase3 and RNase6, but not RNase7, were able to induce the aggregation of all the tested mycobacteria. The results are in accordance with the previous reported data using *M. vaccae*(157). Compared to RNase3 and RNase6, RNase7 lacks an aggregation-prone hydrophobic patch within the primary sequence(167,169,170). It has been reported that the antimycobacterial action of many AMPs is mediated by immune-regulation activities, such as triggering the autophagy pathway to control the proliferation of intracellular resident bacteria in macrophage(45,171,172). Thus, we screened the ability of the seven canonical RNases in inducing autophagy and found that only RNase3 and RNase6 significantly increased *BECN1* and *ATG5* gene expression and LC3 processing. Comparing the effect of wild-type RNase3 and the catalytic defective mutant RNase3-H15A, we found that the catalytic activity of RNase3 is not needed for its antimycobacterial activity and autophagy induction. This is consistent with previous studies on Gram-negative and Gram-positive bacterial species that also observed that the protein enzymatic activity was not require for its antimicrobial activity(155,167,173–175). In addition, we also observed that *M. aurum* infection can modulate the expression of RNase3, suggestion a potential physiological role.

Encouraged by the previous results showing that RNase3 can enter the macrophage and eradicate the intracellular mycobacteria via modulation of autophagy of host macrophage cells(176), we then aimed to broad our understanding of the immune-regulation role of RNase3. In this study, THP1 induced macrophages were treated with the wild-type RNase3 and RNase3-H15A (the catalytic defective mutant) for 4h and 12h and then were characterized by the next generation mRNA sequencing methodology. We identified the regulation pathways related and unrelated to the ribonucleolytic activity of RNase3, by comparing the transcriptomes of macrophage treated with RNase3 and RNase3-H15A. Overall, RNase3 and RNase3-H15A triggered a similar response of macrophages, characterized by a pro-inflammation state, cell growth arrest, and cell duplication inhibition. Moreover, epidermal growth factor receptor (EGFR) was identified as the main hub gene by network analysis of the common response differential expressed genes (DEGs). Interestingly, EGFR is not only a key membrane

receptor involved in cell survival and tissue remodeling(177), EGFR was also reported to be able to mediate the macrophage activation during bacterial(178) and viral infection(179). Specifically, the EGFR signaling induces pro-inflammatory cytokine and chemokine production(178,180,181). Moreover, the homologous protein RNase5 was recently reported to be able to bind to and activate EGFR(129). Those results strongly suggest that EGFR is the key molecule that mediates the macrophage modulation by RNase3. By molecular modeling, taking EGFR-EGF complex as a model, we also predicted a strong binding of RNase3 with EGFR and it is worthy to mention that there is a high sequence identity within the receptor interaction region of EGF with both human RNase A family members. In addition to the common response triggered by RNase3 and RNase3-H15A, we also found a list of DEGs specifically related to the ribonuclease activity. Those DEGs were enriched to viral infection related pathways, of which the top-rated is RIG-I-like receptors (RLRs), consisting of RIG-I, MDA5, and LGP2, play an important role in sensing RNA virus infection to initiate and modulate antiviral immunity. Its necessary to point out that RLRs can also detect self RNA in the cytoplasm to triggers innate immunity and inflammation to control infection in addition to viral RNA molecules(182,183). Thus, we may speculate that RNase3 antiviral activity in macrophage may be mediated by specific RNA cleavage by RNase3. In addition, we found that overexpression of endogenous RNase3 in macrophage significantly reduced both *M. aurum* and RSV infection. To conclude, the results presented in this work highlight that RNase3 plays a crucial role in immunomodulation of human macrophage via interacting with EGFR. Moreover, the ribonucleolytic activity of RNases is required for some but not all of their biological functions. It would be worthwhile to co-crystalize the complex of RNases with the EGFR extracellular domain to further identify the direct interactions and compare with EGF to determine if the activation of EGFR takes place in the same way.

Next, we focused on human RNase2 (EDN), another RNaseA family member that together with RNase3, is one of the main eosinophil derived proteins. In comparison to RNase3 known as a potent antibacterial protein, RNase2 has antiviral activity against RSV, HIV-1, and hepatitis B DNA virus. Nevertheless, RNase2 was also reported to have immune-regulation activity on various host cell types, for example promoting leukocyte activation, maturation, and chemotaxis. In the present study, to further explore the biological role of RNase2 in human macrophages, we first edited a THP1 cell line to knock out RNase2 expression by CRISPR/Cas9. After induction of THP1 into macrophage, we applied next generation sequencing to study the transcriptomic change of macrophages when RNase2 is missing. After DEG analysis, we found that more than 2000 genes were significantly altered when RNase2 is knocked out. We can suggest that RNase2 is crucial in mediating and maintaining the host innate immune response and cell survival, based on the identified DEGs enriched related pathways, such as viral protein interaction, cell cycle, cytokine-cytokine receptor interaction and chemokine signaling. This was further confirmed as we found that knocking out RNase2 resulted in heavier RSV infection burden and severe macrophage cell death. Moreover, EGFR was also identified as the main hub gene by applying those DEGs to network analysis. Based on our recent results on the EGFR activation by the closely related RNase3, we can suggest that the ribonuclease activity of RNase2 is probably not involved in the protein EGFR mediated catalytic immune-regulation activity of macrophages. Small non-coding RNAs (sncRNAs), such as siRNA, miRNA and piRNA, have emerged as key regulatory molecules of the antiviral innate immune response(184). sncRNAs derived from tRNAs, called tRNA-derived RNA fragments (tRFs), have been recently found induced by specific viral infection, such as RSV and hepatitis virus but

not metapneumovirus(185,186). Thus, we next compare the tRNA fragments population in wild-type and RNase2 knocked out macrophages using qPCR based commercial tRFs library screening kit. In total, we detected 5 tRNA fragments that were significantly reduced in RNase2-knocked out macrophages compared to wild-type macrophages. The results indicated that RNase2 is another RNase that may be responsible to cleave tRNA and produce specific tRNA fragments as described for RNase5(187). We then compare tRNA fragments population with or without RSV challenge and we concluded that RSV infection can regulate the production of tRFs in macrophages and the composition of the cell tRFs population is regulated by the presence of RNase2. Overall, our results indicate that RNase2 has a multifaced role in modulating macrophages, either dependent or independent of its catalytic activity. This is consistent with previously reported data that indicated that other features of RNase2 apart from the ribonuclease activity are crucial to its antiviral activity(75).

In order to interpret the potential contribution of tRNA cleavage by RNases in the protein immune-regulatory properties, we decided to further analyze their sequence specificities. Therefore, we decided to compare the catalytic activity of the 7 human canonical RNases. In particular, we focused at the B2 site because a strong specificity was observed at this site in previous studies(98). The kinetic activity on UpA, UpG and UpI was measured by a spectrophotometric assay and the relative preference for the secondary base was estimated for each protein. The results indicated a shift of the secondary base specificity, from a poor A/G discrimination to a pronounced preference for A. By the complementary analysis of the kinetic characterization of other family members available in the literature, we inferred that there has been a shift at the substrate secondary base predilection, from lower to higher order vertebrates, from guanine to adenine (98). Moreover, we carried out a molecular dynamics analysis of RNase-dinucleotide complexes to unravel the structural determinants underlying the observed differentiated kinetic behaviors. Overall, molecular dynamics corroborated the observed shift from guanine to adenine preference by kinetic analysis. Although the main contributors (Asn71 and Glu111 in RNase A and equivalent counterparts) involved in the enzyme B2 sites are present in all the family members, significant differences in L4 loop extension and contribution of complementary residues can facilitate a distinct binding mode that confers discrimination between both purine bases. Asn, Glu/Asp and Arg bidentate side chains provide selective binding to adenine N1/N6 and N6/N7 versus guanine N1/O6, O6/N7 and N1/N2 groups. Moreover, we analyzed the modified base inosine apart from the two natural purine bases in RNA, as inosine is one of the main posttranscriptional modifications in cellular transcripts. We found an overall similar enzymatic activity of RNases on UpG and UpI. Moreover, we identified Glu/Asp residues are important for non-mammalian RNases to recognize N1/N2 group in guanine. RNA modifications can not only regulate the translation pathway, they have also been reported to be involved in the generation of regulatory tRNA fragments(145,188). This specific tRNA cleavage process is associated to the host response to specific stress conditions(147) and the target specificity of endonucleases might be modulated by posttranscriptional modification, such as methyl modifications. For example, m5C modification inhibits RNase5 mediated cleavage of tRNA(145). Noteworthy, RNA posttranslational modification is an important immune-escape mechanism achieved by differential posttranscriptional modification profiles of eukaryotic and prokaryotic RNA(189,190). For example, murine innate immune cells were reported to be able to discriminate between self and nonself RNA (bacterial RNA with ribose 2'-O-methylation)(147). Overall, we speculate here that RNA

posttranscriptional modifications might be important for RNases in discriminating self and non-self RNA.

To summarize, this thesis concluded that human RNases play an important immune-regulation role in regulating macrophages to fight against pathogen infection, through both ribonucleolytic activity dependent and independent ways. Specifically, we identified an activation pathway non-dependent on the RNase catalytic activity mediated through interaction with the EGFR receptor. More studies are needed to completely confirm the interaction of RNases with EGFR, especially to identify the structural interactions. Moreover, it is of special interest to determine the RNase dependent manner activity which may be mediated through the release of selective RNA products, such as regulatory tRNA fragments. To prove that, we need to look closer at the recognition, binding, and cleavage of RNA by human RNase A family members and this can be achieved by applying newly developed methodologies. The next-generation sequencing technologies have been proven a powerful tool in unveiling the cellular transcriptome and the molecular functions of coding and non-coding RNAs. Moreover, some special method, such as "cP-RNA-seq" can achieve to selectively amplify and sequence the cyclic phosphate-containing RNAs. The technique can unambiguously identify the RNA molecules released by a specific enzymatic endonuclease cleavage. Besides, the clustered regularly interspaced short palindromic repeats (CRISPR) based gene editing tool can not only help to conduct RNase-knock in or -knock out comparison experiment but also allows to investigate the effect of RNA modification on RNA cleavage by RNases through specific modification of RNAs. A better knowledge of the mechanism of action of host-defense RNases should set the basis for the design of novel antimicrobial drugs.

4 CONCLUSIONS

4.1

- RNase3, RNase6 and RNase7 achieve the eradication of extracellular and macrophage intracellular infection by *M. aurum* at a low micromolar range.
- RNase3 and RNase6 can agglutinate mycobacteria (*M. aurum*, *M. smegmatis* mc^2 *155*, and *M. bovis BCG*)
- RNase3 and RNase6 can induce autophagy and thereby inhibit intracellular *M. aurum* growth.
- RNase2 is the most abundant RNases expressed in THP1 macrophages followed by RNase3 and RNase6; the expression of RNase3 and RNase6 are regulated by *M. aurum* infection.
- The antimicrobial activity, bacterial agglutination, and autophagy induction ability are not dependent on the RNase enzymatic activity.

4.2

- RNase3 can activate the host immune response of human macrophage through EGFR binding which is not dependent of the ribonuclease activity.
- RNase3 can trigger the antiviral pathway of macrophage, which is dependent of the ribonucleolytic activity.
- *M. aurum* infection can regulate the expression of RNase3 in THP1 induced macrophages while RSV infection cannot.
- Overexpression of RNase3 in human macrophage can inhibit the infection of *M. aurum* and RSV.

4.3

- Overexpression of RNase2 in THP1 leads to cell death.
- Knock-out of RNase2 increases the RSV infection burden of macrophages.
- RSV infection activates the expression of RNase2 in THP1 induced macrophages.
- RNase2 is involved in the activation of EGFR in THP1 induced macrophages.
- RNase2 is another RNase that is involved in specific tRNA fragments release.

4.4

- Among RNase A superfamily, there is an evolutionary trend towards adenine respect to guanine at B2 site from lower to higher order vertebrates.
- The bidentate side chains of Asn, Glu/Asp and Arg, provide selective binding to adenine N1/N6 and N6/N7 versus guanine N1/06, O6/N7 and N1/N2 groups.
- The principal contribution to the distinct binding mode lies in the protein β6 and L4 loop regions, that show significant differences in the orientation and extension.

5 REFERENCES

1. Arora G, Kulshreshtha A, Arora K, Talwar P, Raj R, Grewal G, Sajid A, Kukreti R. "Emerging Themes in Drug Resistance," in *Drug Resistance in Bacteria, Fungi, Malaria, and Cancer* (Cham: Springer International Publishing), 1–24. doi:10.1007/978-3-319-48683-3_1
2. Mahlapuu M, Håkansson J, Ringstad L, Björn C. Antimicrobial Peptides: An Emerging Category of Therapeutic Agents. *Front Cell Infect Microbiol* (2016) **6**:1–12. doi:10.3389/fcimb.2016.00194
3. Hancock REW, Haney EF, Gill EE. The immunology of host defence peptides: beyond antimicrobial activity. *Nat Rev Immunol* (2016) **16**:321–334. doi:10.1038/nri.2016.29
4. Wang G, Li X, Wang Z. APD3: The antimicrobial peptide database as a tool for research and education. *Nucleic Acids Res* (2016) **44**:D1087–D1093. doi:10.1093/nar/gkv1278
5. Hancock REW, Sahl H-G. Antimicrobial and host-defense peptides as new anti-infective therapeutic strategies. *Nat Biotechnol* (2006) **24**:1551–1557. doi:10.1038/nbt1267
6. Conlon JM. Purification of naturally occurring peptides by reversed-phase HPLC. *Nat Protoc* (2007) **2**:191–197. doi:10.1038/nprot.2006.437
7. Rinaldi AC. Antimicrobial peptides from amphibian skin: an expanding scenario. *Curr Opin Chem Biol* (2002) **6**:799–804. Available at: http://www.ncbi.nlm.nih.gov/pubmed/12470734 [Accessed April 24, 2019]
8. B. Hadley E, E.W. Hancock R. Strategies for the Discovery and Advancement of Novel Cationic Antimicrobial Peptides. *Curr Top Med Chem* (2010) **10**:1872–1881. doi:10.2174/156802610793176648
9. Vishnepolsky B, Pirtskhalava M. Comment on: 'Empirical comparison of web-based antimicrobial peptide prediction tools.' *Bioinformatics* (2018) doi:10.1093/bioinformatics/bty1023
10. Torrent M, Di Tommaso P, Pulido D, Nogués MV, Notredame C, Boix E, Andreu D. AMPA: An automated web server for prediction of protein antimicrobial regions. *Bioinformatics* (2012) **28**:130–131. doi:10.1093/bioinformatics/btr604
11. Veltri D, Kamath U, Shehu A. Deep learning improves antimicrobial peptide recognition. *Bioinformatics* (2018) **34**:2740–2747. doi:10.1093/bioinformatics/bty179
12. Chan DI, Prenner EJ, Vogel HJ. Tryptophan- and arginine-rich antimicrobial peptides: Structures and mechanisms of action. *Biochim Biophys Acta - Biomembr* (2006) **1758**:1184–1202. doi:10.1016/j.bbamem.2006.04.006
13. Mowery BP, Lee SE, Kissounko DA, Epand RF, Epand RM, Weisblum B, Stahl SS, Gellman SH. Mimicry of Antimicrobial Host-Defense Peptides by Random Copolymers. *J Am Chem Soc* (2007) **129**:15474–15476. doi:10.1021/ja077288d
14. Hunter HN, Jing W, Schibli DJ, Trinh T, Park IY, Kim SC, Vogel HJ. The interactions of antimicrobial peptides derived from lysozyme with model membrane systems. *Biochim Biophys Acta - Biomembr* (2005) **1668**:175–189. doi:10.1016/j.bbamem.2004.12.004
15. Hilpert K, Elliott MR, Volkmer-Engert R, Henklein P, Donini O, Zhou Q, Winkler DFH, Hancock REW. Sequence Requirements and an Optimization Strategy for Short Antimicrobial Peptides. *Chem Biol* (2006) **13**:1101–1107. doi:10.1016/j.chembiol.2006.08.014
16. Findlay B, Zhanel GG, Schweizer F. Cationic amphiphiles, a new generation of antimicrobials inspired by the natural antimicrobial peptide scaffold. *Antimicrob Agents Chemother* (2010) **54**:4049–58. doi:10.1128/AAC.00530-10
17. Torres MDT, Sothiselvam S, Lu TK, de la Fuente-Nunez C. Peptide Design Principles for Antimicrobial Applications. *J Mol Biol* (2019) doi:10.1016/J.JMB.2018.12.015
18. Giangaspero A, Sandri L, Tossi A. Amphipathic alpha helical antimicrobial peptides. *Eur J Biochem* (2001) **268**:5589–5600. doi:2494 [pii]
19. Fu H, Grimsley GR, Razvi A, Scholtz JM, Pace CN. Increasing protein stability by improving beta-turns. *Proteins Struct Funct Bioinforma* (2009) **77**:491–498. doi:10.1002/prot.22509

20. White D, Drummond J (James T, Fuqua C. *The physiology and biochemistry of prokaryotes*. Fourth Edi. Oxford University Press (2011). Available at: https://global.oup.com/ushe/product/the-physiology-and-biochemistry-of-prokaryotes-9780195393040?cc=es&lang=en& [Accessed August 6, 2019]
21. Niyonsaba F, Nagaoka I, Ogawa H. Human Defensins and Cathelicidins in the Skin: Beyond Direct Antimicrobial Properties. *Crit Rev Immunol* (2006) **26**:545–576. doi:10.1615/CritRevImmunol.v26.i6.60
22. Papanastasiou EA, Hua Q, Sandouk A, Son UH, Christenson AJ, Van Hoek ML, Bishop BM. Role of acetylation and charge in antimicrobial peptides based on human β-defensin-3. *APMIS* (2009) **117**:492–499. doi:10.1111/j.1600-0463.2009.02460.x
23. Pasupuleti M, Walse B, Svensson B, Malmsten M, Schmidtchen A. Rational Design of Antimicrobial C3a Analogues with Enhanced Effects against Staphylococci Using an Integrated Structure and Function-Based Approach †. *Biochemistry* (2008) **47**:9057–9070. doi:10.1021/bi800991e
24. Chen C, Yang C, Chen Y, Wang F, Mu Q, Zhang J, Li Z, Pan F, Xu H, Lu JR. Surface Physical Activity and Hydrophobicity of Designed Helical Peptide Amphiphiles Control Their Bioactivity and Cell Selectivity. *ACS Appl Mater Interfaces* (2016) **8**:26501–26510. doi:10.1021/acsami.6b08297
25. Watson JL, Gillies ER. Amphipathic β-Strand Mimics as Potential Membrane Disruptive Antibiotics. *J Org Chem* (2009) **74**:5953–5960. doi:10.1021/jo900933r
26. Jin Y, Hammer J, Pate M, Zhang Y, Zhu F, Zmuda E, Blazyk J. Antimicrobial activities and structures of two linear cationic peptide families with various amphipathic beta-sheet and alpha-helical potentials. *Antimicrob Agents Chemother* (2005) **49**:4957–64. doi:10.1128/AAC.49.12.4957-4964.2005
27. Pedron CN, Torres MDT, Lima JA da S, Silva PI, Silva FD, Oliveira VX. Novel designed VmCT1 analogs with increased antimicrobial activity. *Eur J Med Chem* (2017) **126**:456–463. doi:10.1016/j.ejmech.2016.11.040
28. Taniguchi M, Ochiai A, Toyoda R, Sato T, Saitoh E, Kato T, Tanaka T. Effects of arginine and leucine substitutions on anti-endotoxic activities and mechanisms of action of cationic and amphipathic antimicrobial octadecapeptide from rice *α* -amylase. *J Pept Sci* (2017) **23**:252–260. doi:10.1002/psc.2983
29. Lum KY, Tay ST, Le CF, Lee VS, Sabri NH, Velayuthan RD, Hassan H, Sekaran SD. Activity of Novel Synthetic Peptides against Candida albicans. *Sci Rep* (2015) **5**:9657. doi:10.1038/srep09657
30. Felício MR, Silva ON, Gonçalves S, Santos NC, Franco OL. Peptides with Dual Antimicrobial and Anticancer Activities. *Front Chem* (2017) **5**:5. doi:10.3389/fchem.2017.00005
31. Takahashi D, Shukla SK, Prakash O, Zhang G. Structural determinants of host defense peptides for antimicrobial activity and target cell selectivity. *Biochimie* (2010) **92**:1236–1241. doi:10.1016/j.biochi.2010.02.023
32. Brogden KA. Antimicrobial peptides: pore formers or metabolic inhibitors in bacteria? *Nat Rev Microbiol* (2005) **3**:238–250. doi:10.1038/nrmicro1098
33. Torres MDT, Pedron CN, Higashikuni Y, Kramer RM, Cardoso MH, Oshiro KGN, Franco OL, Silva Junior PI, Silva FD, Oliveira Junior VX, et al. Structure-function-guided exploration of the antimicrobial peptide polybia-CP identifies activity determinants and generates synthetic therapeutic candidates. *Commun Biol* (2018) **1**:221. doi:10.1038/s42003-018-0224-2
34. Lohner K. New strategies for novel antibiotics: peptides targeting bacterial cell membranes. *Gen Physiol Biophys* (2009) **28**:105–116. doi:10.4149/gpb_2009_02_105
35. Gifford JL, Hunter HN, Vogel HJ. Lactoferricin: a lactoferrin-derived peptide with antimicrobial, antiviral, antitumor and immunological properties. *Cell Mol Life Sci* (2005) **62**:2588–98. doi:10.1007/s00018-005-5373-z
36. Le C-F, Fang C-M, Sekaran SD. Intracellular Targeting Mechanisms by Antimicrobial Peptides. *Antimicrob Agents Chemother* (2017) **61**:e02340-16. doi:10.1128/AAC.02340-16

37. Le C-F, Gudimella R, Razali R, Manikam R, Sekaran SD. Transcriptome analysis of Streptococcus pneumoniae treated with the designed antimicrobial peptides, DM3. *Sci Rep* (2016) **6**:26828. doi:10.1038/srep26828
38. Nijnik A, Hancock R. Host defence peptides: antimicrobial and immunomodulatory activity and potential applications for tackling antibiotic-resistant infections. *Emerg Health Threats J* (2009) **2**:e1. doi:10.3134/ehtj.09.001
39. Hilchie AL, Wuerth K, Hancock REW. Immune modulation by multifaceted cationic host defense (antimicrobial) peptides. *Nat Chem Biol* (2013) **9**:761–8. doi:10.1038/nchembio.1393
40. Achtman AH, Pilat S, Law CW, Lynn DJ, Janot L, Mayer ML, Ma S, Kindrachuk J, Finlay BB, Brinkman FSL, et al. Effective Adjunctive Therapy by an Innate Defense Regulatory Peptide in a Preclinical Model of Severe Malaria. *Sci Transl Med* (2012) **4**:135ra64-135ra64. doi:10.1126/scitranslmed.3003515
41. Scott MG, Dullaghan E, Mookherjee N, Glavas N, Waldbrook M, Thompson A, Wang A, Lee K, Doria S, Hamill P, et al. An anti-infective peptide that selectively modulates the innate immune response. *Nat Biotechnol* (2007) **25**:465–472. doi:10.1038/nbt1288
42. Mookherjee N, Brown KL, Bowdish DME, Doria S, Falsafi R, Hokamp K, Roche FM, Mu R, Doho GH, Pistolic J, et al. Modulation of the TLR-Mediated Inflammatory Response by the Endogenous Human Host Defense Peptide LL-37. *J Immunol* (2006) **176**:2455–2464. doi:10.4049/jimmunol.176.4.2455
43. Nijnik A, Madera L, Ma S, Waldbrook M, Elliott MR, Easton DM, Mayer ML, Mullaly SC, Kindrachuk J, Jenssen H, et al. Synthetic Cationic Peptide IDR-1002 Provides Protection against Bacterial Infections through Chemokine Induction and Enhanced Leukocyte Recruitment. *J Immunol* (2010) **184**:2539–2550. doi:10.4049/jimmunol.0901813
44. Mookherjee N, Lippert DND, Hamill P, Falsafi R, Nijnik A, Kindrachuk J, Pistolic J, Gardy J, Miri P, Naseer M, et al. Intracellular Receptor for Human Host Defense Peptide LL-37 in Monocytes. *J Immunol* (2009) **183**:2688–2696. doi:10.4049/jimmunol.0802586
45. Arranz-Trullén J, Lu L, Pulido D, Bhakta S, Boix E. Host Antimicrobial Peptides: The Promise of New Treatment Strategies against Tuberculosis. *Front Immunol* (2017) **8**:1499. doi:10.3389/fimmu.2017.01499
46. A current view on inflammation. Nature Publishing Group (2017). doi:10.1038/ni.3798
47. Xue J, Schmidt SV, Sander J, Draffehn A, Krebs W, Quester I, De Nardo D, Gohel TD, Emde M, Schmidleithner L, et al. Transcriptome-Based Network Analysis Reveals a Spectrum Model of Human Macrophage Activation. *Immunity* (2014) **40**:274–288. doi:10.1016/J.IMMUNI.2014.01.006
48. Brogden KA, Bates AM, Fischer CL. "Antimicrobial Peptides in Host Defense: Functions Beyond Antimicrobial Activity," in *Antimicrobial Peptides* (Cham: Springer International Publishing), 129–146. doi:10.1007/978-3-319-24199-9_9
49. Yang D, Chen Q, Schmidt AP, Anderson GM, Wang JM, Wooters J, Oppenheim JJ, Chertov O. Ll-37, the Neutrophil Granule–And Epithelial Cell–Derived Cathelicidin, Utilizes Formyl Peptide Receptor–Like 1 (Fprl1) as a Receptor to Chemoattract Human Peripheral Blood Neutrophils, Monocytes, and T Cells. *J Exp Med* (2000) **192**:1069–1074. doi:10.1084/jem.192.7.1069
50. Dürr M, Peschel A. Chemokines meet defensins: the merging concepts of chemoattractants and antimicrobial peptides in host defense. *Infect Immun* (2002) **70**:6515–7. doi:10.1128/iai.70.12.6515-6517.2002
51. Dorschner RA. The mammalian ionic environment dictates microbial susceptibility to antimicrobial defense peptides. *FASEB J* (2006) **20**:35–42. doi:10.1096/fj.05-4406com
52. Tjabringa GS, Ninaber DK, Drijfhout JW, Rabe KF, Hiemstra PS. Human Cathelicidin LL-37 Is a Chemoattractant for Eosinophils and Neutrophils That Acts via Formyl-Peptide Receptors. *Int Arch Allergy Immunol* (2006) **140**:103–112. doi:10.1159/000092305
53. Zhang S-K, Song J, Gong F, Li S-B, Chang H-Y, Xie H-M, Gao H-W, Tan Y-X, Ji S-P. Design of an α-helical antimicrobial peptide with improved cell-selective and potent

anti-biofilm activity. *Sci Rep* (2016) **6**:27394. doi:10.1038/srep27394
54. Nguyen LT, Vogel HJ. Structural perspectives on antimicrobial chemokines. *Front Immunol* (2012) **3**:384. doi:10.3389/FIMMU.2012.00384
55. Pérez-Cañadillas JM, Zaballos Á, Gutiérrez J, Varona R, Roncal F, Albar JP, Márquez G, Bruix M. NMR Solution Structure of Murine CCL20/MIP-3α, a Chemokine That Specifically Chemoattracts Immature Dendritic Cells and Lymphocytes through Its Highly Specific Interaction with the β-Chemokine Receptor CCR6. *J Biol Chem* (2001) **276**:28372–28379. doi:10.1074/jbc.M103121200
56. Niyonsaba F, Ushio H, Nakano N, Ng W, Sayama K, Hashimoto K, Nagaoka I, Okumura K, Ogawa H. Antimicrobial Peptides Human β-Defensins Stimulate Epidermal Keratinocyte Migration, Proliferation and Production of Proinflammatory Cytokines and Chemokines. *J Invest Dermatol* (2007) **127**:594–604. doi:10.1038/sj.jid.5700599
57. Ramos R, Silva JP, Rodrigues AC, Costa R, Guardão L, Schmitt F, Soares R, Vilanova M, Domingues L, Gama M. Wound healing activity of the human antimicrobial peptide LL37. *Peptides* (2011) **32**:1469–1476. doi:10.1016/j.peptides.2011.06.005
58. Carretero M, Escámez MJ, García M, Duarte B, Holguín A, Retamosa L, Jorcano JL, Río M del, Larcher F. In vitro and In vivo Wound Healing-Promoting Activities of Human Cathelicidin LL-37. *J Invest Dermatol* (2008) **128**:223–236. doi:10.1038/sj.jid.5701043
59. Thorburn A. Apoptosis and autophagy: regulatory connections between two supposedly different processes. *Apoptosis* (2008) **13**:1–9. doi:10.1007/s10495-007-0154-9
60. Weiss GG, Schaible UE. Macrophage defense mechanisms against intracellular bacteria. *Immunol Rev* (2015) **264**:182–203. doi:10.1111/imr.12266
61. Hu Z, Murakami T, Suzuki K, Tamura H, Kuwahara-Arai K, Iba T, Nagaoka I. Antimicrobial Cathelicidin Peptide LL-37 Inhibits the LPS/ATP-Induced Pyroptosis of Macrophages by Dual Mechanism. *PLoS One* (2014) **9**:e85765. doi:10.1371/journal.pone.0085765
62. Yuk J-M, Shin D-M, Lee H-M, Yang C-S, Jin HS, Kim K-K, Lee Z-W, Lee S-H, Kim J-M, Jo E-K. Vitamin D3 Induces Autophagy in Human Monocytes/Macrophages via Cathelicidin. *Cell Host Microbe* (2009) **6**:231–43. doi:10.1016/j.chom.2009.08.004
63. Lau YE, Bowdish DME, Cosseau C, Hancock REW, Davidson DJ. Apoptosis of Airway Epithelial Cells. *Am J Respir Cell Mol Biol* (2006) **34**:399–409. doi:10.1165/rcmb.2005-0170OC
64. Chamorro CI, Weber G, Grönberg A, Pivarcsi A, Ståhle M. The Human Antimicrobial Peptide LL-37 Suppresses Apoptosis in Keratinocytes. *J Invest Dermatol* (2009) **129**:937–944. doi:10.1038/jid.2008.321
65. Barnard EA. Biological function of pancreatic ribonuclease. *Nature* (1969) **221**:340–344. doi:10.1038/221340a0
66. Beintema JJ, Kleineidam RG. The ribonuclease A superfamily: General discussion. *Cell Mol Life Sci* (1998) **54**:825–832. doi:10.1007/s000180050211
67. Koczera P, Martin L, Marx G, Schuerholz T. The ribonuclease a superfamily in humans: Canonical RNases as the buttress of innate immunity. *Int J Mol Sci* (2016) **17**:1278. doi:10.3390/ijms17081278
68. Lu L, Li J, Moussaoui M, Boix E. Immune Modulation by Human Secreted RNases at the Extracellular Space. *Front Immunol* (2018) **9**:1012. doi:10.3389/fimmu.2018.01012
69. Parés X, Nogués M V, de Llorens R, Cuchillo CM. Structure and function of ribonuclease A binding subsites. *Essays Biochem* (1991) **26**:89–103. Available at: http://www.ncbi.nlm.nih.gov/pubmed/1778187
70. Futami I, Tsushima Y, Murato Y, Tad H, Sasaki I. Tissue-specific expression of pancreatic-type RNases and RNase inhibitor in humans. *DNA Cell Biol* (1997) **16**:413–419. doi:10.1089/dna.1997.16.413
71. Landre JBP, Hewett PW, Olivot J-M, Friedl P, Ko Y, Sachinidis A, Moenner M. Human endothelial cells selectively express large amounts of pancreatic-type ribonuclease (RNase 1). *J Cell Biochem* (2002) **86**:540–552. doi:10.1002/jcb.10234
72. Fischer S, Nishio M, Dadkhahi S, Gansler J, Saffarzadeh M, Shibamiyama A, Kral N,

Baal N, Koyama T, Deindl E, et al. Expression and localisation of vascular ribonucleases in endothelial cells. *Thromb Haemost* (2011) **105**:345–355. doi:10.1160/TH10-06-0345
73. Rosenberg HF. Eosinophil-Derived Neurotoxin (EDN/RNase 2) and the Mouse Eosinophil-Associated RNases (mEars): Expanding Roles in Promoting Host Defense. *Int J Mol Sci* (2015) **16**:15442–15455. doi:10.3390/ijms160715442
74. Harrison AM, Bonville CA, Rosenberg HF, Domachowske JB. Respiratory syncytical virus–induced chemokine expression in the lower airways. *Am J Respir Crit Care Med* (1999) **159**:1918–1924. doi:10.1164/ajrccm.159.6.9805083
75. Domachowske JB, Dyer KD, Bonville CA, Rosenberg HF. Recombinant Human Eosinophil-Derived Neurotoxin/RNase 2 Functions as an Effective Antiviral Agent against Respiratory Syncytial Virus. *J Infect Dis* (1998) **177**:1458–1464. doi:10.1086/515322
76. Shamri R, Young KM, Weller PF. PI3K, ERK, p38 MAPK and integrins regulate CCR3-mediated secretion of mouse and human eosinophil-associated RNases. *Allergy Eur J Allergy Clin Immunol* (2013) **68**:880–889. doi:10.1111/all.12163
77. Venge P, Byström J, Carlson M, Håkansson L, Karawacjzyk M, Peterson C, Sevéus L, Trulson A, Hâkansson L, Karawacjzyk M, et al. Eosinophil cationic protein (ECP): Molecular and biological properties and the use of ECP as a marker of eosinophil activation in disease. *Clin Exp Allergy* (1999) **29**:1172–1186. doi:10.1046/j.1365-2222.1999.00542.x
78. Bystrom J, Amin K, Bishop-Bailey D. Analysing the eosinophil cationic protein - a clue to the function of the eosinophil granulocyte. *Respir Res* (2011) **12**:10. doi:10.1186/1465-9921-12-10
79. Egesten A, Dyer KD, Batten D, Domachowske JB, Rosenberg HF. Ribonucleases and host defense: Identification, localization and gene expression in adherent monocytes in vitro. *Biochim Biophys Acta - Mol Cell Res* (1997) **1358**:255–260. doi:10.1016/S0167-4889(97)00081-5
80. Boix E, Nogués MV. Mammalian antimicrobial proteins and peptides: overview on the RNase A superfamily members involved in innate host defence. *Mol Biosyst* (2007) **3**:317. doi:10.1039/b617527a
81. Olson KA, Verselis SJ, Fett JW. Angiogenin is regulated in Vivoas an acute phase protein. *Biochem Biophys Res Commun* (1998) **242**:480–483. doi:10.1006/bbrc.1997.7990
82. Koutroubakis IE, Xidakis C, Karmiris K, Sfiridaki A, Kandidaki E, Kouroumalis EA. Serum angiogenin in inflammatory bowel disease. *Dig Dis Sci* (2004) **49**:1758–1762. doi:10.1007/s10620-004-9565-4
83. Rosenberg HF, Dyer KD. Molecular cloning and characterization of a novel human ribonuclease (RNase k6): increasing diversity in the enlarging ribonuclease gene family. *Nucleic Acids Res* (1996) **24**:3507–3513. doi:6a0332 [pii]
84. Becknell B, Eichler TE, Beceiro S, Li B, Easterling RS, Carpenter AR, James CL, McHugh KM, Hains DS, Partida-Sanchez S, et al. Ribonucleases 6 and 7 have antimicrobial function in the human and murine urinary tract. *Kidney Int* (2015) **87**:151–161. doi:10.1038/ki.2014.268
85. Christensen-Quick A, Lafferty M, Sun L, Marchionni L, DeVico A, Garzino-Demo A. Human Th17 Cells Lack HIV-Inhibitory RNases and Are Highly Permissive to Productive HIV Infection. *J Virol* (2016) **90**:7833–47. doi:10.1128/JVI.02869-15
86. Simanski M, Köten B, Schröder JM, Gläser R, Harder J. Antimicrobial RNases in cutaneous defense. *J Innate Immun* (2012) **4**:241–247. doi:10.1159/000335029
87. Harder J, Schröder JM, Gläser R. The skin surface as antimicrobial barrier: Present concepts and future outlooks. *Exp Dermatol* (2013) **22**:1–5. doi:10.1111/exd.12046
88. Spencer JD, Schwaderer AL, Wang H, Bartz J, Kline J, Eichler T, Desouza KR, Sims-Lucas S, Baker P, Hains DS. Ribonuclease 7, an antimicrobial peptide upregulated during infection, contributes to microbial defense of the human urinary tract. *Kidney Int* (2013) **83**:615–625. doi:10.1038/ki.2012.410
89. Harder JJ, Schröder J-MM, Schroder J-M. RNase 7, a Novel Innate Immune Defense

Antimicrobial Protein of Healthy Human Skin. *J Biol Chem* (2002) **277**:46779–46784. doi:10.1074/jbc.M207587200
90. Kenzel S, Mergen M, von Süßkind-Schwendi J, Wennekamp J, Deshmukh SD, Haeffner M, Triantafyllopoulou A, Fuchs S, Farmand S, Santos-Sierra S, et al. Insulin Modulates the Inflammatory Granulocyte Response to Streptococci via Phosphatidylinositol 3-Kinase. *J Immunol* (2012) **189**:4582–4591. doi:10.4049/jimmunol.1200205
91. Zhang J, Dyer KD, Rosenberg HF. RNase 8, a novel RNase A superfamily ribonuclease expressed uniquely in placenta. *Nucleic Acids Res* (2002) **30**:1169–1175. doi:10.1093/nar/30.5.1169
92. Chan CC, Moser JM, Dyer KD, Percopo CM, Rosenberg HF. Genetic diversity of human RNase 8. *BMC Genomics* (2012) **13**:40. doi:10.1186/1471-2164-13-40
93. Raines RT. Ribonuclease A. *Chem Rev* (1998) **98**:1045–1065. doi:10.1021/cr960427h
94. Sorrentino S. Human extracellular ribonucleases: Multiplicity, molecular diversity and catalytic properties of the major RNase types. *Cell Mol Life Sci* (1998) **54**:785–794. doi:10.1007/s000180050207
95. Boix E, Nogues MV, Schein CH, Benner S a, Cuchillo CM. Reverse Transphosphorylation by Ribonuclease A Needs an Intact p2 -binding Site. *J Biol Chem* (1994) **269**:2529–2534.
96. Nogués M V, Moussaoui M, Boix E, Vilanova M, Ribó M, Cuchillo CM. The contribution of noncatalytic phosphate-binding subsites to the mechanism of bovine pancreatic ribonuclease A. *Cell Mol Life Sci* (1998) **54**:766–774. doi:10.1007/s000180050205
97. Moussaoui M, Nogués M V, Guasch A, Barman T, Travers F, Cuchillo CM. The subsites structure of bovine pancreatic ribonuclease A accounts for the abnormal kinetic behavior with cytidine 2',3 '-cyclic phosphate. *J Biol Chem* (1998) **273**:25565–25572. doi:Doi 10.1074/Jbc.273.40.25565
98. Boix E, Blanco JA, Nogués MV, Moussaoui M. Nucleotide binding architecture for secreted cytotoxic endoribonucleases. *Biochimie* (2013) **95**:1087–1097. doi:10.1016/j.biochi.2012.12.015
99. Prats-Ejarque G, Lu L, Salazar VA, Moussaoui M, Boix E. Evolutionary Trends in RNA Base Selectivity Within the RNase A Superfamily. *Front Pharmacol* (2019) **10**:1170. doi:10.3389/fphar.2019.01170
100. Johnson DL, Johnson SAS. CELL BIOLOGY: RNA Metabolism and Oncogenesis. *Science (80-)* (2008) **320**:461–462. doi:10.1126/science.1158680
101. Liu EY, Cali CP, Lee EB. RNA metabolism in neurodegenerative disease. *Dis Model Mech* (2017) **10**:509–518. doi:10.1242/dmm.028613
102. St. Laurent G, Wahlestedt C, Kapranov P. The Landscape of long noncoding RNA classification. *Trends Genet* (2015) **31**:239–251. doi:10.1016/J.TIG.2015.03.007
103. Fabian MR, Sonenberg N, Filipowicz W. Regulation of mRNA Translation and Stability by microRNAs. *Annu Rev Biochem* (2010) **79**:351–379. doi:10.1146/annurev-biochem-060308-103103
104. Li K, Rodosthenous RS, Kashanchi F, Gingeras T, Gould SJ, Kuo LS, Kurre P, Lee H, Leonard JN, Liu H, et al. Advances, challenges, and opportunities in extracellular RNA biology: insights from the NIH exRNA Strategic Workshop. *JCI Insight* (2018) **3**: doi:10.1172/JCI.INSIGHT.98942
105. Tsatsaronis JA, Franch-Arroyo S, Resch U, Charpentier E. Extracellular Vesicle RNA: A Universal Mediator of Microbial Communication? *Trends Microbiol* (2018) **26**:401–410. doi:10.1016/J.TIM.2018.02.009
106. Lee H-H, Wang Y-N, Hung M-C. Functional roles of the human ribonuclease A superfamily in RNA metabolism and membrane receptor biology. *Mol Aspects Med* (2019) **70**:106–116. doi:10.1016/j.mam.2019.03.003
107. Lomax JE, Bianchetti CM, Chang A, Phillips GN, Fox BG, Raines RT. Functional Evolution of Ribonuclease Inhibitor: Insights from Birds and Reptiles. *J Mol Biol* (2014) **426**:3041–3056. doi:10.1016/j.jmb.2014.06.007
108. Zhang J, Dyer KD, Rosenberg HF. Human RNase 7: A new cationic ribonuclease of the

RNase A superfamily. *Nucleic Acids Res* (2003) **31**:602–607. doi:10.1093/nar/gkg157
109. Prats-Ejarque G, Arranz-Trullen J, Blanco JA, Pulido D, Nogues M V., Moussaoui M, Boix E. The first crystal structure of human RNase6 reveals a novel substrate binding and cleavage site arrangement. *Biochem J* (2016) doi:10.1042/BCJ20160245
110. Sorrentino S. The eight human "canonical" ribonucleases: Molecular diversity, catalytic properties, and special biological actions of the enzyme proteins. *FEBS Lett* (2010) **584**:2194–2200. doi:10.1016/j.febslet.2010.04.018
111. Eller CH, Lomax JE, Raines RT. Bovine Brain Ribonuclease Is the Functional Homolog of Human Ribonuclease 1. *J Biol Chem* (2014) **289**:25996–26006. doi:10.1074/jbc.M114.566166
112. Lomax JE, Eller CH, Raines RT. Comparative functional analysis of ribonuclease 1 homologs: molecular insights into evolving vertebrate physiology. *Biochem J* (2017) **474**:2219–2233. doi:10.1042/BCJ20170173
113. Rosenberg HF, Dyer KD, Tiffany HL, Gonzalez M. Rapid evolution of a unique family of primate ribonuclease genes. *Nat Genet* (1995) **10**:219–223. doi:10.1038/ng0695-219
114. Zhang J, Rosenberg HF, Nei M. Positive Darwinian selection after gene duplication in primate ribonuclease genes. *Proc Natl Acad Sci U S A* (1998) **95**:3708–3713. doi:10.1073/pnas.95.7.3708
115. Sorrentino S, Glitz DG. Wibonuclease activity and substrate preference of human eosinophil cationic protein (ECP). *FEBS Lett* (1991) **288**:23–26. doi:10.1016/0014-5793(91)80994-E
116. Yang D, Chen Q, Su SB, Zhang P, Kurosaka K, Caspi RR, Michalek SM, Rosenberg HF, Zhang N, Oppenheim JJ. Eosinophil-derived neurotoxin acts as an alarmin to activate the TLR2–MyD88 signal pathway in dendritic cells and enhances Th2 immune responses. *J Exp Med* (2008) **205**:79–90. doi:10.1084/jem.20062027
117. Schwartz L, Cohen A, Thomas J, Spencer J, Schwartz L, Cohen A, Thomas J, Spencer JD. The Immunomodulatory and Antimicrobial Properties of the Vertebrate Ribonuclease A Superfamily. *Vaccines* (2018) **6**:76. doi:10.3390/vaccines6040076
118. Rosenberg HF. Recombinant human eosinophil cationic protein. Ribonuclease activity is not essential for cytotoxicity. *J Biol Chem* (1995) **270**:7876–7881.
119. Yang D, Chen Q, Rosenberg HF, Rybak SM, Newton DL, Wang ZY, Fu Q, Tchernev VT, Wang M, Schweitzer B, et al. Human ribonuclease A superfamily members, eosinophil-derived neurotoxin and pancreatic ribonuclease, induce dendritic cell maturation and activation. *J Immunol* (2004) **173**:6134–6142. doi:10.4049/jimmunol.173.10.6134
120. Rugeles MT, Trubey CM, Bedoya VI, Pinto LA, Oppenheim JJ, Rybak SM, Shearer GM. Ribonuclease is partly responsible for the HIV-1 inhibitory effect activated by HLA alloantigen recognition. *AIDS* (2003) **17**:481–486. doi:10.1097/00002030-200303070-00002
121. Weller PF, Spencer LA. Functions of tissue-resident eosinophils. *Nat Rev Immunol* (2017) **17**:746–760. doi:10.1038/nri.2017.95
122. Chihara J, Urayama O, Tsuda A, Kakazu T, Higashimoto I, Yamada H. Eosinophil Cationic Protein Induces Insulin-Like Growth Factor I Receptor Expression on Bronchial Epithelial Cells. *Int Arch Allergy Immunol* (1996) **111**:43–45. doi:10.1159/000237414
123. Li S, Sheng J, Hu JK, Yu W, Kishikawa H, Hu MG, Shima K, Wu D, Xu Z, Xin W, et al. Ribonuclease 4 protects neuron degeneration by promoting angiogenesis, neurogenesis, and neuronal survival under stress. *Angiogenesis* (2013) **16**:387–404. doi:10.1007/s10456-012-9322-9
124. Cocchi F, DeVico AL, Lu W, Popovic M, Latinovic O, Sajadi MM, Redfield RR, Lafferty MK, Galli M, Garzino-Demo A, et al. Soluble factors from T cells inhibiting X4 strains of HIV are a mixture of chemokines and RNases. *Proc Natl Acad Sci* (2012) **109**:5411–5416. doi:10.1073/pnas.1202240109
125. Harris P, Johannessen KM, Smolenski G, Callaghan M, Broadhurst MK, Kim K, Wheeler TT. Characterisation of the anti-microbial activity of bovine milk ribonuclease4

and ribonuclease5 (angiogenin). *Int Dairy J* (2010) **20**:400–407. doi:10.1016/j.idairyj.2009.12.018
126. Miyake M, Goodison S, Lawton A, Gomes-Giacoia E, Rosser CJ. Angiogenin promotes tumoral growth and angiogenesis by regulating matrix metallopeptidase-2 expression via the ERK1/2 pathway. *Oncogene* (2015) **34**:890–901. doi:10.1038/onc.2014.2
127. Yamasaki S, Ivanov P, Hu GF, Anderson P. Angiogenin cleaves tRNA and promotes stress-induced translational repression. *J Cell Biol* (2009) **185**:35–42. doi:10.1083/jcb.200811106
128. Tsuji T, Sun Y, Kishimoto K, Olson KA, Liu S, Hirukawa S, Hu GG. Angiogenin Is Translocated to the Nucleus of HeLa Cells and Is Involved in Ribosomal RNA Transcription and Cell Proliferation. *Cancer Res* (2005) **65**:1352–1360. doi:10.1158/0008-5472.CAN-04-2058
129. Wang Y-N, Lee H-H, Chou C-K, Yang W-H, Wei Y, Chen C-T, Yao J, Hsu JL, Zhu C, Ying H, et al. Angiogenin/Ribonuclease 5 Is an EGFR Ligand and a Serum Biomarker for Erlotinib Sensitivity in Pancreatic Cancer. *Cancer Cell* (2018) **33**:752-769.e8. doi:10.1016/j.ccell.2018.02.012
130. Tschesche H, Kopp C, Hörl WH, Hempelmann U. Inhibition of degranulation of polymorphonuclear leukocytes by angiogenin and its tryptic fragment. *J Biol Chem* (1994) **269**:30274–30280.
131. Shcheglovitova ON, Maksyanina E V, Ionova II, Rustam'yan YL, Komolova GS. Cow milk angiogenin induces cytokine production in human blood leukocytes. *Bull Exp Biol Med* (2003) **135**:158–160. doi:10.1023/A:1023871931764
132. Abtin A, Eckhart L, Mildner M, Ghannadan M, Harder J, Schröder JM, Tschachler E. Degradation by stratum corneum proteases prevents endogenous RNase inhibitor from blocking antimicrobial activities of RNase 5 and RNase 7. *J Invest Dermatol* (2009) **129**:2193–2201. doi:10.1038/jid.2009.35
133. Li S, Yu W, Hu G-F. Angiogenin inhibits nuclear translocation of apoptosis inducing factor in a Bcl-2-dependent manner. *J Cell Physiol* (2012) **227**:1639–1644. doi:10.1002/jcp.22881
134. Torrent M, Sánchez D, Buzón V, Nogués MV, Cladera J, Boix E. Comparison of the membrane interaction mechanism of two antimicrobial RNases: RNase 3/ECP and RNase 7. *Biochim Biophys Acta - Biomembr* (2009) **1788**:1116–1125. doi:10.1016/j.bbamem.2009.01.013
135. Torrent M, Badia M, Moussaoui M, Sanchez D, Nogués MV, Boix E. Comparison of human RNase 3 and RNase 7 bactericidal action at the Gram-negative and Gram-positive bacterial cell wall. *FEBS J* (2010) **277**:1713–1725. doi:10.1111/j.1742-4658.2010.07595.x
136. Kopfnagel V, Wagenknecht S, Harder J, Hofmann K, Kleine M, Buch A, Sodeik B, Werfel T. RNase 7 Strongly Promotes TLR9-Mediated DNA Sensing by Human Plasmacytoid Dendritic Cells. *J Invest Dermatol* (2018) **138**:872–881. doi:10.1016/j.jid.2017.09.052
137. Zasloff M. Antimicrobial rnases of human skin. *J Invest Dermatol* (2009) **129**:2091–2093. doi:10.1038/jid.2009.216
138. Rudolph B, Podschun R, Sahly H, Schubert S, Schröder JM, Harder J. Identification of RNase 8 as a novel human antimicrobial protein. *Antimicrob Agents Chemother* (2006) **50**:3194–3196. doi:10.1128/AAC.00246-06
139. Liang S, Acharya KR. Structural basis of substrate specificity in porcine RNase 4. *FEBS J* (2016) **283**:912–928. doi:10.1111/febs.13646
140. Lyons SM, Fay MM, Akiyama Y, Anderson PJ, Ivanov P. RNA biology of angiogenin: Current state and perspectives. *RNA Biol* (2017) **14**:171–178. doi:10.1080/15476286.2016.1272746
141. Fu H, Feng J, Liu Q, Sun F, Tie Y, Zhu J, Xing R, Sun Z, Zheng X. Stress induces tRNA cleavage by angiogenin in mammalian cells. *FEBS Lett* (2009) **583**:437–442. doi:10.1016/j.febslet.2008.12.043
142. Lee YS, Shibata Y, Malhotra A, Dutta A. A novel class of small RNAs: tRNA-derived

RNA fragments (tRFs). *Genes Dev* (2009) **23**:2639–2649. doi:10.1101/gad.1837609
143. Kumar P, Mudunuri SB, Anaya J, Dutta A. tRFdb: A database for transfer RNA fragments. *Nucleic Acids Res* (2015) **43**:D141–D145. doi:10.1093/nar/gku1138
144. Lambertz U, Oviedo Ovando ME, Vasconcelos EJR, Unrau PJ, Myler PJ, Reiner NE. Small RNAs derived from tRNAs and rRNAs are highly enriched in exosomes from both old and new world Leishmania providing evidence for conserved exosomal RNA Packaging. *BMC Genomics* (2015) **16**:151. doi:10.1186/s12864-015-1260-7
145. Li S, Xu Z, Sheng J. tRNA-derived small RNA: A novel regulatory small non-coding RNA. *Genes (Basel)* (2018) **9**: doi:10.3390/genes9050246
146. Lee SR, Collins K. Starvation-induced cleavage of the tRNA anticodon loop in Tetrahymena thermophila. *J Biol Chem* (2005) **280**:42744–9. doi:10.1074/jbc.M510356200
147. Thompson DM, Lu C, Green PJ, Parker R. tRNA cleavage is a conserved response to oxidative stress in eukaryotes. *RNA* (2008) **14**:2095–2103. doi:10.1261/rna.1232808
148. Dhahbi JM, Spindler SR, Atamna H, Yamakawa A, Boffelli D, Mote P, Martin DIK. 5' tRNA halves are present as abundant complexes in serum, concentrated in blood cells, and modulated by aging and calorie restriction. *BMC Genomics* (2013) **14**:1–14. doi:10.1186/1471-2164-14-298
149. Prats-Ejarque G, Blanco JA, Salazar VA, Nogués VM, Moussaoui M, Boix E. Characterization of an RNase with two catalytic centers. Human RNase6 catalytic and phosphate-binding site arrangement favors the endonuclease cleavage of polymeric substrates. *Biochim Biophys Acta - Gen Subj* (2019) **1863**:105–117. doi:10.1016/j.bbagen.2018.09.021
150. Bedoya VI, Boasso A, Hardy AW, Rybak S, Shearer GM, Rugeles MT. Ribonucleases in HIV type 1 inhibition: effect of recombinant RNases on infection of primary T cells and immune activation-induced RNase gene and protein expression. *AIDS Res Hum Retroviruses* (2006) **22**:897–907. doi:10.1089/aid.2006.22.897
151. Li Y, Zhao Y, Liu J, Huang Y, Liu Z, Xue C. A promising alternative anti-HBV agent: The targeted ribonuclease. *Int J Mol Med* (2009) **23**:521–527. doi:10.3892/ijmm
152. Boix E, Pulido D, Moussaoui M, Victòria Nogués M, Russi S. The sulfate-binding site structure of the human eosinophil cationic protein as revealed by a new crystal form. *J Struct Biol* (2012) **179**:1–9. doi:10.1016/j.jsb.2012.04.023
153. Pulido D, Moussaoui M, Andreu D, Nogués MV, Torrent M, Boix E. Antimicrobial action and cell agglutination by the eosinophil cationic protein are modulated by the cell wall lipopolysaccharide structure. *Antimicrob Agents Chemother* (2012) **56**:2378–2385. doi:10.1128/AAC.06107-11
154. Hooper L V., Stappenbeck TS, Hong C V., Gordon JI. Angiogenins: a new class of microbicidal proteins involved in innate immunity. *Nat Immunol* (2003) **4**:269–273. doi:10.1038/ni888
155. Pulido D, Arranz-Trullén J, Prats-Ejarque G, Velázquez D, Torrent M, Moussaoui M, Boix E. Insights into the Antimicrobial Mechanism of Action of Human RNase6: Structural Determinants for Bacterial Cell Agglutination and Membrane Permeation. *Int J Mol Sci* (2016) **17**:552. doi:10.3390/ijms17040552
156. Becknell B, Spencer JD. A Review of Ribonuclease 7's Structure, Regulation, and Contributions to Host Defense. *Int J Mol Sci* (2016) **17**: doi:10.3390/ijms17030423
157. Pulido D, Torrent M, Andreu D, Nogués MV, Boix E. Two Human Host Defense Ribonucleases against Mycobacteria, the Eosinophil Cationic Protein (RNase 3) and RNase 7. *Antimicrob Agents Chemother* (2013) **57**:3797–3805. doi:10.1128/AAC.00428-13
158. Yang D, Rosenberg HF, Chen Q, Dyer KD, Kurosaka K, Oppenheim JJ. Eosinophil-derived neurotoxin (EDN), an antimicrobial protein with chemotactic activities for dendritic cells. *Blood* (2003) **102**:3396–3403. doi:10.1182/blood-2003-01-0151
159. Zagai U, Dadfar E, Lundahl J, Venge P, Sköld CM. Eosinophil cationic protein stimulates TGF-β1 release by human lung fibroblasts in vitro. *Inflammation* (2007) **30**:153–160. doi:10.1007/s10753-007-9032-4

160. Sheng J, Xu Z. Three decades of research on angiogenin: a review and perspective. *Acta Biochim Biophys Sin (Shanghai)* (2016) **48**:399–410. doi:10.1093/abbs/gmv131
161. Rendl M, Mayer C, Weninger W, Tschachler E. Topically applied lactic acid increases spontaneous secretion of vascular endothelial growth factor by human reconstructed epidermis. *Br J Dermatol* (2001) **145**:3–9. doi:10.1046/j.1365-2133.2001.04274.x
162. Li S, Hu G-F. Emerging role of angiogenin in stress response and cell survival under adverse conditions. *J Cell Physiol* (2012) **227**:2822–6. doi:10.1002/jcp.23051
163. Wang Y-N, Lee H-H, Hung M-C. A novel ligand-receptor relationship between families of ribonucleases and receptor tyrosine kinases. *J Biomed Sci* (2018) **25**:83. doi:10.1186/s12929-018-0484-7
164. Kopfnagel V, Wagenknecht S, Brand L, Zeitvogel J, Harder J, Hofmann K, Kleine M, Werfel T. RNase 7 downregulates TH2 cytokine production by activated human T-cells. *Allergy* (2017) doi:10.1111/all.13173
165. Gambichler T, Skrygan M, Tomi NS, Othlinghaus N, Brockmeyer NH, Altmeyer P, Kreuter A. Differential mRNA Expression of Antimicrobial Peptides and Proteins in Atopic Dermatitis as Compared to Psoriasis Vulgaris and Healthy Skin. *Int Arch Allergy Immunol* (2008) **147**:17–24. doi:10.1159/000128582
166. Rademacher F, Simanski M, Harder JJ. RNase 7 in cutaneous defense. *Int J Mol Sci* (2016) **17**: doi:10.3390/ijms17040560
167. Boix E, Salazar VA, Torrent M, Pulido D, Nogués MV, Moussaoui M. Structural determinants of the eosinophil cationic protein antimicrobial activity. *Biol Chem* (2012) **393**:801–815. doi:10.1515/hsz-2012-0160
168. Lu L, Li J, Moussaoui M, Boix E. Immune modulation by human secreted RNases at the extracellular space. *Front Immunol* (2018) **9**:1–20. doi:10.3389/fimmu.2018.01012
169. Pulido D, Moussaoui M, Victòria Nogués M, Torrent M, Boix E. Towards the rational design of antimicrobial proteins: Single point mutations can switch on bactericidal and agglutinating activities on the RNase A superfamily lineage. *FEBS J* (2013) **280**:5841–5852. doi:10.1111/febs.12506
170. Pulido D, Prats-Ejarque G, Villalba C, Albacar M, González-López JJ, Torrent M, Moussaoui M, Boix E. A Novel RNase 3/ECP Peptide for Pseudomonas aeruginosa Biofilm Eradication That Combines Antimicrobial, Lipopolysaccharide Binding, and Cell-Agglutinating Activities. *Antimicrob Agents Chemother* (2016) **60**:6313–6325. doi:10.1128/AAC.00830-16
171. Rekha RS, Rao Muvva SSVJ, Wan M, Raqib R, Bergman P, Brighenti S, Gudmundsson GH, Agerberth B, Sultana Rekha R, Rao Muvva SSVJ, et al. Phenylbutyrate induces LL-37-dependent autophagy and intracellular killing of mycobacterium tuberculosis in human macrophages. *Autophagy* (2015) **11**:1688–1699. doi:10.1080/15548627.2015.1075110
172. Muciño G, Castro-Obregón S, Hernandez-Pando R, Del Rio G. Autophagy as a target for therapeutic uses of multifunctional peptides. *IUBMB Life* (2016) **68**:259–267. doi:10.1002/iub.1483
173. Torrent M, Cuyás E, Carreras E, Navarro S, López O, de la Maza A, Nogués MV, Reshetnyak YK, Boix E. Topography Studies on the Membrane Interaction Mechanism of the Eosinophil Cationic Protein. *Biochemistry* (2007) **46**:720–733. doi:10.1021/bi061190e
174. Huang Y-C, Lin Y-M, Chang T-W, Wu S-J, Lee Y-S, Chang MD-T, Chen C, Wu S-H, Liao Y-D. The Flexible and Clustered Lysine Residues of Human Ribonuclease 7 Are Critical for Membrane Permeability and Antimicrobial Activity. *J Biol Chem* (2007) **282**:4626–4633. doi:10.1074/jbc.M607321200
175. Boix E, Torrent M, Sánchez D, Nogués MV. The antipathogen activities of eosinophil cationic protein. *Curr Pharm Biotechnol* (2008) **9**:141–152. doi:10.2174/138920108784567353
176. Lu L, Arranz-Trullén J, Prats-Ejarque G, Pulido D, Bhakta S, Boix E. Human Antimicrobial RNases Inhibit Intracellular Bacterial Growth and Induce Autophagy in Mycobacteria-Infected Macrophages. *Front Immunol* (2019) **10**:1500.

doi:10.3389/fimmu.2019.01500
177. Herbst RS. Review of epidermal growth factor receptor biology. *Int J Radiat Oncol* (2004) **59**:S21–S26. doi:10.1016/J.IJROBP.2003.11.041
178. Hardbower DM, Singh K, Asim M, Verriere TG, Olivares-Villagómez D, Barry DP, Allaman MM, Washington MK, Peek RM, Piazuelo MB, et al. EGFR regulates macrophage activation and function in bacterial infection. *J Clin Invest* (2016) **126**:3296–3312. doi:10.1172/JCI83585
179. Kalinowski A, Galen BT, Ueki IF, Sun Y, Mulenos A, Osafo-Addo A, Clark B, Joerns J, Liu W, Nadel JA, et al. Respiratory syncytial virus activates epidermal growth factor receptor to suppress interferon regulatory factor 1-dependent interferon-lambda and antiviral defense in airway epithelium. *Mucosal Immunol* (2018) **11**:958–967. doi:10.1038/mi.2017.120
180. Minutti CM, Drube S, Blair N, Schwartz C, McCrae JC, McKenzie AN, Kamradt T, Mokry M, Coffer PJ, Sibilia M, et al. Epidermal Growth Factor Receptor Expression Licenses Type-2 Helper T Cells to Function in a T Cell Receptor-Independent Fashion. *Immunity* (2017) **47**:710-722.e6. doi:10.1016/J.IMMUNI.2017.09.013
181. Rayego-Mateos S, Rodrigues-Diez R, Morgado-Pascual JL, Valentijn F, Valdivielso JM, Goldschmeding R, Ruiz-Ortega M. Role of Epidermal Growth Factor Receptor (EGFR) and Its Ligands in Kidney Inflammation and Damage. *Mediators Inflamm* (2018) **2018**:1–22. doi:10.1155/2018/8739473
182. Zhao Y, Ye X, Dunker W, Song Y, Karijolich J. RIG-I like receptor sensing of host RNAs facilitates the cell-intrinsic immune response to KSHV infection. *Nat Commun* (2018) **9**:4841. doi:10.1038/s41467-018-07314-7
183. Loo Y-M, Gale M. Immune Signaling by RIG-I-like Receptors. *Immunity* (2011) **34**:680–692. doi:10.1016/j.immuni.2011.05.003
184. Ghildiyal M, Zamore PD. Small silencing RNAs: An expanding universe. *Nat Rev Genet* (2009) **10**:94–108. doi:10.1038/nrg2504
185. Selitsky SR, Baran-Gale J, Honda M, Yamane D, Masaki T, Fannin EE, Guerra B, Shirasaki T, Shimakami T, Kaneko S, et al. Small tRNA-derived RNAs are increased and more abundant than microRNAs in chronic hepatitis B and C. *Sci Rep* (2015) **5**: doi:10.1038/srep07675
186. Wang Q, Lee I, Ren J, Ajay SS, Lee YS, Bao X. Identification and Functional Characterization of tRNA-derived RNA Fragments (tRFs) in Respiratory Syncytial Virus Infection. *Mol Ther* (2013) **21**:368–379. doi:10.1038/mt.2012.237
187. Su Z, Kuscu C, Malik A, Shibata E, Dutta A. Angiogenin generates specific stress-induced tRNA halves and is not involved in tRF-3–mediated gene silencing. *J Biol Chem* (2019) **294**:16930–16941. doi:10.1074/jbc.RA119.009272
188. Lyons SM, Fay MM, Ivanov P. The role of RNA modifications in the regulation of tRNA cleavage. *FEBS Lett* (2018) **592**:2828–2844. doi:10.1002/1873-3468.13205
189. Eigenbrod T, Dalpke AH. Bacterial RNA: An Underestimated Stimulus for Innate Immune Responses. *J Immunol* (2015) **195**:411–418. doi:10.4049/jimmunol.1500530
190. Schlee M, Hartmann G. Discriminating self from non-self in nucleic acid sensing. *Nat Rev Immunol* (2016) **16**:566–580. doi:10.1038/nri.2016.78
191. Machado D, Hoffmann J, Moroso M, Rosa-Calatrava M, Endtz H, Terrier O, Paranhos-Baccalà G. RSV Infection in Human Macrophages Promotes CXCL10/IP-10 Expression during Bacterial Co-Infection. *Int J Mol Sci* (2017) **18**: doi:10.3390/IJMS18122654
192. Acharya KR, Ackerman SJ. Eosinophil granule proteins: Form and function. *J Biol Chem* (2014) **289**:17406–17415. doi:10.1074/jbc.R113.546218
193. Lee JJ, Jacobsen EA, McGarry MP, Schleimer RP, Lee NA. Eosinophils in health and disease: the LIAR hypothesis. *Clin Exp Allergy* (2010) **40**:563–575. doi:10.1111/j.1365-2222.2010.03484.x
194. Davoine F, Lacy P. Eosinophil cytokines, chemokines, and growth factors: Emerging roles in immunity. *Front Immunol* (2014) **5**: doi:10.3389/fimmu.2014.00570
195. Boix E, Nogués MV. Mammalian antimicrobial proteins and peptides: overview on the RNase A superfamily members involved in innate host defence. *Mol Biosyst* (2007)

3:317–335. doi:10.1039/b617527a
196. Monteseirín J, Vega A, Chacón P, Camacho MJ, El Bekay R, Asturias JA, Martínez A, Guardia P, Pérez-Cano R, Conde J, et al. Neutrophils as a Novel Source of Eosinophil Cationic Protein in IgE-Mediated Processes. *J Immunol* (2007) **179**:2634–2641. doi:10.4049/jimmunol.179.4.2634
197. Rosenberg H. Eosinophil-Derived Neurotoxin / RNase 2: Connecting the Past, the Present and the Future. *Curr Pharm Biotechnol* (2008) **9**:135–140. doi:10.2174/138920108784567236
198. Oppenheim JJ, Tewary P, de la Rosa G, Yang D. "Alarmins Initiate Host Defense," in (Springer, New York, NY), 185–194. doi:10.1007/978-0-387-72005-0_19
199. Rosenberg HF, Dyer KD. Diversity among the primate eosinophil-derived neurotoxin genes: A specific C-terminal sequence is necessary for enhanced ribonuclease activity. *Nucleic Acids Res* (1997) **25**:3532–3536. doi:10.1093/nar/25.17.3532
200. Kim C-K, Seo JK, Ban SH, Fujisawa T, Kim DW, Callaway Z. Eosinophil-derived neurotoxin levels at 3 months post-respiratory syncytial virus bronchiolitis are a predictive biomarker of recurrent wheezing. *Biomarkers* (2013) **18**:230–235. doi:10.3109/1354750X.2013.773078
201. Al Yacoub N, Romanowska M, Haritonova N, Foerster J. Optimized production and concentration of lentiviral vectors containing large inserts. (2007) doi:10.1002/jgm.1052
202. Kutner RH, Zhang X-Y, Reiser J. Production, concentration and titration of pseudotyped HIV-1-based lentiviral vectors. *Nat Protoc* (2009) **4**:495–505. doi:10.1038/nprot.2009.22
203. Shen B, Zhang J, Wu H, Wang J, Ma K, Li Z, Zhang X, Zhang P, Huang X. Generation of gene-modified mice via Cas9/RNA-mediated gene targeting. *Cell Res* (2013) **23**:720–723. doi:10.1038/cr.2013.46
204. Prats-Ejarque G, Arranz-Trullén J, Blanco JA, Pulido D, Nogués MV, Moussaoui M, Boix E. The first crystal structure of human RNase 6 reveals a novel substrate-binding and cleavage site arrangement. *Biochem J* (2016) **473**:1523–1536. doi:10.1042/BCJ20160245
205. Pertea M, Kim D, Pertea GM, Leek JT, Salzberg SL. Transcript-level expression analysis of RNA-seq experiments with HISAT, StringTie and Ballgown. *Nat Protoc* (2016) **11**:1650–1667. doi:10.1038/nprot.2016.095
206. Durinck S, Spellman PT, Birney E, Huber W. Mapping identifiers for the integration of genomic datasets with the R/Bioconductor package biomaRt. *Nat Protoc* (2009) **4**:1184–1191. doi:10.1038/nprot.2009.97
207. Love MI, Huber W, Anders S. Moderated estimation of fold change and dispersion for RNA-seq data with DESeq2. *Genome Biol* (2014) **15**:550. doi:10.1186/s13059-014-0550-8
208. Yu G, Wang L-G, Han Y, He Q-Y. clusterProfiler: an R Package for Comparing Biological Themes Among Gene Clusters. *Omi A J Integr Biol* (2012) **16**:284–287. doi:10.1089/omi.2011.0118
209. Zhou G, Soufan O, Ewald J, Hancock REW, Basu N, Xia J. NetworkAnalyst 3.0: a visual analytics platform for comprehensive gene expression profiling and meta-analysis. *Nucleic Acids Res* (2019) doi:10.1093/nar/gkz240
210. van Zundert GCP, Rodrigues JPGLM, Trellet M, Schmitz C, Kastritis PL, Karaca E, Melquiond ASJ, van Dijk M, de Vries SJ, Bonvin AMJJ. The HADDOCK2.2 Web Server: User-Friendly Integrative Modeling of Biomolecular Complexes. *J Mol Biol* (2016) **428**:720–725. doi:10.1016/J.JMB.2015.09.014
211. Dominguez C, Boelens R, Bonvin AMJJ. HADDOCK: A protein-protein docking approach based on biochemical or biophysical information. *J Am Chem Soc* (2003) **125**:1731–1737. doi:10.1021/ja026939x
212. Vissers M, Habets MN, Ahout IML, Jans J, de Jonge MI, Diavatopoulos DA, Ferwerda G. An In vitro Model to Study Immune Responses of Human Peripheral Blood Mononuclear Cells to Human Respiratory Syncytial Virus Infection. *J Vis Exp* (2013)e50766. doi:10.3791/50766

213. Sun Y, Jain D, Koziol-White CJ, Genoyer E, Gilbert M, Tapia K, Panettieri RA, Hodinka RL, López CB. Immunostimulatory Defective Viral Genomes from Respiratory Syncytial Virus Promote a Strong Innate Antiviral Response during Infection in Mice and Humans. *PLOS Pathog* (2015) **11**:e1005122. doi:10.1371/journal.ppat.1005122
214. Dewhurst-Maridor G, Simonet V, Bornand J., Nicod L., Pache J. Development of a quantitative TaqMan RT-PCR for respiratory syncytial virus. *J Virol Methods* (2004) **120**:41–49. doi:10.1016/J.JVIROMET.2004.03.017
215. Baker PJ, Masters SL. "Generation of Genetic Knockouts in Myeloid Cell Lines Using a Lentiviral CRISPR/Cas9 System," in *Methods in Molecular Biology*, 41–55. doi:10.1007/978-1-4939-7519-8_3
216. Tiscornia G, Singer O, Verma IM. Production and purification of lentiviral vectors. *Nat Protoc* (2006) **1**:241–245. doi:10.1038/nprot.2006.37
217. Gleich GJ, Loegering D a, Bell MP, Checkel JL, Ackerman SJ, McKean DJ. Biochemical and functional similarities between human eosinophil-derived neurotoxin and eosinophil cationic protein: homology with ribonuclease. *Proc Natl Acad Sci U S A* (1986) **83**:3146–3150. doi:10.1073/pnas.83.10.3146
218. Rosenberg HF. RNase A ribonucleases and host defense: an evolving story. *J Leukoc Biol* (2008) **83**:1079–87. doi:10.1189/jlb.1107725
219. Roskoski R. The ErbB/HER family of protein-tyrosine kinases and cancer. *Pharmacol Res* (2014) **79**:34–74. doi:10.1016/j.phrs.2013.11.002
220. Colomiere M, Ward AC, Riley C, Trenerry MK, Cameron-Smith D, Findlay J, Ackland L, Ahmed N. Cross talk of signals between EGFR and IL-6R through JAK2/STAT3 mediate epithelial-mesenchymal transition in ovarian carcinomas. *Br J Cancer* (2009) **100**:134–144. doi:10.1038/sj.bjc.6604794
221. Chakraborty S, Li L, Puliyappadamba VT, Guo G, Hatanpaa KJ, Mickey B, Souza RF, Vo P, Herz J, Chen MR, et al. Constitutive and ligand-induced EGFR signalling triggers distinct and mutually exclusive downstream signalling networks. *Nat Commun* (2014) **5**: doi:10.1038/ncomms6811
222. Monticelli LA, Osborne LC, Noti M, Tran S V., Zaiss DMW, Artis D. IL-33 promotes an innate immune pathway of intestinal tissue protection dependent on amphiregulin-EGFR interactions. *Proc Natl Acad Sci U S A* (2015) **112**:10762–10767. doi:10.1073/pnas.1509070112
223. Choi HJ, Seo CH, Park SH, Yang H, Do KH, Kim J, Kim HK, Chung DH, Ahn JH, Moon Y. Involvement of epidermal growth factor receptor-linked signaling responses in Pseudomonas fluorescens-infected alveolar epithelial cells. *Infect Immun* (2011) **79**:1998–2005. doi:10.1128/IAI.01232-10
224. Franzke CW, Cobzaru C, Triantafyllopoulou A, Löffek S, Horiuchi K, Threadgill DW, Kurz T, van Rooijen N, Bruckner-Tuderman L, Blobel CP. Epidermal ADAM17 maintains the skin barrier by regulating EGFR ligand- dependent terminal keratinocyte differentiation. *J Exp Med* (2012) **209**:1105–1119. doi:10.1084/jem.20112258
225. Skalsky RL, Cullen BR. Viruses, microRNAs, and Host Interactions. *Annu Rev Microbiol* (2010) **64**:123–141. doi:10.1146/annurev.micro.112408.134243
226. Deng J, Ptashkin RN, Chen Y, Cheng Z, Liu G, Phan T, Deng X, Zhou J, Lee I, Lee YS, et al. Respiratory Syncytial Virus Utilizes a tRNA Fragment to Suppress Antiviral Responses Through a Novel Targeting Mechanism. *Mol Ther* (2015) **23**:1622–1629. doi:10.1038/mt.2015.124
227. Das AT, Klaver B, Berkhout B. Reduced Replication of Human Immunodeficiency Virus Type 1 Mutants That Use Reverse Transcription Primers other than the Natural tRNA 3 Lys. (1995). Available at: http://jvi.asm.org/ [Accessed February 5, 2020]
228. Schorn AJ, Gutbrod MJ, LeBlanc C, Martienssen R. LTR-Retrotransposon Control by tRNA-Derived Small RNAs. *Cell* (2017) **170**:61-71.e11. doi:10.1016/j.cell.2017.06.013
229. Jin D, Musier-Forsyth K. Role of host tRNAs and aminoacyl-tRNA synthetases in retroviral replication. *J Biol Chem* (2019) **294**:5352–5364. doi:10.1074/jbc.REV118.002957
230. Xin X, Wang H, Han L, Wang M, Fang H, Hao Y, Li J, Zhang H, Zheng C, Shen C.

Single-Cell Analysis of the Impact of Host Cell Heterogeneity on Infection with Foot-and-Mouth Disease Virus. *J Virol* (2018) **92**:e00179-18. doi:10.1128/JVI.00179-18
231. Zhang X, Cozen AE, Liu Y, Chen Q, Lowe TM. Small RNA Modifications: Integral to Function and Disease. *Trends Mol Med* (2016) **22**:1025–1034. doi:10.1016/J.MOLMED.2016.10.009
232. Ivanov P, Emara MM, Villen J, Gygi SP, Anderson P. Angiogenin-induced tRNA fragments inhibit translation initiation. *Mol Cell* (2011) **43**:613–623. doi:10.1016/j.molcel.2011.06.022
233. Akiyama Y, Lyons S, Fay MM, Abe T, Anderson P, Ivanov P. Multiple ribonuclease A family members cleave transfer RNAs in response to stress. doi:10.1101/811174

CHAPTER I

frontiers in Immunology

REVIEW
published: 07 November 2017
doi: 10.3389/fimmu.2017.01499

Host Antimicrobial Peptides: The Promise of New Treatment Strategies against Tuberculosis

Javier Arranz-Trullén[1,2†], Lu Lu[1†], David Pulido[1†], Sanjib Bhakta[2] and Ester Boix[1*]*

[1] Faculty of Biosciences, Department of Biochemistry and Molecular Biology, Universitat Autònoma de Barcelona, Cerdanyola del Vallès, Spain, [2] Mycobacteria Research Laboratory, Department of Biological Sciences, Institute of Structural and Molecular Biology, Birkbeck University of London, London, United Kingdom

OPEN ACCESS

Edited by:
Uday Kishore,
Brunel University London,
United Kingdom

Reviewed by:
Suraj Sable,
Centers for Disease Control and Prevention, United States
Kushagra Bansal,
Harvard Medical School,
United States

***Correspondence:**
Ester Boix
Ester.Boix@uab.cat;
Sanjib Bhakta
s.bhakta@bbk.ac.uk

†Present address:
David Pulido,
Nuffield Department of Medicine,
University of Oxford,
Oxford, United Kingdom

‡These authors have contributed equally to this work.

Specialty section:
This article was submitted to Molecular Innate Immunity, a section of the journal Frontiers in Immunology

Received: 26 April 2017
Accepted: 24 October 2017
Published: 07 November 2017

Citation:
Arranz-Trullén J, Lu L, Pulido D, Bhakta S and Boix E (2017) Host Antimicrobial Peptides: The Promise of New Treatment Strategies against Tuberculosis. Front. Immunol. 8:1499. doi: 10.3389/fimmu.2017.01499

Tuberculosis (TB) continues to be a devastating infectious disease and remerges as a global health emergency due to an alarming rise of antimicrobial resistance to its treatment. Despite of the serious effort that has been applied to develop effective antitubercular chemotherapies, the potential of antimicrobial peptides (AMPs) remains underexploited. A large amount of literature is now accessible on the AMP mechanisms of action against a diversity of pathogens; nevertheless, research on their activity on mycobacteria is still scarce. In particular, there is an urgent need to integrate all available interdisciplinary strategies to eradicate extensively drug-resistant *Mycobacterium tuberculosis* strains. In this context, we should not underestimate our endogenous antimicrobial proteins and peptides as ancient players of the human host defense system. We are confident that novel antibiotics based on human AMPs displaying a rapid and multifaceted mechanism, with reduced toxicity, should significantly contribute to reverse the tide of antimycobacterial drug resistance. In this review, we have provided an up to date perspective of the current research on AMPs to be applied in the fight against TB. A better understanding on the mechanisms of action of human endogenous peptides should ensure the basis for the best guided design of novel antitubercular chemotherapeutics.

Keywords: antimicrobial peptides, innate immunity, tuberculosis, infectious diseases, mycobacteria, antimicrobial resistance, host defense

INTRODUCTION

Tuberculosis (TB) is currently one of the most devastating infectious diseases having caused around 1.8 million human deaths, with 10.4 million new cases reported in 2016 and approximately a third of the world's population harboring its persistent form of the disease-causing pathogen, *Mycobacterium tuberculosis* (Mtb) (1). Statistical analysis of epidemiological data have been shown a steady increase of the disease incidences over the past decade and new drug-resistant forms of TB cases are currently more than 5% of the total. TB has represented a major challenge worldwide and is the first/top leading cause of death from a single infectious microorganism (1).

Although the TB causing pathogen was first identified at the end of the nineteenth century, effective drugs against Mtb were only introduced during the second half of the twentieth century XXs: streptomycin first, followed by isoniazid (INH), pyrazinamide (PZA), ethambutol (EMB), and rifampicin (RIF). Unfortunately, the misuse and overuse of antibiotics for human welfare and farming industry have facilitated the emergence of resistant strains (2–4). Multidrug-resistant TB strains

(MDR-TB) do not respond to INH and RIF and extensively drug-resistant strains (XDR-TB) display an added resistance to any fluoroquinolone and at-least one of the three second-line injectable drugs, i.e., amikacin, kanamycin, or capreomycin. Although the development of the first combined anti-TB drug-therapy dramatically improved the disease prognosis outcome, the current alarming rise in multidrug resistance is jeopardizing our early attempt to control the disease (5, 6). Moreover, the current WHO approved treatments impair the patient life quality and have an enormous economic cost (2, 7). Mtb being an extremely successful intracellular pathogen, can remain within the host system by keeping the immune responses under control *via* a wide repertoire of escape pathways (8). To complicate matters further, latent tubercle bacilli infections have become a serious global threat because of the challenge in diagnosing them clinically and their regular conversion from dormancy to active infections in immunocompromised circumstances, due to HIV coinfection, immunosuppressive therapies (9, 10) or diabetes mellitus type 2 conditions (11). Although novel drug susceptibility testing methodologies, such as the GeneXpert® MTB/RIF (12, 13) and HT-SPOTi (14), are enabling the early detection of antibiotic-resistant strains, a complete comprehension of the host immune capability and the mode by which Mtb handles/endures/evades the host defenses will be needed to eradicate this infectious disease (15).

Despite the initial underestimation of the properties of antimicrobial peptides (AMPs) and the difficulties encountered in their attempt to reach the market, nowadays, it is widely accepted that AMPs are multifunctional molecules with key contributions in the mammalian host innate defense (2, 3, 16, 17). In addition, due to the evolution of drug resistance among Mtb strains and their rapid spread across the globe, the use of both natural and synthetic AMPs and their combination with conventional drugs (18, 19) are enabling the creation of a new generation of truly promising antibiotics (20–23). As Mtb can survive and replicate within macrophages, novel anti-TB agents should be able to target the intracellularly dwelling mycobacteria without causing any damage to the host. In this review, we will focus on AMPs, either exploited naturally by our immune system or artificially synthesized, as potential therapeutics to overcome and eradicate the pathogen infection. Special attention will be paid to the diverse mechanisms that can mediate the AMPs' action against TB infection. Finally, we will discuss the advantages, limitations, and challenges of AMPs for its merchandising and clinical use.

A UNIQUE AND PATHOGENIC BACTERIA

Although most mycobacteria (more than 150 species reported to date) are environmental, only a few species can infect both humans and livestock alike. Mtb is an obligate human pathogen with a low mutation rate (24) and no horizontal gene transfer (25). The TB-causing bacilli have coevolved with our civilization over millennia and its indefinite latency periods probably evolved as an adaptation to the sparse geographic distribution of early human settlements. However, our modern one-world globalization might be triggering a worryingly shorter latency in TB (4).

Tuberculosis is mainly an airborne respiratory disease that is conveyed through aerosolized particles. Once in contact with the lung tissues, Mtb can enter and dwell within the host macrophages and other phagocytic immune cells. Immediately after, the infection triggers a complex immune response, and as a result, the pathogens may manage to establish a long-term residence within the host (4, 12, 26). During the primary infection phase, the host defense response sequesters the bacilli in confined cages at the lung alveoli, known as granuloma (**Figure 1**). During this early period the infected alveolar macrophages, the favorite mycobacterial lodge, are actively releasing pro-inflammatory effectors and other signaling molecules to remove the resident pathogens (8, 27). Following, the tubercle bacilli manage to downregulate the host cell expression profile and enter into a dormant state (26, 28). Ultimately, granuloma will mature and endure a necrosis process. Dormancy responses will facilitate the pathogen's long-term intra-host survival, and enable it to withstand the necrotic granuloma environment. Upon reactivation of dormant cells, the bacilli will start growing extracellularly and cover the lung cavities with a biofilm layer enriched with the most drug-resistant cells (29). The spread of reinfection is then mediated by coughing induced granuloma mechanical shear (12, 28).

THE POTENTIAL OF ANTIMICROBIAL PEPTIDES IN THE ANTI-TB CHEMOTHERAPY: UNRAVELING THEIR MECHANISMS OF ACTION

Emergence of extensively antimicrobial resistance toward current anti-TB drugs has drawn back our attention toward alternative once neglected therapeutic strategies, including a resurge in AMPs research (2, 30). Expression of endogenous AMPs represents one of the most ancient host defense strategy of living organisms. Their multifunctional mode of action, natural origin, and effectiveness at low concentration have positioned them as prospective candidates in future antitubercular therapeutics market (3, 7, 31, 32). Notwithstanding, to ensure a successful therapy prior to drug design, we must deepen in the knowledge of the underlying mechanism of action of our own innate immunity players.

Despite a low level of amino acid sequence identity, AMPs adopt similar structural folds, indicating the existence of parallel mechanisms of antimicrobial action among distant living organisms (33). Among a significant variety of AMPs traits, we can outline the main common properties. We will review here the main known human AMPs secreted by innate immunity cells to counterbalance mycobacterial infections along with their mode of action.

Mycobacterial Cell-Wall: A Complex Barrier Particularly Difficult to Overcome

The unusual high antimicrobial resistance in mycobacteria is primarily due to the unique complexity of its cell wall. The complex network of macromolecules such as peptidoglycan, arabinogalactan, and mycolic acids (MAgP complex), which are conglomerated by other proteins and polysaccharides, confirm the main

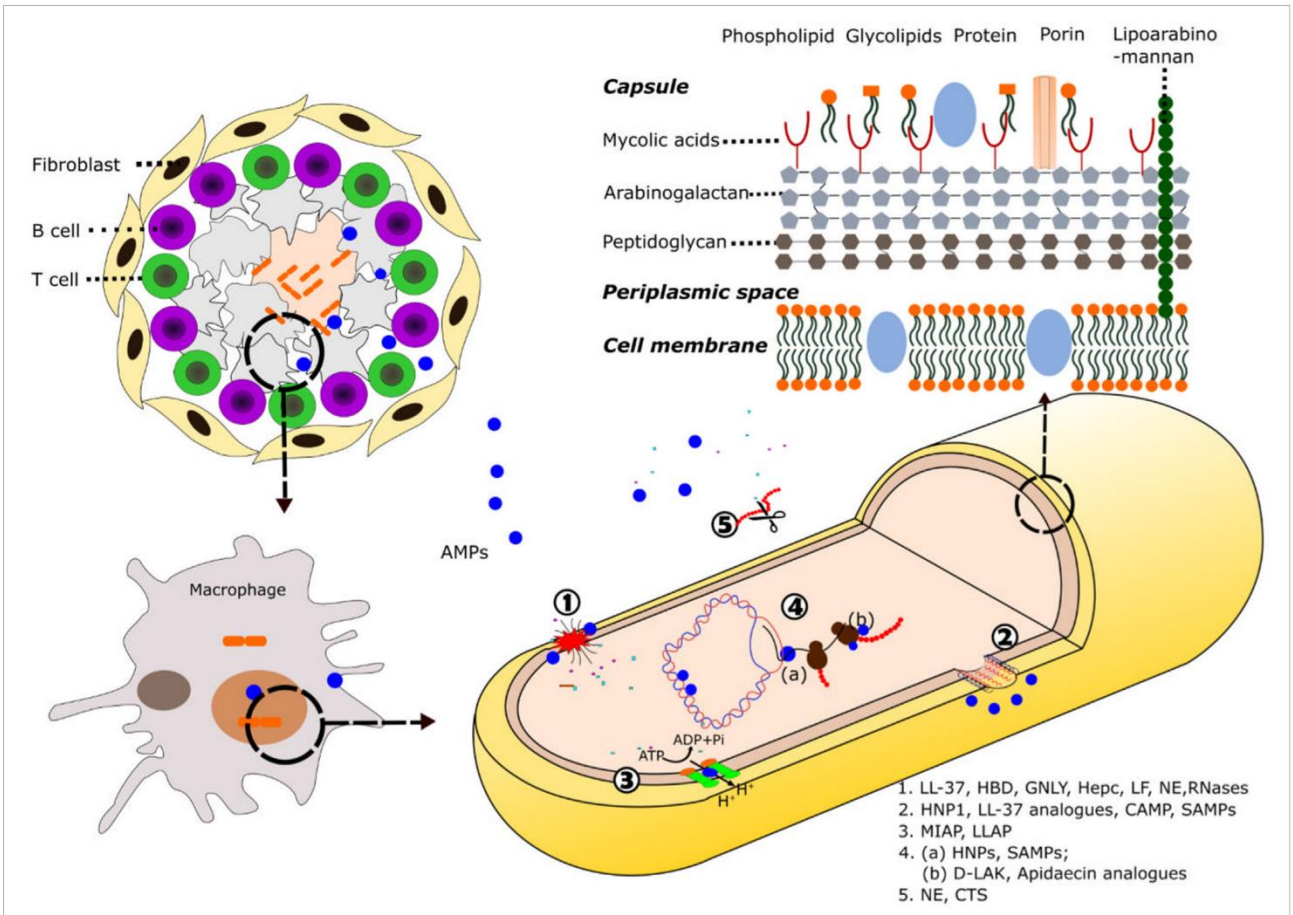

FIGURE 1 | Schematic illustration of AMP mode of action against mycobacteria. Following induction of the immune response by mycobacteria, AMPs are directed toward the area of infection where they can be recruited into the granuloma. At the cellular level, the destruction of the pathogens takes place inside the macrophage phagolysosomes. Composition of the mycobacteria cell wall and the main described mechanisms of action of AMPs against mycobacteria are shown: (1) cell wall and plasmatic membrane disruption, (2) membrane pore formation, (3) inhibition of ATPase, (4) AMP intracellular targets: **(a)** nucleic acids binding, inhibition of replication, and transcription; **(b)** inhibition of translation, and (5) protein degradation. Selected AMPs for each activity are highlighted. See **Tables 1** and **2** for a detailed description of each AMP mechanism of action. *Abbreviation*: LL-37, cathelicidin C-terminus; HBD, human β-defensin; GNLY, granulysin; Hepc, hepcidin; LF, lactoferrin; NE, neutrophil elastase; HNPs, human neutrophil proteins; CAMP, cationic antimicrobial peptides; SAMPs, synthetic antimicrobial peptides; MIAP, magainin-I derived antimicrobial peptide; LLAP, LL-37 derived antimicrobial peptide; D-LAK, D-enantiomeric antimicrobial peptides; CTS, cathepsins.

mycobacterial cell-wall scaffold and constitute a highly difficult crossing-barrier for antimicrobial agents (34–37) (**Figure 1**). The unique covalently-linked MAgP complex of Mtb is a result of mycobacterial adaptation to secure the intracellular survival against continuous selective pressures exerted by the host immune system and other hostile environments. Furthermore, it has been found that the characteristics and composition of the cell wall can be modified during infection (38). The length and structure of the mycolic acids have been related to bacterial intracellular survival and are one of the favorite targets of successful antibiotics (12, 37). Unfortunately, the emergence of Mtb strains with acquired resistance to INH and EMB drugs that target the mycolic acids synthesis, demands novel strategies. Resistant strains have also emerged to PZA, a drug that targets the cell-envelope integrity (2). In this context, dermcidin, a human peptide secreted by sweat glands (39) has been predicted to inhibit the mycolyl transferase enzyme efficiently (40). Other re-emerged research lines target the cell-wall peptidoglycan metabolism (12). On the other hand, one of the main mechanisms by which the AMPs exert their effect is based on the ability to disrupt or permeate the cell membrane (**Figure 1**), either fully disrupting the lipid bilayer or by creating transient pores (41). Numerous AMPs have acquired amphipathic and cationic structures as short β-sheets and α-helices that allow them to establish interactions with bacterial membranes (42). The first step of AMPs interaction with the pathogen is generally mediated by their positive net charge and hydrophobicity. Unlike eukaryotic cells, in which the anionic lipids are predominantly in the inner leaflet of the lipid membrane providing a neutral cell surface, prokaryotic cells expose a negatively charged surface. Many AMPs can exert a direct killing mechanism against mycobacteria through cell membrane disruption. The binding between the mycobacterial anionic surface compounds and

the cationic residues of the peptides promotes the membrane permeabilization (43). Contribution of the peptide cationicity has been corroborated in distinct AMPs by amino acid substitution. As an example, the replacement of lysines by arginines in lactoferrin (LF) variants enhanced their mycobactericidal effect (44). In addition, although the highly hydrophobic scaffold of the mycobacterial envelope offers resistance to AMPs action, the increase in the proportion of α-helical structure and peptide hydrophobicity has being engineered as an alternative strategy to enhance their mycobactericidal features (18). Moreover, some AMPs are directly targeting surface cell-wall proteins to interfere in the cell ion exchange and inhibit the mycobacterial growth. AMPs can interact with the mycobacterial membrane proteins such as ATPases and inhibit the cell pH homeostasis (45, 46). Interestingly, AMPs inducing the membrane permeation can be applied as adjuvants to conventional antibiotics (47).

Intracellular Targets

Although most of the known AMPs exert their action at the bacterial membrane level, there is a growing number of identified peptides endowed with other previously overlooked targets. Many AMPs have the ability to translocate across the membrane and novel methodologies are bringing the opportunity to identify the peptide interactions with intracellular components (48). As an example, human neutrophil peptides can effectively cross the lipid bilayer without causing significant membrane damage and bind to nucleic acids (49, 50). Selective mycobactericidal action has been achieved by synthetic antimicrobial peptides (SAMPs) that can be internalized by mycobacterial cells and bind to DNA, inhibiting replication, and transcription processes (51). Interestingly, the intracellular action can be achieved at very low peptide concentrations, reducing the potential toxicity to host cells.

Phagosome-Lysosomal Pathway and Autophagy Modulation

Mycobacterium tuberculosis has evolved to dwell within one of the most inhospitable cell types, the macrophage. The tubercle bacillus is able to interfere with the phagosomal maturation pathway, blocking the transfer of the phagocytosed compounds to lysosomes (52). At this stage, several mechanisms take place toward the elimination of the pathogen, among them: production of reactive oxygen and nitrogen species, vacuole acidification, lytic enzymes activation, and changes in ion fluxes (53). *Mycobacterium* is able to interfere not only in the recruitment of vesicular ATPase proton pump but also in the acquisition of markers for the endocytic pathway. The TB causing bacilli promote the fusion with early endosomal vesicles but arrest the fusion to the lysosomal compartment, thereby protecting its phagosomal niche from acidification and avoiding the action of lytic enzymes. Moreover, the pathogen inhibits the phosphatidylinositol kinase, reducing the phosphatidyl inositol triphosphate (PIP3) levels and impairing the phagosome maturation (54). The modulation of the phagocytic maturation seems to be carried out by components of the mycobacterial cell wall, such as the mannosylated lipoarabinomannan (7, 54). Altogether, mycobacteria ensure their survival within the host cell by intercepting the autophagic machinery at distinct levels (**Figure 2**) (8, 55). On their side, many AMPs promoting the phagolysosome formation also contribute to remove the pathogen intruder (56). Thereby, one of the strategy undertaken by the mycobacteria is the downregulation of AMP expression within the macrophage (57). Autophagy has other beneficial effects for the host, such as the restriction of inflammation (58). Indeed, one of main currently used anti-TB drug is rapamycin, an autophagy activator, and the search of novel autophagy inducers is a priority (3, 23, 59).

Immunomodulatory Activities

Undoubtedly, immunotherapy is at the frontline of TB eradication programs. Following the bacteria engulfment by alveolar macrophages, the mycobacterial components are identified by several pattern recognition receptors resulting in the activation of signaling pathways and the subsequent leukocyte activation (27, 58). In this scenario, participation of endogenous AMPs during the host immune response (**Figure 2**) is key for a successful eradication of infection (28, 60). We can differentiate two main phases that would mediate the infection process, in the early acute step the AMPs can directly kill the Mtb bacilli, whereas in the secondary late step, the AMPs immunomodulatory action takes the leadership (26). Pro and anti-inflammatory effects can be induced by AMPs mediated by the release of a variety of cytokines (16, 23, 57). Interestingly, the same AMP can have a pro-inflammatory action at an early infection stage, while shifting to anti-inflammatory activity during late infection (3). Indeed, many immune factors play an essential role in the mediation of the infective process (8). For instance, the production of cytokines, which are important for the immune response, such as interferon gamma (IFNγ), are undermined by the mycobacterial infection (61).

HUMAN ENDOGENOUS AMPs INVOLVED IN THE FIGHT AGAINST TB INFECTION

Following mycobacterial infection, a large assortment of antimicrobial peptides is released by our innate immune cells into the affected tissue (62). AMPs as key players of the non-specific immune response (2, 17) have attracted renewed attention as novel therapeutics and several comprehensive databases are now available open to the scientific community (2, 63–65). We describe, here, the main natural human AMPs involved in the fight against TB infection (**Table 1**).

Cathelicidins

Cathelicidins constitute a mammalian family of antimicrobial peptides mostly expressed in leukocytes and epithelial cells in response to different pathogens, contributing to their eradication (7, 37, 72). The human cationic antimicrobial peptide-18 (hCAP-18) is the unique known human member and the leading AMP in TB therapeutics (7, 131). hCAP-18 is essentially conformed by two regions, a highly conserved N-terminal sequence, called cathelin and the bactericidal C-terminal region known as LL-37, released by proteolysis (132, 133). LL-37 contributes to the recruitment of T-cells to the site of infection (66) and displays

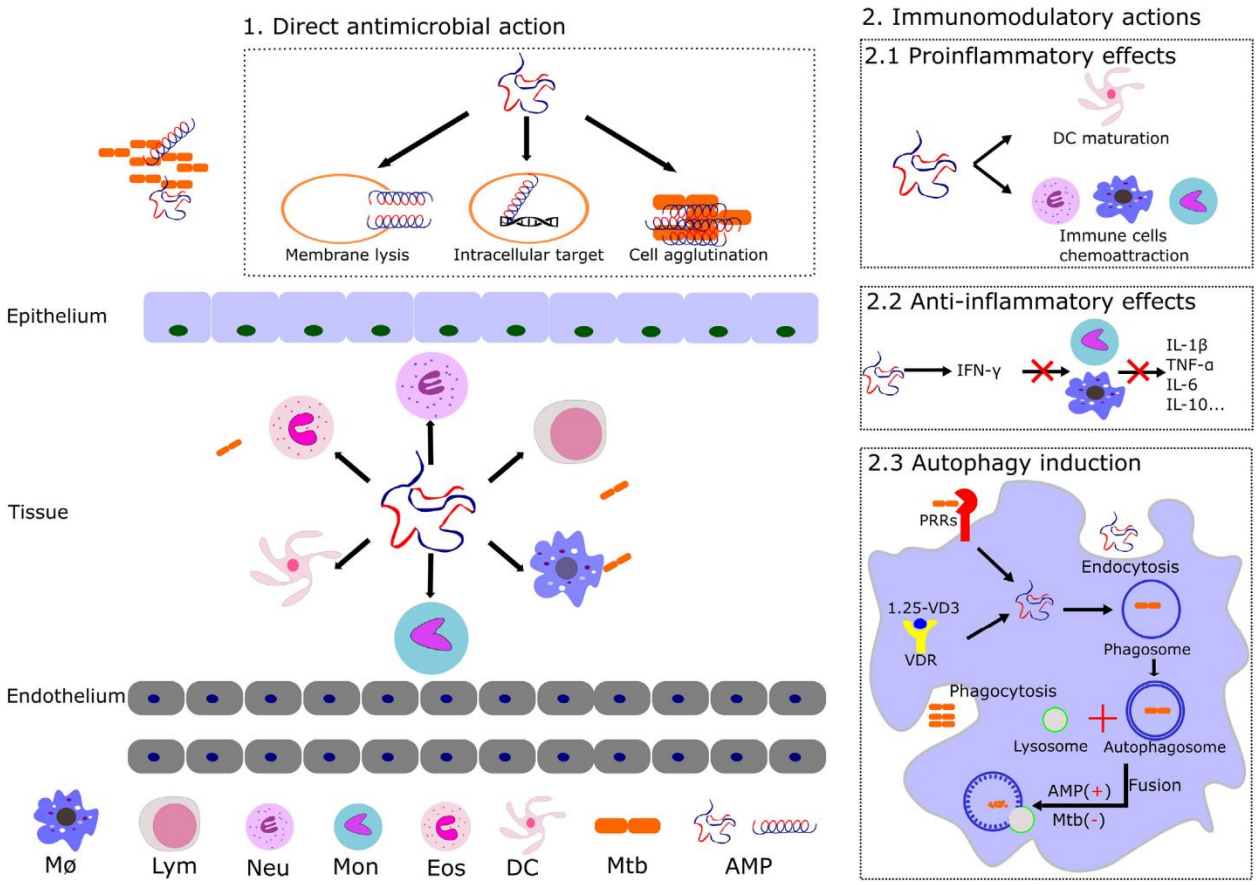

FIGURE 2 | Illustration of the distinct reported mechanism of action of AMPs expressed by the host innate immune cells. The main AMP antimicrobial and immunomodulatory activities are shown: (1) AMPs can trigger the cell lysis, target intracellular key processes (described in **Figure 1**), and/or agglutinate the bacterial cells. (2) Main AMPs' immunomodulatory actions that promote the mycobacterial clearance are illustrated. Induction of pro and anti-inflammatory activities contributes to the host defense by regulation of cytokines and chemokines expression and induction of innate cell maturation. AMPs can also intervene in the autophagosome and phagolysosome formation during autophagy. *Abbreviations*: MØ, macrophages; Lym, lymphocytes; Neu, neutrophils; Mon, monocytes; Eos, eosinophils; DC, dendritic cells; Mtb, *Mycobacterium tuberculosis*; AMP, antimicrobial peptides; VD3, vitamin D3; VDR, vitamin D receptor; PRRs, pattern recognition receptors.

diverse immunomodulatory and antimicrobial activities (57, 73), undertaking a prominent role during mycobacterial infection (57, 69). In particular, a significant overexpression of LL-37 on neutrophils, epithelial cells, and alveolar macrophages has been observed during Mtb infection (67). The infection of mononuclear cells promotes the upregulation synthesis of LL-37 *via* the vitamin D induction pathway (134). Interestingly, vitamin D deficiency correlates with susceptibility to tuberculosis, while supplementation with vitamin D derivatives improves the efficiency to overcome TB (75). Phagosomal pathway is known to be a key defensive procedure to eradicate Mtb and recent studies point to vitamin D3 as an inducer of autophagy in human monocytes as well as an inhibitor of intracellular mycobacterial growth, *via* upregulation of autophagy-related gene expression (3, 76, 134). The LL-37 peptide thereby decreases, directly or indirectly, the rate of intracellular bacteria proliferation. Recently, transcriptome profiling confirmed the direct contribution of LL-37 at the lysosomal compartment (135). Jointly, all these experimental evidences highlight cathelicidin LL-37 not only as a forthright antimicrobial peptide but also as a prominent modulator of autophagy during mycobacterial infection (3, 77).

Defensins

Defensins were the first AMPs related to TB by pioneer researchers (49, 50, 81, 136). Defensins are a set of cationic and cysteine-rich peptides with immunomodulatory and microbicidal properties that constitute one of the major and most diverse group of AMPs in the mammalian pulmonary host defense system (3, 16, 137). They are classified according to their structure into alpha, beta, and theta. They show substantial variation in terms of amino acid sequences, and show a diversity of mechanism of action at membrane and intracellular levels. In addition, defensins can be induced and activated by proteolysis pathways to acquire their antibacterial activity (138). Interestingly, high-throughput gene

TABLE 1 | Human AMPs involved in immune host defense against mycobacteria.

AMP	Cell type source[b]	Reported activities[a]
Cathelicidin (hCAP18/LL-37)	Neutrophils (66, 67[b]) Monocytes (66, 67[b]) Epithelial cells (66, 67[b]) Mast cells (68) Macrophages (67[b], 69) Dendritic cells (70) Natural killer cells (71)	Mycobacterial cell wall lysis (72, 73) Immunomodulation (57, 69) Pro-inflammatory action (74)[a] Autophagy activation (58, 75–78) Chemotaxis (58) Neutrophil extracellular traps (NETs) promotion (73)
Defensins	Eosinophils (HAD) (79)[b] Macrophages (HBD1) (80) Epithelial cells (HBD1, HBD2, HBD3, HBD4) (7, 81[b], 82) Dendritic cells (HBD1, HBD2) (80) Neutrophils (HNPs) (7, 30)	Mycobacterial cell membrane lysis (HBD) (23)[a] (2, 62) Membrane pore formation (HNPs) (7) Mycobacterial growth inhibition (HBD2,3,4) (79, 81, 83[a], 84) Dendritic and macrophage cells chemotaxis (HBD/HNPs) (82, 85[a]) (23)[a] Inflammation regulation (HBD) (62, 82) (HNP1) (7, 82) Intracellular DNA target (HNPs) (49, 50)
Hepcidin	Hepatocytes (86) Macrophages (87)[b] Dendritic cells (88, 89) Lung epithelial cells (89) Lymphocytes (90)	Mycobacterial cell wall lysis (37, 62) Inhibition of mycobacterial infection (91) Iron homeostasis regulation (92, 93) Pro-inflammatory activity (94)
Lactoferrin	Epithelial cells (95) Neutrophils (96) Polymorphonuclear (PMN) leukocytes (97)	Bacterial cell permeation (98) Iron kidnapping (99) Anti-inflammatory activity (100)[a](101)[a](102)[a]
Azurocidin	PMN leukocytes (103) Neutrophils (104)	Mycobacterial cell wall lysis (104) Promotion of phagolysosomal fusion (104)
Elastases	Neutrophil azurophilic granules, bone marrow cells (105) Macrophages (106)	Bacterial cell membrane lysis (107) Serine protease activity (108) Cell chemotaxis induction (108) Immunomodulation (109)[a] NETs formation (110) Macrophage extracellular traps (METs) formation (106, 111)
Antimicrobial RNases	Eosinophils (RNase3/ECP) (79[b], 112, 113) Neutrophils and monocytes (RNase6) (114) Epithelial cells and leukocytes (RNase7) (115, 116)	Mycobacteria cell wall and membrane lysis (117) Mycobacterial cell agglutination (117)
Eosinophil peroxidase	Eosinophils (118)[b]	Bacterial cell wall lysis (119)
Cathepsins	Neutrophils Monocytes (120)[b]	Mediation of apoptosis pathway (120, 121) Immunomodulation (122)[a] (109)[a]
Granulysin	Lymphocytes (37)	Mycobacterial cell lysis (37, 123)
Calgranulin/calprotectin	Neutrophils (124, 125) Monocytes (124, 126[b]) Keratinocytes (124, 127) Leukocytes (128)	Phagolysosomal fusion (30, 126) Pro-inflammatory action (125)
Ubiquitinated peptides	Macrophages (37, 129[b])	Mycobacterial cell lysis (37)
Lipocalin2	Neutrophils (130)[b]	Mycobacterial growth inhibition (37, 130) Immunoregulation (37, 130)

[a]*Reported activities tested in vivo using murine infection models.*
[b]*Reported regulation of AMP expression upon mycobacterial infection.*

expression of peripheral blood mononuclear cells profile analysis from patients with tuberculosis and Mtb-infected healthy donors revealed the existence of an overexpression of defensins levels in TB patients (139). The peptides were observed to bind to Mtb cells within the macrophage phagosome (140). The essential participation of defensins in the host fight against TB infection has also been corroborated in a murine model (23, 85).

Within the defensin family, we find a variety of cellular source types (**Table 1**) (82). Noteworthy, the β-defensin2 (HBD2) and the α-defensin (HAD) expression are inducible by mycobacteria wall components in epithelial cells and eosinophils, respectively (79, 81), and could have a preservative role *in vivo* against TB infection. Upregulation of HDB3 and 4 were also reported effective in Mtb MDR-infected mice (83).

Human Neutrophil Peptides (HNPs)

Human neutrophil peptides are α-defensin type AMPs mainly secreted by neutrophils (50), although low levels of expression

have also been detected in monocytes, eosinophils, and epithelial cells (79). HNP-1–4 expression is induced by TB infection (7, 37, 82). On the other hand, although macrophages express only small amounts of HNPs, high intracellular levels can be reached *via* neutrophil-phagocytosis. Interestingly, HNPs have been observed to colocalize with tuberculosis bacilli in early endosomes (84). Moreover, the administration of HNPs maximizes the antimicrobial capacity of macrophages against Mtb (50) and HNP1 was proven effective in a Mtb-infected mouse model (50). HNP-1 can permeabilize the Mtb cell membrane by forming transmembrane pore and then bind to intracellular DNA (7, 50). Interaction with nucleic acids could subsequently inhibit the main cell functions, as transcription and translation (48). On the other hand, combination studies using HNPs and β-defensins with conventional antitubercular drugs have shown a synergistic effect. Therefore, the AMP adjuvant role can reduce the required drug dose and also significantly diminish the bacterial load in vital organs (141). Overall, these findings together with recent experimental work with tuberculosis animal models entrench the therapeutic application in favor of the whole defensin family (7, 37, 83).

Hepcidin

Hepcidin (Hepc) is a short and highly cationic antimicrobial peptide that was originally detected in serum and urine (142). It adopts a hairpin loop that encompasses two short beta-strands. Hepcidin is predominantly synthesized in hepatocytes and is released from a precursor by proteolysis. Its expression is induced by infectious or inflammatory processes and plays a prominent role in the iron homeostasis, regulating uptake, and mobilization (92, 143). Specifically, hepcidin can downregulate the transmembrane transport of iron through its union with ferroportin, a transmembrane protein that exports iron to the extracellular space (93). The reduction in extracellular iron concentrations makes pathogen invasion conditions more hostile (91). Interestingly, during infection, hepcidin is released into the bloodstream and is considered to be responsible of the anemia associated with inflammation (94). Indeed, anemia is a common difficulty encountered in TB (144). Moreover, Lafuse and coworkers demonstrated that mycobacterial infection induced the emergence of high levels of hepcidin in macrophages phagosomes and confirmed the peptide inhibition of Mtb growth *in vitro* (87). Further research also reported the presence of hepcidin in other innate cell types such as dendritic cells. The peptide expression in non-phagocyte cells suggests an extracellular mycobactericidal activity mediated by iron reduction in both alveolar and interstitial spaces (88). Particularly, due to the hepcidin effect on iron levels, differences in the expression of the peptide could be related to different phenotypes of iron homeostasis in TB patients. A significant correlation was observed between serum hepcidin levels and the promoter polymorphism in TB patients and was suggested to be considered in the diagnosis and prognosis of tuberculosis (145).

Lactoferrin

Lactoferrin is another AMP related to iron homeostasis regulation. It is a multifunctional iron binding glycoprotein present in several tissues and most human body fluids. It has a molecular weight of 80 kDa and belongs to the transferrin family (99). LF and its natural N-terminal fragment released by proteolytic cleavage (*Lactoferricin*, LFcin) participate in host defense and have wide spectra antimicrobial effects (37, 44, 98). Noteworthy, LF is the only AMP given by systemic administration that is currently in clinical trials (146). Diverse studies have demonstrated the presence of LF in macrophages and blood cells and its activity against *Mycobacterium*. Moreover, LF immunomodulatory capacity can also contribute to the eradication of TB. Particularly, it has been observed that mice treated with LF manifest an increase in the proportion of IL-12/IL-10, which results in increased Th1 cells, with a protective role against Mtb (100, 101). The anti-inflammatory properties of human and mouse LF were also corroborated in another Mtb mouse infected model (102). In addition, other studies clearly demonstrated the immunomodulatory role of LF, improving BCG-vaccine efficacy when used as adjuvant (147, 148). Recently, it has been reported that LF expressed in azurophilic granules of neutrophils is capable of killing *M. smegmatis* (104).

Lipocalins

Lipocalins are a family of peptides involved in cellular traffic and inflammation which are also related to the iron homeostasis (149). Lipocalin2, also called neutrophil gelatinase associated lipocalin, is expressed in neutrophils and displays anti-TB activity (130).

Azurocidin

Azurocidin, a leukocyte polymorphonuclear (PMN) granule protein, is a cationic antimicrobial protein of 37 kDa, also called CAP37 or heparin-binding protein, due to its high affinity for heparin (103). Shortly after its discovery it was found that azurocidin, like other antimicrobial proteins, not only displayed an antimicrobial activity but was also capable of exerting a mediating role in the modulation of the host defense system (150). Azurocidin is stored in secretory granules and is released into the endothelial area by PMN cells, rapidly reaching the infected or inflammation area (151). Azurocidin, at the front line of infection, activates monocytes, macrophages, and epithelial cells (152). Moreover, azurocidin has a wide range antimicrobial activity, working efficiently at acidic pH, a condition promoted in mature phagolysosomes (153). Interestingly, it has recently been reported that azurophilic granule proteins are implicated in mycobacterial killing, facilitating the fusion of mycobacteria-containing phagosomes with lysosomes (104).

Elastases

Elastases are serine proteases secreted by neutrophils and macrophages involved in the fight against pulmonary infections (107). One of the best studied elastase is the neutrophil elastase (NE), also known as elastase2, a 29-kDa protein expressed during myeloid development and secreted by neutrophils during episodes of infection and inflammation (107, 108). NE was reported to confer a protective effect against *M. bovis* in mice pulmonary tract (109). Many studies emphasize NE multi-functionality; the protein can break the tight junctions to facilitate the migration of PMN cells to the inflammation/infection area and induce cell chemotaxis (108). The neutrophil granule protein can work

within the macrophage phagosomes (154). Complementarily, NE is also reported to kill mycobacteria extracellularly in a rather peculiar way. Neutrophil granules can release their protein cargo together with chromatin, resulting in the formation of extracellular fibrillar structures that facilitate bacteria arrest. NE colocalizes with the neutrophil extracellular traps and can facilitate the degradation of virulence factors (110, 155). Interestingly, heavily infected macrophages can also explode and form extracellular traps, a process which is also regulated by elastases (106, 111).

Cathepsin (CTS)

Cathepsin is another serine protease involved in the host defense against TB infection that is mainly expressed in neutrophils and macrophages (130, 156). Procathepsins are converted to the mature enzyme in acidic conditions and are active within the lysosomal compartment (30). The Mtb bacilli can downregulate CTSs expression in macrophages to ensure its intracellular survival (120, 156). The antimicrobial protease is proposed to protect the host mostly by an immunoregulatory role rather than a direct bacteria killing activity, as observed in an infection mouse model (122). Recent work using the zebrafish/*M. marinum* model indicates the involvement of macrophage lysosomal CTSs to control the TB infection at the granuloma level (121, 157).

Granulysin (GNLY)

Granulysin is a small cationic human antimicrobial protein expressed by lymphocytes that is upregulated by HIV/TB coinfection (37, 158). GNLY can enter the macrophages and is able to disrupt the bacillus envelope (7).

Calgranulin

Calgranulin, also called calprotectin, is another AMP that is used as a TB infection marker in blood samples (30, 124, 127). Calgranulin is a calcium-binding protein that also interacts avidly with Zn^{2+} cations. Binding to Zn^{2+} activates the peptide antimicrobial activity. Recently, calgranulin overexpression has been associated to anti-TB activity at the macrophage intracellular level by promotion of the phagolysosomal fusion (30, 126).

Ubiquitin-Derived Peptides

Ubiquitin-derived peptides are ubiquitinated proteolytic peptides which can also be classified as AMPs (7, 37, 159). In particular, ubiquitin-conjugated peptides as products of the proteosome degradation activity accumulate in the lysosome and can inhibit Mtb growth within the autophagolysosome (129). Ubiquitin by itself is innocuous while ubiquitinated peptides, such as Ub2, can permeate the mycobacteria membrane (160).

Human Antimicrobial RNases

Human antimicrobial RNases are small secretory proteins (~15 kDa) belonging to the RNaseA superfamily. They are highly cationic and possess a wide range of biological properties, representing an excellent example of multitasking proteins (112, 161). The family comprises eight human members, expressed in diverse epithelial and blood cell types.

RNase3, also known as the eosinophil cationic protein (ECP), is mainly expressed during infection and inflammation in the secondary granules of eosinophils (162) and secondarily in neutrophils (163). Complementarily, the signal peptide of the ECP (ECPsp) was found to promote the migration of macrophages *via* pro-inflammatory molecules to sites of infection and inflammation (164). Interestingly, ECP is secreted, together with α-defensin, in response to *M. bovis* BCG infection (79). Although the recruitment of eosinophils in the respiratory tract during Mtb infection was first regarded as a mere response to inflammation (165), further work has shown that this cell type together with neutrophils can directly participate in the removal of the infection focus (166). Eosinophils are activated *via* TLR2 induction by the specific mycobacterial wall component, the lipomannan (79). Eosinophils, together with neutrophils, would then release the content of their granules into the granuloma macrophages (84, 159). To note, the *eosinophil peroxidase*, another eosinophil protein stored in the secondary granules, is also endowed with antimycobacterial activity (119). On the other hand, macrophages express upon bacterial infection two additional RNases, RNase6 and RNase7 (114). In addition, human RNase7, also called the skin derived RNase, is also secreted by keratinocytes and exerts a protective role against a variety of pathogens at the skin barrier (39, 115). Interestingly, RNase7, together with RNase3, can eradicate mycobacteria *in vitro* (117). Moreover, very recent results indicate that human RNases 3, 6, and 7 can also inhibit the growth of mycobacteria in a macrophage infection model (167). Considering that RNase6 and RNase 7 expression is induced in macrophages upon bacterial infection (114), one might hypothesize that these antimicrobial proteins can also play a physiological role against intracellular dwelling mycobacteria. Eventually, we cannot disregard a complementary contribution of the RNases reported immunomodulatory properties, such as the induction of pro-inflammatory cytokines and the dendritic cell chemoattraction (168, 169).

SYNTHETIC ANTIMICROBIAL PEPTIDES

In the race against TB, novel synthetic AMPs with potent mycobactericidal activities have been developed (2, 19, 22, 37, 170). AMP synthetic analogs are often considered to be the next generation of antibiotics and have attracted the attention of many companies aiming to develop new anti-TB therapies against drug-resistant strains (35). Following, we summarize the main SAMPs successfully designed (**Table 2**).

One of the favorite applied strategies for the design of potent AMPs is the engineering of stabilized amphipathic α-helix that are enriched with selected antimicrobial prone amino acids. Complementarily, peptide modifications are devised to endow them with enhanced resistance to proteolysis; thereby improving their *in vivo* stability and efficacy. The *D-LAK peptides* are a family of serial peptides consisting of 25 D-enantiomer amino acid residues in a primary sequence designed to adopt a left-handed α-helix conformation and containing eight lysine residues (175). The peptides were designed to enhance their antimicrobial activity and decrease their hemolytic effect (188), providing efficient antimycobacterial activity at non-toxic concentrations. Furthermore, D-LAK peptides can be administered as inhalable dry powder (176). Another synthetic α-helical peptide, the

TABLE 2 | Synthetic peptides effective against mycobacteria.

Peptide	Modifications	Source	Mechanism/antimicrobial activity	Reference
1-C13$_{4mer}$	Tetrameric form; oligo-N-substituted glycines (peptoid) and alkylation	Design *de novo*	Pore formation MIC (Mtb H37Rv): 6.6 μM	(171)
A18G5, A24C1ac, A29C5FA, and A38A1guan	D-enantiomer, alkylation, tetramethylguanidinilation, and polyethylene glycol conjugation	Derived from the insect proline-rich peptide Apidaecin	Bacterial membrane permeation/inhibition of protein synthesis	Hoffmann R, Czihal P Patent WO2009013262 A1. 2009 (172)
CAMP/PL-D	–	Short cationic peptides (10 AA) rich in W and R selected from peptide libraries	Pore formation MIC (Mtb H37Rv): 1.1–141 μM	(173)
CP26	–	Derived from cecropin A: mellitin	Bacterial cell wall disruption MIC (Mtb H37Rv): 2 μg/mL	(174)
D-LAK 120	D-enantiomer	Synthetic α-helical peptides	Pore-formation/Inhibition of protein synthesis MIC (Mtb H37Rv): 35.2–200 μg/mL	(175, 176)
D-LL37	D-enantiomer	Derived from LL-37	Pore-formation/Immunomodulatory activity MIC (H37Rv): 100 μg/mL	(170)
E2 and E6	–	Derived from bactenecin (bovine cathelicidin) Bac8c (8 AA)	Bacterial cell wall disruption MIC (Mtb H37Rv): 2–3 μg/mL	(174, 177)
HHC-10	–	Derived from bactenecin	Bacteria membrane lysis MIC (*M. bovis* BCG): 100 μg/mL	(178[a], 179)
hLFcin1-11/ hLFcin17-30	D-enantiomer	Derived from lactoferricin (All-R and All-K substitutions)	Bacterial cell wall and membrane lysis IC90 (*M. avium*): 15–30 μM	(44)
Innate defense regulators [innate defense regulator (IDR)-1002, -HH2, IDR-1018]	–	Derived from macrophage chemotactic protein-1 (MCP-1)	Immunomodulatory activity/anti-inflammatory MIC (Mtb H37Rv): 15–30 μg/mL; *in vivo* [Mtb H37Rv and multidrug resistant TB strain (MDR-TB) infected mice]: 10–71% killing at 32 μg/mouse (3 × week intra-tracheal administration, 30 days)	(180)[a](181)[a](182)
LLAP		Derived from LL-37	Inhibition of ATPase MIC (*M. smegmatis* mc^{2}155): 600 μg/mL	(183)
LLKKK18	Hyaluronic acid nanogel conjugation	Derived from LL-37	Pore formation/Immunomodulatory activity *In vivo* (Mtb H37Rv-infected mice): 1.2-log reduction at 100 μM (10 intra-tracheal administrations)	(184)[a]
MU1140		Derived from *Streptococcus mutans* lantibiotics	Inhibition of cell wall synthesis/On preclinical stage. Effective on active and dormant Mtb MDR	Oragenics Inc Patent WO2013130349A (185)[a]
MIAP	–	Derived from Magainin-I	Inhibition of ATPase MIC (H37Ra): 300 μg/mL	(46)
Pin2 variants		Derived from pandinin2 (short helical peptides)	Membrane disruption Mtb H37Rv and Mtb MDR: 6–14 μg/mL	(186)
RN3(1-45) RN6(1-45) RN7(1-45)	–	Derived from human RNases N-terminus	Bacterial cell wall disruption/cell agglutination and intracellular macrophage killing MIC (*M. vacae; M. aurum; M. smegmatis* mc^{2}155*; M bovis* BCG) *in vitro*: 10–20 μM and *ex vivo* (*M. aurum*): 5–10 μM	(117, 167)
Synthetic AMPs (SAMPs-Dma)	Dimethylamination and imidazolation	Design *de novo*	Cell penetration and DNA binding/ synthetic antimicrobial peptide-Dma10: MIC *(M. smegmatis* mc^{2}155): <20 μM	(51)
X(LLKK) 2X: II-D, II-Orn, IIDab, and IIDap	Peptide D-enantiomer, ornithination, 2,4-diaminobutyric acidation, and 2,3-diaminopropionic acidation	Short stabilized α-helix amphipatic peptides	Pore formation M(LLKK)2M: MIC (Mtb H37Rv): 125 μg/mL; I(LLKK)2I: effective against MDR-TB	(22, 187)

[a]*Reported activities tested in vivo using murine infection models.*

M(LLKK)2M, was proven successful against MDR strains when combined with RIF (187). On the other hand, a short synthetic cathelicidin variant (the *HHC-10*) is able to inhibit the growth of *M. bovis* BCG both *in vitro* and in a mouse model (178).

Interestingly, the N-terminus derived peptides of human antimicrobial RNases can reproduce the parental protein activity against several tested *Mycobacterium* species (117, 167). The *RN(1-45)* peptides encompass a highly cationic and amphipathic region that adopts an extended α-helix in a membrane-like environment (189). In addition, the RN3(1-45) and RN6(1-45) peptides include an aggregation prone sequence which promotes bacterial cell agglutination (117, 167, 190), a property that can facilitate the microbial clearance at the infectious focus (190).

Recently, particular interest has been drawn by a collection of short synthetic peptides with immunomodulatory activities, the *innate defense regulators* (IDRs). The peptides are effective at very low concentration and thereby can elude any toxicity to the host (181). They do not display a direct bactericidal activity but can promote the proper endogenous expression of antimicrobial agents by the host cells. Among others, the peptides enhance the release of chemokines and downregulate the inflammation pathway (181, 182). The IDR peptides, such as the IDR-1018 (**Table 2**), have been tested successfully in a MDR-TB infected mouse model by intra-tracheal administration (180). Likely, immunoregulatory peptides will take a leading role in the treatment of immunocompromised patients in a near future (16).

AMPs TO COMBAT ANTIMICROBIAL RESISTANCE IN TB: A TIME FOR HOPE

In recent years, thousands of antimicrobial peptides have been identified from natural sources, mostly classified as key players of the non-specific host defense response (30, 33, 191). On the other hand, despite the existence of a wide range of successful antibiotics since their entry into the worldwide trade, nowadays there is an increasing demand of novel drugs to tackle multidrug-resistance mycobacteria strains (2, 20, 192). The antimicrobial proteins and peptides (AMPPs), given their direct bacilli killing mechanism and immunomodulatory properties provide an attractive pharmacological potential against mycobacterial infections (see **Table 3** for a summary of main AMP-based therapies). However, despite their appealing properties, AMPs are still facing major challenges to join the pharmaceutical industry (30–32). The main advantages and disadvantages associated with AMPs are listed in **Table 4**. Although the high cost of synthesis is one of the main drawbacks that the manufacturing of peptides faces, some companies are already managing commercial-scale peptide production platforms. For example, recombinant AMPs can be prepared in fungi and plants at high yield and low cost (2). Another drawback of AMPs therapy is their susceptibility to proteolytic cleavage, in particular when delivered by systemic administration (2, 31). In addition, the antimicrobial activity of some peptides appears to be decimated in physiological saline and serum conditions (32, 193). Novel design strategies are focusing on the production of cheaper and reduced-size analogs (2, 194) with improved selectivity toward prokaryotic targets and broaden therapeutic indexes (195). To improve the peptide bioavailability and stability *in vivo* several strategies have been developed such as incorporation of non-natural amino acids, backbone mimetics, conjugation with fatty acids, N and C- terminus modifications (196). The peptide performance can also be improved by intra-tracheal administration (184). In addition, encapsulation within biodegradable particles or liposomes improves the distribution of the drug toward the site of action (31, 196). Fortunately, macrophage nature by itself should promote the engulfment of such nanovehicles (19) and extensive research has been applied to define the parameters that determine the nanoparticles uptake by the phagocytic cells and intracellular traffic (2, 197). Very recently, a novel delivery system has been achieved by a LL-37 analog embedded within a hyaluronic nanogel. The self-assembled polymer stabilizes the peptide inside its hydrophobic core, allows a higher dose cargo and promotes the macrophage uptake, with increased

TABLE 3 | AMPs based strategies to develop novel anti-TB drugs.

Pro-autophagy AMPs[a]	Cathelicidins (56, 58, 78); azurocidin (104); calgranulin (126)
Anti-inflammatory AMPs	Defensins (23, 82); AMP binders to antigenic molecules (23); LL-37 inhibition of TNF-α and other pro-inflammatory cytokines (57); synthetic innate defense regulator (IDR) peptides (181); synthetic LLKKK18 (LL-37 analog) (184); lactoferrin (100)
Pro-inflammatory AMPs	LL-37 (57, 74); defensins (82); hepcidin (94)
Chemotaxis induction by AMPs	Defensins (23); IDR synthetic peptides (23); LL-37 (2, 58, 181); elastases (108)
AMP synergy	*with current antibiotics*: HNP1 + isoniazid/rifamicin (141); HBD1 + isoniazid (217); synthetic α-helix AMP + rifampicin (18)
	with immunomodulators: HNP1 and HBD2 + L-isoleucine (206)
	with nanoparticles (19)
Induction of host AMP expression	Search for novel LL-37 inducers (218); vit D3 and phenylbutirate (PBA) for LL-37 (16, 28, 77, 204); L-isoleucine for β-defensins (83); aroylated phenylenediamine inducers (205)
AMP-based gene therapy	Adenovirus encoding LL-37 or HBD3 (219)
AMP nanodelivery	Nanovehiculation systems: nanoparticle size, surface chemistry, and mechanical properties to enhance macrophage uptake (2); liposomes (2, 196); nanogels (184, 196); aerosolization (176, 196)

[a]*Representative examples are provided for each indicated strategy.*

TABLE 4 | Human anti-TB AMP therapy: advantages and disadvantages.

Application strategy	Advantages	Disadvantages
Exogenous AMP administration	Broad-spectrum activity Multi-functionality Low immunogenicity Rapid direct killing mechanism High affinity toward mycobacterial surface Enhanced uptake by macrophages Very low/none toxicity of natural human AMP Rapid clearance in host tissues Beneficial effects to the host (anti-inflammatory, pro-autophagy, anti-tumoral, etc.) Low rate of bacterial resistance emergence High stability and efficacy of modified peptide derivatives Reduced manufacturing cost by new recombinant methodologies Gene therapy can restore endogenous AMPs levels in immunocompromised patients Synergy with current antibiotics Potential use as antibiotic adjuvants	Rapid degradation following oral/systemic administration Low stability in human biological fluids Potential undesirable side-effects at high concentration (tumorigenesis, angiogenesis, etc) Potential toxicity *via* oral/systemic administration High cost of chemical synthesis
Endogenous AMP induction	Efficient at very low concentrations Reinforcement of the immune response in immunocompromised patients Prevention of latent mycobacterial reactivation	No current information on the long-term effects of endogenous AMP induction. Potential induction of AMP resistance

antimicrobial efficiency and reduced toxicity to host cells. Besides, AMPs are also prone to aggregate and show occasionally poor solubility (198, 199). Luckily, there are currently different strategies and predictive software available to prevent aggregation and improve physicochemical properties (42, 200, 201). Complementarily, cleavage protection can be enhanced through secondary structure stabilization (37, 202). Alternatively, AMPs, as effector players of the host immune system (203) can also be upregulated by immunostimulation therapies (23, 204–206), overcoming the drawbacks inherent to the peptide administration *via*. Furthermore, recent studies on mycobacterial infection reveal how some species such as Mtb are capable of inhibiting the expression and release of endogenous AMPs (30, 77). Thus, the administration of supplementary AMPs, the use of gene therapy (136) or an immunomodulatory hormonal induction would be necessary to achieve an effective dose (207). This approach would be mostly recommended for immunocompromised patients (60, 204, 205). However, researchers should not disregard the unpredictable long-term consequences of exposing the bacteria to an overdose of AMPs. Mycobacteria pathogens exposed to either externally administered or endogenous overexpressed AMPs might develop novel resistance strategies to face back this new affront (2, 146, 208). In fact, the co-evolution of the pathogens with natural AMPs has already induced some bacterial resistance mechanisms (209–212). First, bacteria can alter their cell envelope composition to reduce their affinity toward cationic peptides (82, 209, 212, 213). Pathogenic mycobacteria can also ensure their intracellular survival by the control of the macrophage efflux pump (210, 211). Other observed strategies are the release of extracellular proteases (212, 214, 215) or the downregulation of host AMPs (74). Therefore, resistance to AMPs should be anticipated and might be overcome by innovative peptide variants (216), host-directed therapies or the use of combined synergies (47, 215). Eventually, recent collaborative initiatives have been launched to join efforts in the fight against mycobacterial resistance (TBNET, FightTB, TB-Platform, and TB-PACTS) (2), opening a window of hope.

CONCLUDING REMARKS

Peptide-based therapy to treat infectious diseases is recently experiencing resurgence. AMPs, as mere components of the immune system, promote the direct killing of mycobacteria and often have immunomodulatory effects. Their non-specific pleiotropic mechanisms of action and unique immunomodulatory properties over conventional antibiotics have awakened the pharmaceutical market interest. Moreover, the efficacy of BCG vaccine is highly variable and the alarming increase of extensively drug-resistant strains of Mtb is a major global health emergency to address. In this context and considering the limitations in the current antituberculosis drug treatment, AMPs represent an immediate alternative approach in tackling antimicrobial resistance. Scientific evidences provide a solid basis to ensure that the future development of peptide-based therapy will continue to address the unsolved drawbacks that the pharmaceutical industry is currently facing. Novel research methodologies and integrated interdisciplinary strategies should provide the opportunity to boast current antimicrobial peptide research efforts in the fight against tuberculosis.

AUTHOR CONTRIBUTIONS

JA-T, LL, DP, SB, and EB contributed to the original draft and edited versions. JA-T and LL prepared the graphical material and JA-T, DP, LL, and EB prepared the tables. SB and EB wrote, edited, and revised the final manuscript version. All authors approved the final manuscript version.

FUNDING

Research work was supported by the Ministerio de Economía y Competitividad (SAF2015-66007P) co-financed by FEDER funds. LL is a recipient of a CSC predoctoral fellowship. JA-T was a recipient of a predoctoral fellowship (PIF, UAB). SB is a Cipla distinguished Fellow in Pharmaceutical Sciences.

REFERENCES

1. WHO. Global tuberculosis report 2016. *World Heal Organ Glob Tuberc Rep.* Geneva (2016).
2. Silva JP, Appelberg R, Gama FM. Antimicrobial peptides as novel anti-tuberculosis therapeutics. *Biotechnol Adv* (2016) 34:924–40. doi:10.1016/j.biotechadv.2016.05.007
3. Rodriguez Plaza JG. Prospective tuberculosis treatment: peptides, immunity and autophagy. *J Mol Genet Med* (2014) 8:128. doi:10.4172/1747-0862.1000128
4. Eldholm V, Balloux F. Antimicrobial resistance in *Mycobacterium tuberculosis*: the odd one out. *Trends Microbiol* (2016) 24:637–48. doi:10.1016/j.tim.2016.03.007
5. Zager EM, McNerney R. Multidrug-resistant tuberculosis. *BMC Infect Dis* (2008) 8:10. doi:10.1186/1471-2334-8-10
6. Dye C. Doomsday postponed? Preventing and reversing epidemics of drug-resistant tuberculosis. *Nat Rev Microbiol* (2009) 7:81–7. doi:10.1038/nrmicro2048
7. Khusro A, Aarti C, Agastian P. Anti-tubercular peptides: a quest of future therapeutic weapon to combat tuberculosis. *Asian Pac J Trop Med* (2016) 9:1023–34. doi:10.1016/j.apjtm.2016.09.005
8. Gupta A, Kaul A, Tsolaki AG, Kishore U, Bhakta S. *Mycobacterium tuberculosis*: immune evasion, latency and reactivation. *Immunobiology* (2012) 217:363–74. doi:10.1016/j.imbio.2011.07.008
9. Keane J, Gershon S, Wise RP, Mirabile-Levens E, Kasznica J, Schwieterman WD, et al. Tuberculosis associated with infliximab, a tumor necrosis factor alpha-neutralizing agent. *N Engl J Med* (2001) 345:1098–104. doi:10.1056/NEJMoa011110
10. Yasui K. Immunity against *Mycobacterium tuberculosis* and the risk of biologic anti-TNF-α reagents. *Pediatr Rheumatol Online J* (2014) 12:45. doi:10.1186/1546-0096-12-45
11. Montoya-Rosales A, Castro-Garcia P, Torres-Juarez F, Enciso-Moreno JA, Rivas-Santiago B. Glucose levels affect LL-37 expression in monocyte-derived macrophages altering the *Mycobacterium tuberculosis* intracellular growth control. *Microb Pathog* (2016) 97:148–53. doi:10.1016/j.micpath.2016.06.002
12. Maitra A, Kamil TK, Shaik M, Danquah CA, Chrzastek A, Bhakta S. Early diagnosis and effective treatment regimens are the keys to tackle antimicrobial resistance in tuberculosis (TB): a report from Euroscicon's international TB Summit 2016. *Virulence* (2016) 8(6):1005–24. doi:10.1080/21505594.2016.1256536
13. Catanzaro A, Rodwell TC, Catanzaro DG, Garfein RS, Jackson RL, Seifert M, et al. Performance comparison of three rapid tests for the diagnosis of drug-resistant tuberculosis. *PLoS One* (2015) 10:1–14. doi:10.1371/journal.pone.0136861
14. Danquah CA, Maitra A, Gibbons S, Faull J, Bhakta S. HT-SPOTi: a rapid drug susceptibility test (DST) to evaluate antibiotic resistance profiles and novel chemicals for anti-infective drug discovery. *Curr Protoc Microbiol* (2016) 40:1–12. doi:10.1002/9780471729259.mc1708s40
15. Dheda K, Barry CE, Maartens G. Tuberculosis. *Lancet* (2016) 387(10024):1211–26. doi:10.1016/S0140-6736(15)00151-8
16. Hancock REW, Haney EF, Gill EE. The immunology of host defence peptides: beyond antimicrobial activity. *Nat Rev Immunol* (2016) 16:321–34. doi:10.1038/nri.2016.29
17. Bastos P, Trindade F, da Costa J, Ferreira R, Vitorino R. Human antimicrobial peptides in bodily fluids: current knowledge and therapeutic perspectives in the postantibiotic era. *Med Res Rev* (2017). doi:10.1002/med.21435
18. Khara JS, Lim FK, Wang Y, Ke X-Y, Voo ZX, Yang YY, et al. Designing α-helical peptides with enhanced synergism and selectivity against *Mycobacterium smegmatis*: discerning the role of hydrophobicity and helicity. *Acta Biomater* (2015) 28:99–108. doi:10.1016/j.actbio.2015.09.015
19. Mohanty S, Jena P, Mehta R, Pati R, Banerjee B, Patil S, et al. Cationic antimicrobial peptides and biogenic silver nanoparticles kill mycobacteria without eliciting DNA damage and cytotoxicity in mouse macrophages. *Antimicrob Agents Chemother* (2013) 57:3688–98. doi:10.1128/AAC.02475-12
20. Zumla A, George A, Sharma V, Herbert RHN, Oxley A, Oliver M. The WHO 2014 global tuberculosis report – further to go. *Lancet Glob Heal* (2015) 3:e10–2. doi:10.1016/S2214-109X(14)70361-4
21. Olmo ED, Molina-Salinas GM, Bini EI, González-Hernández S, Bustos LA, Escarcena R, et al. Efficacious in vitro and in vivo effects of dihydrosphingosine-ethambutol analogues against susceptible and multi-drug-resistant *Mycobacterium tuberculosis*. *Arch Med Res* (2016) 47:262–70. doi:10.1016/j.arcmed.2016.07.004
22. Khara JS, Priestman M, Uhía I, Hamilton MS, Krishnan N, Wang Y, et al. Unnatural amino acid analogues of membrane-active helical peptides with anti-mycobacterial activity and improved stability. *J Antimicrob Chemother* (2016) 71:2181–91. doi:10.1093/jac/dkw107
23. Rivas-Santiago CE, Hernández-Pando R, Rivas-Santiago B. Immunotherapy for pulmonary TB: antimicrobial peptides and their inducers. *Immunotherapy* (2013) 5:1117–26. doi:10.2217/imt.13.111
24. Mcgrath M, Gey van Pittius NC, Van Helden PD, Warren RM, Warner DF. Mutation rate and the emergence of drug resistance in *Mycobacterium tuberculosis*. *J Antimicrob Chemother* (2014) 69:292–302. doi:10.1093/jac/dkt364
25. Gröschel MI, Sayes F, Simeone R, Majlessi L, Brosch R. ESX secretion systems: mycobacterial evolution to counter host immunity. *Nat Rev Microbiol* (2016) 14:677–91. doi:10.1038/nrmicro.2016.131
26. Volpe E, Cappelli G, Grassi M, Martino A, Serafino A, Colizzi V, et al. Gene expression profiling of human macrophages at late time of infection with *Mycobacterium tuberculosis*. *Immunology* (2006) 118:449–60. doi:10.1111/j.1365-2567.2006.02378.x
27. Portugal B, Motta FN, Correa AF, Nolasco DO, de Almeida H, Magalhães KG, et al. *Mycobacterium tuberculosis* prolyl oligopeptidase induces in vitro secretion of proinflammatory cytokines by peritoneal macrophages. *Front Microbiol* (2017) 08:155. doi:10.3389/fmicb.2017.00155
28. Wallis RS, Hafner R. Advancing host-directed therapy for tuberculosis. *Nat Rev Immunol* (2015) 15:255–63. doi:10.1038/nri3813
29. Ojha AK, Baughn AD, Sambandan D, Hsu T, Trivelli X, Guerardel Y, et al. Growth of *Mycobacterium tuberculosis* biofilms containing free mycolic acids and harbouring drug-tolerant bacteria. *Mol Microbiol* (2008) 69:164–74. doi:10.1111/j.1365-2958.2008.06274.x
30. Padhi A, Sengupta M, Sengupta S, Roehm KH, Sonawane A. Antimicrobial peptides and proteins in mycobacterial therapy: current status and future prospects. *Tuberculosis (Edinb)* (2014) 94:363–73. doi:10.1016/j.tube.2014.03.011
31. Mahlapuu M, Håkansson J, Ringstad L, Björn C. Antimicrobial peptides: an emerging category of therapeutic agents. *Front Cell Infect Microbiol* (2016) 6:194. doi:10.3389/fcimb.2016.00194
32. Kosikowska P, Lesner A. Antimicrobial peptides (AMPs) as drug candidates: a patent review (2003–2015). *Expert Opin Ther Pat* (2016) 26:689–702. doi:10.1080/13543776.2016.1176149
33. Diamond G, Beckloff N, Weinberg A, Kisich KO. The roles of antimicrobial peptides in innate host defense. *Curr Pharm Des* (2009) 15:2377–92. doi:10.2174/138161209788682325
34. Mishra AK, Driessen NN, Appelmelk BJ, Besra GS. Lipoarabinomannan and related glycoconjugates: structure, biogenesis and role in *Mycobacterium tuberculosis* physiology and host-pathogen interaction. *FEMS Microbiol Rev* (2011) 35:1126–57. doi:10.1111/j.1574-6976.2011.00276.x
35. Abedinzadeh M, Gaeini M, Sardari S. Natural antimicrobial peptides against *Mycobacterium tuberculosis*. *J Antimicrob Chemother* (2015) 70:1285–9. doi:10.1093/jac/dku570
36. Bansal-Mutalik R, Nikaido H. Mycobacterial outer membrane is a lipid bilayer and the inner membrane is unusually rich in diacyl phosphatidylinositol dimannosides. *Proc Natl Acad Sci U S A* (2014) 111:4958–63. doi:10.1073/pnas.1403078111
37. Gutsmann T. Interaction between antimicrobial peptides and mycobacteria. *Biochim Biophys Acta* (2016) 1858:1034–43. doi:10.1016/j.bbamem.2016.01.031
38. Bhamidi S, Shi L, Chatterjee D, Belisle JT, Crick DC, McNeil MR. A bioanalytical method to determine the cell wall composition of *Mycobacterium tuberculosis* grown in vivo. *Anal Biochem* (2012) 421:240–9. doi:10.1016/j.ab.2011.10.046
39. Niyonsaba F, Kiatsurayanon C, Chieosilapatham P, Ogawa H. Friends or foes? Host defense (antimicrobial) peptides and proteins in human skin diseases. *Exp Dermatol* (2017) 26(11):989–98. doi:10.1111/exd.13314
40. Banerjee DI, Gohil TP. Interaction of antimicrobial peptide with mycolyl transferase in *Mycobacterium tuberculosis*. *Int J Mycobacteriol* (2016) 5:83–8. doi:10.1016/j.ijmyco.2015.07.002
41. Wimley WC. Describing the mechanism of antimicrobial peptide action with the interfacial activity model. *ACS Chem Biol* (2010) 5:905–17. doi:10.1021/cb1001558

42. Torrent M, Andreu D, Nogués VM, Boix E. Connecting peptide physicochemical and antimicrobial properties by a rational prediction model. *PLoS One* (2011) 6:e16968. doi:10.1371/journal.pone.0016968
43. Méndez-Samperio P. The human cathelicidin hCAP18/LL-37: a multifunctional peptide involved in mycobacterial infections. *Peptides* (2010) 31:1791–8. doi:10.1016/j.peptides.2010.06.016
44. Silva T, Magalhães B, Maia S, Gomes P, Nazmi K, Bolscher JGM, et al. Killing of *Mycobacterium avium* by lactoferricin peptides: improved activity of arginine- and d-amino-acid-containing molecules. *Antimicrob Agents Chemother* (2014) 58:3461–7. doi:10.1128/AAC.02728-13
45. Rao M, Streur TL, Aldwell FE, Cook GM. Intracellular pH regulation by *Mycobacterium smegmatis* and *Mycobacterium bovis* BCG. *Microbiology* (2001) 147:1017–24. doi:10.1099/00221287-147-4-1017
46. Santos P, Gordillo A, Osses L, Salazar LM, Soto CY. Effect of antimicrobial peptides on ATPase activity and proton pumping in plasma membrane vesicles obtained from mycobacteria. *Peptides* (2012) 36:121–8. doi:10.1016/j.peptides.2012.04.018
47. Wright GD. Antibiotic adjuvants: rescuing antibiotics from resistance. *Trends Microbiol* (2016) 24:862–71. doi:10.1016/j.tim.2016.06.009
48. Le C-F, Fang C-M, Sekaran SD. Beyond membrane-lytic: intracellular targeting mechanisms by antimicrobial peptides. *Antimicrob Agents Chemother* (2017) 61:e02340–16. doi:10.1128/AAC.02340-16
49. Sharma S, Verma I, Khuller GK. Antibacterial activity of human neutrophil peptide-1 against *Mycobacterium tuberculosis* H37Rv: in vitro and ex vivo study. *Eur Respir J* (2000) 16:112–7. doi:10.1034/j.1399-3003.2000.16a20.x
50. Sharma S, Verma I, Khuller GK. Therapeutic potential of human neutrophil peptide 1 against experimental tuberculosis. *Antimicrob Agents Chemother* (2001) 45:639–40. doi:10.1128/AAC.45.2.639-640.2001
51. Sharma A, Pohane AA, Bansal S, Bajaj A, Jain V, Srivastava A. Cell penetrating synthetic antimicrobial peptides (SAMPs) exhibiting potent and selective killing of *Mycobacterium* by targeting its DNA. *Chemistry* (2015) 21:3540–5. doi:10.1002/chem.201404650
52. Goldberg MF, Saini NK, Porcelli SA. Evasion of innate and adaptive immunity by *Mycobacterium tuberculosis*. *Microbiol Spectr* (2014) 2:1–24. doi:10.1128/microbiolspec.MGM2-0005-2013
53. Soldati T, Neyrolles O. Mycobacteria and the intraphagosomal environment: take it with a pinch of salt(s)! *Traffic* (2012) 13:1042–52. doi:10.1111/j.1600-0854.2012.01358.x
54. Vergne I, Fratti RA, Hill PJ, Chua J, Belisle J, Deretic V. *Mycobacterium tuberculosis* phagosome maturation arrest: mycobacterial phosphatidylinositol analog phosphatidylinositol mannoside stimulates early endosomal fusion. *Mol Biol Cell* (2004) 15:751–60. doi:10.1091/mbc.E03-05-0307
55. Cemma M, Brumell JH. Interactions of pathogenic bacteria with autophagy systems. *Curr Biol* (2012) 22:R540–5. doi:10.1016/j.cub.2012.06.001
56. Muciño G, Castro-Obregón S, Hernandez-Pando R, Del Rio G. Autophagy as a target for therapeutic uses of multifunctional peptides. *IUBMB Life* (2016) 68:259–67. doi:10.1002/iub.1483
57. Torres-Juarez F, Cardenas-Vargas A, Montoya-Rosales A, González-Curiel I, Garcia-Hernandez MH, Enciso-Moreno JA, et al. LL-37 immunomodulatory activity during *Mycobacterium tuberculosis* infection in macrophages. *Infect Immun* (2015) 83:4495–503. doi:10.1128/IAI.00936-15
58. Yu X, Li C, Hong W, Pan W, Xie J. Autophagy during *Mycobacterium tuberculosis* infection and implications for future tuberculosis medications. *Cell Signal* (2013) 25:1272–8. doi:10.1016/j.cellsig.2013.02.011
59. Stanley SA, Barczak AK, Silvis MR, Luo SS, Sogi K, Vokes M, et al. Identification of host-targeted small molecules that restrict intracellular *Mycobacterium tuberculosis* growth. *PLoS Pathog* (2014) 10:e1003946. doi:10.1371/journal.ppat.1003946
60. Castañeda-Delgado JE, Frausto-Lujan I, González-Curiel I, Montoya-Rosales A, Serrano CJ, Torres-Juarez F, et al. Differences in cytokine production during aging and its relationship with antimicrobial peptides production. *Immunol Investig* (2017) 46:48–58. doi:10.1080/08820139.2016.1212873
61. Kim B-H, Shenoy AR, Kumar P, Das R, Tiwari S, MacMicking JD. A family of IFN-γ-inducible 65-kD GTPases protects against bacterial infection. *Science* (2011) 332:717–21. doi:10.1126/science.1201711
62. Shin D-M, Jo E-K. Antimicrobial peptides in innate immunity against mycobacteria. *Immune Netw* (2011) 11:245. doi:10.4110/in.2011.11.5.245
63. Wang G, Li X, Wang Z. APD3: the antimicrobial peptide database as a tool for research and education. *Nucleic Acids Res* (2016) 44:D1087–93. doi:10.1093/nar/gkv1278
64. Zhao X, Wu H, Lu H, Li G, Huang Q. LAMP: a database linking antimicrobial peptides. *PLoS One* (2013) 8:6–11. doi:10.1371/journal.pone.0066557
65. Aguilera-Mendoza L, Marrero-Ponce Y, Tellez-Ibarra R, Llorente-Quesada MT, Salgado J, Barigye SJ, et al. Overlap and diversity in antimicrobial peptide databases: compiling a non-redundant set of sequences. *Bioinformatics* (2015) 31:2553–9. doi:10.1093/bioinformatics/btv180
66. De Y, Chen Q, Schmidt AP, Anderson GM, Wang JM, Wooters J, et al. LL-37, the neutrophil granule- and epithelial cell-derived cathelicidin, utilizes formyl peptide receptor-like 1 (FPRL1) as a receptor to chemoattract human peripheral blood neutrophils, monocytes, and T cells. *J Exp Med* (2000) 192:1069–74. doi:10.1084/jem.192.7.1069
67. Rivas-Santiago B, Hernandez-Pando R, Carranza C, Juarez E, Contreras JL, Aguilar-Leon D, et al. Expression of cathelicidin LL-37 during *Mycobacterium tuberculosis* infection in human alveolar macrophages, monocytes, neutrophils, and epithelial cells. *Infect Immun* (2008) 76:935–41. doi:10.1128/IAI.01218-07
68. Di Nardo A, Vitiello A, Gallo RL. Cutting edge: mast cell antimicrobial activity is mediated by expression of cathelicidin antimicrobial peptide. *J Immunol* (2003) 170:2274–8. doi:10.4049/jimmunol.170.5.2274
69. Sonawane A, Santos JC, Mishra BB, Jena P, Progida C, Sorensen OE, et al. Cathelicidin is involved in the intracellular killing of mycobacteria in macrophages. *Cell Microbiol* (2011) 13:1601–17. doi:10.1111/j.1462-5822.2011.01644.x
70. Sigurdardottir SL, Thorleifsdottir RH, Guzman AM, Gudmundsson GH, Valdimarsson H, Johnston A. The anti-microbial peptide LL-37 modulates immune responses in the palatine tonsils where it is exclusively expressed by neutrophils and a subset of dendritic cells. *Clin Immunol* (2012) 142:139–49. doi:10.1016/j.clim.2011.09.013
71. Büchau AS, Morizane S, Trowbridge J, Schauber J, Kotol P, Bui JD, et al. The host defense peptide cathelicidin is required for NK cell-mediated suppression of tumor growth. *J Immunol* (2009) 184:369–78. doi:10.4049/jimmunol.0902110
72. Zanetti M. The role of cathelicidins in the innate host defenses of mammals. *Curr Issues Mol Biol* (2005) 7:179–96.
73. Kai-Larsen Y, Agerberth B. The role of the multifunctional peptide LL-37 in host defense. *Front Biosci* (2008) 13:3760–7. doi:10.2741/2964
74. Gupta S, Winglee K, Gallo R, Bishai WR. Bacterial subversion of cAMP signalling inhibits cathelicidin expression, which is required for innate resistance to *Mycobacterium tuberculosis*. *J Pathol* (2017) 242:52–61. doi:10.1002/path.4878
75. Campbell GR, Spector SA. Autophagy induction by vitamin D inhibits both *Mycobacterium tuberculosis* and human immunodeficiency virus type 1. *Autophagy* (2012) 8:1523–5. doi:10.4161/auto.21154
76. Yuk J-M, Shin D-M, Lee H-M, Yang C-S, Jin HS, Kim K-K, et al. Vitamin D3 induces autophagy in human monocytes/macrophages via cathelicidin. *Cell Host Microbe* (2009) 6:231–43. doi:10.1016/j.chom.2009.08.004
77. Rekha RS, Rao Muvva SSVJ, Wan M, Raqib R, Bergman P, Brighenti S, et al. Phenylbutyrate induces LL-37-dependent autophagy and intracellular killing of *Mycobacterium tuberculosis* in human macrophages. *Autophagy* (2015) 11:1688–99. doi:10.1080/15548627.2015.1075110
78. Bradfute SB, Castillo EF, Arko-Mensah J, Chauhan S, Jiang S, Mandell M, et al. Autophagy as an immune effector against tuberculosis. *Curr Opin Microbiol* (2013) 16:355–65. doi:10.1016/j.mib.2013.05.003
79. Driss V, Legrand F, Hermann E, Loiseau S, Guerardel Y, Kremer L, et al. TLR2-dependent eosinophil interactions with mycobacteria: role of α-defensins. *Blood* (2009) 113:3235–44. doi:10.1182/blood-2008-07-166595
80. Duits LA, Ravensbergen B, Rademaker M, Hiemstra PS, Nibbering PH. Expression of beta-defensin 1 and 2 mRNA by human monocytes, macrophages and dendritic cells. *Immunology* (2002) 106:517–25. doi:10.1046/j.1365-2567.2002.01430.x
81. Rivas-Santiago B, Schwander SK, Sarabia C, Diamond G, Klein-Patel ME, Hernandez-Pando R, et al. Human {beta}-defensin 2 is expressed and associated with *Mycobacterium tuberculosis* during infection of human alveolar epithelial cells. *Infect Immun* (2005) 73:4505–11. doi:10.1128/IAI.73.8.4505-4511.2005
82. Dong H, Lv Y, Zhao D, Barrow P, Zhou X. Defensins: the case for their use against mycobacterial infections. *J Immunol Res* (2016) 2016:7515687. doi:10.1155/2016/7515687

83. Rivas-Santiago CE, Rivas-Santiago B, León DA, Castañeda-Delgado J, Hernández Pando R. Induction of β-defensins by l-isoleucine as novel immunotherapy in experimental murine tuberculosis. *Clin Exp Immunol* (2011) 164:80–9. doi:10.1111/j.1365-2249.2010.04313.x
84. Tan BH, Meinken C, Bastian M, Bruns H, Legaspi A, Ochoa MT, et al. Macrophages acquire neutrophil granules for antimicrobial activity against intracellular pathogens. *J Immunol* (2006) 177:1864–71. doi:10.4049/jimmunol.177.3.1864
85. Biragyn A, Ruffini PA, Leifer CA, Klyushnenkova E, Shakhov A, Chertov O, et al. Toll-like receptor 4-dependent activation of dendritic cells by beta-defensin 2. *Science* (2002) 298:1025–9. doi:10.1126/science.1075565
86. Kanamori Y, Murakami M, Matsui T, Funaba M. Hepcidin expression in liver cells: evaluation of mRNA levels and transcriptional regulation. *Gene* (2014) 546:50–5. doi:10.1016/j.gene.2014.05.040
87. Sow FB, Florence WC, Satoskar AR, Schlesinger LS, Zwilling BS, Lafuse WP. Expression and localization of hepcidin in macrophages: a role in host defense against tuberculosis. *J Leukoc Biol* (2007) 82:934–45. doi:10.1189/jlb.0407216
88. Sow FB, Nandakumar S, Velu V, Kellar KL, Schlesinger LS, Amara RR, et al. *Mycobacterium tuberculosis* components stimulate production of the antimicrobial peptide hepcidin. *Tuberculosis (Edinb)* (2011) 91:314–21. doi:10.1016/j.tube.2011.03.003
89. Sow FB, Sable SB, Plikaytis BB, Lafuse WP, Shinnick TM. Role of hepcidin in the innate immune response to *Mycobacterium tuberculosis*. *FASEB J* (2008) 22:556. doi:10.1096/fj.1530-6860
90. Pinto JP, Dias V, Zoller H, Porto G, Carmo H, Carvalho F, et al. Hepcidin messenger RNA expression in human lymphocytes. *Immunology* (2010) 130:217–30. doi:10.1111/j.1365-2567.2009.03226.x
91. Sow FB, Alvarez GR, Gross RP, Satoskar AR, Schlesinger LS, Zwilling BS, et al. Role of STAT1, NF- B, and C/EBP in the macrophage transcriptional regulation of hepcidin by mycobacterial infection and IFN. *J Leukoc Biol* (2009) 86:1247–58. doi:10.1189/jlb.1208719
92. Yamaji S. Inhibition of iron transport across human intestinal epithelial cells by hepcidin. *Blood* (2004) 104:2178–80. doi:10.1182/blood-2004-03-0829
93. Nemeth E, Ganz T. The role of hepcidin in iron metabolism. *Acta Haematol* (2009) 122:78–86. doi:10.1159/000243791
94. Ganz T. Hepcidin, a key regulator of iron metabolism and mediator of anemia of inflammation. *Blood* (2003) 102:783–8. doi:10.1182/blood-2003-03-0672
95. Close MJ, Howlett AR, Roskelley CD, Desprez PY, Bailey N, Rowning B, et al. Lactoferrin expression in mammary epithelial cells is mediated by changes in cell shape and actin cytoskeleton. *J Cell Sci* (1997) 110:2861–71.
96. Teng CT. Lactoferrin gene expression and regulation: an overview. *Biochem Cell Biol* (2002) 80:7–16. doi:10.1139/o01-215
97. Oseas R, Yang HH, Baehner RL, Boxer LA. Lactoferrin: a promoter of polymorphonuclear leukocyte adhesiveness. *Blood* (1981) 57:939–45.
98. Gifford JL, Hunter HN, Vogel HJ. Lactoferricin: a lactoferrin-derived peptide with antimicrobial, antiviral, antitumor and immunological properties. *Cell Mol Life Sci* (2005) 62:2588–98. doi:10.1007/s00018-005-5373-z
99. Arnold RR, Russell JE, Champion WJ, Brewer M, Gauthier JJ. Bactericidal activity of human lactoferrin: differentiation from the stasis of iron deprivation. *Infect Immun* (1982) 35:792–9.
100. Welsh KJ, Hwang S-A, Boyd S, Kruzel ML, Hunter RL, Actor JK. Influence of oral lactoferrin on *Mycobacterium tuberculosis* induced immunopathology. *Tuberculosis* (2011) 91:S105–13. doi:10.1016/j.tube.2011.10.019
101. Hwang S-A, Wilk KM, Bangale YA, Kruzel ML, Actor JK. Lactoferrin modulation of IL-12 and IL-10 response from activated murine leukocytes. *Med Microbiol Immunol* (2007) 196:171–80. doi:10.1007/s00430-007-0041-6
102. Hwang S-A, Kruzel ML, Actor JK. Oral recombinant human or mouse lactoferrin reduces *Mycobacterium tuberculosis* TDM induced granulomatous lung pathology. *Biochem Cell Biol* (2017) 95:148–54. doi:10.1139/bcb-2016-0061
103. Pereira HA, Spitznagel JK, Winton EF, Shafer WM, Martin LE, Guzman GS, et al. The ontogeny of a 57-Kd cationic antimicrobial protein of human polymorphonuclear leukocytes: localization to a novel granule population. *Blood* (1990) 76:825–34.
104. Jena P, Mohanty S, Mohanty T, Kallert S, Morgelin M, Lindstrøm T, et al. Azurophil granule proteins constitute the major mycobactericidal proteins in human neutrophils and enhance the killing of mycobacteria in macrophages. *PLoS One* (2012) 7:e50345. doi:10.1371/journal.pone.0050345
105. Fouret P, du Bois RM, Bernaudin JF, Takahashi H, Ferrans VJ, Crystal RG. Expression of the neutrophil elastase gene during human bone marrow cell differentiation. *J Exp Med* (1989) 169:833–45. doi:10.1084/jem.169.3.833
106. Wong KW, Jacobs WR. *Mycobacterium tuberculosis* exploits human interferon γ to stimulate macrophage extracellular trap formation and necrosis. *J Infect Dis* (2013) 208:109–19. doi:10.1093/infdis/jit097
107. Bieth J. Elastases: catalytic and biological properties. In: Mecham R, editor. *Regul Matrix Accumulation*. New York: Academic Press (1986). p. 217–320.
108. Pham CTN. Neutrophil serine proteases: specific regulators of inflammation. *Nat Rev Immunol* (2006) 6:541–50. doi:10.1038/nri1841
109. Steinwede K, Maus R, Bohling J, Voedisch S, Braun A, Ochs M, et al. Cathepsin G and neutrophil elastase contribute to lung-protective immunity against mycobacterial infections in mice. *J Immunol* (2012) 188:4476–87. doi:10.4049/jimmunol.1103346
110. Brinkmann V, Reichard U, Goosmann C, Fauler B, Uhlemann Y, Weiss DS, et al. Neutrophil extracellular traps kill bacteria. *Science* (2004) 303:1532–5. doi:10.1126/science.1092385
111. Je S, Quan H, Yoon Y, Na Y, Kim BJ, Seok SH. *Mycobacterium massiliense* induces macrophage extracellular traps with facilitating bacterial growth. *PLoS One* (2016) 11:e0155685. doi:10.1371/journal.pone.0155685
112. Boix E, Nogués MV. Mammalian antimicrobial proteins and peptides: overview on the RNase A superfamily members involved in innate host defence. *Mol Biosyst* (2007) 3:317–35. doi:10.1039/b617527a
113. Boix E, Salazar VA, Torrent M, Pulido D, Nogués MV, Moussaoui M. Structural determinants of the eosinophil cationic protein antimicrobial activity. *Biol Chem* (2012) 393:801–15. doi:10.1515/hsz-2012-0160
114. Becknell B, Eichler TE, Beceiro S, Li B, Easterling RS, Carpenter AR, et al. Ribonucleases 6 and 7 have antimicrobial function in the human and murine urinary tract. *Kidney Int* (2015) 87:151–61. doi:10.1038/ki.2014.268
115. Harder J, Schroder J-M. RNase 7, a novel innate immune defense antimicrobial protein of healthy human skin. *J Biol Chem* (2002) 277:46779–84. doi:10.1074/jbc.M207587200
116. Zhang J, Dyer KD, Rosenberg HF. Human RNase 7: a new cationic ribonuclease of the RNase A superfamily. *Nucleic Acids Res* (2003) 31:602–7. doi:10.1093/nar/gkg157
117. Pulido D, Torrent M, Andreu D, Nogues MV, Boix E. Two human host defense ribonucleases against mycobacteria, the eosinophil cationic protein (RNase 3) and RNase 7. *Antimicrob Agents Chemother* (2013) 57:3797–805. doi:10.1128/AAC.00428-13
118. Gruart V, Truong M-J, Plumas J, Zandecki M, Kusnierz J-P, Prin L, et al. Decreased expression of eosinophil peroxidase and major basic protein messenger RNAs during eosinophil maturation. *Blood* (1992) 79(10):2592–7.
119. Borelli V, Vita F, Shankar S, Soranzo MR, Banfi E, Scialino G, et al. Human eosinophil peroxidase induces surface alteration, killing, and lysis of *Mycobacterium tuberculosis*. *Infect Immun* (2003) 71:605–13. doi:10.1128/IAI.71.2.605-613.2003
120. Rivera-Marrero CA, Stewart J, Shafer WM, Roman J. The down-regulation of cathepsin G in THP-1 monocytes after infection with *Mycobacterium tuberculosis* is associated with increased intracellular survival of bacilli. *Infect Immun* (2004) 72:5712–21. doi:10.1128/IAI.72.10.5712-5721.2004
121. Berg RD, Levitte S, O'Sullivan MP, O'Leary SM, Cambier CJ, Cameron J, et al. Lysosomal disorders drive susceptibility to tuberculosis by compromising macrophage migration. *Cell* (2016) 165:139–52. doi:10.1016/j.cell.2016.02.034
122. Walter K, Steinwede K, Aly S, Reinheckel T, Bohling J, Maus UA, et al. Cathepsin G in experimental tuberculosis: relevance for antibacterial protection and potential for immunotherapy. *J Immunol* (2015) 195:3325–33. doi:10.4049/jimmunol.1501012
123. Stenger S, Hanson DA, Teitelbaum R, Dewan P, Niazi KR, Froelich CJ, et al. An antimicrobial activity of cytolytic T cells mediated by granulysin. *Science* (1998) 282:121–5. doi:10.1126/science.282.5386.121
124. Ross KF, Herzberg MC. Calprotectin expression by gingival epithelial cells. *Infect Immun* (2001) 69:3248–54. doi:10.1128/IAI.69.5.3248-3254.2001
125. Bagheri V. S100A12: friend or foe in pulmonary tuberculosis? *Cytokine* (2017) 92:80–2. doi:10.1016/j.cyto.2017.01.009
126. Dhiman R, Venkatasubramanian S, Paidipally P, Barnes PF, Tvinnereim A, Vankayalapati R. Interleukin 22 inhibits intracellular growth of *Mycobacterium tuberculosis* by enhancing calgranulin a expression. *J Infect Dis* (2014) 209:578–87. doi:10.1093/infdis/jit495

127. Mork G, Schjerven H, Mangschau L, Soyland E, Brandtzaeg P. Proinflammatory cytokines upregulate expression of calprotectin (L1 protein, MRP-8/MRP-14) in cultured human keratinocytes. *Br J Dermatol* (2003) 149:484–91. doi:10.1046/j.1365-2133.2003.05536.x
128. Lusitani D, Malawista SE, Montgomery RR. Calprotectin, an abundant cytosolic protein from human polymorphonuclear leukocytes, inhibits the growth of *Borrelia burgdorferi*. *Infect Immun* (2003) 71:4711–6. doi:10.1128/IAI.71.8.4711-4716.2003
129. Alonso S, Pethe K, Russell DG, Purdy GE. Lysosomal killing of *Mycobacterium* mediated by ubiquitin-derived peptides is enhanced by autophagy. *Proc Natl Acad Sci U S A* (2007) 104:6031–6. doi:10.1073/pnas.0700036104
130. Martineau AR, Newton SM, Wilkinson KA, Kampmann B, Hall BM, Nawroly N, et al. Neutrophil-mediated innate immune resistance to mycobacteria. *J Clin Invest* (2007) 117:1988–94. doi:10.1172/JCI31097
131. Bandurska K, Berdowska A, Barczyńska-Felusiak R, Krupa P. Unique features of human cathelicidin LL-37. *Biofactors* (2015) 41:289–300. doi:10.1002/biof.1225
132. Zanetti M, Gennaro R, Romeo D. Cathelicidins: a novel protein family with a common proregion and a variable C-terminal antimicrobial domain. *FEBS Lett* (1995) 374:1–5. doi:10.1016/0014-5793(95)01050-O
133. Sørensen OE, Follin P, Johnsen AH, Calafat J, Tjabringa GS, Hiemstra PS, et al. Human cathelicidin, hCAP-18, is processed to the antimicrobial peptide LL-37 by extracellular cleavage with proteinase 3. *Blood* (2001) 97:3951–9. doi:10.1182/blood.V97.12.3951
134. Liu PT, Stenger S, Tang DH, Modlin RL. Cutting edge: vitamin D-mediated human antimicrobial activity against *Mycobacterium tuberculosis* is dependent on the induction of cathelicidin. *J Immunol* (2007) 179:2060–3. doi:10.4049/jimmunol.179.4.2060
135. Lin W, Florez de Sessions P, Teoh GHK, Mohamed ANN, Zhu YO, Koh VHQ, et al. Transcriptional profiling of *Mycobacterium tuberculosis* exposed to *in vitro* lysosomal stress. *Infect Immun* (2016) 84:2505–23. doi:10.1128/IAI.00072-16
136. Kisich KO, Heifets L, Higgins M, Diamond G. Antimycobacterial agent based on mRNA encoding human β-defensin 2 enables primary macrophages to restrict growth of *Mycobacterium tuberculosis*. *Infect Immun* (2001) 69:2692–9. doi:10.1128/IAI.69.4.2692-2699.2001
137. Ganz T. Defensins: antimicrobial peptides of innate immunity. *Nat Rev Immunol* (2003) 3:710–20. doi:10.1038/nri1180
138. Faurschou M, Kamp S, Cowland JB, Udby L, Johnsen AH, Calafat J, et al. Prodefensins are matrix proteins of specific granules in human neutrophils. *J Leukoc Biol* (2005) 78:785–93. doi:10.1189/jlb.1104688
139. Jacobsen M, Repsilber D, Gutschmidt A, Neher A, Feldmann K, Mollenkopf HJ, et al. Candidate biomarkers for discrimination between infection and disease caused by *Mycobacterium tuberculosis*. *J Mol Med* (2007) 85:613–21. doi:10.1007/s00109-007-0157-6
140. Kisich KO, Higgins M, Diamond G, Heifets L. Tumor necrosis factor alpha stimulates killing of *Mycobacterium tuberculosis* by human neutrophils. *Infect Immun* (2002) 70:4591–9. doi:10.1128/IAI.70.8.4591
141. Kalita A, Verma I, Khuller GK. Role of human neutrophil peptide-1 as a possible adjunct to antituberculosis chemotherapy. *J Infect Dis* (2004) 190:1476–80. doi:10.1086/424463
142. Park CH, Valore EV, Waring AJ, Ganz T. Hepcidin, a urinary antimicrobial peptide synthesized in the liver. *J Biol Chem* (2001) 276:7806–10. doi:10.1074/jbc.M008922200
143. Michels K, Nemeth E, Ganz T, Mehrad B. Hepcidin and host defense against infectious diseases. *PLoS Pathog* (2015) 11:e1004998. doi:10.1371/journal.ppat.1004998
144. Morris CD, Bird AR, Nell H. The haematological and biochemical changes in severe pulmonary tuberculosis. *Q J Med* (1989) 73:1151–9.
145. Javaheri-Kermani M, Farazmandfar T, Ajami A, Yazdani Y. Impact of hepcidin antimicrobial peptide on iron overload in tuberculosis patients. *Scand J Infect Dis* (2014) 46:693–6. doi:10.3109/00365548.2014.929736
146. Andersson DI, Hughes D, Kubicek-Sutherland JZ. Mechanisms and consequences of bacterial resistance to antimicrobial peptides. *Drug Resist Updat* (2016) 26:43–57. doi:10.1016/j.drup.2016.04.002
147. Hwang S-A, Kruzel ML, Actor JK. CHO expressed recombinant human lactoferrin as an adjuvant for BCG. *Int J Immunopathol Pharmacol* (2015) 28:452–68. doi:10.1177/0394632015599832
148. Thom RE, Elmore MJ, Williams A, Andrews SC, Drobniewski F, Marsh PD, et al. The expression of ferritin, lactoferrin, transferrin receptor and solute carrier family 11A1 in the host response to BCG-vaccination and *Mycobacterium tuberculosis* challenge. *Vaccine* (2012) 30:3159–68. doi:10.1016/j.vaccine.2012.03.008
149. Jensen-Jarolim E, Pacios LF, Bianchini R, Hofstetter G, Roth-Walter F. Structural similarities of human and mammalian lipocalins, and their function in innate immunity and allergy. *Allergy* (2016) 71:286–94. doi:10.1111/all.12797
150. Soehnlein O, Zernecke A, Eriksson EE, Rothfuchs AG, Pham CT, Herwald H, et al. Neutrophil secretion products pave the way for inflammatory monocytes. *Blood* (2008) 112:1461–71. doi:10.1182/blood-2008-02-139634
151. Tapper H, Karlsson A, Mörgelin M, Flodgaard H, Herwald H. Secretion of heparin-binding protein from human neutrophils is determined by its localization in azurophilic granules and secretory vesicles. *Blood* (2002) 99:1785–93. doi:10.1182/blood.V99.5.1785
152. Soehnlein O, Kai-Larsen Y, Frithiof R, Sorensen OE, Kenne E, Scharffetter-Kochanek K, et al. Neutrophil primary granule proteins HBP and HNP1-3 boost bacterial phagocytosis by human and murine macrophages. *J Clin Invest* (2008) 118:3491–502. doi:10.1172/JCI35740
153. Shafer WM, Martin LE, Spitznagel JK. Late intraphagosomal hydrogen ion concentration favors the in vitro antimicrobial capacity of a 37-kilodalton cationic granule protein of human neutrophil granulocytes. *Infect Immun* (1986) 53:651–5.
154. Ribeiro-Gomes FL, Moniz-de-Souza MCA, Alexandre-Moreira MS, Dias WB, Lopes MF, Nunes MP, et al. Neutrophils activate macrophages for intracellular killing of *Leishmania major* through recruitment of TLR4 by neutrophil elastase. *J Immunol* (2007) 179:3988–94. doi:10.4049/jimmunol.179.6.3988
155. Belaaouaj A, McCarthy R, Baumann M, Gao Z, Ley TJ, Abraham SN, et al. Mice lacking neutrophil elastase reveal impaired host defense against gram negative bacterial sepsis. *Nat Med* (1998) 4:615–8. doi:10.1038/nm0598-615
156. Pires D, Marques J, Pombo JP, Carmo N, Bettencourt P, Neyrolles O, et al. Role of cathepsins in *Mycobacterium tuberculosis* survival in human macrophages. *Sci Rep* (2016) 6:32247. doi:10.1038/srep32247
157. Meijer AH. Protection and pathology in TB: learning from the zebrafish model. *Semin Immunopathol* (2016) 38:261–73. doi:10.1007/s00281-015-0522-4
158. Pitabut N, Sakurada S, Tanaka T, Ridruechai C, Tanuma J, Aoki T, et al. Potential function of granulysin, other related effector molecules and lymphocyte subsets in patients with TB and HIV/TB coinfection. *Int J Med Sci* (2013) 10:1003–14. doi:10.7150/ijms.6437
159. Saiga H, Shimada Y, Takeda K. Innate immune effectors in mycobacterial infection. *Clin Dev Immunol* (2011) 2011:347594. doi:10.1155/2011/347594
160. Foss MH, Powers KM, Purdy GE. Structural and functional characterization of mycobactericidal ubiquitin-derived peptides in model and bacterial membranes. *Biochemistry* (2012) 51:9922–9. doi:10.1021/bi301426j
161. Koczera P, Martin L, Marx G, Schuerholz T. The ribonuclease a superfamily in humans: canonical RNases as the buttress of innate immunity. *Int J Mol Sci* (2016) 17:E1278. doi:10.3390/ijms17081278
162. Bystrom J, Amin K, Bishop-Bailey D. Analysing the eosinophil cationic protein – a clue to the function of the eosinophil granulocyte. *Respir Res* (2011) 12:10. doi:10.1186/1465-9921-12-10
163. Monteseirín J, Vega A, Chacón P, Camacho MJ, El Bekay R, Asturias JA, et al. Neutrophils as a novel source of eosinophil cationic protein in IgE-mediated processes. *J Immunol* (2007) 179:2634–41. doi:10.4049/jimmunol.179.4.2634
164. Liu Y-S, Tsai P-W, Wang Y, Fan T, Hsieh C-H, Chang M, et al. Chemoattraction of macrophages by secretory molecules derived from cells expressing the signal peptide of eosinophil cationic protein. *BMC Syst Biol* (2012) 6:105. doi:10.1186/1752-0509-6-105
165. Vijayan VK, Reetha AM, Jawahar MS, Sankaran K, Prabhakar R. Pulmonary eosinophilia in pulmonary tuberculosis. *Chest* (1992) 101:1708–9. doi:10.1378/chest.101.6.1708
166. Kita H. Eosinophils: multifaceted biological properties and roles in health and disease. *Immunol Rev* (2011) 242:161–77. doi:10.1111/j.1600-065X.2011.01026.x
167. Arranz-Trullén J, Lu L, Pulido D, Bhakta S, Boix E. Unveiling the mode of action of human antimicrobial RNases against *Mycobacterium tuberculosis*

using a surrogate macrophage infected model. *TB Summit 2016*. London (2016).
168. Gupta SK, Haigh BJ, Griffin FJ, Wheeler TT. The mammalian secreted RNases: mechanisms of action in host defence. *Innate Immun* (2012) 19:86–97. doi:10.1177/1753425912446955
169. Yang D, Chen Q, Su SB, Zhang P, Kurosaka K, Caspi RR, et al. Eosinophil-derived neurotoxin acts as an alarmin to activate the TLR2-MyD88 signal pathway in dendritic cells and enhances Th2 immune responses. *J Exp Med* (2008) 205:79–90. doi:10.1084/jem.20062027
170. Jiang Z, Higgins MP, Whitehurst J, Kisich KO, Voskuil MI, Hodges RS. Anti-tuberculosis activity of α-helical antimicrobial peptides: de novo designed L- and D-enantiomers versus L- and D-LL-37. *Protein Pept Lett* (2011) 18:241–52. doi:10.2174/092986611794578288
171. Kapoor R, Eimerman PR, Hardy JW, Cirillo JD, Contag CH, Barron AE. Efficacy of antimicrobial peptoids against *Mycobacterium tuberculosis*. *Antimicrob Agents Chemother* (2011) 55:3058–62. doi:10.1128/AAC.01667-10
172. Hoffmann and Czihal. Antibiotic peptides Patent WO2009013262 A1 (2009).
173. Ramón-García S, Mikut R, Ng C, Ruden S, Volkmer R, Reischl M, et al. Targeting *Mycobacterium tuberculosis* and other microbial pathogens using improved synthetic antibacterial peptides. *Antimicrob Agents Chemother* (2013) 57:2295–303. doi:10.1128/AAC.00175-13
174. Rivas-Santiago B, Rivas Santiago CE, Castañeda-Delgado JE, León-Contreras JC, Hancock REW, Hernandez-Pando R. Activity of LL-37, CRAMP and antimicrobial peptide-derived compounds E2, E6 and CP26 against *Mycobacterium tuberculosis*. *Int J Antimicrob Agents* (2013) 41:143–8. doi:10.1016/j.ijantimicag.2012.09.015
175. Lan Y, Lam JT, Siu GKH, Yam WC, Mason AJ, Lam JKW. Cationic amphipathic D-enantiomeric antimicrobial peptides with in vitro and ex vivo activity against drug-resistant *Mycobacterium tuberculosis*. *Tuberculosis* (2014) 94:678–89. doi:10.1016/j.tube.2014.08.001
176. Kwok PCL, Grabarek A, Chow MYT, Lan Y, Li JCW, Casettari L, et al. Inhalable spray-dried formulation of D-LAK antimicrobial peptides targeting tuberculosis. *Int J Pharm* (2015) 491:367–74. doi:10.1016/j.ijpharm.2015.07.001
177. Spindler EC, Hale JDF, Giddings TH, Hancock REW, Gill RT. Deciphering the mode of action of the synthetic antimicrobial peptide bac8c. *Antimicrob Agents Chemother* (2011) 55:1706–16. doi:10.1128/AAC.01053-10
178. Llamas-González YY, Pedroza-Roldán C, Cortés-Serna MB, Márquez-Aguirre AL, Gálvez-Gastélum FJ, Flores-Valdez MA. The synthetic cathelicidin HHC-10 inhibits *Mycobacterium bovis* BCG in vitro and in C57BL/6 mice. *Microb Drug Resist* (2013) 19:124–9. doi:10.1089/mdr.2012.0149
179. Cherkasov A, Hilpert K, Jenssen H, Fjell CD, Waldbrook M, Mullaly SC, et al. Use of artificial intelligence in the design of small peptide antibiotics effective against a broad spectrum of highly antibiotic-resistant superbugs. *ACS Chem Biol* (2009) 4:65–74. doi:10.1021/cb800240j
180. Mansour SC, de la Fuente-Nunez C, Hancock REW. Peptide IDR-1018: modulating the immune system and targeting bacterial biofilms to treat antibiotic-resistant bacterial infections. *J Pept Sci* (2015) 21:323–9. doi:10.1002/psc.2708
181. Rivas-Santiago B, Castañeda-Delgado JE, Rivas Santiago CE, Waldbrook M, González-Curiel I, León-Contreras JC, et al. Ability of innate defence regulator peptides IDR-1002, IDR-HH2 and IDR-1018 to protect against *Mycobacterium tuberculosis* infections in animal models. *PLoS One* (2013) 8:e59119. doi:10.1371/journal.pone.0059119
182. Huante-Mendoza A, Silva-García O, Oviedo-Boyso J, Hancock REW, Baizabal-Aguirre VM. Peptide IDR-1002 inhibits NF-κB nuclear translocation by inhibition of IκBα degradation and activates p38/ERK1/2–MSK1-dependent CREB phosphorylation in macrophages stimulated with lipopolysaccharide. *Front Immunol* (2016) 7:533. doi:10.3389/fimmu.2016.00533
183. Chingaté S, Delgado G, Salazar LM, Soto CY. The ATPase activity of the mycobacterial plasma membrane is inhibited by the LL37-analogous peptide LLAP. *Peptides* (2015) 71:222–8. doi:10.1016/j.peptides.2015.07.021
184. Silva JP, Gonçalves C, Costa C, Sousa J, Silva-Gomes R, Castro AG, et al. Delivery of LLKKK18 loaded into self-assembling hyaluronic acid nanogel for tuberculosis treatment. *J Control Release* (2016) 235:112–24. doi:10.1016/j.jconrel.2016.05.064
185. Ghobrial O, Derendorf H, Hillman JD. Pharmacokinetic and pharmacodynamic evaluation of the lantibiotic MU1140. *J Pharm Sci* (2010) 99:2521–8. doi:10.1002/jps.22015
186. Rodríguez A, Villegas E, Montoya-Rosales A, Rivas-Santiago B, Corzo G. Characterization of antibacterial and hemolytic activity of synthetic pandinin 2 variants and their inhibition against *Mycobacterium tuberculosis*. *PLoS One* (2014) 9:e101742. doi:10.1371/journal.pone.0101742
187. Khara JS, Wang Y, Ke X-Y, Liu S, Newton SM, Langford PR, et al. Anti-mycobacterial activities of synthetic cationic α-helical peptides and their synergism with rifampicin. *Biomaterials* (2014) 35:2032–8. doi:10.1016/j.biomaterials.2013.11.035
188. Vermeer LS, Lan Y, Abbate V, Ruh E, Bui TT, Wilkinson LJ, et al. Conformational flexibility determines selectivity and antibacterial, antiplasmodial, and anticancer potency of cationic α-helical peptides. *J Biol Chem* (2012) 287:34120–33. doi:10.1074/jbc.M112.359067
189. Torrent M, Pulido D, Valle J, Nogués MV, Andreu D, Boix E. Ribonucleases as a host-defence family: evidence of evolutionarily conserved antimicrobial activity at the N-terminus. *Biochem J* (2013) 456:99–108. doi:10.1042/BJ20130123
190. Torrent M, Pulido D, Nogués MV, Boix E. Exploring new biological functions of amyloids: bacteria cell agglutination mediated by host protein aggregation. *PLoS Pathog* (2012) 8:e1003005. doi:10.1371/journal.ppat.1003005
191. Hilchie AL, Wuerth K, Hancock REW. Immune modulation by multifaceted cationic host defense (antimicrobial) peptides. *Nat Chem Biol* (2013) 9:761–8. doi:10.1038/nchembio.1393
192. Fosgerau K, Hoffmann T. Peptide therapeutics: current status and future directions. *Drug Discov Today* (2014) 20:122–8. doi:10.1016/j.drudis.2014.10.003
193. Goldman MJ, Anderson GM, Stolzenberg ED, Kari UP, Zasloff M, Wilson JM. Human beta-defensin-1 is a salt-sensitive antibiotic in lung that is inactivated in cystic fibrosis. *Cell* (1997) 88:553–60. doi:10.1016/S0092-8674(00)81895-4
194. Hilpert K, Volkmer-Engert R, Walter T, Hancock REW. High-throughput generation of small antibacterial peptides with improved activity. *Nat Biotechnol* (2005) 23:1008–12. doi:10.1038/nbt1113
195. Chen Y, Mant CT, Farmer SW, Hancock REW, Vasil ML, Hodges RS. Rational design of alpha-helical antimicrobial peptides with enhanced activities and specificity/therapeutic index. *J Biol Chem* (2005) 280:12316–29. doi:10.1074/jbc.M413406200
196. Nordström R, Malmsten M. Delivery systems for antimicrobial peptides. *Adv Colloid Interface Sci* (2017) 242:17–34. doi:10.1016/j.cis.2017.01.005
197. Zhang J, Zhang X, Liu G, Chang D, Liang X, Zhu X, et al. Intracellular trafficking network of protein nanocapsules: endocytosis, exocytosis and autophagy. *Theranostics* (2016) 6:2099–113. doi:10.7150/thno.16587
198. Hamley I. Peptide fibrillization. *Angw Chem Int Ed Eng* (2007) 46:8128–47. doi:10.1002/anie.200700861
199. Torrent M, Valle J, Nogués MV, Boix E, Andreu D. The generation of antimicrobial peptide activity: a trade-off between charge and aggregation? *Angw Chem Int Ed Eng* (2011) 50:10686–9. doi:10.1002/anie.201103589
200. Mikut R, Ruden S, Reischl M, Breitling F, Volkmer R, Hilpert K. Improving short antimicrobial peptides despite elusive rules for activity. *Biochim Biophys Acta* (2016) 1858:1024–33. doi:10.1016/j.bbamem.2015.12.013
201. Haney EF, Mansour SC, Hilchie AL, de la Fuente-Núñez C, Hancock RE. High throughput screening methods for assessing antibiofilm and immunomodulatory activities of synthetic peptides. *Peptides* (2015) 71:276–85. doi:10.1016/j.peptides.2015.03.015
202. Sim S, Kim Y, Kim T, Lim S, Lee M. Directional assembly of α-helical peptides induced by cyclization. *J Am Chem Soc* (2012) 134:20270–2. doi:10.1021/ja3098756
203. Bowdish DME, Davidson DJ, Lau YE, Lee K, Scott MG, Hancock REW. Impact of LL-37 on anti-infective immunity. *J Leukoc Biol* (2005) 77:451–9. doi:10.1189/jlb.0704380
204. Zumla A, Rao M, Wallis RS, Kaufmann SHE, Rustomjee R, Mwaba P, et al. Host-directed therapies for infectious diseases: current status, recent progress, and future prospects. *Lancet Infect Dis* (2016) 16:e47–63. doi:10.1016/S1473-3099(16)00078-5
205. Ottosson H, Nylén F, Sarker P, Miraglia E, Bergman P, Gudmundsson GH, et al. Highly potent inducers of endogenous antimicrobial peptides for host directed therapy of infections. *Sci Rep* (2016) 6:36692. doi:10.1038/srep36692
206. Rivas-Santiago B, Rivas-Santiago C, Sada E, Hernandez-Pando R. Prophylactic potential of defensins and L-isoleucine in tuberculosis household contacts:

an experimental model. *Immunotherapy* (2015) 7:207–13. doi:10.2217/imt.14.119
207. Liu PT, Stenger S, Li H, Wenzel L, Tan BH, Krutzik SR, et al. Toll-like receptor triggering of a vitamin D-mediated human antimicrobial response. *Science* (2006) 311:1770–3. doi:10.1126/science.1123933
208. Lofton H, Pränting M, Thulin E, Andersson DI. Mechanisms and fitness costs of resistance to antimicrobial peptides LL-37, CNY100HL and wheat germ histones. *PLoS One* (2013) 8:e68875. doi:10.1371/journal.pone.0068875
209. Kraus D, Peschel A. Molecular mechanisms of bacterial resistance to antimicrobial peptides. *Curr Top Microbiol Immunol* (2006) 306:231–50.
210. Adams KN, Takaki K, Connolly LE, Wiedenhoft H, Winglee K, Humbert O, et al. Drug tolerance in replicating mycobacteria mediated by a macrophage-induced efflux mechanism. *Cell* (2011) 145:39–53. doi:10.1016/j.cell.2011.02.022
211. Szumowski JD, Adams KN, Edelstein PH, Ramakrishnan L. Antimicrobial efflux pumps and *Mycobacterium tuberculosis* drug tolerance: evolutionary considerations. *Curr Top Microbiol Immunol* (2013) 374:81–108. doi:10.1007/82_2012_300
212. Rios AC, Moutinho CG, Pinto FC, Del Fiol FS, Jozala A, Chaud MV, et al. Alternatives to overcoming bacterial resistances: state-of-the-art. *Microbiol Res* (2016) 191:51–80. doi:10.1016/j.micres.2016.04.008
213. Gao LY, Laval F, Lawson EH, Groger RK, Woodruff A, Morisaki JH, et al. Requirement for kasB in *Mycobacterium mycolic* acid biosynthesis, cell wall impermeability and intracellular survival: implications for therapy. *Mol Microbiol* (2003) 49:1547–63. doi:10.1046/j.1365-2958.2003.03667.x
214. Gryllos I, Tran-Winkler HJ, Cheng M-F, Chung H, Bolcome R, Lu W, et al. Induction of group A *Streptococcus* virulence by a human antimicrobial peptide. *Proc Natl Acad Sci U S A* (2008) 105:16755–60. doi:10.1073/pnas.0803815105
215. Brown ED, Wright GD. Antibacterial drug discovery in the resistance era. *Nature* (2016) 529:336–43. doi:10.1038/nature17042
216. Bauer ME, Shafer WM. On the in vivo significance of bacterial resistance to antimicrobial peptides. *Biochim Biophys Acta* (2015) 1848:3101–11. doi:10.1016/j.bbamem.2015.02.012
217. Fattorini L, Gennaro R, Zanetti M, Tan D, Brunori L, Giannoni F, et al. In vitro activity of protegrin-1 and beta-defensin-1, alone and in combination with isoniazid, against *Mycobacterium tuberculosis*. *Peptides* (2004) 25:1075–7. doi:10.1016/j.peptides.2004.04.003
218. Nylen F, Bergman P, Gudmundsson GH, Agerberth B. Assays for identifying inducers of the antimicrobial peptide LL-37. *Methods Mol Biol* (2017) 1548:271–81. doi:10.1007/978-1-4939-6737-7_19
219. Ramos-Espinosa O, Hernández-Bazán S, Francisco-Cruz A, Mata-Espinosa D, Barrios-Payán J, Marquina-Castillo B, et al. Gene therapy based in antimicrobial peptides and proinflammatory cytokine prevents reactivation of experimental latent tuberculosis. *Pathog Dis* (2016) 74:ftw075. doi:10.1093/femspd/ftw075

Conflict of Interest Statement: No potential conflicts of interest were disclosed. The authors declare that the research was conducted in the absence of any commercial or financial relationships that could be construed as a potential conflict of interest.

CHAPTER II

frontiers in Immunology

REVIEW
published: 16 May 2018
doi: 10.3389/fimmu.2018.01012

Immune Modulation by Human Secreted RNases at the Extracellular Space

Lu Lu, Jiarui Li, Mohammed Moussaoui and Ester Boix**

Department of Biochemistry and Molecular Biology, Faculty of Biosciences, Universitat Autònoma de Barcelona, Cerdanyola del Vallès, Spain

The ribonuclease A superfamily is a vertebrate-specific family of proteins that encompasses eight functional members in humans. The proteins are secreted by diverse innate immune cells, from blood cells to epithelial cells and their levels in our body fluids correlate with infection and inflammation processes. Recent studies ascribe a prominent role to secretory RNases in the extracellular space. Extracellular RNases endowed with immuno-modulatory and antimicrobial properties can participate in a wide variety of host defense tasks, from performing cellular housekeeping to maintaining body fluid sterility. Their expression and secretion are induced in response to a variety of injury stimuli. The secreted proteins can target damaged cells and facilitate their removal from the focus of infection or inflammation. Following tissue damage, RNases can participate in clearing RNA from cellular debris or work as signaling molecules to regulate the host response and contribute to tissue remodeling and repair. We provide here an overall perspective on the current knowledge of human RNases' biological properties and their role in health and disease. The review also includes a brief description of other vertebrate family members and unrelated extracellular RNases that share common mechanisms of action. A better knowledge of RNase mechanism of actions and an understanding of their physiological roles should facilitate the development of novel therapeutics.

Keywords: ribonucleases, innate immunity, RNA, extracellular, inflammation, infection

OPEN ACCESS

Edited by:
Tobias Schuerholz, Universitätsmedizin Rostock, Germany

Reviewed by:
Lukas Martin, Uniklinik RWTH Aachen, Germany
Caroline Jefferies, Cedars-Sinai Medical Center, United States

****Correspondence:***
Mohammed Moussaoui
mohammed.moussaoui@uab.es;
Ester Boix
ester.boix@uab.es

Specialty section:
This article was submitted to Inflammation, a section of the journal Frontiers in Immunology

Received: *01 February 2018*
Accepted: *23 April 2018*
Published: *16 May 2018*

Citation:
Lu L, Li J, Moussaoui M and Boix E (2018) Immune Modulation by Human Secreted RNases at the Extracellular Space. Front. Immunol. 9:1012. doi: 10.3389/fimmu.2018.01012

INTRODUCTION

Thirty years ago Steven Benner conjectured the existence of extracellular RNA communicators (1, 2). At that time, he was investigating bovine RNaseA activity and expressed skepticism that pancreatic RNases merely removed the large amount of bacterial RNA present in the ruminant digestive tract (3, 4). Based on the diverse biological properties displayed by some RNaseA family members, i.e., anti-tumoural action, angiogenesis, and neurotoxicity, he suggested that the catalytic activity of vertebrate secreted RNases intervened in the regulation of the development of higher organisms. The hypothesis was launched well before the discovery of extracellular vesicles as horizontal nanovehicle carriers and well before the discovery that angiogenin, a member of the vertebrate-specific RNaseA superfamily, generates RNA regulatory fragments (5, 6). RNaseA, the vertebrate secretory RNases' reference family member, is a small and highly stable protein that served as a working model for biochemists during the twentieth century; several Nobel prizes in chemistry were awarded for work with RNaseA (7, 8). Many times, researchers have tried unsuccessfully to

rescue the RNaseA superfamily from its purely academic role (1, 7). Despite extensive knowledge on the mechanism of catalysis (8) and phylogeny (9–12), the biological properties of some family members remained puzzling, and the ultimate physiological roles of these proteins remained elusive. Exhaustive sequencing of RNases within vertebrates and a comparative phylogenetic analysis suggested that the family emerged with a host defense role (11, 13–16). Another interesting hypothesis suggested that granulocyte-secreted proteins could play a primary role in local tissue repair and the removal of macromolecular debris following cell damage during inflammation (17). The authors considered the potential contribution to RNA clearance by eosinophil secreted RNases. Later studies also indicated an RNA scavenging role for pancreatic-type RNases (18, 19). In addition, the secreted proteins displayed immuno-regulatory properties that suggest they could participate in the transmission and amplification of local danger signals (17, 20). Therefore, extracellular RNases are key players that ensure tissue health and body homeostasis. Indeed, we find examples of genetic deficiencies in extracellular RNases that lead to immune-related diseases, such as amyotrophic lateral sclerosis (ALS), associated with human RNase5 mutations (21, 22) and cystic leukoencephalopathy, a neuronal disorder associated with RNaseT2 deficiency (23, 24). Potential RNA-targeted therapeutic applications for secretory RNases were envisaged as far back as two decades ago (25–27).

Recent methodological advances in the cellular biology and RNA fields have facilitated novel approaches to understanding the *in vivo* role of extracellular RNases. Hopefully, knowledge on RNases action and trafficking in biological fluids will give path to translational research from academia to pharmaceutical industry. Indeed, recent experimental trials with animal models, such as those on hematopoiesis regulation by human RNase5 (28) or attenuation of extracellular RNA (exRNA) pro-inflammatory activity by RNaseA (29), are already offering promising therapeutic results.

The review summarizes the current knowledge on the mechanism of action of the RNaseA superfamily members and their contribution to innate immunity, as sentinel proteins at the extracellular space. We also briefly compared RNaseA proteins with other extracellular RNases, such as RNaseT2 family members, which are ancient RNases that are highly conserved through taxa from viruses to humans (30, 31), and bacterial RNases (19, 32) that work as defense weapons in inter-strain warfare.

THE RNase A SUPERFAMILY

The RNaseA superfamily is a vertebrate-specific gene family that has shown great divergence in a short period of time, a characteristic trait of immune-related proteins (11, 16, 33). Despite the low sequence identity between some family members (~30%), they all share a common three-dimensional structural fold and conserved motif signature (CKXXNTF). They are small secretory proteins (13–15 kDa) expressed with a short 25–27 amino acid signal peptide. The mature protein adopts an $\alpha + \beta$ kidney-shaped fold crosslinked by three to four disulfide bonds. A conserved catalytic triad formed by two His and a Lys participates in the endoribonuclease acid–base catalytic mechanism of action (8). A marked preference for cleavage of single-stranded RNA (ssRNA) is observed, with specificity for pyrimidines at the main base and a preference for purines at the secondary base site (7, 34, 35). In addition, other nucleotide-binding sites contribute to RNase-substrate specificities (36–38) and might determine the selectivity of RNases for cellular RNA. Recently, novel methodologies to identify the selective cleavage site for non-coding RNA for some family members, i.e., tRNA, have indicated their direct involvement in main cellular machinery tasks (39–41).

RNaseA superfamily members are mainly expressed in innate cells and display a variety of antimicrobial and immune modulation activities. They can participate in host immune responses, working as alarmins and safeguard molecules against infection and inflammation (16, 42–45). **Table 1** summarizes most of their reported activities and suggested physiological roles. Below, we describe the eight canonical family members in humans. **Table 2** indicates their reported source cell types and summarizes their constitutive and induced expression patterns. Human RNase expression and response processes activated by diverse stimuli are illustrated in **Figure 1**.

hRNase1

hRNase1 is the human homolog of the family reference protein, bovine pancreatic RNaseA. A comparative evolutionary analysis indicates a divergent role for non-ruminant RNase1 family members that are unrelated to digestion (18, 142). Expression of human RNase1 was detected in almost all tissues (143). In particular, human RNase1 is abundantly expressed by endothelial

TABLE 1 | Proposed roles and reported activities for extracellular RNases.

RNases roles	Reported activities	Reference
Cellular immune regulation	– Innate cells' activation and migration	(46–53)
	– Toll-like receptor pattern recognition and receptor activation	(46, 54, 55)
	– Hematopoiesis	(28)
	– Selective processing of non-coding RNA	(6, 40, 56–59)
	– Release of regulatory tRNA fragments	(6, 41, 58)
Tissue homeostasis, repair and remodeling	– Alarm signalling	(17, 54, 60, 61)
	– Activation and chemotaxis of fibroblasts	(51, 52, 62)
	– Activation of epithelial cells	(51, 52)
	– Cell proliferation activity	(63, 64)
	– Angiogenesis and neo-vascularization	(65, 66)
	– Wound healing activity	(67–70)
	– Autophagy induction	(71, 72)
	– Apoptosis induction	(73–75)
Clearance of extracellular RNA (exRNA)	– Clearance of cellular RNA debris following tissue injury	(29)
	– RNA scavenger activity	(76, 77)
	– Removal of blood exRNA released during hypoxia	(76)
	– Reduction of exRNA pro-inflammatory activity	(29, 78)
Epithelial barrier protection	– Antimicrobial activity at the skin and respiratory, urogenital and intestinal epithelial tracts	(43, 44, 70, 79–85)
Body fluid sterility	– Antibacterial activity	(83, 86–91)
	– Antiparasitic activity	(92–99)
	– Antiviral activity	(100–107)

TABLE 2 | Expression profile and location of human secretory RNases.

Human RNase	Main expression tissues and cell types[a]	Presence in biological fluids: rank score or reported level[b]		Subcellular location[c]	Expression regulated by (in comparison with)[d]
1	• Pancreas • Lung • Adipose • Endothelial cells • Erythroblasts	• Amniotic fluid: 629 • Blood: 4.09e^3 • Serum: 0.5 μg/mL • Synovial fluid (108) • Cerebrospinal fluid (109) • Urine (110)		• Extracellular space • Exosomes (111)	† Psoriatic arthritis (vs healthy in synovial fluid) † Sepsis (vs normal in whole blood and monocytes) (112) † Meningococcal sepsis (at 24 h vs normal at 0 h in monocytes) † Leishmaniasis (vs normal) † Systemic lupus erythematosus (vs normal) † Interstitial cystitis (ulcer vs normal) ↓ *Francisella tularensis* novicida (vs uninfect) ↓ *Francisella tularensis* schu S4 (vs uninfect) ↓ *Mycobacterium tuberculosis* (vs none in macrophages at 48 h)
2	• Liver • Lung • Spleen • Bone marrow • Neutrophils • Eosinophils • Monocytes	• Amniotic fluid: 1.41e^4 • Blood: 982 • Cerebrospinal fluid (113) • Urine (114) • Early gut lavage fluid (115) • Late gut lavage fluid (115)	 Healthy: 163 ng/mL Inflammatory bowel disease: 538 ng/mL Healthy: 18 ng/mL Inflammatory bowel disease: 95 ng/mL	• Extracellular space (116) • Exosomes (117) • Azurophil granule lumen	† Septic shock (vs normal) † Meningococcal sepsis — At 8 h, 24 h vs normal at 0 h in lymphocytes; At 24 h vs normal at 0 h in blood; At 0, 8, and 24 h vs normal at 0 h in monocytes; At 24 h vs meningococcal sepsis at 0 h in monocytes † Sepsis (vs normal in whole blood, CD8, and monocytes) † Tuberculosis (vs normal) † Leishmaniasis (vs normal) † Lyme disease at acute phase of infection (vs normal) † Interstitial cystitis (ulcer vs normal) † Psoriasis (at lesional skin vs normal at normal skin) † Burn (vs control at early stage and middle stage) ↓ *Francisella tularensis* novicida (vs uninfect) ↓ *Mycobacterium tuberculosis* (vs none in macrophage at 48 h)
3	• Bone marrow • Neutrophils • Eosinophils • Monocytes • T cells	• Amniotic fluid: 3.17e^4 • Blood: 4.51e^3 • Cerebrospinal fluid (113) • Bronchoalveolar lavage fluid (118) • Sputum (119) • Tear (120) • Early gut lavage fluid (115) • Late gut lavage fluid (115) • Plasma (121)	 Control: 1.7 μg/L Asthma: 2.8 μg/L Healthy: 26.1 ± 4.7 ng/mL Asthma: 142.6 ± 34.2 ng/mL Control: <20 μg/L Vernal keratoconjunctivitis: 470 μg/L Atopic keratoconjunctivitis:215 μg/L Giant papillary conjunctivitis: 53 μg/L Healthy: 5 ng/mL Inflammatory bowel disease: 15 ng/mL Healthy: 1 ng/mL Control: 3.5 ± 4.1 μg/L Reactive eosinophilia with inflammation: 75.0 ± 92.3 μg/L	• Exosomes (111, 124) • Extracellular space (125) • Azurophil granule lumen	† Meningococcal sepsis — At 24 h vs normal at 0 h in blood; At 24 h vs normal at 0 h in lymphocytes; At 0, 8, and 24 h vs normal at 0 h in monocytes † Septic shock (vs normal) (112) † Lyme disease at acute phase of infection (vs normal) † Leishmaniasis (vs normal) † Burn (vs control at early stage and middle stage) † Asthma (118, 119) † Inflammatory bowel disease (115) ↓ Atopic eczema (at normal skin vs normal at normal skin)

(Continued)

TABLE 2 | Continued

Human RNase	Main expression tissues and cell types[a]	Presence in biological fluids: rank score or reported level[b]		Subcellular location[c]	Expression regulated by (in comparison with)[d]
		• Serum (122) • Nasal fluid (123)	Control: 5.4–9.2 μg/L Helminthiases: 46–98 μg/L Atopic dermatitis: 50 μg/L Bacterial infections: 23 μg/L Malaria: 13 μg/L Interstitial cystitis:10 μg/L Normal: 32.6 ± 8.1 ng/mL Chronic non-allergic sinusitis: 87.6 ± 20.8 ng/mL Perennial allergic rhinitis: 84.7 ± 24.7 ng/mL Perennial and seasonal allergy: 112.9 ± 25.6 ng/mL		
4	• Liver • Adipose • Salivary gland • Colon • Endothelial cells • Monocytes • B cells • T cells	• Blood: $9.27e^3$ • Cerebrospinal fluid (113)	• Extracellular space • Exosomes (126)		† Sepsis (vs normal in whole blood) ↓ Visceral Leishmaniasis (vs normal) ↓ Psoriasis (at lesional skin vs normal at normal skin)
5	• Liver • Endothelial cells • Spinal cord neurons • T cells • Mast cells	• Amniotic fluid: $2.60e^4$ • Blood: $7.93e^3$ • Plasma: 96–478 ng/ml (127) • Bronchoalveolar lavage fluid (128) • Serum (129) • Cerebrospinal fluid (130)	Healthy: 394.6 ± 137.6 ng/mL Ulcerative colitis: 526.5 ± 224.1 ng/mL Crohn's disease: 508.8 ± 228.5 ng/mL Crohn's disease: 508.8 ± 228.5 ng/mL Control: 6.197 ± 1.987 ng/ml Amyotrophic lateral sclerosis: 5.582 ± 1.754 ng/mL	• Exosomes (111) • Extracellular space • Growth cone • Basal lamina (131) • Angiogenin–RNase inhibitor complex (132) • Neuronal cell body • Nucleus (133) • Nucleolus (134, 135) • Cytoplasmic vesicle • RNA stress granules (58)	† *Enterococcus faecalis* (vs none at 5 days) † *Mycobacterium tuberculosis* (vs none in macrophage at 48 h) † Meningococcal sepsis (at 24 h vs normal at 0 h in blood) † Asthma (128) † Inflammatory bowel disease (129) ↓ *Francisella tularensis* novicida (vs uninfect) ↓ *Francisella tularensis* schu S4 (vs uninfect) † Psoriasis — Lesional vs non-lesional psoriasis Lesional vs normal
6	• Lung • Heart • Placenta • Kidney • Monocytes • Neutrophils	• Amniotic fluid: $1.49e^4$ • Blood: $1.87e^3$		• Exosomes • Extracellular space • Cytoplasmic vesicle	† Ulcerative colitis † Crohn's disease † Interstitial cystitis (ulcer vs normal) † Tuberculosis (vs normal) † Juvenile dermatomyositis (vs normal) † Interstitial fibrosis and inflammation (vs normal) † Sepsis (vs normal in whole blood) † Periodontitis (vs normal) • Meningococcal sepsis — † At 8 h, 24 h vs normal at 0 h in lymphocytes ↓ At 0 h vs normal at 0 h in monocytes

(Continued)

TABLE 2 | Continued

Human RNase	Main expression tissues and cell types[a]	Presence in biological fluids: rank score or reported level[b]		Subcellular location[c]	Expression regulated by (in comparison with)[d]
					↓ *Francisella tularensis* novicida (vs uninfect) ↓ *Francisella tularensis* schu S4 (vs uninfect) ↓ *Mycobacterium tuberculosis* (vs none in dendritic and macrophage cell at 18 and 48 h) ↓ Newcastle disease virus (at 14, 16, and 18 h vs none at 0 h) ↓ Psoriasis (vs normal) ↓ Septic shock (vs normal) ↓ Burn (middle stage vs control)
7	• Epithelial tissues • Liver • Kidney • Skeletal muscle • Keratinocytes (89, 136) • Basal cells (70)	• Amniotic fluid: $2.69e^3$ • Blood: $3.22e^4$ • Skin washing fluids (44)	Forehead: 0.93 ng/cm^2 Nose: 2.7 ng/cm^2 Arm: 0.94–4.9 ng/cm^2 Palm: 2.0 ng/cm^2 Finger: 1.5 ng/cm^2 Hand back: 2.0 ng/cm^2 Neck: 3.1 ng/cm^2 Calf: 3.4 ng/cm^2	• Exosomes (111, 137, 138) • Extracellular space (43, 84) • Cytoplasm	† Sepsis (vs normal) (112) † Psoriasis (lesional vs normal) † Acute pyelonephritis (84) † Atopic dermatitis (69) † Chronic anal fistula (139) † Nontypeable *Haemophilus influenzae* (70) † *Pseudomonas aeruginosa* (89) † *Staphylococcus aureus* (89) † *E. coli* (89) † *Streptococcus pyogenes* (89) † *Mycobacterium tuberculosis* (140) ↓ Atopic eczema (at skin lesion and normal skin vs normal at normal skin)
8	• Placenta • Spleen (141) • Lung (141) • Testis (141)			• Extracellular space	

[a]*Summary from Uniprot (www.uniprot.org/uniprot/), Genevisible (https://genevisible.com/search), and Human Expression Atlas (https://www.ebi.ac.uk/gxa/home/).*
[b]*Summary from Bgee (https://bgee.org/) (Rank scores of expression calls are normalized across genes, conditions, and species. Low score means that the gene is highly expressed in the condition. Max rank score in all species: $4.10e^4$. Min rank score varies across species).*
[c]*Summary from Uniprot (www.uniprot.org/uniprot/) and Exocarta (www.exocarta.org/).*
[d]*Summary from Human Expression Atlas (https://www.ebi.ac.uk/gxa/home/). Only inflammatory, injury, and infection-related conditions are included (up and downregulation is indicated by arrows).*

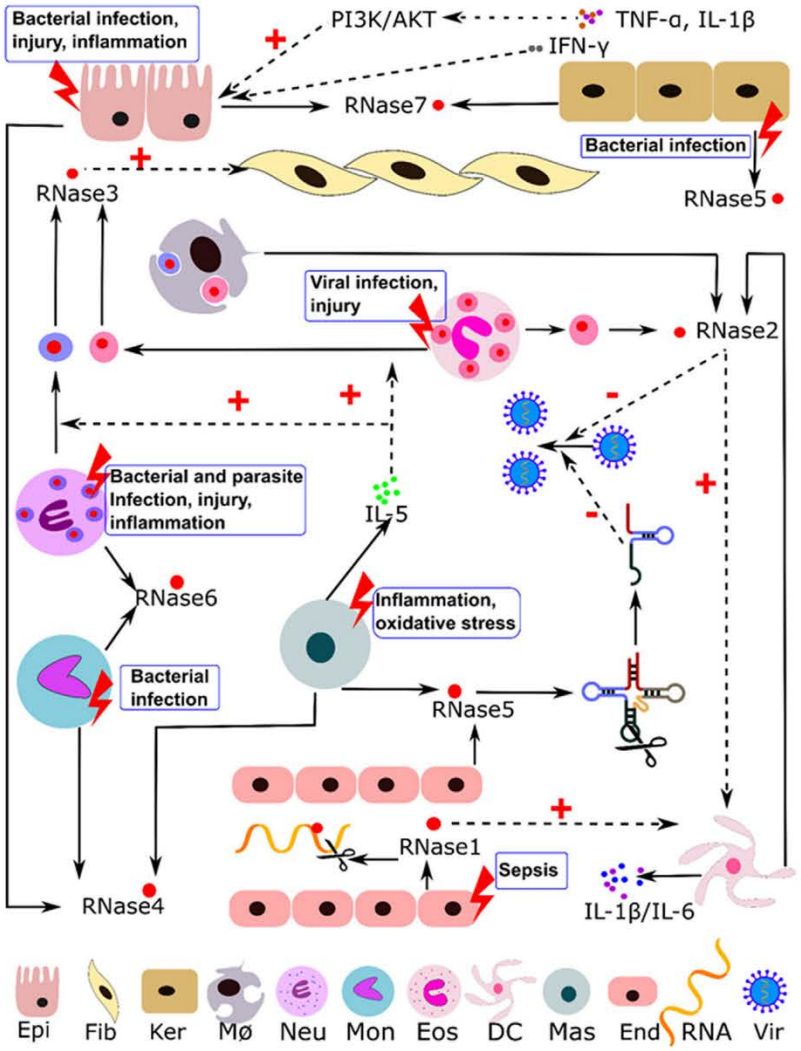

FIGURE 1 | Illustration of the immuno-modulatory properties reported for human RNaseA family members. Induction stimuli, expression cell type, and regulation pathways are indicated. Abbreviations: Epi, epithelial; Fib, fibroblast; Ker, keratinocytes; MØ, macrophages; Neu, neutrophils; Mon, monocytes; Eos, eosinophils; DC, dendritic cells; Mas, mast cells; End, endothelial cells; Vir, virus; dotted line indicates regulation paths and solid line indicates expression and secretion processes.

cells (144, 145), and its presence in blood can modulate the content of exRNA (18, 77). An interesting hypothesis attributes an RNA scavenger role to hRNase1 (77). Supporting this proposal, Raines and co-workers (18) highlight the different optimal conditions for catalysis between ruminant and non-ruminant RNases. Whereas bovine pancreatic RNase shows a slightly acidic optimum pH for catalysis, adapted for working in the digestive tract (4), the observed optimum neutral pH for non-digestive RNases allows their enhanced activity in biological fluids such as blood (18). Likewise, the enhanced capacity to cleave double-stranded RNA (dsRNA) by non-digestive RNases (10, 18) might facilitate the removal of heterogeneous RNAs circulating in blood (18). Interestingly, clearance of exRNA would mitigate its pro-inflammatory activity (76, 77). An excess of exRNA is released in hypoxic conditions, and hRNase1 administration was reported to provide cardiac protection in a mouse model (76). Administration of the protein *in vivo* reduces the release of pro-inflammatory cytokines and provides a multiple-organ protection in mice (29).

hRNase2

hRNase2, together with hRNase3, is one of the main secretory proteins stored within the eosinophil secondary granules (107, 146). This eosinophil protein is partly responsible for eosinophil-induced neurotoxicity, and it is referred to as the eosinophil-derived neurotoxin (EDN), hereafter. In addition, hRNase2/EDN is expressed in other blood cell types (**Table 2**) such as monocytes and dendritic cells (DCs) (107). Expression of the protein is induced by viral infection (100, 107, 147), and

it displays a broad antiviral activity, in particular against ssRNA viruses (104, 107). The protein inhibits the replication of respiratory syncytial (RSV), human immunodeficiency virus (HIV)-1, and hepatitis B DNA virus (100, 102, 103). RNase2 has high catalytic activity, which together with its unique protein structural features (106), is essential for its antiviral action (104). Eosinophil recruitment and degranulation is activated during RSV infection (147), and hRNase2 is a clinical marker for RSV bronchiolitis (148). Interestingly, Weller and co-workers observed the induced release of eosinophil RNases by cytokines such as eosinophil chemotactic proteins (eotaxins CCL11 and CCL24) and through the P13K/MAPK pathway in humans and mice (149). Eosinophil activation by virus infection can be mediated by the toll-like receptor (TLR)7–MyD88 signaling pathway. Likewise, specific expression of the eosinophil RNases following RSV infection in mice is reported to be mediated by the TLR7–MyD88 pathway (55). The TLR7 receptor can be activated by ssRNA, causing the eosinophil RNase to act on viral RNA to enhance the host response against the infection. In addition, viral infection of the respiratory tract is frequently accompanied by lung inflammation and hRNase2 expression. Secondarily, local eosinophil degranulation correlates with tissue damage with eosinophil degranulation activated by tissue injury (**Figure 1**) and the released RNases contributing to the tissue remodeling process (149). Indeed, hRNase2 immuno-regulatory properties can promote leukocyte activation, maturation, and chemotaxis (107). In particular, hRNase2 can contribute to host immunity through interactions with DCs (46, 47). The activation of DCs can be mediated by the TLR2–MyD88 pathway, and hRNase2 is classified as an alarmin (60). Direct protein binding to TLR may occur (107) taking into account the striking shape similarity between the TLR receptor and the RNase inhibitor (RI), both of which have leucine-rich repeat (LRR) domains (150). Human RNase2 and mouse RNases2 are also both expressed in macrophages (**Table 2**) (48, 107). Of note, the mouse eosinophil-associated RNase Ear11 works as a macrophage chemoattractant, although, in this case, the process is not directly mediated by TLR2 activation (48, 107). Because TLRs can interact with ssRNA, we can contemplate a scenario in which RNA pieces bound to RNase2, or, alternatively, the direct action of RNase cleavage products, trigger the TLR signaling cascade. As TLRs can discriminate between self and non-self molecules, cleavage of viral RNA could contribute to the host defense response. Thereby, immune regulation and antimicrobial functions would work cooperatively (151). Eosinophil degranulation during infection and inflammation can contribute locally to both eradicate the infection focus and palliate tissue injury.

hRNase3

hRNase3 is the other eosinophil RNase abundant in the secondary secretory granule, where both RNase2 and 3 together account for about one-third of the total protein content (152). The two human eosinophil RNases share 70% amino acid identity. RNases 2 and 3 emerged from a gene duplication event about 50 million years ago and underwent a divergence process at an extremely rapid rate of evolution (12). During the drift of RNase3 from a common RNase2/3 ancestor, the protein acquired much higher cationicity (pI > 10); therefore, it is called eosinophil cationic protein (ECP). Abundant surface-exposed Arg residues facilitate binding of the protein to bacterial cell membranes and subsequent destabilization through a carpet-like mechanism characteristic of many host defense antimicrobial proteins and peptides (AMPs) (153). RNase3 shares neurotoxic and antiviral activities with RNase2 (105) but it has unique bactericidal properties (86). In particular, hRNase3, together with its high cationicity, has an aggregation-prone region that promotes the protein self-aggregation and mediates the agglutination of bacterial cells (154). Bacterial cell agglutination is further enhanced by high binding affinity of the protein to anionic lipopolysaccharides in the Gram-negative bacterial wall (155). RNase3 release is induced both by infection and inflammation, and several immuno-modulatory activities have been described. The levels of protein circulating in biological fluids (**Table 2**) correlate with eosinophil degranulation, and it is currently used as a routine clinical marker for the diagnosis and monitoring of inflammatory disorders, such as asthma (51, 52). Airway inflammation is closely associated with eosinophil degranulation and local tissue damage follows the deposition of eosinophil secondary granule protein (156, 157). The levels of this protein are also associated with damaged airway epithelia (52). Further, skin ulceration follows eosinophil infiltration, and local protein deposits harm epithelial cells (121, 158, 159). Fortunately, the detrimental side effects of the protein tissue deposits are followed by remodeling processes. RNase3 remodeling activity is partly mediated by the upregulation of the insulin growth factor-1 receptor on epithelial cells. In addition, hRNase3 activation and chemotaxis of fibroblasts can contribute to tissue repair (49, 62, 160). Nevertheless, fibroblast activation can also lead to airway fibrosis, as observed during chronic eosinophil inflammation in asthma (49). Interestingly, a population study identified a natural genotype variant of hRNase3 (ECP97Arg) with enhanced cytotoxicity that was linked to a higher frequency of fibrosis (161). Despite the higher antimicrobial activity of the Arg97 variant, genetic selection toward a less toxic protein must have taken place in a chronic parasite infection in endemic areas of Asia to reduce the incidence of liver fibrosis (162). The Arg to Thr substitution at position 97 of hRNase3 results in a new potential N-glycosylation site at a nearby Asn residue (163). Additional glycosylation at this site blocks the cationic domain that participates in the protein antimicrobial activity (164). Similarly, a correlation between hRNase3 polymorphisms and cerebral malaria susceptibility was observed (165, 166).

Together with direct hRNase3 action on pathogens and host tissues, a series of immune-modulating activities are observed (51, 52). Eotaxin attracts eosinophils to the area of inflammation, i.e., lung in asthma, nasal mucosa in allergic rhinitis, skin in dermatitis, or gut epithelia in intestinal bowel diseases. Eosinophil degranulation is activated by IL-5, leukotriene B4 (LTB4), platelet activating factor (PAF) (52), or the P13K/MAPK pathway (149). Early experimental assays also showed mast cell activation by hRNase3 and the induction of histamine release (50). In turn, mast cells produce and secrete IL-5, PAF, and LTB4, which enhance hRNase3 release from eosinophils. Moreover, hRNase3 induces the synthesis of prostaglandin D2 by mast cells, which then acts as an eosinophil chemoattractant. This process suggests cross talk between mast cells and eosinophils, with RNase able

to promote positive feedback (52). Other leukocyte cells such as neutrophils can also express hRNase3 (**Table 2**). Interestingly, free granules released by both eosinophils and neutrophils maintain their autonomy and functionality (167) and selectively secrete RNases upon cytokine induction (168). Moreover, the extracellular granules can also be engulfed by macrophages (**Figure 1**) and contribute to the immune response.

hRNase4

hRNase4 is one of the oldest representative RNase A family members within mammals, showing a static evolution history in comparison with the other family counterparts (33). RNase 4, together with RNase 5, shares some conserved structural features with non-mammalian vertebrates RNases, such as the first pyroglutamic N-terminal residue (169). Moreover, there are no reported glycosylation forms and no recognition sites for N-glycosylation (169). RNase4 retains the highest inter-species homology, close to 90%, within the family members (33, 170). Nearly ubiquitous distribution suggests a housekeeping role for this protein. The presence of hRNase4 transcripts was detected in most human tissues (143, 171) and was found particularly abundant in the liver (143) and lungs (169). Interestingly, cytoplasmic granules of monocytes also express this RNase (172). Divergence and diversification events within the oldest mammals suggest a strong evolutionary pressure that may respond to host adaptation to an ever-changing pathogen environment. In this scenario, duplication of the RNase4 gene in ancestral mammals may have led to other RNaseA family lineages that acquired a host defense function (33). There is a controversy about the physiological role of the protein. On one side, its conservation among species suggests strong evolutionary pressure to maintain an essential role. Cleaning-up of cellular RNA was first proposed (173). However, the enzyme showed enhanced preference for uridine at the main base binding site (169, 173, 174), suggesting strong selectivity for RNA recognition (169). A structural analysis highlighted particular structural features at the main base binding pocket that determine the protein enhanced preference for uridine over cytidine in comparison to other family members (174, 175). Although considerable work has been undertaken to interpret RNase4 substrate specificity, there are few reports on the biological properties of the protein. Interestingly, RNase4 was identified, along with RNase5, among the soluble factors secreted by T cells showing anti-HIV activity (176).

hRNase5

hRNase5 is considered the most ancient RNaseA family member, and it shares many structural features with non-mammalian vertebrate RNases. It is unique within the family in presenting six paired cysteine residues instead of eight. In addition, it shows rather atypical enzymatic properties, with very low catalytic efficiency for ssRNA but selective cleavage for some non-coding RNA (41, 177, 178). Its expression was detected in many adult and embryonic somatic cells (179). It was also reported in a variety of innate cells, ranging from diverse blood cell types to intestinal and skin epithelial cells (**Table 2**) (28, 67, 129, 180). Further expression of this protein is increased during inflammation (129, 181). RNase5 promotes angiogenesis and is, therefore, termed angiogenin (65). The purified protein was reported to display other activities, such as antimicrobial action (67, 88) and some immuno-regulatory properties (88, 182), in addition to the induction of vascularization. In particular, the protein inhibits neutrophil degranulation, a process that might induce an anti-inflammatory effect during immune response (183, 184). Interestingly, this degranulation inhibitory action was mimicked by a short tryptic peptide (183), indicating a protein activity unrelated to its enzymatic function. On the other hand, angiogenesis relies on hRNase5 catalytic activity and is inhibited by the RI (185). Distinct immuno-regulatory activities were observed to be dependant on the action of the protein on non-coding RNA, i.e., cleavage of tRNA and upregulation of rRNA. Upon nuclear translocation hRNase5 can stimulate the proliferation of several cell types, such as endothelial cells (66), by regulating rRNA transcription (63, 186). In addition, angiogenesis and cell proliferation are mediated by the activation of cellular signaling kinases such as the ERK1/2 (179, 187). In addition, hRNase5 expression is activated in response to cellular stress and promotes the formation of stress granules. The protein generates stress-induced tRNA fragments (tRFs) (tiRNA) (6, 56, 58). In turn, the tiRNA fragments can impede the formation of the translation initiation factor complex, thereby inhibiting translation (188). Accumulation of tiRNA activates the cell response to oxidative stress (59). The release of tRFs associated with hRNase5 activity is also a characteristic feature linked to endoplasmic reticulum (ER) stress, a condition that can be triggered by the accumulation of unfolded/misfolded proteins in the ER lumen (57). Likewise, hRNase5 induces the release of tiRNA by stem cells and activates hematopoietic cell regeneration (28). Generation of tRFs is also observed upon viral infection (189). Using deep sequencing methodologies, the enzyme cleavage target sites are being identified (5, 6, 39). Two tRNA halves can be produced by a unique enzymatic cut at the anticodon loop (5, 6, 58, 190). In addition, Li and co-workers observed a unique cleavage by hRNase5 at the tRNA TΨC loop (39); the resulting 3′-tRNA fragment was complementary to an endogenous human genome sequence, and the fragment was found to downregulate retroviral expression by RNA interference (39). However, potential therapeutic applications for hRNase5, such as hematopoiesis regeneration or antiviral activity (28), should be viewed with caution, considering its protein pro-tumoural properties (65). In particular, upregulation of rRNA transcription has been related to cancer cell proliferation (63, 64). A recent work correlated elevated hRNase5 expression in some tumor cell lines with the promotion of cell proliferation and development of malignant cancer (64). In addition, elevated levels of tiRNA were also observed in some cancers (190) with tRFs inducing tumorigenesis (188).

hRNase6

hRNase6, also named hRNasek6, was identified for the first time by Helen Rosenberg and Kimberly Dyer as a human ortholog of bovine kidney RNasek2 (191). The first tissue screening study to define hRNase6 expression patterns revealed a nearly ubiquitous distribution, including monocytes and neutrophils (191). The expression of this protein is upregulated following genitourinary tract bacterial infections (83) and high antimicrobial activity

against Gram-positive and Gram-negative species was observed (83, 90). Very recently, hRNase6 antiviral activity was reported. Interestingly, the authors observed the protein downregulation in Th17 polarized cells upon HIV infection (192).

hRNase7

hRNase7 is probably the best studied example of an RNase that can work as a tissue safeguard sentinel (**Table 1**). It is also one of the most abundant antimicrobial proteins purified from skin (44, 79). RNase7 is secreted by a variety of epithelial cells (**Table 2**) and mostly contributes to urinary tract sterility and epidermis protection (43, 80–82). Together with high antimicrobial activity against a variety of infective microorganisms (82, 87, 89, 193), some immuno-modulatory properties were reported. RNase7 expression is upregulated during kidney infection (84). Expression is also selectively induced by inflammation signaling molecules, such as IL-1β and IFN-γ (89) or the PI3K/AKT pathway (194). The PI3K/AKT signaling pathway can modulate the innate immune response during inflammation and prevent sepsis (195, 196). Interestingly, expression of this protein in the urinary tract can be upregulated by insulin through the PI3K/AKT pathway (197). Spencer and co-workers correlated expression with increased susceptibility to infection of diabetic patients (197). Indeed, insulin induces the secretion of granulocyte content and impairment of the expression of other AMPs, which are also associated with diabetes (198). Of note, the regulation of protein expression by the P13K/AKT pathway is also observed with eosinophil-associated RNases (EARs) (149). On the other hand, RNase7 is abundantly secreted by keratinocytes (43, 44, 79) and can contribute to wound healing and tissue repair (67, 68). Protein overexpression in skin can be induced by inflammation and infection diseases (69, 81). Interestingly, protease degradation of the RI at the stratum corneum can activate hRNase7 for skin barrier protection (67). Finally, expression of the protein was recently reported to be induced in basal cells of damaged airway epithelia, reinforcing the idea of a protective role for this protein following tissue injury (**Table 1**) (70). A very recent study showed that this protein directly stimulated plasmocytoid DCs following tissue damage and infection, and the authors of the report proposed to classify hRNase7 as an alarmin (54). Interestingly, the immuno-modulatory activity of the RNase correlates with binding to self-DNA and activation of TLR9 receptors. The authors suggest that following tissue damage, hRNase7 detects the host DNA released by dying cells and activates the host response (54).

hRNase8

hRNase8 is the last identified and least well-characterized canonical member of the RNaseA superfamily. It was first uniquely identified in the placenta (199). Wide spectrum antimicrobial activity was observed for this protein (91), suggesting a role in amniotic fluid protection against infection. Indeed, hRNase7, the closest homolog to hRNase8 in the RNaseA family, was found recently among AMPs expressed in prenatal skin, suggesting it may contribute to amniotic cavity sterility (200). However, despite sharing a high sequence identity with hRNase7, hRNase8 shows highly reduced catalytic activity (199). A particular cysteine location within its primary sequence indicates a unique disulfide bonding among the family members. An evolutionary analysis in primates revealed a sequential cysteine gain-and-loss process, representing an unusual example of disulfide bond reshuffling (201). In addition, the protein shows an elevated rate of incorporation of non-silent mutations in its primary structure (202) suggesting functional divergence toward a distinct physiological role (141). Moreover, a unique extension at the hRNase8 N-terminus may indicate that the protein is not undergoing the secretion process shared by all other canonical members of the family (141). Recent evidence of hRNase8 gene expression in other additional tissues, such as the lung, liver, and testes (141), together with controversial reports on its recombinant protein antimicrobial activity (91, 199), urges a reconsideration of the function of this protein.

hRNases 9–13

The RNaseA superfamily was lately expanded with the discovery of several novel mammalian members (11, 203–205). The newcomers share just 15–30% identity with the eight "canonical RNases," and they are associated mainly with male reproductive functions. Some of them, like hRNase9, are endowed with bactericidal activity and are expressed in the epididymis, with evidence of an association with sperm maturation (33, 206). The primary structure of these proteins resembles ancestral RNases, sharing the three most conserved disulfide bonds and a secretion peptide, but not the N-terminus region of mature proteins. In addition, the non-canonical RNases do not include the family signature (CKXXNTF) or the catalytic triad and their biological properties do not seem to require enzymatic activity (207).

Other Vertebrate RNaseA Family Members

The RNaseA superfamily is one of the most extensively studied gene family, since the pioneering studies on molecular evolution (208). As a vertebrate-specific family, it is an excellent working model and a deep analysis has been carried out to understand the main driving force toward a defined function in mammals (11, 33, 209, 210). Further, we will briefly comment on the non-human family members present in the extracellular compartment and displaying immune modulation properties. In particular, bovine proteins are the best characterized, being the RNaseA the bovine counterpart of human RNase1. RNaseA, the bovine pancreatic RNase1, is expressed in large amounts in the pancreas and participates in RNA degradation in the digestive tract (3).

Bovine Seminal RNase (BS-RNase)

Bovine seminal RNase is a close homolog to bovine pancreatic RNase that is solely present in seminal fluid (211), where it plays an immune-protective role (182). BS-RNase, despite sharing an 80% amino acid identity with the pancreatic RNaseA, is the only family member present *in vivo* as a homodimer. Owing to its natural dimeric form, BS-RNase can elude the blockage of the cytosolic RI in case of cellular internalization following endocytosis. The high cytotoxicity of the protein (212) is attributed to the degradation of cellular RNA (213). In addition, the dimerization of BS-RNase and RNaseA constructs correlates with an enhanced catalytic activity and the ability to cleave dsRNA (214–216). Degradation of dsRNA by BS-RNase is induced by IFN (217, 218) and the protein can inhibit HIV-1 replication in leukemia

cells (219). Interestingly, engineered quaternary structures of RNaseA can not only mimic BS-RNase enzymatic cleavage of dsRNA, but also some of its biological properties (220, 221). The seminal RNase also differs from its pancreatic homolog by its ability to inhibit the proliferation of cancer cells mediated by autophagy induction (72). BS-RNase also inhibits the proliferation of T-lymphocytes (222, 223) and can downregulate the T cell IL-2 receptor expression (222). However, the immune-protective mechanism of BS-RNase in the seminal fluid remains unknown (182).

Bovine Milk RNases

Bovine milk RNases are another group of secretory RNases that mediate an extracellular protective role. Two proteins with RNase activity homologous to human RNases 4 and 5 were identified in bovine milk (224, 225). Both RNases were quantified in bovine milk at μM concentrations and reported to display some antimicrobial activity (225). Bovine milk RNases can participate in the host response against infection both by direct antimicrobial action and immune response activation (182). A pro-inflammatory activity is observed in epithelial cells, which is mediated by nucleic acids (53, 226). Both RNases can bind nucleic acids, and milk RNase5 induces cytokine release in leukocytes (53). Recognition of foreign pathogen nucleic acids may facilitate the activation of pattern recognition receptors and promote a pro-inflammatory response (226). Interestingly, the RNase immuno-stimulatory activity is also dependent on the protein catalytic activity (226).

Rodent RNases

Rodent RNases are another well characterized group that can help us to outline the RNaseA family involvement in the host immune response (11). Lineages of RNases 1, 2, 3, and 5 are identified in rat and mouse genomes, presenting an unusual expansion rate (11, 207, 227–229). However, no orthologs of RNases 7 and 8 have been found (11, 33). Particularly, a striking diversity of RNases 2 and 3 counterparts is observed in mice and rats. Two orthologs of the eosinophil RNases lineage were first discovered in 1996 and named EARs (230). Subsequently, up to 13 new eosinophil murine members were identified (231). The phylogenetic analysis of the distinct EAR rodent gene clusters revealed a rapid gene duplication and selection process that resulted in high diversification, a characteristic pattern of host defense protein lineages (232). Many of these EAR proteins, despite their nomenclature, are not solely secreted by eosinophil granules but can also be expressed by other cell types. For example, mEAR11 is expressed in somatic tissues, such as lungs, liver, or spleen, along with macrophages. The protein expression is induced in response to Th2 cytokines and it acts as a potent leukocyte chemoattractant (48). The immune regulation of eosinophil release of granule proteins in mice has been thoroughly studied by Weller and colleagues (149, 168). EARs similar to their human counterparts actively contribute to the host defense and tissue repair and remodeling. However, significant differences are observed in the regulation mechanism of eosinophil degranulation, limiting the use of laboratory animal models in the study of human eosinophil-associated diseases (233–235). Nonetheless, experimental studies in mice corroborate the autonomy of eosinophil cell-free granules and their activation by a common CCR3-mediated signaling pathway (149, 168). EARs can also provide immune protection against virus infection *in vivo* in a mice model, where the eosinophil activation and virus clearance is mediated by a TLR7-signaling pathway (55).

In addition, several homologs to human RNase5 endowed with antimicrobial properties were identified in mouse intestinal epithelium (88). In particular, the upregulation of the mouse RNase Ang4 by commensal bacteria suggests a role for this protein in the gut and systemic innate immunity, where it can establish a host defense barrier against infection (88).

Rosenberg and colleagues went further down the evolution scale and characterized avian and reptilian RNases to deepen the understanding of the role of vertebrate RNaseA family in host immunity (13, 16, 236). As mentioned previously, non-mammalian RNases are evolutionarily closely related to mammalian RNase5 members (11). Two leukocyte-associated homologs were identified in chicken, RNases A1 and A2, the last one displaying both angiogenic and bactericidal properties (13). On the other hand, the *Iguana* RNase is catalytically active but devoid of antimicrobial activity (236).

Frog RNases

Frog RNases are secreted by oocytes and early embryos and might protect the eggs against infection (237–241). The observed anti-proliferative properties of the RNases from early vertebrates have attracted the interest of pharmaceutical companies since their discovery (242, 243). *Rana pipiens* RNase, named Onconase® (ONC) after its anti-tumoural activity, is currently on phase III clinical trial. The anti-proliferative action of ONC on cancer cells is mediated by induction of the autophagy pathway (71), as reported for BS-RNase (72). Recently, its cytotoxicity was enhanced by promoting its dimerization (244). The anti-tumoural activity of ONC has also been attributed to its action on microRNA (miRNA) precursors (40). On the other hand, the frog RNase inhibits the replication of HIV-1 through directly targeting the viral RNA and host cellular tRNA (245, 246). A specific excision on host Lys-tRNA inhibits the virion replication (101). A common tRNA targeting mechanism might be shared with the oldest mammalian RNases. Moreover, a similarity between the structural fold of tRNA and miRNAs that are targeted by the frog RNase suggests that the RNA recognition and cleavage requires specific primary and secondary structures (40).

Finally, identification and characterization of fish RNases completes the overall picture of the vertebrate RNaseA family (15, 247, 248). RNases identified in zebrafish (ZF-RNases) shared the bactericidal, angiogenic and reduced catalytic properties of hRNase5 (247). Catalytic activity for ZF-RNase5 was required for angiogenesis but not for antimicrobial action (247). Interestingly, ZF-RNases 1 to 3 can activate the ERK1/2 kinase pathway similar to hRNase5 (249). Recently, the expression of several RNase2 and RNase3 paralogs in the pond-cultured blunt snout bream fish induced by bacterial infection was reported (250).

OTHER EXTRACELLULAR RNases

RNases T2: A Family of Ancient Extracellular RNases

RNaseT2 family, in contrast with the RNaseA family, comprises a group of proteins conserved from virus to humans, suggesting a shared preserved function (31). The biological properties of human RNaseT2 have been extensively studied. The RNase that works as a signaling molecule and is secreted by damaged tissues has being classified as an alarmin (61). RNaseT2 is stored in the lysosomal compartment and contributes to the clearance of cellular macromolecular debris. Its secretion can be induced by oxidative stress and it participates in the regulation of immune response. RNaseT2 is proposed to work as an RNA scavenger in the extracellular compartment (31). Moreover, the human RNaseT2 shows macrophage chemotaxis (30) and tissue remodeling activities *in vitro*. Similarly, the RNaseT2 secreted by the eggs of the parasite *Schistosoma mansoni*, also named Omega-1, can induce the release of pro-inflammatory cytokines by macrophages during infection (251). Omega-1 can be internalized into DCs and regulates their programming pathway by the RNase-mediated cleavage of rRNAs and mRNAs and subsequent impairment of protein synthesis. Another RNaseT2 family member that has been well characterized is the yeast RNaseT2, named Rny1, which is stored in cell vacuoles, similar to the storage of other RNaseT2 members in lysosomes, and shows a selective tRNA cleavage under oxidative stress equivalent to the activity reported for hRNase5 (56). In addition, yeast RNaseT2 combines its enzymatic action with other non-catalytic properties such as binding to regulatory proteins and the destabilization of lysosomal membrane, a mechanism that can trigger the programmed cell death (56, 252). Overall, we observed common properties between the RNaseA and the RNaseT2 family members, e.g., release of stress-induced tiRNA, leukocyte activation, or exRNA scavenging (30, 31, 56, 250).

Plant Self-Incompatibility RNases (S-RNases)

Plant S-RNases prevent self-fertilization and avoid inbreeding. S-RNases exert cytotoxicity against the growing pollen tube by targeting rRNA (253, 254). Each plant is endowed with specific recognition patterns that can block the RNase activity of all the S-RNases except its own, ensuring the degradation of pollen grains corresponding to its haplotype (255). Interestingly, S-RNases exhibit a specific catalytic activity on tRNA when the plants are exposed to stress (256).

Bacterial RNases as Inter-Strain Competition Toxins

Going further down the evolutionary scale, we can find a wide variety of bacterial RNases that participate in the bacterial defense against external threats, e.g., presence of a competing bacterial species, viral infection, or the defense response of the infected host cell. Bacterial RNases can work as powerful toxins selectively targeting coding and non-coding RNAs (257–259). Among the non-coding RNAs, the specific cleavage of tRNAs is a conserved regulatory mechanism shared from bacterial to mammalian cells (56). Stress-induced tRNA cleavage is reported for the *Escherichia coli* endoribonuclease Prrc in response to bacteriophage infection (260). Colicins are another group of *E. coli* cytotoxic tRNases that block the protein synthesis machinery as a defense mechanism against other microbial competitors (261). Interestingly, comparison among the bacterial RNases suggest an evolutionary convergence to acquire structural features that enable the targeting of the tRNA anticodon loop (261). In simple eukaryotes, such as the protozoa *Tetrahymena*, and the budding yeast *Saccharomyces cerevisiae*, the release of specific tRFs during starvation is also reported (256, 262). We can establish a parallelism between the release of stress-induced tiRNA by prokaryotes, primitive eukaryotes, and human RNase5 (6), as a mechanism to downregulate protein synthesis. An intriguing question arises: have the host defense mechanisms of vertebrate RNases evolved from the ancestral prokaryotic inter-strain competition processes? Although the RNaseA superfamily is vertebrate-specific, the recent report of the structure of a bacterial RNase involved in inter-strain competition highlights a shared protein scaffold shaped for RNA recognition (32). However, the lack of sequence identity between bacterial and vertebrate RNases and the absence of any putative invertebrate intermediate suggests a convergent evolution (32, 263). Thus, the origin of the RNaseA superfamily remains unknown. In contrast, the RNaseT2 family conserves its ancestral lineage from prokaryotes to humans (56).

Similarities between unicellular self-defense and mammalian innate immune mechanisms can provide novel strategies to boost our own immune response. For example, macrophage immune regulation by *Bacillus* RNase (binase) can trigger the host cell antitumor response (19) and the RNaseT2 of the *Schistosoma* parasite can modulate the host response (250) and prevent the outbreak of autoimmune diseases or diabetes (264, 265). Understanding the uniqueness of RNases and their specificity for cellular RNAs will lead to the development of novel therapeutics.

RNase TRAFFIC IN THE EXTRACELLULAR SPACE

Extracellular RNases are released as secretory proteins by diverse pathways into the extracellular compartment. Recent advances in histochemical and cell analytical methodologies have unveiled the structural and functional complexity of the extracellular space. A rich world of secretory storage granules, transport vesicles, and intracellular vacuoles ensures that the organism is fit to respond to external stimuli.

Compartmentalization

Compartmentalization of RNA and RNases is an important regulatory mechanism (266). RNases packed within secretory granules will be selectively released upon action by diverse stimuli (see **Figure 1**). In particular, eosinophil degranulation has been thoroughly investigated and several secretory mechanisms have been described (267). Intracellular granules can undergo piecemeal degranulation, whereby small packets of derived vesicles are mobilized toward the cell surface for secretion (231). Alternatively,

the cell storage granules can be freed as independent entities. Free extracellular eosinophil granules can actively release their content upon cytokine activation (167). Weller and co-workers have extensively characterized the signaling pathways that mediate the release of RNases by the free extracellular eosinophil granules in humans and mice (149, 168). Free eosinophil granules can be internalized by other innate cells, such as macrophages (**Figure 1**) and thereby participate in the regulatory pathways of the recipient cell. Extracellular RNases can also find a way back into cells through the endosomal pathway (240, 268). Fortunately, the cytosolic compartment of cells is protected from the potential toxicity of RNaseA superfamily members by the action of the RI, which constitutes about 0.1% of the total protein content in the cytosol of mammalian cells (269). The RI is expressed in all studied human tissues (143) and binds with an extremely high affinity to mammalian RNaseA family members (in the fM range) (270, 271). Interestingly, Raines and co-workers (270) identified the avian and reptilian counterparts of mammalian RI but no equivalent protein was detected in amphibians and fish, suggesting a specific role for RI in higher order vertebrates (270). Recent RI-knockout experiments confirmed the protective action of RI toward cytosolic RNA against endocytosed RNases (272). The inhibitor structure adopts a horseshoe conformation composed of LRRs and exposed free cysteine residues. The inhibitor is functional in its fully reduced state and is extremely sensitive to cellular oxidative stress. RI inactivation by partial oxidation can work as a mechanism to switch on the RNase-mediated degradation of cellular RNA under stress conditions (56, 270). For example, RI participates in the regulation of hRNase5 subcellular localization during stress conditions. Under stress, the cytosolic hRNase5 is liberated from the RI complex, whereas the nuclear protein is bound to the inhibitor, thereby downregulating cell growth (272). Interestingly, the hRNase5 evasion of the cytosolic RI and migration to the nucleolus is also mediated by phosphorylation (273). RI can also participate in the regulation of RNases expressed at the epidermis (67). The secreted RNases in the skin provide a protective barrier against invading pathogens. Degradation of RI by proteases at the stratum corneum can liberate the RNases' antimicrobial action during infection (67, 274). Regulation of RNase activity by RI in the urinary tract has also been proposed by Spencer and co-workers (275).

Intercellular Communication

Nowadays, novel methodologies have led to better understanding of the functions of the extracellular compartment and have proposed previously undescribed roles for secretory proteins. RNases secreted by diverse stimuli (**Figure 1**) can participate in intercellular communication in an organism (56). Of note, some RNaseA family members have been detected within extracellular vesicles (117, 276, 277) (**Table 2**) and selective RNA packaging into the vesicles has been observed (278). This brings us back to the pioneering biochemical work on the pancreatic RNaseA family (3). The identification of the angiogenic activity of hRNase5 and the suspicion that angiogenic factors might contain RNA (279) hinted that exRNA might work as an intercellular communicator (1). Novel sequencing methodologies confirmed hRNase5 selective cleavage of non-coding RNAs and the involvement of the released products in immune regulation pathways (57). Other pancreatic RNase family members may also have evolved to acquire a non-digestive role and may contribute to the regulation of the circulating exRNA content in blood (18, 280). James Lee proposed that during vertebrate evolution the mechanism of action of granulocyte proteins might have evolved from mere localized action to an organized systemic response mechanism. The increase in size and complexity of multicellular organisms is accompanied by long distance stress signaling processes. In this context, secretory RNases originally recruited at the damaged tissue site to remove cellular RNA debris from dying cells could have acquired a selective anti-pathogen activity to provide the host protection against infection. An amoeboid-type secretory blood cell initially adapted to localized response and tissue repair duties would have acquired novel properties, allowing isolated tissue cells to communicate over an extended distance and participate in the overall systemic response (17).

ROLE IN HEALTH AND DISEASE

Overall, extracellular RNases display a variety of immune-related activities that ensure that the organism is fit for survival. The RNases participate in diverse tasks, from cellular housekeeping to ensuring the sterility of body fluids (**Table 1**). Following tissue damage by an external injury the RNases are expressed as alarm signaling molecules (54, 60, 61). Their secretion at the inflammation site contributes to tissue repair and remodeling (52, 62). To participate in the tissue healing process, the RNases can target and remove the host-damaged cells. Selective cytotoxicity can be mediated by the activation of autophagy or apoptotic pathways (72, 75). To facilitate subsequent tissue remodeling, the RNases also function as cytokines and chemokines, displaying anti-inflammatory activities and inducing chemoattraction of innate cells, such as macrophages or DCs (29, 46–48). Other complementary activities have been reported such as binding to nucleic acids, activation of TLR receptors and removal of exRNA (54, 55, 76).

RNases' expression can also be induced during infections and the secreted RNases can directly participate in the killing of invading microorganisms (42, 84, 89) (**Table 1**). Overall, we observed an organized distribution of tasks among the distinct host innate cells that can ensure the coverage of wide spectra of potential pathogens. On the other hand, there is also a downregulation in RNases' expression after extended periods of infection (**Table 2**). A close inspection of the RNases' expression patterns suggests an adaptive process by the intracellular-dwelling pathogens to inhibit the host response and extend their survival lifespan.

Fortunately, extensive research on secretory RNases is currently setting the basis for applied therapies. Clinicians are already taking advantage of the selective secretion of RNases for monitoring and diagnosing inflammation. RNase3 levels are routinely used to monitor asthma processes (51). Levels of hRNase1, hRNase3, and hRNase7 are increased during sepsis and are proposed as markers for the diagnosis of organ failure (112). Another interesting proposal is the use of RI as a cancer biomarker (281).

Furthermore, successful results achieved using experimental animal models promise therapeutic applications in the near future. Removal of circulating exRNA shows beneficial

anti-inflammatory properties following tissue damage (17, 29, 76). In particular, removal of blood exRNA can protect cardiac tissue in hypoxic conditions (29, 76). Treatment with hRNase1 has been observed to reduce deposits of exRNA and inflammation in a mouse model of atherosclerosis (78). RNases can also determine the fate of RNA stress granules. Under stress conditions, hRNase5 accumulates within stress granules (282). Local accumulation of RNA and alteration of RNA self-assembly is associated with neurodegenerative diseases (283). Selective cleavage of cellular RNAs mediates response to stress stimuli (56, 57). Overall, deregulation of non-coding RNA processing is a major cause of immune-malfunctioning and serious diseases (284).

Some RNaseA members can participate in biological functions such as hematopoiesis and angiogenesis, and show anti-tumoural properties mediated by selective cellular RNA targeting (6, 40, 285). The design of RNase constructs to develop specific immunotoxins that selectively target cancer cells is currently one of the most prioritize research topics. ImmunoRNases are engineered to be internalized by tumor cells, evade RI, and degrade cellular RNA (26, 269, 286–289). A recent nanocarrier delivery system using encapsulated RNaseA effectively achieves inhibition of cancer cell proliferation (290).

RNases can also maintain the sterility of biological fluids (100, 285). Eosinophils are involved in antiviral immunity and eosinophil RNases might mediate host response by TLR7 activation (55). Expression of hRNase2 is induced by HIV-1 infection and recombinant hRNase2 administration is proposed as an anti-HIV-1 therapy (100).

CONCLUSION AND PERSPECTIVES

The overview of the immuno-regulatory properties of secretory RNases highlights the similarities between their mechanisms of action and provides novel approaches to progress toward a deeper understanding of their ultimate *in vivo* biological role. We are confident that any step forward in this direction can consolidate our knowledge of the innate immune system and contribute to the development of novel treatments against immunological deregulations. In particular, the biological roles of RNases, such as in hematopoiesis regulation, tissue remodeling, prevention of infection and inflammation offer promising therapeutic applications.

AUTHOR CONTRIBUTIONS

LL, JL, MM, and EB contributed to the original draft and edited versions. LL and JL prepared the tables and graphical material. MM and EB wrote, edited, and revised the final manuscript version. All authors approved the final manuscript version.

FUNDING

Research work was supported by the *Ministerio de Economía y Competitividad* (SAF2015-66007P) and by *AGAUR*, Generalitat de Catalunya (2016PROD00060; 2017SGR1010), co-financed by FEDER funds. LL and JL are recipients of a CSC predoctoral fellowship.

REFERENCES

1. Benner SA. Extracellular "communicator RNA". *FEBS Lett* (1988) 233:225–8. doi:10.1016/0014-5793(88)80431-9
2. Benner SA, Allemann RK. The return of pancreatic ribonucleases. *Trends Biochem Sci* (1989) 14:396–7. doi:10.1016/0968-0004(89)90282-X
3. Barnard EA. Biological function of pancreatic ribonuclease. *Nature* (1969) 221:340–4. doi:10.1038/221340a0
4. Zendzian EN, Barnard EA. Distributions of pancreatic ribonuclease, chymotrypsin, and trypsin in vertebrates. *Arch Biochem Biophys* (1967) 122:699–713. doi:10.1016/0003-9861(67)90180-4
5. Fu H, Feng J, Liu Q, Sun F, Tie Y, Zhu J, et al. Stress induces tRNA cleavage by angiogenin in mammalian cells. *FEBS Lett* (2009) 583:437–42. doi:10.1016/j.febslet.2008.12.043
6. Yamasaki S, Ivanov P, Hu GF, Anderson P. Angiogenin cleaves tRNA and promotes stress-induced translational repression. *J Cell Biol* (2009) 185:35–42. doi:10.1083/jcb.200811106
7. Raines RT. Ribonuclease A. *Chem Rev* (1998) 98:1045–65. doi:10.1021/cr960427h
8. Cuchillo CM, Nogués MV, Raines RT. Bovine pancreatic ribonuclease: fifty years of the first enzymatic reaction mechanism. *Biochemistry* (2011) 50:7835–41. doi:10.1021/bi201075b
9. Beintema JJ, Gaastra W, Lenstra JA, Welling GW, Fitch WM. The molecular evolution of pancreatic ribonuclease. *J Mol Evol* (1977) 10:49–71. doi:10.1007/BF01796134
10. Jermann TM, Opitz JG, Stackhouse J, Benner SA. Reconstructing the evolutionary history of the artiodactyl ribonuclease superfamily. *Nature* (1995) 374:57–9. doi:10.1038/374057a0
11. Cho S, Beintema JJ, Zhang J. The ribonuclease A superfamily of mammals and birds: identifying new members and tracing evolutionary histories. *Genomics* (2005) 85:208–20. doi:10.1016/j.ygeno.2004.10.008
12. Zhang J, Rosenberg HF, Nei M. Positive Darwinian selection after gene duplication in primate ribonuclease genes. *Proc Natl Acad Sci U S A* (1998) 95:3708–13. doi:10.1073/pnas.95.7.3708
13. Nitto T, Dyer KD, Czapiga M, Rosenberg HF. Evolution and function of leukocyte RNase A ribonucleases of the avian species, *Gallus gallus*. *J Biol Chem* (2006) 281:25622–34. doi:10.1074/jbc.M604313200
14. Pizzo E, D'Alessio G. The success of the RNase scaffold in the advance of biosciences and in evolution. *Gene* (2007) 406:8–12. doi:10.1016/j.gene.2007.05.006
15. Cho S, Zhang J. Zebrafish ribonucleases are bactericidal: implications for the origin of the vertebrate RNase a superfamily. *Mol Biol Evol* (2007) 24:1259–68. doi:10.1093/molbev/msm047
16. Rosenberg HF. RNase A ribonucleases and host defense: an evolving story. *J Leukoc Biol* (2008) 83:1079–87. doi:10.1189/jlb.1107725
17. Lee JJ, Lee NA. Eosinophil degranulation: an evolutionary vestige or a universally destructive effector function? *Clin Exp Allergy* (2005) 35:986–94. doi:10.1111/j.1365-2222.2005.02302.x
18. Lomax JE, Eller CH, Raines RT. Comparative functional analysis of ribonuclease 1 homologs: molecular insights into evolving vertebrate physiology. *Biochem J* (2017) 474:2219–33. doi:10.1042/BCJ20170173
19. Makeeva A, Rodriguez-Montesinos J, Zelenikhin P, Nesmelov A, Preissner KT, Cabrera-Fuentes HA, et al. Antitumor macrophage response to bacillus pumilus ribonuclease (Binase). *Mediators Inflamm* (2017) 2017:4029641. doi:10.1155/2017/4029641
20. Matzinger P. An innate sense of danger the signals that initiate immune responses. *Semin Immunol* (1998) 10:399–415.
21. Wu D, Yu W, Kishikawa H, Folkerth RD, Iafrate AJ, Shen Y, et al. Angiogenin loss-of-function mutations in amyotrophic lateral sclerosis. *Ann Neurol* (2007) 62:609–17. doi:10.1002/ana.21221
22. Thiyagarajan N, Ferguson R, Subramanian V, Acharya R. Structural and molecular insights into the mechanism of action of human angiogenin-ALS variants in neurons. *Nat Commun* (2012) 3:1114–21. doi:10.1038/ncomms2126
23. Henneke M, Diekmann S, Ohlenbusch A, Kaiser J, Engelbrecht V, Kohlschütter A, et al. RNASET2-deficient cystic leukoencephalopathy resembles congenital cytomegalovirus brain infection. *Nat Genet* (2009) 41:773–5. doi:10.1038/ng.398

24. Thorn A, Steinfeld R, Ziegenbein M, Grapp M, Hsiao HH, Urlaub H, et al. Structure and activity of the only human RNase T2. *Nucleic Acids Res* (2012) 40:8733–42. doi:10.1093/nar/gks614
25. Schein CH. From housekeeper to microsurgeon: the diagnostic and therapeutic potential of ribonucleases. *Nat Biotechnol* (1997) 15:529–36. doi:10.1038/nbt0697-529
26. Suzuki M, Saxena SK, Boix E, Prill RJ, Vasandani VM, Ladner JE, et al. Engineering receptor-mediated cytotoxicity into human ribonucleases by steric blockade of inhibitor interaction. *Nat Biotechnol* (1999) 17:265–70. doi:10.1038/7010
27. Rybak SM, Newton DL. Natural and engineered cytotoxic ribonucleases: therapeutic potential. *Exp Cell Res* (1999) 253:325–35. doi:10.1006/excr.1999.4718
28. Goncalves KA, Silberstein L, Li S, Severe N, Hu MG, Yang H, et al. Angiogenin promotes hematopoietic regeneration by dichotomously regulating quiescence of stem and progenitor cells. *Cell* (2016) 166:894–906. doi:10.1016/j.cell.2016.06.042
29. Ma G, Chen C, Jiang H, Qiu Y, Li Y, Li X, et al. Ribonuclease attenuates hepatic ischemia reperfusion induced cognitive impairment through the inhibition of inflammatory cytokines in aged mice. *Biomed Pharmacother* (2017) 90:62–8. doi:10.1016/j.biopha.2017.02.094
30. Acquati F, Lualdi M, Bertilaccio S, Monti L, Turconi G, Fabbri M, et al. Loss of function of Ribonuclease T2, an ancient and phylogenetically conserved RNase, plays a crucial role in ovarian tumorigenesis. *Proc Natl Acad Sci U S A* (2013) 110(20):8140–5. doi:10.1073/pnas.1222079110
31. Luhtala N, Parker R. T2 Family ribonucleases: ancient enzymes with diverse roles. *Trends Biochem Sci* (2010) 35:253–9. doi:10.1016/j.tibs.2010.02.002
32. Batot G, Michalska K, Ekberg G, Irimpan EM, Joachimiak G, Jedrzejczak R, et al. The CDI toxin of *Yersinia kristensenii* is a novel bacterial member of the RNase A superfamily. *Nucleic Acids Res* (2017) 45:5013–25. doi:10.1093/nar/gkx230
33. Goo SM, Cho S. The expansion and functional diversification of the mammalian ribonuclease a superfamily epitomizes the efficiency of multigene families at generating biological novelty. *Genome Biol Evol* (2013) 5:2124–40. doi:10.1093/gbe/evt161
34. Sorrentino S. The eight human "canonical" ribonucleases: molecular diversity, catalytic properties, and special biological actions of the enzyme proteins. *FEBS Lett* (2010) 584:2194–200. doi:10.1016/j.febslet.2010.04.018
35. Boix E, Blanco JA, Nogués MV, Moussaoui M. Nucleotide binding architecture for secreted cytotoxic endoribonucleases. *Biochimie* (2013) 95:1087–97. doi:10.1016/j.biochi.2012.12.015
36. Nogués MV, Moussaoui M, Boix E, Vilanova M, Ribó M, Cuchillo CM. The contribution of noncatalytic phosphate-binding subsites to the mechanism of bovine pancreatic ribonuclease A. *Cell Mol Life Sci* (1998) 54:766–74. doi:10.1007/s000180050205
37. Prats-Ejarque G, Arranz-Trullén J, Blanco JA, Pulido D, Nogués MV, Moussaoui M, et al. The first crystal structure of human RNase 6 reveals a novel substrate-binding and cleavage site arrangement. *Biochem J* (2016) 473:1523–36. doi:10.1042/BCJ20160245
38. Sikriwal D, Seth D, Batra JK. Role of catalytic and non-catalytic subsite residues in ribonuclease activity of human eosinophil-derived neurotoxin. *Biol Chem* (2009) 390:225–34. doi:10.1515/BC.2009.025
39. Li Z, Ender C, Meister G, Moore PS, Chang Y, John B. Extensive terminal and asymmetric processing of small RNAs from rRNAs, snoRNAs, snRNAs, and tRNAs. *Nucleic Acids Res* (2012) 40:6787–99. doi:10.1093/nar/gks307
40. Qiao M, Zu L-D, He X-H, Shen R-L, Wang Q-C, Liu M-F. Onconase down-regulates microRNA expression through targeting microRNA precursors. *Cell Res* (2012) 22:1199–202. doi:10.1038/cr.2012.67
41. Lyons SM, Fay MM, Akiyama Y, Anderson PJ, Ivanov P. RNA biology of angiogenin: current state and perspectives. *RNA Biol* (2017) 14:171–8. doi:10.1080/15476286.2016.1272746
42. Boix E, Nogués MV. Mammalian antimicrobial proteins and peptides: overview on the RNase A superfamily members involved in innate host defence. *Mol Biosyst* (2007) 3:317–35. doi:10.1039/b617527a
43. Köten B, Simanski M, Gläser R, Podschun R, Schröder JM, Harder J. RNase 7 contributes to the cutaneous defense against *Enterococcus faecium*. *PLoS One* (2009) 4:e6424. doi:10.1371/journal.pone.0006424
44. Simanski M, Köten B, Schröder JM, Gläser R, Harder J. Antimicrobial RNases in cutaneous defense. *J Innate Immun* (2012) 4:241–7. doi:10.1159/000335029
45. Koczera P, Martin L, Marx G, Schuerholz T. The ribonuclease a superfamily in humans: canonical RNases as the buttress of innate immunity. *Int J Mol Sci* (2016) 17:E1278. doi:10.3390/ijms17081278
46. Yang D, Rosenberg HF, Chen Q, Dyer KD, Kurosaka K, Oppenheim JJ. Eosinophil-derived neurotoxin (EDN), an antimicrobial protein with chemotactic activities for dendritic cells. *Blood* (2003) 102:3396–403. doi:10.1182/blood-2003-01-0151
47. Yang D, Chen Q, Rosenberg HF, Rybak SM, Newton DL, Wang ZY, et al. Human ribonuclease A superfamily members, eosinophil-derived neurotoxin and pancreatic ribonuclease, induce dendritic cell maturation and activation. *J Immunol* (2004) 173:6134–42. doi:10.4049/jimmunol.173.10.6134
48. Yamada KJ, Barker T, Dyer KD, Rice TA, Percopo CM, Garcia-Crespo KE, et al. Eosinophil-associated ribonuclease 11 is a macrophage chemoattractant. *J Biol Chem* (2015) 290:8863–75. doi:10.1074/jbc.M114.626648
49. Zagai U, Dadfar E, Lundahl J, Venge P, Sköld CM. Eosinophil cationic protein stimulates TGF-β1 release by human lung fibroblasts in vitro. *Inflammation* (2007) 30:153–60. doi:10.1007/s10753-007-9032-4
50. Zheutlin LM, Ackerman SJ, Gleich GJ, Thomas LL. Stimulation of basophil and rat mast cell histamine release by eosinophil granule-derived cationic proteins. *J Immunol* (1984) 133:2180–5.
51. Venge P, Byström J, Carlson M, Håkansson L, Karawacjzyk M, Peterson C, et al. Eosinophil cationic protein (ECP): molecular and biological properties and the use of ECP as a marker of eosinophil activation in disease. *Clin Exp Allergy* (1999) 29:1172–86. doi:10.1046/j.1365-2222.1999.00542.x
52. Bystrom J, Amin K, Bishop-Bailey D. Analysing the eosinophil cationic protein – a clue to the function of the eosinophil granulocyte. *Respir Res* (2011) 12:10. doi:10.1186/1465-9921-12-10
53. Shcheglovitova ON, Maksyanina EV, Ionova II, Rustam'yan YL, Komolova GS. Cow milk angiogenin induces cytokine production in human blood leukocytes. *Bull Exp Biol Med* (2003) 135:158–60. doi:10.1023/A:1023871931764
54. Kopfnagel V, Wagenknecht S, Harder J, Hofmann K, Kleine M, Buch A, et al. RNase 7 strongly promotes TLR9-mediated DNA sensing by human plasmacytoid dendritic cells. *J Invest Dermatol* (2017) 138:872–81. doi:10.1016/j.jid.2017.09.052
55. Phipps S, Lam CE, Mahalingam S, Newhouse M, Ramirez R, Rosenberg HF, et al. Eosinophils contribute to innate antiviral immunity and promote clearance of respiratory syncytial virus. *Blood* (2007) 110:1–3. doi:10.1182/blood-2007-01-071340
56. Thompson DM, Parker R. Stressing out over tRNA cleavage. *Cell* (2009) 138:215–9. doi:10.1016/j.cell.2009.07.001
57. Mesitov MV, Soldatov RA, Zaichenko DM, Malakho SG, Klementyeva TS, Sokolovskaya AA, et al. Differential processing of small RNAs during endoplasmic reticulum stress. *Sci Rep* (2017) 7:1–14. doi:10.1038/srep46080
58. Emara MM, Ivanov P, Hickman T, Dawra N, Tisdale S, Kedersha N, et al. Angiogenin-induced tRNA-derived stress-induced RNAs promote stress-induced stress granule assembly. *J Biol Chem* (2010) 285:10959–68. doi:10.1074/jbc.M109.077560
59. Ivanov P, Emara MM, Villen J, Gygi SP, Anderson P. Angiogenin-induced tRNA fragments inhibit translation initiation. *Mol Cell* (2011) 43:613–23. doi:10.1016/j.molcel.2011.06.022
60. Yang D, Chen Q, Su SB, Zhang P, Kurosaka K, Caspi RR, et al. Eosinophil-derived neurotoxin acts as an alarmin to activate the TLR2-MyD88 signal pathway in dendritic cells and enhances Th2 immune responses. *J Exp Med* (2008) 205:79–90. doi:10.1084/jem.20062027
61. Chan JK, Roth J, Oppenheim JJ, Tracey KJ, Vogl T, Feldmann M, et al. Alarmins: awaiting a clinical response. *J Clin Invest* (2012) 122:2711–9. doi:10.1172/JCI62423
62. Zagai U, Sköld CM, Trulson A, Venge P, Lundahl J. The effect of eosinophils on collagen gel contraction and implications for tissue remodelling. *Clin Exp Immunol* (2004) 135:427–33. doi:10.1111/j.1365-2249.2004.02396.x
63. Tsuji T, Sun Y, Kishimoto K, Olson KA, Liu S, Hirukawa S, et al. Angiogenin is translocated to the nucleus of HeLa cells and is involved in ribosomal RNA transcription and cell proliferation. *Cancer Res* (2005) 65:1352–60. doi:10.1158/0008-5472.CAN-04-2058
64. Xu L, Liao WL, Lu QJ, Li CG, Yuan Y, Xu ZY, et al. ANG promotes proliferation and invasion of the cell of lung squamous carcinoma by directly up-regulating HMGA2. *J Cancer* (2016) 7:862–71. doi:10.7150/jca.14539
65. Fett JW, Strydom DJ, Lobb RR, Alderman EM, Bethune JL, Riordan JF, et al. Isolation and characterization of angiogenin, an angiogenic protein

from human carcinoma cells. *Biochemistry* (1985) 24:5480–6. doi:10.1021/bi00341a030
66. Kishimoto K, Liu S, Tsuji T, Olson KA, Hu G. Endogenous angiogenin in endothelial cells is a general requirement for cell proliferation and angiogenesis. *Oncogene* (2005) 24:445–56. doi:10.1038/sj.onc.1208223
67. Abtin A, Eckhart L, Mildner M, Ghannadan M, Harder J, Schröder J-M, et al. Degradation by stratum corneum proteases prevents endogenous RNase inhibitor from blocking antimicrobial activities of RNase 5 and RNase 7. *J Invest Dermatol* (2009) 129:2193–201. doi:10.1038/jid.2009.35
68. Bernard JJ, Gallo RL. Protecting the boundary: the sentinel role of host defense peptides in the skin. *Cell Mol Life Sci* (2011) 68:2189–99. doi:10.1007/s00018-011-0712-8
69. Harder J, Dressel S, Wittersheim M, Cordes J, Meyer-Hoffert U, Mrowietz U, et al. Enhanced expression and secretion of antimicrobial peptides in atopic dermatitis and after superficial skin injury. *J Invest Dermatol* (2010) 130:1355–64. doi:10.1038/jid.2009.432
70. Amatngalim GD, van Wijck Y, de Mooij-Eijk Y, Verhoosel RM, Harder J, Lekkerkerker AN, et al. Basal cells contribute to innate immunity of the airway epithelium through production of the antimicrobial protein RNase 7. *J Immunol* (2015) 194:3340–50. doi:10.4049/jimmunol.1402169
71. Fiorini C, Cordani M, Gotte G, Picone D, Donadelli M. Onconase induces autophagy sensitizing pancreatic cancer cells to gemcitabine and activates Akt/mTOR pathway in a ROS-dependent manner. *Biochim Biophys Acta* (2015) 1853:549–60. doi:10.1016/j.bbamcr.2014.12.016
72. Fiorini C, Gotte G, Donnarumma F, Picone D, Donadelli M. Bovine seminal ribonuclease triggers Beclin1-mediated autophagic cell death in pancreatic cancer cells. *Biochim Biophys Acta* (2014) 1843:976–84. doi:10.1016/j.bbamcr.2014.01.025
73. Navarro S, Aleu J, Jiménez M, Boix E, Cuchillo CM, Nogués MV. The cytotoxicity of eosinophil cationic protein/ribonuclease 3 on eukaryotic cell lines takes place through its aggregation on the cell membrane. *Cell Mol Life Sci* (2008) 65:324–37. doi:10.1007/s00018-007-7499-7
74. Spalletti-Cernia D, Sorrentino R, Di Gaetano S, Arciello A, Garbi C, Piccoli R, et al. Antineoplastic ribonucleases selectively kill thyroid carcinoma cells via caspase-mediated induction of apoptosis. *J Clin Endocrinol Metab* (2003) 88:2900–7. doi:10.1210/jc.2002-020373
75. Chang KC, Lo CW, Fan TC, Chang MD, Shu CW, Chang CH, et al. TNF-α mediates eosinophil cationic protein-induced apoptosis in BEAS-2B cells. *BMC Cell Biol* (2010) 11. doi:10.1186/1471-2121-11-6
76. Cabrera-Fuentes HA, Ruiz-Meana M, Simsekyilmaz S, Kostin S, Inserte J, Saffarzadeh M, et al. RNase1 prevents the damaging interplay between extracellular RNA and tumour necrosis factor-α in cardiac ischaemia/reperfusion injury. *Thromb Haemost* (2014) 112:1110–9. doi:10.1160/th14-08-0703
77. Zernecke A, Preissner KT. Extracellular ribonucleic acids (RNA) enter the stage in cardiovascular disease. *Circ Res* (2016) 118:469–79. doi:10.1161/CIRCRESAHA.115.307961
78. Simsekyilmaz S, Cabrera-Fuentes HA, Meiler S, Kostin S, Baumer Y, Liehn EA, et al. Role of extracellular RNA in atherosclerotic plaque formation in mice. *Circulation* (2014) 129:598–606. doi:10.1161/CIRCULATIONAHA.113.002562
79. Harder J, Schröder JM, Gläser R. The skin surface as antimicrobial barrier: present concepts and future outlooks. *Exp Dermatol* (2013) 22:1–5. doi:10.1111/exd.12046
80. Zanger P, Holzer J, Schleucher R, Steffen H, Schittek B, Gabrysch S. Constitutive expression of the antimicrobial peptide RNase 7 is associated with *Staphylococcus aureus* infection of the skin. *J Infect Dis* (2009) 200:1907–15. doi:10.1086/648408
81. Rademacher F, Simanski M, Harder J. RNase 7 in cutaneous defense. *Int J Mol Sci* (2016) 560:1–12. doi:10.3390/ijms17040560
82. Becknell B, Spencer JD. A review of ribonuclease 7's structure, regulation, and contributions to host defense. *Int J Mol Sci* (2016) 423:1–10. doi:10.3390/ijms17030423
83. Becknell B, Eichler TE, Beceiro S, Li B, Easterling RS, Carpenter AR, et al. Ribonucleases 6 and 7 have antimicrobial function in the human and murine urinary tract. *Kidney Int* (2015) 87:151–61. doi:10.1038/ki.2014.268
84. Spencer JD, Schwaderer AL, Wang H, Bartz J, Kline J, Eichler T, et al. Ribonuclease 7, an antimicrobial peptide upregulated during infection, contributes to microbial defense of the human urinary tract. *Kidney Int* (2013) 83:615–25. doi:10.1038/ki.2012.410
85. Ganz T. Angiogenin: an antimicrobial ribonuclease. *Nat Immunol* (2003) 4:213–4. doi:10.1038/ni0403-394b
86. Boix E, Salazar VA, Torrent M, Pulido D, Nogués MV, Moussaoui M. Structural determinants of the eosinophil cationic protein antimicrobial activity. *Biol Chem* (2012) 393:801–15. doi:10.1515/hsz-2012-0160
87. Pulido D, Torrent M, Andreu D, Nogues MV, Boix E. Two human host defense ribonucleases against mycobacteria, the eosinophil cationic protein (RNase 3) and RNase 7. *Antimicrob Agents Chemother* (2013) 57:3797–805. doi:10.1128/AAC.00428-13
88. Hooper LV, Stappenbeck TS, Hong CV, Gordon JI. Angiogenins: a new class of microbicidal proteins involved in innate immunity. *Nat Immunol* (2003) 4:269–73. doi:10.1038/ni888
89. Harder J, Schröder JM. RNase 7, a novel innate immune defense antimicrobial protein of healthy human skin. *J Biol Chem* (2002) 277:46779–84. doi:10.1074/jbc.M207587200
90. Pulido D, Arranz-Trullen J, Prats-Ejarque G, Velazquez D, Torrent M, Moussaoui M, et al. Insights into the antimicrobial mechanism of action of human RNase6: structural determinants for bacterial cell agglutination and membrane permeation. *Int J Mol Sci* (2016) 17:552. doi:10.3390/ijms17040552
91. Rudolph B, Podschun R, Sahly H, Schubert S, Schröder JM, Harder J. Identification of RNase 8 as a novel human antimicrobial protein. *Antimicrob Agents Chemother* (2006) 50:3194–6. doi:10.1128/AAC.00246-06
92. Ackerman SJ, Gleich GJ, Loegering DA, Richardson BA, Butterworth AE. Comparative toxicity of purified human eosinophil granule cationic proteins for schistosomula of *Schistosoma mansoni*. *Am J Trop Med Hyg* (1985) 34:735–45. doi:10.4269/ajtmh.1985.34.735
93. Ramos AL, Discipio RG, Ferreira AM. Eosinophil cationic protein damages protoscoleces in vitro and is present in the hydatid cyst. *Parasite Immunol* (2006) 28:347–55. doi:10.1111/j.1365-3024.2006.00842.x
94. Hamann KJ, Gleich GJ, Checkel JL, Loegering DA, McCall JW, Barker RL. In vitro killing of microfilariae of *Brugia pahangi* and *Brugia malayi* by eosinophil granule proteins. *J Immunol* (1990) 144:3166–73.
95. Singh A, Batra JK. Role of unique basic residues in cytotoxic, antibacterial and antiparasitic activities of human eosinophil cationic protein. *Biol Chem* (2011) 392:337–46. doi:10.1515/BC.2011.037
96. Attery A, Batra JK. Mouse eosinophil associated ribonucleases: mechanism of cytotoxic, antibacterial and antiparasitic activities. *Int J Biol Macromol* (2017) 94:445–50. doi:10.1016/j.ijbiomac.2016.10.041
97. Blom K, Elshafie AI, Jönsson UB, Rönnelid J, Håkansson LD, Venge P. The genetically determined production of the alarmin eosinophil-derived neurotoxin is reduced in visceral leishmaniasis. *APMIS* (2018) 126:85–91. doi:10.1111/apm.12780
98. Rajamanickam A, Munisankar S, Bhootra Y, Dolla CK, Nutman TB, Babu S. Elevated systemic levels of eosinophil, neutrophil, and mast cell granular proteins in strongyloides stercoralis infection that diminish following treatment. *Front Immunol* (2018) 9:207. doi:10.3389/fimmu.2018.00207
99. Waters LS, Taverne J, Tai PC, Spry CJ, Targett GA, Playfair JH. Killing of Plasmodium falciparum by eosinophil secretory products. *Infect Immun* (1987) 55:877–81.
100. Bedoya VI, Boasso A, Hardy AW, Rybak S, Shearer GM, Rugeles MT. Ribonucleases in HIV type 1 inhibition: effect of recombinant RNases on infection of primary T cells and immune activation-induced RNase gene and protein expression. *AIDS Res Hum Retroviruses* (2006) 22:897–907. doi:10.1089/aid.2006.22.897
101. Suhasini AN, Sirdeshmukh R. Onconase action on tRNALys3, the primer for HIV-1 reverse transcription. *Biochem Biophys Res Commun* (2007) 363:304–9. doi:10.1016/j.bbrc.2007.08.157
102. Rugeles MT, Trubey CM, Bedoya VI, Pinto LA, Oppenheim JJ, Rybak SM, et al. Ribonuclease is partly responsible for the HIV-1 inhibitory effect activated by HLA alloantigen recognition. *AIDS* (2003) 17:481–6. doi:10.1097/00002030-200303070-00002
103. Li Y, Zhao Y, Liu J, Huang Y, Liu Z, Xue C. A promising alternative anti-HBV agent: the targeted ribonuclease. *Int J Mol Med* (2009) 23:521–7. doi:10.3892/ijmm
104. Domachowske JB, Dyer KD, Bonville CA, Rosenberg HF. Recombinant human eosinophil-derived neurotoxin/RNase 2 functions as an effective antiviral agent against respiratory syncytial virus. *J Infect Dis* (1998) 177:1458–64. doi:10.1086/515322

105. Domachowske JB, Dyer KD, Adams AG, Leto TL, Rosenberg HF. Eosinophil cationic protein/RNase 3 is another RNase A-family ribonuclease with direct antiviral activity. *Nucleic Acids Res* (1998) 26:3358–63. doi:10.1093/nar/26.14.3358
106. Sikriwal D, Seth D, Parveen S, Malik A, Broor S, Batra JK. An insertion in loop L7 of human eosinophil-derived neurotoxin is crucial for its antiviral activity. *J Cell Biochem* (2012) 113:3104–12. doi:10.1002/jcb.24187
107. Rosenberg H. Eosinophil-derived neurotoxin (EDN/RNase 2) and the mouse eosinophil-associated RNases (mEars): expanding roles in promoting host defense. *Int J Mol Sci* (2015) 16:15442–55. doi:10.3390/ijms160715442
108. Roller BL, Monibi F, Stoker AM, Bal BS, Cook JL. Identification of novel synovial fluid biomarkers associated with meniscal pathology. *J Knee Surg* (2016) 29:47–62. doi:10.1055/s-0034-1394165
109. Stark M, Danielsson O, Griffiths WJ, Jörnvall H, Johansson J. Peptide repertoire of human cerebrospinal fluid: novel proteolytic fragments of neuroendocrine proteins. *J Chromatogr B Biomed Sci Appl* (2001) 754:357–67. doi:10.1016/S0378-4347(00)00628-9
110. Sugiyama RH, Blank A, Dekker CA. Multiple ribonucleases of human urine. *Biochemistry* (1981) 20(8):2268–74. doi:10.1021/bi00511a031
111. Prunotto M, Farina A, Lane L, Pernin A, Schifferli J, Hochstrasser DF, et al. Proteomic analysis of podocyte exosome-enriched fraction from normal human urine. *J Proteomics* (2013) 82:193–229. doi:10.1016/j.jprot.2013.01.012
112. Martin L, Koczera P, Simons N, Zechendorf E, Hoeger J, Marx G, et al. The human host defense ribonucleases 1, 3 and 7 are elevated in patients with sepsis after major surgery-A pilot study. *Int J Mol Sci* (2016) 17:1–11. doi:10.3390/ijms17030294
113. Schieven GL, Blank A, Dekker CA. Ribonucleases of human cerebrospinal fluid: detection of altered glycosylation relative to their serum counterparts1. *Biochemistry* (1982) 21:5148–55. doi:10.1021/bi00264a007
114. Reimert CM, Minuva U, Kharazmi A, Bendtzen K. Eosinophil protein X/eosinophil derived neurotoxin (EPX/EDN) detection by enzyme-linked immunosorbent assay and purification from normal human urine. *J Immunol Methods* (1991) 141:97–104. doi:10.1016/0022-1759(91)90214-Z
115. Levy AM, Gleich GJ, Sandborn WJ, Tremaine WJ, Steiner BL, Phillips SF. Increased eosinophil granule proteins in gut lavage fluid from patients with inflammatory bowel disease. *Mayo Clin Proc* (1997) 72:117–23. doi:10.4065/72.2.117
116. Rosenberg HF, Tenen DG, Ackerman SJ. Molecular cloning of the human eosinophil-derived neurotoxin: a member of the ribonuclease gene family. *Proc Natl Acad Sci U S A* (1989) 86:4460–4. doi:10.1073/pnas.86.12.4460
117. Raimondo F, Morosi L, Corbetta S, Chinello C, Brambilla P, Della Mina P, et al. Differential protein profiling of renal cell carcinoma urinary exosomes. *Mol Biosyst* (2013) 9:1220. doi:10.1039/c3mb25582d
118. Robinson DS, Assoufi B, Durham SR, Kay AB. Eosinophil cationic protein(ECP) and eosinophil protein X (EXP) concentrations in serum and bronchial lavage fluid in asthma. effect of prednisolone treatment. *Clin Exp Allergy* (1995) 25:1118–27. doi:10.1111/j.1365-2222.1995.tb03259.x
119. Fahy JV, Liu J, Wong H, Boushey HA. Cellular and biochemical analysis of induced sputum from asthmatic and from healthy subjects. *Am Rev Respir Dis* (1993) 147:1126–31. doi:10.1164/ajrccm/147.5.1132
120. Montan PG, van Hage-Hamsten M. Eosinophil cationic protein in tears in allergic conjunctivitis. *Br J Ophthalmol* (1996) 80:556–60. doi:10.1136/bjo.80.6.556
121. Park YJ, Oh EJ, Park JW, Kim M, Han K. Plasma eosinophil cationic protein, interleukin-5, and ECP/Eo count ratio in patients with various eosinophilic diseases. *Ann Clin Lab Sci* (2006) 36:262–6.
122. Tischendorf FW, Brattig NW, Lintzel M, Buttner DW, Burchard GD, Bork K, et al. Eosinophil granule proteins in serum and urine of patients with helminth infections and atopic dermatitis. *Trop Med Int Health* (2000) 5:898–905. doi:10.1046/j.1365-3156.2000.00649.x
123. Rasp G, Thomas PA, Bujía J. Eosinophil inflammation of the nasal mucosa in allergic and non-allergic rhinitis measured by eosinophil cationic protein levels in native nasal fluid and serum. *Clin Exp Allergy* (1994) 24:1151–6. doi:10.1111/j.1365-2222.1994.tb03321.x
124. Dalli J, Montero-Melendez T, Norling LV, Yin X, Hinds C, Haskard D, et al. Heterogeneity in neutrophil microparticles reveals distinct proteome and functional properties. *Mol Cell Proteomics* (2013) 12:2205–19. doi:10.1074/mcp.M113.028589
125. Tollin M, Bergman P, Svenberg T, Jörnvall H, Gudmundsson GH, Agerberth B. Antimicrobial peptides in the first line defence of human colon mucosa. *Peptides* (2003) 24:523–30. doi:10.1016/S0196-9781(03)00114-1
126. van Herwijnen MJC, Zonneveld MI, Goerdayal S, Nolte-'t Hoen ENM, Garssen J, Stahl B, et al. Comprehensive proteomic analysis of human milk-derived extracellular vesicles unveils a novel functional proteome distinct from other milk components. *Mol Cell Proteomics* (2016) 15:3412–23. doi:10.1074/mcp.M116.060426
127. Liote F, Champy R, Moenner M, Boval-Boizard B, Badet J. Elevated angiogenin levels in synovial fluid from patients with inflammatory arthritis and secretion of angiogenin by cultured synovial fibroblasts. *Clin Exp Immunol* (2003) 132:163–8. doi:10.1046/j.1365-2249.2003.02117.x
128. Simcock DE, Kanabar V, Clarke GW, O'Connor BJ, Lee TH, Hirst SJ. Proangiogenic activity in bronchoalveolar lavage fluid from patients with asthma. *Am J Respir Crit Care Med* (2007) 176:146–53. doi:10.1164/rccm.200701-042OC
129. Koutroubakis IE, Xidakis C, Karmiris K, Sfiridaki A, Kandidaki E, Kouroumalis EA. Serum angiogenin in inflammatory bowel disease. *Dig Dis Sci* (2004) 49:1758–62. doi:10.1007/s10620-004-9565-4
130. McLaughlin RL, Phukan J, McCormack W, Lynch DS, Greenway M, Cronin S, et al. Angiogenin levels and ANG genotypes: dysregulation in amyotrophic lateral sclerosis. *PLoS One* (2010) 5:e15402. doi:10.1371/journal.pone.0015402
131. Pavlov N, Hatzi E, Bassaglia Y, Frendo J-L, Brion DE, Badet J. Angiogenin distribution in human term placenta, and expression by cultured trophoblastic cells. *Angiogenesis* (2003) 6:317–30. doi:10.1023/B:AGEN.0000029412.95244.81
132. Shapiro R, Vallee BL. Human placental ribonuclease inhibitor abolishes both angiogenic and ribonucleolytic activities of angiogenin. *Proc Natl Acad Sci U S A* (1987) 84:2238–41. doi:10.1073/pnas.84.8.2238
133. Hu GF, Xu CJ, Riordan JF. Human angiogenin is rapidly translocated to the nucleus of human umbilical vein endothelial cells and binds to DNA. *J Cell Biochem* (2000) 76:452–62. doi:10.1002/(SICI)1097-4644(20000301)76:3<452::AID-JCB12>3.0.CO;2-Z
134. Moroianu J, Riordan JF. Nuclear translocation of angiogenin in proliferating endothelial cells is essential to its angiogenic activity. *Proc Natl Acad Sci U S A* (1994) 91:1677–81. doi:10.1073/pnas.91.5.1677
135. Moroianu J, Riordan JF. Identification of the nucleolar targeting signal of human angiogenin. *Biochem Biophys Res Commun* (1994) 203:1765–72. doi:10.1006/bbrc.1994.2391
136. Reithmayer K, Meyer KC, Kleditzsch P, Tiede S, Uppalapati SK, Gläser R, et al. Human hair follicle epithelium has an antimicrobial defence system that includes the inducible antimicrobial peptide psoriasin (S100A7) and RNase 7. *Br J Dermatol* (2009) 161:78–89. doi:10.1111/j.1365-2133.2009.09154.x
137. Welton JL, Khanna S, Giles PJ, Brennan P, Brewis IA, Staffurth J, et al. Proteomics analysis of bladder cancer exosomes. *Mol Cell Proteomics* (2010) 9:1324–38. doi:10.1074/mcp.M000063-MCP201
138. Wang Z, Hill S, Luther JM, Hachey DL, Schey KL. Proteomic analysis of urine exosomes by multidimensional protein identification technology (MudPIT). *Proteomics* (2012) 12:329–38. doi:10.1002/pmic.201100477
139. Kiehne K, Fincke A, Brunke G, Lange T, Fölsch UR, Herzig K-H, et al. Antimicrobial peptides in chronic anal fistula epithelium. *Scand J Gastroenterol* (2007) 42:1063–9. doi:10.1080/00365520701320489
140. Torres-Juarez F, Touqui L, Leon-Contreras J, Rivas-Santiago C, Enciso-Moreno JA, Hernandez-Pando R, et al. RNase7 but not psoriasin nor sPLA2-IIA associates to *Mycobacterium tuberculosis* during airway epithelial cells infection. *Pathog Dis* (2018) 76:1–19. doi:10.1093/femspd/fty005
141. Chan CC, Moser JM, Dyer KD, Percopo CM, Rosenberg HF. Genetic diversity of human RNase 8. *BMC Genomics* (2012) 13:40. doi:10.1186/1471-2164-13-40
142. Eller CH, Lomax JE, Raines RT. Bovine brain ribonuclease is the functional homolog of human Ribonuclease 1. *J Biol Chem* (2014) 289:25996–6006. doi:10.1074/jbc.M114.566166
143. Futami I, Tsushima Y, Murato Y, Tad H, Sasaki I, Seno M, et al. Tissue-specific expression of pancreatic-type RNases and RNase inhibitor in humans. *DNA Cell Biol* (1997) 16:413–9. doi:10.1089/dna.1997.16.413
144. Landre JBP, Hewett PW, Olivot J-M, Friedl P, Ko Y, Sachinidis A, et al. Human endothelial cells selectively express large amounts of pancreatic-type

ribonuclease (RNase 1). *J Cell Biochem* (2002) 86:540–52. doi:10.1002/jcb.10234
145. Fischer S, Nishio M, Dadkhahi S, Gansler J, Saffarzadeh M, Shibamiyama A, et al. Expression and localisation of vascular ribonucleases in endothelial cells. *Thromb Haemost* (2011) 105:345–55. doi:10.1160/TH10-06-0345
146. Acharya KR, Ackerman SJJ. Eosinophil granule proteins: form and function. *J Biol Chem* (2014) 289:17406–15. doi:10.1074/jbc.R113.546218
147. Harrison AM, Bonville CA, Rosenberg HF, Domachowske JB. Respiratory syncytical virus-induced chemokine expression in the lower airways. *Am J Respir Crit Care Med* (1999) 159:1918–24. doi:10.1164/ajrccm.159.6.9805083
148. Kim C-K, Seo JK, Ban SH, Fujisawa T, Kim DW, Callaway Z. Eosinophil-derived neurotoxin levels at 3 months post-respiratory syncytial virus bronchiolitis are a predictive biomarker of recurrent wheezing. *Biomarkers* (2013) 18:230–5. doi:10.3109/1354750X.2013.773078
149. Shamri R, Young KM, Weller PF. PI3K, ERK, p38 MAPK and integrins regulate CCR3-mediated secretion of mouse and human eosinophil-associated RNases. *Allergy* (2013) 68:880–9. doi:10.1111/all.12163
150. Botos I, Segal D, Davies D. The structural biology of toll-like receptors. *Structure* (2011) 19:447–59. doi:10.1016/j.str.2011.02.004
151. Percopo CM, Dyer KD, Ochkur SI, Luo JL, Fischer ER, Lee JJ, et al. Activated mouse eosinophils protect against lethal respiratory virus infection. *Blood* (2014) 123:743–52. doi:10.1182/blood-2013-05-502443
152. Olsson I, Venge P, Spitznagel JK, Lehrer RI. Arginine-rich cationic proteins of human eosinophil granules: comparison of the constituents of eosinophilic and neutrophilic leukocytes. *Lab Invest* (1977) 36:493–500.
153. Torrent M, Sánchez D, Buzón V, Nogués MV, Cladera J, Boix E. Comparison of the membrane interaction mechanism of two antimicrobial RNases: RNase 3/ECP and RNase 7. *Biochim Biophys Acta* (2009) 1788:1116–25. doi:10.1016/j.bbamem.2009.01.013
154. Torrent M, Pulido D, Nogués MV, Boix E. Exploring new biological functions of amyloids: bacteria cell agglutination mediated by host protein aggregation. *PLoS Pathog* (2012) 8:e1003005. doi:10.1371/journal.ppat.1003005
155. Pulido D, Moussaoui M, Andreu D, Nogués MV, Torrent M, Boix E. Antimicrobial action and cell agglutination by the eosinophil cationic protein are modulated by the cell wall lipopolysaccharide structure. *Antimicrob Agents Chemother* (2012) 56:2378–85. doi:10.1128/AAC.06107-11
156. Trautmann A, Schmid-Grendelmeier P, Krüger K, Crameri R, Akdis M, Akkaya A, et al. T cells and eosinophils cooperate in the induction of bronchial epithelial cell apoptosis in asthma. *J Allergy Clin Immunol* (2002) 109:329–37. doi:10.1067/MAI.2002.121460
157. Hogan SP, Waddell A, Fulkerson PC. Eosinophils in infection and intestinal immunity. *Curr Opin Gastroenterol* (2013) 29:7–14. doi:10.1097/MOG.0b013e32835ab29a
158. Plager DA, Davis MDP, Andrews AG, Coenen MJ, George TJ, Gleich GJ, et al. Eosinophil ribonucleases and their cutaneous lesion-forming activity. *J Immunol* (2009) 183:4013–20. doi:10.4049/jimmunol.0900055
159. Amin K, Lúdvíksdóttir D, Janson C, Nettelbladt D, Björnsson E, Roomans GM, et al. Inflammation and structural changes in the airways of patients with atopic and nonatopic asthma. BHR Group. *Am J Respir Crit Care Med* (2000) 162:2295–301. doi:10.1164/ajrccm.162.6.9912001
160. Hernnäs J, Särnstrand B, Lindroth P, Peterson CG, Venge P, Malmström A. Eosinophil cationic protein alters proteoglycan metabolism in human lung fibroblast cultures. *Eur J Cell Biol* (1992) 59:352–63.
161. Rubin J, Zagai U, Blom K, Trulson A, Engström A, Venge P. The coding ECP 434(G>C) gene polymorphism determines the cytotoxicity of ECP but has minor effects on fibroblast-mediated gel contraction and no effect on RNase activity. *J Immunol* (2009) 183:445–51. doi:10.4049/jimmunol.0803912
162. Eriksson J, Woschnagg C, Fernvik E, Venge P. A SELDI-TOF MS study of the genetic and post-translational molecular heterogeneity of eosinophil cationic protein. *J Leukoc Biol* (2007) 82:1491–500. doi:10.1189/jlb.0507272
163. Trulson A, Byström J, Engström A, Larsson R, Venge P. The functional heterogeneity of eosinophil cationic protein is determined by a gene polymorphism and post-translational modifications. *Clin Exp Allergy* (2007) 37:208–18. doi:10.1111/j.1365-2222.2007.02644.x
164. Salazar VA, Rubin J, Moussaoui M, Pulido D, Nogués MV, Venge P, et al. Protein post-translational modification in host defense: the antimicrobial mechanism of action of human eosinophil cationic protein native forms. *FEBS J* (2014) 281:5432–46. doi:10.1111/febs.13082
165. Diop G, Derbois C, Loucoubar C, Mbengue B, Ndao BN, Thiam F, et al. Genetic variants of RNASE3 (ECP) and susceptibility to severe malaria in Senegalese population. *Malar J* (2018) 17:1–10. doi:10.1186/s12936-018-2205-9
166. Adu B, Dodoo D, Adukpo S, Gyan BA, Hedley PL, Goka B, et al. Polymorphisms in the RNASE3 gene are associated with susceptibility to cerebral malaria in Ghanaian children. *PLoS One* (2011) 6:e29465. doi:10.1371/journal.pone.0029465
167. Neves JS, Harvard MS, Weller P. Functional extracellular eosinophil granules: novel implications in eosinophil immunobiology. *Curr Opin Immunol* (2009) 21:694–9. doi:10.1016/j.coi.2009.07.011
168. Shamri R, Melo RCN, Young KM, Bivas-Benita M, Xenakis JJ, Spencer LA, et al. CCL11 elicits secretion of RNases from mouse eosinophils and their cell-free granules. *FASEB J* (2012) 26:2084–93. doi:10.1096/fj.11-200246
169. Hofsteenge J, Moldow C, Vicentini AM, Zelenko O, Jarai-Kote Z, Neumann U. A single amino acid substitution changes ribonuclease 4 from a uridine-specific to a cytidine-specific enzyme. *Biochemistry* (1998) 37:9250–7. doi:10.1021/bi9803832
170. Hofsteenge J, Vicentini A, Zelenko O. Ribonuclease 4, an evolutionarily highly conserved member of the superfamily. *Cell Mol Life Sci* (1998) 54:804–10. doi:10.1007/s000180050209
171. Rosenberg HF, Dyer KD. Human ribonuclease 4 (RNase 4): coding sequence, chromosomal localization and identification of two distinct transcripts in human somatic tissues. *Nucleic Acids Res* (1995) 23:4290–5. doi:10.1093/nar/23.21.4290
172. Egesten A, Dyer KD, Batten D, Domachowske JB, Rosenberg HF. Ribonucleases and host defense: identification, localization and gene expression in adherent monocytes in vitro. *Biochim Biophys Acta* (1997) 1358:255–60. doi:10.1016/S0167-4889(97)00081-5
173. Zhou H-M, Strydom DJ. The amino acid sequence of human ribonuclease 4, a highly conserved ribonuclease that cleaves specifically on the 3' side of uridine. *Eur J Biochem* (1993) 217:401–10. doi:10.1111/j.1432-1033.1993.tb18259.x
174. Liang S, Acharya KR. Structural basis of substrate specificity in porcine RNase 4. *FEBS J* (2016) 283:912–28. doi:10.1111/febs.13646
175. Terzyan SS, Peracaula R, de Llorens R, Tsushima Y, Yamada H, Seno M, et al. The three-dimensional structure of human RNase 4, unliganded and complexed with d(Up), reveals the basis for its uridine selectivity. *J Mol Biol* (1999) 285:205–14. doi:10.1006/jmbi.1998.2288
176. Cocchi F, DeVico AL, Lu W, Popovic M, Latinovic O, Sajadi MM, et al. Soluble factors from T cells inhibiting X4 strains of HIV are a mixture of chemokines and RNases. *Proc Natl Acad Sci U S A* (2012) 109:5411–6. doi:10.1073/pnas.1202240109
177. Shapiro R. Structural features that determine the enzymatic potency and specificity of human angiogenin: threonine-80 and residues 58–70 and 116–123. *Biochemistry* (1998) 37:6847–56. doi:10.1021/bi9800146
178. Saxena SK, Rybak SM, Davey RT, Youle RJ, Ackerman EJ. Angiogenin is a cytotoxic, tRNA-specific ribonuclease in the RNase a superfamily. *J Biol Chem* (1992) 267:21982–6.
179. Adams SA, Subramanian V. The angiogenins: an emerging family of ribonuclease related proteins with diverse cellular functions. *Angiogenesis* (1999) 3:189–99. doi:10.1023/A:1009015512200
180. Kulka M, Fukuishi N, Metcalfe DD. Human mast cells synthesize and release angiogenin, a member of the ribonuclease A (RNase A) superfamily. *J Leukoc Biol* (2009) 86:1217–26. doi:10.1189/jlb.0908517
181. Olson KA, Verselis SJ, Fett JW. Angiogenin is regulatedin vivoas an acute phase protein. *Biochem Biophys Res Commun* (1998) 242:480–3. doi:10.1006/bbrc.1997.7990
182. Gupta SK, Haigh BJ, Griffin FJ, Wheeler TT. The mammalian secreted RNases: mechanisms of action in host defence. *Innate Immun* (2013) 19:86–97. doi:10.1177/1753425912446955
183. Tschesche H, Kopp C, Hörl WH, Hempelmann U. Inhibition of degranulation of polymorphonuclear leukocytes by angiogenin and its tryptic fragment. *J Biol Chem* (1994) 269:30274–80.
184. Schmaldienst S, Oberpichler A, Tschesche H, Hörl WH. Angiogenin: a novel inhibitor of neutrophil lactoferrin release during extracorporeal circulation. *Kidney Blood Press Res* (2003) 26:107–12. doi:10.1159/000070992
185. Shapiro R, Ruiz-Gutierrez M, Chen CZ. Analysis of the interactions of human ribonuclease inhibitor with angiogenin and ribonuclease A by mutagenesis:

importance of inhibitor residues inside versus outside the C-terminal "hot spot". *J Mol Biol* (2000) 302:497–519. doi:10.1006/jmbi.2000.4075
186. Xu Z, Tsuji T, Riordan JF, Hu G. Identification and characterization of an angiogenin-binding DNA sequence that stimulates luciferase reporter gene expression. *Biochemistry* (2003) 42:121–8. doi:10.1021/bi020465x
187. Liu S, Yu D, Xu ZP, Riordan JF, Hu GF. Angiogenin activates Erk1/2 in human umbilical vein endothelial cells. *Biochem Biophys Res Commun* (2001) 287:305–10. doi:10.1006/bbrc.2001.5568
188. Honda S, Loher P, Shigematsu M, Palazzo JP, Suzuki R, Imoto I, et al. Sex hormone-dependent tRNA halves enhance cell proliferation in breast and prostate cancers. *Proc Natl Acad Sci U S A* (2015) 112:E3816–25. doi:10.1073/pnas.1510077112
189. Wang Q, Lee I, Ren J, Ajay SS, Lee YS, Bao X. Identification and functional characterization of tRNA-derived RNA fragments (tRFs) in respiratory syncytial virus infection. *Mol Ther* (2013) 21:368–79. doi:10.1038/mt.2012.237
190. Anderson P, Ivanov P. tRNA fragments in human health and disease. *FEBS Lett* (2014) 588:4297–304. doi:10.1016/j.febslet.2014.09.001
191. Rosenberg HF, Dyer KD. Molecular cloning and characterization of a novel human ribonuclease (RNase k6): increasing diversity in the enlarging ribonuclease gene family. *Nucleic Acids Res* (1996) 24:3507–13. doi:10.1093/nar/24.18.3507
192. Christensen-Quick A, Lafferty M, Sun L, Marchionni L, DeVico A, Garzino-Demo A. Human T_h 17 cells lack HIV-inhibitory RNases and are highly permissive to productive HIV infection. *J Virol* (2016) 90:7833–47. doi:10.1128/JVI.02869-15
193. Salazar VA, Arranz-Trullen J, Navarro S, Blanco JA, Sanchez D, Moussaoui M, et al. Exploring the mechanisms of action of human secretory RNase 3 and RNase 7 against *Candida albicans*. *Microbiologyopen* (2016) 5(5):830–45. doi:10.1002/mbo3.373
194. Wanke I, Steffen H, Christ C, Krismer B, Götz F, Peschel A, et al. Skin commensals amplify the innate immune response to pathogens by activation of distinct signaling pathways. *J Invest Dermatol* (2011) 131328:382–90. doi:10.1038/jid.2010.328
195. Williams DL, Li C, Ha T, Ozment-Skelton T, Kalbfleisch JH, Preiszner J, et al. Modulation of the phosphoinositide 3-kinase pathway alters innate resistance to polymicrobial sepsis. *J Immunol* (2004) 172:449–56. doi:10.4049/jimmunol.172.1.449
196. Schabbauer G, Tencati M, Pedersen B, Pawlinski R, Mackman N. PI3K-Akt pathway suppresses coagulation and inflammation in endotoxemic mice. *Arterioscler Thromb Vasc Biol* (2004) 24:1963–9. doi:10.1161/01.ATV.0000143096.15099.ce
197. Eichler TE, Becknell B, Easterling RS, Ingraham SE, Cohen DM, Schwaderer AL, et al. Insulin and the phosphatidylinositol 3-kinase signaling pathway regulate ribonuclease 7 expression in the human urinary tract. *Kidney Int* (2016) 90:568–79. doi:10.1016/j.kint.2016.04.025
198. Kenzel S, Mergen M, von Süßkind-Schwendi J, Wennekamp J, Deshmukh SD, Haeffner M, et al. Insulin modulates the inflammatory granulocyte response to streptococci via phosphatidylinositol 3-kinase. *J Immunol* (2012) 189:4582–91. doi:10.4049/jimmunol.1200205
199. Zhang J, Dyer KD, Rosenberg HF. RNase 8, a novel RNase A superfamily ribonuclease expressed uniquely in placenta. *Nucleic Acids Res* (2002) 30:1169–75. doi:10.1093/nar/30.5.1169
200. Schuster C, Gläser R, Fiala C, Eppel W, Harder J, Schröder JM, et al. Prenatal human skin expresses the antimicrobial peptide RNase 7. *Arch Dermatol Res* (2013) 305:545–9. doi:10.1007/s00403-013-1340-y
201. Zhang J. Disulfide-bond reshuffling in the evolution of an ape placental ribonuclease. *Mol Biol Evol* (2007) 24:505–12. doi:10.1093/molbev/msl177
202. Zhang J, Zhang YP, Rosenberg HF. Adaptive evolution of a duplicated pancreatic ribonuclease gene in a leaf-eating monkey. *Nat Genet* (2002) 30:411–5. doi:10.1038/ng852
203. Penttinen J, Pujianto DA, Sipilä P, Huhtaniemi I, Poutanen M. Discovery *in Silico* and characterization *in Vitro* of novel genes exclusively expressed in the mouse epididymis. *Mol Endocrinol* (2003) 17:2138–51. doi:10.1210/me.2003-0008
204. Castella S, Fouchécourt S, Teixeira-Gomes AP, Vinh J, Belghazi M, Dacheux F, et al. Identification of a member of a new RNase a family specifically secreted by epididymal caput epithelium. *Biol Reprod* (2004) 70:319–28. doi:10.1095/biolreprod.103.022459
205. Cho S, Zhang J. Ancient expansion of the ribonuclease A superfamily revealed by genomic analysis of placental and marsupial mammals. *Gene* (2006) 373:116–25. doi:10.1016/j.gene.2006.01.018
206. Cheng GZ, Li JY, Li F, Wang HY, Shi GX. Human ribonuclease 9, a member of ribonuclease A superfamily, specifically expressed in epididymis, is a novel sperm-binding protein. *Asian J Androl* (2009) 11:240–51. doi:10.1038/aja.2008.30
207. Singhania NA, Dyer KD, Zhang J, Deming MS, Bonville CA, Domachowske JB, et al. Rapid evolution of the ribonuclease A superfamily: adaptive expansion of independent gene clusters in rats and mice. *J Mol Evol* (1999) 49:721–8. doi:10.1007/PL00006594
208. Beintema JJ, Scheffer AJ, van Dijk H, Welling GW, Zwiers H. Pancreatic ribonuclease distribution and comparisons in mammals. *Nat New Biol* (1973) 241:76–8. doi:10.1038/newbio241076a0
209. Rosenberg HF, Dyer KD, Tiffany HL, Gonzalez M. Rapid evolution of a unique family of primate ribonuclease genes. *Nat Genet* (1995) 10:219–23. doi:10.1038/ng0695-219
210. Beintema JJ, Kleineidam RG. The ribonuclease A superfamily: general discussion. *Cell Mol Life Sci* (1998) 54:825–32. doi:10.1007/s000180050211
211. D'Alessio G, Di Donato A, Parente A, Piccoli R. Seminal RNase: a unique member of the ribonuclease superfamily. *Trends Biochem Sci* (1991) 16:104–6. doi:10.1016/0968-0004(91)90042-T
212. D'alessio G. Evolution of oligomeric proteins. The unusual case of a dimeric ribonuclease. *Eur J Biochem* (1999) 266:699–708. doi:10.1046/j.1432-1327.1999.00912.x
213. Kim JS, Soucek J, Matousek J, Raines RT. Catalytic activity of bovine seminal ribonuclease is essential for its immunosuppressive and other biological activities. *Biochem J* (1995) 308:547–50. doi:10.1042/bj3080547
214. Piccoli R, Di Donato A, D'Alessio G. Co-operativity in seminal ribonuclease function. Kinetic studies. *Biochem J* (1988) 253:329–36.
215. Tamburrini M, Piccoli R, Picone D, Di Donato A, D'Alessio G. Dissociation and reconstitution of bovine seminal RNAase: construction of a hyperactive hybrid dimer. *J Protein Chem* (1989) 8:719–31. doi:10.1007/BF01024897
216. Opitz JG, Ciglic MI, Haugg M, Trautwein-Fritz K, Raillard SA, Jermann TM, et al. Origin of the catalytic activity of bovine seminal ribonuclease against double-stranded RNA†. *Biochemistry* (1998) 37:4023–33. doi:10.1021/bi9722047
217. Schein CH, Haugg M, Benner SA. Interferon-gamma activates the cleavage of double-stranded RNA by bovine seminal ribonuclease. *FEBS Lett* (1990) 270:229–32. doi:10.1016/0014-5793(90)81275-S
218. Schein CH, Hauggt M. Deletions at the C-terminus of interferon y reduce RNA binding and activation of double-stranded-RNA cleavage by bovine seminal ribonuclease. *Biochem J* (1995) 307:123–7. doi:10.1042/bj3070123
219. Youle RJ, Wu YN, Mikulski SM, Shogen K, Hamilton RS, Newton D, et al. RNase inhibition of human immunodeficiency virus infection of H9 cells. *Proc Natl Acad Sci U S A* (1994) 91:6012–6. doi:10.1073/pnas.91.13.6012
220. Libonati M, Gotte G. Oligomerization of bovine ribonuclease A: structural and functional features of its multimers. *Biochem J* (2004) 380:311–27. doi:10.1042/bj20031922
221. Gotte G, Mahmoud Helmy A, Ercole C, Spadaccini R, Laurents DV, Donadelli M, et al. Double domain swapping in bovine seminal RNase: formation of distinct N- and C-swapped tetramers and multimers with increasing biological activities. *PLoS One* (2012) 7:e46804. doi:10.1371/journal.pone.0046804
222. Tamburrini M, Scala G, Verde C, Ruocco MR, Parente A, Venuta S, et al. Immunosuppressive activity of bovine seminal RNase on T-cell proliferation. *Eur J Biochem* (1990) 190:145–8. doi:10.1111/j.1432-1033.1990.tb15557.x
223. Souček J, Marinov I, Beneš J, Hilgert I, Matoušek J, Raines RT. Immunosuppressive activity of bovine seminal ribonuclease and its mode of action. *Immunobiology* (1996) 195:271–85. doi:10.1016/S0171-2985(96)80045-3
224. Maes P, Damart D, Rommens C, Montreuil J, Spik G, Tartar A. The complete amino acid sequence of bovine milk angiogenin. *FEBS Lett* (1988) 241:41–5. doi:10.1016/0014-5793(88)81027-5
225. Harris P, Johannessen KM, Smolenski G, Callaghan M, Broadhurst MK, Kim K, et al. Characterisation of the anti-microbial activity of bovine milk

ribonuclease4 and ribonuclease5 (angiogenin). *Int Dairy J* (2010) 20:400–7. doi:10.1016/j.idairyj.2009.12.018
226. Gupta SK, Haigh BJ, Seyfert HM, Griffin FJ, Wheeler TT. Bovine milk RNases modulate pro-inflammatory responses induced by nucleic acids in cultured immune and epithelial cells. *Dev Comp Immunol* (2017) 68:87–97. doi:10.1016/j.dci.2016.11.015
227. Nittoh T, Hirakata M, Mue S, Ohuchi K. Identification of cDNA encoding rat eosinophil cationic protein/eosinophil-associated ribonuclease. *Biochim Biophys Acta* (1997) 1351:42–6. doi:10.1016/S0167-4781(97)00024-9
228. Dubois J-YF, Jekel PA, Mulder PPMFA, Bussink AP, Catzeflis FM, Carsana A, et al. Pancreatic-type ribonuclease 1 gene duplications in rat species. *J Mol Evol* (2002) 55:522–33. doi:10.1007/s00239-002-2347-8
229. Zhao W, Kote-Jarai Z, van Santen Y, Hofsteenge J, Beintema JJ. Ribonucleases from rat and bovine liver: purification, specificity and structural characterization. *Biochim Biophys Acta* (1998) 1384:55–65. doi:10.1016/S0167-4838(97)00213-6
230. Larson KA, Olson EV, Madden BJ, Gleich GJ, Lee NA, Lee JJ. Two highly homologous ribonuclease genes expressed in mouse eosinophils identify a larger subgroup of the mammalian ribonuclease superfamily. *Proc Natl Acad Sci U S A* (1996) 93:12370–5. doi:10.1073/pnas.93.22.12370
231. Shamri R, Xenakis JJ, Spencer LA. Eosinophils in innate immunity: an evolving story Revital. *Cell Tissue Res* (2011) 343:57–83. doi:10.1007/s00441-010-1049-6
232. Zhang J, Dyer KD, Rosenberg HF. Evolution of the rodent eosinophil-associated RNase gene family by rapid gene sorting and positive selection. *Proc Natl Acad Sci U S A* (2000) 97:4701–6. doi:10.1073/pnas.080071397
233. Kumar RK, Foster PS. Modeling allergic asthma in mice: pitfalls and opportunities. *Am J Respir Cell Mol Biol* (2002) 27:267–72. doi:10.1165/rcmb.F248
234. Malm-Erjefält M, Persson CG, Erjefält JS. Degranulation status of airway tissue eosinophils in mouse models of allergic airway inflammation. *Am J Respir Cell Mol Biol* (2001) 24:352–9. doi:10.1165/ajrcmb.24.3.4357
235. Clark K, Simson L, Newcombe N, Koskinen AML, Mattes J, Lee NA, et al. Eosinophil degranulation in the allergic lung of mice primarily occurs in the airway lumen. *J Leukoc Biol* (2004) 75:1001–9. doi:10.1189/jlb.0803391
236. Nitto T, Lin C, Dyer KD, Wagner RA, Rosenberg HF. Characterization of a ribonuclease gene and encoded protein from the reptile, *Iguana iguana*. *Gene* (2005) 352:36–44. doi:10.1016/j.gene.2005.03.002
237. Nitta K, Ozaki K, Ishikawa M, Furusawa S, Hosono M, Kawauchi H, et al. Inhibition of cell proliferation by *Rana catesbeiana* and *Rana japonica* lectins belonging to the ribonuclease superfamily. *Cancer Res* (1994) 54:920–7.
238. Hsu CH, Chang CF, Liao YD, Wu SH, Chen C. Solution structure and base specificity of cytotoxic RC-RNase 2 from *Rana catesbeiana*. *Arch Biochem Biophys* (2015) 584:70–8. doi:10.1016/j.abb.2015.08.010
239. Liao YD, Huang HC, Leu YJ, Wei CW, Tang PC, Wang SC. Purification and cloning of cytotoxic ribonucleases from *Rana catesbeiana* (bullfrog). *Nucleic Acids Res* (2000) 28:4097–104. doi:10.1093/nar/28.21.4097
240. Benito A, Vilanova M, Ribó M. Intracellular routing of cytotoxic pancreatic-type ribonucleases. *Curr Pharm Biotechnol* (2008) 9:169–79. doi:10.2174/138920108784567281
241. Tao P, Fan M, Zhao W, Lin Q, Ma R. A novel cationic ribonuclease with antimicrobial activity from *Rana dybowskii*. *Biochem Genet* (2011) 49:369–84. doi:10.1007/s10528-010-9414-4
242. Ardelt W, Mikulski SM, Shogen K. Amino acid sequence of an anti-tumor protein from Rana pipiens oocytes and early embryos. Homology to pancreatic ribonucleases. *J Biol Chem* (1991) 266:245–51.
243. Ardelt W, Ardelt B, Darzynkiewicz Z. Ribonucleases as potential modalities in anticancer therapy. *Eur J Pharmacol* (2009) 625:181–9. doi:10.1016/j.ejphar.2009.06.067
244. Fagagnini A, Pica A, Fasoli S, Montioli R, Donadelli M, Cordani M, et al. Onconase dimerization through 3D domain swapping: structural investigations and increase in the apoptotic effect in cancer cells. *Biochem J* (2017) 474:3767–81. doi:10.1042/BCJ20170541
245. Saxena SK, Gravell M, Wu YN, Mikulski SM, Shogen K, Ardelt W, et al. Inhibition of HIV-1 production and selective degradation of viral RNA by an amphibian ribonuclease. *J Biol Chem* (1996) 271:20783–8. doi:10.1074/jbc.271.34.20783
246. Suhasini AN, Sirdeshmukh R. Transfer RNA cleavages by onconase reveal unusual cleavage sites. *J Biol Chem* (2006) 281:12201–9. doi:10.1074/jbc.M504488200
247. Pizzo E, Merlino A, Turano M, Russo Krauss I, Coscia F, Zanfardino A, et al. A new RNase sheds light on the RNase/angiogenin subfamily from zebrafish. *Biochem J* (2011) 433:345–55. doi:10.1042/BJ20100892
248. Pizzo E, Varcamonti M, Di Maro A, Zanfardino A, Giancola C, D'Alessio G. Ribonucleases with angiogenic and bactericidal activities from the Atlantic salmon. *FEBS J* (2008) 275:1283–95. doi:10.1111/j.1742-4658.2008.06289.x
249. Monti DM, Yu W, Pizzo E, Shima K, Hu MG, Di Malta C, et al. Characterization of the angiogenic activity of zebrafish ribonucleases. *FEBS J* (2009) 276:4077–90. doi:10.1111/j.1742-4658.2009.07115.x
250. Geng R, Liu H, Wang W. Differential expression of six Rnase2 and three Rnase3 paralogs identified in blunt snout bream in response to aeromonas hydrophila infection. *Genes (Basel)* (2018) 9. doi:10.3390/genes9020095
251. Ferguson BJ, Newland SA, Gibbs SE, Tourlomousis P, Fernandes dos Santos P, Patel MN, et al. The Schistosoma mansoni T2 ribonuclease omega-1 modulates inflammasome-dependent IL-1β secretion in macrophages. *Int J Parasitol* (2015) 45:809–13. doi:10.1016/j.ijpara.2015.08.005
252. Smirnoff P, Roiz L, Angelkovitch B, Schwartz B, Shoseyov O. A recombinant human RNASET2 glycoprotein with antitumorigenic and antiangiogenic characteristics. *Cancer* (2006) 107:2760–9. doi:10.1002/cncr.22327
253. McClure BA, Gray JE, Anderson MA, Clarke AE. Self-incompatibility in *Nicotiana alata* involves degradation of pollen rRNA. *Nature* (1990) 347:757–60. doi:10.1038/347757a0
254. Ramanauskas K, Igić B. The evolutionary history of plant T2/S-type ribonucleases. *PeerJ* (2017) 5:e3790. doi:10.7717/peerj.3790
255. Kubo K-I, Entani T, Takara A, Wang N, Fields AM, Hua Z, et al. Collaborative non-self recognition system in S-RNase-based self-incompatibility. *Science* (2010) 330:796–9. doi:10.1126/science.1195243
256. Thompson DM, Lu C, Green PJ, Parker R. tRNA cleavage is a conserved response to oxidative stress in eukaryotes. *RNA* (2008) 14:2095–103. doi:10.1261/rna.1232808
257. Schifano JM, Cruz JW, Vvedenskaya IO, Edifor R, Ouyang M, Husson RN, et al. TRNA is a new target for cleavage by a MazF toxin. *Nucleic Acids Res* (2016) 44:1256–70. doi:10.1093/nar/gkv1370
258. Chao Y, Li L, Girodat D, Förstner KU, Said N, Corcoran C, et al. In vivo cleavage map illuminates the central role of RNase E in coding and non-coding RNA pathways. *Mol Cell* (2017) 65:39–51. doi:10.1016/j.molcel.2016.11.002
259. Masuda H, Inouye M. Toxins of prokaryotic toxin-antitoxin systems with sequence-specific endoribonuclease activity. *Toxins (Basel)* (2017) 9:1–23. doi:10.3390/toxins9040140
260. Levitz R, Chapman D, Amitsur M, Green R, Snyder L, Kaufmann G. The optional *E. coli* prr locus encodes a latent form of phage T4-induced anticodon nuclease. *EMBO J* (1990) 9:1383–9.
261. Masaki H, Ogawa T. The modes of action of colicins E5 and D, and related cytotoxic tRNases. *Biochimie* (2002) 84:433–8. doi:10.1016/S0300-9084(02)01425-6
262. Lee SR, Collins K. Starvation-induced cleavage of the tRNA anticodon loop in *Tetrahymena thermophila*. *J Biol Chem* (2005) 280:42744–9. doi:10.1074/jbc.M510356200
263. Cuthbert BJ, Burley KH, Goulding CW. Introducing the new bacterial branch of the RNase A superfamily. *RNA Biol* (2018) 15:9–12. doi:10.1080/15476286.2017.1387710
264. Zaccone P, Burton O, Miller N, Jones FM, Dunne DW, Cooke A. *Schistosoma mansoni* egg antigens induce Treg that participate in diabetes prevention in NOD mice. *Eur J Immunol* (2009) 39:1098–107. doi:10.1002/eji.200838871
265. Burton OT, Gibbs S, Miller N, Jones FM, Wen L, Dunne DW, et al. Importance of TLR2 in the direct response of T lymphocytes to *Schistosoma mansoni* antigens. *Eur J Immunol* (2010) 40:2221–9. doi:10.1002/eji.200939998
266. Durdevic Z, Schaefer M. TRNA modifications: necessary for correct tRNA-derived fragments during the recovery from stress? *Bioessays* (2013) 35:323–7. doi:10.1002/bies.201200158
267. Weller PF, Spencer LA. Functions of tissue-resident eosinophils. *Nat Rev Immunol* (2017) 17:746–60. doi:10.1038/nri.2017.95
268. Haigis MC, Raines RT. Secretory ribonucleases are internalized by a dynamin-independent endocytic pathway. *J Cell Sci* (2003) 116:313–24. doi:10.1242/jcs.00214
269. Leland PA, Raines RT. Cancer chemotherapy – ribonucleases to the rescue. *Chem Biol* (2001) 8:405–13. doi:10.1016/S1074-5521(01)00030-8

270. Lomax JE, Bianchetti CM, Chang A, Phillips GN, Fox BG, Raines RT. Functional evolution of ribonuclease inhibitor: insights from birds and reptiles. *J Mol Biol* (2014) 426:3041–56. doi:10.1016/j.jmb.2014.06.007
271. Dickson KA, Haigis MC, Raines RT. Ribonuclease inhibitor: structure and function. *Prog Nucleic Acid Res Mol Biol* (2005) 80:349–74. doi:10.1016/S0079-6603(05)80009-1
272. Thomas SP, Kim E, Kim J-S, Raines RT. Knockout of the ribonuclease inhibitor gene leaves human cells vulnerable to secretory ribonucleases. *Biochemistry* (2016) 55:6359–62. doi:10.1021/acs.biochem.6b01003
273. Hoang TT, Raines RT. Molecular basis for the autonomous promotion of cell proliferation by angiogenin. *Nucleic Acids Res* (2017) 45:818–31. doi:10.1093/nar/gkw1192
274. Zasloff M. Antimicrobial RNases of human skin. *J Invest Dermatol* (2009) 129:2091–3. doi:10.1038/jid.2009.216
275. Spencer JD, Schwaderer AL, Eichler T, Wang H, Kline J, Justice SS, et al. An endogenous ribonuclease inhibitor regulates the antimicrobial activity of ribonuclease 7 in the human urinary tract. *Kidney Int* (2014) 85:1179–91. doi:10.1038/ki.2013.395
276. Mazzeo C, Canas JA, Zafra MP, Rojas Marco A, Fernandez-Nieto M, Sanz V, et al. Exosome secretion by eosinophils: a possible role in asthma pathogenesis. *J Allergy Clin Immunol* (2015) 135:1603–13. doi:10.1016/j.jaci.2014.11.026
277. Xu R, Greening DW, Rai A, Ji H, Simpson RJ. Highly-purified exosomes and shed microvesicles isolated from the human colon cancer cell line LIM1863 by sequential centrifugal ultrafiltration are biochemically and functionally distinct. *Methods* (2015) 87:11–25. doi:10.1016/j.ymeth.2015.04.008
278. Mateescu B, Kowal EJK, van Balkom BWM, Bartel S, Bhattacharyya SN, Buzás EI, et al. Obstacles and opportunities in the functional analysis of extracellular vesicle RNA – an ISEV position paper. *J Extracell Vesicles* (2017) 6:1286095. doi:10.1080/20013078.2017.1286095
279. Folkman J, Merler E, Abernathy C, Williams G. Isolation of a tumor factor responsible for angiogenesis. *J Exp Med* (1971) 133:275–88. doi:10.1084/jem.133.2.275
280. Xu H, Liu Y, Meng F, He B, Han N, Li G, et al. Multiple bursts of pancreatic ribonuclease gene duplication in insect-eating bats. *Gene* (2013) 526:112–7. doi:10.1016/j.gene.2013.04.035
281. Rucksaken R, Pairojkul C, Pinlaor P, Khuntikeo N, Roytrakul S, Selmi C, et al. Plasma autoantibodies against heat shock protein 70, enolase 1 and ribonuclease/angiogenin inhibitor 1 as potential biomarkers for cholangiocarcinoma. *PLoS One* (2014) 9:e103259. doi:10.1371/journal.pone.0103259
282. Pizzo E, Sarcinelli C, Sheng J, Fusco S, Formiggini F, Netti P, et al. Ribonuclease/angiogenin inhibitor 1 regulates stress-induced subcellular localization of angiogenin to control growth and survival. *J Cell Sci* (2013) 126:4308–19. doi:10.1242/jcs.134551
283. Van Treeck B, Protter DSW, Matheny T, Khong A, Link CD, Parker R. RNA self-assembly contributes to stress granule formation and defining the stress granule transcriptome. *Proc Natl Acad Sci U S A* (2018) 4:1–6. doi:10.1073/pnas.1800038115
284. Esteller M. Non-coding RNAs in human disease. *Nat Rev Genet* (2011) 12:861–74. doi:10.1038/nrg3074
285. Tafech A, Bassett T, Sparanese D, Lee CH. Destroying RNA as a therapeutic approach. *Curr Med Chem* (2006) 13:863–81. doi:10.2174/092986706776361021
286. Krauss J, Arndt MAE, Dübel S, Rybak SM. Antibody-targeted RNase fusion proteins (immunoRNases) for cancer therapy. *Curr Pharm Biotechnol* (2008) 9:231–4. doi:10.2174/138920108784567317
287. Newton DL, Rybak SM. Antibody targeted therapeutics for lymphoma: new focus on the CD22 antigen and RNA Introduction: putting them together. *Expert Opin Biol Ther* (2001) 1:995–1003. doi:10.1517/14712598.1.6.995
288. Weber T, Mavratzas A, Kiesgen S, Haase S, Bottcher B, Exner E, et al. A humanized anti-CD22-onconase antibody-drug conjugate mediates highly potent destruction of targeted tumor cells. *J Immunol Res* (2015) 2015:561814. doi:10.1155/2015/561814
289. Jordaan S, Akinrinmade O, Nachreiner T, Cremer C, Naran K, Chetty S, et al. Updates in the development of ImmunoRNases for the selective killing of tumor cells. *Biomedicines* (2018) 6:28. doi:10.3390/biomedicines6010028
290. Wang X, Li Y, Li Q, Neufeld CI, Pouli D, Sun S, et al. Hyaluronic acid modification of RNase A and its intracellular delivery using lipid-like nanoparticles. *J Control Release* (2017) 263:39–45. doi:10.1016/j.jconrel.2017.01.037

Conflict of Interest Statement: The authors declare that the research was conducted in the absence of any commercial or financial relationships that could be construed as a potential conflict of interest.

CHAPTER III

frontiers in Immunology

ORIGINAL RESEARCH
published: 02 July 2019
doi: 10.3389/fimmu.2019.01500

Human Antimicrobial RNases Inhibit Intracellular Bacterial Growth and Induce Autophagy in Mycobacteria-Infected Macrophages

Lu Lu [1], Javier Arranz-Trullén [1,2], Guillem Prats-Ejarque [1], David Pulido [1†], Sanjib Bhakta [2] and Ester Boix [1*]*

[1] Department of Biochemistry and Molecular Biology, Faculty of Biosciences, Universitat Autònoma de Barcelona, Cerdanyola del Vallès, Spain, [2] Mycobacteria Research Laboratory, Department of Biological Sciences, Institute of Structural and Molecular Biology, Birkbeck, University of London, London, United Kingdom

OPEN ACCESS

Edited by:
Alexandre Corthay, Oslo University Hospital, Norway

Reviewed by:
Anthony George Tsolaki, Brunel University London, United Kingdom
Jianguo Liu, Saint Louis University, United States

***Correspondence:**
Sanjib Bhakta
s.bhakta@bbk.ac.uk;
sanjib.bhakta@ucl.ac.uk
Ester Boix
Ester.Boix@uab.cat

†Present Address:
David Pulido, The Jenner Institute, University of Oxford, Oxford, United Kingdom

Specialty section:
This article was submitted to Molecular Innate Immunity, a section of the journal Frontiers in Immunology

Received: 18 March 2019
Accepted: 14 June 2019
Published: 02 July 2019

Citation:
Lu L, Arranz-Trullén J, Prats-Ejarque G, Pulido D, Bhakta S and Boix E (2019) Human Antimicrobial RNases Inhibit Intracellular Bacterial Growth and Induce Autophagy in Mycobacteria-Infected Macrophages. Front. Immunol. 10:1500. doi: 10.3389/fimmu.2019.01500

The development of novel treatment against tuberculosis is a priority global health challenge. Antimicrobial proteins and peptides offer a multifaceted mechanism suitable to fight bacterial resistance. Within the RNaseA superfamily there is a group of highly cationic proteins secreted by innate immune cells with anti-infective and immune-regulatory properties. In this work, we have tested the human canonical members of the RNase family using a spot-culture growth inhibition assay based mycobacteria-infected macrophage model for evaluating their anti-tubercular properties. Out of the seven tested recombinant human RNases, we have identified two members, RNase3 and RNase6, which were highly effective against *Mycobacterium aurum* extra- and intracellularly and induced an autophagy process. We observed the proteins internalization within macrophages and their capacity to eradicate the intracellular mycobacterial infection at a low micro-molar range. Contribution of the enzymatic activity was discarded by site-directed mutagenesis at the RNase catalytic site. The protein induction of autophagy was analyzed by RT-qPCR, western blot, immunofluorescence, and electron microscopy. Specific blockage of auto-phagosome formation and maturation reduced the protein's ability to eradicate the infection. In addition, we found that the *M. aurum* infection of human THP1 macrophages modulates the expression of endogenous RNase3 and RNase6, suggesting a function *in vivo*. Overall, our data anticipate a biological role for human antimicrobial RNases in host response to mycobacterial infections and set the basis for the design of novel anti-tubercular drugs.

Keywords: antimicrobial peptides, ribonucleases, tuberculosis, macrophage, autophagy

INTRODUCTION

Tuberculosis (TB) is an ancient life-threatening infectious disease currently rated among the top ten causes of death worldwide. According to the World Health Organization (WHO), TB is responsible for about 1.6 million TB deaths and 10 million (5.8 million men, 3.2 million women, and 1.0 million children) new cases have been detected in 2017 and more than a third of the world population is hosting *Mycobacterium tuberculosis*, the causative pathogen of TB, in its latent form (1, 2). In recent

years, we have seen a general decline in the TB incidence rate as well as in the absolute number of registered cases of tuberculosis. Nonetheless, the emergence of a growing number of new cases of multi-drug resistant TB (MDR-TB) and even more alarming extensively drug-resistant TB (XDR-TB) cases have placed the eradication of TB as one of the major global challenges to overcome in the twenty-first century. Furthermore, TB prognosis is significantly aggravated during human immunodeficiency virus (HIV) co-infection. A complex cellular machinery is activated during the host immune response against *M. tuberculosis* (Mtb) bacilli; unfortunately, their underlying mechanisms remain poorly understood. Hence, enlargement of novel and effective therapies to battle mycobacteria are urgently required (3, 4). Mtb is an intracellular pathogen able to survive indefinitely under unfavorable conditions inside primary host immune cells, preferably residing in human alveolar macrophages (5, 6). Several studies have recently shown that features such as its high infectivity, slow growth, and complex cell-wall structure, make *M. tuberculosis* a major challenge to be faced, since the specific mechanisms that reinforce the high virulence of Mtb remain largely unknown (4, 7). Despite the antimicrobial activity of macrophages, Mtb has been able to establish a series of strategies to handle the host immune machinery, interfere with, and arrest the phagosome maturation, counteract mycobactericidal molecules and ultimately survive in a hostile intracellular environment (8–10). Therefore, the search for new anti-TB agents that are able to safely penetrate the host immune cells and eradicate the pathogen intracellularly is now one of the priorities of global health action programs to tackle tuberculosis.

The eventual outcome of a mycobacterial infection largely depends on the readiness of the host immune system to counter the pathogen. During infection a large assortment of antimicrobial protein and peptides (AMPs) are released by host immune cells to the bloodstream and nearby tissues to the infected areas (11, 12). At the same time, neutrophil, and eosinophil granules, loaded with lytic enzymes, and antimicrobial molecules, can be acquired by macrophages to counter bacterial invasion (13–15). Because AMPs exert a potent anti-infective effect against a wide range of human pathogens and the likelihood of microbial resistance is mostly reduced in comparison to conventional antibiotics, they are emerging as a new generation of natural lead candidates and its administration in combination with or without other drugs is showing highly promising results (16).

Abbreviations: DOPC, 1,2-dioleoyl-sn-glycero-3-phosphocholine; DOPG, 1,2-dioleoyl-sn-glycero-3-phosphoglycerol); 3MA, 3 Methyadenine; MTT, 3-(4,5-Dimethylthiazol-2-yl)-2,5-diphenyltetrazolium bromide; AO, Acridine orange; AMPs, Antimicrobial protein and peptides; BA, Bafilomycin A; CFU, Colony forming unit; XDR, Extensively drug-resistant; FBS, Fetal bovine serum; HTS, High-throughput screening; LUVs, Large unilamellar vesicles; MB, Middlebrook; MAC, Minimum agglutination activity; MBC, minimum bactericidal concentration; MIC, minimum inhibitory concentration; MOI, Multiplicity of infection; MDR, Multi-drug resistant; Mtb, *Mycobacterium tuberculosis*; NCTC, National Collection of Type Cultures; PMA, Phorbol myristate acetate; SPOTi, Spot-culture growth inhibition assay; TEM, Transmission electron microscopy; TB, Tuberculosis; ZN, Ziehl-Neelsen.

Our research group works on the mechanism of action of human antimicrobial RNases, a group of proteins that belong to the RNase-A superfamily. The family encompasses eight functional members in humans, referred as the "canonical RNases" (17). Among them, there are proteins secreted by epithelial and blood cell types during host-defense response that are endowed with the characteristic biophysical features of AMPs (12, 18, 19). In particular, human RNase3, RNase6, and RNase7 are highly cationic proteins with reported antimicrobial activity against a variety of microbes (20–23). Interestingly, secretion of RNases 3 and 7 was associated to *Mycobacterium bovis* (*M. bovis*) BCG and *M. tuberculosis* infection, respectively (14, 24). Indeed, both RNases displayed antimycobacterial activity *in vitro* (25).

In this work, we aimed to study the antimycobacterial activity of the human canonical RNases by applying an integrated surrogate model for screening of anti-tubercular drugs against *M. tuberculosis* (8). The semi-solid agar-based spot-culture growth inhibition assay (SPOTi) has facilitated a rapid high-through screening of antimicrobial agents against *Mycobacterium aurum* (*M. aurum*) using a macrophage infected model (8, 26, 27). *M. aurum* was chosen as a relatively fast-growing and stable intracellular dwelling species within infected macrophages, previously validated as an appropriate surrogate model for Mtb (8). RNases with positive antimycobacterial activity were further characterized by exploring their mechanism of action in macrophages. The present results indicate that the protein antimycobacterial action is partly mediated by the induction of an autophagy process.

MATERIALS AND METHODS

Protein Expression and Purification

The cDNA for RNase1 was a gift from Prof. Maria Vilanova (Universitat de Girona, Spain) and RNase5 from Prof. Demetres Leonidas (University of Thessaly, Greece). RNase4 synthetic gene was purchased from Nzytech company and RNase6 was obtained from DNA 2.0 (Menlo Park, CA, USA). RNase2, RNase3, and RNase7 genes were obtained as previously described (20). Active site mutations into the RNases genes were introduced using the Quick change™ site-directed mutagenesis kit (Agilent, 200523) following the manufacturers procedure (28). *Escherichia coli (E. coli)* BL21 (DE3) (Novagen, 69450) competent cells were transformed with the pET11c/RNase plasmids. Recombinant proteins were expressed and purified in *E. coli* BL21 (DE3) by an adaptation of the protocol previously described (20). Briefly, *E. coli* BL21(DE3) cells were induced by 1 mM isopropyl β-D-1-thiogalactopyranoside (G Bioscience, RC-063) and the inclusion bodies enriched pellet was resuspended in 80 mL of 10 mM Tris-HCl pH 8.5, 2 mM EDTA and left incubating 30 min with 40 μg/mL of lysozyme prior to sonication. Then, the sample was centrifuged at 30.000 × *g* for 30 min at 4°C and the pellet was resuspended in 25 mL of the same buffer supplemented with 1% triton X-100 and 1 M urea and was left stirring at room temperature for 30 min and centrifuged 30 min at 22.000 × *g*. Following, 200 mL of 10 mM Tris-HCl pH 8.5, 2 mM EDTA was added to the pellet, and then the sample was centrifuged at 22.000 × *g* for 30 min (4°C). The resulting pellet solubilized

in 6 M guanidine hydrochloride and rapidly 80-fold diluted in the refolding buffer was left in gentle stirring for 48–72 h at 4°C. The folded protein was then concentrated, dialyzed against the chromatography buffer and purified by cation exchange chromatography on a Resource S column (GE Healthcare Life Sciences, GE17118001). The identity and homogeneity of the purified proteins were checked by SDS-PAGE, MALDI-TOF, and N-terminal sequencing.

Macrophage Cell Culture

Mouse RAW 264.7 cells (NCTC, #91062702) and human THP-1 cells (NCTC, #88081201) were maintained or passaged in 25 cm^2 tissue culture flasks (BD Biosciences, 353108) using DMEM (Lonza, BE04-687F/U1) and RPMI-1640 (Lonza, BE12-702F) medium with 10% heat-inactivated fetal bovine serum (FBS, Gibco, 26140079) respectively at 37°C and humidified 5% CO_2 conditions. RAW 264.7 cells were seeded at 5×10^5 per well and allowed to attach for 2 h before infection and treatment. THP-1 cells were treated with 100 nM phorbol myristate acetate (PMA, Sigma-Aldrich, P8139) for 48 h to induce differentiation into macrophage-like cells and allowed to rest for 24 h before further treatment. The number of viable cells was counted using a Trypan blue (Invitrogen, 15250-061) exclusion assay.

Growth of Mycobacteria Culture and Macrophage Infection

Mycobacterium aurum was purchased from the UK National Collection of Type Cultures (NCTC). Cells cultures of *M. aurum* (NCTC, 10437), *Mycobacterium smegmatis* mc^2155 (ATCC, 700084) and *M. bovis* BCG Pasteur (ATCC, 35734) were grown in Middlebrook (MB) 7H9 broth (BD Biosciences, 271310) enriched with 10% (v/v) albumin/dextrose/catalase (ADC; BD Biosciences, 212352) containing 0.05% Tween 80 and 0.05% Glycerol for liquid growth at 37°C for BCG, and in MB7H10 (BD Biosciences, 262710) with 10% (v/v) oleic acid/albumin/dextrose/catalase (OADC; BD Biosciences, 212240) for semi-solid agar growth at 37°C. Stock cultures of log-phase cells were maintained in glycerol (25% final concentration of glycerol) at −80°C. The bacteria were vortexed and sonicated using ultrasound sonication bath to obtain a single cell suspension, and then the bacterial concentration was determined by measuring the optical density (OD) of the culture at 600 nm (1 OD $=10^9$ CFU/mL). Mid-log phase *M. aurum* cells, harvested in RPMI-1640 complete medium, were co-cultured with RAW264.7 or THP-1 at a multiplicity of infection (MOI) of 10:1 and were incubated at 37°C for 3 h, then were washed 3 times with PBS and replaced with fresh media supplied with 50 μg/mL gentamycin (Apollo Scientific, BIG0124) to remove extracellular mycobacteria during further treatment.

High Throughput SPOTi Assay, Minimum Inhibitory Concentration (MIC), and Minimum Bactericidal Concentration (MBC) Assays

Antimicrobial activity of RNases was evaluated by calculating the 100% minimum bactericidal concentration (MBC_{100}) and 100% minimum inhibitory concentration (MIC_{100}) in mycobacteria cultures. The semi-solid agar-based SPOTi assay system was applied for fast and high throughput screening and the colony forming unit (CFU) counting assay for the validation and accurate MBC/MIC_{100} determination (8). The MBC_{100} and MIC_{100} of each protein was determined from two independent experiments performed in triplicate for each concentration. Briefly, log-phase cultures of mycobacteria ($OD_{600} \approx 1$) were first checked for quality control using cold Ziehl–Neelsen (ZN) staining (also called "acid fast staining"; TB-color staining kit, Merck Millipore, 116450) according to the manufacturer's protocol. For extracellular analysis, the mycobacterial cultures were then diluted to 2×10^5 CFUs/mL and directly incubated with proteins at 37°C for 4 h in PBS in 1 mL. For intracellular analysis, the mycobacterial cultures diluted to 2×10^5 CFUs/mL were used to infect macrophages and then treated with the proteins for up to 72 h in RPMI-1640 medium with 10% FBS. MIC_{100} were calculated at final incubation time. Uptake of mycobacteria by RAW macrophages was confirmed using the ZN staining assay, as described (8). No significant reduction in the number of live macrophages was observed during the experiment. Macrophage infection was monitored by CFUs counting. Following the treatment, to evaluate the activity at the protein extracellular activity the cultures were centrifuged and suspended in 50 μL of distilled water and 5 μL of the sample was spotted onto wells of a 24-well plate containing MB7H10/OADC/agar. For evaluation of the protein intracellular activity, the macrophages were washed twice with RPMI-1640 and lysed in water to harvest intracellular mycobacteria for plating in 24-well plate (SPOTi) or 10 mm petri dish (CFU assay). Initial infection was adjusted to 2×10^5 CFU/mL for all samples. Mycobacterial cell growth at 37°C was recorded after 2 days for *M. smegmatis*, 4–5 days for *M. aurum*, and 14 days for *M. bovis* BCG.

Minimum Agglutination Activity (MAC) Assay

Mycobacterial cells were grown at 37°C to an OD600 of 1.0 and diluted ten times. Then, cells were centrifuged at 5,000 × g for 2 min, and resuspended in M7H9/ADC media containing 0.05% Tween-80 and 0.05% glycerol. An aliquot of 100 μl of the mycobacterial suspension was treated with increasing protein concentrations (from 0.01 to 25 μM) and incubated at 37°C for 1 h. The aggregation behavior was observed by visual inspection with a stereomicroscope at 50x, and the agglutinating activity was calculated as the minimum agglutinating concentration of the protein, as previously described Pulido et al. (22).

Cytotoxicity Assay

To assay the toxicity of RNases to RAW264.7 macrophages, the assay was performed in 96-well cell culture flat-bottom plates (Costar; Appleton Woods) in triplicate. To each well, 100 μL of diluted macrophage cells (5×10^5 cells/mL) were dispensed in 96-well plates and then proteins were added serially at final concentrations ranging from 0.01 to 50 μM (100 μL/well) and incubated for 48 h; cells were then washed twice with 1X PBS, and fresh RPMI-1640 complete medium was added. Plates were

then treated with 30 μL of a freshly prepared 0.01% resazurin solution and incubated overnight at 37°C. The following day the change in color was observed and the fluorescence intensity was measured (λ_{em}560, λ_{ex}590 nm, FLUOstar OPTIMA microplate reader; BMG LABTECH GmbH). The 50% growth inhibitory concentration (IC_{50}) was determined.

Tracking of RNases Internalization Into RAW264.7 Macrophages by Confocal Microscopy

RNase3, RNase6, and RNase7 were labeled with Alexa Fluor 488 Labeling kit (Invitrogen, A10235), following the manufacturer's instruction as previously described (21). To 0.5 mL of 2 mg/mL protein solution in PBS, 50 μL of 1 M sodium bicarbonate, pH 8.3, was added. The protein was incubated for 1 h at room temperature with the reactive dye, with stirring, and the labeled protein was separated from the free dye by PD-10 desalting column (GE Healthcare, 17-0851-01). Labeled protein distribution in cell cultures was followed by confocal microscopy. About 2.5 × 10^5 RAW cells were harvested in 3 cm diameter microscopy plates (MatTek, P35G-1.5-14-C) 2–3 h before the assay. Macrophages were washed with RPMI and labeled with Hoescht 33342 (Thermo Fisher Scientific, 62249) and Cell Mask Deep Red Plasma membrane Stain (Thermo Fisher Scientific, C10046) at 0.5 μg/mL for 5–10 min before observation in Leica TCS SP5 AOBS equipped with a PL APO 63 × 1.4–0.6 CS oil immersion objective (Leica Microsystems, Mannheim, Germany). Following, Alexa Fluor labeled proteins were added at 2 μM to the cultures and time lapse was recorded at intervals of 30 s for 30 min. Fluorochromes were excited by 405 nm (Hoechst 33342), 649 nm (CellMask Deep Red), and 488 nm (Alexa Fluor 488). Emissions were collected with a HyD detector.

Real-Time qPCR Assays

Total RNA was extracted using mirVanaTM miRNA Isolation Kit as described by the manufacturer (Ambion, Life Technologies, AM1560) at each time point (4, 24, 48, 72 h). Total RNA was quantified by NanoDropTM spectrophotometer (Thermo Fisher Scientific, Wilmington, DE USA), and cDNA was synthesized using iScriptTM cDNA Synthesis Kit (Bio-Rad, 170-8891). The unique ID of the primers used (synthesized by Bio-Rad, Hercules, CA, USA) is shown in **Table S1**. Transcripts of human *RNase2*, *RNase3*, *RNase6*, and *RNase7* genes relative to the human housekeeping *GAPDH*, and mouse *BECN1* and *ATG5* genes relative to mouse housekeeping *β-actin* were measured in triplicate from cDNA samples by real-time quantitative PCR using CFX96 Real-Time PCR detection system (Bio-Rad, Hercules, CA, USA). The results were analyzed by using the relative standard method (29).

Western-Blot Analysis

Expression level of the autophagy marker LC3 in RAW264.7 macrophages was evaluated by western blot analysis. Autophagy was inhibited by addition of either 100 nM of Bafilomycin A (BA, Sigma-Aldrich, 19-148) or 5 mM of 3 Methyladenine (3MA, Sigma-Aldrich, M9281) (30, 31). Rapamycin (Sigma-Aldrich, R0395) at 100 nM was used as a positive control. When the treatment was finished, cells were lysed by RIPA buffer and the protein concentration was determined with the Pierce BCA Protein Assay kit (Thermo Fisher Scientific, 23225). Equal amounts of protein (50 μg) for each sample were loaded onto a 15% SDS–PAGE gel. After the electrophoresis, proteins were transferred to PVDF membrane. The membranes were blocked and incubated with the primary antibody of interest. The primary antibodies used were rabbit polyclonal anti-LC3 (1:1,000, Abcam, ab48394) and chicken polyclonal anti-GAPDH (1:2,000, Abcam, ab9483). After washing, a horseradish peroxidase-conjugated antibody (Goat Anti-Rabbit IgG antibody, Sigma Aldrich, 12-348 and Goat anti-chicken IgY H&L, Abcam, ab6877) was applied for detection using an enhanced chemiluminescent detection system (Supersignal West Pico Chemiluminescent Substrate, ThermoFisher Scientific, 32209). Densitometry analysis was performed using Quantity One software.

Immunofluorescence Microscopy

RAW264.7 cells were grown, plated, and infected as above on glass coverslip (5 × 10^5 cells each one). After fixation and blocking, cells were incubated with the primary antibodies anti-LC3 (1:200, Abcam, ab48394); the cultures were incubated for 1 h at room temperature with labeled secondary antibodies (1:500, anti-rabbit IgG-Alexa Fluor 488, ThermoFisher Scientific, A-11008) and then washed 3 times with PBS. Cells were incubated with Hoechst (ThermoFisher Scientific, 62249) and Cell Mask Deep Red (Invitrogen, C10046) to visualize the nuclei and membrane, and then were loaded with mounting media and sealed with nail oil. Images were captured by Leica TCS SP5 AOBS microscope equipped with a PL APO 63 × 1.4–0.6 CS oil immersion objective (Leica Microsystems, Mannheim, Germany). Quantification of fluorescence intensity was performed by using *Imaris* software.

Alternatively, to quantify LC3 accumulation RAW264.7 cells were plated on glass coverslip (5 × 10^5 cells each one) and treated with RNase3 and/or Bafilomycin A. After treatment, cells were fixed with 2% paraformaldehyde, permeabilized with 0.05% triton-X100, and blocked with 5% non-fat milk. Cells were incubated with the primary antibodies anti-LC3 at 4°C overnight (1:200, Abcam, ab48394), and room temperature 2 h with secondary anti-rabbit IgG-Alexa 488 antibody(ThermoFisher Scientific, A-11008) and then washed 3 times with PBS. Cells were stained with DAPI (ThermoFisher Scientific, 62248) to visualize the nuclei for 30 min at room temperature and then were loaded with mounting media and sealed with nail oil. Images were captured by Leica DM RB equipped with a Leica DFC 500 camera under 100-fold oil objective. LC3 puncta vesicle quantification was performed using *Image J*.

Transmission Electron Microscopy

For transmission electron microscopy (TEM) analysis, 10^6 infected RAW264.7 macrophages cells were seeded in 6-well tissue culture plates and were treated with 10 μM RNase3 or RNase3-H15A for 24 h. After treatment, macrophages were fixed with 2% (w/v) paraformaldehyde and 2.5% (v/v) glutaraldehyde in PBS for 1 h. The samples were then dehydrated in acetone (50,

70, 90, 95, and 100%) and were immersed in Epon resin (32). The ultrathin sections were examined in a JEOL JEM 2011 instrument (JEOL, Ltd., Tokyo, Japan).

Acidic Vesicular Compartment Quantification by the Acridine Orange Assay

To quantify the volume/amount of the acidic vesicular compartment, RAW264.7 macrophage cells were treated with the proteins and were stained with acridine orange (AO, ThermoFisher Scientific, A1301) as previously described (33). Briefly, cells were seeded in 96-well plates (10^4 cells/well) and treated with RNases for 24 h. Rapamycin (100 nM) was used as a positive control and BA (100 nM) was used as an inhibitor of acidification of vesicular content. At the end of the treatments, cells were washed with pre-warmed PBS and stained with 5 μg/mL AO for 10 min in PBS. After washing with PBS three times, the increase in the amount of the acidic vesicular compartment was quantified by measuring the red/green fluorescence intensity ratio of AO staining (AO green fluorescence λ_{exc} 485 and λ_{em} 535 nm; AO red fluorescence λ_{exc} 430 and λ_{em} 590 nm). Values were normalized by cell proliferation count by the Thiazolyl Blue Tetrazolium Bromide (MTT, Sigma-Aldrich, M5655-100MG) assay.

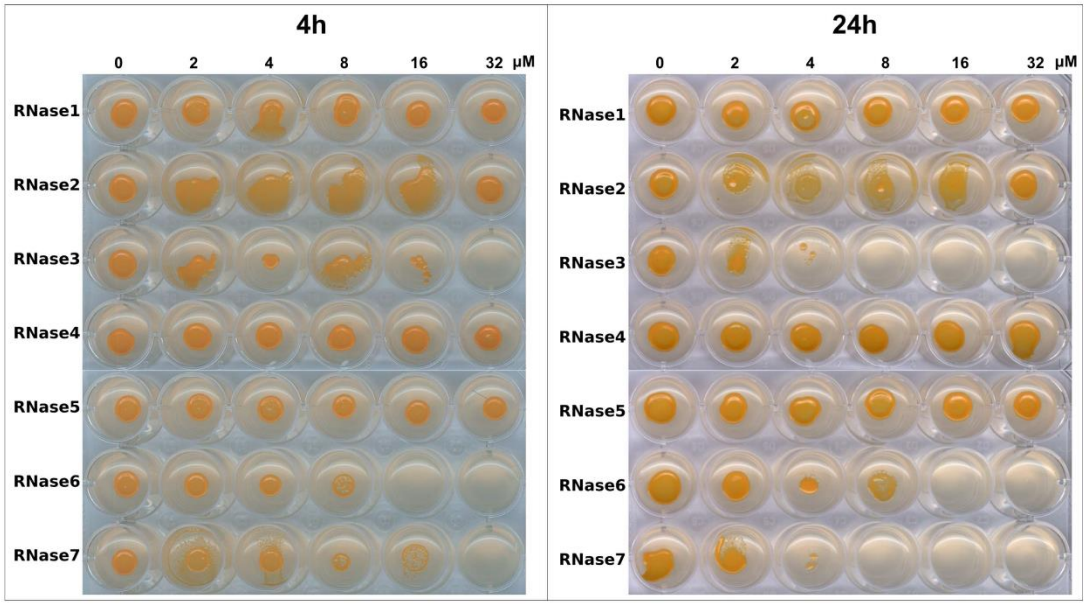

FIGURE 1 | A representative SPOTi image comparing human RNases activity on *Mycobacterium aurum* infected macrophages. RAW 264.7 macrophages were infected with *M. aurum* at 10:1 MOI for 3 h at 37°C. The culture was washed with RPMI-1640 thrice and incubated with different concentrations of the proteins in RPMI-1640 complete medium for 4 h (**Left**) or 24 h (**Right**). Macrophages were washed twice with RPMI-1640 and lysed. Then, an aliquot was spotted onto wells of a 24-well plate containing MB7H10/OADC/agar and incubated at 37°C for 4–5 days to determine intracellular survival.

TABLE 1 | Comparison of the antimycobacterial activity of RNase3, RNase6, and RNase7 and their respective active center mutants (H15A).

Protein	Extracellular MBC (μM)			MAC (μM)			Intracellular MIC (μM)	IC_{50} (μM)
	M. aurum	*M. smegmatis* mc^2155	*M. bovis* BCG	*M. aurum*	*M. smegmatis* mc^2155	*M. bovis* BCG	*M. aurum*	RAW264.7
RNase3	18.75 ± 0.05	9.37 ± 0.05	18.75 ± 0.05	2.34 ± 0.5	1.17 ± 0.3	4.68 ± 1.0	5 ± 0.05	> 25
RNase3-H15A	18.75 ± 0.05	18.75 ± 0.05	18.75 ± 0.05	4.68 ± 0.5	4.68 ± 1.0	4.68 ± 1.0	10 ± 0.05	> 25
RNase6	18.75 ± 0.05	18.75 ± 0.05	18.75 ± 0.05	4.68 ± 1.0	2.34 ± 0.5	4.68 ± 1.0	10 ± 0.05	> 25
RNase6-H15A	18.75 ± 0.05	18.75 ± 0.05	37.5 ± 0.05	4.68 ± 1.0	2.34 ± 0.5	4.68 ± 1.0	10 ± 0.05	> 25
RNase7	18.75 ± 0.05	18.75 ± 0.05	18.75 ± 0.05	> 10	> 10	> 25	10 ± 0.05	> 25
RNase7-H15A	18.75 ± 0.05	18.75 ± 0.05	18.75 ± 0.05	> 10	> 10	> 25	10 ± 0.05	> 25

Extracellular minimum bactericidal concentration (MBC_{100}) and intracellular minimum inhibitory concentration (MIC_{100}) were calculated at 72 h incubation time using the SPOTi assay. Minimum agglutination concentration (MAC) and Inhibitory Concentration (IC_{50}) for RAW 264.7 mouse macrophages were assayed as described in the methodology. Results are an average of three independent repeated experiments. Mean average values ± SD are indicated.

Liposome Aggregation Assay

Large unilamellar vesicles (LUVs) were prepared as previously described (20). Briefly, 1,2-dioleoyl-sn-glycero-3-phosphocholine (DOPC, Avanti, 850375) and 1,2-dioleoyl-sn-glycero-3-phospho-(1'-rac-glycerol) (DOPG, Avanti, 840445P) were mixed in chloroform with 3:2 molar ratio and used to prepare LUVs by Rotavapor. Then the liposomes were resuspended with 10 mM Tris/HCl, pH7.4 and generated a defined size (100 nm) by extrusion through 100 nm polycarbonate membranes.

Aggregation of liposomes was monitored by recording the scattering intensity with the excitation and emission wavelengths at 470 nm using Cary Eclypse spectrofluorimeter. Liposomes were incubated with proteins for indicated time at room temperature, the signal was read 90 degree from the excitation beam with slits at 2.5 and 5 nm.

Statistical Analysis

Data are presented as mean ± SD and comparisons between groups were analyzed by paired Student *t*-test and one-way ANOVA for comparing more than 2 groups. $p < 0.05$ was considered as statistically significant.

RESULTS

Screening of Human Canonical RNases Identifies Three Members With Antimycobacterial Activity at Extracellular and Intracellular Levels

In this work we have evaluated for the first time the antimicrobial potency of the seven human RNases from the RNase A superfamily using the SPOTi surrogate model adapted for the screening of novel anti-TB drug candidates (8). Previous work in our laboratory selected *M. aurum* as a fast non-pathogenic species suitable for the screening of anti-tubercular drugs at the extracellular (directly on mycobacterial culture) and intracellular (on mycobacteria residing inside infected macrophage cell-line) levels, referred in this article as *in vitro* and *ex vivo* assays, respectively. Screening results indicated that RNase3, RNase6 and RNase7 can completely inhibit the growth of *M. aurum* cultures at a low micromolar concentration range, while the rest of the RNases did not reduce the mycobacteria population even at the highest concentration tested (**Figure S1**). Next, we assayed the antimicrobial activity of the seven human RNaseA protein family members against *M. aurum* within RAW 264.7 mouse macrophages. Results from the screening of the seven human secreted RNases confirmed that only RNase3, RNase6 and RNase7 are active against mycobacterial infection (**Figure 1**). Interestingly, when comparing the reduction of CFU counts in comparison to control untreated samples for *in vitro* and *ex vivo* conditions we observed that the effectiveness of the protein was higher at the intracellular level (*ex vivo* assay) (**Table 1**). Besides, comparison of the macrophage intracellular antimycobacterial activity at 4 and 24 h indicated that the protein activity is enhanced at longer incubation times. Total inhibition of intracellular *M. aurum* growth was achieved at about 2-fold lower protein concentration at 24 h incubation time in comparison to 4 h (**Figure 1**). Monitoring of the protein activity within infected macrophages up to 72 h also revealed an increase of the antimicrobial efficiency at longer exposure times. The results suggested that other mechanisms, together with a direct killing of the bacilli, are taking place.

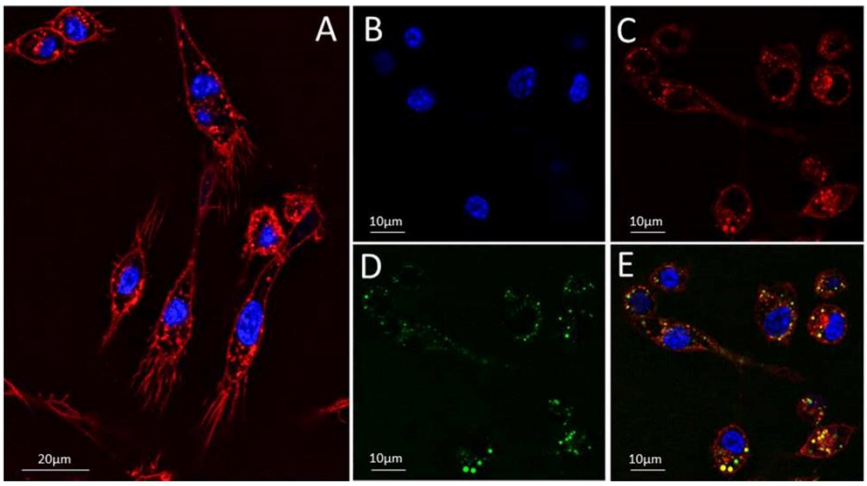

FIGURE 2 | Tracking the translocation of Alexa Fluor 488-labeled RNase3 into RAW 264.7 mouse macrophages. **(A)** macrophages cells were stained with Hoechst and Deep Red to visualize the nuclei (blue) **(B)** and membranes (red) **(C)**, respectively. **(D)** The protein location was registered after 30 min of macrophages post-treatment with Alexa Fluor 488-RNase3 (green). A panel showing merged images is shown in **(E)**. Protein tracking assays were performed using 2.5×10^5 cells/mL and adding 2 μM of labeled protein final concentration. The images were taken using a Leica TCS SP5 AOBS microscope (see Materials and Methods section for more details).

The Enzymatic Activity Is Not Involved in the RNases Antimycobacterial Activity

Following, RNase3, RNase6, and RNase7 were chosen to further investigate whether the enzymatic activity contributes to the antimycobacterial properties of human RNases by comparing the recombinant native proteins with their catalytic inactive mutants. Previous work from our laboratory confirmed that the H15A substitution fully removed the catalytic activity without altering the protein 3D-structure (28). First, the three antimicrobial proteins (RNases 3, 6, and 7) together with their respective active site mutants (H15A) were tested *in vitro* against *M. smegmatis* mc^{2}155, *M. aurum* and *M. bovis* BCG. As summarized in **Table 1**, RNase3, RNase6, and RNase7 showed similar antimicrobial activities against the three mycobacteria species. Then, *M. aurum* species was chosen for macrophage intracellular studies, being among the three tested species the only one that provides a fast growing profile together with an efficient macrophage uptake (8). Overall, no significant differences were observed between the native proteins and their respective active site mutants against *M. aurum*, both at the extracellular and intracellular levels. Therefore, we can conclude that the three RNases can eradicate *M. aurum* dwelling within the macrophage at a low micromolar concentration range. To note, RNase3 stands out as the most active, achieving mycobacterial growth inhibition at 5 μM (**Table 1**).

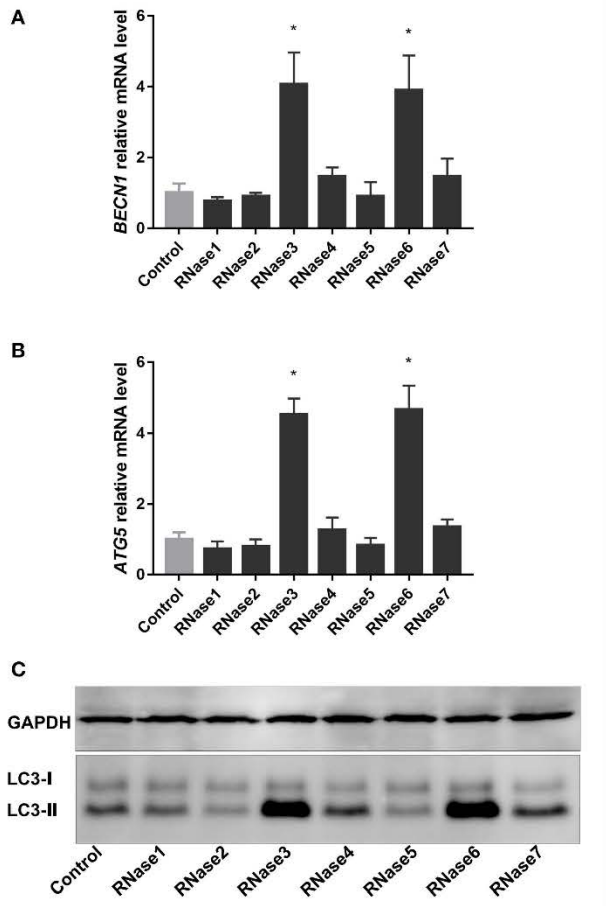

FIGURE 3 | Human RNases 3 and 6 induce macrophage autophagy. RAW 264.7 macrophages were infected with *M. aurum* and treated with 10 μM of proteins (RNase1 to RNase7) for 24 h. Real-time qPCR measured the relative expression of *BECN1* **(A)** and *ATG5* **(B)** genes normalized by housekeeping gene *β-actin*. Results are shown from 3 independent experiments (mean ± SD); **(C)** Immunoblot of LC3-processing and the housekeeping GAPDH control. Results are shown from 3 independent experiments (mean ± SD). *Statistically significant differences compared with the control sample are indicated (p value < 0.05).

Next, we tested the agglutinating activity of the RNases against the three assayed mycobacterial species. The agglutinating activity was calculated as the minimum agglutinating concentration (MAC). Results indicated that RNase3 and RNase6 can agglutinate mycobacteria within the same concentration range, while RNase7 is not active even at the maximum concentration tested. Besides, there were no significant differences among the MAC values of the wild type and active site mutants (**Table 1**). From our findings, we can infer that catalytic activity of the ribonucleases is not involved in their antimycobacterial mode of action.

Tracking the Protein Internalization Within Macrophages

Following, the RNases internalization within macrophages was visualized by confocal microscopy. Results confirmed that the three RNases are able to internalize within the mouse macrophages through a vesicle-mediated mechanism (**Figure 2**). Analysis of the profiles of selected regions of interest confirmed the protein confined location within macrophage vesicles (**Figures S2**, **S3**). In addition, time-lapse assays indicated that internalization is a fast process, where most of the protein enters into the macrophage within the first 30 min. Examples of internalization fluorescence profiles of labeled RNase3, RNase6, and RNase7 were recorded at several time intervals (**Figure S4**). Confocal microscopy images confirmed that no damage to the macrophage cells at the assayed conditions was taking place. Besides, the protein toxicity on the mouse macrophages in the assayed conditions was also discarded by using the resazurin assay; no significant cytotoxicity was observed at the maximum concentration tested (25 μM) (**Table 1**).

M. aurum Infection Modulates the Expression of RNases in THP1 Macrophage Differentiated Cells

Encouraged by positive results on the antimycobacterial activity of recombinant RNases we decided to test whether the mycobacteria infection can induce the protein expression in human macrophages. We selected the human monocyte THP1 cell line differentiated to macrophages and infected it with *M. aurum*. Levels of expression of human RNases were evaluated by real time qPCR. Primers of the four known antimicrobial RNases expressed in blood cell type were used to quantify their transcription levels (**Table S1**). Transcription levels were quantified in relation to the *GAPDH* housekeeping

gene. Results indicated that both control macrophage derived THP1 cells and *M. aurum* infected cells expressed the tested RNase genes (**Figure S5**). However, the protein transcription rates differed significantly among the RNases. Results of non-infected THP1 cells were in agreement with previous expression profile reports showing the predominant transcription of *RNase2* (18). Comparison of the relative expression levels highlighted also the significant quantities of *RNase6* followed by *RNase3*. On the contrary, *RNase7* expression was very scarce, more than 1,000-fold lower than *RNase2*. Interestingly, *M. aurum* infection modulated the expression of *RNase3* and *RNase6*, while *RNase2* transcription levels remained unaffected (**Figure S5**). In addition, analysis of the expression profiles as a function of time also highlighted significant differences between early and late infection periods. Overall, *M. aurum* infection significantly inhibited the THP1 cells expression of RNases at the beginning of the infection (24 h), but triggered their expression at longer infection periods (48–72 h).

RNases 3 and 6 Induce Autophagy in Macrophages

Autophagy is one of the main mechanisms activated by infected macrophages to remove intracellular resident mycobacteria (34). Considering that some AMPs are known to participate in the host immune response against mycobacteria by the activation of autophagy (12), we decided to explore the action of human RNases on infected macrophages. RAW 264.7 mouse macrophages were chosen as a stable well-characterized cell line for the analysis of the recombinant proteins. First, we tested whether the human RNases could induce the expression of the autophagy markers *BECN1* and *ATG5*, two essential genes involved in autophagosome formation and maturation, respectively. Analysis of qPCR results indicated that RNase3 and RNase6, out of the seven screened RNases, significantly upregulated the mRNA expression of *BECN1* and *ATG5* in RAW 264.7 macrophages (**Figures 3A,B**). These positive results were corroborated by analysis of LC3 processing and detection of the LC3II form, involved in the autophagosome formation (35). LC3 transformation was also evaluated by immunoblotting, confirming an increase in the LC3II fraction in detriment of LC3I in RNase3 and RNase6 treated samples in comparison to control (**Figure 3C**). Therefore, we conclude that both RNases activate an autophagy process in the treated macrophages.

RNase Catalytic Activity Is Not Required for the Protein Autophagy Activation

We then analyzed in more details the protein activation of the autophagy pathway by using as a reference RNase3, the most active family member. First, the RNase3 wild-type ability to induce autophagy was compared with the RNase3-H15A enzymatically inactive variant by following the expression of *BECN1* and *ATG5* and monitoring the LC3II/LC3I ratio (**Figure 4**). Equivalent activity of both wild-type and H15A mutant proteins discards any contribution of the enzyme catalytic activity in the autophagy pathway activation.

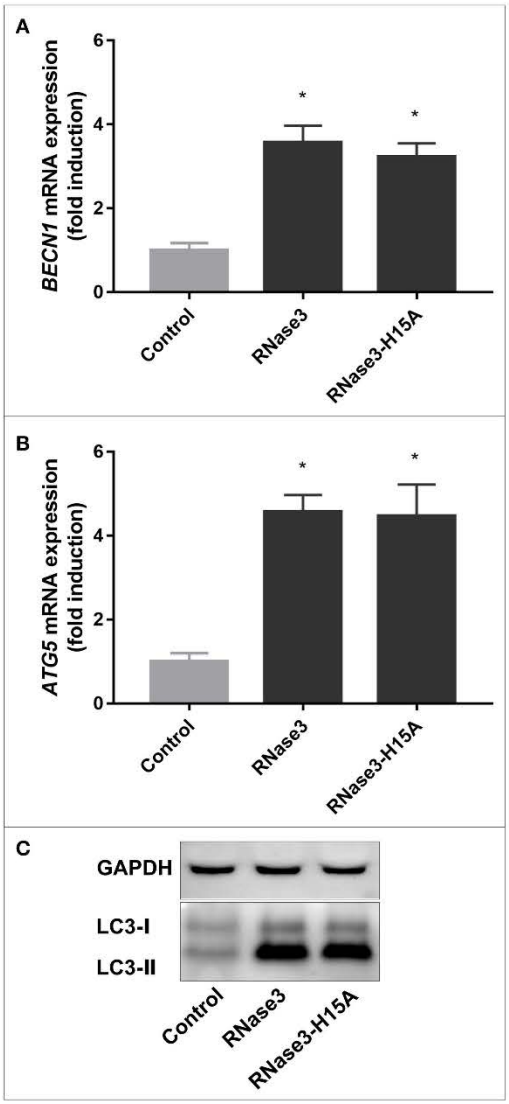

FIGURE 4 | Both RNase3 and the RNase-H15A active site mutant induce autophagy in macrophages. RAW 264.7 mouse macrophages were infected with *M. aurum* and treated with 10 μM of protein (RNase3 and RNase3-H15A). Real-time qPCR measured the relative expression of *BECN1* **(A)** and *ATG5* **(B)** genes normalized by the housekeeping gene *β-actin*. Results are shown from 3 independent experiments (mean ± SD); **(C)** Immunoblot of LC3-processing and the housekeeping GAPDH control. Results are shown from 3 independent experiments (mean ± SD). *Statistically significant differences compared with the control sample are indicated (p value < 0.05).

In addition, LC3 transformation was monitored by immunofluorescence microscopy after treatment of *M. aurum* infected RAW macrophage cells with either RNase3, RNase3-H15A, or rapamycin, used as a positive control of autophagy induction, observing in all cases a significant increase of LC3 intensity (**Figures 5A,C**). Complementarily, we applied TEM to visualize the ultrastructure of mouse macrophages infected with *M. aurum* and treated with RNase3 and RNase3-H15A.

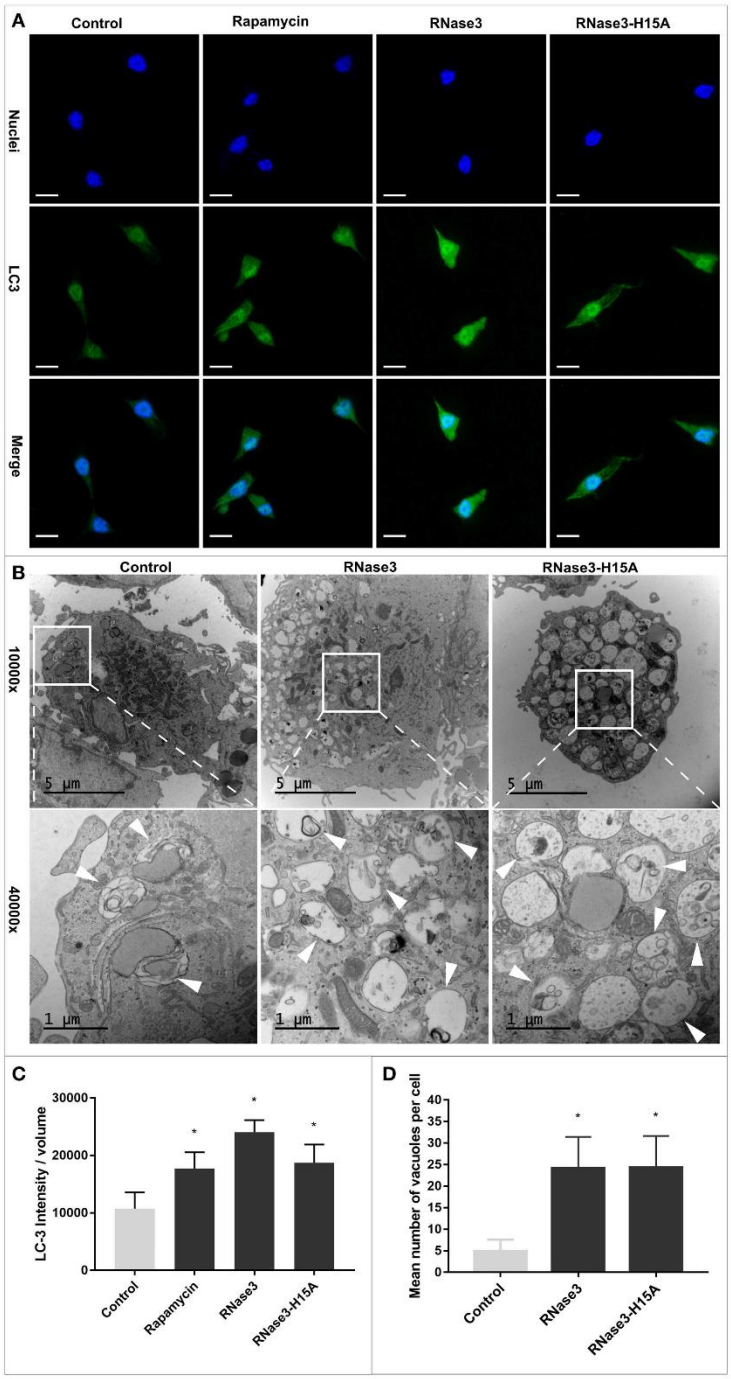

FIGURE 5 | RNase3 and RNase3-H15A induce autophagic vacuole formation and LC3 processing. **(A)** Immunofluorescence microscopy analysis of LC3 processing, Mouse macrophages were infected with *M. aurum* and treated with 10 μM of RNase3, or 10 μM RNase3-H15A mutant, or 100 nM Rapamycin for 24 h. After treatment, the cells were fixed and stained with Hoechst to visualize the nuclei (blue), and with anti-LC3 followed by the addition of Alexa Fluor 488-conjugated anti-rabbit IgG (green). One representative immunofluorescence image out of 3 independent replicates are shown; scale bars: 10 μm; **(B)** Representative transmission electron microscopy images of *M. aurum* infected RAW264.7 cells treated with 10 μM RNase3 or 10 μM RNase3-H15A. Autophagic vacuoles are indicated by white arrow; **(C)** Quantitative analysis of LC3 intensity normalized with cell volume from 3 replicates. Results are shown from 3 independent experiments (mean ± SD). *Statistically significant differences compared with the control sample are indicated (p value ≤ 0.05). **(D)** total number of autophagic vacuoles per cell for 30 cells randomly selected per each treated sample. Autophagic vacuoles were defined as double-membrane vacuolar structures containing recognizable cytoplasmic contents. *Statistically significant differences compared with the control sample are indicated (p-value ≤ 0.05).

Inspection of electron micrographs revealed a higher number of double-membrane vacuoles in both RNase3 and RNase3-H15A treated macrophages in comparison with the control group (**Figures 5B,D**). Thus, the enzymatic activity is not been involved in the RNases autophagy induction process.

The Protein Autophagy Induction Correlates With Vesicles Agglutination Activity

Accumulation of double-membrane vacuoles, associated to the autophagosome formation, constitutes a characteristic trait of the autophagy pathway (36). Together with the initial autophagic vacuoles we could also identify abundant single-membrane degradative vacuoles, that could be ascribed to autolysosomes and are characteristic of the later steps of the autophagy process (**Figure 5B**). Moreover, macrophage incubation with RNase3 presented a dose dependent increase in the total volume of acidic vesicular compartments, as quantified by registering the AO acidotropic dye signal, a trait associated to autolysosome formation (**Figure S6**). In contrast, no significant change in AO signal was recorded for the none-autophagic RNase7, used here as a negative control. Rapamycin was used as a positive control and addition of BA, an inhibitor of the vacuolar H^+ -ATPase, resulted in a significant reduction of the AO signal.

To note, the two RNases that activate autophagy, RNase3 and RNase6, can agglutinate liposome vesicles, in contrast to RNase7 (**Figure S7**). Likewise, RNases 3 and 6, but not RNase7, have mycobacteria cell agglutination activity (**Table 1**). The results suggest that the protein agglutination activity might be involved in the autophagy induction process.

Induction of Macrophage Autophagy Contributes to RNase Antimycobacterial Activity

Next, the induction of the autophagy process was confirmed for wild-type and mutant proteins in both infected a non-infected macrophages. The levels of the autophagy markers in RNase3 treated samples were also compared to rapamycin, observing in all cases comparable levels of *BECN1* and *ATG5* expression and LC3II/LC3I ratio (**Figure 6**). Induction of autophagy by RNase3 was reproduced on both control and infected macrophages (**Figure 6**). Results also corroborated that there were no significant differences between the effect induced by wild-type RNase3 and the H15A mutant variant on both infected and non-infected macrophage populations.

Following, we evaluated whether the RNase induction of autophagy mediates the protein macrophage intracellular killing of mycobacteria. First, the levels of autophagy markers (*BECN1*, *ATG5*, and LC3-II) were quantified following RNase3 treatment in the absence and presence of autophagy inhibitors (3methyladenine and bafilomycin A1). 3MA is an early inhibitor of the autophagy pathway and works by blocking the autophagosome formation, whether BA arrest the autophagic process in a later step by impeding the autophagosome maturation and subsequent fusion with the lysosome compartment. Accordingly, while the presence of 3MA blocked the RNase3 induction of autophagy, no reduction in the expression levels of the autophagy markers were observed in the samples treated with BA (**Figures 7A–C**). In fact, quantification of LC3 accumulation by immunofluorescence microscopy revealed a significant increase of LC3 puncta per cell when macrophages were incubated with RNase3 in the presence of BA (**Figure 8**).

More interestingly, both autophagy inhibitors reduced significantly the protein ability to kill mycobacteria within macrophages (**Figure 7D**, **Figure S8**). The fact that 3MA inhibits RNase3 induction of autophagy, but not BA treatment,

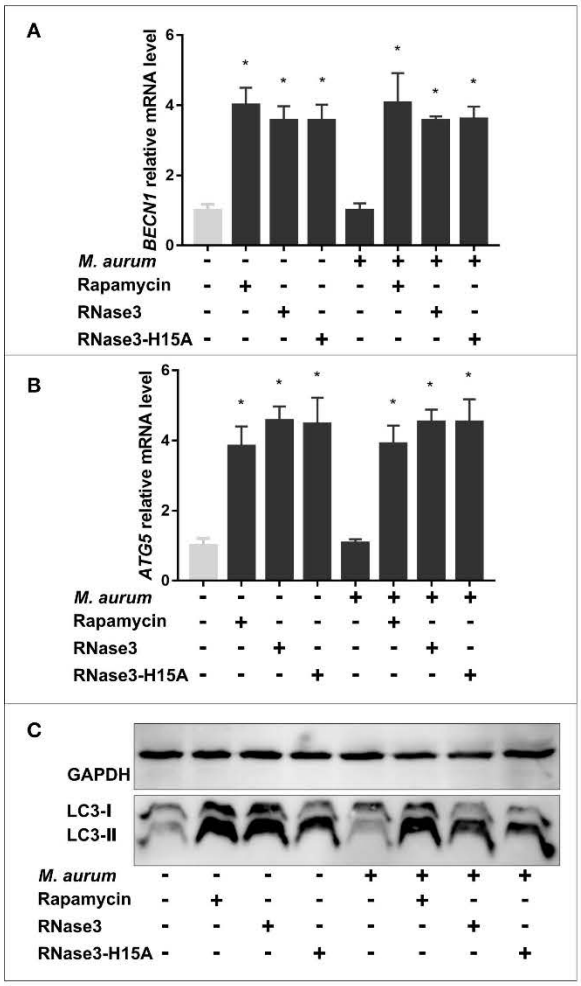

FIGURE 6 | RNase3 and RNase3-H15A induce autophagy in control and *M. aurum* infected macrophages. Mouse macrophages were uninfected or infected with *M. aurum* and treated with 10 μM of protein (RNase3, RNase3-H15A) or 100 nM Rapamycin for 24 h. Real-time qPCR measured the relative expression of **(A)** *BECN1* and **(B)** *ATG5* genes normalized by the housekeeping gene *β-actin*. Results are shown from 3 independent experiments (mean ± SD); **(C)** Immunoblot of LC3-processing and the housekeeping GAPDH control. Results are shown from 3 independent experiments (mean ± SD). *Statistically significant differences compared with the control sample are indicated (p-value < 0.05).

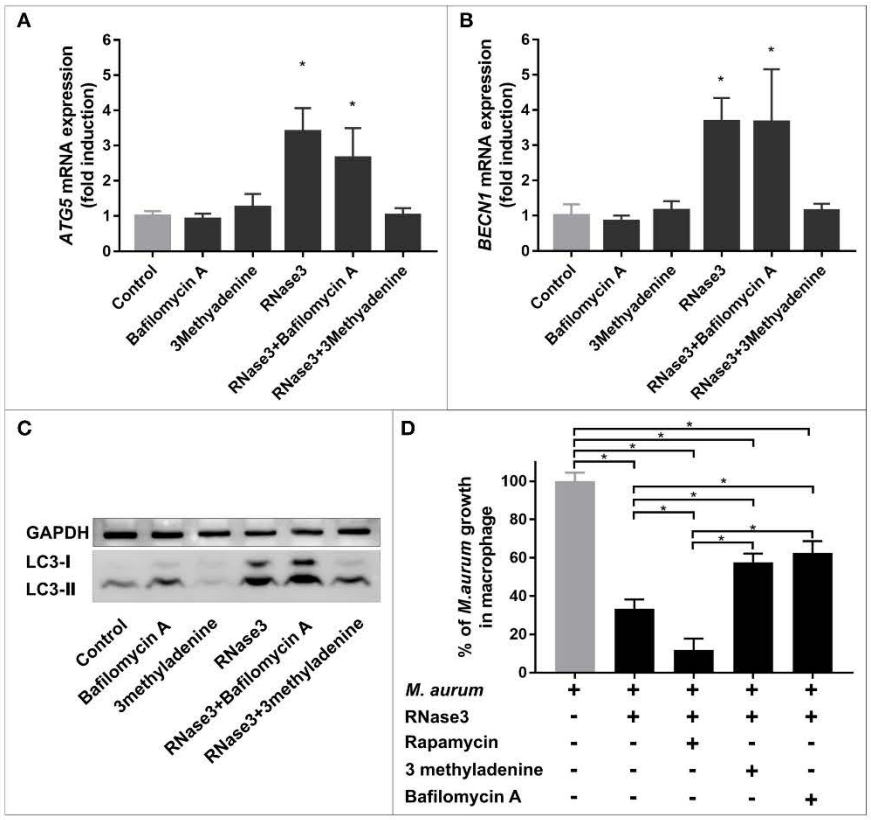

FIGURE 7 | Autophagy induction by RNase3 contributes to its antimycobacterial activity against *M. aurum*. Mouse macrophages were infected with *M. aurum* and treated with 5 μM of RNase3 and/or 100 nM of rapamycin, and/or 100 nM of bafilomycin A1, and/or 5 mM of 3 methyladenine for 24 h. Real-time qPCR measured the relative expression of *BECN1* **(A)** and *ATG5* **(B)** genes normalized by the housekeeping gene *β-actin*. Results are shown from 3 independent experiments (mean ± SD); **(C)** A representative immunoblot of LC3 and housekeeping GAPDH control; **(D)** Intracellular mycobacterial viability was determined based on the number of CFUs. Relative percentages to control samples are indicated. Results are shown from 3 independent experiments (mean ± SD). *Significant differences between pairs is indicated (p value < 0.05).

suggests that the protein triggers the onset of the autophagy process. Moreover, BA reduced the protein ability to kill the intracellular mycobacteria, indicating that the RNase anti-infective activity is partly dependent on the maturation of the autophagosome. Likewise, rapamycin co-treatment with RNase3 enhanced the protein antimicrobial effectivity (**Figure 7D**). An equivalent pattern was reproduced by the RNase3-H15A mutant (**Figure S8**). Therefore, the results confirm that the induction of autophagy participates in the RNase3 antimycobacterial activity within infected macrophages.

DISCUSSION

Previous studies have demonstrated that macrophages serve as a major protecting niche for dormant mycobacteria that can trigger a later reactivation from the disease latency. This scenario is one of the main hindrances in developing effective eradication of tuberculosis. Antimicrobial peptides participate in the host innate immunity against macrophage dwelling TB bacilli (12). Currently, the fight against emergent MDR-TB-forms is at the top priority of global health action programs (1). Within this context, the search for novel anti-TB agents is a priority. In this work, we have taken profit of our developed screening platform adapted for testing the drug efficacy within infected macrophage cells. The SPOTi high-throughput screening (HTS) assay system uses a non-pathogenic fast-growing mycobacterial species (*M. aurum*) able to survive within RAW 264.7 mouse macrophages, as a surrogate model for host TB infection. *M. aurum* is an appropriate substitute for *M. tuberculosis* among other non-pathogen mycobacteria candidates sharing a similar cell-wall structure, gene organization, and drug resistance pattern (8, 26, 27). The SPOTi assay was applied to screen the seven main canonical human members of the RNase A superfamily. The human canonical RNases, although sharing a high sequence identity and a conserved structural fold (**Figure S9**), differ considerably in their biological properties. Overall, RNases are secreted by different types of innate immune cells and participate in a variety of endogenous processes involved in the host defense (18, 28, 37, 38). One of the main ascribed tasks for human secretory RNases is the safeguard of the body

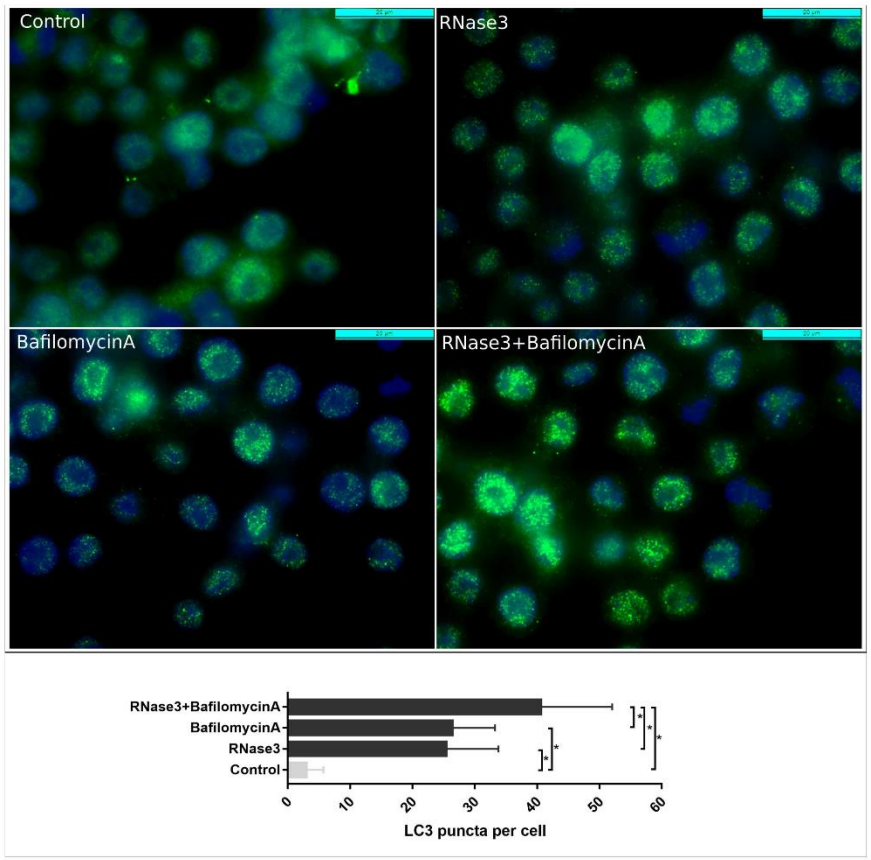

FIGURE 8 | Comparative analysis by immunofluorescence microscopy of LC3 accumulation following RNase3 treatment in the absence and presence of Bafilomycin A. Mouse RAW264.7 cells were incubated with 10 μM RNase3 and/or 100 nM of Bafilomycin A1. Primary anti-LC3 antibody and Alexa-488 labeled secondary antibody were used to detect LC3 (green). Nuclei were labeled with DAPI (blue). Following immunostaining, 100 cells from each treatment were analyzed and the number of LC3 puncta per cell was calculated by *Image J*. *Statistically significant differences are indicated, $p < 0.05$.

fluid sterility. A diversity of anti-infective activities have been reported for some family members (18, 39–42). Among them, the protein mechanism of action on bacterial cells is probably one of the best studied processes (37, 38, 43). In particular, previous works identified the involvement of RNases 3 and 7 in mycobacterial infection. Expression of RNase3 together with α-defensin in *M. bovis* BCG infection was first reported by Capron and coworkers (14). Interestingly, the researchers observed the specific recruitment and induction of eosinophils by lipomannan, a unique mycobacterial cell-wall component. Very recently, Rivas-Santiago and coworkers reported the overexpression of RNase7 in airway epithelial cells infected by *M. tuberculosis* (24). In our laboratory we have confirmed the antimycobacterial activity of recombinant RNase3 and RNase7 on *M. vaccae in vitro* and characterized the protein mechanism of action at the bacterial cell-wall (25).

In this work, we have screened the antimycobacterial activity of the seven main canonical RNases. Taking advantage of the SPOTi-HTS, the protein activities were simultaneously assayed *in vitro* and *ex vivo* (8, 26, 27). Results indicated that out of the seven tested human RNases only three were active against both extracellular and intracellular macrophages-dwelling mycobacteria (**Figures 1**, **2**). A high antimycobacterial activity was observed for RNases 3, 6 and 7, while RNases 1, 2, 4 and 5 were found inactive even at the highest concentration tested. The three active RNases (RNases 3, 6, and 7) correspond to the family members with previously reported antimicrobial activity against Gram-negative and Gram-positive species (37, 38, 41). The present data corroborate that RNase3 is the most active among the family members.

Following, the three active RNases (RNases 3, 6, and 7) were selected for further analysis. First, the minimum bactericidal activity was determined *in vitro* against three distinct *Mycobacterium* species: *M. smegmatis* mc^2155, *M. aurum* and *M. bovis* BCG (**Table 1**). In addition, the protein cell agglutination activity was tested against the three assayed mycobacteria species (*M. smegmatis* mc^2155, *M. aurum*, and *M. bovis* BCG). Interestingly, RNases 3 and 6 were able to induce the aggregation of all the tested mycobacteria, but not RNase7 (**Table 1**). The results are in accordance with our previously published data

using *M. vaccae* cultures, where RNase3, but not RNase7, showed a significant mycobacterial cell agglutination activity (25). Previous works from our laboratory on Gram-negative species also revealed the agglutination ability of RNases 3 and 6 in contrast with RNase7 (21, 38). Likewise, RNases 3 and 6 can agglutinate phospholipid vesicles but not RNase7 (**Figure S7**) (20, 38). Positive agglutination was correlated with the presence of an aggregation-prone hydrophobic patch within the primary sequences of RNases 3 and 6 (37, 44–46). Comparative scanning of the three RNases profiles using the AGGRESCAN 3D software (47) also highlighted the absence of an aggregation patch at the RNase7 structure surface (**Figure S9**). On the other hand, no significant differences were observed between the wild-type and H15A mutants of the three RNases showing antimycobacterial activity (**Table 1**). The present results on mycobacteria confirm previous studies on Gram-negative and Gram-positive bacterial species that indicated that the RNases catalytic activity did not participate in their antimicrobial action (37, 38, 48–51).

To evaluate the potential translational significance of our results in an *in vivo* scenario, we analyzed the expression levels of the RNases in human macrophage THP1 cells following *M. aurum* infection. To this end, we synthesized primers for the four human family members with described anti-pathogen activities and previously reported to be expressed in granulocytes (18). Our data highlighted that the human monocyte-derived THP1 macrophages primarily expresses RNase2 and secondarily RNase3 and RNase6, while a very scarce expression of RNase7 is detected (**Figure S5**). This expression pattern corroborates previous studies that highlighted a predominant expression of RNase2 in human monocytes. On the other hand, RNase7 was reported to be abundantly expressed in epithelial cells (52) but poorly in macrophages (23). In addition, Becknell and co-workers reported a regulation of RNase6 expression in macrophages in response to uropathogenic *E. coli* infection (23). The present data indicates that *M. aurum* infection is only altering the expression profile of cultured macrophages for *RNase3* and *RNase6* genes. However, further work would be needed to characterize the RNases expression pattern in primary macrophages. The results are in accordance with the previously observed anti-pathogen properties of the three detected RNases. RNase2 has a high antiviral activity but no antibacterial activity *in vitro*, and is regulated during viral infection (40). On their turn, RNases 3 and 6 have a high bactericidal activity and their expression is regulated by bacterial infections (18, 23, 42). The present time-course expression profiles in *M. aurum* infected THP1 macrophages indicates a downregulation of RNase3 and RNase6 after a short infection period followed by a significant upregulation at longer incubation times. Modulation of antimicrobial RNases following *M. aurum* infection are in agreement with previously reported results using *M. tuberculosis* (18, 24). In the literature there are other examples of AMPs downregulated upon mycobacteria infection, a process induced by the Mtb bacilli as a protection mechanism against the host innate armory (12, 30). On its turn, upon infection, the host immune cells activate the expression of antimicrobial proteins and peptides (12, 53). Many stimuli have been reported to regulate the expression of human RNases, such as bacterial, viral or parasite infection together with inflammation, sepsis and tissue damage (18, 42, 54). Intriguingly, the comparative expression pattern of the distinct RNaseA members reveals a clear specialization in regard to innate cell and infection types (18, 55). In this context, RNase7 is mainly secreted by epithelial tissues and conforms a protection barrier against bacterial intruders, whereas RNases 3 and 6 are abundant in blood cell types. In particular RNase 3 is highly expressed in eosinophils while RNase6 predominates in neutrophils and monocytes (18). In addition, free secretory granules from eosinophils and neutrophils can be engulfed by macrophage cells and release their content within (18, 56, 57).

Our present results using murine RAW macrophages infected with *M. aurum* highlighted that the three antimicrobial RNases can effectively eradicate the macrophage intracellular resident mycobacteria at a 5 to 10 μM range (**Table 1**). The fact that the RNases could more easily eradicate the mycobacteria resident within macrophages than free in extracellular cultures suggested us that the proteins might combine a direct bacterial cell killing action with some other biological properties.

Immunomodulatory activities mediate the antimycobacterial action of many AMPs (12, 58–60). One of the main strategies undertaken by AMPs to control the proliferation of macrophage intracellular resident bacteria relies on the triggering of the autophagy pathway (12, 30, 34, 61–63). Selective autophagy targeting invading pathogens contributes to maintain the host tissue homeostasis (64). On its turn, the Mtb bacilli ensure their intracellular survival within macrophages by arresting the autophagosome maturation (65, 66). Therefore, autophagy inducers are among the favorite drug candidates against resistant TB strains (12, 34, 58, 59, 62, 67). Interestingly, out of the seven screened RNases, RNase3, and RNase6 significantly increased *BECN1* and *ATG5* gene expression and LC3 processing was observed (**Figure 3**). Subsequent analysis using RNase3 as a reference indicated that the autophagy induction process is unrelated to the protein catalytic activity (**Figures 4**, **5**). Moreover, the autophagy induction was reproduced in both infected and non-infected macrophages (**Figure 6**).

The contribution of autophagy induction on the RNase3 antimycobacterial activity was corroborated by evaluating the protein effect on *M. aurum* growth upon blockage of the autophagy pathway. The blockage of the autophagosome formation or maturation was induced by either addition of 3MA, an inhibitor of the PI3K class III kinase (68), or BA, an ATPase inhibitor that prevents the lysosome fusion with the autophagic vesicles (69). When the infected macrophages were treated with RNase3 in the presence of either 3MA or BA we observed a reduction in the protein inhibitory activity of *M. aurum* growth (**Figure 7** and **Figure S8**). On the other hand, rapamycin enhanced the antimycobacterial activity of RNase3. The same pattern was reproduced when assaying the RNase3-H15A mutant action in the presence of the autophagy inhibitor or activator (**Figure S8**).

The fact that BA does not inhibit the RNase induction of autophagy but reduces its antimycobacterial activity suggests that the protein action is dependent on the late autophagosome maturation process. Moreover, upon cell incubation with RNase3 we observed an increase in the acidic vesicle content (**Figure S6**),

a process that can be associated to autolysosome formation. To note, other AMPs, such as azurodicin and calgranulin, activate autophagy by promoting the autophagosome fusion with lysosomes (12, 53, 70, 71). Overall, our results confirm that autophagy contributes to the RNase antimycobacterial mechanism of action. However, the fact that addition of the autophagy inhibitors does not fully abolishes the antimicrobial activity of the protein indicates that other biological properties are also participating in its antimycobacterial activity. In addition, considering that RNases 3 and 6 induce autophagy, but not RNase7, and that no significant differences are observed between the wild type and the active site mutant proteins, we can suspect that the protein aggregation-prone ability might be involved in the autophagy pathway. Indeed, our previous results correlated the protein self-aggregation capacity with the proteins lipid vesicle agglutination and membrane disruption ability (20). We can speculate that the formation of protein aggregates could promote the autophagosome formation and later fusion with the lysosomal compartment. Complementarily, other protein properties, such as high cationicity, were considered to underlie the autophagy process. The predicted isoelectric point (pI) for all tested seven RNases, ranging from 9 to 10.7 (**Table S2**), emphasizes their prominent cationicity, a characteristic trait of AMPs (72–74). However, although RNase3 is the most cationic of all the proteins, we cannot find a direct correlation between the pI and antimicrobial or autophagy induction abilities among the seven tested human RNases. Likewise, the protein hydrophobicity was analyzed, obtaining very similar calculated GRAVY values (**Table S2**). Further work is ongoing to unravel the structural determinants underlying the RNase antimycobacterial mechanism of action.

Interestingly, two RNaseA family homologs (bovine seminal RNase and onconase) were recently reported to exert their anti-tumoral activity by the selective induction of the autophagic cancer cell death (33, 75). Bovine seminal RNase (BS-RNase) triggers an autophagic cell death process in pancreatic cancer cells mediated by *BECN1* induction; and onconase, a RNaseA superfamily member proposed for chemotherapy, inhibits the proliferation of cancer cells through the ROS/Akt/mTOR pathway (33, 75). Surprisingly, the bovine pancreatic RNaseA, displaying a high catalytic activity and sharing about a 82% sequence identity with BS-RNase, could not reproduce the induction of autophagy. The authors associated the activation of the autophagic pathway to the protein cationicity and oligomer formation, discarding any correlation between the RNase catalytic activity and the autophagic process (75). Two main factors, protein net charge, and stability of the oligomers were considered to explain the difference between RNaseA and BS-RNase in inducing autophagy. Last but not least, there is another human RNase, the RNase L, unrelated to the RNaseA superfamily, which can also trigger the autophagy pathway. RNase L expression is induced during viral infection. The protein can initiate autophagy and suppress thereby the virus replication (31, 76). In all cases, we can outline a convergent mechanism where the RNases induction of autophagy is activated by a cell stress condition: oxidative injury, presence of protein aggregation, or infection (18, 77).

In summary, the present results have revealed the potentiality of human secretory RNases to work as antimicrobial agents in the fight against tuberculosis, extendable to other intracellular infectious bacterial diseases that are difficult to eradicate (78). AMPs that display a multifaceted mechanism of action (12, 16, 79–85), like human antimicrobial RNases, deserve a special attention for their pharmacological potential. Our ongoing inter-disciplinary investigation warrants the understanding of RNases' antimicrobial mechanism of action and can pave the design of novel anti-infective therapies.

CONCLUSIONS

Screening of the seven main human canonical members of the RNaseA superfamily identified three RNases (RNase3, RNase6, and RNase7) that achieved the eradication of *M. aurum* infection within macrophages at a low micromolar range. The protein antimicrobial activity was found not dependent on the RNase enzymatic activity. Out of the three antimycobacterial RNases, two of them (RNase3 and RNase6) demonstrated their ability to induce macrophage autophagy and thereby inhibit *M. aurum* intracellular growth. The expression of both RNases in human THP1 derived macrophage cells is regulated by the mycobacterial infection, suggesting an *in vivo* physiological role.

DATA AVAILABILITY

The raw data supporting the conclusions of this manuscript will be made available by the authors, without undue reservation, to any qualified researcher.

AUTHOR CONTRIBUTIONS

EB and SB contributed in funding acquisition. DP, EB, and SB conceived and designed the experiments. LL, GP-E, and JA-T performed the experiments. EB, GP-E, DP, and SB supervised the experimental work. LL, JA-T, EB, and SB contributed to the original draft preparation. LL, DP, EB, and SB participated in the manuscript revision and final edition.

FUNDING

Experimental work was supported by the *Ministerio de Economía y Competitividad* (SAF2015-66007P to EB), AGAUR (2016PROD00060) co-financed by FEDER funds and *Fundació La Marató de TV3* (ref. 20180310).

ACKNOWLEDGMENTS

The authors wish to thank the *Laboratori d'Anàlisi i Fotodocumentació* (UAB), where spectrofluorescence assays were performed. LL is a recipient of a CSC predoctoral fellowship. JA-T and GP-E were recipients of a predoctoral fellowship (Personal Investigador en Formación, Universitat Autònoma de Barcelona). Authors thank Drs. Esther Julián, Estela Noguera-Ortega, Maria Goetz, José Miguel Lizcano, and

Pau Muñoz-Guardiola, UAB for their technical help. SB is a Cipla Distinguished Fellow in Pharmaceutical Sciences.

SUPPLEMENTARY MATERIAL

The Supplementary Material for this article can be found online at: https://www.frontiersin.org/articles/10.3389/fimmu.2019.01500/full#supplementary-material

Figure S1 | A representative SPOTi image comparing human RNases activity on *M. aurum* cultures. *M. aurum* was incubated with serially diluted recombinant human RNases (ranging from 2 to 32 μM) for 4 h in phosphate-buffered saline (PBS). Next, an aliquot was spotted onto wells of a 24-well plate containing MB7H10/OADC/agar and incubated at 37°C for 4–5 days to determine survival.

Figure S2 | Confocal microscopy analysis of RAW 264.7 cell culture (2.5×10^5 cells/mL) incubated with 2 μM of RNase3 labeled with Alexa Fluor 488. Cells were stained with Hoechst and Deep Red following the assay incubation conditions detailed in the experimental procedures section. After addition of Alexa Fluor 488 labeled protein (green), the evolution of the fluorescence signals was analyzed by confocal microscopy. A total of 20 cells were analyzed by regions of interest (ROIs) using Leica TCS software. The images were taken using a Leica TCS SP5 AOBS microscope.

Figure S3 | 3D reconstruction of RAW 264.7 macrophages post-treatment with RNase3. Confocal microscopy analysis of RAW 264.7 cell culture incubated with 2 μM of RNase3 labeled with Alexa Fluor 488 (green). Cells were stained with Hoechst and Deep Red following the assay incubation conditions detailed in the experimental procedures section. After 45 min of protein addition, the fluorescence signals of Hoechst and AlexaFluor **(A)** and Hoechst, AlexaFluor and Deep Red **(B)** were analyzed by confocal microscopy. The images were taken using a Leica TCS SP5 AOBS microscope.

Figure S4 | Confocal microscopy analysis of RAW 264.7 cell culture incubated with human RNases labeled with Alexa Fluor 488. Cells were stained with Hoechst and Deep Red following the assay incubation conditions detailed in the experimental procedures section. After labeled protein addition (green), the evolution of the fluorescence signals was analyzed by confocal microscopy for 30 min. A total of 20 cells were analyzed by regions of interest (ROIs) using Leica TCS software. The images were taken using a Leica TCS SP5 AOBS microscope. Each panel indicates the RNase assayed.

Figure S5 | Expression pattern of human RNases in THP-1 derived macrophage cells infected with *M. aurum*. Human THP-1 macrophage derived cells were infected with *M. aurum* for 4, 24, 48, and 72 h. The transcriptional expression of human *RNase2*, *RNase3*, *RNase6*, and *RNase7* were detected by real-time qPCR and all samples were normalized with the GAPDH housekeeping gene. **(A)** relative expression of *RNase2*, *RNase3*, *RNase6*, and *RNase7* at 0 h without infection; **(B–D)** The monitoring of RNases' expression upon infection was presented as the fold change of relative expression in infected group compared with the corresponding control group at each time point. Results are shown from 3 independent experiments (mean ± SD), *indicates a significant difference compared with control (p value < 0.05).

Figure S6 | Quantification of acidic vesicular compartment measured by AO staining. The total amount of acidic vesicles was assessed as an estimate of autolysosome formation. Mouse RAW 264.7 macrophage cells were treated with RNases 3 and 7 for 24 h. Values are presented as means ± SD of 8 replicates. *indicates significant difference compared with control group ($p \leq 0.05$).

Figure S7 | Comparison of aggregation of DOPG/DOPC liposomes by RNases. The incubation time of protein with liposomes is 30 min for all assay. The proteins were 2-fold serially diluted (from 1.6 to 0.05 μM).

Figure S8 | RNase3 and RNase3-H15A antimycobacterial activity in the presence of autophagy regulators. RAW 264.7 macrophages were infected with *M. aurum* and treated with different concentration of the proteins, and/or 100 nM of rapamycin (Rapa), and/or 100 nM of bafilomycin A (BA), and/or 5 mM of 3 methyladenine (3MA) for 24 h in RPMI-1640 complete medium. Macrophages were washed twice with RPMI-1640 and lysed, and then an aliquot was spotted onto wells of a 24-well plate containing MB7H10/OADC/agar and incubated at 37°C for 4–5 days to determine intracellular survival.

Figure S9 | Sequence alignment and prediction of aggregation propensity of eight human RNases. **(A)** Alignment of the eight human canonical RNases using the ESPript3 software (espript.ibcp.fr/), the N-terminal domain is highlighted in blue. Sequence allocation was performed following the homology between RNases. **(B)** 3D structure of RNases by *Aggrescan3D* (*A3D*). *A3D* exploits an experimentally derived intrinsic aggregation propensity scale for natural amino acids. This structure-based approach identifies aggregation patches (in red) at the protein surface. **(C)** Aggregation profile propensity of RNase3, RNase6, and RNase7 based on *A3D* score for protein residues.

Table S1 | Primer sequences for real-time qPCR. Primers of human *GAPDH*, *RNase2*, *RNase3*, *RNase6*, and *RNase7*, and human and mouse *β-actin, Beclin-1, and ATG5*.

Table S2 | Comparison of physicochemical parameters of human secretory RNases. pI and Grand average of hydropathy (GRAVY) were predicted using the ProtParam tool (https://web.expasy.org/translate/).

REFERENCES

1. WHO. *Global Tuberculosis Report 2018*. Geneva (2018).
2. Accelerating efforts to end TB. *Nat Microbiol.* (2018) 3:257–7. doi: 10.1038/s41564-018-0126-6
3. Pai M, Schito M. Tuberculosis diagnostics in 2015: landscape, priorities, needs, and prospects. *J Infect Dis.* (2015) 211:S21–8. doi: 10.1093/infdis/jiu803
4. Maitra A, Kamil TK, Shaik M, Danquah CA, Chrzastek A, Bhakta S. Early diagnosis and effective treatment regimens are the keys to tackle antimicrobial resistance in tuberculosis (TB): a report from Euroscicon's international TB Summit 2016. *Virulence.* (2016) 1–20. doi: 10.1080/21505594.2016.1256536
5. Maitra A, Danquah CA, Scotti F, Howard TK, Kamil TK, Bhakta S. Tackling tuberculosis: Insights from an international TB Summit in London. *Virulence.* (2015) 6:561–72. doi: 10.1080/21505594.2015.1060396
6. Eldholm V, Balloux F. Antimicrobial resistance in *Mycobacterium tuberculosis*: the odd one out. *Trends Microbiol.* (2016) 24:637–48. doi: 10.1016/j.tim.2016.03.007
7. Siegrist MS, Bertozzi CR. Mycobacterial lipid logic. *Cell Host Microbe.* (2014) 15:1–2. doi: 10.1016/j.chom.2013.12.005
8. Gupta A, Bhakta S. An integrated surrogate model for screening of drugs against *Mycobacterium tuberculosis*. *J Antimicrob Chemother.* (2012) 67:1380–91. doi: 10.1093/jac/dks056
9. Pieters J. *Mycobacterium tuberculosis* and the macrophage: maintaining a balance. *Cell Host Microbe.* (2008) 3:399–407. doi: 10.1016/j.chom.2008.05.006
10. Welin A, Raffetseder J, Eklund D, Stendahl O, Lerm M. Importance of phagosomal functionality for growth restriction of *Mycobacterium tuberculosis* in primary human macrophages. *J Innate Immun.* (2011) 3:508–18. doi: 10.1159/000325297
11. Saiga H, Shimada Y, Takeda K. Innate immune effectors in mycobacterial infection. *Clin Dev Immunol.* (2011) 2011:1–8. doi: 10.1155/2011/347594
12. Arranz-Trullén J, Lu L, Pulido D, Bhakta S, Boix E. Host antimicrobial peptides: the promise of new treatment strategies against tuberculosis. *Front Immunol.* (2017) 8:1499. doi: 10.3389/fimmu.2017.01499
13. Lasco TM, Turner OC, Cassone L, Sugawara I, Yamada H, McMurray DN, et al. Rapid accumulation of eosinophils in lung lesions in guinea pigs infected with *Mycobacterium tuberculosis*. *Infect Immun.* (2004) 72:1147–9. doi: 10.1128/IAI.72.2.1147-1149.2004
14. Driss V, Legrand F, Hermann E, Loiseau S, Guerardel Y, Kremer L, et al. TLR2-dependent eosinophil interactions with mycobacteria: role of alpha-defensins. *Blood.* (2009) 113:3235–44. doi: 10.1182/blood-2008-07-166595
15. Soehnlein O. Direct and alternative antimicrobial mechanisms of neutrophil-derived granule proteins. *J Mol Med.* (2009) 87:1157–64. doi: 10.1007/s00109-009-0508-6

16. Lázár V, Martins A, Spohn R, Daruka L, Grézal G, Fekete G, et al. Antibiotic-resistant bacteria show widespread collateral sensitivity to antimicrobial peptides. *Nat Microbiol.* (2018) 3:718–31. doi: 10.1038/s41564-018-0164-0
17. Sorrentino S. The eight human "canonical" ribonucleases: molecular diversity, catalytic properties, and special biological actions of the enzyme proteins. *FEBS Lett.* (2010) 584:2194–200. doi: 10.1016/j.febslet.2010.04.018
18. Lu L, Li J, Moussaoui M, Boix E. Immune modulation by human secreted RNases at the extracellular space. *Front Immunol.* (2018) 9:1–20. doi: 10.3389/fimmu.2018.01012
19. Jordaan S, Akinrinmade O, Nachreiner T, Cremer C, Naran K, Chetty S, et al. Updates in the development of immunoRNases for the selective killing of tumor cells. *Biomedicines.* (2018) 6:28. doi: 10.3390/biomedicines6010028
20. Torrent M, Sánchez D, Buzón V, Nogués MV, Cladera J, Boix E. Comparison of the membrane interaction mechanism of two antimicrobial RNases: RNase 3/ECP and RNase 7. *Biochim Biophys Acta.* (2009) 1788:1116–25. doi: 10.1016/j.bbamem.2009.01.013
21. Torrent M, Badia M, Moussaoui M, Sanchez D, Nogués MV, Boix E. Comparison of human RNase 3 and RNase 7 bactericidal action at the Gram-negative and Gram-positive bacterial cell wall. *FEBS J.* (2010) 277:1713–25. doi: 10.1111/j.1742-4658.2010.07595.x
22. Pulido D, Moussaoui M, Andreu D, Nogués MV, Torrent M, Boix E. Antimicrobial action and cell agglutination by the eosinophil cationic protein are modulated by the cell wall lipopolysaccharide structure. *Antimicrob Agents Chemother.* (2012) 56:2378–85. doi: 10.1128/AAC.06107-11
23. Becknell B, Eichler TE, Beceiro S, Li B, Easterling RS, Carpenter AR, et al. Ribonucleases 6 and 7 have antimicrobial function in the human and murine urinary tract. *Kidney Int.* (2015) 87:151–61. doi: 10.1038/ki.2014.268
24. Torres-Juarez F, Touqui L, Leon-Contreras J, Rivas-Santiago C, Enciso-Moreno JA, Hernández-Pando R, et al. RNase 7 but not psoriasin nor sPLA2-IIA associates with *Mycobacterium tuberculosis* during airway epithelial cell infection. *Pathog Dis.* (2018) 76:fty005. doi: 10.1093/femspd/fty005
25. Pulido D, Torrent M, Andreu D, Nogués MV, Boix E, Nogues MV, et al. Two human host defense ribonucleases against mycobacteria, the eosinophil cationic protein (RNase 3) and RNase 7. *Antimicrob Agents Chemother.* (2013) 57:3797–805. doi: 10.1128/AAC.00428-13
26. Guzman JD, Evangelopoulos D, Gupta A, Birchall K, Mwaigwisya S, Saxty B, et al.. Antitubercular specific activity of ibuprofen and the other 2-arylpropanoic acids using the HT-SPOTi whole-cell phenotypic assay. *BMJ Open.* (2013) 3:1–13. doi: 10.1136/bmjopen-2013-002672
27. Danquah CA, Maitra A, Gibbons S, Faull J, Bhakta S. HT-SPOTi: A rapid drug susceptibility test (DST) to evaluate antibiotic resistance profiles and novel chemicals for anti-infective drug discovery. *Curr Protoc Microbiol.* (2016) 40:17.8.1–17.8.12. doi: 10.1002/9780471729259.mc1708s40
28. Salazar VA, Arranz-Trullén J, Navarro S, Blanco JA, Sánchez D, Moussaoui M, et al. Exploring the mechanisms of action of human secretory RNase 3 and RNase 7 against Candida albicans. *Microbiologyopen.* (2016) 5:830–45. doi: 10.1002/mbo3.373
29. Zhang L, Lu L, Li S, Zhang G, Ouyang L, Robinson K, et al. 1,25-Dihydroxyvitamin-D3 induces avian β-defensin gene expression in chickens. *PLoS ONE.* (2016) 11:e0154546. doi: 10.1371/journal.pone.0154546
30. Rekha RS, Rao Muvva SSVJ, Wan M, Raqib R, Bergman P, Brighenti S, et al. Phenylbutyrate induces LL-37-dependent autophagy and intracellular killing of *Mycobacterium tuberculosis* in human macrophages. *Autophagy.* (2015) 11:1688–99. doi: 10.1080/15548627.2015.1075110
31. Siddiqui MA, Malathi K. RNase L induces autophagy via c-Jun N-terminal kinase and double-stranded RNA-dependent protein kinase signaling pathways. *J Biol Chem.* (2012) 287:43651–64. doi: 10.1074/jbc.M112.399964
32. Brambilla C, Llorens-Fons M, Julián E, Noguera-Ortega E, Tomàs-Martínez C, Pérez-Trujillo M, et al. Mycobacteria clumping increase their capacity to damage macrophages. *Front Microbiol.* (2016) 7:1562. doi: 10.3389/fmicb.2016.01562
33. Fiorini C, Cordani M, Gotte G, Picone D, Donadelli M, Fiorini C, et al. Onconase induces autophagy sensitizing pancreatic cancer cells to gemcitabine and activates Akt/mTOR pathway in a ROS-dependent manner. *Biochim Biophys Acta.* (2015) 1853:549–60. doi: 10.1016/j.bbamcr.2014.12.016
34. Muciño G, Castro-Obregón S, Hernandez-Pando R, Del Rio G. Autophagy as a target for therapeutic uses of multifunctional peptides. *IUBMB Life.* (2016) 68:259–67. doi: 10.1002/iub.1483
35. Klionsky DJ. Guidelines for the use and interpretation of assays for monitoring autophagy (3rd edition). *Autophagy.* (2016) 12:1–222. doi: 10.1080/15548627.2015.1100356
36. Yuan K, Huang C, Fox J, Laturnus D, Carlson E, Zhang B, et al. Autophagy plays an essential role in the clearance of Pseudomonas aeruginosa by alveolar macrophages. *J Cell Sci.* (2012) 125:507–15. doi: 10.1242/jcs.094573
37. Boix E, Salazar VA, Torrent M, Pulido D, Nogués MV, Moussaoui M. Structural determinants of the eosinophil cationic protein antimicrobial activity. *Biol Chem.* (2012) 393:801–15. doi: 10.1515/hsz-2012-0160
38. Pulido D, Arranz-Trullen J, Prats-Ejarque G, Velazquez D, Torrent M, Moussaoui M, et al. Insights into the antimicrobial mechanism of action of human RNase6: structural determinants for bacterial cell agglutination and membrane permeation. *Int J Mol Sci.* (2016) 17:552. doi: 10.3390/ijms17040552
39. Singh A, Batra JK. Role of unique basic residues in cytotoxic, antibacterial and antiparasitic activities of human eosinophil cationic protein. *Biol Chem.* (2011) 392:337–46. doi: 10.1515/bc.2011.037
40. Rosenberg HF. Eosinophil-derived neurotoxin (EDN/RNase 2) and the mouse eosinophil-associated RNases (mEars): expanding roles in promoting host defense. *Int J Mol Sci.* (2015) 16:15442–55. doi: 10.3390/ijms160715442
41. Becknell B, Spencer JD. A Review of Ribonuclease 7's structure, regulation, and contributions to host defense. *Int J Mol Sci.* (2016) 17:423. doi: 10.3390/ijms17030423
42. Koczera P, Martin L, Marx G, Schuerholz T. The ribonuclease a superfamily in humans: canonical RNases as the buttress of innate immunity. *Int J Mol Sci.* (2016) 17:E1278. doi: 10.3390/ijms17081278
43. Torrent M, Pulido D, Nogués MV, Boix E. Exploring new biological functions of amyloids: bacteria cell agglutination mediated by host protein aggregation. *PLoS Pathog.* (2012) 8:2012–4. doi: 10.1371/journal.ppat.1003005
44. Pulido D, Moussaoui M, Victòria Nogués M, Torrent M, Boix E. Towards the rational design of antimicrobial proteins: single point mutations can switch on bactericidal and agglutinating activities on the RNase A superfamily lineage. *FEBS J.* (2013) 280:5841–52. doi: 10.1111/febs.12506
45. Pulido D, Prats-Ejarque G, Villalba C, Albacar M, Gonzalez-Lopez JJ, Torrent M, et al. A novel RNase 3/ECP peptide for Pseudomonas aeruginosa biofilm eradication. Combining antimicrobial, lipopolysaccharide binding and cell agglutinating activities. *Antimicrob Agents Chemother.* (2016) 60:6313–25. doi: 10.1128/AAC.00830-16
46. Torrent M, Pulido D, Valle J, Nogués MVV, Andreu D, Boix E. Ribonucleases as a host-defence family: evidence of evolutionarily conserved antimicrobial activity at the N-terminus. *Biochem J.* (2013) 456:99–108. doi: 10.1042/BJ20130123
47. Zambrano R, Jamroz M, Szczasiuk A, Pujols J, Kmiecik S, Ventura S. AGGRESCAN3D (A3D): server for prediction of aggregation properties of protein structures. *Nucleic Acids Res.* (2015) 43:W306–13. doi: 10.1093/nar/gkv359
48. Torrent M, Cuyás E, Carreras E, Navarro S, López O, De La Maza A, et al. Topography studies on the membrane interaction mechanism of the eosinophil cationic protein. *Biochemistry.* (2007) 46:720–33. doi: 10.1021/bi061190e
49. Huang Y-C, Lin Y-M, Chang T-W, Wu S-J, Lee Y-S, Chang MD-T, et al. The flexible and clustered lysine residues of human ribonuclease 7 are critical for membrane permeability and antimicrobial activity. *J Biol Chem.* (2007) 282:4626–33. doi: 10.1074/jbc.M607321200
50. Boix E, Torrent M, Sánchez D, Nogués MV. The antipathogen activities of eosinophil cationic protein. *Curr Pharm Biotechnol.* (2008) 9:141–52. doi: 10.2174/138920108784567353
51. Prats-Ejarque G, Arranz-Trullen J, Blanco JA, Pulido D, Nogues MV, Moussaoui M, et al. The first crystal structure of human RNase 6 reveals a novel substrate-binding and cleavage site arrangement. *Biochem J.* (2016) 473:1523–36. doi: 10.1042/BCJ20160245
52. Harder JJ, Schröder JM, Schroder J-M. RNase 7, a novel innate immune defense antimicrobial protein of healthy human skin. *J Biol Chem.* (2002) 277:46779–84. doi: 10.1074/jbc.M207587200
53. Padhi A, Sengupta M, Sengupta S, Roehm KH, Sonawane A. Antimicrobial peptides and proteins in mycobacterial therapy: current status and future prospects. *Tuberculosis.* (2014) 94:363–73. doi: 10.1016/j.tube.2014.03.011

Supplementary Material

Human Antimicrobial RNases Inhibit Intracellular Bacterial Growth and Induce Autophagy in Mycobacteria-Infected Macrophages

Lu Lu[1], Javier Arranz-Trullén [1,2], Guillem Prats-Ejarque [1], David Pulido [1,3], Sanjib Bhakta[2]* and Ester Boix [1]*

*** Correspondence:** Ester Boix: Ester.Boix@uab.cat (EB); Sanjib Bhakta: s.bhakta@bbk.ac.uk (SB)

Specie	Gene	Sequence	Unique ID / Reference
Human	*GAPDH*		qHsaCED0038674
Human	*RNase2*		qHsaCED0020010
Human	*RNase3*		qHsaCED0001992
Human	*RNase6*		qHsaCED0046630
Human	*RNase7*		qHsaCID0020296
Human	*β-actin-F*	ATCTGGCACCACACCTTCTACAATGAGC TGCG	(1)
Human	*β-actin-R*	ACACCAGACATAGTAGCAGAAATCAAG	
Human	*ATG5-F*	TGGGATTGCAAAATGACAGA	(1)
Human	*ATG5-R*	TTTCCCCATCTTCAGGATCA	
Human	*Beclin-1-F*	CCAGGATGGTGTCTCTCGCA	(1)
Human	*Beclin-1-R*	CTGCGTCTGGGCATAACGCA	
Mouse	*β-actin-F*	GGCACCACACCTTCTACAATG	(2)
Mouse	*β-actin-R*	GGGGTGTTGAAGGTCTCAAAC	
Mouse	*ATG5-F*	GACAAAGATGTGCTTCGAGATGTG	(3)
Mouse	*ATG5-R*	GTAGCTCAGATGCTCGCTCAG	
Mouse	*Beclin-1-F*	GTGCTCCTGTGGAATGGAAT	(4)
Mouse	*Beclin-1-R*	GCTGCACACAGTCCAGAAAA	

Table S1. Primer sequences for real-time qPCR. Primers of human GAPDH, RNase2, RNase3, RNase6 and RNase7, and human and mouse *β-actin, Beclin-1 and ATG5*.

References

1. Yuk J-M, Shin D-M, Lee H-M, Yang C-S, Jin HS, Kim K-K, Lee Z-W, Lee S-H, Kim J-M, Jo E-K. Vitamin D3 Induces Autophagy in Human Monocytes/Macrophages via Cathelicidin. *Cell Host Microbe* (2009) **6**:231–43. doi:10.1016/j.chom.2009.08.004
2. Seldin MM, Lei X, Tan SY, Stanson KP, Wei Z, Wong GW. Skeletal Muscle-derived Myonectin Activates the Mammalian Target of Rapamycin (mTOR) Pathway to Suppress Autophagy in Liver. *J Biol Chem* (2013) **288**:36073–36082. doi:10.1074/jbc.M113.500736
3. Pua HH, Dzhagalov I, Chuck M, Mizushima N, He Y-W. A critical role for the autophagy gene Atg5 in T cell survival and proliferation. *J Exp Med* (2007) **204**:25–31. doi:10.1084/jem.20061303
4. Wang J-D, Cao Y-L, Li Q, Yang Y-P, Jin M, Chen D, Wang F, Wang G-H, Qin Z-H, Hu L-F, et al. A pivotal role of FOS-mediated BECN1/Beclin 1 upregulation in dopamine D2 and D3 receptor agonist-induced autophagy activation. doi:10.1080/15548627.2015.1100930

	RNase1	RNase2	RNase3	RNase4	RNase5	RNase6	RNase7
Theoretical pI	8.98	9.2	10.7	9.18	9.73	9.22	9.83
GRAVY	-0.916	-0.669	-0.598	-0.726	-0.907	-0.543	-0.860

Table S2. Comparison of physicochemical parameters of human secretory RNases. pI and Grand average of hydropathy (GRAVY) were predicted using the ProtParam tool (https://web.expasy.org/translate/).

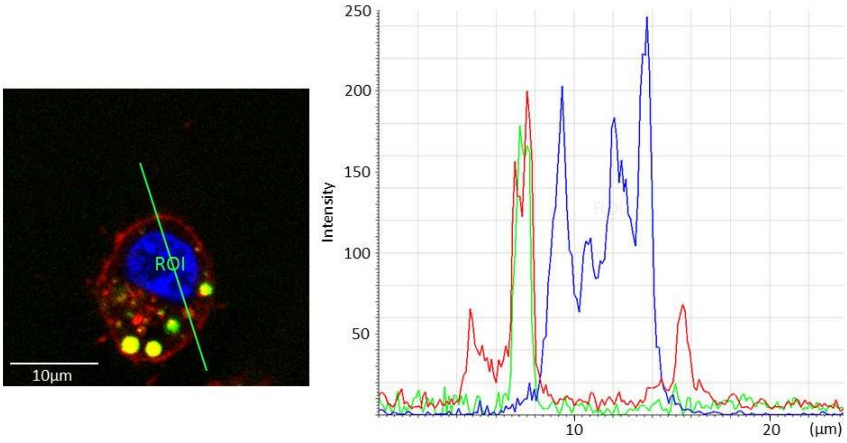

Figure S1. **Confocal microscopy analysis of RAW 264.7 cell culture (2.5x10^5 cells/mL) incubated with 2 µM of RNase3 labelled with Alexa Fluor 488.** Cells were stained with Hoechst and Deep Red following the assay incubation conditions detailed in the experimental procedures section. After addition of Alexa Fluor 488 labelled protein (green), the evolution of the fluorescence signals was analysed by confocal microscopy. A total of 20 cells were analysed by regions of interest (ROIs) using Leica TCS software. The images were taken using a Leica TCS SP5 AOBS microscope.

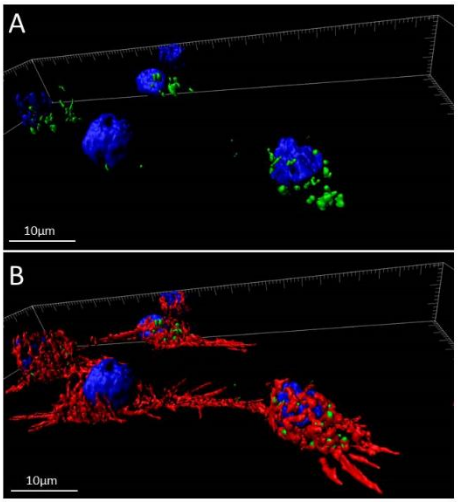

Figure S2. 3D reconstruction of RAW 264.7 macrophages post-treatment with RNase3. Confocal microscopy analysis of RAW 264.7 cell culture incubated with 2 µM of RNase3 labelled with Alexa Fluor 488 (green). Cells were stained with Hoechst and Deep Red following the assay incubation conditions detailed in the experimental procedures section. After 45 min of protein addition, the fluorescence signals of Hoechst and AlexaFluor (A) and Hoechst, AlexaFluor and Deep Red (B) were analyzed by confocal microscopy. The images were taken using a Leica TCS SP5 AOBS microscope.

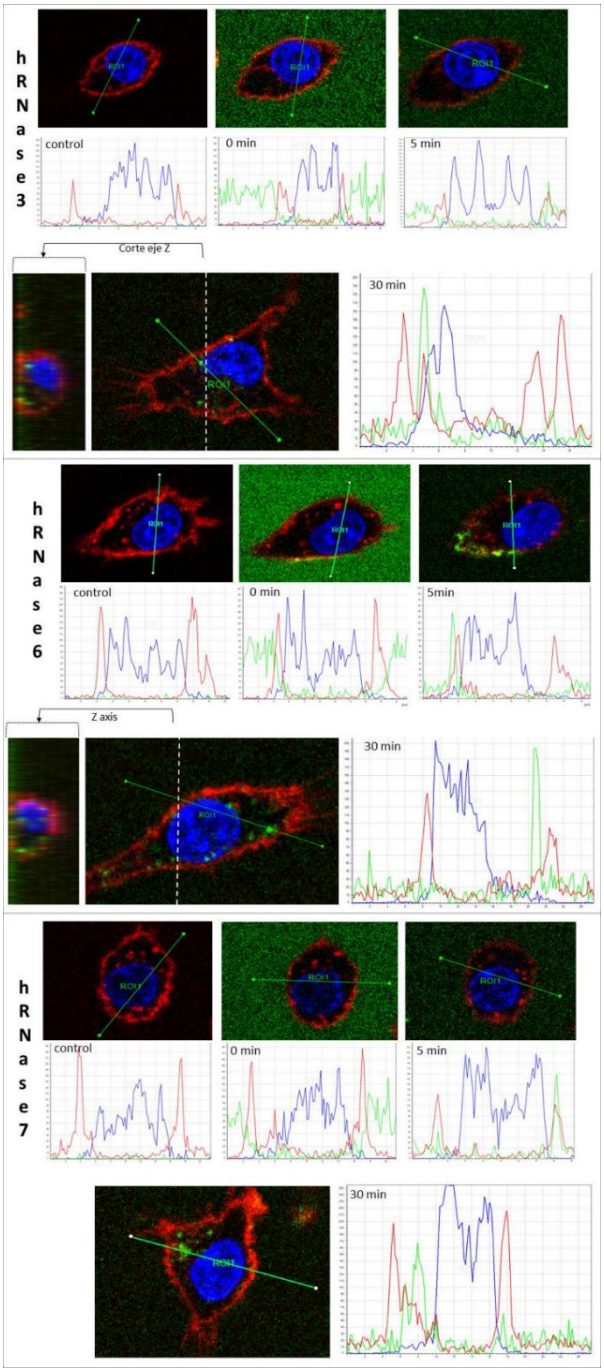

Figure S3. Confocal microscopy analysis of RAW 264.7 cell culture incubated with human RNases labelled with Alexa Fluor 488. Cells were stained with Hoechst and Deep Red following the assay incubation conditions detailed in the experimental procedures section. After labelled protein addition (green), the evolution of the fluorescence signals was analyzed by confocal microscopy for 30 min. A total of 20 cells were analyzed by regions of interest (ROIs) using Leica TCS software. The images were taken using a Leica TCS SP5 AOBS microscope. Each panel indicates the RNase assayed.

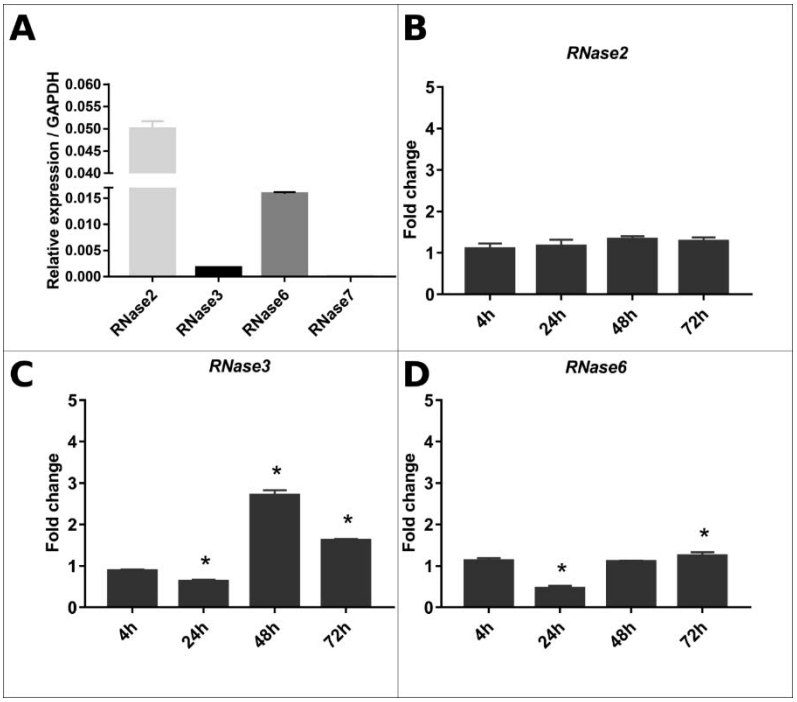

Figure S4. Expression pattern of human RNases in THP-1 derived macrophage cells infected with *M. aurum*. Human THP-1 macrophage derived cells were infected with *M. aurum* for 4, 24, 48 and 72h, the transcriptional expression of human *RNase2*, *RNase3*, *RNase6* and *RNase7* were detected by real-time qPCR, all samples were normalized with GAPDH housekeeping gene. (A) relative expression of *RNase2*, *RNase3*, *RNase6* and *RNase7* at 0h without infection; (B, C, D) The kinetic of RNases' expression upon infection were presented as the fold change of relative expression in infected group compared with the corresponding control group at each time point. Results are shown from 3 independent experiments (mean ± SD), *indicates a significant difference with control with P value is 0.05.

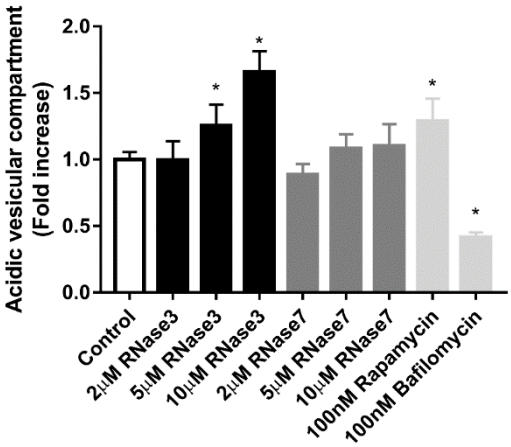

Figure S5. Quantification of acidic vesicular compartment measured by AO staining. The total amount of acidic vesicles was assessed as an estimate of autolysosome formation. Mouse RAW 264.7 macrophage cells were treated with RNases 3 and 7 for 24 h. Values are presented as means ± SD of 8 replicates. * indicates significant difference compared with control group ($p < 0.05$).

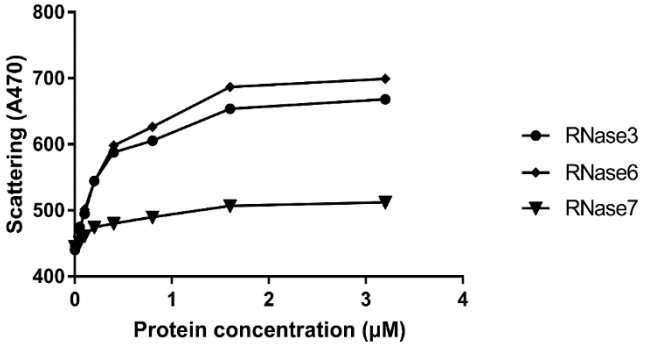

Figure S6. Comparison of aggregation of DOPG/DOPC liposomes by RNases. The incubation time of protein with liposomes is 30 min for all assay. The proteins were 2-fold serially diluted (from 1.6 μM to 0.05 μM).

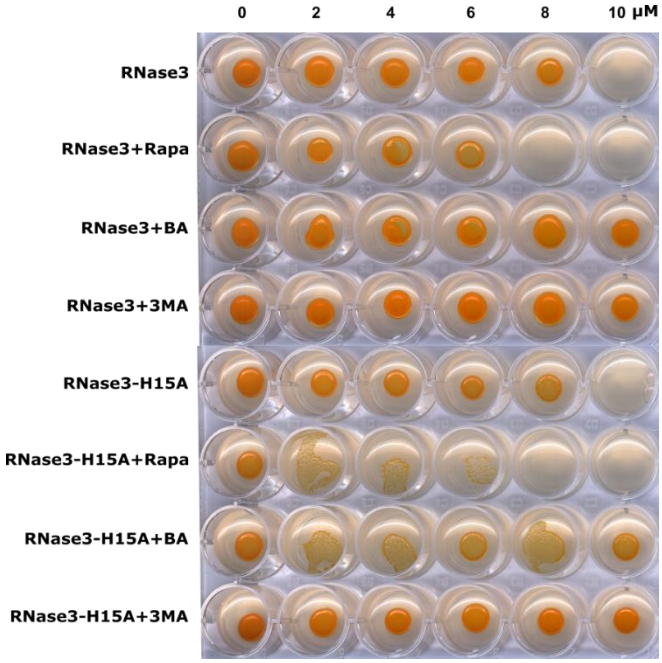

Figure S7. RNase3 and RNase3-H15A antimycobacterial activity in the presence of autophagy regulators. RAW 264.7 macrophages were infected with *M. aurum* and treated with different concentration of the proteins, and/or 100 nM of rapamycin (Rapa), and/or 100 nM of bafilomycin A (BA), and/or 5 mM of 3 methyladenine (3MA) for 24h in RPMI-1640 complete medium. Macrophages were washed twice with RPMI-1640 and lysed, and then an aliquot was spotted onto wells of a 24-well plate containing MB7H10/OADC/agar and incubated at 37ºC for 4-5 days to determine intracellular survival.

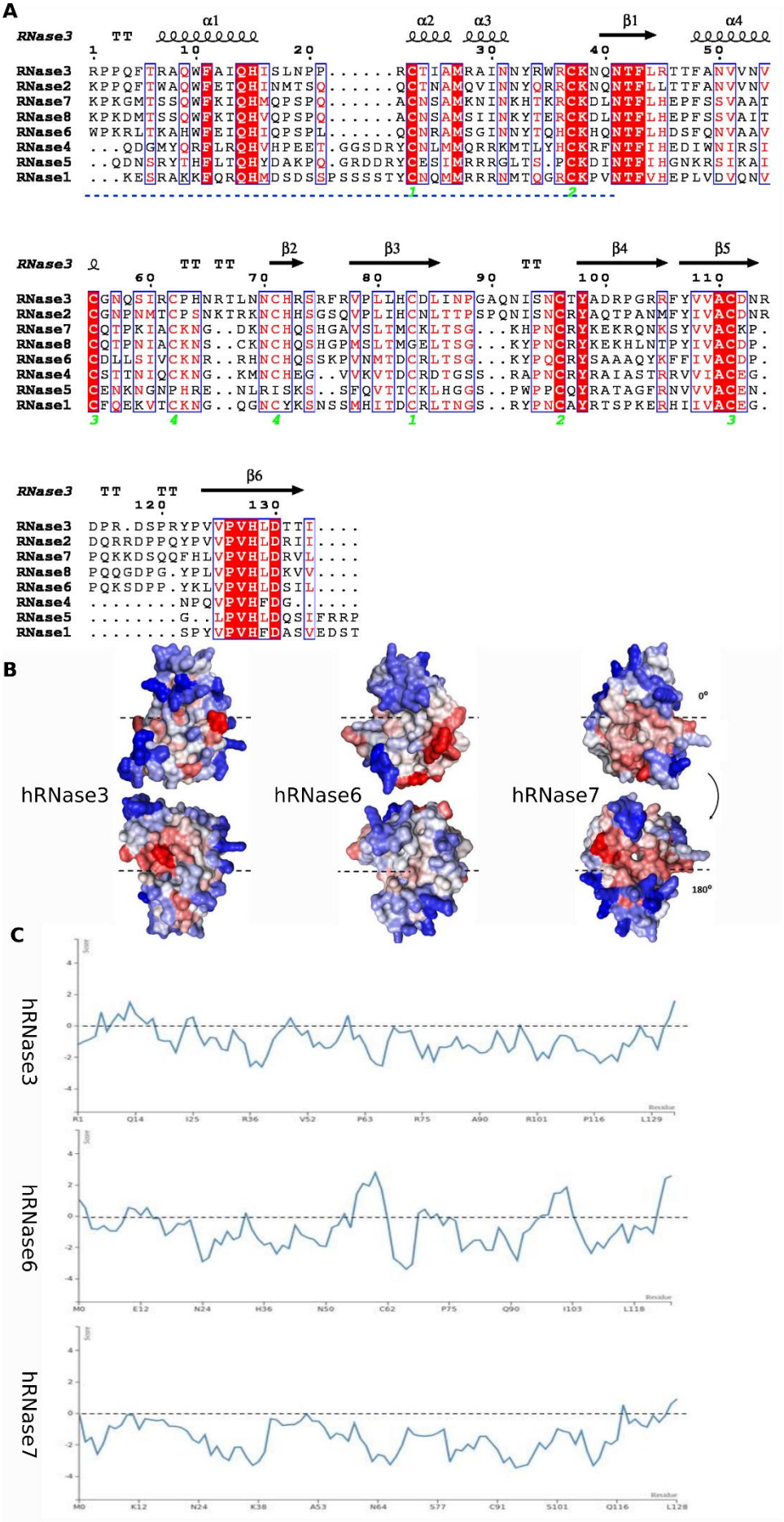
A
RNase3
RNase2
RNase7
RNase8
RNase6
RNase4
RNase5
RNase1
B
hRNase3
hRNase6
hRNase7
0°
180°
C
hRNase3
hRNase6
hRNase7

Figure S8. Sequence alignment and prediction of aggregation propensity of eight human RNases. A) Alignment of the eight human canonical RNases using the ESPript3 software (*espript.ibcp.fr/)*, the N-terminal domain is highlighted in blue. Sequence allocation was performed following the homology between RNases. B) 3D structure of RNases by Aggrescan3D (A3D) [50]. A3D exploits an experimentally derived intrinsic aggregation propensity scale for natural amino acids. This structure-based approach identifies aggregation patches (in red) at the protein surface. C) Aggregation profile propensity of RNase3, RNase6 and RNase7 based on A3D score for protein residues.

CHAPTER IV

Title: Immunomodulatory action of RNase3/ECP in a macrophage infection model related and unrelated to catalytic activity

Authors: Lu Lu[1], RanLei Wei[2], Maria Goetz[1], Guillem Prats-Ejarque[1], Gang Wang[2], Marc Torrent[1], Ester Boix[1#]

[1]Department of Biochemistry and Molecular Biology, Faculty of Biosciences, Universitat Autonomous de Barcelona, Cerdanyola del Vallès, Spain

[2]Center of Precision Medicine& Precision Medicine Key Laboratory of Sichuan Province, West China Hospital, Sichuan University, Chengdu, China

[#]corresponding authors: Ester Boix, Ester.Boix@uab.cat

ORCID: 0000-0003-1790-2142 (EB); 0000-0002-0960-1529(LL); 0000-0002-0257-1603(RLW)

Abstract:

The human RNase3, also named the Eosinophil Cationic protein (ECP), is a member of the pancreatic RNaseA superfamily, involved in host immunity. RNase3 is expressed by leukocytes and show broad-spectrum antimicrobial activity. Together with a direct antimicrobial action, RNase3 also exhibits immunomodulatory properties. To gain a better understanding of RNase3 role, we have analysed here the transcriptome of macrophages exposed to both the wild-type protein and a catalytically defective mutant (RNase3-H15A). The analysis of differently expressed genes (DEGs) in treated THP1 derived macrophages highlighted a common pro-inflammatory "core-response" independent of the protein ribonucleolytic activity. Network analysis identified epidermal growth factor receptor (EGFR) as the main central regulatory protein. Structural analysis suggested that RNase3 can activate the EGFR pathway by direct interaction with the receptor, as recently reported for the homologous human RNase5/Angiogenin. In addition, we identified a subset of DEGs specifically related to the protein ribonucleolytic activity, which are characteristic of virus infection response and interferon signalling. Transcriptome profile comparison at 4 and 12h revealed an early pro-inflammatory response, not dependant on the protein catalytic activity, followed by a late activation of the interferon pathway in a ribonucleolytic dependant manner. Next, we demonstrated that overexpression of the macrophage endogenous RNase3 can protect the cells against intracellular infection by both *Mycobacterium aurum* and the human respiratory syncytial virus (RSV). Eventually, comparative analysis of *M. aurum* and RSV infection profiles of the RNase3 overexpression cell line in the presence of Erlotinib, an inhibitor of the EGFR, revealed that the receptor activation is required for the antibacterial but not for the antiviral protein action. Moreover, the DEGs profiles related and unrelated to the protein catalytic activity are associated to the immune response to and viral infection respectively. We can conclude that RNase3 participates in the macrophage pro-inflammatory immune response against infection. A better knowledge of RNase3 anti-infective mechanism of action would provide the basis for applied therapeutics.

Keywords: RNase3, ribonucleases, macrophage, immunomodulation, EGFR, *Mycobacterium aurum*, Respiratory Syncytial Virus, transcriptome

Introduction:

Human RNase3, also known as Eosinophil Cationic Protein (ECP), is a member of the ribonuclease A superfamily. It is a small and highly cationic protein that participates in the immune defence response. RNase3 is mainly expressed in eosinophils, the mature protein is stored in the eosinophil secondary granules and is secreted upon infection and inflammation [1–3]. Together with its main production source, the protein is also reported to be expressed in other leukocytes, such as neutrophils and macrophages [4]. The importance of the selective expression and secretion of RNase3 has been emphasized due to its association with multiple diseases, such as asthma, intestinal tract inflammation or autoimmune disorders [1, 2, 4, 5]. The protein is routinely used as a clinical diagnostic marker of eosinophil activation during inflammatory processes [2]. Secretion of RNase3 is also induced by damaged epithelia and the protein can also participate in tissue healing and remodelling [4]. In addition, RNase3 expression is induced by infection and might contribute to the protection of biological fluids. The protein exhibits antimicrobial activity against a wide range of microorganisms, such as bacteria, yeast, viruses, and parasites [3, 6–10]. Abundance of surface-exposed cationic and hydrophobic residues can mediate the protein binding and subsequent destabilization of bacterial membranes through a carpet-like mechanism characteristic of many host defence antimicrobial peptides (AMPs) [10–12]. Although the protein triggers the pathogen death mainly through a direct mechanical action at the cell envelope, the targeting of intracellular components, such as nucleic acids cannot be disregarded. Indeed, RNase3 internalization is observed in treated yeast cells and protozoa [8, 13]. Besides, RNase3 can enter the macrophage and eradicate the intracellular dwelling bacteria [14]. On the other hand, the protein antiviral activity on single stranded RNA virus has been directly correlated to its ribonucleolytic action [9].

Together with the RNase3 direct antimicrobial activity, a series of evidences illustrated that RNase3 also plays an immunomodulatory role during host defence [2, 4]. Early studies showed that RNase3 can activate rat mast cell and induce histamine release, mediating the cross talk between mast cells and eosinophils [15]. RNase3 displays remodelling activity partly mediated by inducing the expression of epithelial insulin-like growth factor 1 (IGF1) [5] and the fibroblast chemotaxis can be enhanced by RNase3 release into the injured tissue site [2, 16]. Recently, we observed that RNase3 expression in macrophages is regulated by mycobacteria infection. Moreover, we demonstrated the protein ability to enter macrophage cells and induce autophagy, contributing thereby to the eradication of the intracellular infection [14]. However, how RNase3 regulates the macrophage function and whether the protein immunomodulatory properties are dependent on its ribonucleolytic activity remains to be clarified.

In the present study, we have investigated how RNase3 modulates the transcriptome profile of the macrophage cell. Towards this end, we used the human monocytic cell line THP1 derived to macrophage and applied the next generation RNAseq methodology to analyse the cell response to protein treatment. In addition, we explored the potential contribution of the protein catalytic activity on macrophages by using a mutant enzymatically defective mutant (RNase3-H15A). To note, this is the first systematic study to investigate the biological function of human RNase3 in macrophages by the whole transcriptome analysis. Complementarily, we built an

RNase3 overexpression THP1 cell line by CRISPRa, to validate the transcriptome results and evaluated the direct contribution of endogenous RNase3 in the eradication of intracellular infection by *M. aurum* and the human respiratory syncytial virus (RSV). The results revealed that RNase3 can inhibit both bacterial and viral infection through the modulation of the macrophage immune response in both ribonucleolytic dependent and independent ways.

Materials and methods

Cell culture

Human THP-1 cells (NCTC #88081201) were maintained or passaged in 25 or 75 cm^2 tissue culture flasks (BD Biosciences) using RPMI-1640 (Lonza, BE12-702F) medium with 10% heat-inactivated fetal bovine serum (FBS) at 37°C, humidified 5% CO_2 conditions. THP-1 cells using in this study were controlled below passage 25. THP-1 cells were treated with 50 nM phorbol myristate acetate (PMA, Sigma-Aldrich, P8139) for 48h to induce differentiation into macrophage-like cells and allowed to rest for 24h before further treatment.

Recombinant protein expression

RNase3 and RNase3-H15A recombinant proteins were produced as previously reported [8]. Briefly, *E. coli* BL21(DE3) cells were induced by 1 mM Isopropyl β-d-1-thiogalactopyranoside (IPTG, St. Louis, MO, USA) and the inclusion bodies enriched pellet was resuspended in 80 mL of 10 mM Tris-HCl pH 8.5, 2 mM EDTA and left incubating 30 min with 40 μg/mL of lysozyme prior to sonication. Following, the sample was centrifuged at 30.000×g for 30min at 4°C and the pellet was resuspended in 25 mL of the same buffer with 1% triton X-100 and 1 M urea and was left stirring at room temperature for 30min and then centrifuged 30 min at 22.000×g. Following, 200 mL of 10 mM Tris-HCl pH 8.5, 2 mM EDTA was added to the pellet, and then the sample was centrifuged at 22.000×g for 30min (4°C). The resulting pellet solubilized in 6 M guanidine hydrochloride and rapidly 80-fold diluted in the refolding buffer was left in gentle stirring for 48-72h at 4°C. The folded protein was then concentrated, dialyzed against the chromatography buffer and purified first by cation chromatography using a Resource S (GE Healthcare Life Sciences) column and then by reverse phase chromatography on a Vydac C4 (ThermoFisher Scientific) column. Sample purity was checked by SDS-PAGE and MS spectrometry.

Treatment of THP1 cells derived to macrophages with RNase3 and RNase3-H15A

THP1 cells were differentiated into macrophages by 50 nM of PMA treatment as previously described [14]. The cells were then washed 3 times with prewarmed PBS and replaced with fresh RPMI+10%FBS medium. THP1-derived macrophages were then treated with 10 μM of the recombinant proteins, wild-type (wt) RNase3 or the RNase3-H15A mutant. Previous work confirmed that the selected protein concentration ensured an effective antimicrobial activity and was non-toxic to the macrophage cells [14]. After 4 and 12 h of treatment, the cells were washed 3 times with pre-warmed PBS and collected for further RNA extraction. Three biological repeats were carried out for each experiment.

RNA isolation and sequencing

Total RNA was extracted using the mirVanaTM miRNA Isolation Kit (Ambion, Life Technologies, AM1560) as described by the manufacturer. RNA purity was determined by spectrophotometry and RNA integrity (RIN) was analysed using Agilent 2100 Bioanalyzer (Table S1). Following RNA extraction, total RNAs were submitted to the CRG genomics unit (*Centre for Genomic Regulation*, Barcelona) for cDNA library preparation, polyA enrichment and NGS sequencing. Sequencing libraries were prepared according to protocols provided by Illumina. 50bp-long single-end sequencing was carried out in an Illumina HiSeq2500 sequencer with a depth of >20 million reads per sample. Raw sequence reads have been deposited in the NCBI Sequence Read Archive (SRA) under accession number PRJNA574982.

Transcriptome Analysis

FastQC was used to carry out the quality assessment of reads, assessing the distribution of phred quality scores and mean percentage GC content across each read. Reads were aligned to the latest human genome assembly from the Genome Reference Consortium (GRCh38) using HISAT2 [17]. Aligned reads were stored in the SAM file format. StringTie was used to assemble the alignments into transcripts and estimate the expression levels of all genes and transcripts [17]. Low expression (sum count less than 10) and non-coding genes were filtered out using biomaRT [18] before passing to the Bioconductor package DESeq2 [19]. The resulting P-values were adjusted using Benjamini and Hochberg's approach for controlling the false discovery rate (FDR). Genes with an adjusted P-value (Q-value) < 0.01 & log2fc absolute value >1 found by DESeq2 were assigned as differentially expressed genes (DEGs).

GO enrichment and KEGG pathway enrichment analysis of the differential expression of genes across the samples was carried out using the clusterProfiler R package [20]. Protein-protein-interactions between DEGs were analysed using NetworkAnalyst which integrates the experimentally validated interactions database, InnateDB database [21]. The network was visualized using Cytoscape software (https://cytoscape.org).

Molecular Modeling

HADDOCK2.2 (Utrecht Bioinformatics Center, University of Utrecht) was applied to perform the modelling of the protein complexes and predict the associated free energies [22, 23].

Construction of an RNase3 overexpression THP1 cell line

We applied CRISPRa to activate the endogenous expression of RNase3 in THP1 [24]. Five distinct sgRNAs targeting the region from 100 to 500 bp relative to the transcription start sites (TSS) of the RNase3 gene were designed by using Cas9 Activator Tool (http://sam.genome-engineering.org/database/) [24]; the sgRNA sequence is listed in Table S2. The pLenti239G plasmid, used to co-express the dCas9-VP64 fusion protein and EGFP, was constructed by inserting the T2A-EGFP cassette from the LentiCRISPRv2-GFP-puro (gifted by Manuel Kaulich) in place of the T2A-BSD cassette of the lenti-dCAS-VP64-Blast (Addgene61425, gifted by Manuel Kaulich). The pLenti239R, used to co-express the gRNA, cherry red fluorescence

protein, and puromycin resistance gene, was constructed by displacing the Cas9-T2A-EGFP of LentiCRISPRv2-GFP-puro (gifted by Manuel Kaulich) with Cherry red fluorescent gene (gifted by Marcos Gil García, UAB). The sgRNA sequences were inserted in pLenti239R at downstream of the U6 promoter using the BbsI cloning sites. The correct construction of the plasmids was validated by Sanger sequencing.

Following, HEK293T cells were used for lentiviral production. HEK293T cells were maintained in DMEM + 10% FBS complete medium in a 5% CO_2 humidified incubator at 37°C. Cells were co-transfected with psPAX2 (Addgene#35002, gifted by Marina Rodriguez Muñoz) packaging plasmid, pMD2.G (Addgene#12259, gifted by Marina Rodriguez Muñoz) envelope plasmid, and pLenti-239G (encoding dCAS9 and eGFP) or pLenti-239R (encoding sgRNA and Cherry red fluorescent marker) using calcium phosphate precipitation protocol [25]. The transfection medium was replaced with fresh medium after overnight. Supernatants were collected 24, 48 and 72 hours after transfection, centrifuged to remove cell debris, passed through 0.45 μm filter and concentrated using PEG6000 precipitation method [26]. Viral pellets were resuspended in PBS, aliquoted and stored at -80°C until use. THP1 monocytes were infected with 20 μl concentrated lentivirus in the presence of 8 μg/mL polybrene for overnight. Next day, the cells were replaced with fresh medium and cultured for 72h. Fluorescence positive monocytes were checked by fluorescence microscopy and then sorted by Cell sorter. The fluorescence positive cells were evaluated by suspending the cells in PBS and fixing them with 2% paraformaldehyde for 10 min prior to flow cytometer. The fluorescence positive cells were sorted into single cells by Cell sorter BD FACSJazz.

Real -Time qPCR Assays

The transcriptional expression profiles of selected genes were measured by RT-qPCR with *GAPDH* as the internal control gene. Primers used for RT-qPCR validation are listed in Table S2. The same total RNA was reverse transcribed into cDNA by using iScriptTM cDNA Synthesis Kit (Bio-Rad, 1708891). RT-qPCR assays were performed in 20 μL using the iTaq Universal SYBR Green Supermix (Bio-Rad, 1725121) according to the manufacturer's instructions. The reactions were conducted using CFX96 Real-Time PCR detection system (Bio-Rad, Hercules, CA, USA) under the following conditions: 95°C for 2 min; 40 cycles of 95°C for 15 s and 60°C for 30 s; melting curve generation (60°C to 95°C). The relative expression ratios were calculated using the $2^{-\Delta\Delta CT}$ method [27, 28].

Western blot

For the western blot assays, cells were harvested and lysed with RIPA buffer. The samples were separated by 10% SDS-PAGE, transferred to polyvinylidene difluoride membranes, blocked with 5% non-fat milk in TBST, and incubated with anti-RNase3 primary antibody (Abcam, ab207429) overnight at 4°C. After washing, the membranes were treated with horseradish peroxidase (HRP)-conjugated goat anti-rabbit IgG (Sigma Aldrich, 12-348) for 1 h at room temperature (RT). Finally, the membranes were exposed to an enhanced chemiluminescent detection system (Supersignal West Pico Chemiluminescent Substrate, ThermoFisher Scientific, 32209) for detection. As a control, GAPDH was detected with chicken anti-GAPDH antibodies (Millipore).

Macrophage infection by mycobacteria and CFU assay

Infection of THP1 cells derived to macrophage by mycobacteria was performed as previously described [14]. *M. aurum* was purchased from the UK National Collection of Type Cultures (NCTC). Cells cultures of *M. aurum* (NCTC, 10437 were grown in Middlebrook (MB) 7H9 broth (BD Biosciences, 271310) enriched with 10% (v/v) albumin/dextrose/catalase (ADC; BD Biosciences, 212352) containing 0.05% Tween 80, and in MB7H10 (BD Biosciences, 262710) with 10% (v/v) oleic acid/albumin/dextrose/catalase (OADC; BD Biosciences, 212240) for semi-solid agar growth at 37°C. Stock cultures of log-phase cells were maintained in glycerol (25% final concentration of glycerol) at −80°C. The bacteria were vortexed and sonicated using ultrasound sonication bath to obtain a single cell suspension, and then the bacterial concentration was determined by measuring the optical density (OD) of the culture at 600 nm (OD = 10^9 CFU/mL). Mid-log phase *M. aurum* cells, harvested in RPMI-1640 complete medium, were co-cultured with macrophages at a multiplicity of infection (MOI) of 10:1 and were incubated at 37°C for 3 h, then were washed 3 times with PBS and replaced with fresh media supplied with 50 μg/mL gentamycin (Apollo Scientific, BIG0124) to remove extracellular mycobacteria during further treatment.

Colony forming units (CFU) counting assay was applied to compare the infectivity and living rate of *M. aurum* toward THP1 derived macrophages with or without RNase3 overexpression. $2x10^5$ THP1 cells were seeded in 24 well plates per well and induced to macrophages by 50 nM of PMA treatment. Next, log-phase cultures of *M. aurum* ($OD_{600}\approx1$) were diluted to $2x10^6$ CFUs/mL and were used to infect macrophages derived from wild type macrophage (WT) or RNase3-overexpression macrophage cells (OX) at a multiplicity of infection of 10:1 at 37 degree for 3h. Then the cells were washed 3 times with PBS and replaced with fresh media supplied with 50 μg/mL gentamycin to remove extracellular mycobacteria, taken as the "0h post-infection" reference time. At 0h, 24h, 48h, and 72h, the cells were washed, collected, lysed with distilled water, and plated in 10mm petri dish containing MB7H10/OADC/agar. The CFU were counted after 2 weeks. Five independent experiments were conducted for this assay.

Macrophage infection by viruses & viral quantification

Human respiratory syncytial virus (RSV, ATCC, VR-1540) stock was ordered from ATCC. Hela cells were used to produce RSV under biosafety level II conditions [29]. Briefly, Hela cells are plated in 75 cm^2 culture flask and incubated at 37ºC in DMEM+10% FBS until they are approximately 50% confluent. The cells were then washed and infected with RSV stock under a MOI of 0.1. After 3h infection, the cells were washed and replaced with fresh medium (DMEM+ 10%FBS) and incubated for 4 days at 37ºC, 5% CO_2. The cells and the virus suspension were collected when the cytopathology appeared, with scraping and vortexing of the cells to release more viral particles. The virus suspension was centrifuged for 10 min at 1800×g to remove the cell debris. The virus suspension without cell debris were either frozen immediately and stored at -80ºC as seeding stock or concentrated using Amicon Ultra-15 centrifugal filters (Millipore, UFC910024). The produced viruses were titrated using TCID50 (median tissue culture infectious dose) method in Hela cells [30].

Before RSV infection, THP1 cells were induced to macrophage by 50 nM of PMA treatment for 48h. Cells were washed three time with prewarmed PBS and replaced with

fresh RPMI+10% FBS medium for 24h incubation. After that, macrophages were washed and incubated with RSV, mixing every 15 min for the first 2h. All virus treatment tests were performed using RSV at a MOI of 1 TCID50/cell.

RSV was detected by RT-qPCR [31]. After the indicated post-infection time, the extracellular RSV virus was collected by the PEG6000 precipitation methodology [26, 32] and intracellular RSV virus were collected by lysing the macrophage cells with the lysis buffer from mirVanaTM miRNA Isolation Kit (Ambion, Life Technologies, AM1560). Total RNA from RSV infected macrophage cells as well as stock virus was extracted using mirVanaTM miRNA Isolation Kit according to the manufacturer's instructions. cDNA was synthesized using iScriptTM cDNA Synthesis Kit (Bio-Rad, 170-8891). The synthesis was performed using random hexamers, starting with 1 µg of total cell RNA. The RT-qPCR was performed using ddPCR^{TM} Supermix for Probes (Bio-Rad, 1863024). Samples with a cycle threshold value of more than 40 were recorded as negative. A standard curve was prepared using serially diluted RNA extracts from a known quantity and used to quantify RSV as TCID50/mL. In parallel with the RSV probe assays, an endogenous glyceraldehyde-3-phosphate dehydrogenase (*GAPDH*) control was used for relative quantification of the intracellular virus. The primers and probe used were listed in Table S2.

Cell viability assay

Cell viability was measured using MTT assay as previously reported [33]. After each time point of post of infection, cells were incubated with 100 µL of MTT reagent. The media were then removed and 200 µL of DMSO was added per well. The absorbance of the formazan was determined at 570 nm in an ELISA reader.

Results:

Comparative transcriptome analysis of THP1 derived macrophages treated with wild-type RNase3 and catalytically defective RNase3-H15A mutant

In order to explore the immunomodulatory properties of RNase3 on macrophages we incubated THP1 derived cells in the presence of the protein and analysed the cell transcriptome at 4h and 12h incubation time. Macrophage response to wild-type RNase3 exposure was compared with a protein mutant variant devoid of ribonucleolytic activity. Our previous work indicated that the H15A substitution fully abolishes the RNase3 catalytic activity without any alteration of the 3D protein structure [8]. Besides, we recently observed how both wild-type RNase3 and H15A mutant can induce the autophagy pathway and mediate the eradication of intracellular mycobacteria within macrophages [14]. Therefore, we decided to carry out a whole transcriptome analysis to identify the putative cell pathways associated to the protein exposure.

For each condition, three biological replicates were prepared for control, RNase3 and RNase3-H15A treatment of THP1 derived macrophage cells. Sample points were taken at 4h and 12h incubation time. Total RNA was purified for each condition and cDNA libraries were prepared for poly(A) mRNA sequencing 50 nt single read by NGS Illumina Hiseq2500. The raw sequencing data can be found in NCBI Sequence Read Archive (SRA) under accession number PRJNA574982. A total of 511 million reads (mReads) were obtained, providing about 28 mReads per sample. Approximately 96%

of the reads were uniquely mapped to the Homo sapiens genome (Table S3). Expression of 14801 protein coding genes were detected in at least one individual (filtered by sum count more than 10) (Additional file 1). The Principal Components Analysis (PCA) plot shows tight clustering within the control group and the protein treated groups (either RNase3 or RNase3H15A treatment) for mRNA expression (Figure S1). Additionally, RNase3 and RNase3-H15A treated samples clustered separately from each other, indicating temporal alterations in gene expression driven by different protein treatment.

Following, Differently Expressed Genes (DEGs) were identified for RNase3 versus control, RNase3-H15A versus control, and RNase3-H15A versus RNase3. Using DESeq2, we identified 4930 (2563 up regulated and 2367 down regulated) and 4933 (2584 up regulated and 2349 down regulated) DEGs at 4h and 12h, respectively, between RNase3 treated cells and untreated control cells. When comparing RNase3H15A treated cells to untreated control cells at 4h and 12h respectively, 4869 (2516 up regulated and 2353 down regulated), and 4986 DEGs were identified (2585 up regulated gene and 2401 down regulated) (Figure 1A). Next, we identified DEGs by comparing 4h and 12h timing for each treatment, 18 (10 up regulated and 8 down regulated), 351 (223 up regulated and 128 down regulated) and 198 (81 up regulated and 117 down regulated) DEGs were found in control, RNase3, and RNase3-H15A treatment as a function of time, respectively. The small amount of DEGs between 4h and 12h found in control samples indicated that the biology status of the cells has been stable during all the experiment. A direct comparison between RNase3 and RNase3-H15A treated cells found 30 (22 up regulated and 8 down regulated) and 125 (115 up regulated and 10 down regulated) DEGs at 4h and 12h post of treatment, respectively. All the DEGs described above are listed in Additional file 2.

RNase3 modulates the macrophage global innate immune response in a ribonuclease independent manner

Given the high overlapping rate of DEGs between RNase3 and RNase3-H15A treated cells either at 4h or 12h (Figure 1B & 1C), we sought to identify the genes with similar response profiles. Profiles with overlap between RNase3 and RNase3-H15A treated cells, comprising a total of 3818 genes, were identified to confirm the core response of macrophage modulated by both RNase3 and RNase3-H15A. Core response genes not related to the protein ribonucleolytic activity are listed in Additional file 3 (1972 and 1846 are up-regulated and down-regulated, respectively; see Figures 1B and 1C).

KEGG pathway enrichment of the up-regulated DEGs indicated that both RNase3 and RNase3-H15A treatment triggered the cells overall immune response. In total, 58 KEGG pathways were significantly enriched (padj<0.01) (see Figure 2A and Additional file 4). The top 10 listed pathways included TNF signal pathway, Cytokine-cytokine receptor interaction, NF-kappa B signal pathway, Chemokine signalling pathway, Toll-like receptor signal pathway and MAPK signalling pathway. To examine more closely the correlations between the genes of the core response to RNase3 and RNase3H15A treatment, we incorporated a network based approach using the NetworkAnalyst3.0 with InnateDB database [21]. Ranked by connectivity and betweenness centrality, *EGR1*, *EGFR*, *SRC*, *STAT1*, *NFkB1*, and *JUN* were identified as the primary hub and bottleneck genes of macrophages induced upon RNase3 and RNase3-H15A exposure

(Figure 3A). Among them, the Epithelial Growth Factor Receptor (EGFR) is the main connector, followed by a second group composed by EGR1, SRC, STAT1 and NFkB1 and last the JUN gene. Moreover, EGFR shares direct or indirect interaction with all the other central hub genes: EGR1, SRC, STAT1, NFkB1, and JUN and SRC transcription regulator. EGFR activation positively regulates EGR1, STAT1, NFkB1 and JUN transcription factors. EGFR upregulates the expression of the signal transducer and activator of transcription STAT1, a transcription factor responding to cell stress injuries, such as infection, and regulating genes involved in the inflammatory response [34]; EGFR signalling is an important mechanism of NF-kB activation, which controls pro-inflammatory cytokine production and cell survival [35] and SRC is a regulatory protein kinase that also mediates the inflammatory response via EGFR transactivation [36]. Likewise, EGR1 is a transcription factor that promotes inflammation activated by EGFR. Therefore, we can conclude from the network analysis results that EGFR is the main determinant of shared pathways induced by both wt RNase3 and the RNase3-H15A mutant.

Next, we explored the down regulated DEGs in THP1 derived macrophages upon exposure of both wt and the catalytically defective RNase3. We identified 1846 DEGs counts associated to RNase3/RNase3-H15A common response (Figure 1C), 13pathways were significantly enriched (Figure 2B; Additional file4). Downregulated pathways include cell cycle, DNA replication, homologous recombination and mismatch repair among others, which are indicators of a cellular growth inhibition and duplication arrest response. To note, CDK1, BRCA1, PCNA, CDK1 and KIAA0101, were considered the hub and bottleneck genes by network analysis (Figure 3B). As illustrated by their key connectivity we can highlight CDK1 and BRCA1, followed by CDK2 and PCNA, and last KIAA0101. Interestingly, BRCA1, CDK1 and CDK2 are also downregulated by EGFR activation. Moreover, PCNA is involved in the direct response to EGFR related to DNA damage.

Following, we studied the macrophage cell response upon protein exposure as a function of time. Considering that cytokine-cytokine receptor interaction is within the top common enriched pathway upon RNase3 and RNase3-H15A treatment, with more than 78 genes significantly up-regulated (Figure 2A, Additional file 4), we decided to compare their dynamic changes at 4h and 12h time points. Compared to control, RNase3 or RNase3-H15A triggered a fast inflammatory response of the macrophage cell, as witnessed by a significant up-regulation of 20 hallmark inflammatory genes, such as *TNFα* (210 fold), *IL1β* (1422 fold), *CD40* (14 fold), *CXCL8* (760 fold), *CCL4L2* (1594 fold). Moreover, 19 hallmark TNFα-signalling via NFkB genes were also significantly upregulated, such as *CXCL1* (133 fold), *CXCL2* (183 fold), *CXCL3* (596 fold), *IL7R* (62 fold), *LIF* (366 fold), *CCL3L1* (570 fold), *CCL4* (1771 fold), *TNFRSF12A* (11 fold) (see Additional file 5). Likewise, we identified a group of significantly down-regulated genes, such as *CXCR4*, *IL31RA*, *IL1RAP*, *PRLR*, *CCL28*, *IL12RB1*, *CXCR2*, *CXCR1*, *GDF11*, *CCL23*, *CX3CR1*, *CCR2*, *BMP8B*, and *CSF3R*. According to the timeline, the gene counts of most pro-inflammatory genes decreased by 12h in comparison to a 4h (Figure 4), indicating that the pro-inflammatory effect triggered by RNase3 is a short-term effect and is reduced upon time. Figure 5 illustrates the main activated transcription factors and their associated response. To note, together

with pro-inflammatory cytokines, we can identify up-regulated chemokines related to leukocyte recruitment, such as CCL1 and CCL2 for monocytes, CCL20 for lymphocytes, CCL21 for activated T cells, CXCL3 for neutrophils and tissue remodelling, such as ICAM1, VCAM1, MMP9 and TGFβ. Overall, the observed immune-metabolic response is characteristic of a M1 macrophage activation type [37].

RNase3 modulates the macrophage antiviral pathway in a catalytic dependent manner

Although RNase3 and RNase3-H15A elicited an overall similar transcriptional response of macrophage, a direct comparison between macrophage cells treated with the wt and mutant proteins identified significant changes related to the RNase catalytic activity. Transcriptome analysis of wt versus H15A mutant revealed 30 and 143 DEGs at 4 and 12h, respectively (Figure 1). Within the DEGs paired set we found only 6 genes activated at both 4 and 12h time points: *CXCL10*, *IFIT1*, *LAMTOR1*, *SOCS3*, *OASL*, and *IFIT2* (Figure 6). Interestingly, several of these genes are activated by the interferon pathway, such as the 2'5' oligoadenylate synthase like protein (OASL), the CXCL10 chemokine and the interferon induced RNA binding proteins (IFIT1 and 2) [38–40]. On its side, SOCS3 activation is usually observed following infection and plays a tissue protecting role against inflammation side effects [41].

On the other hand, when all the DEGs were analysed by connectivity and betweenness centrality, we observed 31 seed genes connected by 44 edges. The network analysis clearly pointed out to STAT1 and ISG15 as the hub genes (Figure 6). ISG15 expression is regulated by STAT1 transcription factor (Figure 5), which is characteristic of the macrophage activation by the interferon pathway and adaptation to an antiviral state. The connectivity map outlined the contribution of other interferon induced regulatory proteins, such as IFIT1-3 and the CXCL10 chemokine. By applying the KEGG pathway enrichment analysis, we mostly obtained at 12h signalling pathways related to infection sensing and in particular associated to antiviral response (see table 1 and Additional file 5). In contrast, no significant pathway was found when applying the DEGs at 4h. In any case, according to GO term annotation analysis "response to virus" is the single significantly enriched at 4h. Moreover, analysis of the DEGs at 12h, identified diverse biological processes but in all the cases related to the cell defence response to virus" (Table 3, Additional file 6). In addition, the comparative heatmap of DEGs highlighted that significant changes of wt versus H15A mutant are mostly prominent at 12h. Overall, we can conclude that the late immune-regulatory action (12h) induced by RNase3 dependent on the protein catalytic activity would complement the first short-term response (4h), mostly mediated by EGFR activation. Results suggest that both RNase3 activated pathways, catalytically dependent and independent, might work by complementing each other. In addition, the activation of STAT1, via ISG15 and IFIT1-3, can mediate the endosomal EGFR internalization and macrophage cell response (Figure 5). Indeed, by inspection of DEGs network analysis we observed the induction of the endosomal TLR7-9 mediated pathways dependant on RNase activity (Figure 5). In this context, we observed how STAT1 mediated activation is reinforced by a catalytic activity dependent mechanism at a late (12h) response. We can hypothesize that activation of STAT1 by RNase3 might be mediated by the release of specific RNA products, such as dsRNA. Interestingly, STAT1 is activated by both the IFN and EGFR signalling pathways. Indeed, the initial increase of IFNα and IFNβ would be induced by

the NF-kB pathway, which was observed to be activated by an RNase independent manner (see figure 5). Based on our data, we can suggest that the IFN pathway, might be reinforcing the short term signalling paths induced by a direct targeting of EGFR by RNase3.

Analysis of the putative RNase3-EGFR interaction by Molecular modelling

Considering that our whole transcriptome analysis pointed out to a direct activation of EGFR by RNase3 (Figure 3), we decided to further explore the protein-receptor binding process. Interestingly, it was recently demonstrated that RNase5/Ang, another member from the RNase A superfamily, is a direct ligand of EGFR [42]. The authors identified a C-terminal region in RNase5 needed for EGFR interaction, with significant homology to EGF binding region to the receptor. Interestingly, we observed here how the four conserved residues shared by RNase5 and EGF (C81, C92, Q93, Y94) are mostly conserved in RNase3 (Figure 7A and Additional file 7). In particular, the QYRD sequence was confirmed to participate in EGF interaction with the receptor by site-directed mutagenesis [43]. Considering that the region of RNase 5 involved in the interaction with EGFR is partially conserved in RNase3, we decided to explore the potential protein interaction to the receptor. We applied HADDOCK software to predict the complex structures of RNase3 with the EGFR extracellular domain (Figure 7B). High binding of RNase3 to EGFR was estimated (see Table 2). To note, we obtained for RNase3 similar or even slightly higher binding energies, as calculated for EGF. Besides, our calculated values by HADDOCK are in accordance to the binding energies predicted for EGF by molecular dynamics [44]. A close inspection of the predicted complex revealed that the interaction of RNase3 with EGFR might be mediated by residues regions 1-4, 19-28, 33-35, 86-87 and 94-100. In particular, we can identify the key role of N95, R97, Y98 and D100 of RNase3 that can interact within the 417-470 region of the EGF receptor (see Additional file 7 for a full list of predicted protein-protein interactions). The molecular modelling also indicates that the RNase active site residues (H15, K38 and H128) would not be involved in the receptor binding, in agreement with our transcriptomic results. Besides, the main region identified in RNase3 overlaps with the RNase 5, and EGF counterparts (Figure 7A). However, we also observed significant differences in the main interacting region from EGF and RNases, where residues 45-51 in EGF are not conserved in RNases sequence. This suggests that the RNases mechanism is not fully equivalent to EGF functioning and might indicate a distinct target within the EGFR family. Notwithstanding, we do observed conservation of main key interacting residues, specifically within the CQYRD segment (residues 96-100 and 92-96 in RNase3 and EGF respectively). In particular, Hung and co-workers confirmed that residues Q93 and Y94 were essential for the receptor binding to RNase5. Here, in our model for RNase3, we observed the putative binding of R97 to the receptor extracellular domain. Interestingly, RNase3 presents a single nucleotide polymorphism (SNP) at position 97 with two alternate substitutions (R/T) [45] and molecular modelling predicted a significantly higher affinity to the receptor for the R97 variant respect to the T97 one (Table 2). Previous work by Venge and co-workers indicated that substitution of R97 by a T correlated with a loss of the protein cytotoxicity [46, 47]. The present data might explain the previously observed differences in the biological properties of the two RNase3 variants.

Characterization of an RNase3 overexpression THP1 cell line

In order to corroborate our transcriptomic results and evaluate the potential contribution *in situ* of the macrophage endogenous RNase3, we decided to obtain a THP1 cell line that overexpresses the protein. As quantified in our previous work, basal levels of RNase3 in the monocytic THP1 cell line are detectable but considerably low (estimated about 1/500 respect to the GAPDH control gene) [14]. Therefore, the overexpression of RNase3 in THP1 cells could serve to analyse the protein action within the macrophage –derived cells. CRIPSRa methodology was applied to overexpress RNase3 in THP1 cells. The plasmids encoding CRISPRa components were delivered to THP1 cells by lentiviral infection. An empty lentiviral plasmid was used for the control reference cells. The GFP and Cherry red both positive cells successfully transduced by lenti239G (encoding dCas9-VP64-GFP) and lenti239R (encoding sgRNA-Cherry red) were sorted by FACS (Figure 8A). After induction of THP1 to macrophage, the expression of RNase3 was quantified by qPCR, observing an increase from about 1.5 to 3-fold in all the analysed cell lines (Figure S2). The best performance cell line (OX5) was selected for final characterization. RNase3 levels in relation to wild-type THP1 cells were quantified by both qPCR and WB, confirming a significant increase of RNase3 both at the gene and protein level (Figure 8B & C). On the other hand, we confirmed that overexpression of RNase3 did not alter the macrophage cell viability (Figure 9).

To validate the transcriptome results obtained by NGS sequencing, we analysed the expression profile of the RNase3 overexpression THP1 cell line. A total of 18 genes from the previously obtained DEGs libraries were selected for further qPCR analysis. The results confirmed similar expression levels induced by both endogenous and recombinant proteins (Figure 8D).

Overexpression of endogenous RNase3 inhibits the macrophage intracellular infection by both M. aurum and RSV

Next, we evaluated the efficacy of the macrophage endogenous RNase3 against infection. We selected two models of macrophage intracellular infection. *M. aurum* and the RSV. Both intracellular pathogens have been previously proven to be effectively eradicated within the macrophages by recombinant RNase3 addition [9, 14].

First, we infected both wild-type (WT) and RNase3-overexpression (OX) THP1 cells derived to macrophages with *M. aurum* and monitored the cell lines for 3 days. Intracellular infection was quantified by Colony Forming Unit counting (CFUs) in lysed cells after removal of extracellular mycobacteria. No significant differences in *M. aurum* initial CFUs between WT and OX cell lines were observed at the initial time point (Figure 9A). However, *M. aurum* can easily proliferate in wild type macrophage as indicated by an exponential CFU count increase as a function of time. On the contrary, mycobacteria cannot proliferate in the RNase3-overexpression cell line. A significant growth inhibition of *M. aurum* in RNase3 overexpression macrophages was detected at 24 h post-infection compared to WT macrophage. Noteworthy, the growth inhibition was even more prominent as the infection progressed (48h and 72h). The present data corroborate our previous results showing that recombinant RNase3 can efficiently mediate the eradication of macrophage intracellular infection by mycobacteria [14].

Likewise, both WT and OX THP1 cells derived to macrophages were infected with the RSV virus and the cell lines were monitored for 3 days. Probe-qPCR was applied to quantify the RSVs both extracellularly and intracellularly using an internal RSV quantification standard curve built by serially dilutions from a RSV stock (Figure S3). Starting from an equivalent RSV initial titer in both WT and OX cell lines we observed the increase as a function of time of RSV at extracellular and intracellular levels (Figure 9B and S4). Intracellular and extracellular RSV reached a maximum peak at 24h and 48h post of infection, respectively. Importantly, we found that overexpression of RNase3 in macrophage can significantly inhibit the RSV duplication at 24-72h poi (Figure 9B and S4). In addition, overexpression of RNase3 reduced the macrophage cell death rate caused by *M. aurum* and RSV infection (Figure 9C).

Moreover, the transcriptional expression levels of *RNase3* were quantified in both cell lines (WT and OX) in the absence and presence of *M. aurum* and RSV infection. Overall, we confirmed that the OX cell line expresses significantly higher level of *RNase3* than WT cells at all the time points (Figure 9D). In addition, we explored whether the cell infection by *M. aurum* and RSV could regulate the macrophage endogenous RNase3 expression. The results indicate that short term *M. aurum* infection is downregulating RNase3 whether a longer term exposure (48-72h) induced the protein expression. The data corroborate down and upregulation profile previously reported upon mycobacteria infection [14]. On the contrary, the expression of RNase3 in WT macrophage was not significantly altered by RSV infection. On its side, the OX cell line kept the expression levels of *RNase3* stable during all the 3 days' experiment in both *M. aurum and* RSV infection studies.

Blockage of the EGFR receptor by Erlotinib inhibits the RNase3 antibacterial activity

We next assessed the effect of adding an inhibitor of EGFR activity on the antimicrobial action of RNase3. Erlotinib inhibits EGFR activation by blocking the receptor tyrosine kinase [51]. The RNase3 overexpression macrophages were treated with Erlotinib for 24h before infection of either *M. aurum* or RSV. As illustrated in Figure 10A, upon addition of 10 μM of Erlotinib, we observed a significant increase of *M. aurum* growth within the macrophages. On the contrary, this scenario was not observed in RSV infection even after addition of 100 μM of Erlotinib (Figure 10B). Moreover, we quantified and compared the fold change of a set of 18 selected genes in RNase3 overexpressed cell line in the presence and absence of Erlotinib treatment. The selected genes had previously been quantified as DEGs by both recombinant RNase3 addition and endogenous protein overexpression (see Figure 8D). Moreover, by comparison between wild-type and catalytic defective RNase3 we identified the DEGs dependent or independent of the protein catalytic activity (see figures 3, 5 and 6). Here, following Erlotinib treatment we observed how gene expression is uniquely altered for the genes not dependent on the protein catalytic activity (Figure 10C). That is, addition of 10 μM of Erlotinib significantly inhibited RNase3's induction of the expression of genes such as *CXCL10*, *CEBPB*, *TNF*, *BCL3*, *IL1*, *NFKIBA*, *SRC*, *TLR4*, *ATP6V1H*, *GABARAP*. On the contrary, *MDA5*, *ISG15* and *RIG1* that are dependent on RNase3's catalytic activity, did not response to Erlotinib treatment. The results corroborated the presence of two distinct type of pathways that are regulated by RNase3 and are associated to

either catalytic or non-catalytic dependent mechanisms of action (see Figure 5 for a schematic overview).

Discussion

Antimicrobial peptides (AMPs) are important components of natural defence against a wide range of pathogens [52]. AMPs, originally reported to work by a direct action at the microbial cell wall, were later ascribed a diversity of immune modulatory properties that can contribute to the infection eradication [53, 54]. Human antimicrobial RNases from the RNaseA superfamily can be regarded as multifaceted AMPs that combine a microbial membrane destabilization action with immune regulatory properties [4, 55, 56]. In our recent work, we have reported how RNase3 induction of macrophage autophagy mediated the eradication of *M. aurum* intracellular infection [14]. Here, we have applied the NGS RNA sequencing methodology to explore the immune-regulatory mechanism of action of RNase3 within macrophages. The comparative transcriptomic profile of macrophages treated with wild-type and catalytically defective RNase3 has enabled us to identify the regulation pathways related and unrelated to the protein ribonucleolytic activity. Overall, we observed that treatment with both RNase3 and RNase3-H15A triggered a common immune response. The shared transcriptome profile pattern outlined an up-regulation core response characteristic of a macrophage pro-inflammation condition [37]. On its side, downregulation core response indicated that the protein addition promoted the cell growth arrest and duplication inhibition.

Protein-protein network analysis identified EGFR as the main hub gene, followed by a group of five other genes (JUN, NFkB1, STAT1, EGR1, SRC), which are on their turn directly or indirectly interacting with EGFR (Figure 5). On its side, inspection of central hub downregulated genes (Figure 3) also revealed an association to EGFR receptor activation. Interestingly, EGFR, the epidermal growth factor receptor, is not only a key membrane receptor involved in cell survival and tissue remodelling [57, 58], but it can also mediate the macrophage activation during bacterial [59] and virus infection [60]. Specifically, EGFR signalling is critical for pro-inflammatory cytokine and chemokine production [59, 61, 62]. Therefore, our present results suggest that RNase3 mostly modulates the macrophage response via direct EGFR activation. Taking into consideration the very recent report of human RNase5 direct binding to EGFR [63], we envisaged here a structural analysis of the putative interaction of RNase3 to the receptor. Human RNase5/Ang sharing with RNase3 a common three-dimensional structure fold, was taken as a reference to model a putative RNase3-receptor complex using the EGF-receptor complex as a reference (Figure 7). The results predicted a strong binding of RNase3 to the EGFR extracellular domain. Structural dynamics suggested no involvement of the protein catalytic site in the receptor interaction, as indicated by our transcriptome results. Likewise, EGFR activation by RNase5/Ang was not dependent on the protein catalytic activity [64]. Interestingly, we found a high sequence homology between both RNases at the conserved key target sequence previously identified at RNase5 and EGF C-terminus [64]. In particular, by structural alignment with the EGF molecule in complex with the extracellular domain of the receptor [65] the authors identified in RNase5 four conserved residues: two cysteines (C81 and C92), a glutamine (Q93) and a tyrosine (Y94) [63]. C81 and C92 are conserved in most of the RNaseA family members and participate in the disulphide bonding that connects the protein N

and C ends and stabilizes the overall three dimensional structure. On their turn, Q93 and Y94 counterparts in EGF were reported to bind to the receptor [66] and were confirmed by site-directed mutagenesis to participate in RNase5 -EGFR interaction. Pairwise sequence alignment indicated that Y94 is conserved in all RNase members. On the other hand, we found partially conserved substitutions for RNase5 Q93. To note, in RNase3 the glutamine is substituted by a threonine (T97). Interestingly, RNase3 displays a polymorphism at this position (R/T97), which has been correlated to the protein properties. In particular, R97 shows an enhanced cytotoxicity on several tested cancer cell lines [46]. On the contrary, the presence of a T at this position creates an N-glycosylation site and native N-glycosylated forms display a reduced cytotoxicity and antimicrobial activity [49, 67, 68]. Particular attention to R/T97 SNP in RNase3 was drawn due to the specific distribution within the population [69]. Presence of an R at 97 position has been linked to an enhanced severity of malaria and schistosomiasis side-effects [70, 71], such as hepatic fibrosis or neurological disorders that might be associated to an overabundance of the secreted RNase3 at the infectious focus [72, 73]. The protein overproduction at the infected tissue could be detrimental to the host health, as also observed in allergic asthma and other chronic inflammatory diseases. Evolutionary studies indicated that R is the amino acid present in RNase3 lineage ancestor and is shared by most of the other primate homologues [74]. The current results that highlight the potential contribution of R97 in EGFR activation would provide a novel explanation on the protein potential cytotoxicity and might explain the R/T SNP distribution as a function of the areas of the infection disease predominance. On the other hand, if we analyse the CQYRD region within the family context, we observed a high variability in position 97. Interestingly, while a glutamine is present in RNase5/Ang and ancestral family members, shared by most fish RNases, amphibians have lost the Q residue at this position and a high variability is found in mammalian RNases, where R is the predominant substitution [74, 75]. The importance of this residue was highlighted by Hung and co-workers, who demonstrated that human RNase1 homologue, where position 97 is occupied by an Ala does not activate the EGFR [64]. Additional variability is observed within the last two residues.

Arginine at position 99, present at EGF and RNase5 is substituted by an Ala in some RNases, like RNase2 and RNase3 [74]. To note, A99 in human RNase3 is conserved in all primates [74]. In addition, our modelling study identified another residue key for RNase3 interaction to the receptor, D100. The D residue at position 100 is also key for EGF binding but is not present in RNase5. The residue is conserved in all RNase3 primates but absent in RNase2, its closest homologue counterpart. Therefore, structural analysis revealed subtle differences that might significantly alter the receptor recognition pattern. We can speculate that the observed variability within the interacting sequence is indicating the targeting of distinct receptor subtypes within the EGFR family.

In any case, our results are in agreement with the characterization of the RNase5-EGFR interaction, where the protein catalytic activity was not required for the receptor activation [63]. In addition, the present results highlight the induction by both wild-type RNase3 and RNase3-H15A of pro-inflammatory cytokines. Complementarily, we also identified the release of tissue remodelling chemokines, such as VCAM, MMPs and TGFβ, in a catalytically independent manner (Figure 5). The present data would

reinforce the RNase3 role in tissue remodelling processes reported by *in vitro* wound healing models [2, 16, 76–78].

Although transcriptome analysis indicates that the majority of the macrophage response is common to both RNase3/RNase-H15A treatment, we also identified a group of genes specifically associated to the protein ribonucleolytic activity (see Figures 5 and 6). Overall, the main bulk of identified genes are related to interferon induced pathways, such as CXCL10, a leukocyte chemoattractant during viral infection, IFIT1 and 2, antiviral RNA binding proteins [39] and OASL [79, 80]; OASL is a 2'-5' oligoadenylate synthetase like gene which can bind double-stranded RNA and displays antiviral activity through mediating RIG-I activation [81, 82].

Accordingly, the top-rated KEGG pathways are related to host response to virus infection. Among them, the RIG-I-like receptors (RLRs), consisting of RIG-I, MDA5, and LGP2, play a major role in pathogen sensing of RNA virus infection to initiate and modulate the antiviral immunity [83]. Importantly, not only viral RNA ligands but also processed self RNA can be detected by RLRs in the cytoplasm to triggers innate immunity and inflammation and to impart gene expression that serves to control infection [83, 84]. Our network analysis identified ISG15 as a hub gene dependent on RNase3 catalytic activity (Figure 6B), ISG15 is regarded as the hallmark gene of RIG-I like receptor signalling pathway which is mainly activated by viral RNA and DNA. In addition, a specific processing of the host noncoding RNA and release of dsRNA can also activate the cell intrinsic immune response through RIG-I, MDA5or OASL sensors [84]. Complementarily, the RNA products can work as intercellular signalling molecules to mediate a prompt host response to infection [85]. A complex interplay between the host ncRNA and the RNA virus might determine the final outcome during infection [86]. We can speculate that RNase3 antiviral immune response may be mediated by the generation of specific RNA cleavage products. Our transcriptome results also highlighted that most of the significant DEGs related to RNase3 catalytic activity were visualized at the late (12h) exposure time rather than at the early (4h) time point (figure 6). Moreover, among the activated pathways associated to the protein ribonucleolytic we found the activation of endosomal receptors, such as the TLRs 7-9, which are associated to endosomal detection of both foreign and host signalling nucleic acid molecules [85]. On its turn, TLR8 activated by self RNAs might reinforce the NFkB pathway (see Figure 5).

Interestingly, we find in the literature reference to other members of the RNaseA superfamily that have been related to interferon-mediated response and endosomal TLR activation [87–89]. RNase7 was recently reported to activate the TLR9 signalling pathway [90, 91]. Earlier, Schein and coworkers related BS- RNase activity to a direct interaction with IFN and the cleavage of dsRNA [92, 93]. Besides, IFN is reported to activate the expression of RNase L, another RNase that belongs to a protein family totally unrelated to the RNaseA superfamily. RNase L is also induced by IFN and can release small RNA products that reinforce the IFN mediated response [94]. Both RNase L and RNase3induce the OAS gene, which is related to dsRNA and antiviral response pathways. The present results suggest that both protein families might cooperate to fight infection by shared convergent mechanisms of RNA processing. Indeed, recent work

highlighted the importance of coordinated signalling pathways that mediate the macrophage defence mechanism against infection [95, 96].

In order to complement our comparative transcriptome analysis, we decided to analyse in situ the potential role of the RNase3 endogenously expressed by macrophages. Characterization of a THP1 macrophage derived cell line that overexpresses RNase3 corroborated the protein gene activation profile. The observed gene expression pattern (Figure 8) is characteristic of both EGFR and IFN induction pathways, which can participate in the macrophage response to bacterial and viral infection respectively [59, 96, 97]. Moreover, our results confirmed that native RNase3 expressed within the macrophages can mediate the eradication of *M. aurum* or RSV infection. Our previous work using recombinant RNases highlighted the protein antimicrobial activity against both extracellular and macrophage intracellular dwelling mycobacteria [6, 14]. The present results indicate that overexpression of endogenous RNase3 within macrophages can inhibit both *M. aurum* and RSV intracellular proliferation (Figure 9). Moreover, we observed how the mycobacteria infection is modulating the expression of RNase3, as reported for other host defence peptides [98–100]. Last, with the final aim to confirm RNase3 activation of the EGFR pathway, we treated the THP1 cell lines with Erlotinib, an inhibitor of the EGFR receptor. Results suggests that the receptor is required for RNase3 antibacterial but not for antiviral activity. Accordingly, the receptor blockage only altered the expression profile of genes unrelated to RNase3 catalytic activity (Figure 10). This data is in agreement with previous results by Rosenberg and co-workers that demonstrated how RNase3 catalytic activity directly participates in its antiviral action [9]. Besides, it also reinforces previous report on RNase3 antibacterial action in infected macrophages not dependent on its enzymatic activity [14].

RNase3 has been reported to contribute against persistent intracellular pathogens, such as the tuberculosis bacilli or the HIV virus, that frequently coexist and threaten immune-depressed patients [96, 98]. Therefore, it is crucial to understand the protein mechanism of action against macrophage intracellular infections. Unfortunately, RNase3 pro-inflammatory action following infection might also have a detrimental effect on the host tissues. On the other hand, the protein action at the infection focus might also promote the tissue remodelling and healing [4, 16, 77]. RNase3 leukocyte recruitment activity can reinforce the role of other blood cell type. In particular, RNase3 is abundantly expressed and secreted by eosinophils during inflammation and infection. In this context, we should regard the contribution of RNase3 within the overall host defence response as a reinforcement of the macrophage role that can also be promoted by eosinophil activation. Upon eosinophil degranulation, pro-inflammatory cytokines and chemokines are released to the infected tissue. On its turn, the eosinophil secretory proteins can be engulfed by macrophages and contribute to the eradication of intracellular infection. Therefore, the protein would mediate a positive feedback and will ensure an efficient host response. A better, understanding of the regulatory pathways that mediate the host response processes induced by the secreted RNase3 should facilitate the design of alternative anti-infective drugs. The present results recall once again the importance of understanding the functioning of host defence proteins to take advantage of their therapeutic potentialities.

Conclusions

Comparative transcriptome profile analysis of macrophages treated with wild-type RNase3 and the catalytically defective mutant (RNase3-H15A) revealed that the protein triggers an early pro-inflammatory response in a ribonuclease-independent manner. Moreover, protein-protein network analysis of comparative gene expression profiles indicated that the overall cell response is triggered by a direct activation of the EGFR. By structural analysis we have identified the protein region potentially involved in the receptor binding. Complementarily, transcriptome analysis revealed that RNase3 catalytic activity would participate in the activation of interferon dependent pathways, associated to antiviral host defence. Moreover, the specific blockage of EGFR by Erlotinib indicates that the receptor-associated pathways participate in the protein antibacterial but not antiviral actions. Last, we demonstrated that endogenous overexpression of RNase3 in macrophages can inhibit *M. aurum* and RSV intracellular proliferation, which advances novel strategies in the design of alternative anti-infective drugs.

Acknowledgement

Experimental work was supported by the Ministerio de Economía y Competitividad (SAF2015-66007P to EB), co-financed by FEDER funds and Fundació La Marató de TV3 (ref. 20180310).

The authors wish to thank Francisco Cortes (UAB, SCAC), Maria Rodrigues Muños (UAB) for helping with lentiviral production. Thank Manuel Kaulich (Goethe University Medical School) and Marcos Gil Garcia (UAB, IBB) for gifting gene and plasmids. We Thank Yundong Peng (Max Planck Institute for Heart and Lung Research) for offering help with CRISPR gene editing experiment. Lu Lu is a recipient of a CSC predoctoral fellowship.

Figures and Tables legends:

Table 1. KEGG pathway enrichment analysis of DEGs comparing RNase3-H15A treatment with RNase3 at 12h.

Table 2. Predicted free energies for EGFR-protein modelled complexes. The binding affinities ΔG (kcal/mol) and dissociation constants Kd (M) were predicted using HADDOCK2.2.

Table 3. Top 10 significant GO terms enriched comparing RNase3H15A treatment with RNase3 at 12h.

Figure 1. DEseq2 analysis Count of differential expressing genes. (A). Genes with an adjusted P-value (Q-value) < 0.01 & log2fc absolute value >1 found by DESeq were assigned as differentially expressed (DE). The common DEGs responded to RNase3 and RNase3H15A treatment at 4h and 12h was identified by overlapping. Venn plot of the DEGs from paired comparison, **(B)** common up regulated and **(C)** common down regulated DEGs.

Figure 2. KEGG pathway enrich map of the common response DEGs to RNase3 and RNase3H15A treatment. KEGG pathways enriched by **(A)** common up-regulated DEGs and **(B)** common down-regulated DEGs.

Figure 3. Protein-protein-interaction (PPI) analysis of common response DEGs. The common DEGs were applied to NetworkAnalyst3.0 online tool. **(A)**. The PPI network of upregulated DEGs; **(B)**. The PPI network of downregulated DEGs.

Figure 4. Heatmap of DEGs enriched in cytokine-cytokine receptor interaction pathway.

Figure 5. Schematic illustration of the molecular mechanism of RNase3 modulating in human macrophage. The genes related to ribonucleases activities were label with red color in word.

Figure 6. Ribonuclease specific response. (A). Overlap of the DEGs identified by directly comparing RNase3 with RNase3H15A at 4h and 12h, respectively; **(B)**. Network analysis of ribonuclease dependent protein interaction of DEGs identified by comparing RNase3 and RNase3H15A at 12h.

Figure 7. Schematic illustration of the molecular mechanism of RNase3 modulating in human macrophage.

Figure 8. Overexpression of RNase3 in human THP1 derived macrophages. (A). FACS selection of GFP (indicates the successful transduction of lenti239G-dCas9-VP64) and RFP (indicates the successful transduction of lenti239R-sgRNA) both positive cells; **(B)**. Comparison of the transcriptional expression of *RNase3* gene in wild type (WT) THP1 macrophages and RNase3 overexpression (OX) THP1 macrophages by qPCR; **(C)**. Comparison of the expression of RNase3 protein in wild type (WT) THP1 macrophages and RNase3 overexpression (OX) THP1 macrophages by WB. **(D)**. Comparison of 18 gene expression levels between RNAseq and qPCR. 18 DEGs identified from transcriptome sequencing was validated by qPCR, using wildtype (WT) THP1 induced macrophages and RNase3 overexpression (OX) THP1 macrophages.

Figure 9. RNase3 controls bacterial and viral infection within macrophages. (A). Overexpression of RNase3 in macrophage inhibits *M. aurum* proliferation, the number of *M. aurum* inside of macrophage was counted by CFU assay and compared with wild-type (WT) THP1-induced macrophages and RNase3 overexpression (OX) THP1-induced macrophages for up to 3 days; **(B)** RSV was quantified by probe-qPCR, the intracellular RSV was normalized using *GAPDH* gene; **(C)** MTT assay was applied to measure the cell viability, 0h WT group was used for normalization (100%). **(D)**. Comparison of the relative transcriptional expression of RNase3 gene in WT, OX, WT infected with *M. aurum* (WT+ *M. aurum*), and OX infected with *M. aurum* (OX+ *M. aurum*) cells with by qPCR using GAPDH as reference; Significance was indicated as "*" $p < 0.05$, "**" $p < 0.01$.

Figure 10. EGFR inhibitor, Erlotinib, blocks RNase3 induced antimicrobial activity. Before infection, the EGFR inhibitor, erlotinib, was used to treat RNase3 overexpressed macrophages for 24h under three concentrations, 0 μM, 10 μM and 100 μM. At the indicated time post of infection, the intracellular *M. aurum* **(A)** and RSV **(B)** was quantified by CFU assay and probe-qPCR assay, respectively, the intracellular RSV was normalized using *GAPDH* gene. **(C)**. The relative expression of genes was quantified by qPCR with or without erlotinib treatment (10 μM, 24h), and the fold change was calculated by comparing erlotinib treatment with control. Significance was indicated as "*" $p < 0.05$, "**" $p < 0.01$.

Table S1. Total RNA quality. The concentration of total RNA was measured by nanodrop and the integrity of the RNA was evaluated by bioanalyzer 2100.

Table S2. Oligos of sgRNA, and primers for PCR

Table S3. Basic information on sequencing output and processing

Figure S1. PCA plot.

Figure S2. Selection of THP1/RNase3 overexpression cell lines obtained by CRISPRa.

Figure S3. Standard curve of RSV quantification by probe qPCR. A RSV stock with known concentration was serially diluted and used to build the standard curve.

Figure S4. Extracellular RSV was quantified by probe-qPCR.

References:

1. Acharya KR, Ackerman SJ (2014) Eosinophil granule proteins: Form and function. J Biol Chem 289:17406–17415. https://doi.org/10.1074/jbc.R113.546218

2. Venge P, Byström J, Carlson M, et al (1999) Eosinophil cationic protein (ECP): Molecular and biological properties and the use of ECP as a marker of eosinophil activation in disease. Clin Exp Allergy 29:1172–1186. https://doi.org/10.1046/j.1365-2222.1999.00542.x

3. Bystrom J, Amin K, Bishop-Bailey D (2011) Analysing the eosinophil cationic protein - a clue to the function of the eosinophil granulocyte. Respir Res 12:10. https://doi.org/10.1186/1465-9921-12-10

4. Lu L, Li J, Moussaoui M, Boix E (2018) Immune Modulation by Human Secreted RNases at the Extracellular Space. Front Immunol 9:1012. https://doi.org/10.3389/fimmu.2018.01012

5. Chihara J, Urayama O, Tsuda A, et al (1996) Eosinophil Cationic Protein Induces Insulin-Like Growth Factor I Receptor Expression on Bronchial Epithelial Cells. Int Arch Allergy Immunol 111:43–45. https://doi.org/10.1159/000237414

6. Pulido D, Torrent M, Andreu D, et al (2013) Two Human Host Defense Ribonucleases against Mycobacteria, the Eosinophil Cationic Protein (RNase 3) and RNase 7. Antimicrob Agents Chemother 57:3797–3805. https://doi.org/10.1128/AAC.00428-13

7. Torrent M, Badia M, Moussaoui M, et al (2010) Comparison of human RNase 3 and RNase 7 bactericidal action at the Gram-negative and Gram-positive bacterial cell wall. FEBS J 277:1713–1725. https://doi.org/10.1111/j.1742-4658.2010.07595.x

8. Salazar VA, Arranz-Trullén J, Navarro S, et al (2016) Exploring the mechanisms of action of human secretory RNase 3 and RNase 7 against Candida albicans. Microbiologyopen 5:830–845. https://doi.org/10.1002/mbo3.373

9. Domachowske JB, Dyer KD, Adams AG, et al (1998) Eosinophil cationic protein/RNase 3 is another RNase A-family ribonuclease with direct antiviral activity. Nucleic Acids Res 26:3358–3363. https://doi.org/10.1093/nar/26.14.3358

10. Boix E, Salazar VA, Torrent M, et al (2012) Structural determinants of the eosinophil cationic protein antimicrobial activity. Biol Chem 393:801–815. https://doi.org/10.1515/hsz-2012-0160

11. Torrent M, Cuyás E, Carreras E, et al (2007) Topography studies on the membrane interaction mechanism of the eosinophil cationic protein. Biochemistry 46:720–733. https://doi.org/10.1021/bi061190e

12. Carreras E, Boix E, Rosenberg HF, et al (2003) Both aromatic and cationic residues contribute to the membrane-lytic and bactericidal activity of eosinophil cationic protein. Biochemistry 42:6636–6644. https://doi.org/10.1021/bi0273011

13. Abengozar MA, Torrent M, Fernandez-Reyes M, et al (2012) Deconvolution of eosinophyl cationic protein (ECP) for cell-penetrating and microbicidal activities on Leishmania. The FEBS Journal, p 279

14. Lu L, Arranz-Trullén J, Prats-Ejarque G, et al (2019) Human Antimicrobial RNases Inhibit Intracellular Bacterial Growth and Induce Autophagy in Mycobacteria-Infected Macrophages. Front Immunol 10:1500. https://doi.org/10.3389/fimmu.2019.01500

15. Zheutlin LM, Ackerman SJ, Gleich GJ, Thomas LL (1984) Stimulation of basophil and rat mast cell histamine release by eosinophil granule-derived cationic proteins. J Immunol 133:2180–2185

16. Zagai U, Lundahl J, Klominek J, et al (2009) Eosinophil cationic protein stimulates migration of human lung fibroblasts in vitro. Scand J Immunol 69:381–386. https://doi.org/10.1111/j.1365-3083.2009.02233.x

17. Pertea M, Kim D, Pertea GM, et al (2016) Transcript-level expression analysis of RNA-seq experiments with HISAT, StringTie and Ballgown. Nat Protoc 11:1650–1667. https://doi.org/10.1038/nprot.2016.095

18. Durinck S, Spellman PT, Birney E, Huber W (2009) Mapping identifiers for the integration of genomic datasets with the R/Bioconductor package biomaRt. Nat Protoc 4:1184–1191. https://doi.org/10.1038/nprot.2009.97

19. Love MI, Huber W, Anders S (2014) Moderated estimation of fold change and dispersion for RNA-seq data with DESeq2. Genome Biol 15:550. https://doi.org/10.1186/s13059-014-0550-8

20. Yu G, Wang L-G, Han Y, He Q-Y (2012) clusterProfiler: an R Package for Comparing Biological Themes Among Gene Clusters. Omi A J Integr Biol 16:284–287. https://doi.org/10.1089/omi.2011.0118

21. Zhou G, Soufan O, Ewald J, et al (2019) NetworkAnalyst 3.0: a visual analytics platform for comprehensive gene expression profiling and meta-analysis. Nucleic Acids Res. https://doi.org/10.1093/nar/gkz240

22. van Zundert GCP, Rodrigues JPGLM, Trellet M, et al (2016) The HADDOCK2.2 Web Server: User-Friendly Integrative Modeling of Biomolecular Complexes. J Mol Biol 428:720–725. https://doi.org/10.1016/J.JMB.2015.09.014

23. Dominguez C, Boelens R, Bonvin AMJJ (2003) HADDOCK: A protein-protein docking approach based on biochemical or biophysical information. J Am Chem Soc 125:1731–1737. https://doi.org/10.1021/ja026939x

24. Konermann S, Brigham MD, Trevino AE, et al (2015) Genome-scale transcriptional activation by an engineered CRISPR-Cas9 complex. Nature 517:583–588. https://doi.org/10.1038/nature14136

25. Al Yacoub N, Romanowska M, Haritonova N, Foerster J (2007) Optimized production and concentration of lentiviral vectors containing large inserts. https://doi.org/10.1002/jgm.1052

26. Kutner RH, Zhang X-Y, Reiser J (2009) Production, concentration and titration of pseudotyped HIV-1-based lentiviral vectors. Nat Protoc 4:495–505. https://doi.org/10.1038/nprot.2009.22

27. Livak KJ, Schmittgen TD (2001) Analysis of Relative Gene Expression Data Using Real-Time Quantitative PCR and the 2−ΔΔCT Method. Methods 25:402–408. https://doi.org/10.1006/METH.2001.1262

28. Zhang L, Jie H, Xiao Y, et al (2019) Genomic Identification and Expression Analysis of the Cathelicidin Gene Family of the Forest Musk Deer. Anim an open access J from MDPI 9:. https://doi.org/10.3390/ani9080481

29. Vissers M, Habets MN, Ahout IML, et al (2013) An In vitro Model to Study Immune Responses of Human Peripheral Blood Mononuclear Cells to Human Respiratory Syncytial Virus Infection. J Vis Exp e50766. https://doi.org/10.3791/50766

30. Sun Y, Jain D, Koziol-White CJ, et al (2015) Immunostimulatory Defective Viral Genomes from Respiratory Syncytial Virus Promote a Strong Innate Antiviral Response during Infection in Mice and Humans. PLOS Pathog 11:e1005122. https://doi.org/10.1371/journal.ppat.1005122

31. Dewhurst-Maridor G, Simonet V, Bornand J., et al (2004) Development of a quantitative TaqMan RT-PCR for respiratory syncytial virus. J Virol Methods 120:41–49. https://doi.org/10.1016/J.JVIROMET.2004.03.017

32. Sun Y, López CB (2016) Respiratory Syncytial Virus Infection in Mice and Detection of Viral Genomes in the Lung Using RT-qPCR. Bio-protocol 6:. https://doi.org/10.21769/BioProtoc.1819

33. Ferrari M, Fornasiero MC, Isetta AM (1990) MTT colorimetric assay for testing macrophage cytotoxic activity in vitro. J Immunol Methods 131:165–172. https://doi.org/10.1016/0022-1759(90)90187-Z

34. Han W, Carpenter RL, Cao X, Lo H-W (2013) STAT1 gene expression is enhanced by nuclear EGFR and HER2 via cooperation with STAT3. Mol Carcinog 52:959–69. https://doi.org/10.1002/mc.21936

35. Guo G, Gong K, Wohlfeld B, et al (2015) Ligand-Independent EGFR Signaling. Cancer Res 75:3436–3441. https://doi.org/10.1158/0008-5472.CAN-15-0989

36. El-Hashim AZ, Khajah MA, Renno WM, et al (2017) Src-dependent EGFR transactivation regulates lung inflammation via downstream signaling involving ERK1/2, PI3Kδ/Akt and NFκB induction in a murine asthma model. Sci Rep 7:9919. https://doi.org/10.1038/s41598-017-09349-0

37. Murray PJ, Allen JE, Biswas SK, et al (2014) Macrophage Activation and Polarization: Nomenclature and Experimental Guidelines. Immunity 41:14–20

38. Der SD, Zhou A, Williams BRG, Silverman RH (1998) Identification of genes differentially regulated by interferon , , or using oligonucleotide arrays. Proc Natl Acad Sci 95:15623–15628. https://doi.org/10.1073/pnas.95.26.15623

39. Fensterl V, Sen GC (2015) Interferon-induced Ifit proteins: their role in viral pathogenesis. J Virol 89:2462–8. https://doi.org/10.1128/JVI.02744-14

40. Leisching G, Wiid I, Baker B (2017) The Association of OASL and Type I Interferons in the Pathogenesis and Survival of Intracellular Replicating Bacterial Species. Front Cell Infect Microbiol 7:. https://doi.org/10.3389/fcimb.2017.00196

41. Carow B, Rottenberg ME (2014) SOCS3, a Major Regulator of Infection and Inflammation. Front Immunol 5:. https://doi.org/10.3389/fimmu.2014.00058

42. Wang Y-N, Lee H-H, Chou C-K, et al (2018) Angiogenin/Ribonuclease 5 Is an EGFR Ligand and a Serum Biomarker for Erlotinib Sensitivity in Pancreatic Cancer. Cancer Cell 33:752-769.e8. https://doi.org/10.1016/j.ccell.2018.02.012

43. Mehrabi M, Mansouri K, Soleymani B, et al (2017) Development of a human epidermal growth factor derivative with EGFR-blocking and depleted biological activities: A comparative in vitro study using EGFR-positive breast cancer cells. Int J Biol Macromol 103:275–285. https://doi.org/10.1016/j.ijbiomac.2017.05.035

44. Sanders JM, Wampole ME, Thakur ML, Wickstrom E (2013) Molecular Determinants of Epidermal Growth Factor Binding: A Molecular Dynamics Study. PLoS One 8:e54136. https://doi.org/10.1371/journal.pone.0054136

45. Zhang J, Rosenberg HF (2000) Sequence in variation at two eosinophil-associated ribonuclease loci in humans. Genetics 156:1949–1958

46. Rubin J, Zagai U, Blom K, et al (2009) The Coding ECP 434(G>C) Gene Polymorphism Determines the Cytotoxicity of ECP but Has Minor Effects on Fibroblast-Mediated Gel Contraction and No Effect on RNase Activity. J Immunol 183:445–451. https://doi.org/10.4049/jimmunol.0803912

47. Eriksson J, Woschnagg C, Fernvik E, Venge P (2007) A SELDI-TOF MS study of the genetic and post-translational molecular heterogeneity of eosinophil cationic protein. J Leukoc Biol 82:1491–1500. https://doi.org/10.1189/jlb.0507272

48. Boix E, Nikolovski Z, Moiseyev GP, et al (1999) Kinetic and Product Distribution Analysis of Human Eosinophil Cationic Protein Indicates a Subsite Arrangement That Favors Exonuclease-type Activity. J Biol Chem 274:15605–15614. https://doi.org/10.1074/jbc.274.22.15605

49. Trulson A, Byström J, Engström Å, et al (2007) The functional heterogeneity of eosinophil cationic protein is determined by a gene polymorphism and post-translational modifications. Clin Exp allergy 37:208–218. https://doi.org/10.1111/j.1365-2222.2007.02644.x

50. Woschnagg C, Rubin J, Venge P (2009) Eosinophil cationic protein (ECP) is processed during secretion. J Immunol 183:3949–54. https://doi.org/10.4049/jimmunol.0900509

51. Welch SA, Moore MJ (2007) Erlotinib: Success of a molecularly targeted agent for the treatment of advanced pancreatic cancer. Futur Oncol 3:247–254. https://doi.org/10.2217/14796694.3.3.247

52. Zasloff M (2002) Antimicrobial peptides of multicellular organisms. Nature 415:389–395. https://doi.org/10.1038/415389a

53. Hancock REW, Sahl H-G (2006) Antimicrobial and host-defense peptides as new anti-infective therapeutic strategies. Nat Biotechnol 24:1551–1557. https://doi.org/10.1038/nbt1267

54. Yeung ATY, Gellatly SL, Hancock REW (2011) Multifunctional cationic host defence peptides and their clinical applications. Cell Mol Life Sci 68:2161–2176. https://doi.org/10.1007/s00018-011-0710-x

55. Boix E, Nogués MV (2007) Mammalian antimicrobial proteins and peptides: overview on the RNase A superfamily members involved in innate host defence. Mol Biosyst 3:317–335. https://doi.org/10.1039/b617527a

56. Rosenberg HF (2008) RNase A ribonucleases and host defense: an evolving story. J Leukoc Biol 83:1079–87. https://doi.org/10.1189/jlb.1107725

57. Herbst RS (2004) Review of epidermal growth factor receptor biology. Int J Radiat Oncol 59:S21–S26. https://doi.org/10.1016/J.IJROBP.2003.11.041

58. Sigismund S, Avanzato D, Lanzetti L (2018) Emerging functions of the EGFR in cancer. Mol Oncol 12:3–20. https://doi.org/10.1002/1878-0261.12155@10.1002/(ISSN)1878-0261.REVIEWS

59. Hardbower DM, Singh K, Asim M, et al (2016) EGFR regulates macrophage activation and function in bacterial infection. J Clin Invest 126:3296–3312. https://doi.org/10.1172/JCI83585

60. Kalinowski A, Galen BT, Ueki IF, et al (2018) Respiratory syncytial virus activates epidermal growth factor receptor to suppress interferon regulatory factor 1-dependent interferon-lambda and antiviral defense in airway epithelium. Mucosal Immunol 11:958–967. https://doi.org/10.1038/mi.2017.120

61. Minutti CM, Drube S, Blair N, et al (2017) Epidermal Growth Factor Receptor Expression Licenses Type-2 Helper T Cells to Function in a T Cell Receptor-Independent Fashion. Immunity 47:710-722.e6. https://doi.org/10.1016/J.IMMUNI.2017.09.013

62. Rayego-Mateos S, Rodrigues-Diez R, Morgado-Pascual JL, et al (2018) Role of Epidermal Growth Factor Receptor (EGFR) and Its Ligands in Kidney Inflammation and Damage. Mediators Inflamm 2018:1–22. https://doi.org/10.1155/2018/8739473

63. Wang Y-N, Lee H-H, Hung M-C (2018) A novel ligand-receptor relationship between families of ribonucleases and receptor tyrosine kinases. J Biomed Sci 25:83. https://doi.org/10.1186/s12929-018-0484-7

64. Wang Y-N, Lee H-H, Chou C-K, et al (2018) Angiogenin/Ribonuclease 5 Is an EGFR Ligand and a Serum Biomarker for Erlotinib Sensitivity in Pancreatic Cancer. Cancer Cell 33:752-769.e8. https://doi.org/10.1016/j.ccell.2018.02.012

65. Ogiso H, Ishitani R, Nureki O, et al (2002) Crystal Structure of the Complex of Human Epidermal Growth Factor and Receptor Extracellular Domains. Cell 110:775–787. https://doi.org/10.1016/S0092-8674(02)00963-7

66. Li S, Schmitz KR, Jeffrey PD, et al (2005) Structural basis for inhibition of the epidermal growth factor receptor by cetuximab. Cancer Cell 7:301–311. https://doi.org/10.1016/j.ccr.2005.03.003

67. Blom K, Rubin J, Halfvarson J, et al (2012) Eosinophil associated genes in the inflammatory bowel disease 4 region: Correlation to inflammatory bowel disease revealed. World J Gastroenterol 18:6409–6419. https://doi.org/10.3748/wjg.v18.i44.6409

68. Salazar VA, Rubin J, Moussaoui M, et al (2014) Protein post-translational modification in host defense: The antimicrobial mechanism of action of human eosinophil cationic protein native forms. FEBS J 281:5432–5446. https://doi.org/10.1111/febs.13082

69. Diop G, Derbois C, Loucoubar C, et al (2018) Genetic variants of RNASE3 (ECP) and susceptibility to severe malaria in Senegalese population. Malar J 17:61. https://doi.org/10.1186/s12936-018-2205-9

70. Adu B, Dodoo D, Adukpo S, et al (2011) Polymorphisms in the RNASE3 gene are associated with susceptibility to cerebral malaria in Ghanaian children. PLoS One 6:. https://doi.org/10.1371/journal.pone.0029465

71. Eriksson J, Reimert CM, Kabatereine NB, et al (2007) The 434(G>C) polymorphism within the coding sequence of Eosinophil Cationic Protein (ECP) correlates with the natural course of Schistosoma mansoni infection. Int J Parasitol 37:1359–1366. https://doi.org/10.1016/j.ijpara.2007.04.001

72. Blanchard C, Rothenberg ME (2009) Chapter 3 Biology of the Eosinophil, 1st ed. Elsevier Inc.

73. Rosenberg HF, Dyer KD, Foster PS (2013) Eosinophils: changing perspectives in health and disease. Nat Rev Immunol 13:9–22. https://doi.org/10.1038/nri3341

74. Zhang J, Rosenberg HF, Nei M (1998) Positive Darwinian selection after gene duplication in primate ribonuclease genes. Proc Natl Acad Sci U S A 95:3708–3713. https://doi.org/10.1073/pnas.95.7.3708

75. Prats-Ejarque G, Lu L, Salazar VA, et al (2019) Evolutionary Trends in RNA Base Selectivity Within the RNase A Superfamily. Front Pharmacol 10:1170. https://doi.org/10.3389/fphar.2019.01170

76. Altman L, Ayars G, Baker C, Luchtel D (1993) Cytokines and eosinophil-derived cationic proteins upregulate intercellular adhesion molecule-1 on human nasal epithelial cells. J Allergy Clin Immunol 92:527–536. https://doi.org/10.1016/0091-6749(93)90077-S

77. Zagai U, Sköld CM, Trulson A, et al (2004) The effect of eosinophils on collagen gel contraction and implications for tissue remodelling. Clin Exp Immunol 135:427–433. https://doi.org/10.1111/j.1365-2249.2004.02396.x

78. Zagai U, Dadfar E, Lundahl J, et al (2007) Eosinophil cationic protein stimulates TGF-β1 release by human lung fibroblasts in vitro. Inflammation 30:153–160. https://doi.org/10.1007/s10753-007-9032-4

79. Sidahmed AME, León AJ, Bosinger SE, et al (2012) CXCL10 contributes to p38-mediated apoptosis in primary T lymphocytes in vitro. Cytokine 59:433–441. https://doi.org/10.1016/j.cyto.2012.05.002

80. Abbas YM, Pichlmair A, Górna MW, et al (2013) Structural basis for viral 5′-PPP-RNA recognition by human IFIT proteins. Nature 494:60–64. https://doi.org/10.1038/nature11783

81. Zhu J, Zhang Y, Ghosh A, et al (2014) Antiviral Activity of Human OASL Protein Is Mediated by Enhancing Signaling of the RIG-I RNA Sensor. Immunity 40:936–948. https://doi.org/10.1016/J.IMMUNI.2014.05.007

82. Kristiansen H, Gad HH, Eskildsen-Larsen S, et al (2011) The Oligoadenylate Synthetase Family: An Ancient Protein Family with Multiple Antiviral Activities. J Interf Cytokine Res 31:41–47. https://doi.org/10.1089/jir.2010.0107

83. Loo Y-M, Gale M, Jr. (2011) Immune signaling by RIG-I-like receptors. Immunity 34:680–92. https://doi.org/10.1016/j.immuni.2011.05.003

84. Zhao Y, Ye X, Dunker W, et al (2018) RIG-I like receptor sensing of host RNAs facilitates the cell-intrinsic immune response to KSHV infection. Nat Commun 9:4841. https://doi.org/10.1038/s41467-018-07314-7

85. Tsatsaronis JA, Franch-Arroyo S, Resch U, Charpentier E (2018) Extracellular Vesicle RNA: A Universal Mediator of Microbial Communication? Trends Microbiol 26:401–410. https://doi.org/10.1016/J.TIM.2018.02.009

86. Damas ND, Fossat N, Scheel TKH (2019) Functional Interplay between RNA Viruses and Non-Coding RNA in Mammals. Non-Coding RNA 5:7. https://doi.org/10.3390/ncrna5010007

87. Rademacher F, Dreyer S, Kopfnagel V, et al (2019) The Antimicrobial and Immunomodulatory Function of RNase 7 in Skin. 10:1–11. https://doi.org/10.3389/fimmu.2019.02553

88. Schein CH (2001) Producing soluble recombinant RNases and assays to measure their interaction with interferon-gamma in vitro. Methods Mol. Biol. 160:113–137

89. Schein CH (1997) From housekeeper to microsurgeon: The diagnostic and therapeutic potential of ribonucleases. Nat Biotechnol 15:529–536. https://doi.org/10.1038/nbt0697-529

90. Kopfnagel V, Wagenknecht S, Harder J, et al (2018) RNase 7 Strongly Promotes TLR9-Mediated DNA Sensing by Human Plasmacytoid Dendritic Cells. J Invest Dermatol 138:872–881. https://doi.org/10.1016/j.jid.2017.09.052

91. Kopfnagel V, Wagenknecht S, Brand L, et al (2017) RNase 7 downregulates TH2 cytokine production by activated human T-cells. Allergy. https://doi.org/10.1111/all.13173

92. Schein CH, Haugg M, Benner SA (1990) Interferon-gamma activates the cleavage of double-stranded RNA by bovine seminal ribonuclease. FEBS Lett 270:229–32. https://doi.org/10.1016/0014-5793(90)81275-S

93. Schein CH, Hauggt M (1995) Deletions at the C-terminus of interferon y reduce RNA binding and activation of double-stranded-RNA cleavage by bovine seminal ribonuclease. Biochem J 307:123–127. https://doi.org/10.1042/bj3070123

94. Chakrabarti A, Jha BK, Silverman RH (2011) New Insights into the Role of RNase L in Innate Immunity. J Interf Cytokine Res 31:49–57. https://doi.org/10.1089/jir.2010.0120

95. Wang X, Iyer A, Lyons AB, et al (2019) Emerging roles for G-protein coupled receptors in development and activation of macrophages. Front Immunol 10:. https://doi.org/10.3389/fimmu.2019.02031

96. Chai Q, Lu Z, Liu CH (2019) Host defense mechanisms against Mycobacterium tuberculosis. Cell. Mol. Life Sci.

97. Chattopadhyay S, Veleeparambil M, Poddar D, et al (2015) EGFR kinase activity is required for TLR4 signaling and the septic shock response. EMBO Rep 16:1535–1547. https://doi.org/10.15252/embr.201540337

98. Arranz-Trullén J, Lu L, Pulido D, et al (2017) Host Antimicrobial Peptides: The Promise of New Treatment Strategies against Tuberculosis. Front Immunol 8:1499. https://doi.org/10.3389/fimmu.2017.01499

99. Rivas-Santiago B, Hernandez-Pando R, Carranza C, et al (2008) Expression of cathelicidin LL-37 during Mycobacterium tuberculosis infection in human alveolar macrophages, monocytes, neutrophils, and epithelial cells. Infect Immun 76:935–41. https://doi.org/10.1128/IAI.01218-07

100. Rivas-Santiago CE, Rivas-Santiago B, León DA, et al (2011) Induction of β-defensins by l-isoleucine as novel immunotherapy in experimental murine tuberculosis. Clin Exp Immunol 164:80–9. https://doi.org/10.1111/j.1365-2249.2010.04313.x

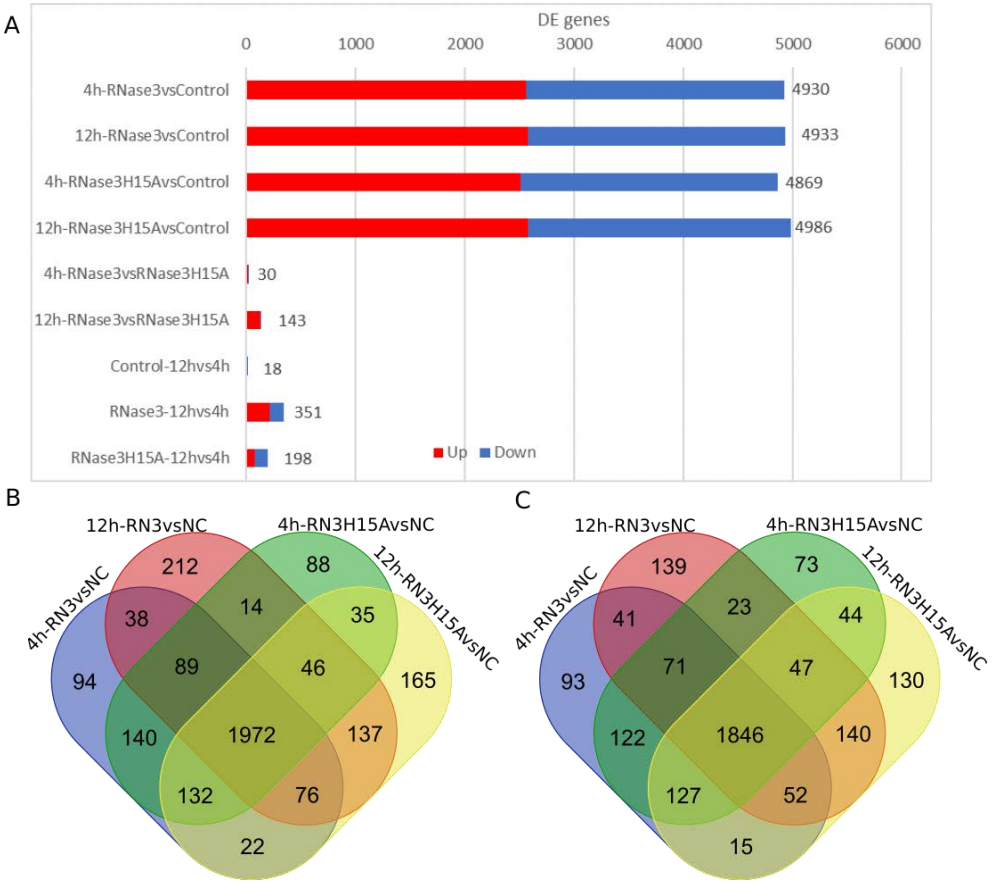

Figure 1. DEseq2 analysis Count of differential expressing genes. (A). Genes with an adjusted P-value (Q-value) < 0.01 & log2fc absolute value >1 found by DESeq were assigned as differentially expressed (DE). The common DEGs responded to RNase3 and RNase3H15A treatment at 4h and 12h was identified by overlapping. Venn plot of the DEGs from paired comparison; **(B)**. common up regulated and **(C)**. common down-regulated DEGs.

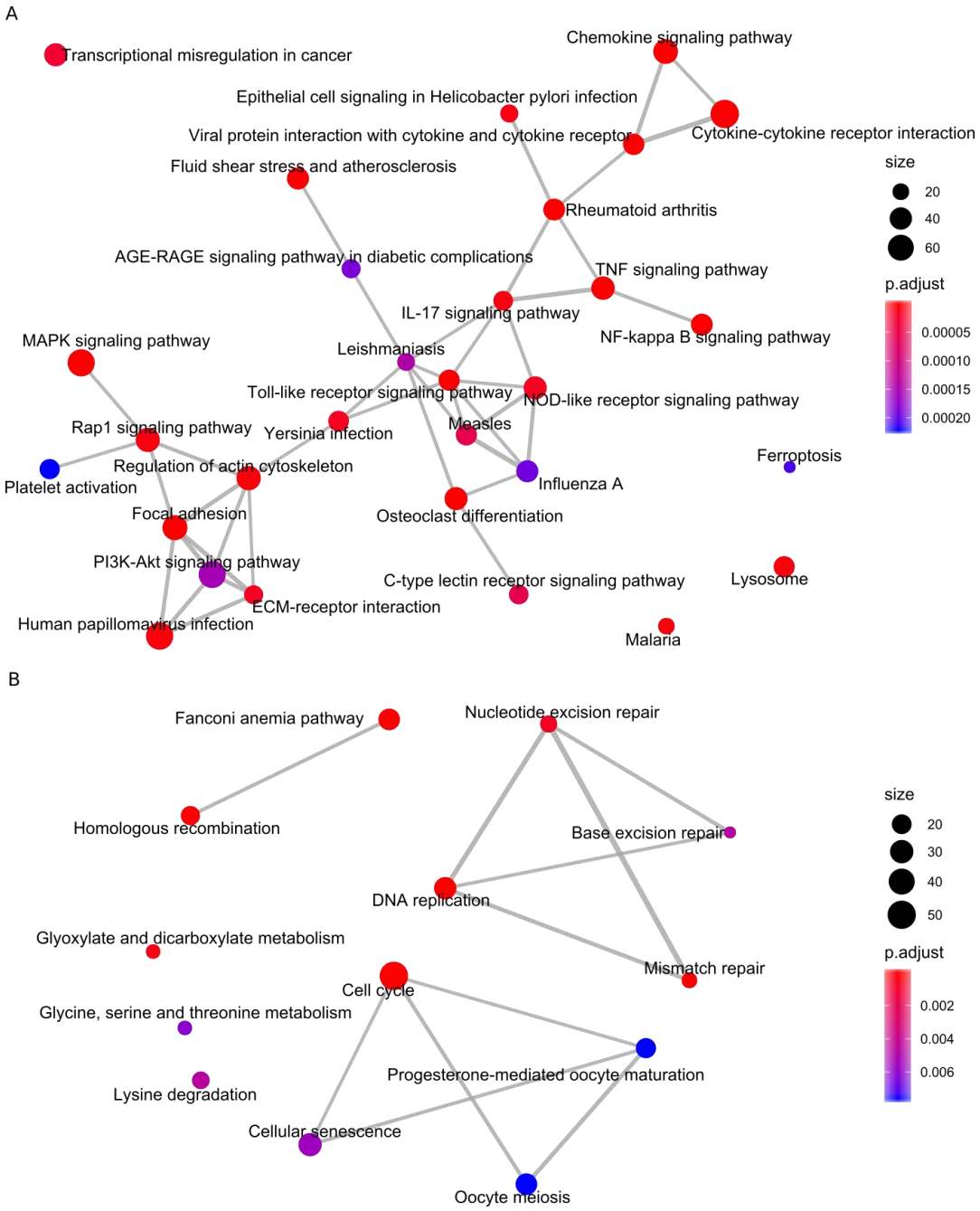

Figure 2. KEGG pathway enrich map of the common response DEGs to RNase3 and RNase3H15A treatment. KEGG pathways enriched by **(A)** common up-regulated DEGs and **(B)** common down-regulated DEGs.

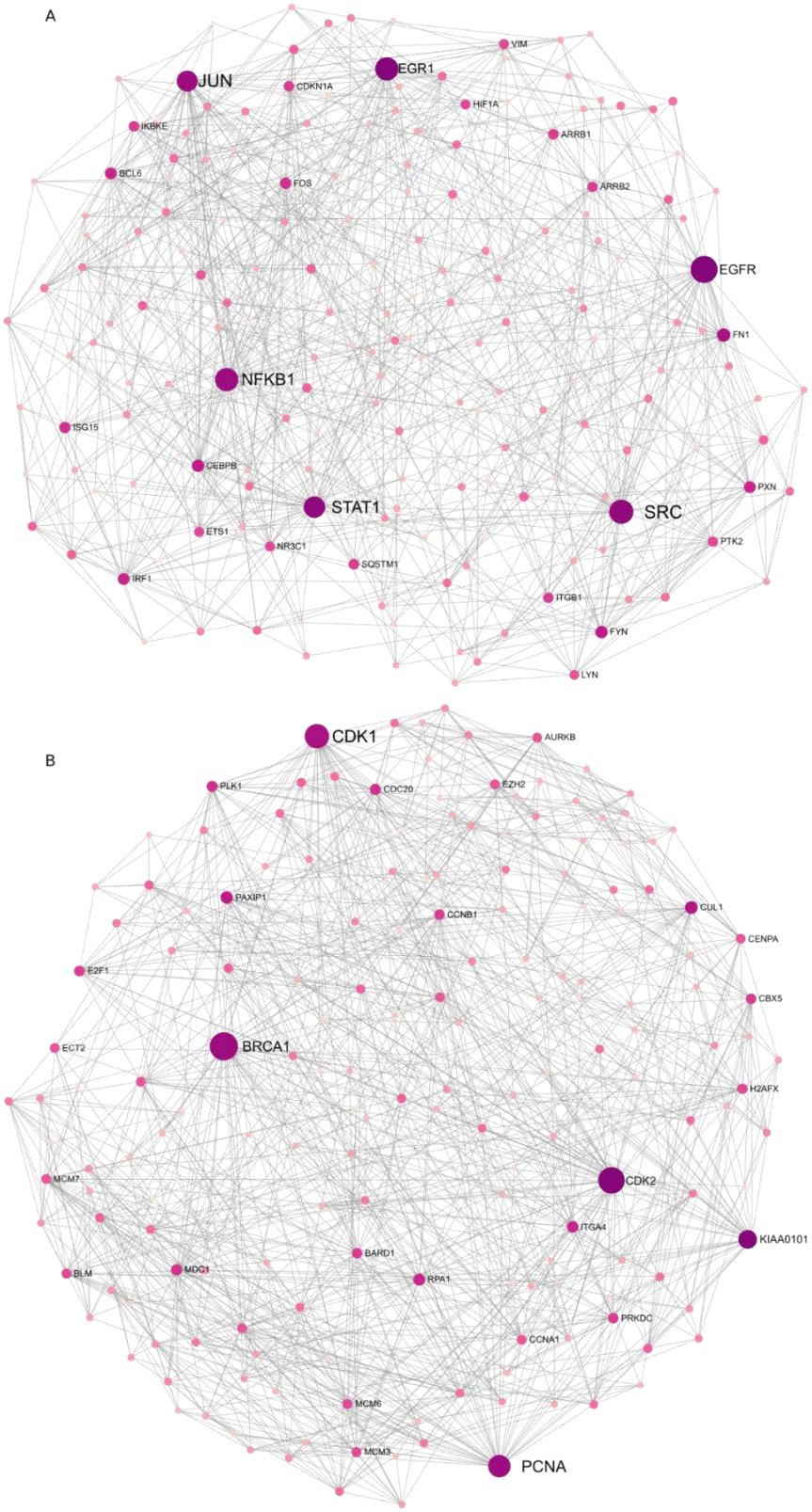

Figure 3. Protein-protein-interaction (PPI) analysis of common response DEGs. The common DEGs were applied to NetworkAnalyst3.0 online tool. A. The PPI network of upregulated DEGs; B. The PPI network of downregulated DEGs. The interaction between each protein pair is indicated with lines, the circle size is proportional to the betweenness and centrality score.

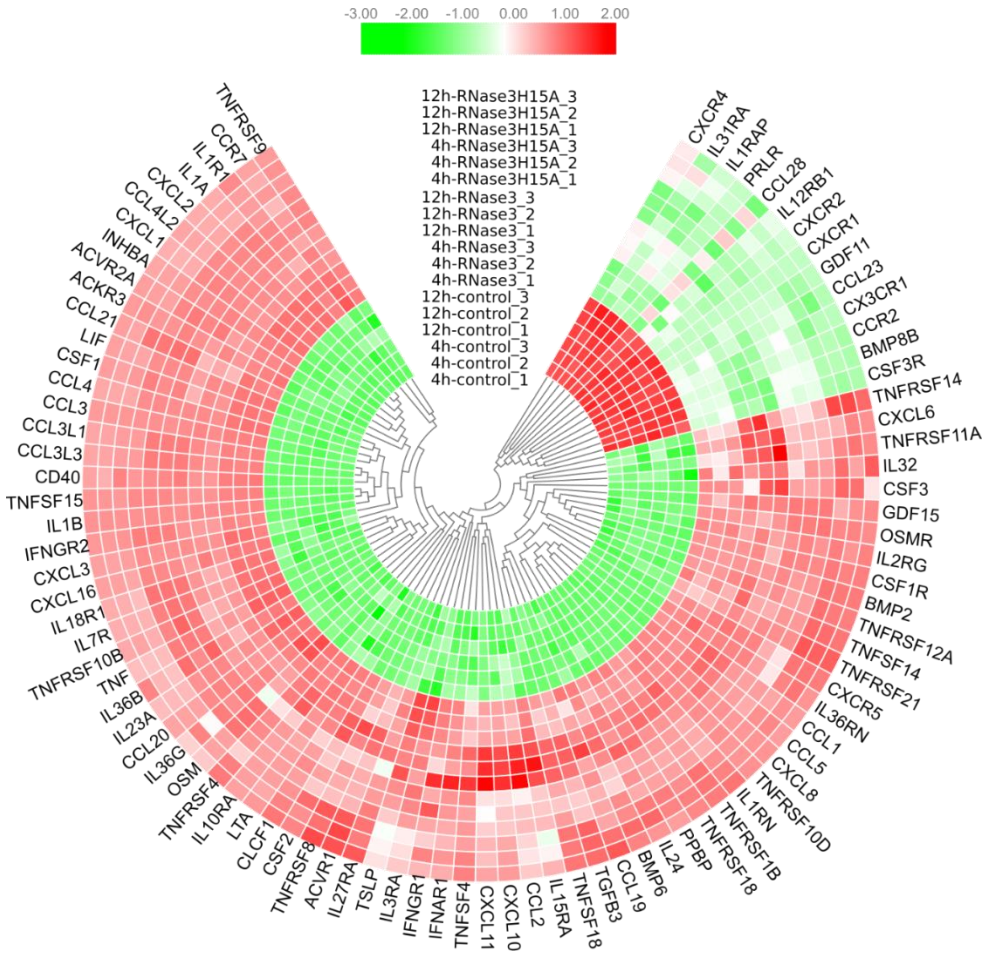

Figure 4. Heatmap of DEGs enriched in cytokine-cytokine receptor interaction pathway.

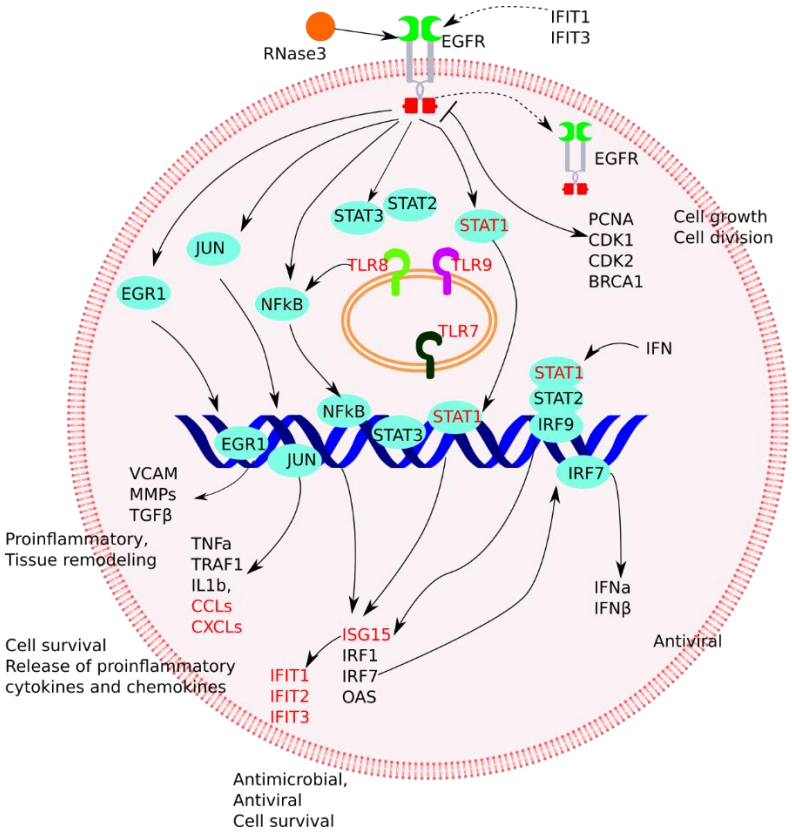

Figure 5. Schematic illustration of the identified pathways activated by macrophage treatment by RNase3. The genes related to RNase catalytic activity are labelled with red color. EGFR, epidermal growth factor receptor; IFIT, interferon induced protein with tetratricopeptide repeats; EGR1, early growth response 1; Jun, jun proto-oncogene, AP-1 transcription factor subunit; NFκB, nuclear factor Kappa B, transcription regulator; STAT, signal transducer and activator of transcription; IRF, interferon regulatory factor; VCAM, vascular cell adhesion molecule; MMP, matrix metallopeptidase; TGF, transforming growth factor; TNF, tumor necrosis factor; TRAF, TNF receptor associated factor; IL, interleukin; CCL, C-C motif chemokine ligand; CXCL, C-X-C motif chemokine ligand; ISG15, interferon induced 15kDa protein; OAS, 2'-5'-oligoadenylate synthetase, interferon induced, dsRNA-activated antiviral enzyme; IFN, interferon; PCNA, proliferating cell nuclear antigen, CDK, cyclin dependent kinase; BRCA1, BRCA1 DNA repair associated, maintaining genomic stability.

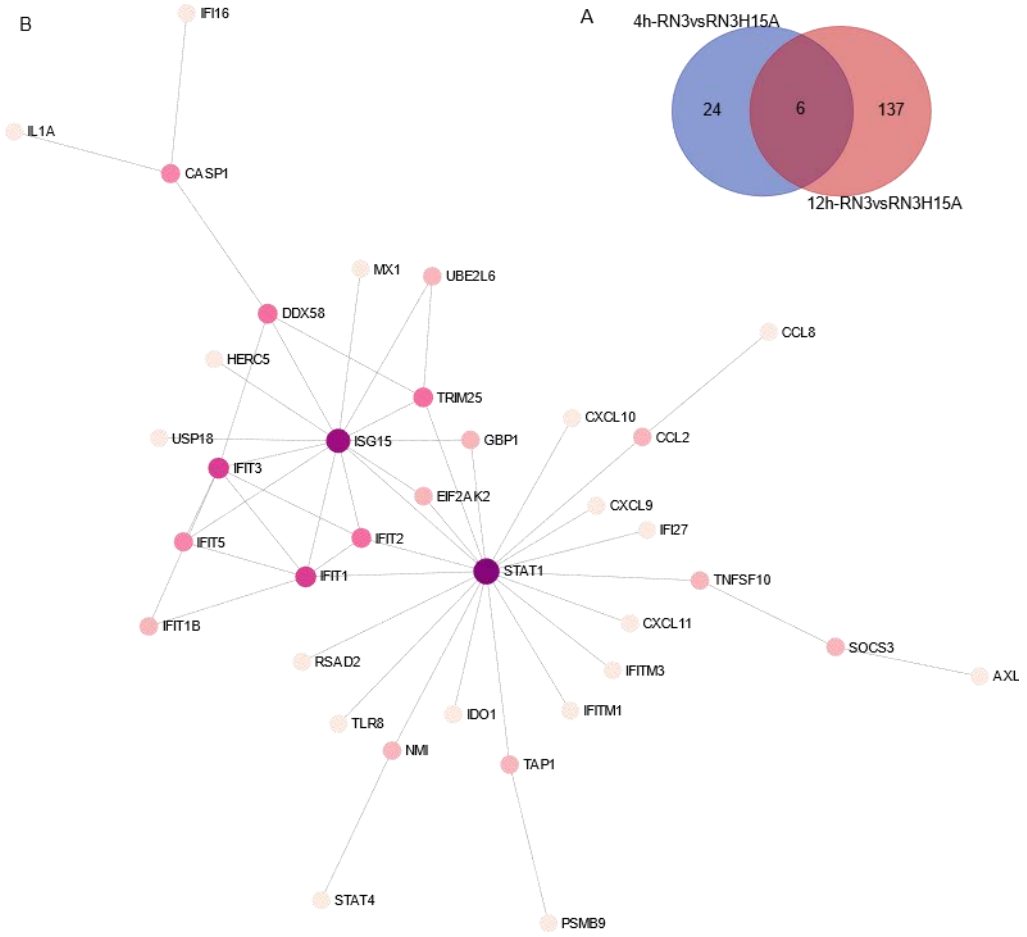

Figure 6. Ribonuclease specific response. (A). Overlap of the DEGs identified by direct comparison of RNase3 with RNase3-H15A at 4h and 12h, respectively; **(B)**. Network analysis of ribonuclease dependent protein interaction of DEGs identified by comparing RNase3 and RNase3-H15A at 12h.

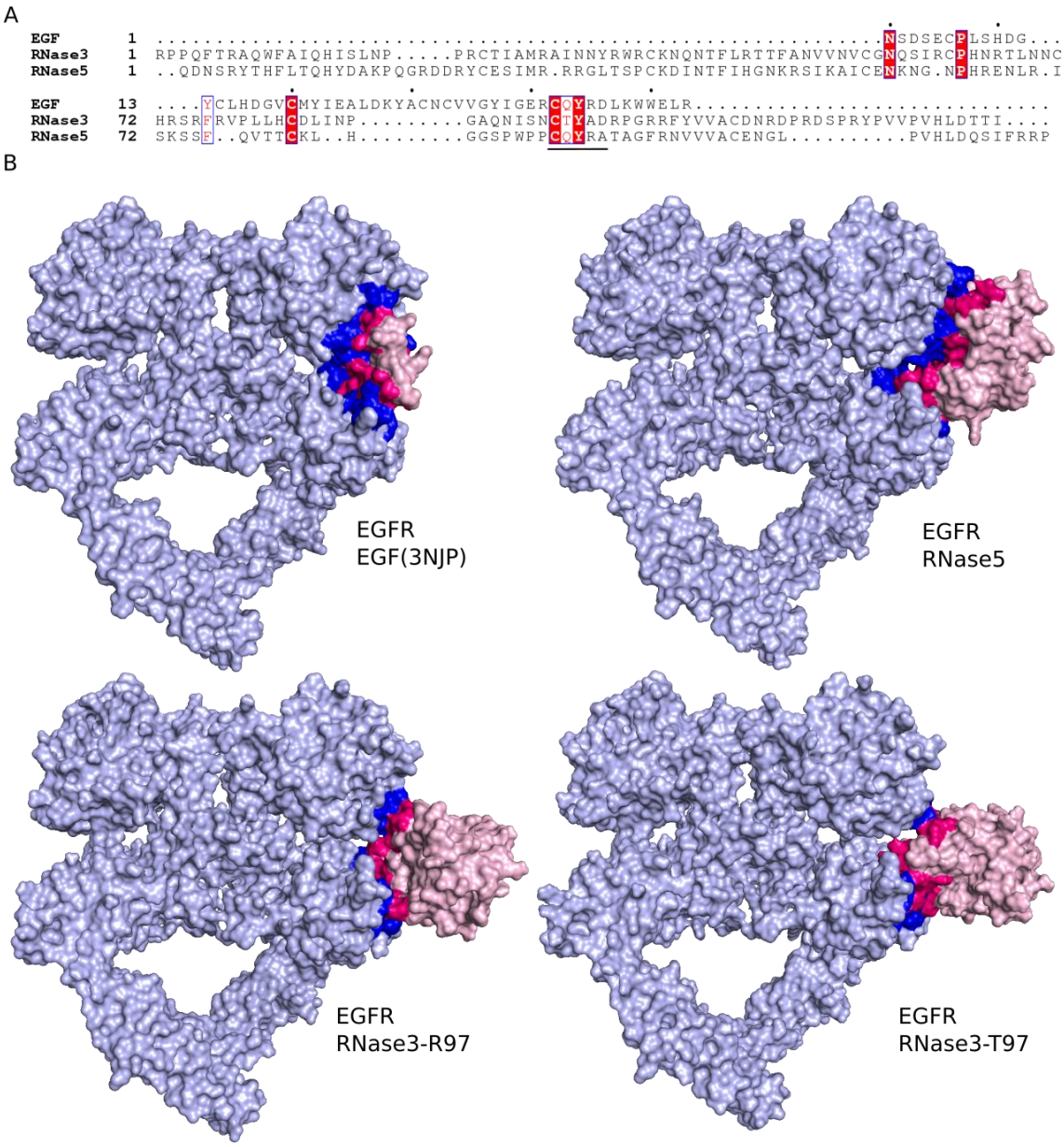

Figure 7. Comparison of the interaction of EGFR with RNase3 (R97 and T97), RNase5 and EGF by molecular modelling. (A). Primary sequence alignment of EGF, RNase3 and RNase5. The common interacting region is underlined. **(B)**. Representative binding of EGFR with EGF, RNase5, and RNase3 single nucleotide polymorphisms:(RNase3-R97) and RNase3-T97). The crystal complex of EGFR with EGF (PDB ID: 3NJP) is depicted. EGFR is coloured in grey, the protein ligands were coloured in pink, the interacting residues from EGFR and the ligands were coloured in blue and red, respectively.

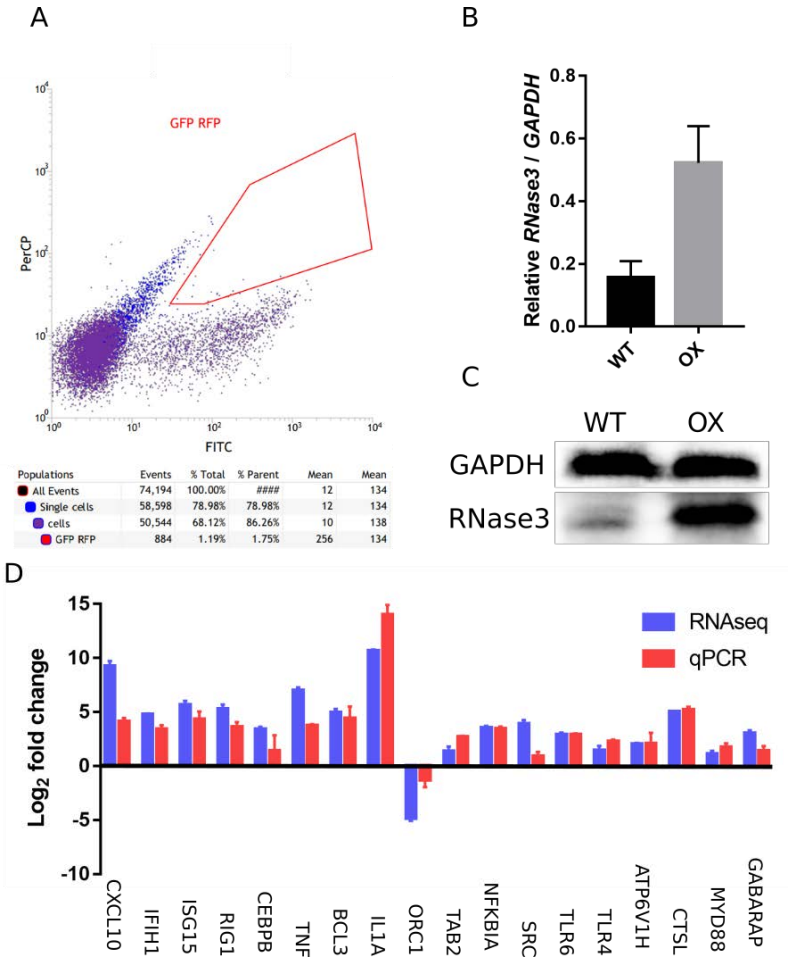

Figure 8. Overexpression of RNase3 in human THP1 derived macrophages. (A). FACS selection of GFP (indicating the successful transduction of lenti239G-dCas9-VP64) and RFP (indicating the successful transduction of lenti239R-sgRNA) both positive cells; **(B)**. Comparison of the transcriptional expression of *RNase3* gene in wild type (WT) THP1 macrophages and RNase3 overexpression (OX5) THP1 macrophages by qPCR; **(C)**. Comparison of the expression of RNase3 protein in wild type (WT) THP1 macrophages and RNase3 overexpression (OX) THP1 macrophages by WB. **(D)**. Comparison of 18 gene expression levels between RNAseq and qPCR. 18 DEGs identified from transcriptome sequencing were validated by qPCR, using wild-type (WT) THP1 induced macrophages and RNase3 overexpression (OX) THP1 macrophages.

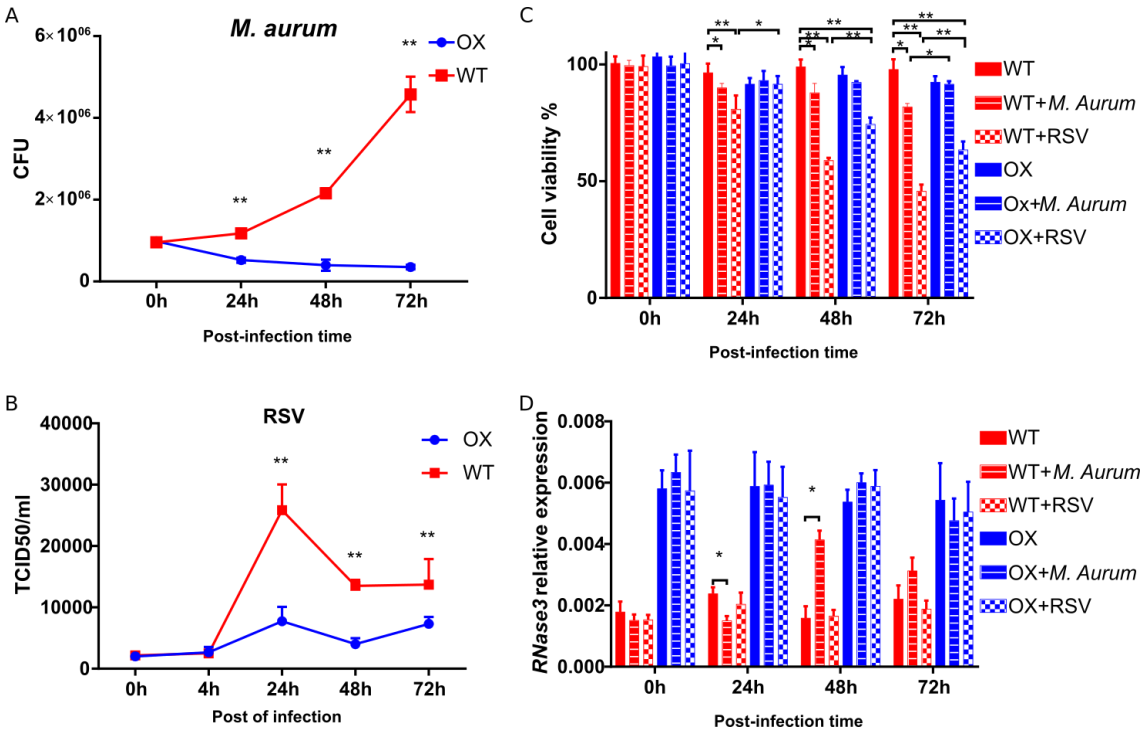

Figure 9. RNase3 controls bacterial and viral infection within macrophages. (A). Overexpression of RNase3 in macrophage inhibits *M. aurum* proliferation. The number of *M. aurum* inside of macrophage was counted by CFU assay and compared with wild-type (WT). THP1-induced macrophages and RNase3 overexpression (OX) THP1-induced macrophages for up to 3 days; **(B)** RSV was quantified by probe-qPCR, the intracellular RSV was normalized using *GAPDH* gene; **(C)** MTT assay was applied to measure the cell viability, 0h WT group was used for normalization (100%). **(D)**. Comparison of the relative transcriptional expression of RNase3 gene in WT, OX, WT infected with *M. aurum* (WT+ *M. aurum*), and OX infected with *M. aurum* (OX+ *M. aurum*) cells with by qPCR using GAPDH as reference; Significance was indicated as "*" $p < 0.05$, "**" $p < 0.01$.

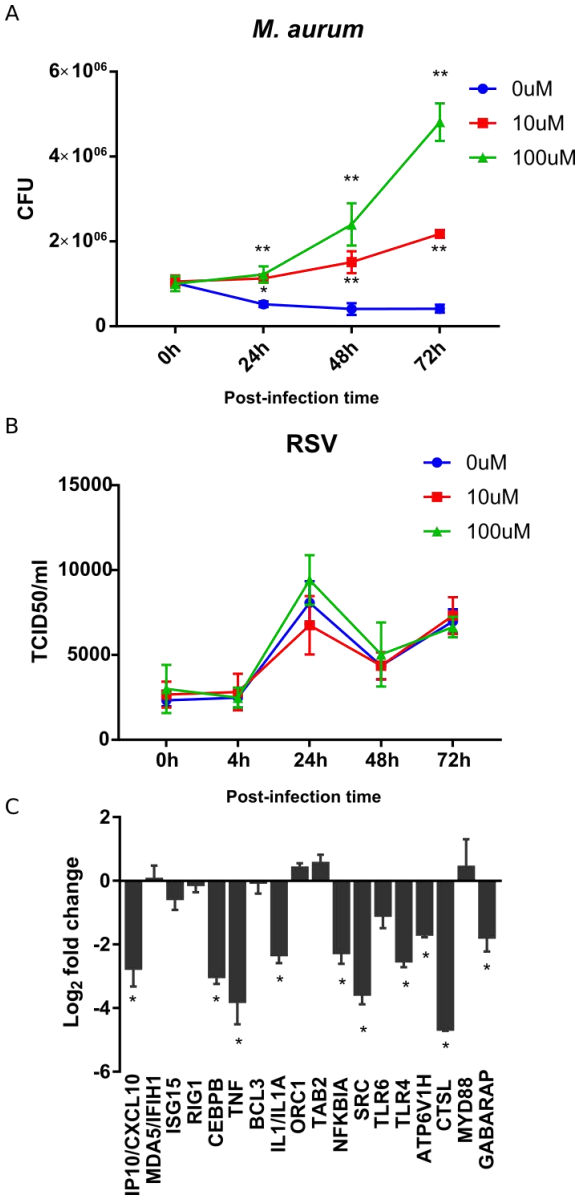

Figure 10. EGFR inhibitor Erlotinib blocks the RNase3 induction of antimycobacterial activity. Before infection, the EGFR inhibitor, Erlotinib, was used to treat RNase3 overexpressed macrophages for 24h under three concentrations, 0 μM, 10 μM and 100 μM. At the indicated time post of infection, the intracellular *M. aurum* **(A)** and RSV **(B)** was quantified by CFU assay and probe-qPCR assay, respectively, the intracellular RSV was normalized using *GAPDH* gene. **(C)**. The relative expression of genes was quantified by qPCR with or without Erlotinib treatment (10 μM, 24h), and the fold change was calculated by comparing Erlotinib treatment with control. Significance was indicated as "*" $p < 0.05$, "**" $p < 0.01$.

Table 1. KEGG pathway enrichment analysis of DEGs comparing RNase3-H15A treatment with RNase3 at 12h.

Description	GeneRatio	BgRatio	*p* adjust	Count
Influenza A	16/82	170/7925	1.60E-09	16
Hepatitis C	13/82	155/7925	3.40E-07	13
Viral protein interaction with cytokine and cytokine receptor	10/82	100/7925	2.88E-06	10
NOD-like receptor signalling pathway	12/82	181/7925	9.50E-06	12
Cytokine-cytokine receptor interaction	14/82	294/7925	4.10E-05	14
Chemokine signalling pathway	11/82	189/7925	6.41E-05	11
Cytosolic DNA-sensing pathway	7/82	63/7925	6.41E-05	7
Toll-like receptor signalling pathway	8/82	104/7925	0.000177	8
Measles	8/82	138/7925	0.001219	8
RIG-I-like receptor signalling pathway	5/82	70/7925	0.009897	5

Significant enriched pathway list was filtered using *p* adjust <0.01.

Table 2. Predicted free energies for EGFR-protein modelled complexes. The binding affinities ΔG (kcal/mol) and dissociation constants Kd (M) were predicted using HADDOCK2.2.

	ΔG (kcal/mol)	**Kd (M) at 25º C**
EGF (docking)	-10,3	$2{,}9 \cdot 10^{-8}$
EGF (crystal)	-15,8	$2{,}5 \cdot 10^{-12}$
RNase5	-12,4	$8{,}2 \cdot 10^{-10}$
RNase3 (R97)	-12,0	$1{,}5 \cdot 10^{-9}$
RNase3 (T97)	-10,2	$3{,}4 \cdot 10^{-8}$

Table 3. Top 10 significant GO terms enriched comparing RNase3-H15A treatment with RNase3 at 12h.

Description	GeneRatio	BgRatio	*p* adjust	Count
defence response to virus	39/130	224/17653	7.32E-40	39
response to virus	42/130	310/17653	8.42E-39	42
negative regulation of viral process	21/130	95/17653	9.30E-23	21
negative regulation of viral life cycle	19/130	79/17653	2.78E-21	19
negative regulation of viral genome replication	16/130	55/17653	3.21E-19	16
regulation of multi-organism process	28/130	391/17653	2.00E-17	28
negative regulation of multi-organism process	21/130	172/17653	2.00E-17	21
regulation of viral life cycle	19/130	137/17653	9.75E-17	19
response to interferon-gamma	21/130	191/17653	1.43E-16	21
regulation of viral process	21/130	196/17653	2.21E-16	21

Supplementary Information

for

Immunomodulatory action of RNase3/ECP in a macrophage infection model related and unrelated to catalytic activity

Lu Lu[1], RanLei Wei[2], Maria Goetz[1], Guillem Prats-Ejarque[1], Gang Wang[2], Marc Torrent[1], Ester Boix[1#]

Table S1. Total RNA quality. The concentration of total RNA was measured by nanodrop and the integrity of the RNA was evaluated by bioanalyzer 2100.

Reference	Treatment	Type of sample	Concentration(ng/μL)	RIN
A1	Control-4h	RNA	261	9.3
A2	Control-4h	RNA	171	10
A3	Control-4h	RNA	151	10
A4	RNase3-4h	RNA	73	9.9
A5	RNase3-4h	RNA	74	10
A6	RNase3-4h	RNA	114	10
A7	RNase3H15A-4h	RNA	96	10
A8	RNase3H15A-4h	RNA	81	10
A9	RNase3H15A-4h	RNA	90	10
A10	Control-12h	RNA	78	10
A11	Control-12h	RNA	66	10
A12	Control-12h	RNA	61	10
A13	RNase3-12h	RNA	66	10
A14	RNase3-12h	RNA	65	10
A15	RNase3-12h	RNA	101	8.8
A16	RNase3H15A-12h	RNA	77	10
A17	RNase3H15A-12h	RNA	80	10
A18	RNase3H15A-12h	RNA	80	10

Table S2. Oligos of sgRNA, and primers for PCR.

Category	Name	Sequence
Guide RNA	sgRNA1	GGCAGCTGGTCTCCCCTACTTGG
	sgRNA2	AGAGCAGCAGGGCTGTCCTTGGG
	sgRNA3	TCAATCTGTGGGTTTCTGCATGG
	sgRNA4	AAAAAGGATGATTGCACAAGTGG
	sgRNA5	TGTTTAAATAAAGCTTCCCTTGG
Sequencing Primer	U6-seq	GAGGGCCTATTCCCATGATT
PCR primers	CXCL10-Fw	GCCATTCTGATTTGCTGCCT
	CXCL10-Rv	GCAGGTACAGCGTACAGTTCT
	IFIH1-Fw	GCATATGCGCTTTCCCAGTG
	IFIH1-Rv	CTCTCATCAGCTCTGGCTCG
	ISG15-Fw	GCGCAGATCACCCAGAAGAT
	ISG15-Rv	GTTCGTCGCATTTGTCCACC
	RIG1-Fw	TGATTGCCACCTCAGTTGCT
	RIG1-Rv	CTGCTTTGGCTTGGGATGTG
	CEBPB-Fw	AAGCACAGCGACGAGTACAA
	CEBPB-Rv	CCCCAAAAGGCTTTGTAACCA
	TNF-Fw	CTGGGCAGGTCTACTTTGGG
	TNF-Rv	CTGGAGGCCCCAGTTTGAAT
	BCL3-Fw	GCCTACACCCCTATACCCCA
	BCL3-Rv	GATGTCGATGACCCTGCGG
	IL1A-Fw	TGAGCTCGCCAGTGAAATGA
	IL1A-Rv	AACACGCAGGACAGGTACAG
	ORC1-Fw	AAGCTTTGGAGCCGGCCAT
	ORC1-Rv	TGATCTCCGAGAAGGCCACT
	TAB2-Fw	TACGAATGGCCCAAGGAAGC
	TAB2-Rv	CACAGCAGGCATCCAGGTTA
	NFKBIA-Fw	TGTGCTTCGAGTGACTGACC

	NFKBIA-Rv	TCACCCCACATCACTGAACG
	SRC-Fw	AACAAGTGCGGCCATTTCAC
	SRC-Rv	GGAGTTGAAGCCTCCGAACA
	TLR6-Fw	GCAGGGGACAATCCATTCCA
	TLR6-Rv	AGAATCAGGCCAGCCCTCTA
	TLR4-Fw	TGCCGTTTTATCACGGAGGT
	TLR4-Rv	GGGCTAAACTCTGGATGGGG
	ATP6V1H-Fw	GAGACGCCTACTTGGCTCTGA
	ATP6V1H-Rv	TTCAACAGCAACACCGCTAC
	CTSL-Fw	CTGCTGGCCTTGAGGTTTTA
	CTSL-Rv	GCAGCCTTCATTGCCTTGAG
	MYD88-Fw	ACCCAGCATTGGTGCCG
	MYD88-Rv	GGTTGGTGTAGTCGCAGACA
	GABARAP-Fw	CTCCCTTATTCAGGACCGGC
	GABARAP-Rv	TGCCAACTCCACCATTACCC
	RSV-A-Probe	TCCCATTATGCCTAGGCCAGCAGCA
RSV-A	RSV-A-Fw	CTCAATTTCCTCACTTCTCCAGTGT
	RSV-A-Rv	CTTGATTCCTCGGTGTACCTCTGT

Table S3. Basic information on sequencing output and processing.

Refer ence	Treatment	Total reads	Total raw base pair(fastq)	Sam base	Mapping reads percentage
A1	Control-4h	28433026	4.2GB	7.8GB	96.69%
A2	Control-4h	28164308	4.3GB	7.7GB	96.97%
A3	Control-4h	28470445	4.3GB	7.8GB	97.09%
A4	RNase3-4h	28535014	4.3GB	7.5GB	96.69%
A5	RNase3-4h	27749512	4.2GB	7.3GB	96.36%
A6	RNase3-4h	28306352	4.3GB	7.5GB	96.63%
A7	RNase3H15A-4h	28752432	4.3GB	7.6GB	96.81%
A8	RNase3H15A-4h	28535256	4.3GB	7.5GB	96.77%
A9	RNase3H15A-4h	28373650	4.3GB	7.6GB	96.53%
A10	Control-12h	28163110	4.3GB	7.7GB	96.92%
A11	Control-12h	28508004	4.3GB	7.8GB	96.65%
A12	Control-12h	28581025	4.4GB	7.8GB	96.84%
A13	RNase3-12h	27864433	4.3GB	7.3GB	96.59%
A14	RNase3-12h	28659039	4.3GB	7.5GB	95.16%
A15	RNase3-12h	28791962	4.4GB	7.8GB	96.79%
A16	RNase3H15A-12h	28618105	4.3GB	7.6GB	96.65%
A17	RNase3H15A-12h	28341850	4.3GB	7.5GB	96.81%
A18	RNase3H15A-12h	28456211	4.3GB	7.6GB	96.51%

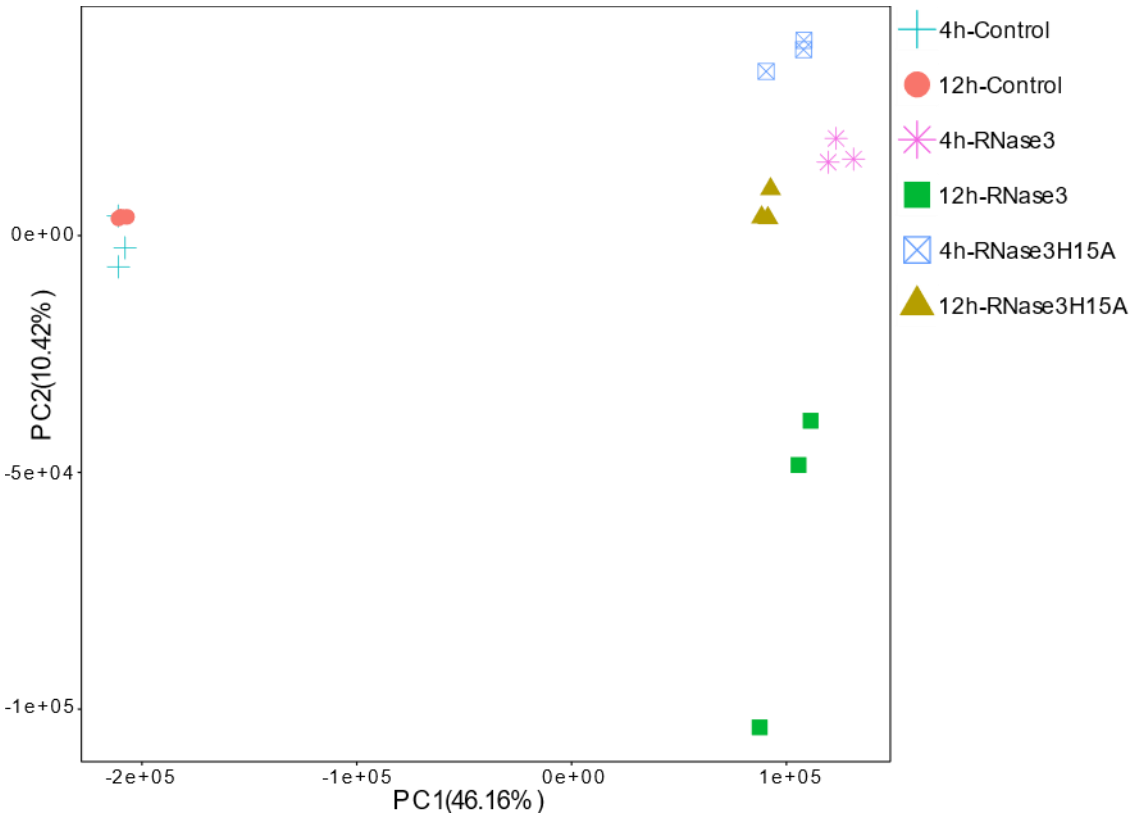

Figure S1. PCA plot.

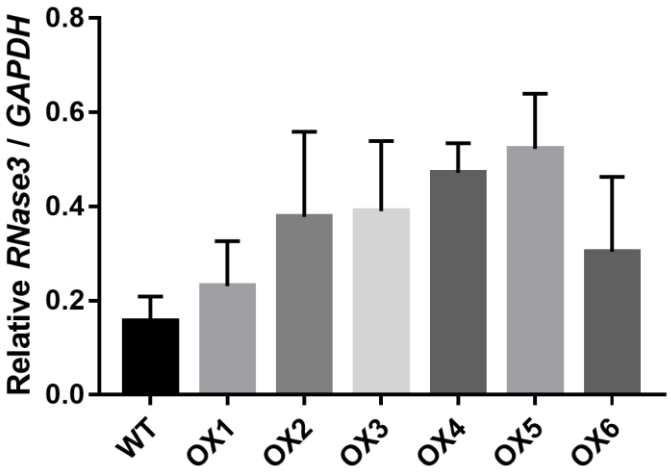

Figure S2. Selection of THP1/RNase3 overexpression THP1 cell lines obtained by CRISPRa. RNase3 and GAPDH genes expression were quantified by qPCR.

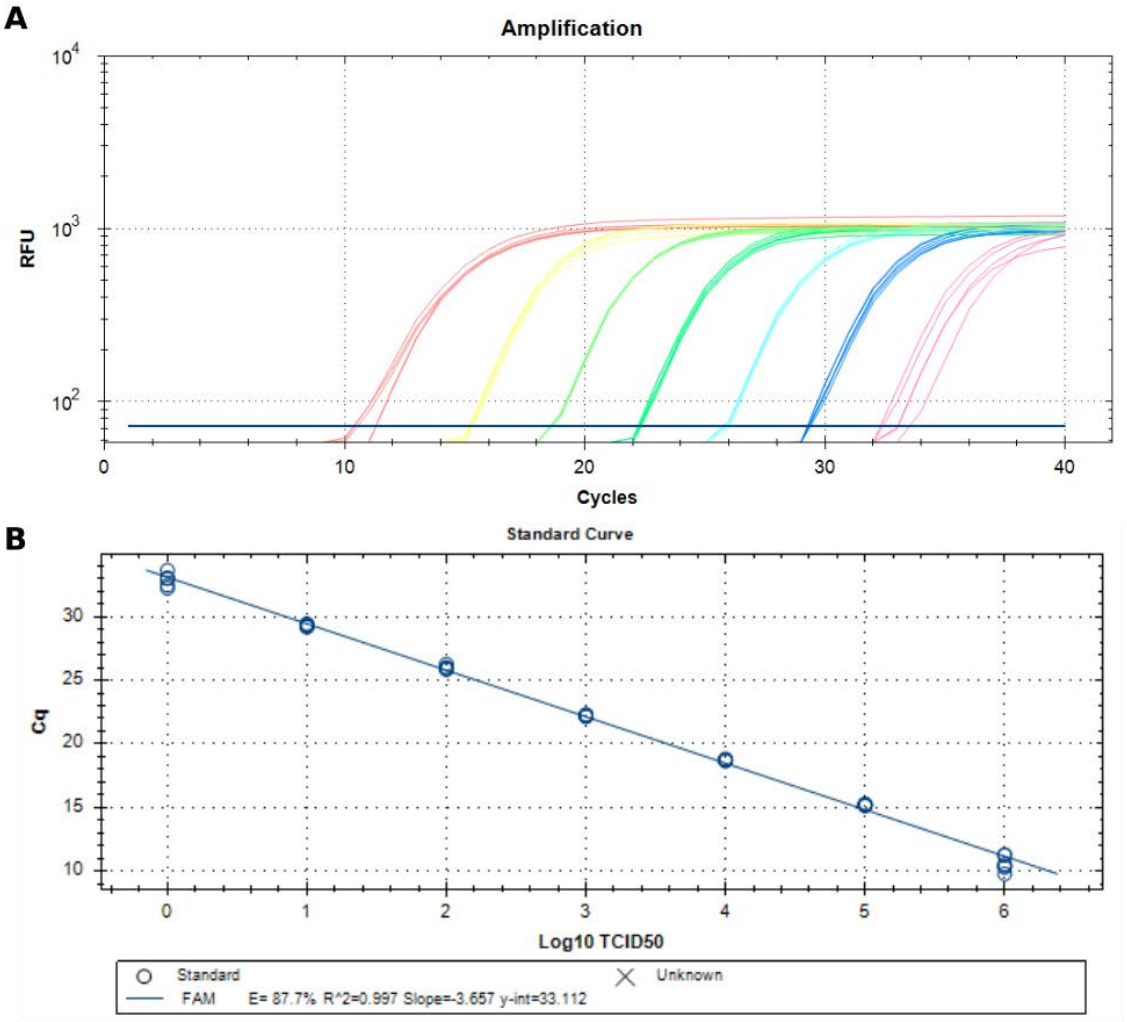

Figure S3. Standard curve of RSV quantification by probe qPCR. A RSV stock with known concentration was serially diluted and used to build the standard curve.

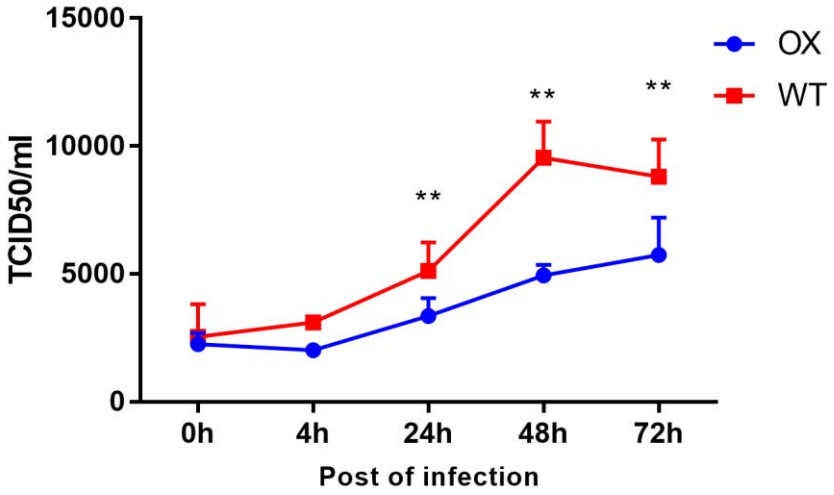

Figure S4. RT-PCR quantification of extracellular RSV. At each time point after infection, the supernatant was collected by centrifugation (4000×g, 5min) and filtration (0.45 μm filter) to removed cell debris. The RSV in the supernatant was precipitated by PEG6000 method and used for RNA extraction. The extracted RNA was then used for probe RT-PCR to quantify.

CHAPTER V

RNase2 antiviral activity against human respiratory syncitial virus through macrophage immunomodulation and targeting of tRNA

Lu Lu[1], Ranlei Wei[2], Maria Goetz-Antico[1], Pablo Fernandez-Millan[1], Ester Boix[1#]

[1]Department of Biochemistry and Molecular Biology, Faculty of Biosciences, Universitat Autonomous de Barcelona, Cerdanyola del Vallès, Spain

[2]Center of Precision Medicine& Precision Medicine Key Laboratory of Sichuan Province, West China Hospital, Sichuan University, Chengdu, China

[#]corresponding authors: Ester Boix, Ester.Boix@uab.cat

Key words: RNase2, macrophage, antivirals, RSV

Abstract:

RNase2, also named the Eosinophil derived Neurotoxin (EDN), is one of the main proteins secreted by the eosinophil secondary granules. RNase2 is also expressed in other leukocyte cells and is the member of the human ribonuclease A family most abundant in macrophages. The protein is endowed with a high ribonuclease catalytic activity and participates in the host antiviral activity. Although RNase2 displays a broad antiviral activity, it is mostly associated to the targeting of single stranded RNA viruses. In particular, its expression is induced upon respiratory viral infection and has been used as a diagnosis marker. Here, we aimed to explore RNase2 mechanism of action in antiviral host defense. Towards this end, we knocked out RNase2 expression in the THP1 monocyte cell line by using the CRISPR/Cas9 editing tool methodology and characterized the transcriptome profile. By comparative transcriptome analysis using NGS RNAseq of native and RNase2 defective THP1-derived macrophages we identified more than 2000 differentially expressed genes. More than 20 significantly enriched pathways were detected, of which the associated top enriched pathways are related to viral infection. Protein-protein interaction network analysis highlighted the EGFR as the main hub gene. Molecular modelling indicated that RNase2 can directly interacts with the EGFR, as recently reported for RNase5. Activation of the EGFR might be associated to cellular response to stress conditions, such as viral infection.

Next, we characterized the native and RNase2 defective THP1 cell lines in the presence of the human Respiratory Syncytial Virus (RSV). First, we observed that RSV infection can induce the *RNase2* expression and protein secretion in THP1 macrophage-derived cells. Moreover, knockout of RNase2 resulted in higher RSV burden in macrophage cells and subsequent cell death. Last, with the final aim to investigate how RNase activity can contribute to the protein antiviral activity, we analyzed the ncRNA digestion product population in infected and none-infected cells. In particular, tRNA derived fragments have been reported to participate in the host response against external injuries, such as infection. Screening of a tRF&tiRNA PCR array identified the specific tRNA fragments associated to RNase2 expression and RSV infection. The present results confirm the key role of EDN in macrophage response against virus infectivity

and contribute to the understanding of the mechanism of action of RNase2 antiviral host defense role towards the design of novel antiviral drugs.

Introduction

Respiratory syncytial virus (RSV) is the most important cause of death in infants. Although RSV infections involve several types of cells in the lung, the central role of macrophages in the host response against respiratory pathogens has been demonstrated (Machado et al., 2017).

RNase2 is a member of the ribonuclease A superfamily that has been associated to innate immunity and mostly to the host response against pathogenic respiratory viruses (Lu et al., 2018; Rosenberg, 2015). In particular, RNase2 was proposed to have a role in RNA viruses, such as the host the human Respiratory Syncytial Virus (RSV). RNase2 is mainly found in the eosinophil secondary granules and is also named Eosinophil Derived Neurotoxin (EDN) (Acharya and Ackerman, 2014; Davoine and Lacy, 2014; Lee et al., 2010; Weller and Spencer, 2017). Eosinophils can migrate into various epithelial tissues, including the gastrointestinal, genitourinary and respiratory tracts in response to chemokine signals produced during diverse types of infection (Davoine and Lacy, 2014; Lee et al., 2010; Weller and Spencer, 2017). Eosinophils will release a number of effector proteins, such as RNase2, which contribute to neutralize the pathogen upon activation. Apart from eosinophils, RNase2 is also expressed in epithelial cells, liver and spleen, together with other leukocyte cell types, such as neutrophils and monocytes (Boix and Nogués, 2007; Monteseirín et al., 2007; Rosenberg, 2008a). Although RNase2's immunomodulatory and antiviral properties have been extensively studied, we still lack a deep knowledge on its underlying mechanism of action.

RNase2 has been reported to participate in the innate host defense, for example, by activation and modulation of the host immune system, working like an alarmin (Oppenheim et al., 2007; Yang et al., 2008). Specifically, RNase2 was observed to induce the TLR2-MyD88 pathway and induce the migration and activation of dendritic cells (Yang et al., 2008). Complementarily, RNase2 can directly target the single stranded RNA virus RSV (Domachowske et al., 1998). Interestingly, the protein ribonucleolytic activity is required to remove the RSV virion, but some structural specificity for RNase2 is mandatory as other family homologues endowed with a high catalytic activity are devoid of antiviral activity. Besides, RNase2 is active against several viral types, such as rhinoviruses, adenoviruses and retroviruses, such as the HIV. On the contrary, no action is reported against the tested bacterial species (Domachowske et al., 1998; Harrison et al., 1999; Rosenberg and Dyer, 1997). In particular, among respiratory viruses, which activate eosinophil recruitment and degranulation, the RSV is probably the most studied model for RNase2 antiviral action. RNase2 levels have predictive value for the development of recurrent wheezing post-RSV bronchiolitis (Kim et al., 2013). Even though it is accepted that RNase2 plays a key role in leukocyte immunomodulation and antiviral activity against RSV infection *in vitro* (Domachowske et al., 1998; Rosenberg, 2008a; Yang et al., 2004), we know very little about the target molecules, the nature of the interactions and its mechanism of action. Moreover, most work was performed on the recombinant protein or the native

form purified from eosinophils, but no information is currently available on the endogenous RNase2 expressed by macrophages. In our previous work in a macrophage infection model, we observed that RNase2 is the most abundantly expressed RNaseA superfamily member in the monocytic THP1 cell line (Lu et al., 2019).

To broaden the knowledge of the immunomodulatory role and potential targeting of cellular RNA population by RNase2 in human macrophages, we first built a RNase2-knockout THP1 monocyte cell line using CRIPSR/Cas9 (clustered regularly interspaced short palindromic repeats) gene editing tool. Next, we compared the transcriptome of the RNase2 knocked out macrophage cells with the unedited macrophages and we found that the top differently expressed pathways are associated to antiviral host defense. Following, we selected a macrophage RSV infection model to explore in situ the protein antiviral action. The comparative infection study conducted indicated that the knockout of RNase2 in macrophage resulted in heavier RSV burden and more cell death. Last, the screening of a regulatory tRNA halves (tiRNA) and tRNA fragment (tRFs) PCR array proved that RNase2 expression in macrophage is correlated to selective tRNA fragment production, as several tiRNA and tRFs were significantly reduced by RNase2 removal. These findings provide increasing understanding on the mechanisms by which RNase2 participates in the macrophage response to viral infection.

Materials and Methods

Plasmid Construction

For long term consideration, we used the two plasmid system to run the CRISPR gene editing experiments instead of using all-in-one CRISPR system. Thus, we constructed a pLenti-239S coding Cas9, GFP and Puromycin resistance gene for knock out assay by replacing the sgRNA expression cassette of LentiCRISPRv2-GFP-puro (gifted by Manuel Kaulich) short annealed oligos; for activation assay, we cloned the eGFP into lenti-dCAS-VP64-Blast (Addgene61425, gifted by Manuel Kaulich), the new plasmid was named pLenti-239G. Lastly, plenti-239R, a new lentiGuide plasmid coding sgRNA expression cassette and Cherry fluorescence gene was created by using the Cherry gene (gifted by Marcos Gil García, UAB) to replace the Cas9 of LentiCRISPRv2-GFP-puro (gifted by Manuel Kaulich). The primers used for PCR was listed in Table S1.

sgRNA design and clone into pLentiGuide (pLenti239R) vector

N20NGG motifs in the RNase2 locus were scanned, and candidate sgRNAs that fit the rules for U6 Pol III transcription and the PAM recognition domain of Streptococcus pyogenes Cas9 were identified. From CRISPOR (http://crispor.tefor.net/) and CRISPR-ERA, the top 2 sgRNA were selected for knockout RNase2. Using the same procedure, potential OT sites were also predicted. The sequences are listed in TableS2. Oligonucleotides were annealed and cloned into BbsI-digested pLenti-239R. The resulting plasmids containing sgRNAs were further confirmed by Sanger sequencing.

Cell Culture

HEK293T cell line was kindly provided by Raquel Pequerul Pavón (UAB). HEK293T cell line was maintained in DMEM (Corning Life Science) supplemented with 10%

fetal bovine serum (FBS) (Gibico). The culture media were replaced every 2–3 days, and the cells were passaged using EDTA solution containing 0.25% trypsin (Corning).

Human THP-1 cells (NCTC #88081201) were maintained or passaged in 25 or 75 cm^2 tissue culture flasks (BD Biosciences) using RPMI-1640 (Lonza, BE12-702F) medium with 10% heat-inactivated FBS at 37°C, humidified 5% CO_2 conditions. The culture media were replaced every 3 days.

Generation of Lentiviral Vectors

To make the cell reach 90% confluence for transfection, 7.5×10^6 of HEK293T cells were seeded in T75 culture flask with 15ml DMEM + 10% FBS complete medium one day before transfection. The lentiviral plasmids were transfected into HEK293T cells using calcium phosphate protocol (Al Yacoub et al., 2007). Briefly, 36 μg transfer plasmid, 18 μg psPAX2 (Addgene#35002, gifted by Marina Rodriguez Muñoz) packaging plasmid, 18 μg pMD2.G (Addgene#12259, gifted by Marina Rodriguez Muñoz) envelope plasmid were mixed and then 93.75 μl of 2 M $CaCl_2$ was added and the final volume was adjusted to 750 μL with H_2O. Then, 750 μL of 2×HBS buffer was added dropwise and vortexed to mix. After 15 min at room temperature, 1.5 mL of the mixture was added dropwise to HEK293T cells and the cells were incubated at 37 °C at 5% CO_2 for 6h, then the medium was replaced with pre-warmed fresh medium. After 24h, 48h, and 72h, the supernatant was collected and cleared by centrifugation at 4000×g for 5 min and passed through 0.45 μm filter. Then, the supernatant fraction was concentrated by PEG6000 precipitate method (Kutner et al., 2009) and the concentrated virus stock was aliquoted and stored in -80 °C freezer.

Cell Transduction

5×10^5 THP1 monocytes were infected with 20 μl concentrated lentivirus in the presence of 8 μg/mL polybrene for overnight. Next day, the cells were replaced with fresh medium and cultured for 72h. Fluorescence positive monocytes were checked by fluorescence microscopy and then sorted by Cell sorter. The percentages of GFP+ HEK293T，THP1 cells were evaluated by suspending the cells in PBS and fixing them with 2% paraformaldehyde for 10 min prior to flow cytometer. Single cells were sorted by Cell sorter BD FACSJazz.

Sanger Sequencing

Briefly, the genomic DNA of THP1 cells was extracted using GenJET Genomic DNA purification kit (ThermoFisher, K0721) and was further used to amplify RNase2 using NZYTaq II 2×Green master mix (nzytech, MB358). Genomic DNA was subjected to PCR (BioRad) using primers listed in Table S2. The general reaction conditions were 95°C for 10 min followed by 30 cycles of 95°C for 30 s, annealing at 60°C for 30 s, and extension at 72°C for 30 s. The pairs of primers were designed to amplify the region that covers the two possible double breaking sites. The PCR product is 410bp. After each reaction, 200 ng of the PCR products was purified using a QIAquick PCR Purification Kit (QIAGEN), subjected to T7E I assays, and then analyzed by agarose gel electrophoresis. The indel mutation was confirmed by Sanger Sequencing.

T7 Endonuclease I Assay-gene editing detection

As illustrated above, 200 ng of the purified *RNase2* PCR products was denatured and re-annealed in 1× T7EI Reaction Buffer and then were incubated with or without T7E I (Alt-R® Genome Editing Detection Kit, IDT). The reaction mixtures were then separated by 2% agarose gel electrophoresis. The knockout efficiency (KO%) was determined using the following formula: KO% = 100 × (1−[1−b]/[a+b])1/2, where a is the integrated intensity of the undigested PCR product and b is the combined integrated intensity of the cleavage products (Shen et al., 2013).

Protein detection by Western Blot and ELISA

For the western blot assays, 5×10^5 cells with or without transduction and their supernatants were harvested with RIPA buffer and the protein concentration was determined with the Pierce BCA Protein Assay Kit (Thermo Fisher Scientific, 23225). Equal amounts of protein (50 μg) for each sample were loaded and separated by 15% SDS-PAGE, transferred to polyvinylidene difluoride membranes. Then the membrane was blocked with 5% non-fat milk in TBST for 1 h at room temperature, and incubated with rabbit source anti-RNase2 primary antibody (abcam, ab103428) overnight at 4°C. After washing, the membranes were treated with horseradish peroxidase (HRP)-conjugated goat anti-rabbit IgG (Sigma Aldrich, 12-348) for 1 h at room temperature (RT). Finally, the membranes were exposed to an enhanced chemiluminescent detection system (Supersignal West Pico Chemiluminescent Substrate, ThermoFisher Scientific, 32209). As a control, GAPDH was detected with chicken anti-GAPDH antibodies (Abcam, ab9483) and goat anti-chicken secondary antibody (Abcam, ab6877)

Secretory RNase2 in cell culture was detected by using human Ribonuclease2, RNase A family, (Liver, Eosinophil-Derived Neurotoxin) (RNASE2) ELISA Kit (MyBioSource, MBS773233). Before applying ELISA, the supernatant of the culture was concentrated 50 times using 15kDa cut-off centrifugal filter unit (Amicon, C7715). Following, the standard and the concentrated culture supernatants were loaded to wells pre-coated with anti-RNase2 antibody, then the HRP-conjugated reagent was added. After incubation and washing for the removal of unbound enzyme, the substrate was added to develop the colorful reaction. The color depth or light was positively correlated with the concentration of RNase2. Triplicates were performed for all assays.

Zymogram/ Ribonuclease activity staining assay

Zymograms were performed as previously described (Prats-Ejarque et al., 2016). 15% polyacrylamide-SDS gels were casted with 0.3 mg/mL of poly(U) (Sigma Aldrich, P9528-25MG). Then, cells were collected by centrifugation and resuspended in 10^6 cells/ml with 1% SDS buffer. After sonication, cell lysate with indicated number of cells was loaded using a loading buffer that does not contain 2-mercaptoethanol. Electrophoresis was run at a constant current of 100 V for 1.5 h. Following, the SDS was removed by washing with 10 mM Tris/HCl, pH 8, and 10% (v/v) isopropanol for 30min. The gel was then incubated for 1 h in the activity buffer (100 mM Tris/HCl, pH 8) to allow ribonuclease digestion of the embedded substrate and then stained with 0.2% (w/v) toluidine blue in 10 mM Tris/HCl, pH 8, for 10 min. Positive bands appeared white against the blue background after distaining.

tRF&tiRNA PCR Array

Total RNA was extracted by using mirVana miRNA Isolation Kit (ambion, AM1556), then 2 μg of purified total RNA was used to create cDNA libraries from small RNAs for qPCR detection using rtStar First-Strand cDNA Synthesis Kit (Arraystar, AS-FS-003). This method sequentially ligate 3'-adaptor with its 5'-end to the 3'-end of the RNAs, and 5'-adaptor with its 3'-end to the 5'-end of the RNAs. After cDNA synthesis, 185 (tRNA-derived fragments) tRFs & (tRNA halves) tiRNAs were profiled and quantified by qPCR method using nrStar Human tRF&tiRNA PCR Array (Arraystar, AS-NR-002).

RNAseq

Total RNA was extracted using mirVanaTM miRNA Isolation Kit as described by the manufacturer (Ambion, Life Technologies, AM1560). RNA purity was determined by spectrophotometry and RNA integrity was analyzed using Agilent 2100 Bioanalyzer and calculated as an RNA integrity number. Following RNA extraction, total RNAs (4 wild-type macrophage samples and 4 RNase2 knocked out macrophage samples) were submitted to CRG genomics (Centre for Genomic Regulation, Barcelona) for cDNA library preparation, polyA enrichment and NGS sequencing. Sequencing libraries were prepared according to protocols provided by Illumina. 50bp-long single-end sequencing was carried out in an Illumina HiSeq2500 sequencer with a depth of >20 million reads per sample.

Transcriptome Assembly and Differential Expression Analysis

FastQC was used to carry out the quality assessment of reads, assessing the distribution of phred quality scores and mean percentage GC content across each read. Reads were aligned to the latest human genome assembly from the Genome Reference Consortium (GRCh38) using HISAT2 (Pertea et al., 2016). Aligned reads were stored in the SAM file format. StringTie was used to assemble the alignments into transcripts and estimate the expression levels of all genes and transcripts (Pertea et al., 2016). Low expression (sum count less than 10) and non-coding genes were filtered out using biomaRT (Durinck et al., 2009) before passing to the Bioconductor package DESeq2 (Love et al., 2014). The resulting P-values were adjusted using Benjamini and Hochberg's approach for controlling the false discovery rate (FDR). Genes with an adjusted P-value (Q-value) < 0.01 & log2fc absolute value >1 found by DESeq were assigned as differentially expressed genes (DEGs).

Gene annotation and network analysis

GO enrichment and KEGG pathway enrichment analysis of the differential expression of genes across the samples was carried out using the clusterProfiler R package (Yu et al., 2012). Protein-protein-interactions between DEGs were analyzed using NetworkAnalyst which integrates the experimentally-validated interactions database, InnateDB database (Zhou et al., 2019). The network was visualized using Cytoscape software.

Molecular docking

HADDOCK2.2 (Utrecht Bioinformatics Center, University of Utrecht) was applied to perform the modelling of the protein complexes with EGFR and predict the associated free energies (Dominguez et al., 2003; van Zundert et al., 2016).

RSV production

Human respiratory syncytial virus (RSV, ATCC, VR-1540) stock was ordered from ATCC. Hela cells were used to produce RSV under biosafety level II conditions (Vissers et al., 2013). Briefly, Hela cells are plated in 75 cm^2 culture flask and incubated at 37°C degree in DMEM+10%FBS until they are approximately 50% confluent. The cells were then washed and infected with RSV stock under multiplicity of infection (MOI) of 0.1. After 3h infection, the cells were washed and replaced with fresh medium (DMEM+10%FBS) and incubate for 4days at 37 degree, 5% CO_2. The cells and the virus suspension were collected when the cytopathology appeared, with scraping and vortexing of the cells to release more viral particles. The virus suspension was centrifuged for 10 min at 1800×g to remove the cell debris. The virus suspension without cell debris were either frozen immediately and stored at -80°C as seeding stock or concentrated using Amicon. The produced viruses were titrated using TCID50 (median tissue culture infectious dose) method in Hela cells (Sun et al., 2015).

RSV infection THP1 induced macrophage

Before RSV infection, THP1 cells were induced to macrophage by 50 nM of PMA treatment for 48h as previously described (Lu et al., 2019). Cells were washed three time with pre-warmed PBS and replaced with fresh RPMI+10%FBS medium for 24h incubation. After that, macrophages were washed and incubated RSV, mixing at every 15 min for the first 2h. All virus treatment tests were performed using RSV at a MOI of 1 TCID50/cell.

Real-time quantitative PCR

RSV quantification were detected by real-time quantitative PCR. After the indicated time post of infection, the extracellular RSV virus were collected by PEG6000 precipitation method and intracellular RSV virus were collected by lysing the macrophage cells with the lysis buffer from mirVanaTM miRNA Isolation Kit (Ambion, Life Technologies, AM1560). Total RNA from RSV infected macrophage cells as well as stock virus was extracted using mirVanaTM miRNA Isolation Kit according to the manufacturer's instructions. cDNA was synthesized using iScriptTM cDNA Synthesis Kit (Bio-Rad, 170-8891). The synthesis was performed using random hexamers, starting with 1 μg or lee of total cell RNA. The RT-qPCR was performed using ddPCR ^{TM} Supermix for Probes (Bio-Rad, 1863024). Samples with a cycle threshold value of more than 40 were recorded as negative. A standard curve was prepared using serially diluted RNA extracts from a known quantity and used to quantify RSV as TCID50/mL. In parallel with the RSV probe assays, an endogenous glyceraldehyde-3-phosphate dehydrogenase (*GAPDH*) control was used for relative quantification of the intracellular virus. The relative expression of *GAPDH* and *RNase2* gene in macrophage was quantified by real-time PCR using iTaq Universal SYBR Green Supermix (Bio-Rad, 1725120). The primers and probe (Dewhurst-Maridor et al., 2004) used were listed in Table S1.

Cell viability assay

THP1 monocytes (wild type or RNase2 knockout) were seeded at 5×10^4 cells/well in 96 well plates and differentiated in macrophages as described (Lu et al., 2019). After infection with RSV under MOI=1 for different times, dynamic cell viability was measured using MTT assay.

Results

RSV infection activated the expression of RNase2 in macrophage

RSV virus stock was obtained at a titration of 2.8×10^6 $TCID_{50}$/mL, as previously described (Lu et al., submitted). THP1 macrophages were exposed to the RSV at a selected MOI of 1:1 up to 72h post of infection (poi). Following, we examined whether RSV infection induced the *RNase2* expression in THP1-derived macrophages. The *GAPDH* gene was used as a housekeeping gene control. Figure 1A shows that unstimulated macrophage cells had a constant and stable transcriptional expression of RNase2 and the *RNase2* gene was significantly upregulated in a time-dependent manner upon RSV infection. The significant *RNase2* gene levels upregulation can be detected as early as at 4h poi, with a 7-fold increase at 72 h poi. Furthermore, to determine whether the induction of *RNase2* mRNA levels correlated with an increase in protein expression, ELISA and WB were conducted to detect intracellular and secreted RNase2 protein of THP1-derived macrophages. At indicated poi time, culture medium and whole-cell extracts of macrophages infected with RSV were collected for ELISA and WB, respectively. As indicated in Figure 1B, the secreted protein levels of RNase2 was detected in human macrophages stimulated with RSV and was enhanced in response to RSV in a time-dependent manner, while no significant change of secreted RNase2 was detected in macrophage without RSV exposure. However, the maximum concentration of secreted RNase2 protein in macrophage culture was detected at 48h poi, with a slight decrease at 72h poi. Likewise, a similar profile was obtained by WB (Figure 1C). Taken together, our results suggest that RSV induces both RNase2 protein expression and secretion in human THP1 induced macrophages.

Construction of RNase2-knockouted THP1 cell line

Myeloid cells are poorly transfected using lipid-based transfection agents. Moreover, they are prone to potent cytokine and cell-death responses induced through intracellular nucleic acid-sensing receptors such as AIM2 and STING (Baker and Masters, 2018). Therefore, we adopted a lentiviral system to deliver CRISPR components into hematopoietic cells, THP1. Cas9 and sgRNAs lentiviral particles were produced in HEK293T cells by Calcium phosphate precipitation method as previously reported (Al Yacoub et al., 2007; Kutner et al., 2009; Tiscornia et al., 2006). THP1 cells were then transduced with the concentrated lentiviral particles with 10 μg/mL of polybrene, the overall transduction efficiency is about 7% (Figure S1). We designed 2 single guide RNAs (sgRNAs) (Table S2) targeting the RNase2 locus to generate double strand breaks (DSBs) (Figure S2A). T7EI assay was employed to select the more active guide RNA, achieving the knockout efficiencies of about 40% (Figure S2B and S2C). The GFP and cherry red double fluorescence positive cells were then sorted by FACS into single cells and were further allowed to grow into a single cell derived clonal cell line.

Following, the genomic DNA was extracted from the single cell derived cell lines and further used as a template to amplify RNase2 using the primers covering the potential mutation sites. After Sanger sequencing validation, we confirmed that *RNase2* gene had been successfully knocked out in 2 out of 32 single cells derived THP1 cell lines, named as KO18 and KO28 (Figure 2A). Both of KO18 and KO28 express a 15aa in length peptide comparing the wild type THP1 which encodes the full length 134aa protein.

Although the successful replacement was confirmed, we needed to ensure that the expression of functional RNase2 has effectively been abolished. According to the WB assay, we can barely detect RNase2 in the KO18 cell lysate sample compared to the control sample and a total absence of signal is achieved in KO28 sample (Figure 2B). Moreover, the release of RNase2 from THP1 cells were quantified by ELISA and we found no significant levels of RNase2 in culture supernatant for KO28, where no detectable differences in absorbance were registered between the KO28 culture supernatant and the RPMI+10%FBS medium (Figure 2C). Last, we conducted the ribonuclease activity staining assay to evaluate the ribonucleolytic activity of the samples from cell lysates and culture supernatants. According to the activity staining electrophoresis, two main activity bands can be visualized in wild-type macrophage lysate sample, with molecular weight sizes are around 15 and 20kDa, respectively. Compared to the WT control, both activity bands were missing in the RNase2 knockout cell lines (Figure 2D). In addition, as recent studies suggested that CRISPR/Cas9 frequently induces unwanted off-target mutations, we evaluated the off-target effects on these transduced monocytes. Here, we examined the top 4 potential off-target sites for the sgRNA1(Table S2), and we did not detect off-target mutation in the T7EI assay (Figure S3). Overall, we confirmed that the RNase2 gene has been both structurally and functionally been knocked out. The KO28 THP1 cell line as that achieved full RNase2-knockout was selected for all the downstream experiments.

Knockout of RNase2 alters the transcriptome of THP1

After knocking out of RNase2 in THP1 cells, next generation sequencing was performed and the whole transcriptomes from wild-type (WT) and knockout (KO) macrophages were compared. Transcriptomic data have been deposited at the NCBI Sequence Read Archive database (PRJNA590650). Expression of up to 19957 protein coding genes were detected (Additional file 1). A tight clustering within the WT group and KO group was observed by PCA plot (Figure S4). Differential expressed gene (DEGs) analysis illustrated that KO of RNase2 in THP1 macrophages resulted in 2009 (1415 up regulated, 594 down regulated) DEGs compared to WT group (Additional file2). Applied DEGs to KEGG pathway enrichment, 23 pathways were significantly enriched ($p.adj<0.05$) (Additional file 3) and listed in Figure 3A. The significantly enriched KEGG pathways were mainly clustered in 3 groups, including Group1: Viral protein interaction with cytokine and cytokine receptor, Cytokine-cytokine receptor interaction and Chemokine signaling pathway; Group2: TNF signaling pathway, NF-kappa B signaling pathway, TNF signaling pathway and Influenza A; and Group3: Oocyte meiosis, maturation and cell cycle. Five top enriched pathways (ranked by p.adj value) are identified: viral protein interaction, cell cycle, cytokine-cytokine receptor, chemokine signaling pathway, and DNA replication. We observed that the DEGs

related to cytokine and chemokines were down-regulated while the DEGs related to cell cycle and DNA replication were up-regulated upon removal of RNase2 expression (Figure3B). A set of 11 selected genes were also used to validate the RNAseq data by qPCR, the result indicated a consistent agreement between RNAseq and qPCR (Figure S5). In addition, the DEGs were applied to network analysis to explore the protein - protein interactions. In total, the network analysis yielded 756 nodes (each node standing for one protein) with 1547 edges (interactions), and SRC, STAT1, EGFR, CDK1, and KIAA0101 were the five top 5 hub genes ranked by betweenness and centrality scores (Figure 4). Interestingly, all the five top central genes associated to RNase2 expression were also identified as hub genes in THP1-derived macrophages in response to RNase3 treatment (Lu et al., unpublished results). Human RNase3 is the closest RNase2 family homologue, sharing about a 70% sequence identity. To note, all the five spotted genes were observed in our previous work to be induced in a none related to catalytic activity manner: an equivalent common response was evidenced by the transcriptome analysis of macrophage cells treatment with both wild-type RNase3 and the H15A catalytically defective mutant (Lu et al. unpublished results). Likewise, in both RNases 2 and 3 the network centrality expressed genes are directly or indirectly related to the EGF receptor (EGFR). Surprisingly, a recent report indicated that RNase5 can work as a direct EGFR ligand (Wang et al., 2018a) and our very recent structural characterization of RNase3 also predicted a high affinity protein-receptor binding. Therefore, we modelled here a putative RNase2- EGFR complex taking the published EGF-EGFR structure as a reference (Wang et al., 2018a). Molecular modelling predicted that RNase2 is a strong ligand of EGFR（Figure 5, Table 1）. Comparing RNase2, RNase3, and RNase5 with EGF sequence, the CQYRD region is mostly conserved, especially the cysteine and tyrosine residues (Figure 5). A close inspection of the predicted complex revealed that the interaction of RNase2 with EGFR might be mediated by residues regions 19-25, 28-35, 79-81, 84-88, and 97-103 (Additional file 4). R97, Y98 of RNase2 were identified as the key residues that interact within the 412-468 region of the EGFR. A side-by-side comparison of RNase2 with its closest homologue RNase3 highlighted conserved features that might account for slightly distinct binding modes. For example, substitution of residue D100, shared by RNase3 and EGF, by a Q in RNase2 might reduce the binding affinity. To note, both D and Q are conserved in the two RNases respective primate lineages (Zhang et al., 1998).

Knocking out RNase2 increases RSV infection burden in macrophage

Next, we investigated whether RNase2 expression within macrophages contributes to the cell antiviral activity. First, THP1 cells (WT and RNase2 KO) were induced into macrophages as described above. Macrophages were then exposed to RSV at MOI=1 to investigate the kinetics of infection by monitoring both intracellular and extracellular RSV amplicon using probe RT-qPCR, the standard curve built by serial diluting of a known RSV stock (Figure S5). Intracellularly (Figure 6A), RSV increased at beginning of the infection (24h) but decreased at longer infection periods (48-72h), with a slow increase (0h-4h) followed by an exponential increase (4h-24h) and reaching a maximum at 24h. At 24h, RNase2 KO macrophages had significantly more RSV inside than WT macrophages. The RSV out of macrophages were also determined (Figure 6B). We observed that RSV increased in KO macrophages' cultures until 48h and then stabilized

at 48-72h. While in WT macrophages' culture, RSV increased and reached the peak at 48h and followed the decreasing, significantly higher RSV were detected in KO macrophages' culture than in WT macrophages' culture at 24h-72h. Moreover, we monitored cell death during RSV infection using MTT assay and our results confirmed that RSV infection can increase cell death in either WT or KO macrophages. However, significant differences were detected, where KO macrophage cell death upon RSV infection was higher than in the WT macrophage (Figure 6C). All together, we concluded that RNase2 KO macrophages burdening is significantly higher for RSV infection and cell death in comparison to WT macrophages.

Knock out of RNase2 alters the tRNA fragment population

Previous work by Rosenberg and coworkers indicated that RNase2 antiviral action was dependent on its catalytic activity (Domachowske et al., 1998). Therefore, we decided to explore here the changes in RNA population in both RSV infected and none infected THP1-derived macrophage cells. First, we decided to analysis the RNase activity on the cell tRNA population. Taking into account that single stranded RNA viral replication had been associated to host tRNA accessibility and that RNase5 homologue was reported to specifically cleave the host self tRNAs, we decided to analyze here RNase2 action on the macrophage tRNA population. In order to find out whether the RNase2 catalytic activity is specifically targeting the tRNA population we screened a tRNAs fragment library.

Using the nrStar Human tRF&tiRNA PCR assay, which includes regulatory tRNA halves (tiRNA) and tRFs, we found that out of a total of 185 tRNA fragments 5 were significantly decreased in RNase2 KO macrophage in comparison to the WT control group: 2 tiRNAs, 1 tRF-5, 1 tRF-3, 1 tRF-1 (see Table 2 and Figure S7). Under RSV infection condition, KO of RNase2 significantly caused the reduction of 22 tRNA fragments (8 tiRNAs, 8 tRF-5, 3 tRF-3, 3 tRF-1). Comparing the tRNA population from WT macrophages with or without RSV infection, we observed that RSV infection can promote the production of 4 tRNA fragments (2 tiRNAs, 2 tRF-5). Cleavage of LysCTT, LysTTT, ArgCCT and GluTTC are commonly released by RNase2 in both infected and non-infected cell cultures. Specifically, the release of the tRNA fragment 1039, is shared in both cases. In total, there are 26 tRFs downregulated by RNase2-KO either with or without RSV infection (Table 2). Upon inspection of sequence of the putative cleavage sites we observed all sites at or near any of the tRNA loops (10 at anticodon, 9 at D loop, 4 at T loop), except 3 tRF-1s which are released from the precursor of tRNA (Table S3). Moreover, we identified the preferable target sequences are enriched with U or A by comparing the cleavage site of 13 tRFs which located strictly within any of the tRNA loops (3 at anticodon loop, 6 at D loop, 4 at T loop), such as XUUX, XAAX. However, there are more G or C appeared in the target sequences when the cleavage site is outside of any of the tRNA loops. A full analysis of exposed cleavage sequences should also consider the final adopted tRNA 3D fold that will hide some regions from the RNase action. Notwithstanding, we still lack information here on the contribution of nucleotide posttranscriptional modifications that might partially protect the processing of the tRNA and play a key role during infection. Besides, prediction of the RNA secondary structure potentially adopted by the tRNA fragments products, indicated that some of the main fragment sequences associated to

RNase2 presence, such as the tiRNA released from LysCTT and LysTTT parental tRNA, can form a very stable hairpin like structure (Figure S7). We can speculate that the adopted hairpin structures might play some key role in the cell response to virus infection, by either interfering in the virus replication or inhibiting the translation machinery. In addition, together with the release of regulatory fragments from mature tRNAs, we also observed few RNA species released from pre-tRNAs transcripts. Further work needs to be performed in order to identify the specific location of expressed RNase2 within the infected macrophages in order to better interpret the present results.

Discussion

RNase2 antiviral activity against RSV within macrophage

Expression of human RNase2 is widely distributed in diverse body tissues such as kidney, liver and spleen together with leukocyte cells. Among the blood cell types, eosinophils are undoubtedly the main source of RNase2 expression, which first gave its name upon the protein discovery, name thereafter as the Eosinophil Derived Neurotoxin (EDN) (Gleich et al., 1986). Apart from its main source, the eosinophils, RNase2 is also expressed in other blood cell types, such as monocytes, basophils, and neutrophils (Rosenberg, 2015).

A number of host defense-associated activities have been proposed for RNase2, mostly associated to the targeting of RNA viral infection. In particular, the protein has been reported to reduce the infectivity of the human respiratory syncytial virus (RSV) and HIV in cell cultures (Domachowske et al., 1998; Rugeles et al., 2003). Moreover, RNase2 has been suggested as a biomarker in RSV induced bronchiolitis (Kim et al., 2013; Rosenberg, 2015).

In this study, we first monitored the dynamic change of RNase2 expression in human THP1-derived macrophage with RSV infection. We chose THP1 induced macrophage to investigate the dynamic expression of RNase2 upon RSV infection because RNase2 is the most abundant RNaseA family member expressed in this cell line (Lu et al., 2019) (https://www.proteinatlas.org/). Viruses can manipulate cell biology to utilize macrophages as vessels for dissemination, long term persistence within tissues and virus replication. Endocytosis, phagocytosis, micropinocytosis, and membrane fusion are the major ways that viruses enter cells. In this study, we observed that RSV can enter human THP1 induced macrophages within 2 hours' infection. A fast proliferation of RSV can be found after 4h post of infection and the number of RSV viruses reached the highest peak at 24h, following a decrease at 48h and 72h in macrophages. Without RSV infection, human THP1 induced macrophages stably express a basic level of RNase2. However, RSV infection can significantly activate transcriptional *RNase2* expression in the macrophage cell as early as 4h post of infection, and the significant increase of protein expression can be detected after 24h post of infection (Figure 1). Its worthy to mention there is a correlation between RSV population and RNase2 expression level at the timeline. It was previously demonstrated that human monocyte-derived macrophages challenged with a combination of LPS and TNF-a produced RNase2 in time-dependent manner (Yang et al., 2004). However, we did not find any significant change of transcriptional expression of RNase2 upon *Mycobacteria aurum* infection (Lu

et al., 2019). Discrepancy of expression induction is also found for RNase2 secretion by eosinophils upon distinct bacterial infections. For example, *Clostridium difficile* and *Staphylococcus aureus* infection caused release of RNase2 while Bifidobacteria, Hemophilus, and Prevotella species infection did not (Rosenberg, 2015). In agreement, our previous work on THP1 derived macrophages infected by mycobacteria also discarded any induction of *RNase2* expression (Lu et al., 2019). In contrast, RSV infection significantly activated the expression of *RNase2* in the same THP1 macrophage derived cell line. Considering the present study and previous reports on RNase2 association to viral infections (Rosenberg, 2015), we may speculate that RNase2 is involved in the immune antiviral response. In particular, our work highlighted the protein role in macrophage cells challenged by RSV infection. This result was further corroborated by knocking out of RNase2 by CRIPSPR/Cas9 and observation of macrophages suffering a heavier RSV infection burden and subsequent cell death. Our present results reinforce the potential role of RNase2 in the host antiviral response.

RNase2 participates in the macrophage overall immune response

Although RNase2 expression is commonly associated to the host antiviral response, no direct characterization was previously performed on the protein endogenously expressed by macrophages. Previous work reported a broad antiviral activity, including inhibition of the replication of the RSV, human immunodeficiency (HIV)-1, and hepatitis B DNA viruses (Bedoya et al., 2006; Domachowske et al., 1998; Li et al., 2009; Rugeles et al., 2003). Beside the antiviral activity on viruses, RNase2 was also reported to mediate an immunomodulatory action on various host cells, promoting leukocyte activation, maturation, and chemotaxis (Rosenberg, 2008b, 2015; Yang et al., 2008). Here, to gain knowledge on how RNase2 exerts its effects on host immune cells, we performed a comparative transcriptome analysis of human THP1 induced macrophages with and without expression of endogenous RNase2. Our results indicated that RNase2 is crucial in maintaining macrophage's immune response, i.e., the knockout of RNase2 resulted in more than 2000 genes significantly differently expressed and those DEGs enriched into pathways related to innate immune response and cell cycle (Figure 3, Additional files 2-3). Specifically, most of the down regulated DEGs upon RNase2 removal, such as cytokines, chemokines, are related to innate immune response, while the main up regulated DEGs when RNase2 is knocked out are related to cell cycle. It was previously reported that RNase2 can activate dendritic cells through TLR2-MyD88 pathway (Yang et al., 2008). However, the main DEGs observed here for THP1 macrophages were not significantly enriched into Toll-like receptor signaling pathway. Notwithstanding, we cannot discard that the present discrepancy with previous results is merely due to intrinsic differences on the working cell lines. Instead, we identified by network analysis based on protein-protein interactions the epidermal growth factor receptor (EGFR) as the main hub gene. The EGFR, also called ErbB1, is a membrane-bound tyrosine kinase, which, together with ErbB2, ErbB3 and ErbB4, constitute the ErbB family (Roskoski, 2014). The receptor activation can trigger downstream signaling via several major pathways, including MAPK, phosphoinositide 3 kinase (PI3K), nuclear factor kappa light chain enhancer of activated B cells (NF-kB) and janus kinase/signal transducer and activator of transcription (JAK/STAT) pathways (Chakraborty et al., 2014; Colomiere et al., 2009). EGFR signaling can result in a number of outcome

primarily associated with growth, including cell proliferation, survival, angiogenesis, adhesion, differentiation and motility. A wide variety of viruses and bacteria are known to exploit EGFR functions for infection and replicative benefit. However, EGFR also functions to protect the host during disease (Choi et al., 2011; Monticelli et al., 2015) and can contribute to the maintenance of epithelial barriers and immune defense (Franzke et al., 2012; Monticelli et al., 2015). It is worthy to mention that RNase5 had been reported very recently to function as a ligand of EGFR (Wang et al., 2018b). Besides, our recent transcriptomic analysis of the THP1 derived macrophages grown in the presence of recombinant RNase3 also identified the network centrality of the EGFR in the cell response (Lu et al., unpublished results). In this work, we have performed a molecular modelling and corroborated the potential direct binding of RNase2 with the receptor (Figure 5). Our molecular docking data suggests that there is a direct interaction of RNase2 with EGFR, and that the key binding region is conserved with RNase3 and RNase5. However, local divergence in the spotted interaction domain among the three RNases suggest that there might be subtle differences in the activation mechanism that could explain the proteins' distinct biological properties. Interestingly, the catalytic activity in both RNase3 and RNase5 is not required for interaction with the receptor (Wang et al., 2018a) (Lu et al., unpublished results). Further work is mandatory to confirm whether this is also the case for RNase2 immunomodulatory activity mediated by EGFR. Future structural analysis will also be required to identify the structural features that contribute to the interaction of RNase2 with EGFR and the similarities and potential specificities respect to the other family homologue proteins. Taking into account that EGFR activation can participate in the host anti-infective response, further work should explore whether some of RNase2 biological properties are mediated by EGFR activation.

RNase2 alters the cellular ncRNA population

Considering previous reports on the contribution of RNase2 enzymatic activity in the protein antiviral activity (Domachowske et al., 1998), we decided to analyze here the effect of the macrophage endogenous RNase2 on the ncRNA population. Increasing data demonstrates that small noncoding RNAs (sncRNAs) play important roles in regulating antiviral innate immune responses (Ghildiyal and Zamore, 2009; Skalsky and Cullen, 2010). In particular, small ncRNAs derived from tRNAs, also called regulatory tRNA halves (tiRNAs) and tRNA-derived fragments (tRFs), have been recently identified and proven as functional molecules. Cellular stress, cell proliferation, or RSV infection can regulate the population of tiRNAs and tRFs. For example, it has been demonstrated that RSV infection and hepatitis viral infection can induce the production of tRFs and tRNA-halves, and their release has been related to RNase5/angiogenin activity (Selitsky et al., 2015; Wang et al., 2013). Interestingly, the release of a specific tRF, tRF5-GluCTC, which targets and suppresses the apolipoprotein E receptor 2 (APOER2), can also promote the RSV replication (Deng et al., 2015; Wang et al., 2013). In the present study, although the tRF5-GluCTC was not significantly changed upon RSV infection alone, we observed a significant reduction in the RNase2 knockout cell line challenged with RSV infection (Table 2). Besides, tiRNA-5034-ValCAC-3, the tRF originated from ValCAC, was found in both the present data and the previous work. Moreover, we found that RSV infection on WT cell line induced the production of 4 tRFs in macrophages in agreement to the previous study that indicated that RSV

infection (moi=3) induced the release of tRFs in epithelial cells (A549 cell line) (Wang et al., 2013). Moreover, the difference of experimental conditions and source cell line should be responsible for the converse results. Moreover, tRFs production was observed to be regulated by specific viral infection, for example, human metapneumovirus did not induce tRFs (Wang et al., 2013). In any case, among the identified tRFs by the array screening, we find the tRF3 from tRNALysTTT, which is reported to block retroviruses replication, such as in HIV-1, by direct binding to the virus priming binding site (Das et al., 1995; Jin and Musier-Forsyth, 2019; Schorn et al., 2017).

RNase5, also known as Angiogenin, is one of the most well-known ribonucleases that are responsible for ribonucleolytic activity-dependent endonucleolytic cleavage of tRNA (Fu et al., 2009; Yamasaki et al., 2009). Under certain conditions of cellular stress, such as nutrition deficiency, oxidative stress, or hypothermia, RNase5 stimulates the formation of cytoplasmic stress granules and cleaves tRNA at positions close to the anticodon loop, producing tRNA-derived stress-induced small RNA (tiRNA, or tRNA halves) (Li and Hu, 2012; Xin et al., 2018; Zhang et al., 2016). Those tiRNA fragments functionally enhance damage repair and cellular survival through suppressing the formation of the translation initiation factor complex or associating with the translational silencer (Ivanov et al., 2011; Yamasaki et al., 2009). In the present study, we found that KO of RNase2 abolishes the tRFs release in human macrophages, and this scenario is more pronounced upon RSV challenge. In particular, the present results indicated that RNase2 expression in macrophages is associated to the enrichment of selective tRNA fragments (Figure 7; Tables 2 and S3). Our result is consistent with the recently published studies, which have suggested that there may be other ribonucleases from the RNaseA superfamily apart from RNase5 that target tRNA and procure regulatory tRNA fragments (Akiyama et al.; Su et al., 2019). Further work is in progress to fully identify the selective cleavage sites within the cell ncRNA population targeted by RNase2 and their role during viral infection.

Conclusions

This is the first characterization of the RNase2 expressed in macrophages and its direct targeting of tRNA. Moreover, the characterization of THP1-derived macrophages defective in RNase2 in a RSV infection model confirms its participation in the macrophage host antiviral defense. In addition, comparative transcriptomic suggests the direct protein activation of EGFR. Last, the screening of a tRNA regulatory fragments library indicates RNase2 specific targeting of tRNA population. Future work should unravel the contribution of the protein catalytically dependent and independent activities in its antiviral action. The results should contribute in the design of novel antiviral drugs.

Acknowledgement

This research was founded by Research work was supported by the Ministerio de Economía y Competitividad (SAF2015-66007P), co-financed by FEDER funds, and by Fundació La Marató de TV3 (2080310). LL is supported by China Scholarship Council (CSC) Grant. PFM has a Juan de la Cierva Postdoctoral Research Contract (MINECO). We thank Yundong Peng (Max Planck Institute for Heart and Lung Research, Bad Nauheim, Germany), Manuel Kaulich (Goethe University Frankfurt, Germany) for technical supporting with CRIPSR design. We would also like to show our gratitude to

Laura Tussel, Anna Genesca, Marina Rodriguez Muñoz, and David Soler from UAB for helping in lentiviral production and Guillem Prats-Ejarque for molecular modeling studies.

References

Acharya, K. R., and Ackerman, S. J. (2014). Eosinophil granule proteins: Form and function. *J. Biol. Chem.* 289, 17406–17415. doi:10.1074/jbc.R113.546218.

Akiyama, Y., Lyons, S., Fay, M. M., Abe, T., Anderson, P., and Ivanov, P. Multiple ribonuclease A family members cleave transfer RNAs in response to stress. doi:10.1101/811174.

Al Yacoub, N., Romanowska, M., Haritonova, N., and Foerster, J. (2007). Optimized production and concentration of lentiviral vectors containing large inserts. doi:10.1002/jgm.1052.

Baker, P. J., and Masters, S. L. (2018). "Generation of Genetic Knockouts in Myeloid Cell Lines Using a Lentiviral CRISPR/Cas9 System," in *Methods in Molecular Biology*, 41–55. doi:10.1007/978-1-4939-7519-8_3.

Bedoya, V. I., Boasso, A., Hardy, A. W., Rybak, S., Shearer, G. M., and Rugeles, M. T. (2006). Ribonucleases in HIV type 1 inhibition: effect of recombinant RNases on infection of primary T cells and immune activation-induced RNase gene and protein expression. *AIDS Res Hum Retroviruses* 22, 897–907. doi:10.1089/aid.2006.22.897.

Boix, E., and Nogués, M. V. (2007). Mammalian antimicrobial proteins and peptides: overview on the RNase A superfamily members involved in innate host defence. *Mol. Biosyst.* 3, 317–335. doi:10.1039/b617527a.

Chakraborty, S., Li, L., Puliyappadamba, V. T., Guo, G., Hatanpaa, K. J., Mickey, B., et al. (2014). Constitutive and ligand-induced EGFR signalling triggers distinct and mutually exclusive downstream signalling networks. *Nat. Commun.* 5. doi:10.1038/ncomms6811.

Choi, H. J., Seo, C. H., Park, S. H., Yang, H., Do, K. H., Kim, J., et al. (2011). Involvement of epidermal growth factor receptor-linked signaling responses in Pseudomonas fluorescens-infected alveolar epithelial cells. *Infect. Immun.* 79, 1998–2005. doi:10.1128/IAI.01232-10.

Colomiere, M., Ward, A. C., Riley, C., Trenerry, M. K., Cameron-Smith, D., Findlay, J., et al. (2009). Cross talk of signals between EGFR and IL-6R through JAK2/STAT3 mediate epithelial-mesenchymal transition in ovarian carcinomas. *Br. J. Cancer* 100, 134–144. doi:10.1038/sj.bjc.6604794.

Das, A. T., Klaver, B., and Berkhout, B. (1995). Reduced Replication of Human Immunodeficiency Virus Type 1 Mutants That Use Reverse Transcription Primers other than the Natural tRNA 3 Lys. Available at: http://jvi.asm.org/ [Accessed February 5, 2020].

Davoine, F., and Lacy, P. (2014). Eosinophil cytokines, chemokines, and growth factors: Emerging roles in immunity. *Front. Immunol.* 5. doi:10.3389/fimmu.2014.00570.

Deng, J., Ptashkin, R. N., Chen, Y., Cheng, Z., Liu, G., Phan, T., et al. (2015). Respiratory Syncytial Virus Utilizes a tRNA Fragment to Suppress Antiviral Responses

Through a Novel Targeting Mechanism. *Mol. Ther.* 23, 1622–1629. doi:10.1038/mt.2015.124.

Dewhurst-Maridor, G., Simonet, V., Bornand, J. ., Nicod, L. ., and Pache, J. . (2004). Development of a quantitative TaqMan RT-PCR for respiratory syncytial virus. *J. Virol. Methods* 120, 41–49. doi:10.1016/J.JVIROMET.2004.03.017.

Domachowske, J. B., Dyer, K. D., Bonville, C. A., and Rosenberg, H. F. (1998). Recombinant Human Eosinophil-Derived Neurotoxin/RNase 2 Functions as an Effective Antiviral Agent against Respiratory Syncytial Virus. *J. Infect. Dis.* 177, 1458–1464. doi:10.1086/515322.

Dominguez, C., Boelens, R., and Bonvin, A. M. J. J. (2003). HADDOCK: A protein-protein docking approach based on biochemical or biophysical information. *J. Am. Chem. Soc.* 125, 1731–1737. doi:10.1021/ja026939x.

Durinck, S., Spellman, P. T., Birney, E., and Huber, W. (2009). Mapping identifiers for the integration of genomic datasets with the R/Bioconductor package biomaRt. *Nat. Protoc.* 4, 1184–1191. doi:10.1038/nprot.2009.97.

Franzke, C. W., Cobzaru, C., Triantafyllopoulou, A., Löffek, S., Horiuchi, K., Threadgill, D. W., et al. (2012). Epidermal ADAM17 maintains the skin barrier by regulating EGFR ligand- dependent terminal keratinocyte differentiation. *J. Exp. Med.* 209, 1105–1119. doi:10.1084/jem.20112258.

Fu, H., Feng, J., Liu, Q., Sun, F., Tie, Y., Zhu, J., et al. (2009). Stress induces tRNA cleavage by angiogenin in mammalian cells. *FEBS Lett.* 583, 437–442. doi:10.1016/j.febslet.2008.12.043.

Ghildiyal, M., and Zamore, P. D. (2009). Small silencing RNAs: An expanding universe. *Nat. Rev. Genet.* 10, 94–108. doi:10.1038/nrg2504.

Gleich, G. J., Loegering, D. a, Bell, M. P., Checkel, J. L., Ackerman, S. J., and McKean, D. J. (1986). Biochemical and functional similarities between human eosinophil-derived neurotoxin and eosinophil cationic protein: homology with ribonuclease. *Proc. Natl. Acad. Sci. U. S. A.* 83, 3146–3150. doi:10.1073/pnas.83.10.3146.

Harrison, A. M., Bonville, C. A., Rosenberg, H. F., and Domachowske, J. B. (1999). Respiratory syncytical virus–induced chemokine expression in the lower airways. *Am. J. Respir. Crit. Care Med.* 159, 1918–1924. doi:10.1164/ajrccm.159.6.9805083.

Ivanov, P., Emara, M. M., Villen, J., Gygi, S. P., and Anderson, P. (2011). Angiogenin-induced tRNA fragments inhibit translation initiation. *Mol. Cell* 43, 613–623. doi:10.1016/j.molcel.2011.06.022.

Jin, D., and Musier-Forsyth, K. (2019). Role of host tRNAs and aminoacyl-tRNA synthetases in retroviral replication. *J. Biol. Chem.* 294, 5352–5364. doi:10.1074/jbc.REV118.002957.

Kim, C.-K., Seo, J. K., Ban, S. H., Fujisawa, T., Kim, D. W., and Callaway, Z. (2013). Eosinophil-derived neurotoxin levels at 3 months post-respiratory syncytial virus

bronchiolitis are a predictive biomarker of recurrent wheezing. *Biomarkers* 18, 230–235. doi:10.3109/1354750X.2013.773078.

Kutner, R. H., Zhang, X.-Y., and Reiser, J. (2009). Production, concentration and titration of pseudotyped HIV-1-based lentiviral vectors. *Nat. Protoc.* 4, 495–505. doi:10.1038/nprot.2009.22.

Lee, J. J., Jacobsen, E. A., McGarry, M. P., Schleimer, R. P., and Lee, N. A. (2010). Eosinophils in health and disease: the LIAR hypothesis. *Clin. Exp. Allergy* 40, 563–575. doi:10.1111/j.1365-2222.2010.03484.x.

Li, S., and Hu, G.-F. (2012). Emerging role of angiogenin in stress response and cell survival under adverse conditions. *J. Cell. Physiol.* 227, 2822–6. doi:10.1002/jcp.23051.

Li, Y., Zhao, Y., Liu, J., Huang, Y., Liu, Z., and Xue, C. (2009). A promising alternative anti-HBV agent: The targeted ribonuclease. *Int. J. Mol. Med.* 23, 521–527. doi:10.3892/ijmm.

Love, M. I., Huber, W., and Anders, S. (2014). Moderated estimation of fold change and dispersion for RNA-seq data with DESeq2. *Genome Biol.* 15, 550. doi:10.1186/s13059-014-0550-8.

Lu, L., Arranz-Trullén, J., Prats-Ejarque, G., Pulido, D., Bhakta, S., and Boix, E. (2019). Human Antimicrobial RNases Inhibit Intracellular Bacterial Growth and Induce Autophagy in Mycobacteria-Infected Macrophages. *Front. Immunol.* 10, 1500. doi:10.3389/fimmu.2019.01500.

Lu, L., Li, J., Moussaoui, M., and Boix, E. (2018). Immune Modulation by Human Secreted RNases at the Extracellular Space. *Front. Immunol.* 9, 1012. doi:10.3389/fimmu.2018.01012.

Machado, D., Hoffmann, J., Moroso, M., Rosa-Calatrava, M., Endtz, H., Terrier, O., et al. (2017). RSV Infection in Human Macrophages Promotes CXCL10/IP-10 Expression during Bacterial Co-Infection. *Int. J. Mol. Sci.* 18. doi:10.3390/IJMS18122654.

Monteseirín, J., Vega, A., Chacón, P., Camacho, M. J., El Bekay, R., Asturias, J. A., et al. (2007). Neutrophils as a Novel Source of Eosinophil Cationic Protein in IgE-Mediated Processes. *J. Immunol.* 179, 2634–2641. doi:10.4049/jimmunol.179.4.2634.

Monticelli, L. A., Osborne, L. C., Noti, M., Tran, S. V., Zaiss, D. M. W., and Artis, D. (2015). IL-33 promotes an innate immune pathway of intestinal tissue protection dependent on amphiregulin-EGFR interactions. *Proc. Natl. Acad. Sci. U. S. A.* 112, 10762–10767. doi:10.1073/pnas.1509070112.

Oppenheim, J. J., Tewary, P., de la Rosa, G., and Yang, D. (2007). "Alarmins Initiate Host Defense," in (Springer, New York, NY), 185–194. doi:10.1007/978-0-387-72005-0_19.

Pertea, M., Kim, D., Pertea, G. M., Leek, J. T., and Salzberg, S. L. (2016). Transcript-level expression analysis of RNA-seq experiments with HISAT, StringTie and Ballgown. *Nat. Protoc.* 11, 1650–1667. doi:10.1038/nprot.2016.095.

Prats-Ejarque, G., Arranz-Trullén, J., Blanco, J. A., Pulido, D., Nogués, M. V., Moussaoui, M., et al. (2016). The first crystal structure of human RNase 6 reveals a novel substrate-binding and cleavage site arrangement. *Biochem. J.* 473, 1523–1536. doi:10.1042/BCJ20160245.

Rosenberg, H. (2008a). Eosinophil-Derived Neurotoxin / RNase 2: Connecting the Past, the Present and the Future. *Curr. Pharm. Biotechnol.* 9, 135–140. doi:10.2174/138920108784567236.

Rosenberg, H. F. (2008b). RNase A ribonucleases and host defense: an evolving story. *J. Leukoc. Biol.* 83, 1079–87. doi:10.1189/jlb.1107725.

Rosenberg, H. F. (2015). Eosinophil-Derived Neurotoxin (EDN/RNase 2) and the Mouse Eosinophil-Associated RNases (mEars): Expanding Roles in Promoting Host Defense. *Int. J. Mol. Sci.* 16, 15442–15455. doi:10.3390/ijms160715442.

Rosenberg, H. F., and Dyer, K. D. (1997). Diversity among the primate eosinophil-derived neurotoxin genes: A specific C-terminal sequence is necessary for enhanced ribonuclease activity. *Nucleic Acids Res.* 25, 3532–3536. doi:10.1093/nar/25.17.3532.

Roskoski, R. (2014). The ErbB/HER family of protein-tyrosine kinases and cancer. *Pharmacol. Res.* 79, 34–74. doi:10.1016/j.phrs.2013.11.002.

Rugeles, M. T., Trubey, C. M., Bedoya, V. I., Pinto, L. A., Oppenheim, J. J., Rybak, S. M., et al. (2003). Ribonuclease is partly responsible for the HIV-1 inhibitory effect activated by HLA alloantigen recognition. *AIDS* 17, 481–486. doi:10.1097/00002030-200303070-00002.

Schorn, A. J., Gutbrod, M. J., LeBlanc, C., and Martienssen, R. (2017). LTR-Retrotransposon Control by tRNA-Derived Small RNAs. *Cell* 170, 61-71.e11. doi:10.1016/j.cell.2017.06.013.

Selitsky, S. R., Baran-Gale, J., Honda, M., Yamane, D., Masaki, T., Fannin, E. E., et al. (2015). Small tRNA-derived RNAs are increased and more abundant than microRNAs in chronic hepatitis B and C. *Sci. Rep.* 5. doi:10.1038/srep07675.

Shen, B., Zhang, J., Wu, H., Wang, J., Ma, K., Li, Z., et al. (2013). Generation of gene-modified mice via Cas9/RNA-mediated gene targeting. *Cell Res.* 23, 720–723. doi:10.1038/cr.2013.46.

Skalsky, R. L., and Cullen, B. R. (2010). Viruses, microRNAs, and Host Interactions. *Annu. Rev. Microbiol.* 64, 123–141. doi:10.1146/annurev.micro.112408.134243.

Su, Z., Kuscu, C., Malik, A., Shibata, E., and Dutta, A. (2019). Angiogenin generates specific stress-induced tRNA halves and is not involved in tRF-3–mediated gene silencing. *J. Biol. Chem.* 294, 16930–16941. doi:10.1074/jbc.RA119.009272.

Sun, Y., Jain, D., Koziol-White, C. J., Genoyer, E., Gilbert, M., Tapia, K., et al. (2015). Immunostimulatory Defective Viral Genomes from Respiratory Syncytial Virus Promote a Strong Innate Antiviral Response during Infection in Mice and Humans. *PLOS Pathog.* 11, e1005122. doi:10.1371/journal.ppat.1005122.

Tiscornia, G., Singer, O., and Verma, I. M. (2006). Production and purification of lentiviral vectors. *Nat. Protoc.* 1, 241–245. doi:10.1038/nprot.2006.37.

van Zundert, G. C. P., Rodrigues, J. P. G. L. M., Trellet, M., Schmitz, C., Kastritis, P. L., Karaca, E., et al. (2016). The HADDOCK2.2 Web Server: User-Friendly Integrative Modeling of Biomolecular Complexes. *J. Mol. Biol.* 428, 720–725. doi:10.1016/J.JMB.2015.09.014.

Vissers, M., Habets, M. N., Ahout, I. M. L., Jans, J., de Jonge, M. I., Diavatopoulos, D. A., et al. (2013). An In vitro Model to Study Immune Responses of Human Peripheral Blood Mononuclear Cells to Human Respiratory Syncytial Virus Infection. *J. Vis. Exp.*, e50766. doi:10.3791/50766.

Wang, Q., Lee, I., Ren, J., Ajay, S. S., Lee, Y. S., and Bao, X. (2013). Identification and Functional Characterization of tRNA-derived RNA Fragments (tRFs) in Respiratory Syncytial Virus Infection. *Mol. Ther.* 21, 368–379. doi:10.1038/mt.2012.237.

Wang, Y.-N., Lee, H.-H., Chou, C.-K., Yang, W.-H., Wei, Y., Chen, C.-T., et al. (2018a). Angiogenin/Ribonuclease 5 Is an EGFR Ligand and a Serum Biomarker for Erlotinib Sensitivity in Pancreatic Cancer. *Cancer Cell* 33, 752-769.e8. doi:10.1016/j.ccell.2018.02.012.

Wang, Y.-N., Lee, H.-H., and Hung, M.-C. (2018b). A novel ligand-receptor relationship between families of ribonucleases and receptor tyrosine kinases. *J. Biomed. Sci.* 25, 83. doi:10.1186/s12929-018-0484-7.

Weller, P. F., and Spencer, L. A. (2017). Functions of tissue-resident eosinophils. *Nat. Rev. Immunol.* 17, 746–760. doi:10.1038/nri.2017.95.

Xin, X., Wang, H., Han, L., Wang, M., Fang, H., Hao, Y., et al. (2018). Single-Cell Analysis of the Impact of Host Cell Heterogeneity on Infection with Foot-and-Mouth Disease Virus. *J. Virol.* 92, e00179-18. doi:10.1128/JVI.00179-18.

Yamasaki, S., Ivanov, P., Hu, G. F., and Anderson, P. (2009). Angiogenin cleaves tRNA and promotes stress-induced translational repression. *J. Cell Biol.* 185, 35–42. doi:10.1083/jcb.200811106.

Yang, D., Chen, Q., Rosenberg, H. F., Rybak, S. M., Newton, D. L., Wang, Z. Y., et al. (2004). Human ribonuclease A superfamily members, eosinophil-derived neurotoxin and pancreatic ribonuclease, induce dendritic cell maturation and activation. *J. Immunol.* 173, 6134–6142. doi:10.4049/jimmunol.173.10.6134.

Yang, D., Chen, Q., Su, S. B., Zhang, P., Kurosaka, K., Caspi, R. R., et al. (2008). Eosinophil-derived neurotoxin acts as an alarmin to activate the TLR2–MyD88 signal pathway in dendritic cells and enhances Th2 immune responses. *J. Exp. Med.* 205, 79–90. doi:10.1084/jem.20062027.

Yu, G., Wang, L.-G., Han, Y., and He, Q.-Y. (2012). clusterProfiler: an R Package for Comparing Biological Themes Among Gene Clusters. *Omi. A J. Integr. Biol.* 16, 284–287. doi:10.1089/omi.2011.0118.

Zhang, J., Rosenberg, H. F., and Nei, M. (1998). Positive Darwinian selection after gene duplication in primate ribonuclease genes. *Proc. Natl. Acad. Sci. U. S. A.* 95, 3708–3713. doi:10.1073/pnas.95.7.3708.

Zhang, X., Cozen, A. E., Liu, Y., Chen, Q., and Lowe, T. M. (2016). Small RNA Modifications: Integral to Function and Disease. *Trends Mol. Med.* 22, 1025–1034. doi:10.1016/J.MOLMED.2016.10.009.

Zhou, G., Soufan, O., Ewald, J., Hancock, R. E. W., Basu, N., and Xia, J. (2019). NetworkAnalyst 3.0: a visual analytics platform for comprehensive gene expression profiling and meta-analysis. *Nucleic Acids Res.* doi:10.1093/nar/gkz240.

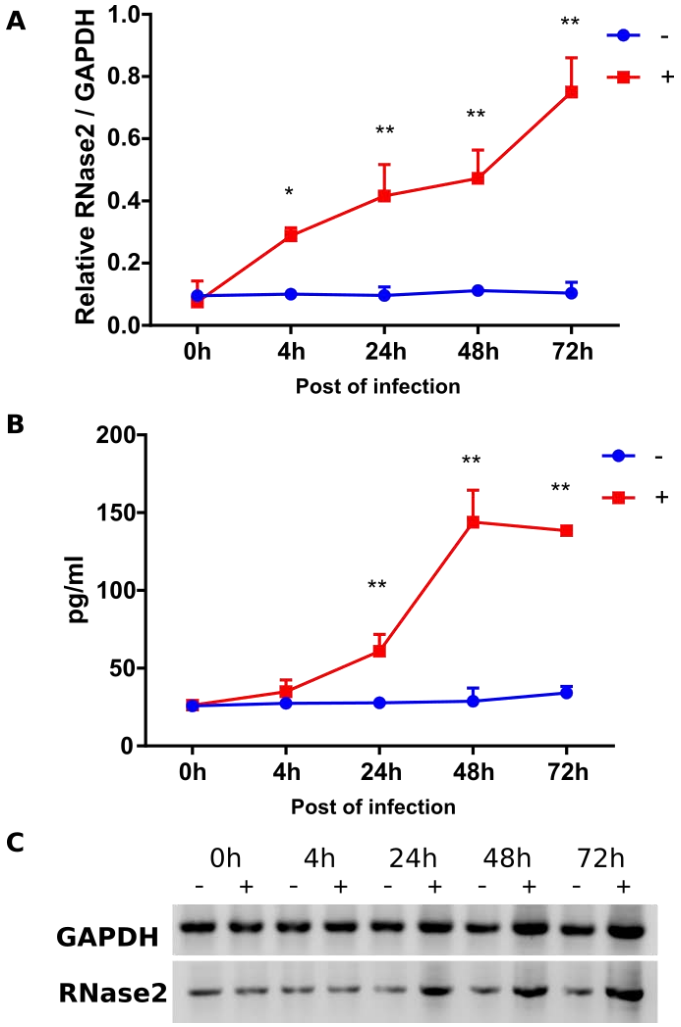

Figure 1. RSV infection activates the expression of RNase2 in THP1 induced macrophages. 10^6 THP1 cells were seeded in 6-well tissue culture plate per well and induced by 50 nM of PMA treatment. After induction, macrophages with infected with RSV under MOI=1 for 2h and then cells were washed and replaced with fresh RPMI+10%FBS (0h time point post of infection). At each time point post of infection, the supernatant and cells were collected to quantify the expression of RNase2. **(A)**. qPCR detection of relative expression of *RNase2* gene; **(B)**. Secreted RNase2 in culture supernatant was measured by ELISA and normalized with alive cell number, Significance was indicated as "*" $p < 0.05$, "**" $p < 0.01$. **(C)**. The intracellular RNase2 protein in macrophage was detected by WB. "+" and "-" indicate with or without RSV infection, respectively.

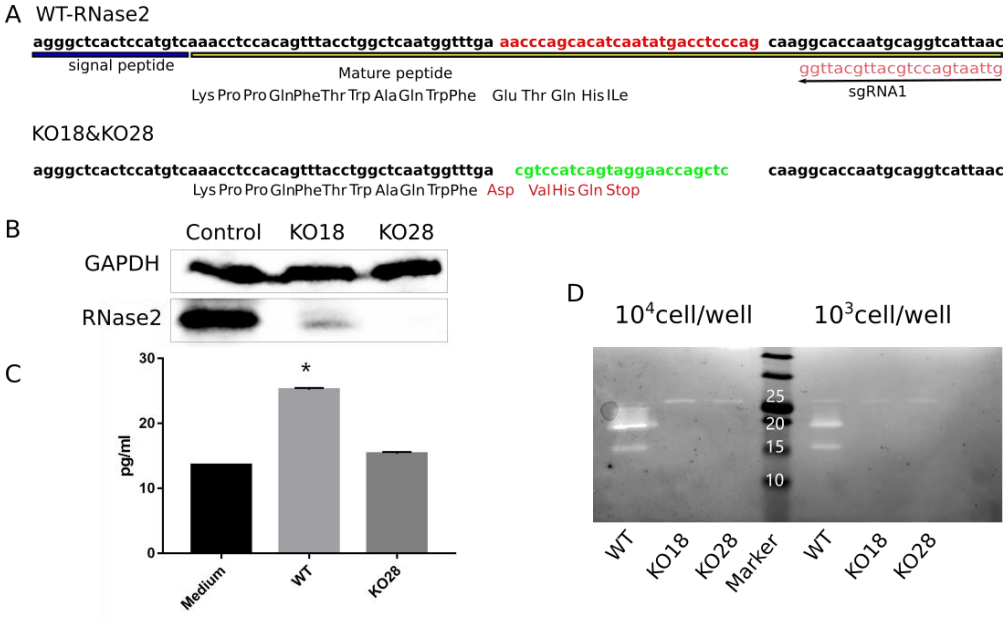

Figure 2. CRISPR/Cas9 mediated knock out of *RNase2* gene in THP1 derived macrophages. (A). Schematic of the mutation of *RNase2* caused by sgRNA1, the sequence if validated by Sanger sequencing; a replacement happened, where the deep red labeled sequence in wild type was replaced by the green labeled sequence, resulting in the coding frame change; **(B)**. Western blot assay was applied to detect the RNase2 protein; **(C)**. The secreted RNase2 in supernatant was measured by ELISA, the RPMI+10%FBS complete culture medium was used as a negative control, all the supernatant was concentrated 50 times; **(D)**. Ribonuclease activity staining assay was used to confirm the removal of functional ribonuclease protein. Cells were collected and resuspended in water and sonicated, cell lysates were loaded in each well at the indicated quantity. Significance was indicated as "*" $p < 0.05$.

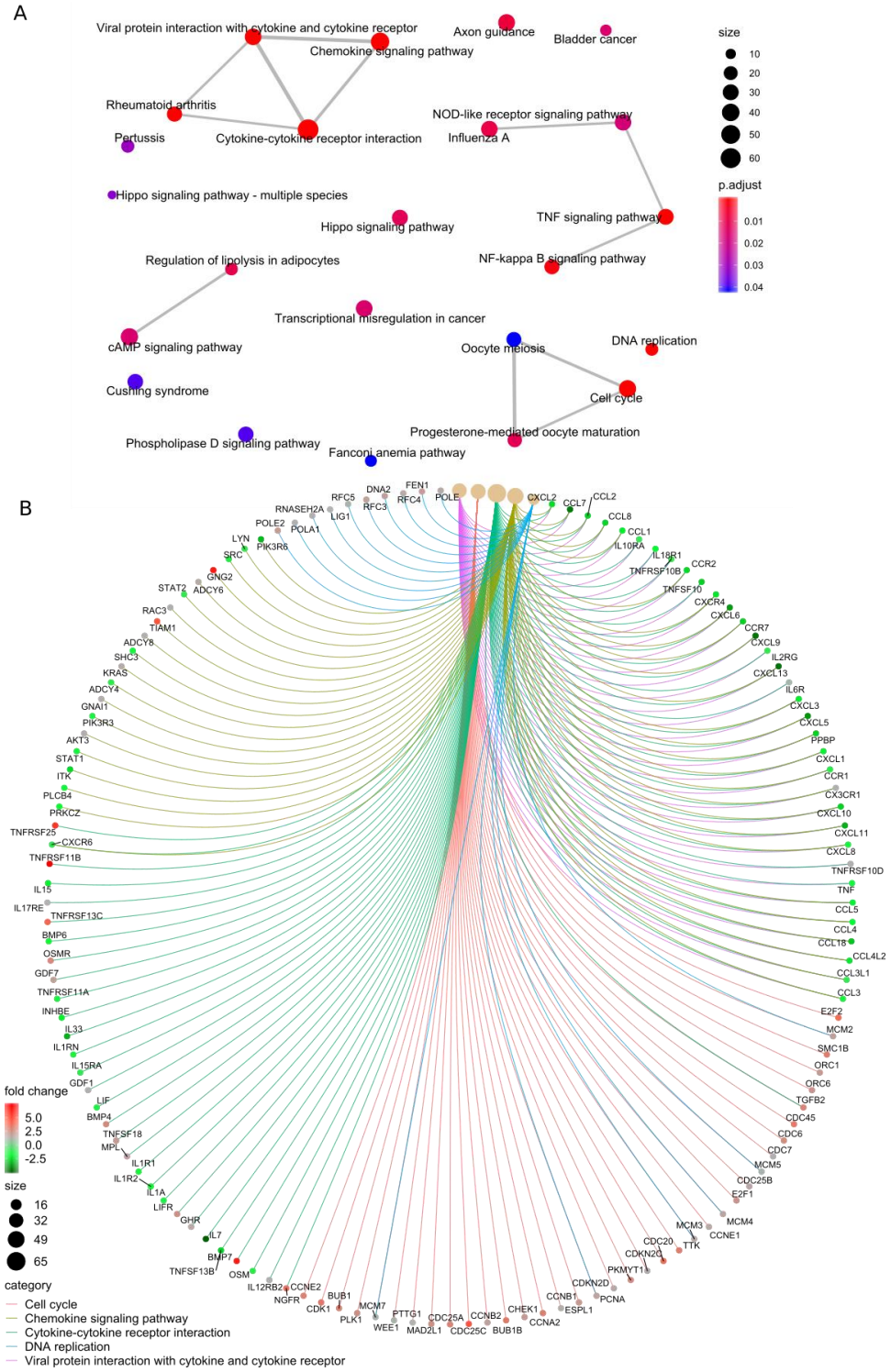

Figure 3. KEGG pathway enrichment analysis. (A). Enrichment map of significant pathways. The DEGs identified from differential expressed gene analysis were applied to KEGG enrichment, p.adj<0.05 was set as the cut-off. Each circle represents one pathway, and pathways shared DEGs were connected with lines, the color indicates the significance and the size of circle indicates the number of DEGs enriched in the specific pathway; **(B)**. Top 5 most significant pathways (labeled with different size of circles, in brown color) were chosen to illustrate in more detail the DEGs, the individual DEG was shown in small colorful circle (the fold change of DEGs, Red, up-regulated; Green, down-regulated).

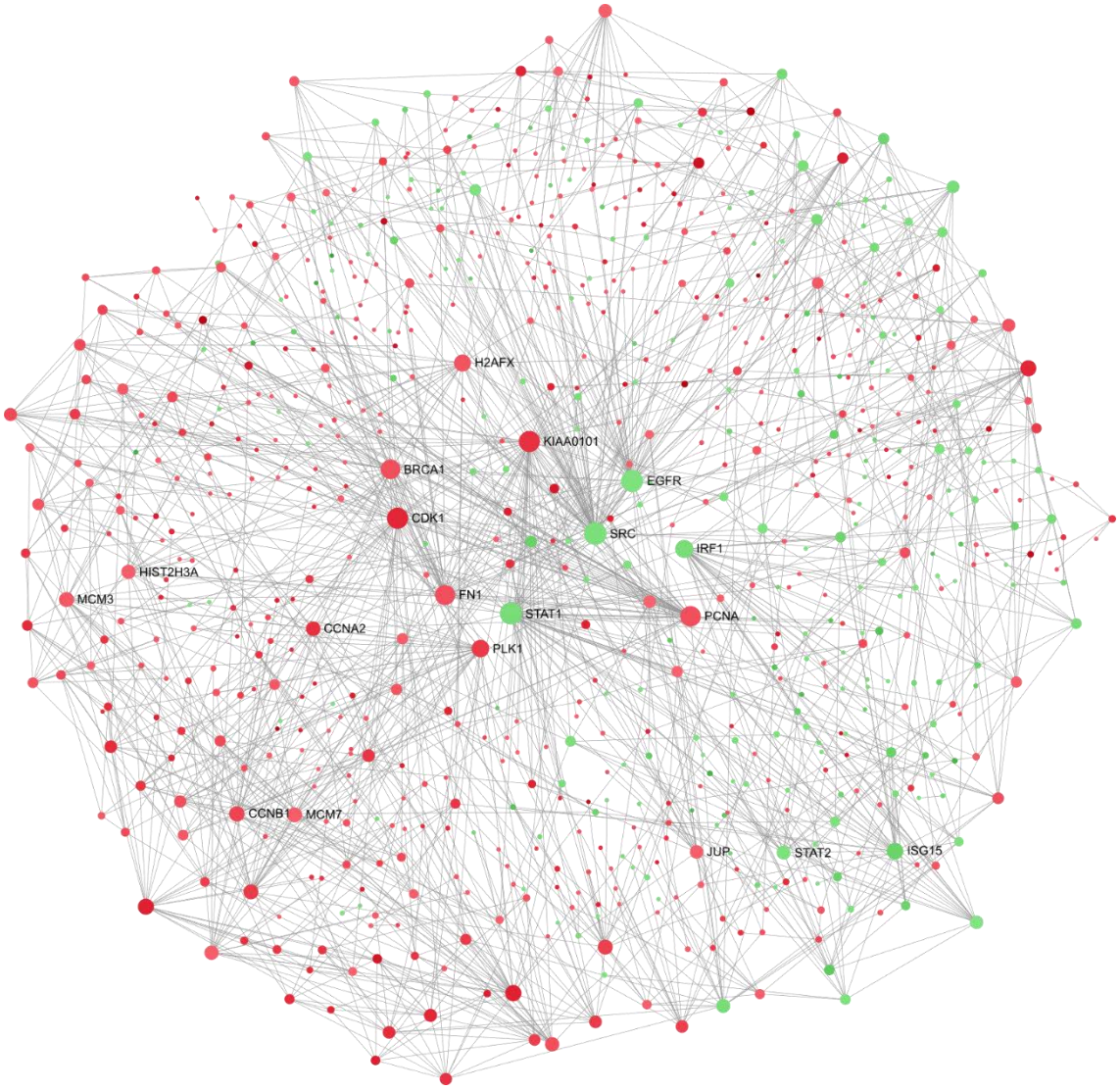

Figure 4. Protein-protein interaction analysis of the DEGs. The DEGs identified by comparing the transcriptome of macrophages (wild-type and RNase2 knockout) was applied to NetworkAnalyst 3.0 tool. Each circle represents one DEG annotated protein, and the line represents the protein-protein interaction. The up regulated DEGs and down regulated DEGs were colored in red and green, respectively. The genes with higher scores by calculating the betweenness and centrality were identified as hub genes and the top rated were labeled with their protein name.

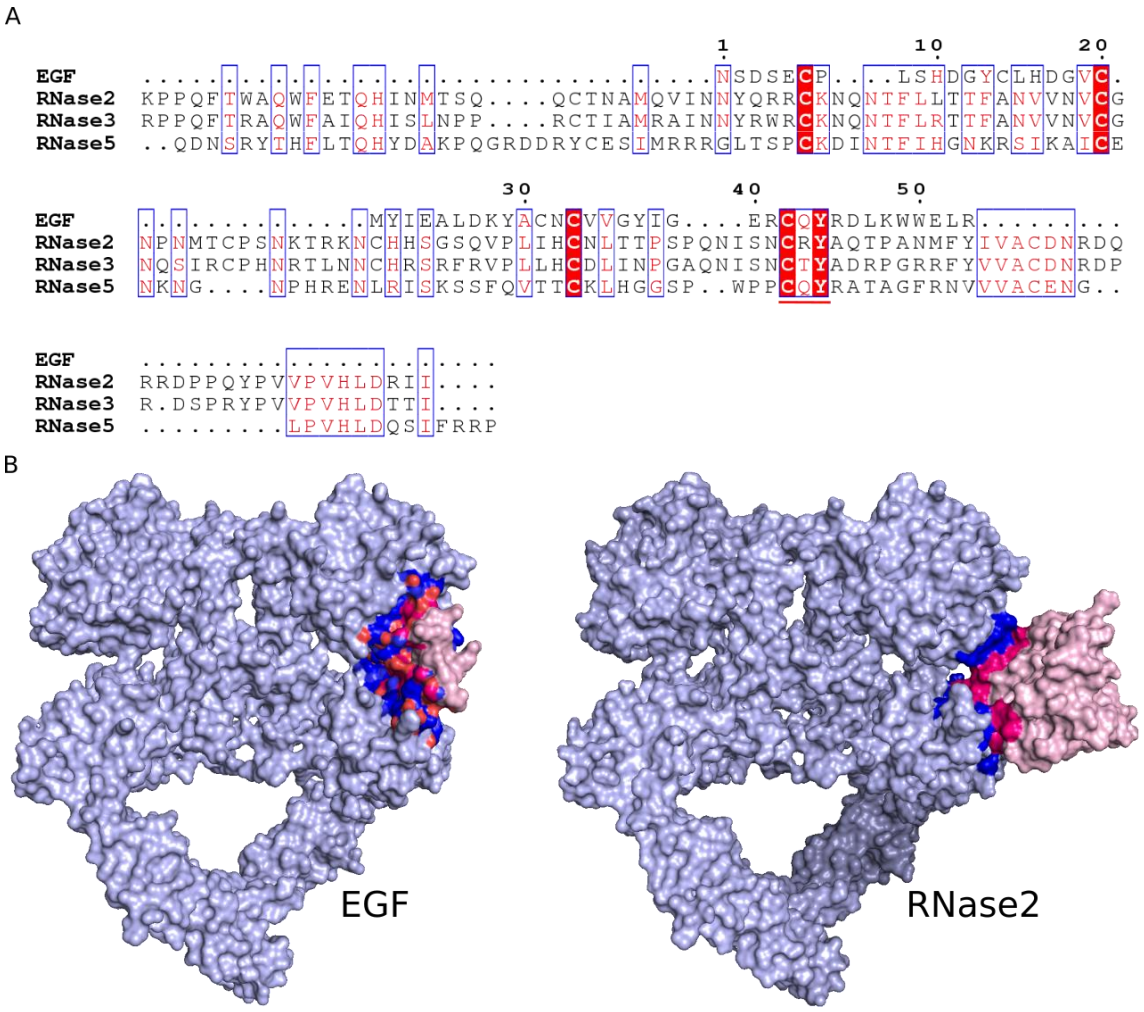

Figure 5. Comparison of the interaction of EGFR with RNase2 and EGF by molecular modeling. (A). Primary sequence alignment of EGF, RNase2, RNase3 and RNase5. The conserved interaction region (CQYRD) is underlined. **(B)**. Representative binding of EGFR with EGF and RNase2. The crystal complex of EGFR with EGF (PDB ID: 3NJP) is depicted. EGFR is colored in grey, the ligands were colored in pink, the interacted residues from EGFR and the ligands were colored in blue and red, respectively.

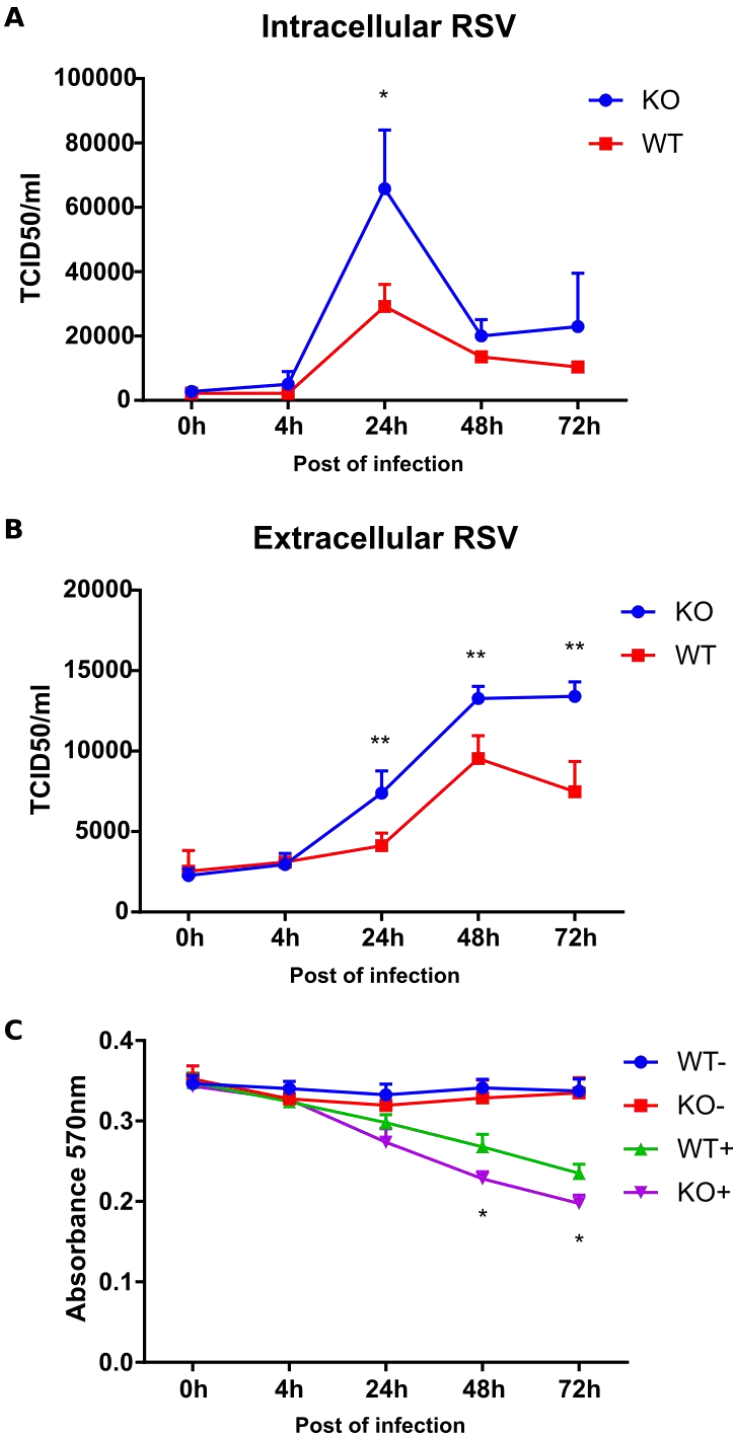

Figure 6. Knocking out of RNase2 resulted in macrophages suffering heavier RSV burden and more cell death. The intracellular **(A)** and extracellular **(B)** RSV was quantified by probe qPCR. **(C)**. MTT assay was applied to monitor the proliferation of macrophages, the star indicates the significance between KO+ and WT+. "+" and "-" indicate with or without RSV infection, respectively. Significance was indicated as "*" $p < 0.05$, "**" $p < 0.01$.

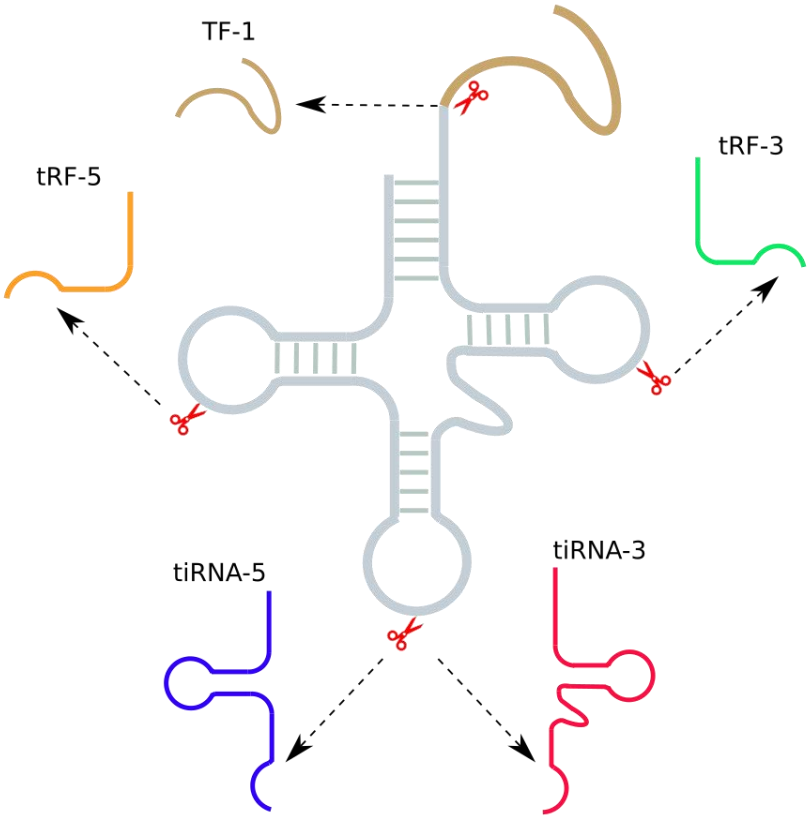

Figure 7. Scheme of identified cleavage of tRNA by RNase2. The cleavage sites are indicated by red scissors.

Table 1. Free energy of the complex and residues involved in direct interaction.

	ΔG (kcal/mol)	Kd (M) at 25º C
EGF	-11.8	$2.3 \cdot 10^{-9}$
RNase2	-9.9	$5.5 \cdot 10^{-8}$

Table 2. tRNA fragment population changes upon RNase2 knockout and/or RSV infection. 185 tRNA fragments from four groups (WT, wild-type macrophage; KO, RNase2-knockout macrophage; WT+RSV, WT macrophage infected RSV; KO+RSV, KO macrophage infected with RSV) were detected by using nrStar Human tRF&tiRNA PCR Array and compared between each other. P value <0.05 and absolute value of the fold change >2 was set as the significant threshold.

Comparison	Transcript name	p value	Fold change	Type	tRF&tiRNA Precursor
KO vs WT	3'tiR_088_LysCTT (n)	0.008549	-4.11511	3-half	LysCTT (n)
	tiRNA-5033-LysTTT-1	0.010405	-16.544	5-half	LysTTT
	1039	0.018261	-80.5836	tRF-1	ArgCCT
	3002A	0.010849	-8.03351	tRF-3	ProAGG
	5028/29A	0.035238	-2.41112	tRF-5	GluTTC GluTTC
KO+RSV vs WT+RSV	3'tiR_060_MetCAT (n)	0.009106	-3.62243	3-half	MetCAT (n)
	TRF62	0.035978	-2.38937	5-half	MetCAT
	TRF315	0.018585	-3.28841	5-half	LysCTT
	TRF353	0.024323	-3.8968	5-half	GlnTTG
	TRF419	0.021386	-2.15623	5-half	LeuTAG
	tiRNA-5030-LysCTT-2	0.03224	-2.93952	5-half	LysCTT
	tiRNA-5031-HisGTG-1	0.034538	-2.78883	5-half	HisGTG
	tiRNA-5031-GluCTC-1	0.015486	-3.05342	5-half	GluCTC
	1001	0.047471	-2.92261	tRF-1	SerTGA
	1013	0.048765	-4.36482	tRF-1	AlaCGC
	1039	0.010483	-2.38917	tRF-1	ArgCCT
	3004B	0.001669	-5.38453	tRF-3	GlnTTG
	3006B	0.047336	-2.12999	tRF-3	LysTTT
	3016/18/22B	0.011578	-2.20447	tRF-3	LysCTT MetCAT
	5024A	0.011785	-3.8361	tRF-5	LeuTAA
	5032A	0.03463	-2.42302	tRF-5	AspGTC
	TRF356/359	0.039843	-3.63021	tRF-5	ArgTCG

					ArgTCG
	TRF366	0.028509	-2.84655	tRF-5	ThrTGT
	TRF365	0.025314	-7.96473	tRF-5	ThrTGT
	TRF396	0.046282	-2.39119	tRF-5	AlaAGC
	TRF457	0.042069	-4.42785	tRF-5	SerAGA
	TRF550/551	0.039843	-4.83758	tRF-5	GluTTC GluCTC
RSV vs WT	tiRNA-5034-ValCAC-3	0.006083	5.48561	5-half	ValCAC
	tiRNA-5029-ProAGG	0.034864	2.19859	5-half	ProAGG
	TRF354	0.012413	2.97669	tRF-5	ThrTGT
	TRF374	0.019808	25.9252	tRF-5	ThrCGT

Supplementary Information

for

RNase2 antiviral activity against human respiratory syncitial virus through macrophage immunomodulation and targeting of tRNA

Lu Lu[1], Ranlei Wei[2], Maria Goetz-Antico[1], Pablo Fernandez-Millan[1], Ester Boix[1#]

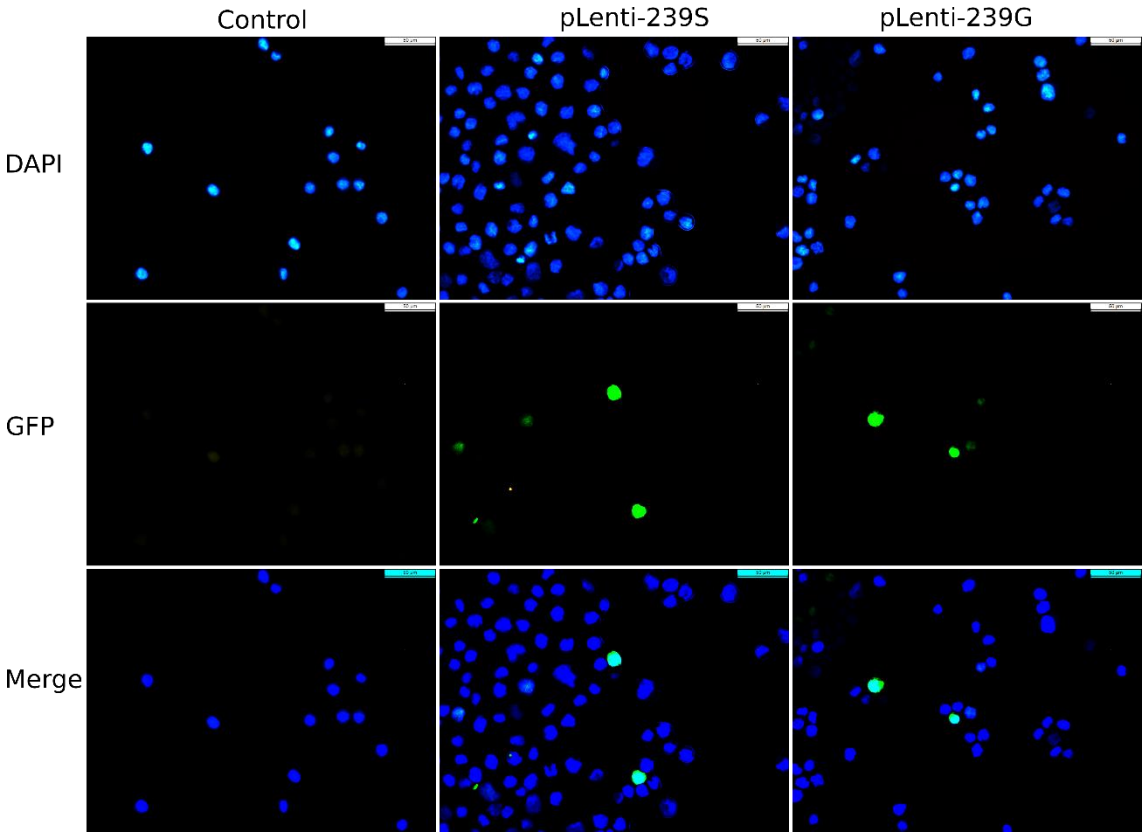

Figure S1. Representative image of THP1 cells tranduced by CRISPR lentiviral. 1x10^6 of THP1 cells were resuspended in 2mL of RPMI+10%FBS and incubated in 37 ℃ at 5% CO_2 for 2h before the transduction. 20 µl of the concentrated virus and 8 ug/mL polybrene were added into THP1 culture in 6-well plate. After overnight's culture, the medium was changed with fresh medium and the cells were continually grown. After 72h post of the infection, the cell samples were fixed by 4% paraformaldehyde and dyed with DAPI and the fluorescence images were captured using Olympus BX50 fluorescence microscopy. The GFP positive cells were calculated to evaluate the transduction efficiency of lentiviral with THP1 cells from 15 randomly chosen images.

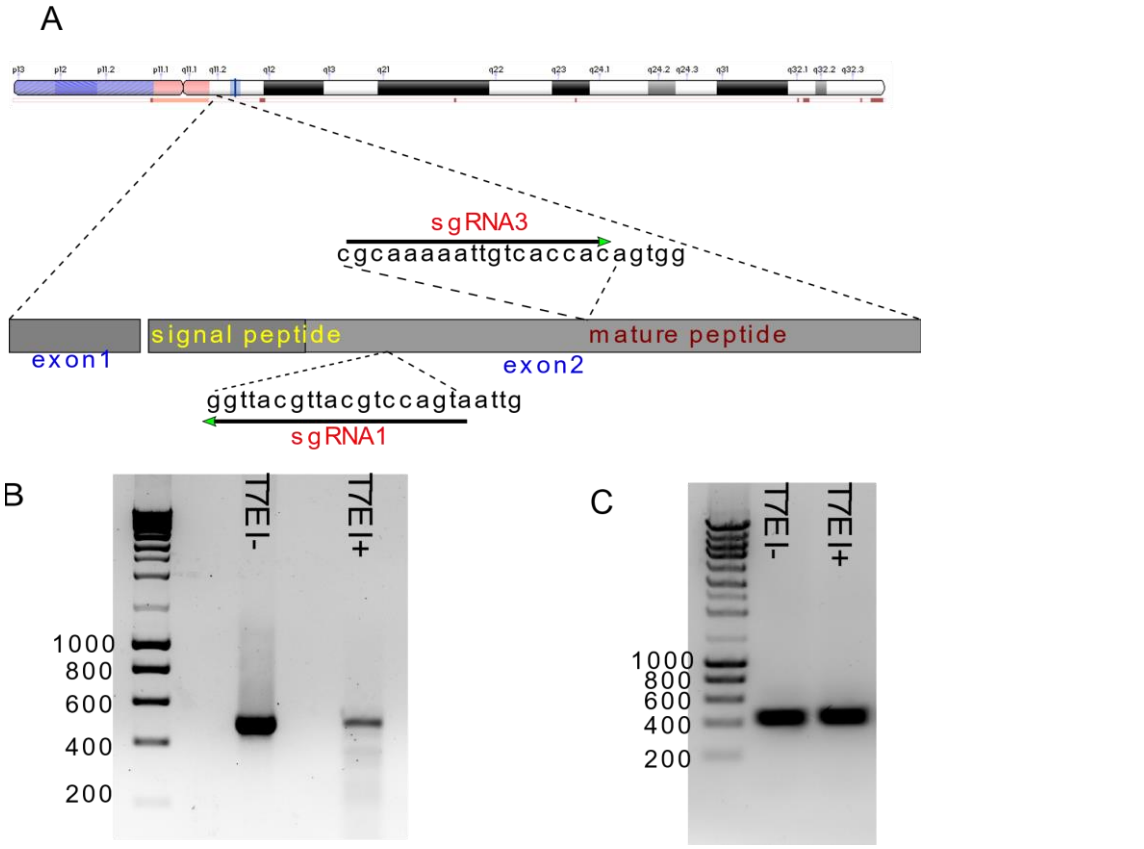

Figure S2. Evaluation of the knockout efficiency of sgRNA1-6 targeting the AAVS1 locus in HeLa cells. (A). Schematic of sgRNA1&3 designed to target the RNase2 locus; **(B)** and **(C)** Detection of the knockout efficiency of sgRNA1 and sgRNA3 using a T7E I assay, respectively. Amplicons of sgRNA1&3 that were treated with T7E I (T7E I+) or without T7E I (T7E I+) were separated by 2% agarose gel electrophoresis. DSB sites were recognized and digested by T7E I. Undigested and digested bands were consistent with the predicted sizes from the RNase2 locus.

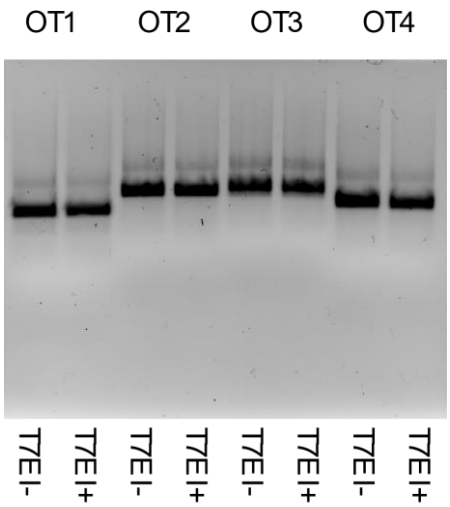

Figure S3. Analysis of the potential off-target effects of sgRNA1. The sgRNA1 mediated off-target sites OT1-4 were predicted and analysed by T7EI assays.

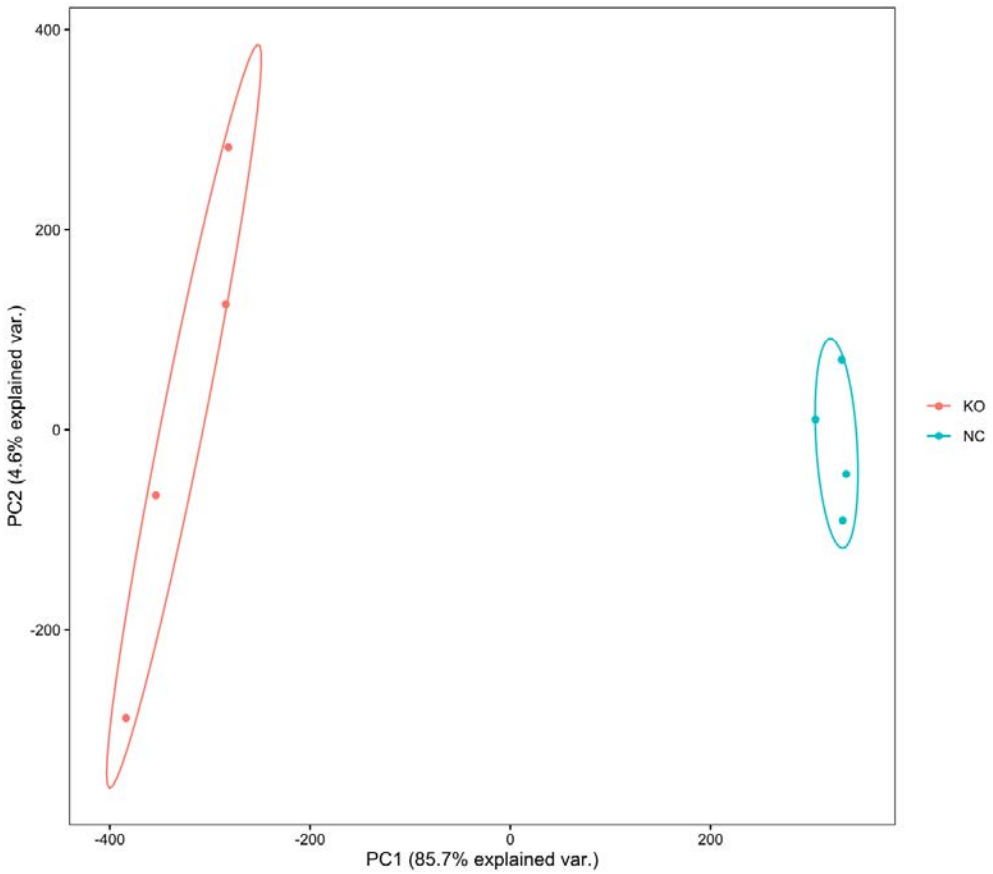

Figure S4. PCA plot. NC, wild-type THP1 macrophage; KO, RNase2 knockout THP1 macrophage.

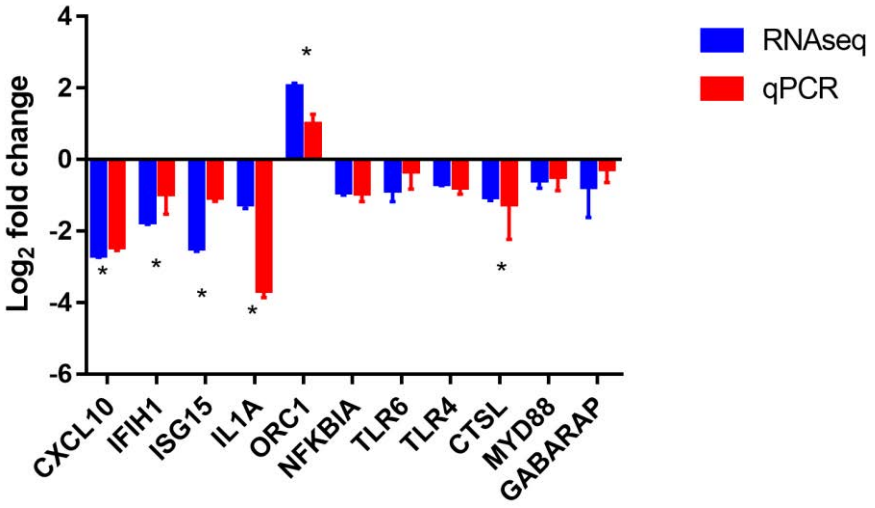

Figure S5. Comparison of gene expression between RNAseq and qPCR.

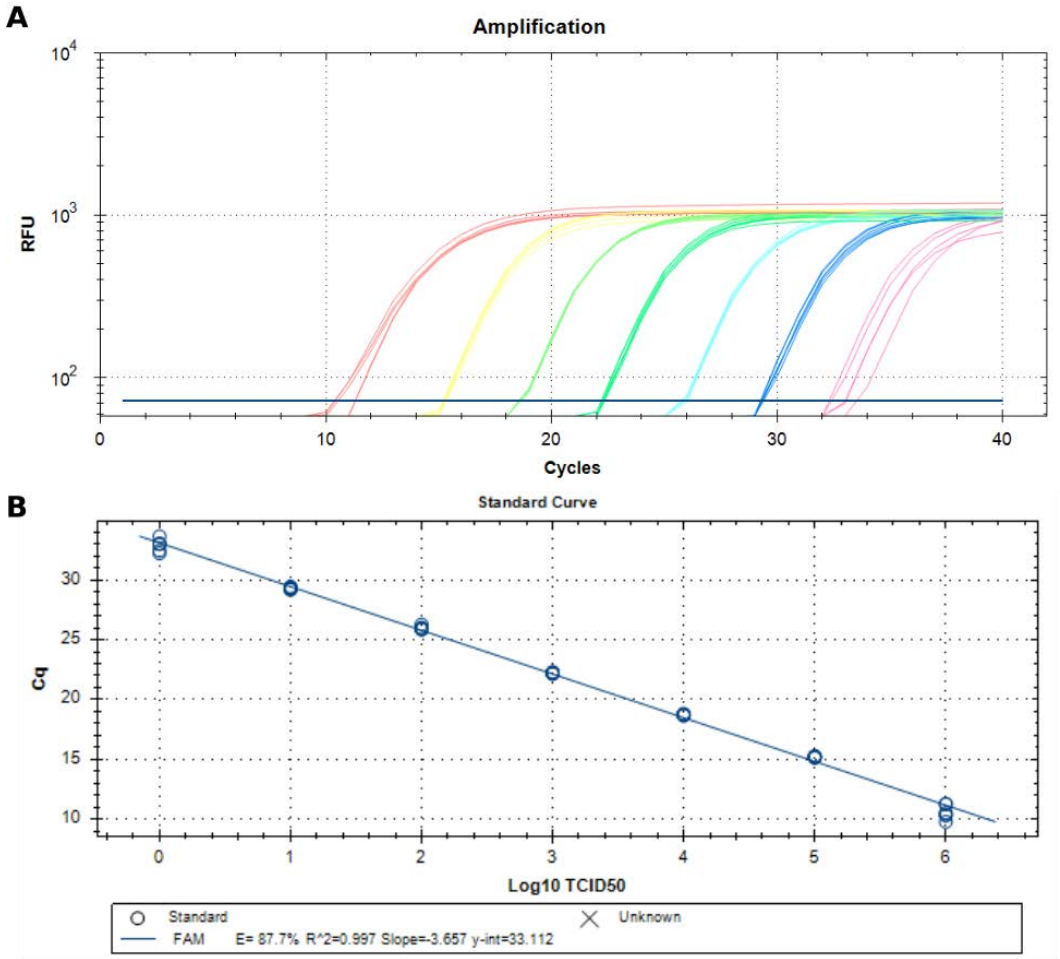

Figure S6. Standard curve of RSV quantification by probe qPCR.

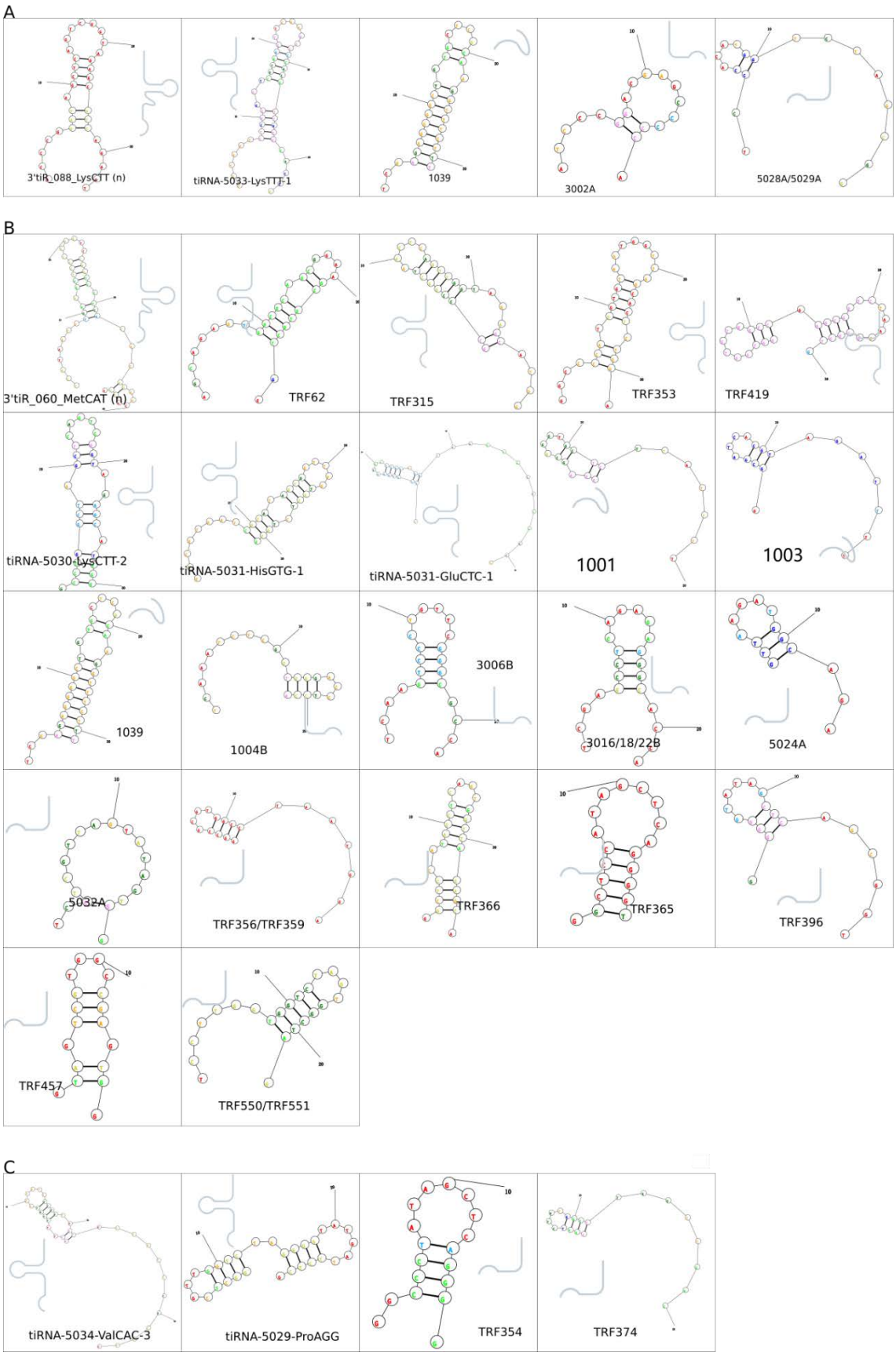

Figure S7. Secondary structure prediction of the tRNA fragments. The tRNA fragment type is indicated on the side. The secondary structure of the significantly expressed tRNA fragments were predicted using RNAstructure online tool

(https://rna.urmc.rochester.edu/RNAstructureWeb/Servers/Predict1/Predict1.html). **(A)**. The significantly differential expressed tRNA fragments comparing RNase2-knockout macrophage cells with wild-type cells; **(B)**. The significantly differential expressed tRNA fragments comparing RNase2-knockout macrophage cells with wild-type cells under RSV infection condition; **(C)**. The significantly differential expressed tRNA fragments comparing wild-type macrophage cells infected with RSV with wild-type macrophage cells without RSV infection.

Table S1. Primers used for PCR.

Name	Sequences
Short-Fw	CCACCGGGTCTTCGAAGACTGTTTG
Short-Rv	CATGGGTGGCCCAGAACCTTCTGACAAACGATC
Cherry-Kosak-AgeI	TATAACCGGTGCCACCATGGTGAGCAAGGGCGAGGA
Cherry-BamHI	ATAAGGATCCCTTGTACAGCTCGTCCATGC
GFP-BsrGI	ATATTGTACAGAGGGCAGAGGAAGTCTGCT
GFP-EcoRI	TTAGAATTCTTACAGCTCGTCCATGCCGAGAG
RSV-A-Fw	CTCAATTTCCTCACTTCTCCAGTGT
RSV-A-Rv	CTTGATTCCTCGGTGTACCTCTGT
RSV-A-Probe	TCCCATTATGCCTAGGCCAGCAGCA

The fluorogenic probe was labeled with 6-carboxyfluorescein (FAM) and 6-carboxytetramethylrhodamine (TAMRA).

Table S2. Oligos of the sgRNAs, and primers for PCRs

Target name	Sequence	
SgRNA1	GTTAATGACCTGCATTGCATTGG	
sgRNA3	CGCAAAAATTGTCACCACAGTGG	
Off-target name		Chromosome location
OT-1	GTTAATGACCTGCATTGCATTGG	chr10:116445782-116445804:+
OT-2	CTTAATGATATGCATTGCAT AGG	chr4:95875569-95875591:-
OT-3	GATAATGAGATACATTGCAT TGG	chr2:211644633-211644655:+
OT-4	TTTTATGACCTGTATAGCAT AGG	chr6:22605178-22605200:+
PCR primers		
sgRNA-x-Fw	TCTTCTGTTGGGGCTTCTGGCTG	482
sgRNA-x-Rv	GATGAGTGATGATGAGGAGTGCT	
sgRNA3-Fw	TCTTCTGTTGGGGCTTCTGGCTG	482
sgRNA3-Rv	GATGAGTGATGATGAGGAGTGCT	
OT1-Fw	TCAGGGGCTAAAATAGGGTGC	107
OT1-Rv	TATTGGATTGCCTGCTCCCC	
OT2-Fw	ACAAACTCTGCAGCTTTGGC	123
OT2-Rv	TCTATGTAAACAGAGTCTTTGGCA	
OT3-Fw	AGGGGCTTGACTCAGAGAGT	129
OT3-Rv	GGCATGCATCCATTGAGCTG	
OT4-Fw	TCCATGTAATCTGCCAGCCA	115
OT4-Rv	AATTGGGTGGCTGAGGTGAC	
Sequencing primers		
U6-seq	GAGGGCCTATTCCCATGATT	
Fw-seq	GCTTCTTCTGTTGGGGCTTC	
Rv-seq	TCAACGACGAGACCCTCCAC	
qPCR primers		
CXCL10-Fw	GCCATTCTGATTTGCTGCCT	
CXCL10-Rv	GCAGGTACAGCGTACAGTTCT	

IFIH1-Fw	GCATATGCGCTTTCCCAGTG	
IFIH1-Rv	CTCTCATCAGCTCTGGCTCG	
ISG15-Fw	GCGCAGATCACCCAGAAGAT	
ISG15-Rv	GTTCGTCGCATTTGTCCACC	
IL1A-Fw	TGAGCTCGCCAGTGAAATGA	
IL1A-Rv	AACACGCAGGACAGGTACAG	
ORC1-Fw	AAGCTTTGGAGCCGGCCAT	
ORC1-Rv	TGATCTCCGAGAAGGCCACT	
TAB2-Fw	TACGAATGGCCCAAGGAAGC	
TAB2-Rv	CACAGCAGGCATCCAGGTTA	
NFKBIA-Fw	TGTGCTTCGAGTGACTGACC	
NFKBIA-Rv	TCACCCCACATCACTGAACG	
TLR6-Fw	GCAGGGGACAATCCATTCCA	
TLR6-Rv	AGAATCAGGCCAGCCCTCTA	
TLR4-Fw	TGCCGTTTTATCACGGAGGT	
TLR4-Rv	GGGCTAAACTCTGGATGGGG	
CTSL-Fw	CTGCTGGCCTTGAGGTTTTA	
CTSL-Rv	GCAGCCTTCATTGCCTTGAG	
MYD88-Fw	ACCCAGCATTGGTGCCG	
MYD88-Rv	GGTTGGTGTAGTCGCAGACA	
GABARAP-Fw	CTCCCTTATTCAGGACCGGC	
GABARAP-Rv	TGCCAACTCCACCATTACCC	

Table S3. Predicted cleavage sites of the tRNA.

Transcript name	Type	Identified sequence in tiRNA&tRF library	Remaining sequence from parental tRNAsequence	Predicted cleavage site[1]
3'tiR_088_LysCTT (n)	3-half	CUUAAUCUCAGGGUCGUGGGUUCGAGCCCCACGUUGGGCGCCA	GCCCGGCUAGCUCAGUCGGUAGAGCAUGGGACU	GGA(CU↓CUU)AA
tiRNA-5033-LysTTT-1	5-half	GCCCGGAUAGCUCAGUCGGUAGAGCAUCAGACU	UUUAAUCUGAGGGUCCAGGGUUCAAGUCCCUGUUCGGGCG	AGA(CU↓UUUAA)
1039	tRF-1	UCGAGAGGGGCUGUGCUCGCAAGGUUUCUUU		
3002A	tRF-3	AUCCCGGACGAGCCCCCA	GGCUCGUUGGUCUAGGGGUGUGGUUCUCGCUUAGGGCGGGAGACCCAAGAGGUCCCGGGUUCAA	(UUCAA↓AU)CCC
5028/29A	tRF-5	UCCCACAUGGUCUAGCGG	UUAGGAUUCCUGGUUUUCACCCAGGUGGCCCGGGUUCGACUCCCGGUAUGGGAA	(AGCGG↓UUA)GG
3'tiR_060_MetCAT (n)	3-half	UCAUAAUCUGAAGGUCGUGAGUUCGAUCCUCACACGGGGCACCA	GCCCUCUUAGUGCAGCUGGCAGCGCGUCAGUU	CAG(UU↓UCAUAAU)
TRF62	5-half	AGCAGAGUGGCGCAGCGGAAGCGUGCUGG	GCCCAUAACCCAGAGGUCGAUGGAUCGAAACCAUCCUCUGCUA	GCUGG↓G(CCCAUAA)
TRF315	5-half	GCCCGGCUAGCUCAGUCGGUAGAGCAUGG	GACUCUUAAUCUCAGGGUCGUGGGUUCGAGCCCCACGUUGGGCG	CAUGG↓GA(CUCUUAA)
TRF353	5-half	GGCCCCAUGGUGUAAUGGUUAGCACUCUGGA	CUUUGAAUCCAGCAAUCCGAGUUCGAAUCUCGGUGGGACCU	CUGGA↓(CUUUGAA)
TRF419	5-half	GGUAGUGUGGCCGAGCGGUCU	GAUUUAGGCUCCAGUCUCUUCGGAGGCGUGGGUU	CGCUG↓GA(UU

		AAGGCGCUG	CGAAUCCCACCGCUGCCA	UAGGC)
tiRNA-5030-LysCTT-2	5-half	GCCCGGCUAGCUCAGUCGGUAGAGCAUGGG	ACUCUUAAUCUCAGGGUCGUGGGUUCGAGCCCCACGUUGGGCG	AUGGG↓A(CUCUUAA)
tiRNA-5031-HisGTG-1	5-half	GCCGUGAUCGUAUAGUGGUUAGUACUCUGCG	UUGUGGCCGCAGCAACCUCGGUUCGAAUCCGAGUCACGGCA	CUGCG↓(UUGUGGC)
tiRNA-5031-GluCTC-1	5-half	UCCCUGGUGGUCUAGUGGUUAGGAUUCGGCG	CUCUCACCGCCGCGGCCCGGGUUCGAUUCCCGGUCAGGAAA CUCUCACCGCCGCGGCCCGGGUUCGAUUCCCGGUCAGGGAA	CGGCG↓(CUCUCAC)
1001	tRF-1	GAAGCGGGUGCUCUUAUUUU		
1013	tRF-1	GGCGAUCACGUAGAUUUU		
1039	tRF-1	UCGAGAGGGGCUGUGCUCGCAAGGUUUCUUU		
3004B	tRF-3	UCAAAUCUCGGUGGGACCUCCA	GGCCCCAUGGUGUAAUGGUUAGCACUCUGGACUUUGAAUCCAGCGAUCCGAGU GGUCCCAUGGUGUAAUGGUUAGCACUCUGGACUUUGAAUCCAGCGAUCCGAGU	CGAGU↓(UCAAAU)
3006B	tRF-3	UCAAGUCCCUGUUCGGGCGCCA	GCCCGGAUAGCUCAGUCGGUAGAGCAUCAGACUUUUAAUCUGAGGGUCCGGGGU GCCCGGAUAGCUCAGUCGGUAGAGCAUCAGACUUUUAAUCUGAGGGUCCAGGGU	GGGG(U↓UCAAGU)
3016/18/22B	tRF-3	UCGAGCCCCACGUUGGGCGCCA	GCCCGGCUAGCUCAGUCGGUAGAGCAUGGGACUCUUAAUCUCAGGGUCGUGG	UGGG(U↓UCG

			GU	AGC)
5024A	tRF-5	GUUAAGAUGGCAGA	ACCUGGCAGUUUCAUAAAACUUAAAGUUUAUAAUCAGAGGUUCAACUCCUCUUCUUAACA GCCCGGUAAUCGCAUAAAACUUAAAACUUUACAGUCAGAGGUUCAAGUCCUCUUCUUAACA	GCAG(A↓ACCUGGCAG) GCAG(A↓GCCCGGUAA)
5032A	tRF-5	UCCUCGUUAGUAUAGUGG	UGAGUGUCCCCGUCUGUCACGCGGGAGACCGGGGUUCGAUUCCCCGACGGGGAG UUAGUAUCCCCGCCUGUCACGCGGGAGACCGGGGUUCAAUUCCCCGACGGGGAG UGAGUAUCCCCGCCUGUCACGCGGGAGACCGGGGUUCGAUUCCCCGACGGGGAG	(AGUGG↓UGA)GU (AGUGG↓UUA)GU
TRF356/359	tRF-5	GGCCGCGUGGCCUAAUGGA	UAAGGCGUCUGACUUCGGAUCAGAAGAUUGCAGGUUCGAGUCCUGCCGCGGUCG	(AAUGGA↓UA)AGG
TRF366	tRF-5	GGCUCCAUAGCUCAGUGGUUAGAGCA	CUGGUCUUGUAAACCAGGGGUCGCGAGUUCGAUCCUCGCUGGGGCCU	(AGUGGUUA)GAGCA↓CUGGU
TRF365	tRF-5	GGCUCCAUAGCUCAGGGGU	UAGAGCGCUGGUCUUGUAAACCAGGGGUCGCGAGUUCAAUUCUCGCUGGGGCCU UAGAGCACUGGUCUUGUAAACCAGGGGUCGCGAGUUCAAAUCUCGCUGGGGCCU	(AGGGGU↓UA)GAG
TRF396	tRF-5	GGGGGUAUAGCUCAGCGGU	AGAGCGCGUGCUUAGCAUGCACGAGGUCCUGGGGUUCAAUCCCCAAUACCUCC	(AGCGGU↓A)GA

			A	GC
TRF457	tRF-5	GUAGUCGUGGCCGAGUGG	UUAAGGCGAUGGACUAGAAAUCCAUUGGGGUUUCCCCACGCAGGUUCGAAUCCUGCCGACUACG	(GAGUGG↓UUAA)G
TRF550/551	tRF-5	UCCUUGGUGGUCUAGUGGCUAGUCCUUGAUGUCUAGUGGUUAG	GAUUCGGCGCUUUCACCGCCGCGGCCCGGGUUCGAUUCCCGGCCAGGGAA GAUUCGGCGCUUUCACCGCCGCGGCCCGGGUUCGAUUCCCGGUCAGGGAA GAUUCGGCGCUUUCACCGCUGCGGCCCGGGUUCGAUUCCCGGUCAGGGAA GAUUUGGUGCUCUCACUGCAGCAGCCUGGGUUCAUUUCUCAGUCAGGGAA	(AGUGGCUA)G↓GAUUC (AGUGGUUA)G↓GAUUC (AGUGGUUA)G↓GAUUU
tiRNA-5034-ValCAC-3	5-half	GUUUCCGUAGUGUAGCGGUUAUCACAUUCGCCUC	ACACGCGAAAGGUCCCCGGUUUGAAACCAGGCGGAAACA ACACGCGAAAGGUCCCCGGUUCGAAACUGGGCGGAAACA ACACGCGAAAGGUCCCCGGUUCGAAACCGGGCGGAAACA ACACGCGUAAAGGUCCCCGGUUCGAAACCGGGCGGAAAACA	GC(CUC↓ACAC)G
tiRNA-5029-ProAGG	5-half	GGCUCGUUGGUCUAGGGGUAUGAUUCUCG	CUUAGGGUGCGAGAGGUCCCGGGUUCAAAUCCCGGACGAGCCC CUUAGGAUGCGAGAGGUCCCGGGUUCAAAUCCCGGACGAGCCC	UCUCG↓C(UUAGGGU)
TRF354	tRF-5	GGCCCUAUAGCUCAGGGG	UUAGAGCACUGGUCUUGUAAACCAGGGGUCGCGAGUUCAAAUCUCGCUGGGGCCU	(AGGGG↓UUA)GA

TRF374	tRF-5	GGCUCUGUGGC UUAGUUGGC	UAAAGCGCCUGUCUCGU AAACAGGAGAUCCUGGG UUCGAAUCCCAGCGGGGC CU	(AGUU GGC↓U A)AAG

[1]the potential cleavage site of the tRNAs are indicated according to the sequences detected in the tiRNA&tRFs library screening. Complementarily, we include in the next column the remaining tRNA sequence from the parental tRNA. The tRNA fragments at the 5' and 3' sides are colored in red and blue, respectively. The cleavage site is marked with an arrow and the corresponding loop region in the parental tRNA is enclosed by parenthesis. See figure S7 for a schematic drawing of the identified fragment and a prediction of the adopted secondary structure.

CHAPTER VI

frontiers in Pharmacology

ORIGINAL RESEARCH
published: 09 October 2019
doi: 10.3389/fphar.2019.01170

Evolutionary Trends in RNA Base Selectivity Within the RNase A Superfamily

*Guillem Prats-Ejarque, Lu Lu, Vivian A. Salazar, Mohammed Moussaoui and Ester Boix**

Department of Biochemistry and Molecular Biology, Faculty of Biosciences, Universitat Autònoma de Barcelona, Barcelona, Spain

There is a growing interest in the pharmaceutical industry to design novel tailored drugs for RNA targeting. The vertebrate-specific RNase A superfamily is nowadays one of the best characterized family of enzymes and comprises proteins involved in host defense with specific cytotoxic and immune-modulatory properties. We observe within the family a structural variability at the substrate-binding site associated to a diversification of biological properties. In this work, we have analyzed the enzyme specificity at the secondary base binding site. Towards this end, we have performed a kinetic characterization of the canonical RNase types together with a molecular dynamic simulation of selected representative family members. The RNases' catalytic activity and binding interactions have been compared using UpA, UpG and UpI dinucleotides. Our results highlight an evolutionary trend from lower to higher order vertebrates towards an enhanced discrimination power of selectivity for adenine respect to guanine at the secondary base binding site (B2). Interestingly, the shift from guanine to adenine preference is achieved in all the studied family members by equivalent residues through distinct interaction modes. We can identify specific polar and charged side chains that selectively interact with donor or acceptor purine groups. Overall, we observe selective bidentate polar and electrostatic interactions: Asn to N1/N6 and N6/N7 adenine groups in mammals versus Glu/Asp and Arg to N1/N2, N1/O6 and O6/N7 guanine groups in non-mammals. In addition, kinetic and molecular dynamics comparative results on UpG versus UpI emphasize the main contribution of Glu/Asp interactions to N1/N2 group for guanine selectivity in lower order vertebrates. A close inspection at the B2 binding pocket also highlights the principal contribution of the protein β6 and L4 loop regions. Significant differences in the orientation and extension of the L4 loop could explain how the same residues can participate in alternative binding modes. The analysis suggests that within the RNase A superfamily an evolution pressure has taken place at the B2 secondary binding site to provide novel substrate-recognition patterns. We are confident that a better knowledge of the enzymes' nucleotide recognition pattern would contribute to identify their physiological substrate and eventually design applied therapies to modulate their biological functions.

Keywords: RNase, RNA, purine, catalysis, molecular dynamics, evolution, RNase A superfamily

OPEN ACCESS

Edited by:
Olga N. Ilinskaya, Kazan Federal University, Russia

Reviewed by:
Arun Malhotra, University of Miami, United States
Vladimir Alexandrovich Mitkevich, Engelhardt Institute of Molecular Biology (RAS), Russia

****Correspondence:***
Ester Boix
Ester.Boix@uab.es

Specialty section:
This article was submitted to Translational Pharmacology, a section of the journal Frontiers in Pharmacology

Received: *16 April 2019*
Accepted: *12 September 2019*
Published: *09 October 2019*

Citation:
Prats-Ejarque G, Lu L, Salazar VA, Moussaoui M and Boix E (2019) Evolutionary Trends in RNA Base Selectivity Within the RNase A Superfamily. Front. Pharmacol. 10:1170. doi: 10.3389/fphar.2019.01170

INTRODUCTION

The interest to solve a biological problem is frequently correlated to its inherent difficulty. When entering the RNA world we are faced with a wide diversity of secondary and tertiary structures. An even higher level of complexity is encountered when trying to identify the rules that guide the RNA binding protein recognition process. During the last decades, many efforts have been applied to unravel the structural determinants for protein RNA recognition (Draper, 1999; Allers and Shamoo, 2001; Draper, 2015; Terribilini et al., 2007). We are currently witnessing significant advances within the RNA field thanks to the novel RNA sequencing methodologies that have laid the path to an RNA-omics era. Nowadays, we have access to many protein-RNA binding predictors (Miao and Westhof, 2016) and the main basic rules that drive the protein–nucleotide interaction process have been identified (Luscombe, 2001; Denessiouk and Johnson, 2003; Morozova et al., 2006; Kondo and Westhof, 2011). The study of RNA cleaving enzymes poses additional complexity. Efficient RNases should first recognize a specific RNA target, and then provide a proper active site configuration to promote catalysis and ensure the proper cleavage of the substrate. A particular pharmacological interest relies on the design of tailored enzymes with specific RNA cleavage targets (Tamkovich et al., 2016). Recent work on RNases' action within a cellular environment is helping to unravel their natural *in vivo* substrates (Honda et al., 2015; Lyons et al., 2017; Mesitov et al., 2017). A proper knowledge of the RNases' active site architecture should lead to the design of specific inhibitors of their biological functions (Chatzileontiadou et al., 2015; Chatzileontiadou et al., 2018).

In this work, we have explored the nucleotide base preference within the vertebrate-specific RNase A superfamily. The bovine pancreatic enzyme RNase A was one of the earliest enzymes to be studied in the 20th century and is still one of the best characterized (Cuchillo et al., 2011). All the family members share a common three-dimensional fold, catalytic triad and mechanism of action on single-stranded RNA. During the last decades, the modular subsite arrangement of RNase A for the recognition of bases, ribose and phosphates has been characterized (Parés et al., 1991; Nogués et al., 1998). The enzyme cleaves the 3′5′ phosphodiester bonds with specificity for pyrimidines at the main anchoring site (B1) and preference for purines at the secondary site (B2) (Richards and Wyckoff, 1971; Raines, 1998). In a previous work, we analyzed the enzyme residues that were reported to participate in the specific binding of adenine (A) and guanine (G) bases at the B2 site among the RNase A superfamily members (Boix et al., 2013). A high evolutionary conservation was observed for B1, whereas a significant variability was visualized for the secondary base selectivity. Interestingly, the observed structural differences at the secondary base site correlate with their substrate specificity and catalytic efficiency (Tarragona-Fiol et al., 1993; Sorrentino, 1998; Boix et al., 2013). Likewise, the analysis of the protein conformational changes induced upon nucleotide binding by NMR and molecular dynamics highlighted an evolutionary trend in base interaction selectivity (Gagné and Doucet, 2013; Narayanan et al., 2017; Narayanan et al., 2018a). Conserved conformational rearrangements upon ligand binding within closely related members suggested a link between shared protein networks and their characteristic biological properties (Narayanan et al., 2018a). The RNase A superfamily includes a series of proteins with antimicrobial and immune-modulatory activities and is considered to have emerged with an ancestral host-defense role (Boix and Nogués, 2007; Rosenberg, 2008; Lu et al., 2018). Family members were classified according to their structural, enzymatic and biological properties into eight canonical types (Sorrentino and Libonati, 1997; Sorrentino, 2010). A better understanding of the structural determinants that govern the RNases' substrate specificity can help us to explain the divergent functionalities within the family.

Here, we have committed ourselves to undertake a comprehensive comparative analysis of representative family members and explore the structural drift that has taken place through evolution to shape the substrate specificity of the secondary base binding site. First, we have performed a kinetic characterization of the first seven human canonical RNases using dinucleotides. Secondly, we have selected representative RNase A superfamily members from lower to higher order vertebrates and have performed molecular dynamics simulations of the protein-dinucleotide complexes.

MATERIALS AND METHODS

Expression and Purification of the Recombinant Proteins

RNase A was purchased from Sigma Aldrich. The cDNA for RNase 1 was a gift from Prof. Maria Vilanova (University of Girona, Spain) and cDNA for RNase 5 was provided by Prof. Demetres Leonidas (University of Thessaly, Greece). RNase 4 synthetic gene was purchased from NZYtech (Lisboa, Portugal) and RNase 6 was obtained from DNA 2.0 (Menlo Park, CA, USA). RNase 2, RNase 3 and RNase 7 genes were obtained as previously described (Torrent et al., 2010). The recombinant proteins were expressed and purified as previously described (Boix, 2001; Prats-Ejarque et al., 2016). Briefly, the gene was cloned into the pET11c expression vector (Novagen), the protein was expressed in *Escherichia coli* BL21(DE3) cells (Novagen) and then purified from inclusion bodies. Finally, the protein was purified by cationic exchange FPLC on a Resource S column (GE Healthcare) and lyophilized. Protein purity was confirmed by SDS-PAGE and mass spectrometry.

Spectrophotometric Kinetic Analysis

UpA, UpG and UpI (Biomers, Söflinger, Germany) were used as substrates, and the kinetic parameters were determined by a spectrophotometric method as described (Boix et al., 1999b). Assays were carried out in 50 mM sodium acetate, 1 mM EDTA, pH 5.5, at 25°C, using 1 cm path length cuvette. Substrate concentration was determined spectrophotometrically using the following extinction coefficients: ε_{260} = 24,600 M^{-1} cm^{-1} for UpA, ε_{261} = 20,600 M^{-1} cm^{-1} for UpG and ε_{260} = 16,400 M^{-1} cm^{-1} for UpI. The activity was measured by following the initial reaction velocities using the difference molar absorbance coefficients, in relation to cleaved phosphodiester bonds during

the transphosphorylation reaction: $\Delta\varepsilon_{286}$ = 570 M^{-1} cm^{-1} for UpA, $\Delta\varepsilon_{280}$ = 480 M^{-1} cm^{-1} for UpG (Imazawa et al., 1968), $\Delta\varepsilon_{280}$ = 316 M^{-1} cm^{-1} for UpI (experimentally determined). Final enzyme concentrations were adjusted depending on the RNase activity for each assayed substrate in a range between 0.005 and 10 μM. The reactions were performed in triplicate with 100 μM of substrate and the activity was normalized at an enzyme/substrate ratio of 1:100.

Molecular Dynamics Simulations

All the molecular dynamics (MD) simulations were performed using GROMACS 2016.2 (Abraham et al., 2015). The force field used was a modification of AMBER99SB (Best and Hummer, 2009). Charges of inosine were derived by R.E.D server (Vanquelef et al., 2011). The modifications of the force field to include inosine parametrization are detailed in the Supplemental Materials (**Figure S1**). All the complexes were centred in a dodecahedral cell with a minimum distance box-solute of 1.0 nm. The unit cell was filled with TIP3P (transferable intermolecular potential 3P) water (Jorgensen et al., 1983) in neutral pH conditions supplemented with 150 mM of NaCl.

Neighbor search was performed using a Verlet cut-off scheme (Páll and Hess, 2013) with a cut-off of 0.9 nm for both Van der Waals and coulombic interactions. For long range interactions, smooth particle mesh of Ewald (PME) (Darden et al., 1993; Essmann et al., 1995) was used with a fourth-order interpolation scheme and 0.1125 nm grid spacing for FFT. The bonds were constrained with the P-LINCS algorithm (Hess, 2008), with an integration time step of 2 fs.

The energy of the systems was minimized using the steepest descendant algorithm and equilibrated in two steps. First, an initial constant volume equilibration (NVT) of 1 ns was performed with a temperature of 300 K using a modified velocity rescaling thermostat (Bussi et al., 2007). Then, 1 ns of constant pressure equilibration (NPT) was run at 1 bar with a Berendsen barostat (Berendsen et al., 1984) at 300 K and the same thermostat. Finally, 100 ns production runs were performed under an NPT ensemble without applying restraints. Three independent simulations in periodic boundary conditions were conducted for each complex. Dinucleotides were generated by modifying the dCpA ligand of an RNase A–d(CpA) complex (Zegers et al., 1994), maintaining the same initial coordinates.

RESULTS

Comparison of Canonical RNases' Catalytic Activity on Dinucleotide Substrates: A Trend From Guanine to Adenine Selectivity At the B2 Secondary Base Site

In an effort to deepen into our knowledge of the evolutionary pressure that has guided the nucleotide base preference within the RNase A superfamily, we have compared the catalytic activity of the human canonical members on dinucleotides (**Figure 1**).

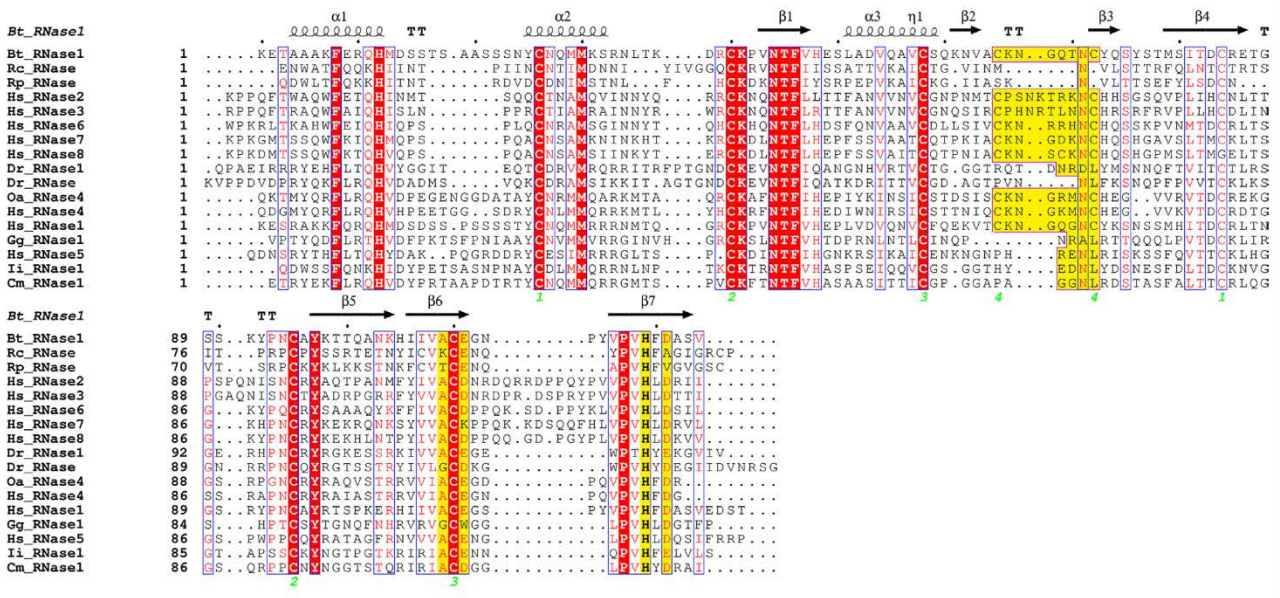

FIGURE 1 | Sequence alignment of the eight canonical human RNases together with the RNase A superfamily members analyzed by molecular dynamics (sequences correspond to mature proteins, without the signal peptide). Protein regions identified to participate in B2 site are highlighted in yellow: L4, spanning from b2 to b3, end of β6 (residues 109 and 111) and one of the two catalytic histidines together with a close by residue at β7 (residues 119 and 121). TT indicates the presence of a β-turn. Dots label every 10 residues of the reference protein used (Bt-RNase 1, known as RNase A). The disulphide bonds are labeled with green numbers. Full species names are included in **Table S1**. Labels are as follows: red box with white character for strict identity; red character for similarity within a group; and character with blue frame for similarity across groups. The alignment was performed using *Clustal Omega* (Sievers and Higgins, 2018), and the picture was drawn using *ESPript* (Robert and Gouet, 2014).

First, each canonical RNase was expressed using a prokaryote recombinant expression system. We successfully expressed and purified with high yield the first seven human canonical RNases using the T7 promotor and the pET expression system. Unfortunately, using the same prokaryote expression system we were unable to obtain a properly folded and catalytically active human RNase 8. In fact, inspection of the RNase 8 coding transcript by Rosenberg and co-workers revealed an unusual gene organization and protein disulphide pairing, suggesting a significant functional divergence from the canonical characteristic structure of the family (Chan et al., 2012). The authors do not discard the possibility that RNase 8 is not expressed as a standard secretory RNase. Therefore, we decided to perform our kinetic study using the first seven human canonical RNases. This is the first simultaneous comparison of the catalytic activity of all seven proteins within a single laboratory.

The catalytic activity of the RNases was assayed using dinucleotide substrates, where the first pyrimidine was kept invariable as a uridine and the secondary base was substituted by the natural standard purines and the modified base inosine. Together with the two natural purines incorporated in RNA during transcription, we have also selected inosine, a modified base frequently present in cellular RNA, as one of the main post-transcriptional modifications. Kinetic activity on UpA, UpG and UpI was measured by a spectrophotometric assay and the relative preference for the secondary base was estimated for each protein. Bovine pancreatic RNase A was taken as a reference control.

Interestingly, the respective catalytic activities of the seven human canonical RNases indicate a shift of the secondary base specificity, from a poor A/G discrimination to a pronounced preference for A (**Table 1**). In particular, the human RNase 5, which is the canonical member more closely related to ancestral RNases (Sorrentino, 2010), shows only a mild preference for adenine over guanine. In turn, the pancreatic-type RNase 1 shows a significant preference for adenine at B2 position. Last, the more evolved RNase subgroups (types 2/3 and 6/7) do not have any detectable activity using UpG as a substrate (**Table 1**, **Figure 2**).

On the other hand, when we analyze the kinetic characterization of other family members available in the literature, we can infer a shift at the substrate secondary base predilection, from lower to higher order vertebrates, from guanine to adenine (Boix et al., 2013). Basically, the characterized fish, amphibian and reptile RNases show a marked preference for G at B2 site (Hsu et al., 2003; Ardelt et al., 2008), while mammalian prefer A (Richards and Wyckoff, 1971; Zhao et al., 1998; Prats-Ejarque et al., 2016). We can group the family members, according to their relative activity on dinucleotide substrates, within three main subcategories by their base preference at the B2 site: G > A, G ~ A and A > G (**Figure 2**). The results suggest that an evolutionary pressure has taken place to promote selectivity for the adenine base within the family's more recently evolved members, coming from an ancestral precursor with a marked preference for guanine.

Last, we have studied the RNases' activity on UpI dinucleotides. Inosine (I) was selected as an appropriate model to inspect the particular effect of the presence of a C=O group at the purine C6 atom and the influence of the NH_2 group at the C2 position, in comparison to the other two purine base structures. Detectable activity for the inosine dinucleotide was mainly registered for the RNases 1, 2, 4 and 5 (**Table 1**). Overall, kinetic results indicate that no important differences are observed between the proteins' enzymatic activity on UpG and UpI, although a slight preference for I over G is shown. Interestingly, the family members that have a closer relationship to lower order vertebrates (RNases 1, 4 and 5) present a significant activity against dinucleotides with inosine at the B2 position, but no detectable activity in the presence of a guanine. The results suggest that A/G discrimination within the RNase A superfamily relies partly in the recognition of N1/N2 group.

B2 Base Selectivity Within the RNase A Superfamily by Molecular Dynamics

Following, to complement the enzymatic characterization of the canonical RNases, we performed a comparative analysis within the RNase A superfamily by molecular dynamics. To gain insight into the structural determinants of the protein recognition pattern at the B2 site, we have selected here representative members for each vertebrate family subgroup. Ten representative RNases were chosen and their binding mode to dinucleotides was predicted by MD simulations. **Figure 2** illustrates the selected proteins and their evolutionary relationships. When no

TABLE 1 | Kinetic activity of RNase A and the human RNases 1–7.

	V_0 (μmol/min)			B2 ratio	
	UpA	UpG	UpI	A/G	G/I
Bt-RNase A	0.783 ± 0.033	$1.49{\cdot}10^{-2} \pm 9.99{\cdot}10^{-4}$	$3.62{\cdot}10^{-2} \pm 2.22{\cdot}10^{-3}$	52.65	0.411
Hs-RNase 1	$0.108 \pm 3.93{\cdot}10^{-3}$	$1.15{\cdot}10^{-3} \pm 6.09{\cdot}10^{-6}$	$7.87{\cdot}10^{-3} \pm 5.54{\cdot}10^{-4}$	93.63	0.146
Hs-RNase 2	$2.57{\cdot}10^{-3} \pm 1.32{\cdot}10^{-4}$	n.d.	$5.53{\cdot}10^{-4} \pm 1.56{\cdot}10^{-4}$	∞	0
Hs-RNase 3	$2.39{\cdot}10^{-3} \pm 4.96{\cdot}10^{-5}$	n.d.	n.d.	∞	∞
Hs-RNase 4	$5.92{\cdot}10^{-2} \pm 3.97{\cdot}10^{-3}$	$2.38{\cdot}10^{-3} \pm 2.86{\cdot}10^{-4}$	$6.86{\cdot}10^{-3} \pm 1.7{\cdot}10^{-4}$	24.85	0.348
Hs-RNase 5	$2.39{\cdot}10^{-4} \pm 3.74{\cdot}10^{-5}$	$1.94{\cdot}10^{-5} \pm 2.5{\cdot}10^{-6}$	$5.33{\cdot}10^{-5} \pm 8.19{\cdot}10^{-6}$	12.29	0.365
Hs-RNase 6	$6.74{\cdot}10^{-3} \pm 1.90{\cdot}10^{-4}$	n.d.	n.d.	∞	∞
Hs-RNase 7	$4.25{\cdot}10^{-5} \pm 6.21{\cdot}10^{-6}$	n.d.	n.d.	∞	∞

The reactions were performed using 100 μM of substrate. Initial velocity (V_0) of dinucleotide phosphodiester bond cleavage is indicated. The average of three replicates is shown. Standard error of the mean is shown. n.d.: not detected at the assayed conditions. Bt, Bos taurus; Hs, Homo sapiens.

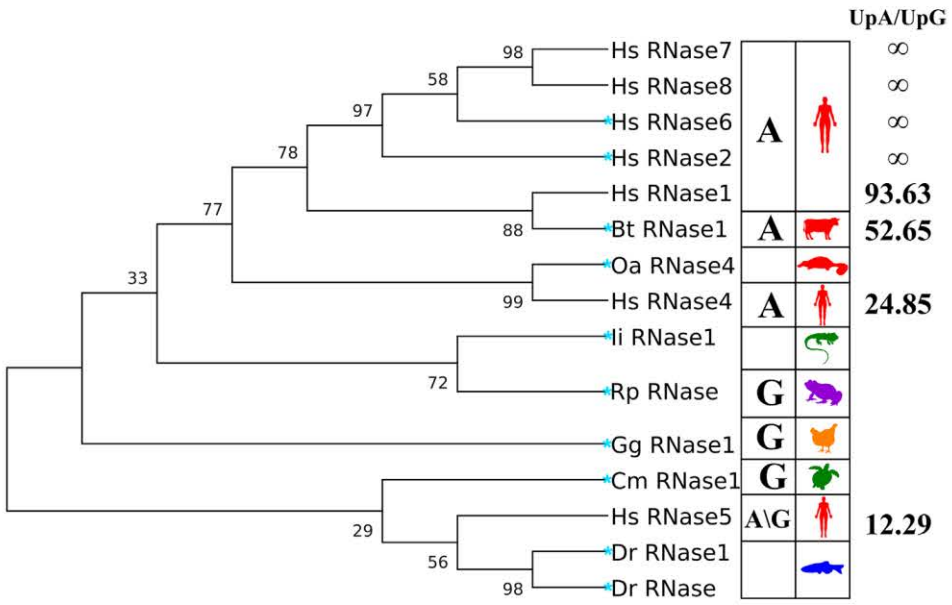

FIGURE 2 | Phylogenetic tree of the RNases studied in the kinetic and molecular dynamics analysis. Right column indicates the UpA/UpG preference ratio according to kinetic results (see **Table 1**). Left column includes the A/G preference at B2 according to the literature. The evolutionary history tree was inferred by using the maximum likelihood method and JTT matrix-based model (Jones et al., 1992). The tree with the highest log likelihood (–3745.36) is shown. The percentage of trees in which the associated taxa clustered together is shown next to the branches. Initial tree(s) for the heuristic search were obtained automatically by applying Neighbour-Join and BioNJ algorithms to a matrix of pairwise distances estimated using a JTT model, and then selecting the topology with superior log likelihood value. The tree is scaled, with branch lengths measured as the number of substitutions per site. Evolutionary analyses were conducted in MEGA X (Kumar et al., 2018). A more complete phylogenetic tree of RNase A family members is included in **Figure S2**. Blue star highlights the selected representative RNases to perform MD simulation runs.

solved 3D structure was available (RNase 4 of *Ornithorhynchus anatinus* and RNase 1 of *Iguana iguana*), a prediction model was generated using the *Modeller* software by the *ModWeb* server (Webb and Sali, 2016). From lower to higher order vertebrates, the following organisms were analyzed: *Danio rerio* (Dr), *Rana pipiens* (Rp), *Iguana iguana* (Ii), *Chelonia mydas* (Cm), *Gallus gallus* (Gg), *Ornithorhynchus anatinus* (Oa), *Bos taurus* (Bt) and *Homo sapiens* (Hs). Representative organisms were selected based on the available information on the evolutionary relationships and previous structure-functional characterization studies (Goo and Cho, 2013). We also indicate, when known, the canonical type of each selected RNase (Sorrentino and Libonati, 1997). Within the placental mammals, we have included two representative human members (RNases 2 and 6; UniProtKB P10153 and Q93091), which are expressed during infection and inflammation and are endowed with a high catalytic activity. We have also selected the bovine pancreatic RNase, or RNase A (UniProtKB P61823), which is the family reference member and one of the best characterized enzymes (Cuchillo et al., 2011). Bovine pancreatic RNase belongs to the RNase 1 type. On the other hand, for early mammals, we selected the platypus (*O. anatinus)*, an egg-laying animal and precursor to higher order vertebrates, before divergence of placental RNases. Accordingly, the platypus RNase belongs to type 4 (UniProtKB F6ZXU1), and was previously identified as the predecessor of higher order mammalian RNase types (Goo and Cho, 2013). Following, representative members of avian, reptiles, amphibian and fishes were chosen, based on the availability of previously solved 3D structures. Chicken RNase 1 was taken (UniProtKB P27043) as the only member with a known 3D structure (Lomax et al., 2014). In turn, reptiles have been represented by turtle (UniProtKB P84844) and iguana (UniProtKB P80287) (Nitto et al., 2005). Next, we selected the northern leopard frog (*R. pipiens)* RNase (also named Onconase, UniProtKB P22069), which has been extensively characterized because of its antitumoral properties (Boix et al., 1996; Lee and Raines, 2003; Lee et al., 2008). Lastly, for fish representative sequences, we selected *D. rerio* RNases (Dr-RNase 1 and Dr-RNase; UniProtKB A5HAK0 and E7FH77), also named as zebrafish RNases 3 and 5 respectively. Both RNases were previously reported to display a high catalytic activity in comparison to other fish homologues (Cho and Zhang, 2007; Pizzo et al., 2011). In particular, the zebrafish 5 (Dr-RNase) was classified as one of the most ancestral family members, showing a high catalytic activity along with both antimicrobial and angiogenic properties (Pizzo et al., 2011). In all cases, previously reported 3D structures were taken as a reference, except for the platypus RNase, where a prediction model had to be generated.

To compare the RNases' selectivity at the B2 site, the three dinucleotides, UpA, UpG and UpI, were selected (see **Figure S3** for atom nomenclature). Molecular dynamics were performed using GROMACS software as detailed in the methodology. Triplicates for each protein complex were carried out at 100

ns. The RMSD between the dinucleotide positioning during the simulation is shown in **Figure S4**. The following common criteria were established to confirm at the end of each modelling run that the nucleotide is positioned in a productive orientation, favorable for catalysis: phosphate location at the RNase catalytic triad and pyrimidine proximity to B1 site. Equivalent residues to RNase A (H12/K41/H119 at the catalytic triad and T45 at B1 site) were taken as a reference for each protein.

The dinucleotides' RMSD fluctuations during each production run indicate a reduced substrate mobility, oscillating within a value range of 0.1–0.4 nm (**Figure S4**). The total hydrogen bond interactions per residue were calculated for each simulation and expressed as a fraction of occurrence. **Figure S5** illustrates the interacting residues with the purine moieties.

Overall, we observe at the end of each simulation run a similar productive positioning of the dinucleotides at the active site cleft for most of the studied proteins (**Figures 3** and **S6**). However, comparison between all different RNase–nucleotide complexes and among triplicates highlights that most variability is located at the purine moiety (**Figure 4**). Likewise, time course analysis for each dynamic run shows significantly much higher mobility for the purine nucleoside in comparison to the pyrimidine main nucleoside and phosphate portions. We can confirm that the protein phosphate p1 and base B1 sites are mostly conserved among all the family members and provide stronger and more specific interactions.

Following, we have analyzed the specific binding interactions at the B2 purine portion. Specific binding residues at the B2 site were identified. In the majority of complexes, the purine base is fixed by the L4 loop and β6 strand structures (**Figure 4**). Contribution of each interacting residue was monitored as a function of time. Each run was subdivided into initial, central and late periods. Although some mobility of the substrate positioning is observed during the 100 ns MD production runs (**Figure S4**), overall no major significant differences are identified as a function of time. The most representative interacting residues and atom types involved in each modelled complex are summarized in **Figure 5**.

Figure 5 illustrates the main residues that contribute to B2 base recognition. The figure indicates the main residues that were found involved in interactions with the purine ligand for at least one third of the total 100 ns molecular dynamics run. We observe the contribution of polar and charged residues that act as acceptors/donors to purine representative groups. We can identify the protein residues that can provide a bidentate anchoring with the purine base and selectively interact with unique base groups. In particular, we find specific discriminators for adenine (N1/N6 and N6/N7 groups) versus guanine (N1/O6 and N1/N2 groups). Likewise, discrimination between guanine and inosine binding was identified by looking for the residues with specific interactions at the base N1/N2 group, unique to guanine.

Each studied family member was analyzed taking bovine pancreatic RNase A sequence numbering as a reference (see **Table S2** and **Figure 1**) (Raines, 1998; Boix et al., 2013). The adenine base is fixed in bovine RNase by residues Asn67, Gln69, Asn71, Glu111 and His119 (see **Figure 5**). The reliability of the dynamic simulation was first evaluated by comparing the obtained results for RNase A using UpA with the previous structural work by

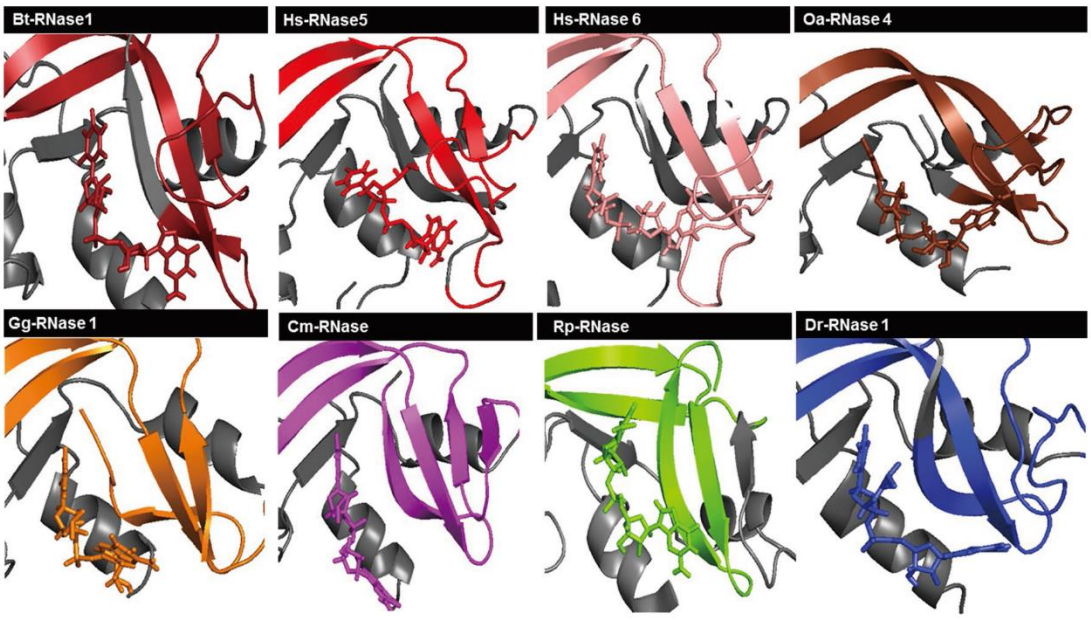

FIGURE 3 | Schematic illustration of RNase–UpA complexes obtained at the end of the MD 100 ns simulation run. Colors of each vertebrate group are taken according to the family phylogenetic tree selection (see **Figure S2**). Mammal RNases are shown in shades of red, turtle RNase in magenta, chicken RNase in orange, frog RNase in green and fish RNase in blue. Some parts of the RNase are colored in gray to allow better visualization of the ligand and the interaction regions of the protein. The picture was generated using PyMOL 1.7.2 (Schrödinger, Inc).

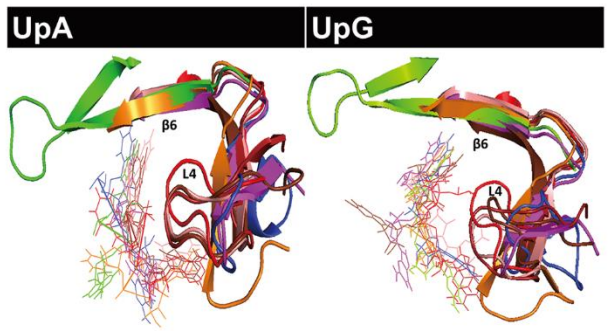

FIGURE 4 | Overlapping of all RNase-UpA and RNase-UpG complexes obtained by molecular dynamics (see **Figures 3** and **S6**). The secondary base binding site (B2) is highlighted (loop L4 and strand β6). As shown in **Figure 3**, the molecules are colored according to vertebrate groups as indicated in the family phylogenetic tree (see **Figure S2**). Mammal RNases are shown in shades of red, turtle RNase in magenta, chicken RNase in orange, frog RNase in green and fish RNase in blue.

X-ray crystallography on RNase A–dinucleotide complexes (Boix et al., 2013). In particular the adenine binding residues identified by molecular dynamics were compared with the RNase A–d(CpA) complex (Zegers et al., 1994), where the same residues for adenine binding had been identified (Asn67, Gln69, Asn71, Glu111 and His119). Specific bidentate interactions for adenine are provided by Asn71/Gln69 at N1/N6, Asn67 at N6/N7 and Glu111 at N6. In particular, our molecular dynamics results corroborate the key contribution of all Asn71 counterparts in mammalian members for adenine specificity. On the other hand, we observe the flexibility of residues such as Glu111, which can offer a bidentate anchoring at either the NH_2 group at C6 position in adenine or at N2/N1 groups in guanine (**Figure 5**).

In addition, we observe the contribution of the His119 catalytic residue by π-π interactions with the purine 5-membered ring in all the predicted complexes for any of the three assayed dinucleotides (**Figure 5**). Previous structural studies have revealed that the catalytic His119 in the free protein can adopt two conformations (A and B), where only one rotamer (A) is compatible with catalysis and purine interaction (Berisio et al., 1999; Merlino et al., 2002). Favored stacking interactions of the His imidazole with the purine ring are suggested to participate in nucleotide discrimination (Gagné and Doucet, 2013). In our molecular dynamics study we cannot find any significant differences between the complexes obtained with any of the three dinucleotide types. On the other hand, significant differences are observed for some particular RNases, where the purine ring is also establishing cation-π interactions with other residues, in particular arginine (such as Arg68 in Hs-RNase 2, Arg66 in Gg-RNase, Arg117 in Cm-RNase and Arg8 in Dr-RNase 1 (see

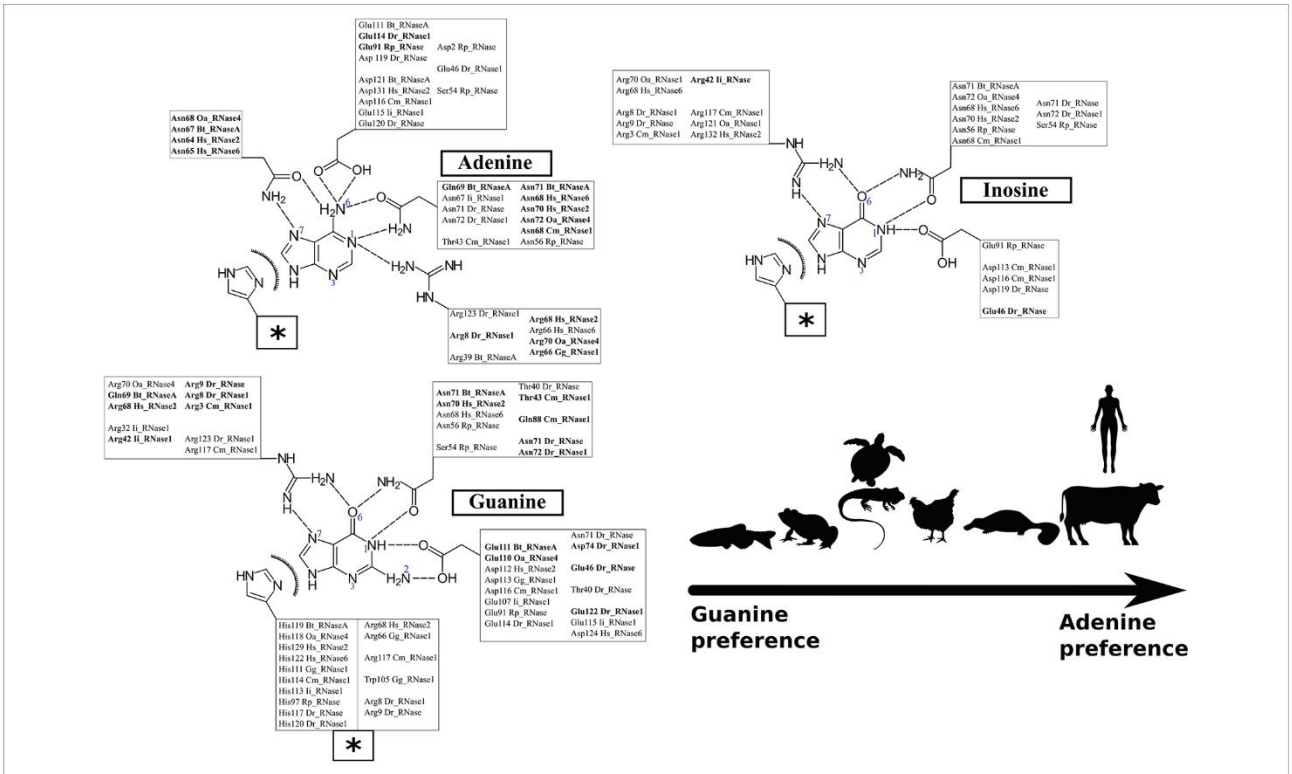

FIGURE 5 | Schematic representation of the predominant interactions observed during the 100 ns of each simulation run. Only the interactions present during more than 30% of the total dynamic runs were considered. The interactions observed in more than 50% of the total dynamic runs are highlighted in bold. Protein residues are listed according to RNase A numbering reference (see **Table S2** for structural residues overlapping between the analyzed homologues). Polar and electrostatic interactions are detailed for each location. The box labeled with a star includes the shared common van der Waals interactions for the three base types.

Figure 5). Overall, we observe that most differences among the studied family members are located at the L4 Loop. The loop mobility is restricted by a disulphide bridge (Cys65–Cys72 pair in RNase A), that is conserved in most mammalian RNases (except in RNase type5/angiogenin-like), but absent in all the non-mammalian vertebrate groups (see **Figure 1**).

We can conclude from the analysis of predicted protein–dinucleotide complexes that the main key residues for purine interactions (Asn71 and Glu111) are mostly conserved among all the studied family members, although distinct binding modes are identified depending on the nature of the purine base. Asn71 in RNase A, and equivalent residues both in human and platypus proteins, specifically bind by a bidentate interaction at the N1/N6 of the adenine ring. Likewise, the Asn side chain can establish equivalent interactions for guanine or inosine binding, by shifting their NH and C=O amide groups and thereby interacting with the respective N1/O6 groups. However, these interactions are not so often observed for guanine/inosine interaction and frequently only the Asn binding to the O6 group is identified.

When we inspect the non-mammalian vertebrate members, we find a similar scenario: an Asn residue (Asn71 RNase A counterpart) can also interact with both N1/N6 groups for A and N1/O6 in G/I in turtle, frog and fish proteins. Significant differences are found in chicken RNase, where an Arg is located at the same position. On its turn, the nearby residue Gln69 would contribute to provide a specificity for adenine. A Gln at this position is only present in the pancreatic RNase 1 type. Substitutions of Gln by an Argin Hs-RNases 2 and 6 and platypus RNase favor the bidentate interaction with G/I at the N7/O6 group. The equivalent counterpart in fish is an Asn (), which shows a preference for guanine/inosine binding. No equivalent residues are found in any other lower order vertebrates, due to a deletion in the loop L4 region from residues 65 to 71 (see **Figures 1** and **S7–S11**). In addition, we find another Asn residue in mammalian RNases that is also favoring the adenine versus guanine binding: Asn67 (**Figure 5**). In this case, the Asn is providing a bidentate interaction to N6/N7 adenine groups. The presence of an additional Asn is also found in zebrafish RNase 5 (Dr-RNase) but is missing in all the other studied lower order vertebrates. Interestingly, the shorter L4 loop version in the fish protein still permits the appropriate Asn positioning.

The molecular dynamics results also highlight two other protein regions, which are also participating in the purine binding: residues 109–111 (β5) and 119–121 (β6). In particular, we observe the main contribution of Glu111 in Bt-RNase A and the respective Glu/Asp counterparts in the other studied family members (**Figure 5** and **Table S2**). Both the Glu/Asp bidentate anionic side chains are observed to bind at both the NH_2/N6 adenine and the N2/N1 guanine specific groups. However, Glu substitution by an Asp residue (found in Hs-RNases 2 and 6) prevents, or reduces drastically, the base interactions. Similar interactions at the adenine N6 NH_2 group and the guanine N2/N1 group are established by Asp121 at Bt-RNase A and their counterparts in mammals and chicken RNases. Although a Glu/Asp is present in all the studied proteins, frog RNases show significant differences. Interestingly, the zebrafish 3 counterpart (Glu122) interacts with guanine base but is not involved in adenine binding. Finally, another substitution that is observed to favor guanine binding in non-mammalian RNases is Ala122 to Arg. The Arg counterpart residues in fish and turtle RNases can interact by bidentate interactions with the O6/N7 group of the guanine/inosine bases (**Figure 5**).

Overall, although key residues for purine binding are mostly conserved in all the studied members, such as Asn71, His119 and Glu111, our molecular dynamics analysis indicates that distinct binding modes could promote a shift from G to A at the B2 site.

An Evolutionary Trend Shaping the B2 Selectivity Within the RNase A Superfamily Lineage

To validate the significance of the residues identified by MD to participate in purine recognition, we have supplemented our study with the comparative analysis of other family member close homologues. Accordingly, each representative member analyzed by MD simulations has been compared within its own vertebrate subgroup. By close inspection of sequence alignments, we have identified the counterpart to the key residues for binding of a purine at B2 location. **Figures S7–S11** include the respective sequence alignments within each vertebrate subgroup. The relationships between all the aligned sequences of family homologues are illustrated in the phylogenetic tree included in **Figure S2**.

First, we have analyzed the fish RNase sequences, taking as a reference *D. rerio* RNase 1 (Pizzo et al., 2011), also named zebrafish RNase 3 (ZF3). Acharya and co-workers solved the crystal structure of this RNase together with a polymorphism variant (Kazakou et al., 2008). The chosen protein structure corresponds to the variant identified as ZF3e. Overall, the researchers identified five protein variants, with substitutions at six sequence locations. Among them, we observe that one of the residues involved in the purine binding (Arg123) is only present in the ZF3e polymorphism and is substituted by a Lys in the other variant. On the other hand, comparison with the other fish RNase sequences (**Figure S7**) highlights the presence of one or two conserved Asn residues at L4 loop region. The loop is present in fishes in a short-reduced version in comparison to the extended version present in more evolved mammal RNase types: 2/3–6/7/8 (**Figure 1**). However, the Asn residue at position 72/74 (corresponding to positions 67 and 71 in RNase A) can also participate in the adenine interaction but would preferably interact with the N1-O6 group of a guanine. Noteworthy, several fish RNase sequences display an Asp at 74 position, which according to molecular dynamics results is a suitable binder for guanine. Two other anionic residues at the protein C-terminus are key for the studied RNase complexes; that is Glu114 and Glu122 (corresponding to Glu111 and Asp121 in RNase A counterparts). While most fish RNases show a Glu at 114 position, we also find in some cases the presence of an Asp. This is the case of zebrafish 5 (Pizzo et al., 2011), which was reported to have a relative much higher catalytic activity than the other characterized fish RNases (Pizzo et al., 2011). Likewise, residue Glu122 is either conserved or substituted by an Asp residue. Finally, molecular dynamics reveal the presence of an Arg residue at the zebrafish proteins'

N-terminus that shows favored interactions to guanine and inosine. The Arg is only present in about 50% of the analyzed fish sequences.

Following, we inspected the residues potentially involved in purine binding in amphibians. In this vertebrate group we also observed a short version of the L4 loop. However, in comparison to fish RNases, the analyzed amphibian members show a less optimal loop conformation. The loop is orientated to the opposite direction respect to RNase A, and lacks one of the key Asn found in mammalian RNases. In particular, in northern leopard frog *R. pipiens* RNase (Onconase) we can identify Asn56 (counterpart of Asn71 in Bt-RNase A) but no other equivalent residues in the region (**Figure 1**). Comparative structural alignment only reveals the presence of a conserved Glu residue at position 91 (Glu111 counterpart in RNase A). Molecular dynamics results on Onconase interaction with dinucleotides have been compared with the previous reported solved crystal structure in complex with a tetranucleotide (Lee et al., 2008). Raines and co-workers studied in detail the enzyme binding to the d(AUGA) substrate analogue and observed that while an equivalent binding pocket is conserved for the pyrimidine base at B1, significant differences are found for the B2 site. In particular, specific bidentate interactions of Glu91 with the guanine base were identified at B2 position. Moreover, the authors confirmed by site-directed mutagenesis that this residue was responsible for the frog RNase preference of guanine over adenine. In addition, the authors also highlighted the importance of the nature of the nearby residue located at position 89 (Onconase counterpart of Ala109 in RNase A). Ala109 is conserved in all mammalian and most reptile sequences but shows a significant variability in fishes and amphibians. Interestingly, ZF3 presents an Ala at this position, as observed in mammals, whereas other fish RNases have a polar or cationic residue (Thr/Lys or Arg), as observed in frog RNases. Substitution of Thr89 in Onconase by an Asn residue reduced the enzyme's G > A preference. The authors suggested that long-range electrostatic interactions were key for the enzyme turnover activity on cellular RNA substrate in physiological conditions (Lee et al., 2008). The hypothesis was further backed up by recent NMR and molecular dynamics studies by Doucet and collaborators, that emphasized the key role of network interactions connecting distant protein residues (Narayanan et al., 2018a). Interestingly, site-directed mutagenesis in Onconase revealed also the contribution of the N-terminus in the B2 base discrimination (Lee et al., 2008). In particular, insertion of an Arg at position 5 is significantly enhancing the frog RNase catalytic activity. Likewise, in our molecular dynamics analysis we observe equivalent Arg residues at the protein N-terminus of turtle and fish RNases that contribute to purine binding (**Figure 5** and **Table S2**).

Molecular dynamics results of Onconase were also compared with the structural information reported for bullfrog (*R. catesbeiana*) RNase purified from oocytes (RC-RNase), the most catalytically active frog RNase (Chang et al., 1998; Lee and Raines, 2003). A structural study by NMR of bullfrog oocyte RNase analyzed the enzyme interaction with tetranucleotides (Hsu et al., 2015). The authors reported a much higher catalytic activity for oocyte RC-RNase in comparison to RC-RNase 2 and RC-RNase 4. The contribution of the L4 loop to guanine binding was also highlighted, although distinct conformations are observed among the bullfrog RNases that could account for the higher catalytic activity displayed by the oocyte RC-RNase. When we overlap the reported NMR structures with our modelled structures in complex with dinucleotides, we also observe that the oocyte RC-RNase is the only one that has an Asn residue at an equivalent position to Asn71 in RNase A, that can establish interactions with the N1-O6 group of the guanine. Therefore, the higher catalytic efficiency of bullfrog oocyte RNase respect to Onconase could be mostly attributed to residue Asn57, which is substituted by a Ser in the latter. When we compare the sequence identities of the distinct frog RNases, we observe a high variability at the loop L4, where Asn residues are mostly substituted by either a Ser or an Asp (**Figure S8**). Besides, presence of Pro and short amino acid insertions in other amphibian RNases might also modify significantly the interaction at this site. Interestingly, whereas most *R. catesbeiana* RNases show a particular four amino acid insertion, we found several *Xenopus* species that display an alternative loop version, with a slightly extended insert (**Figure S8**).

In turn, reptiles present a short version of the L4 loop (see **Figure S9**), with a similar length to the one observed in fishes, although encompassing a higher sequence divergence at the region. In particular, most species include only one Asn within the region. In our molecular dynamics study of iguana and turtle RNase-dinucleotide complexes we can identify one Asn (Asn68 in turtle RNase and Asn67 in iguana) equivalent to the Asn71 counterpart in RNase A (Table S2). Close inspection of sequence alignment identifies few reptile species with two Asn residues at 67/71 positions (such as the species of the *Micrurus* or *Boiga* genera), whereas other species show an Asn to Asp substitution at position 71. However, we observe an overall higher variability at L4 loop, which incorporates non-conserved substitutions (**Figure S8**). We have also analyzed within reptiles the other residues that were identified in turtle or iguana to potentially participate in binding at the B2 site (**Figure 5**). Rosenberg and co-workers characterized the RNase from iguana, which is mostly expressed in the pancreas and displays a significantly high catalytic activity (Nitto et al., 2005). In the present work, productive binding conformations obtained by molecular dynamics of turtle RNase with dinucleotides highlight the contribution at the protein C-terminus of Asp116 and Arg117 (Asp116, counterpart of Asp121 in RNase A, is only present in few reptile sequences). In turn, the presence of an Arg at position 117, not shared by all the family homologues, is rare.

Avian RNases present the shortest L4 loop version that incorporates the most significant deviation from the L4 loop consensus sequence (**Figure S10**). Most L4 sequences do not include any Asn residue. In our modelled complex of chicken RNase, Asn65 is equivalent to Asn67 in RNase A. However, we did not observe any direct participation of Asn65 in purine binding. In turn, the neighboring residue Arg66 is significantly participating in B2 binding and was observed to bind to any of the three purine bases. Arg66 position can be equated to Bt-RNase A Asn71 counterpart, although the loop conformation is very divergent at this region (Table S2). Arg66 is only found in few bird sequences but is located close to Arg66/70 in some other mammalian RNases (Hs-RNase 2, Hs-RNase 6 and Oa-RNase

in our study; **Figure 5** and **Table S2**). Most strikingly, there is no equivalent Glu/Asp counterpart to Bt-RNase A Glu111. On the contrary, a Trp is present at that location in the studied chicken RNase (**Figure 1**). Trp is conserved in some chicken and snake (*Boiga*) RNase sequences (**Figures S9**, **S10**). In other avian sequences we find another bulky hydrophobic residue, followed by Asp, which might substitute the Glu111 function. Interestingly, in our molecular dynamics study we find the contribution of stacking interaction of Trp105 with the purine base. On the other hand, the presence of a residue equivalent to Asp121 is only observed in some of the sequences, whereas others show a substitution by an Ala. In any case, a higher proportion of non-productive dinucleotide binding is obtained by molecular dynamics (>75% of all run assays) in relation to the other studied members (<30% in fish, frog, turtle or platypus), which might be attributed to the chicken RNase's different conformations of the L4 loop and the presence of Arg66 and Trp105, that tend to establish stacking interactions with the purine base. Noteworthy, Rosenberg and co-workers performed a comparative study of available sequences for chicken RNases and concluded that the evolution within this group of proteins might not respond to functional constraints directly related to the enzyme catalytic activity (Nitto et al., 2006). Comparison of two chicken leukocyte RNases identified key regions for either antimicrobial or angiogenic activity. By construction of hybrid proteins, they concluded that following a duplication event, a selective evolutionary pressure unrelated to the protein enzymatic activity had taken place. In our study, we have selected the only available 3D structure of a chicken RNase. Unfortunately, this RNase corresponds to the angiogenin-type RNase instead of the other characterized chicken RNase (leukocyte RNase-A2 or RSFR-RNase), which displays a much higher catalytic activity (Nitto et al., 2006).

In contrast to lower order vertebrates, we observe that all mammalian RNases, except the RNase 5 type, share an extended L4 loop fixed by a disulphide bridge (Cys65 and Cys72 in RNase A). In contrast, all the non-mammalian vertebrate RNases have either a single Cys or none at this location (**Figure 1**). Mammalian RNases' extended L4 loop includes in all cases the RNase A Asn71 counterparts and, in the majority of cases, the RNase A Asn67 residue. On the other hand, more variability is observed at 69 position, where either a Gln, Ser or Arg is found (**Figure S11**). On its side, Glu in position 111 is mostly conserved but can also be substituted by an Asp or even a Lys residue. Our MD results indicate that the presence of the shorter Asp residue is associated in Hs-RNase 2 and Hs-RNase 6 with scarce or null interactions with the purine (**Figure 5**). Structural crystallographic data on Hs-RNases 2 and 3 complexes (Mohan et al., 2002) also highlighted the different interaction mode of Asp at this position. Hs-RNase 6 structural studies also indicated that the Glu to Asp substitution might significantly modify substrate specificity (Prats-Ejarque et al., 2016). On the other hand, it is also interesting to note the presence of an Arg at position 122 (Arg132 in RNase 2), which is shared with some fish and other lower order vertebrates (**Table S2**) and might provide a significantly differentiated specificity. Overall, we can conclude that counterpart residues to Asn71 and Glu111 in Bt-RNase A, shared by all the mammalian RNases, were already present in most ancestral RNases; but the observed purine selective specificity is modulated in each family member by complementary interactions of environment residues.

DISCUSSION

The RNase A superfamily is currently a reference model for evolutionary and enzymology studies. Although a wealth of information is available on ruminant evolution and the pancreatic-type RNases (Beintema and Kleineidam, 1998; Goo and Cho, 2013; Xu et al., 2013; Lomax et al., 2017), a comprehensive full understanding of the whole family is still missing. Following a pattern characteristic of host-defense proteins, the RNase A family has undergone frequent duplication and gene sorting events (Rosenberg et al., 1995; Zhang et al., 2000; Zhang et al., 2002; Liu et al., 2015). Many studies have tried to unveil the structural determinants for the distinct RNases' biological activities (Lu et al., 2018); however, we find much less information on the evolutionary trends that shaped the family's enzymatic diversity. Nonetheless, the understanding of the evolutionary processes that determined the enzymes' substrate selectivity is key to unravel their physiological roles. Distinct nucleotide specificities should respond to an adaptation to their respective biological functions (Narayanan et al., 2018b). Undoubtedly, mastering the structural basis for protein nucleotide recognition is essential to assist the design of novel anti-infective and immunomodulatory drugs.

Here, we have compared for the first time the catalytic activity of the human canonical RNases. The analysis of all the recombinant proteins, obtained by the same expression system and using the same kinetic characterization methodology, ensures a reliable comparative evaluation of their respective efficiencies. To unravel the enzyme specificity for the binding of the purine secondary base, we have tested the respective catalytic activity of the distinct canonical RNases using UpA, UpG and UpI dinucleotides as a substrate. Interestingly, when we compare the A/G ratio at B2 site for the studied seven canonical RNases (**Figure 2**), we observe a pronounced evolutionary tendency from guanine to adenine preference. Previous evolutionary studies identified within the RNase A superfamily the phylogenetic relationship between the eight canonical subtypes (Cho and Zhang, 2007). By comparative analysis of the family coding sequences we can order the different RNase types from ancestral to modern as follows: 5, 4, 1 and 6/7/8–2/3 group (Zhang, 2007; Sorrentino, 2010) (see the family phylogenetic tree in **Figure S2**). Kinetic results of human canonical RNases follow the same ordering when considering the UpA/UpG ratio (Table 1). The present result is in agreement with previously reported kinetic data, where lower order vertebrates, such as amphibians and reptiles, show a preference for G (Liao, 1992; Irie et al., 1998), while mammalian RNases have a clear preference for A (Boix et al., 2013). In addition, the recent kinetic characterization of human RNase 6 corroborated the previously reported preference for adenine at B2 for human RNases 2 and 3 (Boix et al., 1999a; Sikriwal et al., 2007; Prats-Ejarque et al., 2016). On its turn, human RNase type 5 shows a much less pronounced preference

for adenine over guanine (Acharya et al., 1994; Shapiro, 1998). Early kinetic characterization of human RNase 5 (angiogenin) already reported its poor discriminating ability on the purine located at B2 position (Shapiro et al., 1986; Harper and Vallee, 1989). Vallee and co-workers engineered an RNase 5 hybrid protein by replacing the L4 loop residues 60-70 with the RNase A counterparts, successfully enhancing the enzyme catalytic activity on UpA dinucleotides (Harper and Vallee, 1989). Further work by site-directed mutagenesis in angiogenin suggested that an Asn at Gln69 position in RNase A would provide most of the purine selective binding. On the contrary, replacement of the Glu111 RNase A counterpart (Glu108 in RNase 5) did not significantly alter the enzyme B2 selectivity (Curran et al., 1993). Indeed, structural and molecular dynamics simulation studies indicate that Glu111 in RNase A could contribute to either adenine or guanine binding by alternative modes, by direct or water-mediated interactions. The nature of the nearby residue (109 in RNase A) could determine the potential participation of the corresponding Glu residue (Glu111 in RNase A) in the purine binding. The hypothesis was elegantly confirmed by site-directed mutagenesis studies in Onconase (Lee et al., 2008). Raines and co-workers demonstrated that the B2 site specificity could be shifted from guanine to adenine preference by impeding the long distance network interactions that Glu establishes for the purine recognition (Lee et al., 2008). Likewise, substitution of Glu111 by the shorter Asp side chain in human RNases 2 and 6 could enhance the adenine versus guanine discriminating power in relation to ancestral RNases, such as RNase-type 4 and 5, as observed in our kinetic comparison studies (**Table 1**, **Figure 2**).

In an effort to unravel the structural determinants underlying the observed differentiated kinetic behaviors, we have carried out a molecular dynamics analysis of RNase-dinucleotide complexes. Representative family members were chosen from lower order vertebrates to placental mammals. Overall, molecular dynamics corroborate the observed shift from guanine to adenine preference by kinetic analysis (**Table 1**, **Figure 2**). Notwithstanding, results also highlight that conservative sequence identities are frequently not accompanied by equivalent substrate binding. A similar conclusion was reached by NMR analysis of RNases' nucleotide binding (Narayanan et al., 2018a). Therefore, no straightforward conclusions can be directly inferred from the identification of individual interactions to nucleotides by mere structural overlapping analysis. On the other hand, although molecular dynamics considers the protein–ligand complex as an entity in motion and provides the equivalent freedom and flexibility that could be found in experimental conditions, the methodology has also its own limitations when trying to simulate the enzyme behavior. Fortunately, Bt-RNase A, the family reference member, has been one of the best enzymes ever characterized (Raines, 1998; Cuchillo et al., 2011). RNase A was classified by earlier studies as an almost "perfect" enzyme, where the transphosphorylation state is not limited by the transition state (Albery and Knowles, 1976). Raines and coworkers analyzed the behaviour of RNase A on UpA substrate by experimental kinetics and concluded that the cleavage efficiency is mostly limited by the substrate desolvation (Thompson et al., 1995). Early crystallographic and NMR studies of RNase A in complex with mono-, di- and tetranucleotides identified the main residues that conformed the RNase A substrate binding subsites (Fontecilla-Camps et al., 1994; Nogués et al., 1998; Hsu et al., 2015).

Notwithstanding, despite the RNase protein small size and structure stability, that facilitated the pioneer biochemistry works during the first half of the 20th century, the polymeric nature and structural complexity of the substrate is still challenging the enzymologists. In this context, it is important to analyze the protein family members as a whole dynamic entity. The protein has a kidney-shaped structure conformed by two domains that delimitate the catalytic active site groove. The open and closed conformation of enzymes were compared in the presence of nucleotide ligands (Watt et al., 2011; Gagné and Doucet, 2013). Key residues involved in the RNase protein motion would have co-evolved to shape the enzyme catalytic efficiencies, as described for other enzyme families (Maguid et al., 2006; Ramanathan and Agarwal, 2011; Narayanan et al., 2018a). Within the RNase A superfamily we observed the conservation of key domains involved the protein motion (Merlino et al., 2003; Gagné and Doucet, 2013). Notwithstanding, comparative studies from lower to higher order family members infer an inverse relationship between the protein's structural rigidity and its catalytic efficiency (Merlino et al., 2005; Holloway et al., 2011).

Although our molecular dynamics runs using dinucleotides are overall in agreement with the reported crystal complex structures (Fontecilla-Camps et al., 1994; Zegers et al., 1994; Leonidas et al., 2001; Mohan et al., 2002; Lee et al., 2008), we do observe some significant differences. This might be due to the allowed protein flexibility during the molecular dynamics simulations, a fact that could enable a better accommodation of the nucleotide substrates. Besides, MD studies permitted us to work with the natural enzyme substrates, rather than the analogues, commonly used in crystallographic studies. On the other hand, NMR titration studies using mononucleotides could only mimic the enzyme interactions that were to take place with the enzyme reaction product (Narayanan et al., 2018a). Interestingly, when we analyze the results of our molecular simulation, we can observe significant differences among the residues that participate in the distinct periods of the reaction. Mostly, interactions with the purine base are frequently lost at the end of the production run. Interestingly, in our modelling studies we observe how the substitution of Glu111 by an Asp residue in human RNases 2 and 6 is only participating in the purine binding at the initial step of the reaction. In contrast, the positioning of the pyrimidine base, located at the main B1 site, and the phosphate are mostly retained during all the simulation run, as reported in previous molecular dynamics using RNase A or angiogenin (Madhusudhan and Vishveshwara, 2001). Indeed, Raines and co-workers' kinetic studies indicated that the RNase A catalytic mechanism relies mostly on the substrate association step (delCardayre and Raines, 1994). A high catalytic efficiency would mostly be associated to the enzyme facility to throw away the product from the catalytic site. In this context, previous studies emphasized the importance of the active site flexibility for substrate recognition, catalysis and product release (Sanjeev and Vishveshwara, 2005; Gagné et al., 2012; Gagné and Doucet, 2013). The authors identified two main clusters involved in the protein

motion that participate in substrate recognition and product release. In particular, L4 loop plays a key role in the protein motion (Gagné et al., 2012). In addition, a distant residue, Ala109, was identified in RNase A to work as a hinge and promote the active cleft opening and product release (Gagné et al., 2015). Ala109 is conserved in almost all the studied vertebrate members, except in frog and chicken RNases. To note, chicken family members are characterized by a much lower catalytic efficiency. On the other hand, comparison of zebrafish proteins indicates that presence of an Ala or Gly at this position is associated to high catalytic efficiency (Kazakou et al., 2008). On the other hand, a network of sequential hydrogen bond interactions was found mostly dependent on His48 protonation state, where deprotonation is associated to product release (Doucet et al., 2009; Watt et al., 2011). Interestingly, His48 is close to the protein family signature CKXXNTF and is conserved in most members, except in fish and amphibian sequences (**Figures S7–S11**).

Early dynamic predictions could also clearly differentiate between the main B2 residue (Asn71), which directly interacted with the adenine base, and other contributing residues, such as residues Gln69 and Glu111, which participated through water-mediated interactions (Seshadri et al., 1995; Madhusudhan and Vishveshwara, 2001). The results helped to interpret previous results obtained by site-directed mutagenesis and kinetic characterization (Tarragona-Fiol et al., 1993). Likewise, the NMR analysis of several frog RNases in complex with a deoxytetranucleotide also highlighted the key role of Asn71 counterparts for guanine binding, even if the respective L4 loops are significantly shortened in contrast to the bovine RNase A structure (Hsu et al., 2015). Moreover, the studies by Hsu and Chen corroborated the importance of Glu111 counterpart in specific guanine recognition at the N1/N2 group (Hsu et al., 2015).

On the other hand, significant divergence is evidenced at the guanine-binding mode between the present molecular dynamics analysis and previous structural characterization by X-ray crystallography. Mostly, although our data emphasizes the preference for adenine at B2 site in mammal RNases, we do not observe any impediment for guanine positioning at the enzyme base secondary site, nor any tendency of guanine to bind at the main B1 base site. Surprisingly, RNase A crystallographic studies using 2′5′-UpG and d(UpG), both in soaking and co-crystallization conditions, showed an unusual binding mode (Lisgarten et al., 1995). Specifically, the guanine was located at B1 instead of B2 site; this peculiar non-productive positioning was classified as a "retrobinding" mode (Aguilar et al., 1992). In addition, not only was "retrobinding" reported by independent researchers for RNase A for both d(CpG) and d(UpG) (Aguilar et al., 1992; Lisgarten et al., 1995; Vitagliano et al., 2000), but also for bullfrog RNase binding to d(CpA) (Chang et al., 1998). Noteworthy, the present kinetic results are also emphasizing a much more pronounced substrate selectivity at B2 site than the MD data reveal (**Table 1**, **Figure 2**).

Overall, our molecular dynamics study using UpA and UpG enabled us to outline the main residues involved in the RNases' distinct specificities for B2. **Figure 5** illustrates the main interactions that participate in the purine recognition. First, bidentate interactions can mainly discriminate between binding to either adenine or guanine at N1/N6 or N1/O6 groups respectively. In addition, we observe specific interactions at N7/N6 for adenine versus N7/O6 for guanine; and eventually specific binding at guanine N1/N2 group. A summary of the most representative residues that provide selectivity for each base is shown in **Figure 6**. Although no universal rules can be written for protein-nucleotide base binding, the residues identified in our study for RNase A superfamily members match most of the previously reported in the literature (Luscombe, 2001; Kondo and Westhof, 2011). Our previous statistical analysis of protein–nucleotide complexes available at the Protein Data Bank also highlighted the main contribution of Asn/Gln, Arg and Glu/Asp that provide bidentate interactions at N1/N6 and N1/O6 or N1/N2 groups, respectively (Boix et al., 2013). Other polar or charged secondary residues, such as Thr, Ser or Lys could also be identified (Luscombe, 2001; Boix et al., 2013). Complementarily, stacking interactions are also significantly influencing the protein binding mode (Luscombe, 2001; Boix et al., 2013). Interestingly, another structural feature reported by Westhof and co-workers as characteristic for adenine binding is the combined contribution of amino acid side chain and the peptide backbone atoms (Kondo and Westhof, 2011). Our molecular dynamics analysis highlights the conserved binding mode for adenine of Asn71 in RNase A, and counterparts, together with L4 loop main chain atoms. This emphasizes the importance of Asn and loop L4 conformation in RNase A superfamily to favor adenine binding in mammals (**Figure 4**). On their turn, lower order vertebrates tend to present an Arg that facilitates the interactions at N7/O6 for guanine recognition, as reported for other nucleotide-binding proteins (Luscombe, 2001).

Last, together with the two natural purine bases found in RNA we decided here to analyse the modified base inosine. Inosine molecular structure was used as a purine binding model that served to visualize unique interactions at N7/O6 and N1/O6, in relation to guanine. Comparison of kinetic and MD results on UpG and UpI highlights the importance of specific Glu/Asp residues

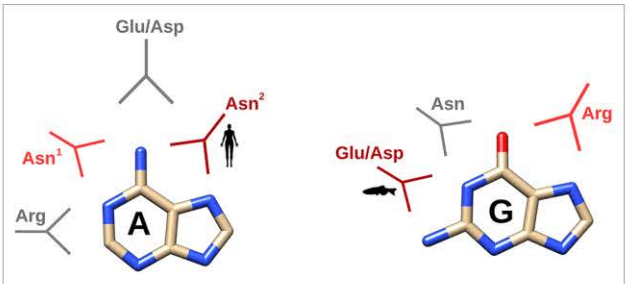

FIGURE 6 | Schematic depiction of the main interactions identified by molecular dynamics according to the two main family classes (mammalian versus non-mammalian RNases). In dark and light red, the main and secondary specific interactions characteristic for either mammalian or non-mammalian RNases and in grey, the other interactions observed in all the RNases analyzed. Representative icon labels for humans and fishes illustrate the predominant interaction mode for each RNase class. Asn¹ corresponds to Asn71 and Asn² to Asn 67 in RNase A.

in non-mammalian RNases involved in guanine N1/N2 group recognition. Interestingly, we find in the literature an inosine-specific RNase that can accommodate the base in its active site groove and provides specificity by discriminating the modified base against the two natural purines (Versées et al., 2002). To note, the contribution of Trp side chain in packing the inosine base by stacking interactions is observed. Inosine represents one of the main posttranscriptional modifications in cellular transcripts. RNA modifications not only contribute to regulate the translation pathway, they are also involved in the generation of regulatory tRNA fragments (Lyons et al., 2018). It is important to highlight that specific tRNA cleavage participates in the host response in stress conditions (Thompson et al., 2008) and RNA posttranscriptional modification can alter the target specificity for cellular endonucleases. For example, base methylation can protect tRNA from cleavage by human RNase 5 (angiogenin) (Lyons et al., 2017). Overall, RNA modifications not only alter their own processing rate but also influence their association to selective binding proteins, participating in the cellular metabolism and physiology (Boccaletto et al., 2017). Besides, the complexity of cellular RNA structure and its organization into supramolecular complexes within the cell further difficult our understanding of the cellular RNA metabolism (Van Treeck et al., 2018). Definitely, we are still facing important methodological limitations to interpret the RNases' behavior in physiological conditions.

On the other hand, a comprehensive analysis of the protein nucleotide recognition pattern cannot disregard the existence of an extended substrate binding site architecture as demonstrated by many structural and kinetic studies (Boix et al., 1994; Fontecilla-Camps et al., 1994; Irie et al., 1998; Nogués et al., 1998; Raines, 1998; Hsu et al., 2015; Prats-Ejarque et al., 2019). Interestingly, recent work on the protein motion and ligand binding energies using a pentanucleotide suggests that induced conformational changes take place upon RNA interaction with secondary binding sites and can eventually provide a synergistic addition effect (Narayanan et al., 2017). The cooperative participation of secondary substrate binding sites could explain the enzyme low binding affinity for mono- and dinucleotides and is also significantly limiting the potency of molecular dynamics predictions, when working with such probes. However, our present results, together with previously reported data, are definitely indicating an evolutionary trend in B2 base selectivity within the vertebrate-specific RNase A superfamily that should respond to changing environmental conditions and adaptation to novel physiological needs. There is still a long path to walk to unveil the RNases' substrate selectivity *in vivo*. We are confident that the identification of the structural patterns for nucleotide recognition in host defense RNases would provide valuable tools for structure-based drug design.

CONCLUSIONS

In this work, we have analysed the base selectivity at B2 site within the RNase A superfamily by kinetic assays and molecular dynamics simulations using dinucleotide substrates. Our results indicate an evolutionary drift tendency from guanine to adenine preference. Interestingly, a close inspection of the residues potentially involved in the enzyme B2 site reveals that the main contributors (Asn71 and Glu111 in RNase A and equivalent counterparts) are present in all the family members. Notwithstanding, significant differences in L4 loop extension and contribution of complementary residues can facilitate a distinct binding mode that confers discrimination between both purine bases. Overall, Asn, Glu/Asp and Arg bidentate side chains provide selective binding to adenine N1/N6 and N6/N7 versus guanine N1/O6, O6/N7 and N1/N2 groups.

DATA AVAILABILITY STATEMENT

All datasets generated for this study are included in the manuscript/**Supplementary Files**.

AUTHOR CONTRIBUTIONS

EB and GP-E conceived and designed the experiments. GP-E, LL, VS and MM performed the experimental work. EB, GP-E and LL analysed the data. EB and GP-E drafted the manuscript. EB, GP-E, LL, VS and MM revised the final manuscript. All authors approved the final manuscript version.

FUNDING

Research work was supported by the Ministerio de Economía y Competitividad (SAF2015-66007P) and by AGAUR, Generalitat de Catalunya (2016PROD00060; 2017SGR1010), co-financed by FEDER funds and by Fundació La Marató de TV3 (20180310). GP-E is a recipient of a PIF (UAB) predoctoral fellowship. LL is a recipient of a CSC predoctoral fellowship.

ACKNOWLEDGMENTS

The authors wish to thank Helena Carbó for laboratory technical support, Clara Villalba for her careful revision of the manuscript and the *Laboratori d'Anàlisi i Fotodocumentació*, Universitat Autònoma de Barcelona for providing the necessary infrastructure. We also wish to thank Dr. Marc Torrent for his help in molecular dynamic studies.

SUPPLEMENTARY MATERIAL

The Supplementary Material for this article can be found online at: https://www.frontiersin.org/articles/10.3389/fphar.2019.01170/full#supplementary-material

SUPPLEMENTARY FIGURE 1 | Modifications of the force field to include inosine parametrization.

SUPPLEMENTARY FIGURE 2 | Phylogenetic tree of representative sequences of pancreatic ribonucleases. The evolutionary history was inferred by using the Maximum Likelihood method and JTT matrix-based model (Jones et al., 1992).

The tree with the highest log likelihood (–27534.43) is shown. The percentage of trees in which the associated taxa clustered together is shown next to the branches. Initial tree(s) for the heuristic search were obtained automatically by applying Neighbour-Join and BioNJ algorithms to a matrix of pairwise distances estimated using a JTT model, and then selecting the topology with superior log likelihood value. The tree is drawn to scale, with branch lengths measured in the number of substitutions per site. This analysis involved 160 amino acid sequences. There were a total of 212 positions in the final dataset. Evolutionary analyses were conducted in MEGA X (Kumar et al., 2018). RNases are labeled with the species abbreviation (see **Table S1**) and its UNIPROT code, or, in its absence, with its NCBI code.

SUPPLEMENTARY FIGURE 3 | Atom nomenclature of the three dinucleotides used in the molecular dynamics simulations.

SUPPLEMENTARY FIGURE 4 | Mobility of the dinucleotides, calculated in RMSD (nm), during each 100 ns simulation run. Each color represents a different replicate.

SUPPLEMENTARY FIGURE 5 | Fraction of hydrogen bond interaction occurrence of the key protein residues involved in the binding to the purine base during each MD simulation run.

SUPPLEMENTARY FIGURE 6 | Schematic illustration of RNase-UpG complexes obtained by molecular dynamics simulations using GROMACS. The picture was generated using PyMOL 1.7.2 (Schrödinger, Inc).

SUPPLEMENTARY FIGURE 7 |Sequence alignment of representative sequences of fish RNases. Protein regions identified to participate in B2 site are highlighted in yellow (L4, spanning from b2 to b3, end of β6 and one of the two catalytic histidines together with a close by residue at β7). Main conserved key residues are: Asn 72/74, Glu 114 and Glu 122/Arg123. TT indicates the presence of a β-turn. Dots label every 10 residues of the reference protein used (Dr-RNase 1). The disulphide bonds are labeled with green numbers. The alignment was performed using Clustal Omega (Sievers and Higgins, 2018), and the picture was drawn using ESPript (Robert and Gouet, 2014). Labels are as follows: red box, white character for strict identity; red character for similarity within a group; and character with blue frame for similarity across groups.

SUPPLEMENTARY FIGURE 8 | Sequence alignment of representative sequences of amphibian RNases. Protein regions identified to participate in B2 site are highlighted in yellow (L4, spanning from b2 to b3, end of β6 and one of the two catalytic histidines together with a close by residue at β7). Main conserved key residues are: Arg5, Asn56 and Thr89/Glu91. TT indicates the presence of a β-turn. Dots label every 10 residues of the reference protein used (Rp-RNase). The disulphide bonds are labelled with green numbers. The alignment was performed using Clustal Omega (Sievers and Higgins, 2018), and the picture was drawn using ESPript (Robert and Gouet, 2014). Labels are as follows: red box, white character for strict identity; red character for similarity within a group; and character with blue frame for similarity across groups.

SUPPLEMENTARY FIGURE 9 | Sequence alignment of representative sequences of reptilian RNases. Protein regions identified to participate in B2 site are highlighted in yellow (L4, spanning from b2 to b3, end of β6 and one of the two catalytic histidines together with a close by residue at β7). Main conserved key residues are: Asn68 and Asp116/Arg117. TT indicates the presence of a β-turn. Dots label every 10 residues of the reference protein used (Cm-RNase 1). The disulphide bonds are labelled with green numbers. The alignment was performed using Clustal Omega (Sievers and Higgins, 2018), and the picture was drawn using ESPript (Robert and Gouet, 2014). Labels are as follows: red box, white character for strict identity; red character for similarity within a group; and character with blue frame for similarity across groups.

SUPPLEMENTARY FIGURE 10 | Sequence alignment of representative sequences of bird RNases. Protein regions identified to participate in B2 site are highlighted in yellow (L4, spanning from b2 to b3, end of β6 and one of the two catalytic histidines together with a close by residue at β7). Main conserved key residues are: Asn65, Arg66 and Trp105. TT indicates the presence of a β-turn. Dots label every 10 residues of the reference protein used (Gg-RNase 1). The disulphide bonds are labelled with green numbers. The alignment was performed using Clustal Omega (Sievers and Higgins, 2018), and the picture was drawn using ESPript (Robert and Gouet, 2014). Labels are as follows: red box, white character for strict identity; red character for similarity within a group; and character with blue frame for similarity across groups.

SUPPLEMENTARY FIGURE 11 | Sequence alignment of representative sequences of mammalian RNases. Protein regions identified to participate in B2 site are highlighted in yellow (L4, spanning from b2 to b3, end of β6 and one of the two catalytic histidines together with a close by residue at β7). Main conserved key residues are: Asn67/Gln69/Asn71, Ala109, Glu111 and Arg122. TT indicates the presence of a β-turn. Dots label every 10 residues of the reference protein used (Bt-RNase 1). The disulphide bonds are labelled with green numbers. The alignment was performed using Clustal Omega (Sievers and Higgins, 2018), and the picture was drawn using ESPript (Robert and Gouet, 2014). Labels are as follows: red box, white character for strict identity; red character for similarity within a group; and character with blue frame for similarity across groups.

SUPPLEMENTARY TABLE 1 | Phylogenetic classification and abbreviations used for the analysed species.

SUPPLEMENTARY TABLE 2 | Main key residues identified by molecular dynamic simulations of the studied RNase complexes with UpA, UpG and UpI. Equivalent residues by structural superposition are indicated. Cationic residues are indicated in blue, anionic residues in red and polar residues in black. Histidine residues involved in stacking interactions with the purine base are coloured in orange. Only specific interactions with purine atoms are included. Specific interaction to purine atoms are illustrated in **Figure 5**.

REFERENCES

Abraham, M. J., Murtola, T., Schulz, R., Páll, S., Smith, J. C., Hess, B. et al. (2015). GROMACS: High performance molecular simulations through multi-level parallelism from laptops to supercomputers, *SoftwareX*, 1–2. 19–25. doi: 10.1016/j.softx.2015.06.001

Acharya, K. R., Allen, S. C., Riordan, J. F., Valleeo, B. L., Shapiro, R., Allen, S. C., et al. (1994). Crystal structure of human angiogenin reveals the structural basis for its functional divergence from ribonuclease. *Proc. Natl. Acad. Sci. U. S. A.* 91, 2915–2919. doi: 10.1073/pnas.91.8.2915

Aguilar, C. F., Thomas, P. J., Mills, A., Moss, D. S., and Palmer, R. A. (1992). Newly observed binding mode in pancreatic ribonuclease. *J. Mol. Biol.* 224, 265–267. doi: 10.1016/0022-2836(92)90589-C

Albery, W. J., and Knowles, J. R. (1976). Evolution of enzyme function and the development of catalytic efficiency. *Biochemistry* 15, 5631–5640. doi: 10.1021/bi00670a032

Allers, J., and Shamoo, Y. (2001). Structure-based analysis of protein–RNA interactions using the program ENTANGLE. *J. Mol. Biol.* 311, 75–86. doi: 10.1006/jmbi.2001.4857

Ardelt, W., Shogen, K., and Darzynkiewicz, Z. (2008). Onconase and amphinase, the antitumor ribonucleases from *Rana pipiens* oocytes. *Curr. Pharm. Biotechnol.* 9, 215–225. doi: 10.2174/138920108784567245

Beintema, J. J., and Kleineidam, R. G. (1998). The ribonuclease A superfamily: general discussion. *Cell. Mol. Life Sci.* 54, 825–832. doi: 10.1007/s000180050211

Berendsen, H. J. C., Postma, J. P. M., Van Gunsteren, W. F., Dinola, A., and Haak, J. R. (1984). Molecular dynamics with coupling to an external bath. *J. Chem. Phys.* 81, 3684–3690. doi: 10.1063/1.448118

Berisio, R., Lamzin, V. S., Sica, F., Wilson, K. S., Zagari, A., and Mazzarella, L. (1999). Protein titration in the crystal state. *J. Mol. Biol.* 292, 845–854. doi: 10.1006/jmbi.1999.3093

Best, R. B., and Hummer, G. (2009). Optimized molecular dynamics force fields applied to the helix-coil transition of polypeptides. *J. Phys. Chem. B.* 113, 9004–9015. doi: 10.1021/jp901540t

Boccaletto, P., Magnus, M., Almeida, C., Żyła, A., Astha, A., Pluta, R., et al. (2017). RNArchitecture: a database and a classification system of RNA families, with a focus on structural information. *Nucleic Acids Res.* 46, D202–D205. doi: 10.1093/nar/gkx966

Boix, E. (2001). "Eosinophil cationic protein," in *Methods in Enzymology* CA, USA: Academic Press, 287–305. doi: 10.1016/S0076-6879(01)41159-1

Boix, E., Blanco, J., Nogués, M. V., and Moussaoui, M. (2013). Nucleotide binding architecture for secreted cytotoxic endoribonucleases. *Biochimie* 95, 1087–1097. doi: 10.1016/j.biochi.2012.12.015

Boix, E., Leonidas, D. D., Nikolovski, Z., Nogués, M. V., Cuchillo, C. M., and Acharya, K. R. (1999a). Crystal structure of eosinophil cationic protein at 2.4 Å resolution. *Biochemistry* 38, 16794–16801. doi: 10.1021/bi9919145

Boix, E., Nikolovski, Z., Moiseyev, G., Rosenberg, H. F., Cuchillo, C. M., and Nogues, M. V. (1999b). Kinetic and product distribution analysis of human eosinophil cationic protein indicates a subsite arrangement that favors exonuclease-type activity. *J. Biol. Chem.* 274, 15605–15614. doi: 10.1074/jbc.274.22.15605

Boix, E., and Nogués, M. V. (2007). Mammalian antimicrobial proteins and peptides: overview on the RNase A superfamily members involved in innate host defence. *Mol. Biosyst.* 3, 317–335. doi: 10.1039/b617527a

Boix, E., Nogués, M. V., Schein, C. H., Benner, S. A., and Cuchillo, C. M. (1994). Reverse transphosphorylation by ribonuclease a needs an intact p2-binding site: point mutations at LYS-7 and ARG-10 alter the catalytic properties of the enzyme. *J. Biol. Chem.* 269, 2529–2534.

Boix, E., Wu, Y., Vasandani, V. M., Saxena, S. K., Ardelt, W., Ladner, J., et al. (1996). Role of the N terminus in RNase A homologues: differences in catalytic activity, ribonuclease inhibitor interaction and cytotoxicity. *J. Mol. Biol.* 257, 992–1007. doi: 10.1006/jmbi.1996.0218

Bussi, G., Donadio, D., and Parrinello, M. (2007). Canonical sampling through velocity rescaling. *J. Chem. Phys.* 126, 1–7. doi: 10.1063/1.2408420

Chan, C. C., Moser, J. M., Dyer, K. D., Percopo, C. M., and Rosenberg, H. F. (2012). Genetic diversity of human RNase 8. *BMC Genomics* 13, 40. doi: 10.1186/1471-2164-13-40

Chang, C. F., Chen, C., Chen, Y. C., Hom, K., Huang, R. F., and Huang, T. H. (1998). The solution structure of a cytotoxic ribonuclease from the oocytes of I (bullfrog). *J. Mol. Biol.* 283, 231–244. doi: 10.1006/jmbi.1998.2082

Chatzileontiadou, D. S. M., Parmenopoulou, V., Manta, S., Kantsadi, A. L., Kylindri, P., Griniezaki, M., et al. (2015). Triazole double-headed ribonucleosides as inhibitors of eosinophil derived neurotoxin. *Bioorg. Chem.* 63, 152–165. doi: 10.1016/j.bioorg.2015.10.007

Chatzileontiadou, D. S. M., Tsika, A. C., Diamantopoulou, Z., Delbé, J., Badet, J., Courty, J., et al. (2018). Evidence for novel action at the cell-binding site of human angiogenin revealed by heteronuclear NMR spectroscopy, *in silico* and *in vivo* studies. *Chem. Med. Chem.* 13, 259–269. doi: 10.1002/cmdc.201700688

Cho, S., and Zhang, J. (2007). Zebrafish ribonucleases are bactericidal: implications for the origin of the vertebrate RNase a superfamily. *Mol. Biol. Evol.* 24, 1259–1268. doi: 10.1093/molbev/msm047

Cuchillo, C. M., Nogueś, M. V., and Raines, R. T. (2011). Bovine pancreatic ribonuclease: fifty years of the first enzymatic reaction mechanism. *Biochemistry* 50, 7835–7841. doi: 10.1021/bi201075b

Curran, T. P., Shapiro, R., and Riordan, J. F. (1993). Alteration of the enzymatic specificity of human angiogenin by site-directed mutagenesis. *Biochemistry* 32, 2307–2313. doi: 10.1021/bi00060a023

Darden, T., York, D., and Pedersen, L. (1993). Particle mesh Ewald: an N·log(N) method for Ewald sums in large systems. *J. Chem. Phys.* 98, 10089. doi: 10.1063/1.464397

delCardayre, S. B., and Raines, R. T. (1994). Structural determinants of enzymic processivity. *Biochemistry* 33, 6031–6037. doi: 10.1021/bi00186a001

Denessiouk, K. A., and Johnson, M. S. (2003). Acceptor–donor–acceptormotifs recognize the Watson–Crick, Hoogsteen and sugardonor–acceptor–donoredges of adenine and adenosine-containing ligands. *J. Mol. Biol.* 333, 1025–1043. doi: 10.1016/j.jmb.2003.09.017

Doucet, N., Watt, E. D., and Loria, J. P. (2009). The flexibility of a distant loop modulates active site motion and product release in ribonuclease A. *Biochemistry* 48, 7160–7168. doi: 10.1021/bi900830g

Draper, D. E. (1999). Themes in RNA-protein recognition. *J. Mol. Biol.* 293, 255–270. doi: 10.1006/jmbi.1999.2991

Draper, D. E. (2015). Reflections on 20 years of RNA. *RNA* 21, 601–602. doi: 10.1261/rna.050930.115

Essmann, U., Perera, L., Berkowitz, M. L., Darden, T., Lee, H., and Pedersen, L. G. (1995). A smooth particle mesh Ewald method. *J. Chem. Phys.* 103, 8577. doi: 10.1063/1.470117

Fontecilla-Camps, J. C., De Llorens, R., Le Du, M. H., and Cuchillo, C. M. (1994). Crystal structure of ribonuclease A·d(ApTpApApG) complex. Direct evidence for extended substrate recognition. *J. Biol. Chem.* 269, 21526–21531. doi: 10.2210/pdb1rcn/pdb

Gagné, D., Charest, L. A., Morin, S., Kovrigin, E. L., and Doucet, N. (2012). Conservation of flexible residue clusters among structural and functional enzyme homologues. *J. Biol. Chem.* 287, 44289–44300. doi: 10.1074/jbc.M112.394866

Gagné, D., and Doucet, N. (2013). Structural and functional importance of local and global conformational fluctuations in the RNase A superfamily. *FEBS J.* 280, 5596–5607. doi: 10.1111/febs.12371

Gagné, D., French, R. L., Narayanan, C., Simonović, M., Agarwal, P. K., and Doucet, N. (2015). Perturbation of the conformational dynamics of an active-site loop alters enzyme activity. *Structure* 23, 2256–2266. doi: 10.1016/j.str.2015.10.011

Goo, S. M., and Cho, S. (2013). The expansion and functional diversification of the mammalian ribonuclease a superfamily epitomizes the efficiency of multigene families at generating biological novelty. *Genome Biol. Evol.* 5, 2124–2140. doi: 10.1093/gbe/evt161

Harper, J. W., and Vallee, B. L. (1989). A covalent angiogenin/ribonuclease hybrid with a fourth disulfide bond generated by regional mutagenesis. *Biochemistry* 28, 1875–1884. doi: 10.1021/bi00430a067

Hess, B. (2008). P-LINCS: a parallel linear constraint solver for molecular simulation. *J. Chem. Theory Comput.* 4, 116–122. doi: 10.1021/ct700200b

Holloway, D. E., Singh, U. P., Shogen, K., and Acharya, K. R. (2011). Crystal structure of onconase at 1.1 ?? resolution—insights into substrate binding and collective motion. *FEBS J.* 278, 4136–4149. doi: 10.1111/j.1742-4658.2011.08320.x

Honda, S., Loher, P., Shigematsu, M., Palazzo, J. P., Suzuki, R., Imoto, I., et al. (2015). Sex hormone-dependent tRNA halves enhance cell proliferation in breast and prostate cancers. *Proc. Natl. Acad. Sci.* 112, E3816–E3825. doi: 10.1073/pnas.1510077112

Hsu, C.-H., Liao, Y.-D., Pan, Y.-R., Chen, L.-W., Wu, S.-H., Leu, Y.-J., et al. (2003). Solution structure of the cytotoxic RNase 4 from oocytes of bullfrog *Rana catesbeiana*. *J. Mol. Biol.* 326, 1189–1201. doi: 10.1016/S0022-2836(02)01472-9

Hsu, C. H., Chang, C. F., Liao, Y., Wu, S. H., and Chen, C. (2015). Solution structure and base specificity of cytotoxic RC-RNase 2 from *Rana catesbeiana*. *Arch. Biochem. Biophys.* 584, 70–78. doi: 10.1016/j.abb.2015.08.010

Imazawa, M., Irie, M., and Ukita, T. (1968). Substrate specificity of ribonuclease from *Aspergillus saitoi*. *J. Biochem.* 64, 595–602. doi: 10.1093/oxfordjournals.jbchem.a128936

Irie, M., Nitta, K., and Nonaka, T. (1998). Biochemistry of frog ribonucleases. *Cell Mol. Life Sci.* 54, 775–784. doi: 10.1007/s000180050206

Jones, D. T., Taylor, W. R., and Thornton, J. M. (1992). The rapid generation of mutation data matrices. *Bioinformatics* 8, 275–282. doi: 10.1093/bioinformatics/8.3.275

Jorgensen, W. L., Chandrasekhar, J., Madura, J. D., Impey, R. W., and Klein, M. L. (1983). Comparison of simple potential functions for simulating liquid water. *J. Chem. Phys.* 79, 926. doi: 10.1063/1.445869

Kazakou, K., Holloway, D. E., Prior, S. H., Subramanian, V., and Acharya, K. R. (2008). Ribonuclease A homologues of the zebrafish: polymorphism, crystal structures of two representatives and their evolutionary implications. *J. Mol. Biol.* 380, 206–222. doi: 10.1016/j.jmb.2008.04.070

Kondo, J., and Westhof, E. (2011). Classification of pseudo pairs between nucleotide bases and amino acids by analysis of nucleotide-protein complexes. *Nucleic Acids Res.* 39, 8628–8637. doi: 10.1093/nar/gkr452

Kumar, S., Stecher, G., Li, M., Knyaz, C., and Tamura, K. (2018). MEGA X: Molecular evolutionary genetics analysis across computing platforms. *Mol. Biol. Evol.* 35, 1547–1549. doi: 10.1093/molbev/msy096

Lee, J. E., Bae, E., Bingman, C. A., Phillips, G. N., and Raines, R. T. (2008). Structural basis for catalysis by onconase. *J. Mol. Biol.* 375, 165–177. doi: 10.1016/j.jmb.2007.09.089

Lee, J. E., and Raines, R. T. (2003). Contribution of active-site residues to the function of onconase, a ribonuclease with antitumoral activity. *Biochemistry* 42, 11443–11450. doi: 10.1021/bi035147s

Leonidas, D. D., Boix, E., Prill, R., Suzuki, M., Turton, R., Minson, K., et al. (2001). Mapping the ribonucleolytic active site of eosinophil-derived neurotoxin (EDN): High resolution crystal structures of EDN complexes with adenylic nucleotide inhibitors. *J. Biol. Chem.* 276, 15009–15017. doi: 10.1074/jbc.M010585200

Liao, Y.-D. (1992). A pyrimidine-guanine sequence-specific ribonuclease from *Rana catesbeiana* (bullfrog) oocytes. *Nucleic Acids Res.* 20, 1371–1377. doi: 10.1093/nar/20.6.1371

Lisgarten, J. N., Maes, D., Wyns, L., Aguilar, C. F., and Palmer, R. A. (1995). Structure of the crystalline complex of deoxycytidylyl-3',5'-guanosine (3',5'-dCpdG) cocrystallized with ribonuclease at 1.9 Angstrom resolution. *Acta Crystallogr.–Sect. D Biol. Crystallogr.* 51, 767–771. doi: 10.1107/S0907444995001570

Liu, J., Wang, X., Cho, S., Lim, B. K., Irwin, D. M., Ryder, O. A., et al. (2015). Evolutionary and functional novelty of pancreatic ribonuclease: a study of Musteloidea (order Carnivora). *Sci. Rep.* 4, 5070. doi: 10.1038/srep05070

Lomax, J. E., Bianchetti, C. M., Chang, A., Phillips, G. N., Fox, B. G., and Raines, R. T. (2014). Functional evolution of ribonuclease inhibitor: insights from birds and reptiles. *J. Mol. Biol.* 426, 3041–3056. doi: 10.1016/j.jmb.2014.06.007

Lomax, J. E., Eller, C. H., and Raines, R. T. (2017). Comparative functional analysis of ribonuclease 1 homologs: molecular insights into evolving vertebrate physiology. *Biochem. J.* 2219–2233. doi: 10.1042/BCJ20170173

Lu, L., Li, J., Moussaoui, M., and Boix, E. (2018). Immune modulation by human secreted RNases at the extracellular space. *Front. Immunol.* 9, 1–20. doi: 10.3389/fimmu.2018.01012

Luscombe, N. M. (2001). Amino acid-base interactions: a three-dimensional analysis of protein-DNA interactions at an atomic level. *Nucleic Acids Res.* 29, 2860–2874. doi: 10.1093/nar/29.13.2860

Lyons, S. M., Fay, M. M., Akiyama, Y., Anderson, P. J., and Ivanov, P. (2017). RNA biology of angiogenin: current state and perspectives. *RNA Biol.* 14, 171–178. doi: 10.1080/15476286.2016.1272746

Lyons, S. M., Fay, M. M., and Ivanov, P. (2018). The role of RNA modifications in the regulation of tRNA cleavage. *FEBS Lett.* 592, 2828–2844. doi: 10.1002/1873-3468.13205

Madhusudhan, M. S., and Vishveshwara, S. (2001). Computer modeling of human angiogenin-dinucleotide substrate interaction. *Proteins Struct. Funct. Genet.* 42, 125–135. doi: 10.1002/1097-0134(20010101)42:1<125::AID-PROT120>3.0.CO;2-K

Maguid, S., Fernández-Alberti, S., Parisi, G., and Echave, J. (2006). Evolutionary conservation of protein backbone flexibility. *J. Mol. Evol.* 63, 448–457. doi: 10.1007/s00239-005-0209-x

Merlino, A., Mazzarella, L., Carannante, A., Di Fiore, A., Di Donato, , A., et al., et al. (2005). The importance of dynamic effects on the enzyme activity. *J. Biol. Chem.* 280, 17953–17960. doi: 10.1074/jbc.M501339200

Merlino, A., Vitagliano, L., Antoine Ceruso, M., Di Nola, A., and Mazzarella, L. (2002). Global and local motions in ribonuclease A: a molecular dynamics study. *Biopolymers* 65, 274–283. doi: 10.1002/bip.10225

Merlino, A., Vitagliano, L., Ceruso, M. A., and Mazzarella, L. (2003). Subtle functional collective motions in pancreatic-like ribonucleases: from ribonuclease A to angiogenin. *Proteins Struct. Funct. Bioinform.* 53, 101–110. doi: 10.1002/prot.10466

Mesitov, M. V., Soldatov, R. A., Zaichenko, D. M., Malakho, S. G., Klementyeva, T. S., Sokolovskaya, A. A., et al. (2017). Differential processing of small RNAs during endoplasmic reticulum stress. *Sci. Rep.* 7, 1–14. doi: 10.1038/srep46080

Miao, Z., and Westhof, E. (2016). *RBscore&NBench*: a high-level web server for nucleic acid binding residues prediction with a large-scale benchmarking database. *Nucleic Acids Res.* 44, W562–W567. doi: 10.1093/nar/gkw251

Mohan, C. G., Boix, E., Evans, H. R., Nikolovski, Z., Nogués, M. V., Cuchillo, C. M., et al. (2002). The crystal structure of eosinophil cationic protein in complex with 2',5'-ADP at 2.0 Å resolution reveals the details of the ribonucleolytic active site †, ‡. *Biochemistry* 41, 12100–12106. doi: 10.1021/bi0264521

Morozova, N., Allers, J., Myers, J., and Shamoo, Y. (2006). Protein-RNA interactions: exploring binding patterns with a three-dimensional superposition analysis of high resolution structures. *Bioinformatics* 22, 2746–2752. doi: 10.1093/bioinformatics/btl470

Narayanan, C., Bernard, D. N., Bafna, K., Gagné, D., Agarwal, P. K., and Doucet, N. (2018a). Ligand-induced variations in structural and dynamical properties within an enzyme superfamily. *Front. Mol. Biosci.* 5, 1–12. doi: 10.3389/fmolb.2018.00054

Narayanan, C., Bernard, D. N., Bafna, K., Gagné, D., Chennubhotla, C. S., Doucet, N., et al. (2018b). Conservation of dynamics associated with biological function in an enzyme superfamily. *Structure* 26, 426–436.e3. doi: 10.1016/j.str.2018.01.015

Narayanan, C., Gagné, D., Reynolds, K. A., and Doucet, N. (2017). Conserved amino acid networks modulate discrete functional properties in an enzyme superfamily. *Sci. Rep.* 7, 3207. doi: 10.1038/s41598-017-03298-4

Nitto, T., Dyer, K. D., Czapiga, M., and Rosenberg, H. F. (2006). Evolution and function of leukocyte RNase A ribonucleases of the avian species, *Gallus gallus*. *J. Biol. Chem.* 281, 25622–25634. doi: 10.1074/jbc.M604313200

Nitto, T., Lin, C., Dyer, K. D., Wagner, R. A., and Rosenberg, H. F. (2005). Characterization of a ribonuclease gene and encoded protein from the reptile, *Iguana iguana*. *Gene* 352, 36–44. doi: 10.1016/j.gene.2005.03.002

Nogués, M. V., Moussaoui, M., Boix, E., Vilanova, M., Ribó, M., and Cuchillo, C. M. (1998). The contribution of noncatalytic phosphate-binding subsites to the mechanism of bovine pancreatic ribonuclease A. *Cell. Mol. Life Sci.* 54, 766–774. doi: 10.1007/s000180050205

Páll, S., and Hess, B. (2013). A flexible algorithm for calculating pair interactions on SIMD architectures. *Comput. Phys. Commun.* 184, 2641–2650. doi: 10.1016/j.cpc.2013.06.003

Parés, X., Nogués, M. V., de Llorens, R., and Cuchillo, C. M. (1991). Structure and function of ribonuclease A binding subsites. *Essays Biochem.* 26, 89–103.

Pizzo, E., Merlino, A., Turano, M., Russo Krauss, I., Coscia, F., Zanfardino, A., et al. (2011). A new RNase sheds light on the RNase/angiogenin subfamily from zebrafish. *Biochem. J.* 433, 345–355. doi: 10.1042/BJ20100892

Prats-Ejarque, G., Arranz-Trullén, J., Blanco, J. A., Pulido, D., Nogués, M. V., Moussaoui, M., et al. (2016). The first crystal structure of human RNase 6 reveals a novel substrate-binding and cleavage site arrangement. *Biochem. J.* 473, 1523–1536. doi: 10.1042/BCJ20160245

Prats-Ejarque, G., Blanco, J. A., Salazar, V. A., Nogués, V. M., Moussaoui, M., and Boix, E. (2019). Characterization of an RNase with two catalytic centers. Human RNase6 catalytic and phosphate-binding site arrangement favors the endonuclease cleavage of polymeric substrates. *Biochim. Biophys. Acta–Gen. Subj.* 1863, 105–117. doi: 10.1016/j.bbagen.2018.09.021

Raines, R. T. (1998). Ribonuclease A. *Chem. Rev.* 98, 1045–1066. doi: 10.1021/cr960427h

Ramanathan, A., and Agarwal, P. K. (2011). Evolutionarily conserved linkage between enzyme fold, flexibility, and catalysis. *PLoS Biol.* 9, e1001193. doi: 10.1371/journal.pbio.1001193

Richards, F. M., and Wyckoff, H. W. (1971). "Bovine pancreatic ribonuclease," in *Hydrolysis The Enzymes*. Ed. P. D. Boyer NY, USA: Academic Press, 647–806. doi: 10.1016/S1874-6047(08)60384-4

Robert, X., and Gouet, P. (2014). Deciphering key features in protein structures with the new ENDscript server. *Nucleic Acids Res.* 42, 320–324. doi: 10.1093/nar/gku316

Rosenberg, H. F. (2008). RNase A ribonucleases and host defense: an evolving story. *J. Leukoc. Biol.* 83, 1079–1087. doi: 10.1189/jlb.1107725

Rosenberg, H. F., Dyer, K. D., Tiffany, H. L., and Gonzalez, M. (1995). Rapid evolution of a unique family of primate ribonuclease genes. *Nat. Genet.* 10, 219–223. doi: 10.1038/ng0695-219

Sanjeev, B. S., and Vishveshwara, S. (2005). Dynamics of the native and the ligand-bound structures of eosinophil cationic protein: network of hydrogen bonds at the catalytic site. *J. Biomol. Struct. Dyn.* 22, 657–671. doi: 10.1080/07391102.2005.10507033

Seshadri, K., Rao, V. S., and Vishveshwara, S. (1995). Interaction of substrate uridyl 3',5'-adenosine with ribonuclease A: a molecular dynamics study. *Biophys. J.* 69, 2185–2194. doi: 10.1016/S0006-3495(95)80094-9

Shapiro, R. (1998). Structural features that determine the enzymatic potency and specificity of human angiogenin: threonine-80 and residues 58-70 and 116-123. *Biochemistry* 37, 6847–6856. doi: 10.1021/bi9800146

Shapiro, R., Fett, J. W., Strydom, D. J., and Vallee, B. L. (1986). Isolation and characterization of a human colon carcinoma-secreted enzyme with pancreatic

ribonuclease-like activity. *Biochemistry* 25, 7255–7264. doi: 10.1021/bi00371a002

Sievers, F., and Higgins, D. G. (2018). Clustal Omega for making accurate alignments of many protein sequences. *Protein Sci.* 27, 135–145. doi: 10.1002/pro.3290

Sikriwal, D., Seth, D., Dey, P., and Batra, J. K. (2007). Human eosinophil-derived neurotoxin: involvement of a putative non-catalytic phosphate-binding subsite in its catalysis. *Mol. Cell. Biochem.* 303, 175–181. doi: 10.1007/s11010-007-9471-0

Sorrentino, S. (1998). Human extracellular ribonucleases: multiplicity, molecular diversity and catalytic properties of the major RNase types. *Cell Mol. Life Sci.* 54, 785–794. doi: 10.1007/s000180050207

Sorrentino, S. (2010). The eight human "canonical" ribonucleases: molecular diversity, catalytic properties, and special biological actions of the enzyme proteins. *FEBS Lett.* 584, 2194–2200. doi: 10.1016/j.febslet.2010.04.018

Sorrentino, S., and Libonati, M. (1997). Structure-function relationships in human ribonucleases: main distinctive features of the major RNase types. *FEBS Lett.* 404, 1–5. doi: 10.1016/S0014-5793(97)00086-0

Tamkovich, N., Koroleva, L., Kovpak, M., Goncharova, E., Silnikov, V., Vlassov, V., et al. (2016). Design, RNA cleavage and antiviral activity of new artificial ribonucleases derived from mono-, di- and tripeptides connected by linkers of different hydrophobicity. *Bioorganic Med. Chem.* 24, 1346–1355. doi: 10.1016/j.bmc.2016.02.007

Tarragona-Fiol, A., Eggelte, H. J., Harbron, S., Sanchez, E., Taylorson, C. J., Ward, J. M., et al. (1993). Identification by site-directed mutagenesis of amino acids in the subsite of bovine pancreatic ribonuclease A. *Protein Eng. Des. Sel.* 6, 901–906. doi: 10.1093/protein/6.8.901

Terribilini, M., Sander, J. D., Lee, J. H., Zaback, P., Jernigan, R. L., Honavar, V., et al. (2007). RNABindR: a server for analyzing and predicting RNA-binding sites in proteins. *Nucleic Acids Res.* 35, 578–584. doi: 10.1093/nar/gkm294

Thompson, D. M., Lu, C., Green, P. J., and Parker, R. (2008). tRNA cleavage is a conserved response to oxidative stress in eukaryotes. *RNA* 14, 2095–2103. doi: 10.1261/rna.1232808

Thompson, J. E., Kutateladze, T. G., Schuster, M. C., Venegas, F. D., Messmore, J. M., and Raines, R. T. (1995). Limits to catalysis by ribonuclease A. *Bioorg. Chem.* 23, 471–481. doi: 10.1006/bioo.1995.1033

Torrent, M., Badia, M., Moussaoui, M., Sanchez, D., Nogués, M. V., and Boix, E. (2010). Comparison of human RNase 3 and RNase 7 bactericidal action at the Gram-negative and Gram-positive bacterial cell wall. *FEBS J.* 277, 1713–1725. doi: 10.1111/j.1742-4658.2010.07595.x

Van Treeck, B., Protter, D. S. W., Matheny, T., Khong, A., Link, C. D., and Parker, R. (2018). RNA self-assembly contributes to stress granule formation and defining the stress granule transcriptome. *Proc. Natl. Acad. Sci.* 115, 2734–2739. doi: 10.1073/pnas.1800038115

Vanquelef, E., Simon, S., Marquant, G., Garcia, E., Klimerak, G., Delepine, J. C., et al. (2011). R.E.D. Server: a web service for deriving RESP and ESP charges and building force field libraries for new molecules and molecular fragments. *Nucleic Acids Res.* 39, 511–517. doi: 10.1093/nar/gkr288

Versées, W., Decanniere, K., Van Holsbeke, E., Devroede, N., and Steyaert, J. (2002). Enzyme-substrate interactions in the purine-specific nucleoside hydrolase from *Trypanosoma vivax*. *J. Biol. Chem.* 277, 15938–15946. doi: 10.1074/jbc.M111735200

Vitagliano, L., Merlino, A., Zagari, A., and Mazzarella, L. (2000). Productive and nonproductive binding to ribonuclease A: X-ray structure of two complexes with uridylyl(2′,5′)guanosine. *Protein Sci.* 9, 1217–1225. doi: 10.1110/ps.9.6.1217

Watt, E. D., Rivalta, I., Whittier, S. K., Batista, V. S., and Loria, J. P. (2011). Reengineering rate-limiting, millisecond enzyme motions by introduction of an unnatural amino acid. *Biophys. J.* 101, 411–420. doi: 10.1016/j.bpj.2011.05.039

Webb, B., and Sali, A. (2016). Comparative protein structure modeling using MODELLER. *Curr. Protoc. Bioinform.* 54, 5.6.1-5.6.37. doi: 10.1002/cpbi.3

Xu, H., Liu, Y., Meng, F., He, B., Han, N., Li, G., et al. (2013). Multiple bursts of pancreatic ribonuclease gene duplication in insect-eating bats. *Gene* 526, 112–117. doi: 10.1016/j.gene.2013.04.035

Zegers, I., Maes, D., Dao-Thi, M. H., Wyns, L., Poortmans, F., and Palmer, R. (1994). The structures of rnase a complexed with 3′-CMP and d(CpA): active site conformation and conserved water molecules. *Protein Sci.* 3, 2322–2339. doi: 10.1002/pro.5560031217

Zhang, J. (2007). Disulfide-bond reshuffling in the evolution of an ape placental ribonuclease. *Mol. Biol. Evol.* 24, 505–512. doi: 10.1093/molbev/msl177

Zhang, J., Dyer, K. D., and Rosenberg, H. F. (2000). Evolution of the rodent eosinophil-associated RNase gene family by rapid gene sorting and positive selection. *Proc. Natl. Acad. Sci.* 97, 4701–4706. doi: 10.1073/pnas.080071397

Zhang, J., Zhang, Y., and Rosenberg, H. F. (2002). Adaptive evolution of a duplicated pancreatic ribonuclease gene in a leaf-eating monkey. *Nat. Genet.* 30, 411–415. doi: 10.1038/ng852

Zhao, W., Kote-Jarai, Z., van Santen, Y., Hofsteenge, J., and Beintema, J. J. (1998). Ribonucleases from rat and bovine liver: purification, specificity and structural characterization. *Biochim. Biophys. Acta* 1384, 55–65. doi: 10.1016/S0167-4838(97)00213-6

Conflict of Interest: The authors declare that the research was conducted in the absence of any commercial or financial relationships that could be construed as a potential conflict of interest.

Supplementary Material

Evolutionary Trends in RNA Base Selectivity Within the RNase A Superfamily

Prats-Ejarque, Guillem; Lu, Lu; Salazar, Vivian A.; Moussaoui, Mohammed; Boix, Ester
Correspondence: Ester Boix: Ester.Boix@uab.cat (EB)

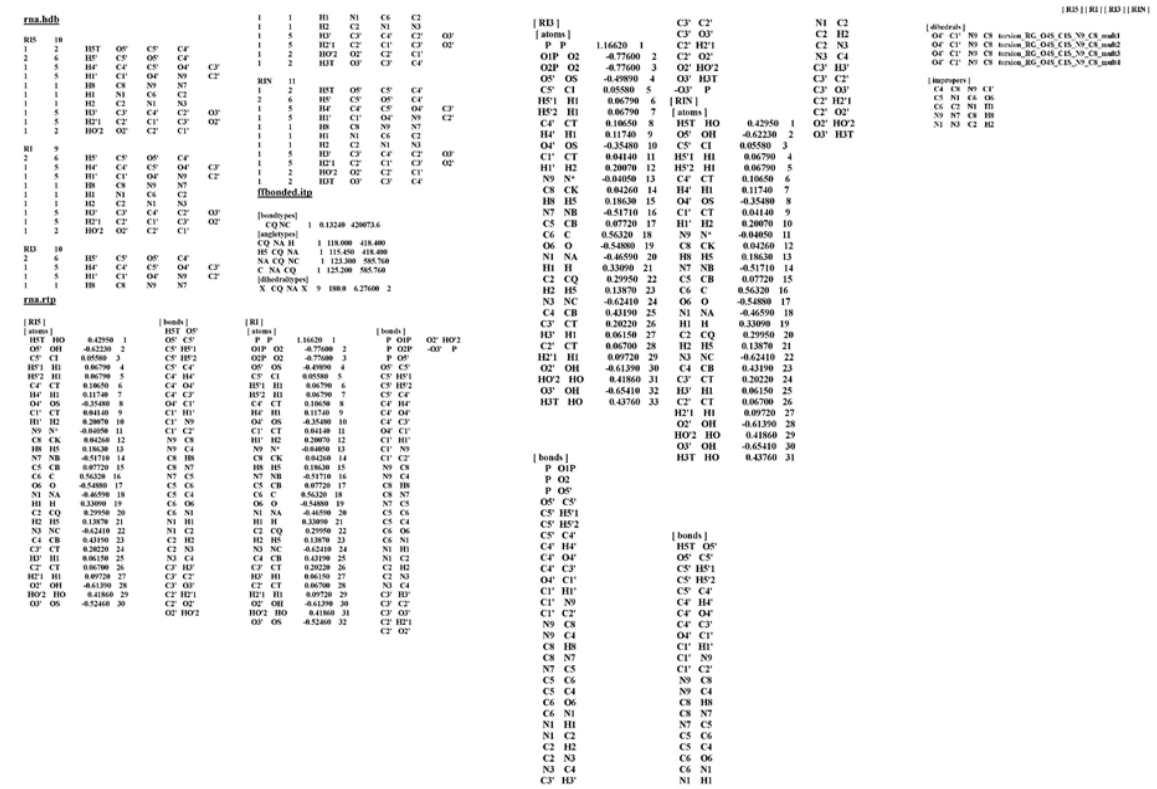

Supplementary Figure 1 | Modifications of the force field to include inosine parametrization.

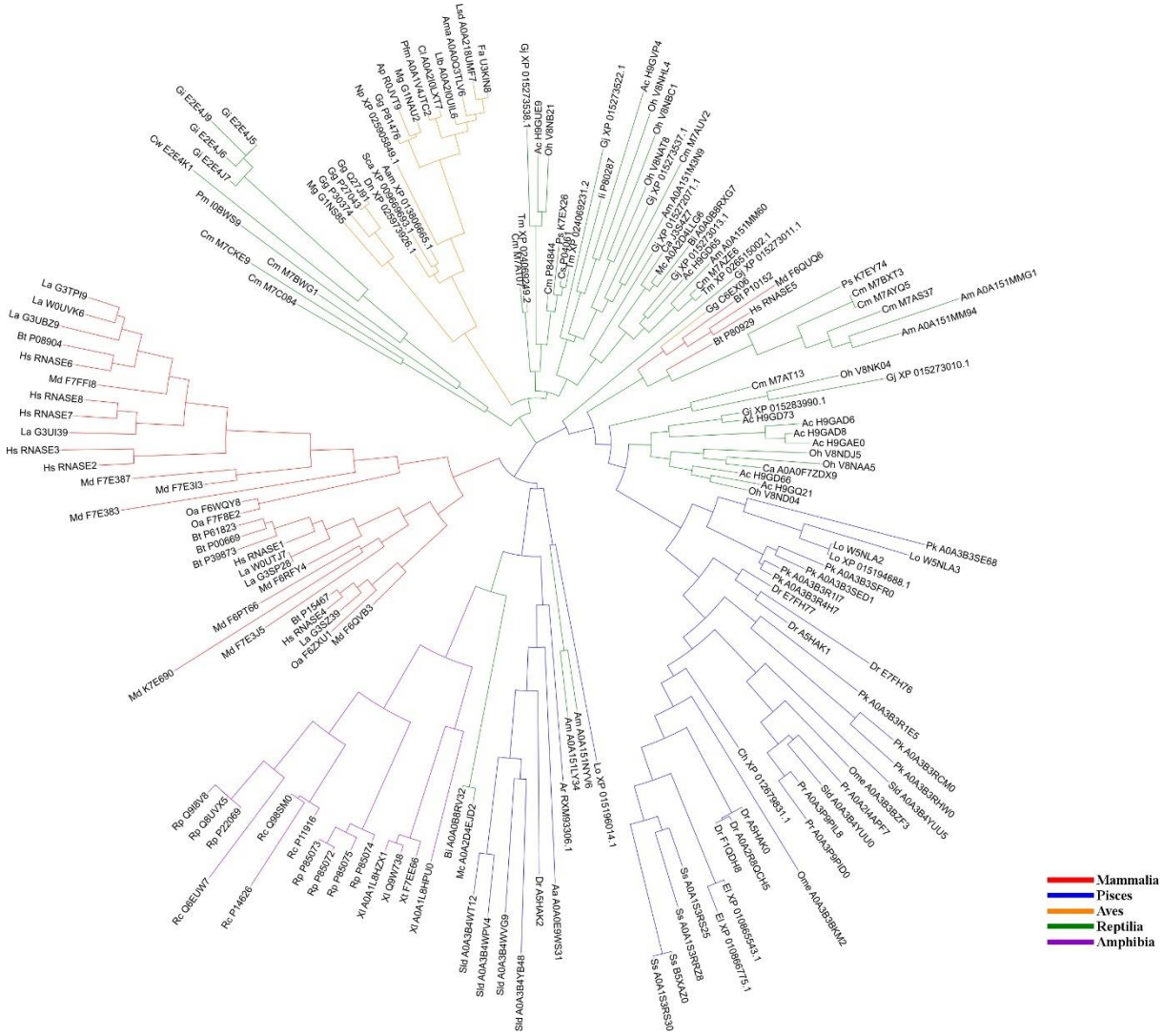

Supplementary Figure 2 | Phylogenetic tree of representative sequences of pancreatic ribonucleases. The evolutionary history was inferred by using the Maximum Likelihood method and JTT matrix-based model (Jones et al., 1992). The tree with the highest log likelihood (−27534.43) is shown. The percentage of trees in which the associated taxa clustered together is shown next to the branches. Initial tree(s) for the heuristic search were obtained automatically by applying Neighbour-Join and BioNJ algorithms to a matrix of pairwise distances estimated using a JTT model, and then selecting the topology with superior log likelihood value. The tree is drawn to scale, with branch lengths measured in the number of substitutions per site. This analysis involved 160 amino acid sequences. There were a total of 212 positions in the final dataset. Evolutionary analyses were conducted in MEGA X (Kumar et al., 2018). RNases are labeled with the species abbreviation (see Table S1) and its UNIPROT code, or, in its absence, with its NCBI code.

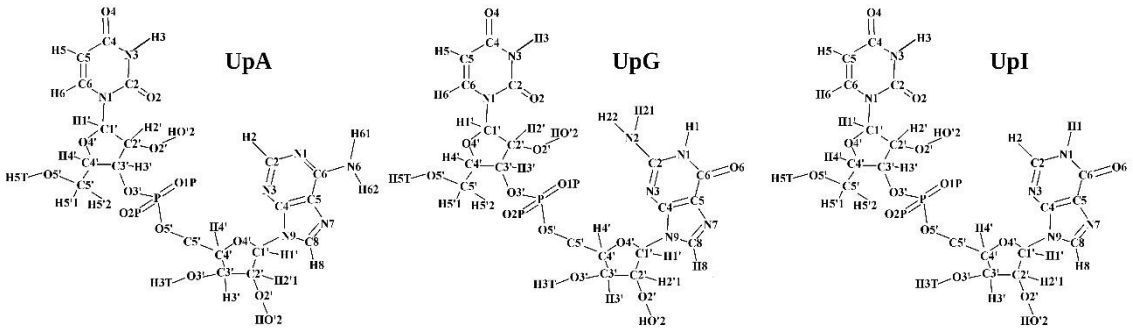

Supplementary Figure 3 | Atom nomenclature of the three dinucleotides used in the molecular dynamics simulations.

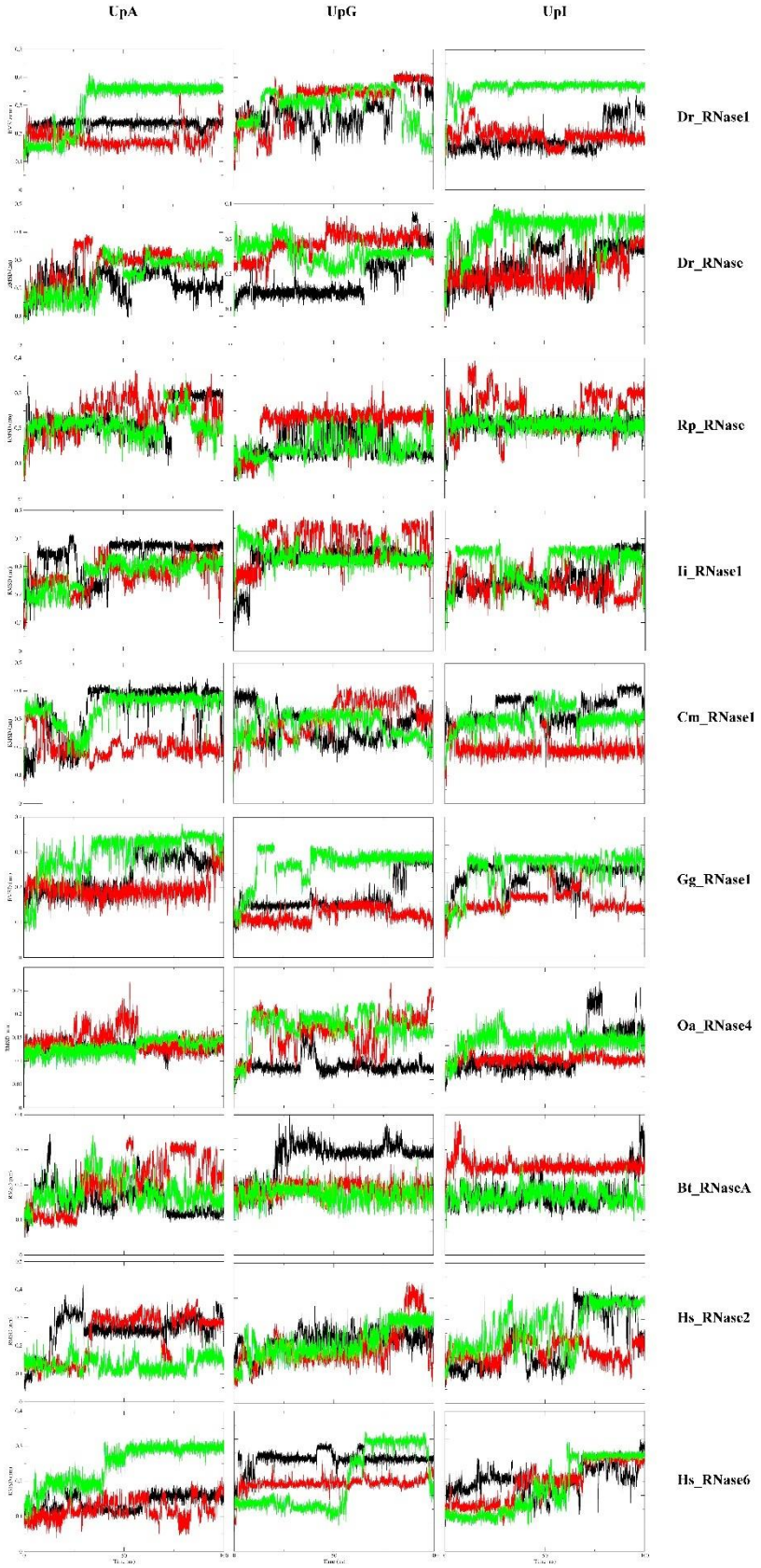

Supplementary Figure 4 | Mobility of the dinucleotides, calculated in RMSD (nm), during each 100 ns simulation run. Each color represents a different replicate.

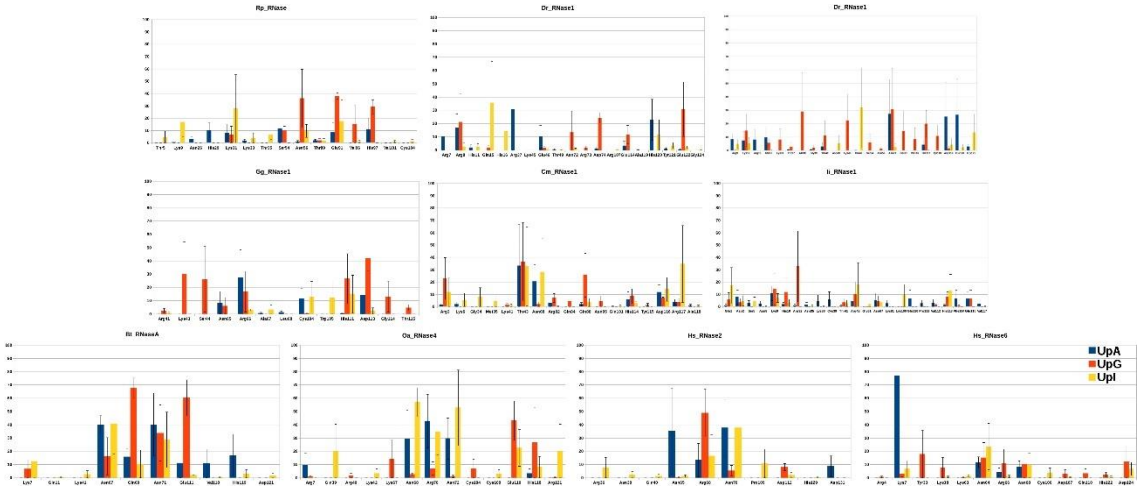

Supplementary Figure 5 | Fraction of hydrogen bond interaction occurrence of the key protein residues involved in the binding to the purine base during each MD simulation run.

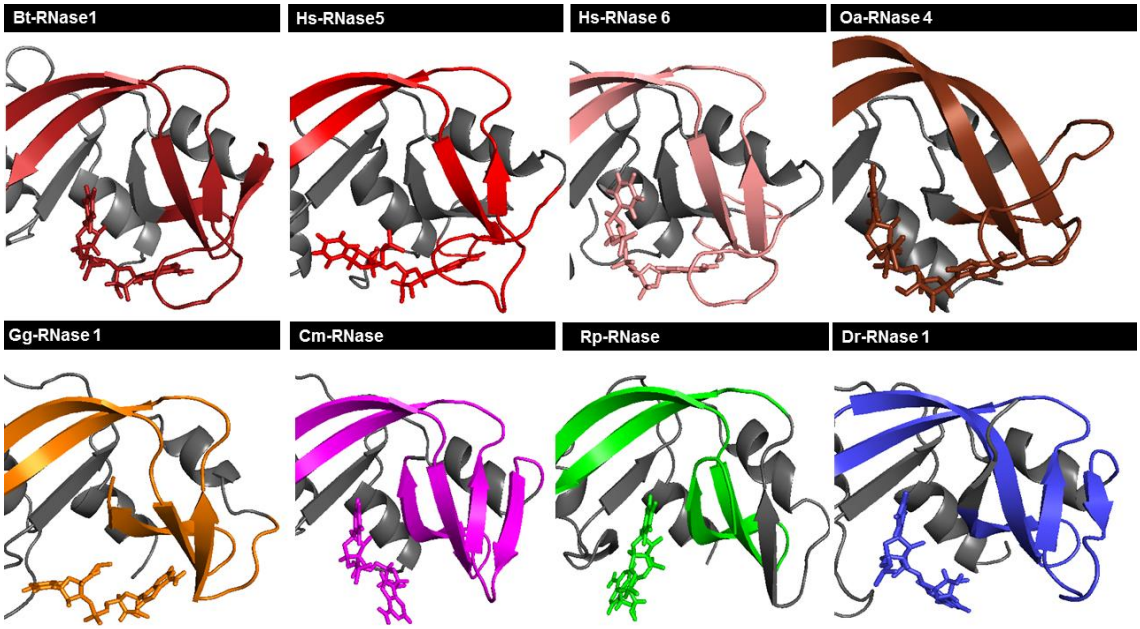

Supplementary Figure 6 | Schematic illustration of RNase-UpG complexes obtained by molecular dynamics simulations using GROMACS. The picture was generated using PyMOL 1.7.2 (Schrödinger, Inc).

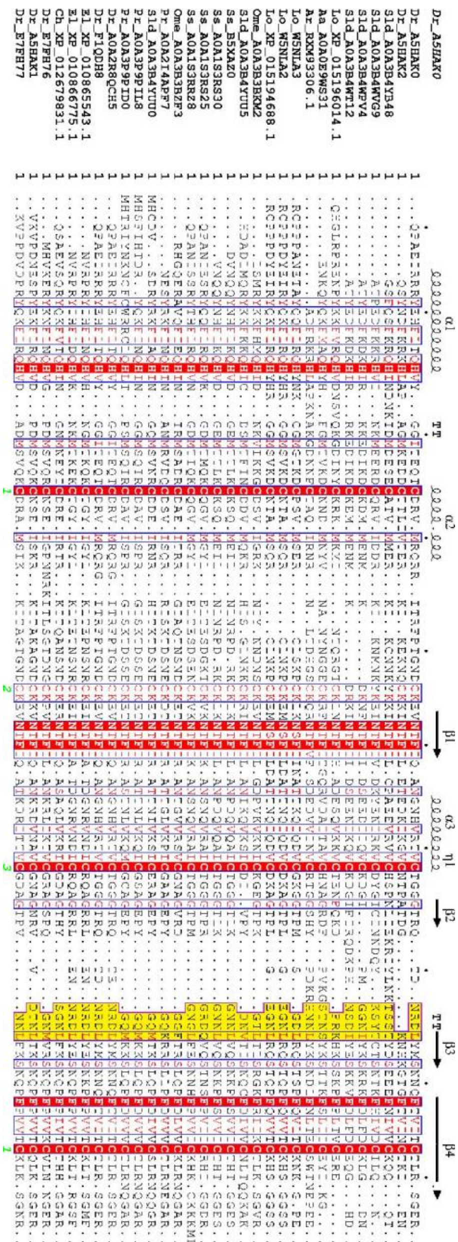

Supplementary Figure 7 | Sequence alignment of representative sequences of fish RNases. Protein regions identified to participate in B2 site are highlighted in yellow (L4, spanning from b2 to b3, end of ß6 and one of the two catalytic histidines together with a close by residue at ß7). Main conserved key residues are: Asn 72/74, Glu 114 and Glu 122/Arg123. TT indicates the presence of a ß-turn. Dots label every 10 residues of the reference protein used (Dr-RNase 1). The disulphide bonds are labeled with green numbers. The alignment was performed using Clustal Omega (Sievers and Higgins, 2018), and the picture was drawn using ESPript (Robert and Gouet, 2014). Labels are as follows: red box, white character for strict identity; red character for similarity within a group; and character with blue frame for similarity across groups.

Rp_P22069
Rp_P22069
X1_A0A1L8HPU0
Xt_F7EE66
X1_Q9W738
X1_A0A1L8HZX1
Rc_Q9DFY6
Rp_Q8UVX5
Rp_Q91BV8
Rc_Q9DFY8
Rc_Q6EUW7
Rc_Q9DFY7
Rc_Q6EUW8
Rc_Q6EUW9
Rc_Q9DFY5
Rc_A0A2G9S8L3
Rp_P85072
Rc_P14626
Rc_Q9DF78
Rc_Q98SL8
Rc_Q98SL9
Rc_Q98SM1
Rc_Q98SM2
Rc_P11916
Rc_Q98SM0
Rc_A0A2G9RDT1
Rc_C1C425

Supplementary Figure 8 | Sequence alignment of representative sequences of amphibian RNases. Protein regions identified to participate in B2 site are highlighted in yellow (L4, spanning from b2 to b3, end of ß6 and one of the two catalytic histidines together with a close by residue at ß7). Main conserved key residues are: Arg5, Asn56 and Thr89/Glu91. TT indicates the presence of a ß-turn. Dots label every 10 residues of the reference protein used (Rp-RNase). The disulphide bonds are labelled with green numbers. The alignment was performed using Clustal Omega (Sievers and Higgins, 2018), and the picture was drawn using ESPript (Robert and Gouet, 2014). Labels are as follows: red box, white character for strict identity; red character for similarity within a group; and character with blue frame for similarity across groups.

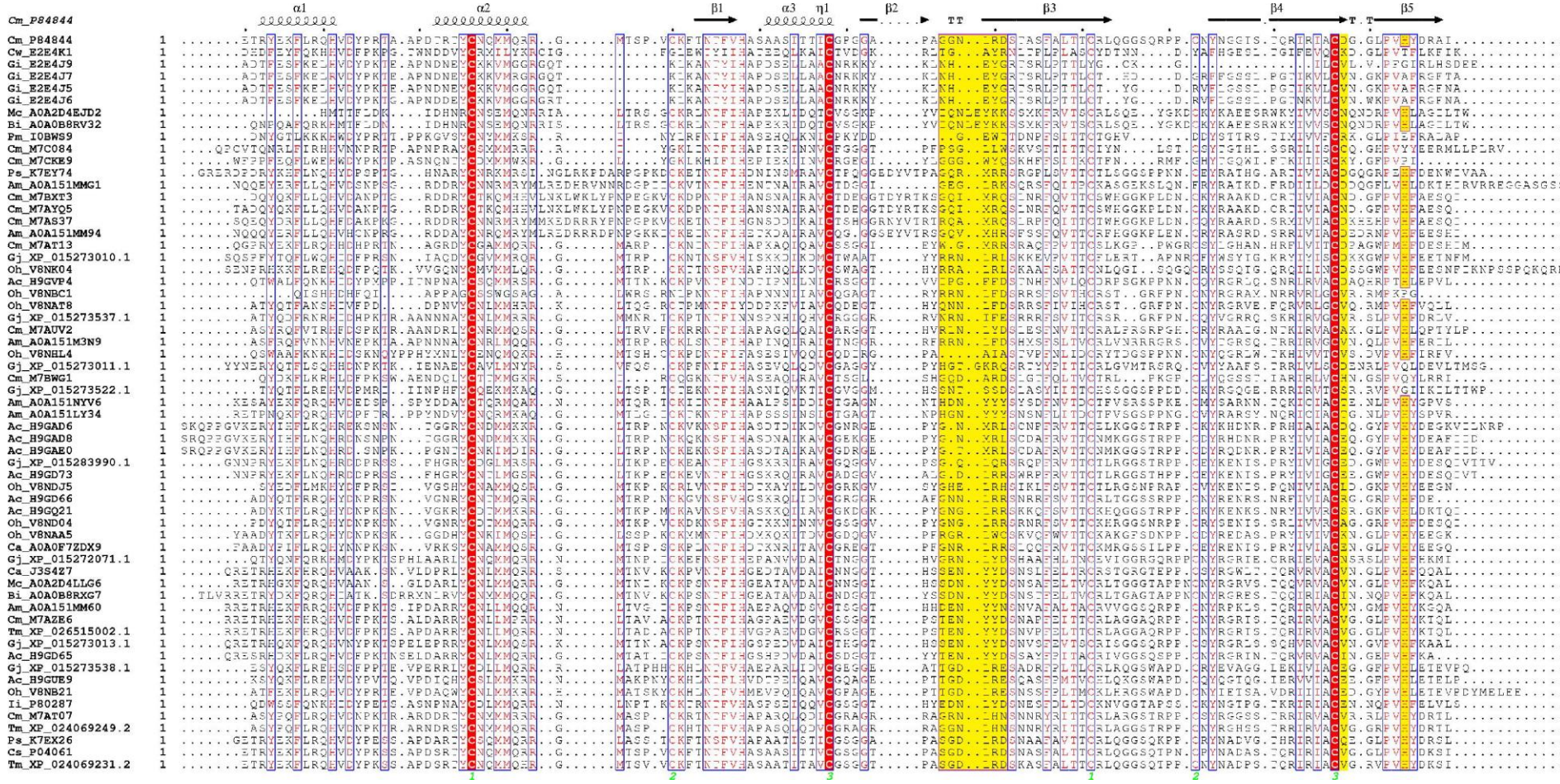
α1
α2
β1
α3
η1
β2
β3
β4
β5
Cm_P84844
Cm_P84844
Cw_E2E4K1
Gi_E2E4J9
Gi_E2E4J7
Gi_E2E4J5
Gi_E2E4J6
Mc_A0A2D4EJD2
Bi_A0A0B8RV32
Pm_I0BWS9
Cm_M7C084
Cm_M7CKE9
Ps_K7EY74
Am_A0A151MMG1
Cm_M7BXT3
Cm_M7AYQ5
Cm_M7AS37
Am_A0A151MM94
Cm_M7AT13
Gj_XP_015273010.1
Oh_V8NK04
Ac_H9GVP4
Oh_V8NBC1
Oh_V8NAT8
Gj_XP_015273537.1
Cm_M7AUV2
Am_A0A151M3N9
Oh_V8NHL4
Gj_XP_015273011.1
Cm_M7BWG1
Gj_XP_015273522.1
Am_A0A151NYV6
Am_A0A151LY34
Ac_H9GAD6
Ac_H9GAD8
Ac_H9GAE0
Gj_XP_015283990.1
Ac_H9GD73
Oh_V8NDJ5
Ac_H9GD66
Ac_H9GQ21
Oh_V8ND04
Oh_V8NAA5
Ca_A0A0F7ZDX9
Gj_XP_015272071.1
Ca_J3S4Z7
Mc_A0A2D4LLG6
Bi_A0A0B8RXG7
Am_A0A151MM60
Cm_M7AZE6
Tm_XP_026515002.1
Gj_XP_015273013.1
Ac_H9GD65
Gj_XP_015273538.1
Ac_H9GUE9
Oh_V8NB21
Ii_P80287
Cm_M7AT07
Tm_XP_024069249.2
Ps_K7EX26
Cs_P04061
Tm_XP_024069231.2

Supplementary Figure 9 | Sequence alignment of representative sequences of reptilian RNases. Protein regions identified to participate in B2 site are highlighted in yellow (L4, spanning from b2 to b3, end of ß6 and one of the two catalytic histidines together with a close by residue at ß7). Main conserved key residues are: Asn68 and Asp116/Arg117. TT indicates the presence of a ß-turn. Dots label every 10 residues of the reference protein used (Cm-RNase 1). The disulphide bonds are labelled with green numbers. The alignment was performed using Clustal Omega (Sievers and Higgins, 2018), and the picture was drawn using ESPript (Robert and Gouet, 2014). Labels are as follows: red box, white character for strict identity; red character for similarity within a group; and character with blue frame for similarity across groups.

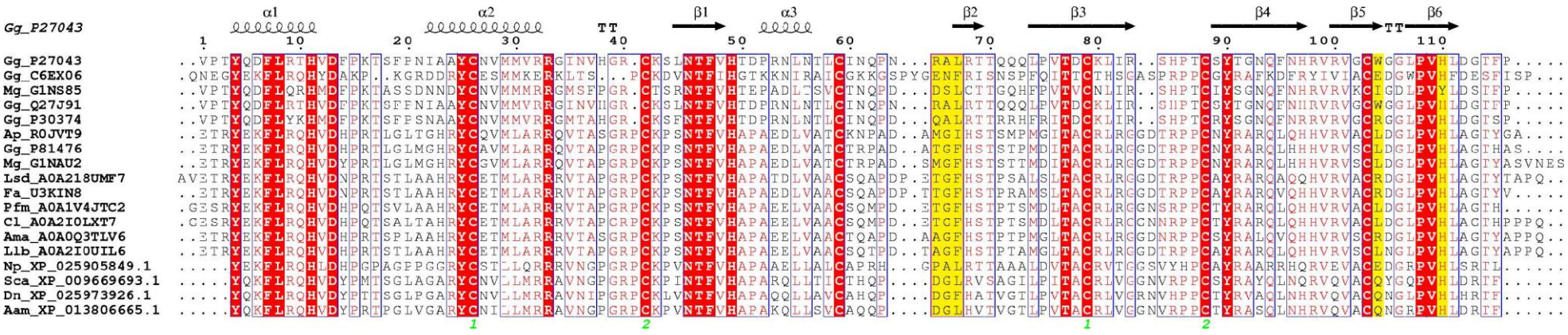
Gg_P27043
α1
α2
TT
β1
α3
β2
β3
β4
β5
TT
β6
1
10
20
30
40
50
60
70
80
90
100
110
Gg_P27043
Gg_C6EX06
Mg_G1NS85
Gg_Q27J91
Gg_P30374
Ap_R0JVT9
Gg_P81476
Mg_G1NAU2
Lsd_A0A218UMF7
Fa_U3KIN8
Pfm_A0A1V4JTC2
Cl_A0A2I0LXT7
Ama_A0A0Q3TLV6
Llb_A0A2I0UIL6
Np_XP_025905849.1
Sca_XP_009669693.1
Dn_XP_025973926.1
Aam_XP_013806665.1
1
2
1
2

Supplementary Figure 10 | Sequence alignment of representative sequences of bird RNases. Protein regions identified to participate in B2 site are highlighted in yellow (L4, spanning from b2 to b3, end of ß6 and one of the two catalytic histidines together with a close by residue at ß7). Main conserved key residues are: Asn65, Arg66 and Trp105. TT indicates the presence of a ß-turn. Dots label every 10 residues of the reference protein used (Gg-RNase 1). The disulphide bonds are labelled with green numbers. The alignment was performed using Clustal Omega (Sievers and Higgins, 2018), and the picture was drawn using ESPript (Robert and Gouet, 2014). Labels are as follows: red box, white character for strict identity; red character for similarity within a group; and character with blue frame for similarity across groups.

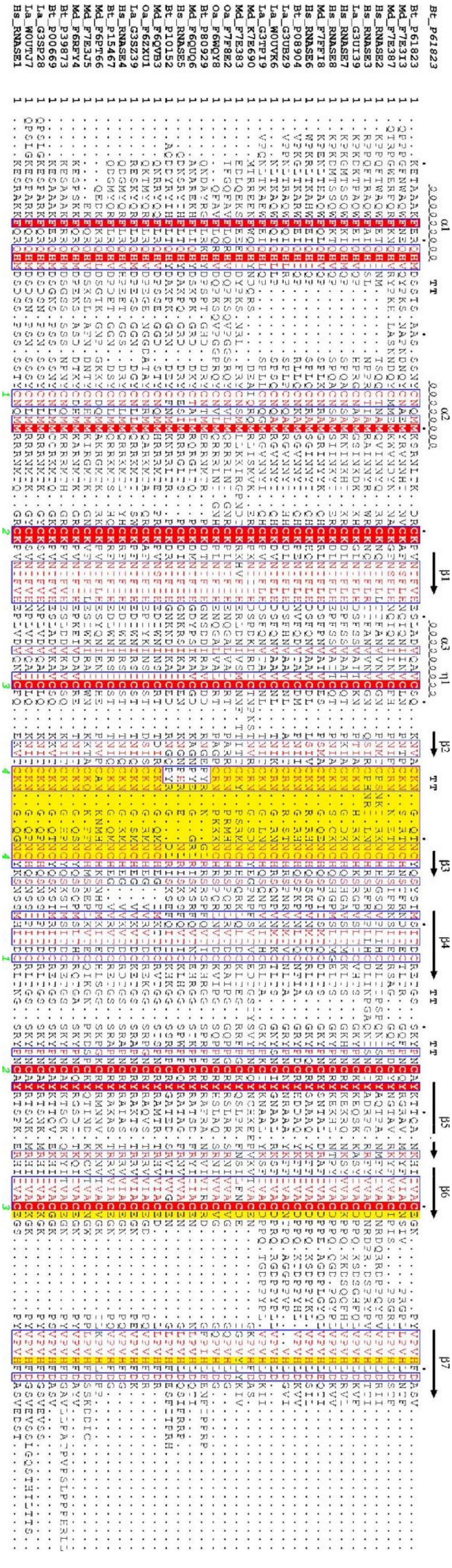

Supplementary Figure 11 | Sequence alignment of representative sequences of mammalian RNases. Protein regions identified to participate in B2 site are highlighted in yellow (L4, spanning from b2 to b3, end of ß6 and one of the two catalytic histidines together with a close by residue at ß7). Main conserved key residues are: Asn67/Gln69/Asn71, Ala109, Glu111 and Arg122. TT indicates the presence of a ß-turn. Dots label every 10 residues of the reference protein used (Bt-RNase 1). The disulphide bonds are labelled with green numbers. The alignment was performed using Clustal Omega (Sievers and Higgins, 2018), and the picture was drawn using ESPript (Robert and Gouet, 2014). Labels are as follows: red box, white character for strict identity; red character for similarity within a group; and character with blue frame for similarity across groups.

Class	Subclass	Cohort	Subcohort	Order	Suborder/ Infraorder	Family	Species	Abb.
Actinopteri (Pisces)	*Neopterygii*	Elopomorpha	-	Anguilliformes	-	Anguillidae	*Anguilla anguilla*	Aa
		Otomorpha	Ostariophysi	Cypriniformes	Cyprinoidei	Cyprinidae	*Danio rerio*	Dr
			Clupei	Clupeiformes	Clupeoidei	Clupeidae	*Clupea harengus*	Ch
		Euteleostei	Protacanthopterygii	Salmoniformes	-	Salmonidae	*Salmo salar*	Ss
				Esociformes	-	Esocidae	*Esox lucius*	El
			Neoteleostei	*Cyprinodontiformes*	Cyprinodontoidei	Poeciliidae	*Poecilla reticulata*	Pr
				Carangiformes	-	Carangidae	*Seriola lalandi dorsalis*	Sld
				Beloniformes	Adrianichthyoidei	Adrianichthyidae	*Oryzias melastigma*	Ome
		-		Lepisosteiformes	-	Lepisosteidae	*Lepisosteus oculatus*	Lo
	Chondrostei	-		Acipenseriformes	-	Acipenseridae	*Acipenser ruthenus*	Ar
Amphibia	Lissamphibia	-		Anura	Sokolanura	Ranidae	*Rana catesbeiana*	Rc
							Rana pipiens	Rp
					Xenoanura	Pipidae	*Xenopus laevis*	Xl
Reptilia	Diapsida	-		Squamata	Gekkota	Gekkonidae	*Gekko japonicus*	Gj
					Diploglossa	Diploglossidae	*Celestus warreni*	Cw
						Anguidae	*Gerrhonotus infernalis*	Gi
					Iguania	Iguanidae	*Iguana iguana*	Ii
						Dactyloidae	*Anolis carolinensis*	Ac
					Ophidia	Elapidae	*Ophiophagus hannah*	Oh
							Micrurus corallinus	Mc
						Lamprophiidae	*Psammophis mossambicus*	Pm
						Viperidae	*Crotalus adamanteus*	Ca
	Anapsida	-		Testudines	Cryptodira	Cheloniidae	*Chelonia mydas*	Cm
						Emydidae	*Terrapene mexicana*	Tm
						Chelydridae	*Chelydra serpentina*	Cs
				Crocodylia	Eusuchia	Alligatoridae	*Alligator mississippiensis*	Am
	Aves	Neognathae	Galloanserae	Galliformes	-	Phasianidae	*Gallus gallus*	Gg
							Meleagris gallopavo	Mg
				Anseriformes	-	Anatidae	*Anas platyrhynchos*	Ap
			Neoaves	Passeriformes	-	Muscicapidae	*Ficedula albicollis*	Fa
						Estrildidae	*Lonchura striata domestica*	Lsd
				Psittaciformes	-	Psittacidae	*Amazona aestiva*	Ama
				Charadriiformes	-	Scolopacidae	*Limosa lapponica baueri*	Llb
				Columbiformes	-	Columbidae	*Patagioenas fasciata monilis*	Pfm
							Columba livia	Cl

				Apterygiformes	-	Apterygidae	*Apteryx australis mantelli*	Aam
		Paleognathae	-	Tinamiformes	-	Tinamidae	*Nothoprocta perdicaria*	Np
Mammalia	Prototheria	-	-	Monotremata	-	Ornithorhynchidae	*Ornithorhynchus anatinus*	Oa
	Metatheria	-	-	Didelphimorphia	-	Didelphidae	*Monodelphis domestica*	Md
	Theria	Placentalia	-	Proboscidea	Elephantiformes	*Elephantidae*	*Loxodonta africana*	La
				Primates	Euprimates	Hominidae	*Homo sapiens*	Hs
				Artiodactyla	Ruminantia	Bovidae	*Bos taurus*	Bt

Supplementary Table 1 | Phylogenetic classification and abbreviations used for the analysed species.

RNaseA Reference numbering	Bt-RNaseA	Hs-RNase6	Hs-RNase2	Oa-RNase4	Cm-RNase	Ii-RNase	Gg-RNase	Rp-RNase	Dr-RNase1	Dr-RNase
A4					R3			D2	R8	R9
R39	R39									
P42						R42			E46	E46
V47					T43					
N67	N67	N64	N65	N68						
Q69	Q69	R66	R68	R70				S54	N72	
N71	N71	N68	N70	N72	N68	N67	R66	N56	D74	N71
G85					Q88					
E111	E111	D107	D112	E110		E107		E91	E114	
H119	H119	H122	H129	H118	H114	H113	H111	H97	H120	H117
D121	D121	D124	D131		D116		D113		E122	D119
A122			R132	R121	R117	E115			R123	E120

Supplementary Table 2. Main key residues identified by molecular dynamic simulations of the studied RNase complexes with UpA, UpG and UpI. Equivalent residues by structural superposition are indicated. Cationic residues are indicated in blue, anionic residues in red and polar residues in black. Histidine residues involved in stacking interactions with the purine base are coloured in orange. Only specific interactions with purine atoms are included. Specific interaction to purine atoms are illustrated in Figure 5.